FORCES ON BODIES IN AN OSCILLATORY FLOW

BY

SHYAMCHARAN SINGH

DEPARTMENT OF AERONAUTICS

IMPERIAL COLLEGE

UNIVERSITY OF LONDON

THESIS SUBMITTED FOR THE DEGREE OF DOCTOR OF PHILOSOPHY IN THE FACULTY OF ENGINEERING, UNIVERSITY OF LONDON.

MAY, 1979.

SUMMARY

A U-tube water tank and drive mechanism were designed, which produced stable sinusoidal oscillations of the water in the tank; these oscillations were capable of attaining a maximum amplitude of about 12". A force measuring system, capable of measuring both in-line and transverse forces was designed. This was used to measure the forces on a circular cylinder, a diamond section cylinder, and a square section cylinder, in the Keulegan and Carpenter number range from 3 to 70. Flow visualisation revealed the presence of large discrete vortices on three of the sections; but these were not observed on the square section cylinder. On these sections where large vortices were formed, they set up clearly defined flow patterns which were generally similar. The similarity in flow pattern on the three sections leads to some similarity in the in-line force. The transverse force on the circular cylinder and diamond section is also similar in its variation during a cycle, for the same Keulegan and Carpenter number. On the square section cylinder, the absence of any clearly defined vortex patternfor values of the Keulegan and Carpenter number less than about 25, leads to a different behaviour of both the in-line and transverse forces. However for values of the Keulegan and Carpenter number greater than about 25, the flows past all the sections are similar as they become quasi-steady and a Karman vortex street is formed. In thisregion therefore the behaviour of both the in-line and transverse forces on the square section cylinder is more or less similar to that observed on the other sections, except that some turbulence is produced by the square section. On all these sections, for small values of the Keulegan and Carpenter number, their inertia coefficients tend towards their corresponding attached flow values. For large values of the Keulegan and Carpenter number the tendency of the flow to become quasi-steady is reflected in the drag coefficients all tending towards their corresponding steady flow values, except on the square section cylinder where the presence of turbulence results in a drag coefficient lower than the smooth, steady flow value. Both the in-line and transverse forces are

related to the vortex strengths and positions, and since these tend to show some variation from cycle to cycle, both forces show some cycle to cycle variation. However the variation is more pronounced on the transverse force since this force is entirely due to the vortices; as a matter of fact the transverse force on all the sections occurs in irregular bursts. The transverse force also occurs over a wide band of frequencies which in general increases with NKC, though the Strouhal number formed from the centre frequency appears to tend towards a constant value as NKC increases. Blockage has been shown to be important in oscillatory flows, causing a marked increase in the in-line force for values of the Keulegan and Carpenter number greater than about 5. Finally Morison's equation has been shown to result in poor prediction for sharp-edged bodies and for circular cylinders when large vortices are present which remains close to the body. However for values of the Keulegan and Carpenter number greater than about 25 to 30 a fairly good prediction by Morison's equation is obtained for all the sections tested.

ACKNOWLEDGEMENTS

I would like to thank both the academic and non-academic staff of the Aeronautics Department for their help and friendship during my time at Imperial College. Of the non-academic staff, I am particularly grateful to Mr McAra and Mr. John Coles for their assistance in the workshop, and to Mr. John O'Leary for his help with photography.

Of the academic staff I am especially grateful for the excellent supervision provided by Dr. P.W. Bearman and Dr. J.M.R. Graham, which has been extremely useful and interesting throughout.

I would also like to express my sincerest thanks and appreciation to my wife, Anne for her support and encouragement throughout, and for typing this thesis.

This research was supported by the Science Research Council and forms part of their Marine Technology Research programme. Finally I would also like to thank the University of London for providing a studentship which enabled me to carry out this research.

CONTENTS

		Page No.
Summary		i
Acknowledgements		iii
Contents		iv
List of Symbols		vi
CHAPTER: 1	INTRODUCTION	
1.1	Review Of The Problem	1
1.2	Some Previous Studies In The Drag/Inertia Regime.	11
1.3	Aims of Present Study	22
CHAPTER: 2	EXPERIMENTAL EQUIPMENT AND TECHINIQUE	
2.1.	The 'U' Tube Water Tank	26
2.1.1	Preliminary Considerations	26
2.1.2	Design Of The Tank	29
2.1.3	Driving Mechanism and Water Displacement Gauge.	32
2.1.4	Characteristics Of The Tank	33
2.2	Force Measuring System	35
2.2.1	The Design	35
2.2.2	Dynamic Response of Load Cells & Models	39
2.3	Data Logging	45
CHAPTER: 3	DATA ANALYSIS	
3.1	Data Reduction	47
3.2	Blockage Correction	54
3.3	The Computer Programs	55
CHAPTER: 4	RESULTS OF FORCE MEASUREMENTS	
4.1	In-Line Force	59
4.1.1	The Circular Cylinder	59
4.1.2	The Flat Plates	70
4.1.2 (A)	The 1.5" Diameter Flat Plate	70
4.1.2 (B)	Blockage	75
4.1.3	The Diamond Section	78
4.1.4	The Square Section	81
4.2	Transverse Force	83
4.2.1	The Circular Cylinder	83
4.2.2	The Diamond Section	87
4.2.3	The Square Section	89

Page No.

CHAPTER: 5 FLOW VISUALISATION

5.1 Introduction 92
5.2 Visualisation Technique 92
5.3 The Circular Cylinder 96
5.4 The Flat Plates 101
5.5 The Diamond Section 105
5.6 The Square Section 109
5.7 Conclusion 112

CHAPTER: 6 DISCUSSION

6.1 In-Line Force 113
6.2 Morison's Equation 123
6.3 Transverse Force 131
6.4 Some Important Effects 141
6.4.1 Body Geometry 141
6.4.2 Blockage 142
6.5 Representation of the Forces 143

CHAPTER: 7 CONCLUSIONS 147

References 152

Appendix: 1 Response Of Load Cells and Models 158

Appendix: 2 Phase Shift Analysis 165

Appendix: 3 In-Line Force Coefficients 168

Appendix: 4 R.M.S. Force From Morison's Equation 171

Appendix: 5 In-Line Force Coefficients - Data 173

Appendix: 6 Vortex Positions During a Cycle 180

Figures

LIST OF SYMBOLS

a	Semi-wave height
A	Amplitude of water oscillation
An, Bn, Bn'	Fourier coefficients
c	Structural damping
C	Single total force coefficient
C_a	Added mass coefficient
C_D	Drag coefficient
C_{Dc}	Corrected drag coefficient
C_{Ds}	Drag coefficient for force with phase shift
C_F	General in-line force coefficient
C_{Fc}	In-line force coefficient predicted by Morison's equation.
C_{Fmax}	Maximum in-line force coefficient
C_{Frem}	Remainder term equal to difference between C_F and C_{Fc}
C_{Frms}	Root mean square in-line force coefficient
C'_{Frms}	Root mean square force coefficient but now with force nondimensionalised by $\frac{1}{2}\rho D^3/T^2$
C_{Frms_c}	Root mean square force coefficient calculated from Morison's equation.
C_h	History coefficient
C_L	Lift or transverse force coefficient
C_{Lmax}	Maximum lift force coefficient
C_{Lmin}	Minimum lift force coefficient
C_{Lrms}	Root mean square lift force coefficient
C_m	Inertia coefficient
C_{ms}	Inertia coefficient but for force with a phase shift
C_{Pb}	Base pressure coefficient
C_{PF}	Pressure coefficient on front face
D	Diameter of body
e	Distance between cylinder and wall
E	Modulus of elasticity; Difference between measured force and that calculated by Morison's equation.
EI	Flexural stiffness
f	Frequency of water oscillations
f_n	Natural frequency of model and load cell combination

f_T	Frequency used in description of the transverse force
F	In-line force per unit length
F_a	Force due to added mass
F_I	Inertial force
F_k	Froude - Krylov force
F_T	Total in line force
g	Acceleration due to gravity.
I	Moment of inertia
k	{Added mass coefficient (C_a); Structural stiffness; base pressure parameter
l	Measuring element of load cell
L	{Length of model; Lift force; total length of fluid in tank
m	Mass of model
m_a	Added mass
M	Mass of model and added mass
n	Selection parameter to determine no. of points used to describe a cycle.
NKC	Keulegan and Carpenter number
r	Volume ratio , = ratio of volume of model to volume of a notional cylinder based on the maximum transverse dimension of the body
S	Frontal area of body
t	time
T	Natural period of oscillation
U	Ambient velocity
U_m	Maximum free-stream velocity or velocity amplitude
v	Vertical velocity
v_{max}	Amplitude of vertical velocity
V	Volume of fluid displaced by a notional circular cylinder of diameter equal to the maximum transverse dimension of the body.
x	Horizontal distance between a vortex and its image
y	Vertical distance between a vortex and its image
β	Viscous parameter = $D^2/\nu T$
γ	Damping coefficient
Γ	Vortex strength
δ_m	Added mass
ϵ	Phase shift

ν	Kinematic viscosity
ϕ	Phase of maximum force
μ	Viscosity
ρ	Fluid density
λ	Wave length
θ	$= 2\pi\, t/_T$ = angle in radians
ω	= cyclic frequency

CHAPTER: 1

INTRODUCTION

1.1. REVIEW OF THE PROBLEM

In recent years, the rapid development of the offshore industry has provided a major impetus to the study of fluid loading on offshore structures. However, after substantial research, both the designer and researcher still face considerable problems in the prediction of loads on these structures. These problems arise for a number of reasons, but probably the most fundamental of all is a lack of understanding of the fluid mechanics associated with these complex unsteady flows generated in the sea. A brief description of the commonly used fluid loading regimes, and the prediction methods used therein will help to illustrate some typical problems. Detailed accounts may be found in a rather comprehensive review paper by Hogben (1974) and also in another paper by Milgram (1976).

These regimes may be broadly classified under the headings of, pure reflection, diffraction, inertia, and drag; the importance of which will depend on two parameters relating to the size of the structure and to the flow conditions. The first of these parameters is the ratio of the diameter of the body (D) to the wavelength (λ) of the wave; which serves as a measure of the disturbance of the incident wave. The second is the Keulegan and Carpenter number (NKC), which by definition is $U_m T/D$; where U_m = Amptitude of the orbital velocity, T = period of the motion, and D is the diameter of the body. This was first introduced by Keulegan and Carpenter (1958), who used it to correlate their force data. The Keulegan and Carpenter number may be viewed as a parameter which compares the path length of an orbiting fluid particle, with the body diameter and gives an indication of the flow development. It thus gives a measure of the relative

importance of drag and inertia forces, (see Appendix:1 of Hogben et al (1977)). There are no distinct boundaries separating these loading regimes and quite often a structure experiences loads of different types. However within certain ranges of flow conditions one type of loading may prevail over another.

Pure reflection of waves occur when $D/\lambda > 1$, and is of more significance in the design of coastal structures such as sea walls and breakwaters rather than in the design of offshore structures.

Diffraction forces arise when $D/\lambda > 0.2$; then, the presence of the body causes significant scattering of the incident wave, (a condition which usually occurs on gravity type platform structures) and this effect must be taken into account in the calculation of the loads. In this analysis, viscous effects and hence drag is usually neglected; in a typical analysis the structure is represented mathematically by a series of grids or elements, over which there are a distribution of sources, the nature of which depends on the type of structure and sea conditions. The velocity potential obtained from this source distribution must satisfy the boundary conditions on the body, at the sea surface, at the sea-bed and at large distances from the body. Further, the velocity potential includes a contribution due to the undisturbed incident wave (i.e. in the absence of the body), which gives rise to the Froude - Krylov force. The remaining part is the disturbance potential which includes the effect of wave scattering and a part which includes the local flow disturbance caused by the body, giving rise to the added mass effect. Further details and applications of this method are found in the works of Garrison and Chow (1972), Hogben and Standing (1974), Hogben (1976) and more recently by Isaacson (1978). Since its inception, considerable progress has been made in the diffraction analysis technique, and programs are now available which calculate the loads on and responses of

both fixed and floating structures, e.g. Standing (1978), and usually good agreement with experimental results is achieved. One of the problems in using this analysis is that quite often, parts of a structure may be in different loading regimes, and experiencing forces of different types, also the flow is locally modified. In general such analyses are done numerically on a large computer and are rather costly. Considerable care must therefore be taken, which includes the above mentioned effects, if adequate modelling is to be achieved.

The diffraction analysis technique can also be used to calculate inertia coefficients of bodies of arbitrary cross-sectional shapes, e.g. Hogben, Standing and Osborne (1974). When the body is no longer large compared with the wave length, wave scattering may be neglected, and in the absence of the body, the pressure gradient due to the undisturbed flow, and hence the acceleration may be assumed uniform over the body. The calculated force is then all inertial from which the inertia coefficient may be obtained.

Inertial loads are dominant when $D/\lambda < 0.2$, and NKC less than about 15, then the above two assumptions are justified. These loads are composed of two parts, the Froude Krylov force (F_k) and an added mass effect. The Froude-Krylov force is the force that the fluid would exert on the body, had the presence of the body not disturbed the flow, i.e. due to the pressure gradient of the undisturbed flow which maintains the fluid acceleration in the absence of the body. Thus the Froude-Krylov force is given as:

$$F_k = \rho \dot{V} \dot{U} \qquad (1.1)$$

where ρ = density of fluid, $\dot{V}$ = volume of fluid displaced by the body, and $\dot{U}$ is the acceleration of the fluid; an infinitesimally thin flat plate will therefore experience no such force. The added mass effect however, is caused by the presence of the body which locally disturbs the fluid and gives rise to increased fluid accelerations. These resulting local fluid accelerations causes the body to

experience an extra force (F_a) which may be considered as equivalent to an extra or added mass (δm) with the ambient fluid acceleration. Thus the added mass force is given as:

$$F_a = \delta m \dot{U} = k\rho V\dot{U} \qquad (1.2)$$

where k is usually referred to as the added mass coefficient, and it is usual to define V as the volume of fluid displaced by a notional circular cylinder circumscribing the body, i.e. $V = \pi D^2/4$ where D is the maximum body width. The total inertial force (F_I) is then:

$$F_I = F_k + F_a = \rho V\dot{U} + k\rho V\dot{U} = (\frac{\nu'}{\nu}+k)\rho V\dot{U}$$
$$= C_m \rho V\dot{U} \qquad (1.3)$$

As stated earlier, the predominance of inertia over drag at small values of NKC, leads to prediction methods which usually neglect viscous effects. However Graham (1978) has shown that for sharp edged bodies this assumption may not be justified, due to the formation of vortices. Graham also states that the effect of the growing vortices may be significant even in the diffraction regime. Here he showed that at low NKC, the vortex induced drag component of the force is related to the internal angle of the shedding edge of the body and to NKC. For NKC less than about 5 however, viscous forces, i.e. drag arising from separation and vortex formation, though significant for sharp edged bodies are not as important as inertial forces. As NKC increases, these effects become more important, vortex formation and shedding occurs which leads to asymmetry in the flow which generates lift and torque on the body. In the region $5<NKC<25$ both inertia and drag are important and for this reason, it is commonly referred to as the drag/inertia regime. As NKC increases above about 25, the flow approaches a quasi-steady situation, and inertial effects are less important.

The drag/inertia regime is very important as numerous offshore structures, e.g. jacket type platforms, are in this fluid loading region. For this reason, considerable attention and studies have been focussed on fluid loading and prediction

methods in this regime. Unfortunately, however this region presents the greatest problems, as there is no clear understanding of the fluid mechanics associated with flow reversal, together with the numerous other effects which occur; these effects will be mentioned later.

Most prediction methods currently used rely heavily on Morison's equation proposed by Morison et al (1950). Here it is assumed that the force on a fixed body in unsteady flow can be represented by the sum of two independent components; one in phase with the velocity, the drag force and the other in phase with the acceleration known as the inertia force. Estimation of the forces is then possible by using empirically obtained values of the drag coefficient (C_D) and the inertia coefficient (C_m) in the equation. Morison's equation has been used extensively, in predictions of loads on structures, in field experiments and in controlled laboratory experiments, resulting in an abundance of available drag and inertia coefficients. However, in spite of the wide experience gained from the use of Morison's equation, considerable disagreement and uncertainties still exist about its applicability as a tool for prediction, and on the reliability of the coefficients to be used with it. One of the problems arises from the fact that the coefficients for full scale use cannot be obtained from laboratory tests, as these are usually at a lower Reynolds number. In addition, the incident flow during laboratory tests is not usually representative of real sea conditions as these tests are commonly done in regular waves or in planar oscillatory flow. Oscillatory flow represents a simpler case where the orbit is flat as opposed to elliptical,in waves. Field tests are therefore carried out to determine these coefficients and unfortunately, but not surprisingly, the data exhibits considerable scatter. This scatter is amply demonstrated in figures 1.1a, 1.1b and 1.2 taken from Wiegel (1964). Figures

1.1a and 1.1b show the scatter in the drag and inertia coefficients, obtained from field tests and are compared with Keulegan and Carpenter's data. In figure 1.2, which was obtained from field experiments by Wiegel, Beebe and Moon (1957), the drag coefficients were plotted as a function of Reynolds number and still exhibit considerable scatter. They attributed this scatter to the variation of turbulence in the flow, cylinder roughness, interference from other cylinders and the effect of the vortices sweeping back against the cylinder. Another reason for the scatter in the data of Wiegel et al is that the Keulegan and Carpenter number variation was not taken into account; it is now widely accepted that both the drag and inertia coefficients are functions of Reynolds number and NKC. Scatter in field data and laboratory experiments is also discussed by Dean (1976) and by Hogben et al (1977).

In addition to the effects mentioned above, other factors such as irregularity of the incident wave, three dimensionality of the flow and different spanwise correlation all contribute to the scatter in field data. The methods used in data analysis, both, in field tests and laboratory studies could also induce scatter in the available data. This is particularly relevant to experiments where water particle velocities and accelerations are calculated from measurements of surface elevations coupled with some wave theory. The accuracy of the data thus obtained will depend on the choice of the wave theory, (Dean (1970)) and even if the best available theory is used, there is no guarantee that the wave structure will be the same from cycle to cycle, especially in field tests.

Most of the available data, in field tests and laboratory experiments were obtained on circular cylinders as it is the most commonly used shape in offshore structures. Unfortunately, however the circular cylinder, as compared with sharp-edged bodies, is extremely sensitive to most of the above mentioned factors, especially turbulence, roughness and Reynolds number.

In steady flow, results obtained from experiments by Fage and Warsap (1929), up to Reynolds numbers of 2.5×10^5 showed a distinct effect of both free stream turbulence and roughness on the drag of circular cylinders. The effect of free stream turbulence is to promote transition of the shear layers, at a Reynolds number lower than that which would occur in smooth flow; the resulting shear layers remain attached longer at supercritical Reynolds number, and gives a narrower wake width and hence a lower drag. Roughness on circular cylinders was also studied by Achenbach (1971), in steady flow at Reynolds numbers of up to 3×10^6. The work of Fage and Warsap and Achenbach, viewed together shows that, in steady flow, in the subcritical Reynolds number range, the local surface roughness, promotes early transition in the shear layers, and as before enables them to remain attached longer, resulting in a lower drag. As the Reynolds number is increased, in the supercritical range, roughness results in earlier separation of the turbulent shear layers, leading to an increased drag, compared with smooth cylinders. In steady flow, therefore, roughness may be seen to result in an earlier critical region, so the drag drops earlier to a value below the corresponding smooth cylinder value and then rises above this, as the Reynolds number is increased.

In planar oscillatory flow Sarpkaya (1976a, 1976b and 1977a), examined the effect of surface roughness on several circular cylinders and at high Reynolds numbers. In this study considerable effects of roughness on the in line force coefficients were observed; the transverse or lift force did not reflect any significant influence. As in steady flow, the drag coefficient exhibited a similar drop below its equivalent smooth cylinder value, then rose to an asymptotic value well above the smooth cylinder value as the Reynolds number was increased. Sarpkaya noted that this asymptotic value was larger than its corresponding equivalent, with the same roughness in steady flow, and was a function of the relative roughness and Keulegan and Carpenter number. This effect was observed for Keulegan and Carpenter numbers as low as 20, and in the range of Reynolds number of 10^4 to 10^6.

The inertia coefficient also shows considerable influence of roughness, and changes in the opposite direction to the drag coefficient. This coefficient first rises and then drops, again to an asymptotic value below the corresponding smooth cylinder value. Here again the asymptotic value depends on the relative roughness and NKC. Although no significant effect of roughness on the transverse force was observed, probably because of the large scatter that occurs anyway, Sarpkaya reported that for Reynolds numbers greater than about 2×10^4, the Strouhal number remained constant at about 0.22, whereas for smooth cylinders it was a function of NKC and Reynolds number.

Tests on the effect of roughness on cylinders in waves have also been carried out by Matten (1977), who found considerable increase in the total force on rough cylinders for the larger NKC values. The increase in drag due to surface roughness in these unsteady flow situations can be accounted for by two main effects. Firstly, the increased roughness results in a physical increase in the size of the cylinder, which results in a higher drag force. The second reason lies in the effect of roughness on the boundary layer of the cylinder. In these unsteady flows the incident stream is usually turbulent with the degree of turbulence increasing as NKC increases. A rough cylinder in such a flow will therefore experience a higher drag because, both turbulence in the free stream and local surface roughness promotes earlier separation of the boundary layer leading to a larger wake and hence higher drag.

Another possible reason for the scatter in field data, and incidentally also a problem experienced in predicting loads on offshore structures, is the influence of neighbouring elements. In steady flow, because of the numerous practical applications, such as in condenser tubes and cooling towers, this interference effect on circular cylinders has been extensively studied . Some of these effects, have been highlighted in a review of flow interference between two circular cylinders in several possible arrangements by Zdravkovich (1977). Interference effects on other shapes have received

much less attention, but a recent paper by Ball and Cox (1978) showed that interference effects are just as important on flat plates.

By oscillating several cylinders in various arrangements, Laird, Johnson and Walker (1960) observed signigicant influence of neighbouring cylinders on a test cylinder. Both the drag and transverse forces were affected to an extent depending on the spacing of the cylinders, but for a spacing of 10 diameters little influence was noted. For a group of 24 cylinders oscillating in still water, Laird and Warren (1963), observed that the overall drag on the group was less than the sum of the individual drags of the cylinders in a uniform stream of the same maximum velocity as the group. They also found that the drag of the group was a function of the spacing; fluctuations of both the drag and transverse forces which were functions of the Reynolds number were also reported. In an oscillating flow, Sarpkaya (1978) examined the variation of the drag and inertia coefficients on two groups of cylinders, and found that these coefficients were independent of Reynolds numbers. However these tests were conducted for a limited Reynolds number range. Further he noted that these coefficients approached a terminal value at NKC of about 150. Bushnell (1977) also examined interference effects of two circular cylinders and of a group in oscillating flow. Here the angle of the configuration, relative to the flow was also varied and he examined the effect of interference on cylinders with and without trip wires. His results show considerable effect on both the drag and transverse force, which increases with the Keulegan and Carpenter number. He also observed that the magnitude of the interference varied with the orientation of the configuration and that no dependence of Reynolds number on the interference was noted. Reynolds number dependence was examined in this case by attaching trip wires to the cylinders. For the array of cylinders tested, Bushnell's results showed that the transverse force interference was much higher when trip wires were used compared with the smooth cylinders. However he had reason to doubt the validity of this technique to simulate high Reynolds

number flow situation; and his conclusion on the Reynolds number dependence was based on results of the two cylinder arrangement.

Examination of the above-mentioned studies reveal that interference can be considered as the result of two separate effects. For moderately large spacing ratios, the wakes of the upstream cylinders are more or less fully developed at large NKC, with vortices being shed, and these considerably influence the flow development on the remaining cylinders. For smaller spacing ratios, the group acts almost like a single porous body, and the wake development of the upstream cylinders is inhibited.

Further problems in the prediction of loads on offshore structures arise because of cylinder orientation, and variation of flow conditions along the length of the cylinder. In waves, the incident flow is usually orbital with the type of orbit depending on the ratio of the wavelength to the depth; the orbit typically being near-circular for deep water waves towards the surface and elliptical lower down. A vertical cylinder will therefore be subjected to different flow conditions including a spanwise velocity component if it is long enough. A horizontal cylinder on the other hand may have the same incident flow along its span but the wake interaction would be different to that of a vertical cylinder; unless the orbit is flat. For the vertical cylinder, regardless of the orbit, the wake will be swept back against the cylinder; but for the horizontal cylinder the wake will in general follow the orbital path. Depending on the orbit, the vortices shed from the previous half cycle on a horizontal cylinder may be swept far enough away from the cylinder, so that when the flow reverses they may not significantly affect the forces on the cylinder. The horizontal and vertical cylinder in waves therefore represent two different flow situations. For cylinders inclined and yawed, the situation is even more complex, with wake interactions that are totally different to either of the two cases mentioned above.

These factors together with the very complex sea state,

makes fluid loading prediction on offshore structures a very complex problem. In order therefore to achieve a better understanding of the fluid mechanics associated with these flows, these factors must be separated, and individually studied under laboratory conditions. Unfortunately, however experiments and investigations in laboratories are usually carried out at Reynolds numbers too low to be representative of real conditions. Information thus obtained cannot usually be confidently extrapolated to real sea conditions. The present study will therefore mainly concentrate on bodies with fixed separation points, i.e. sharp edged bodies, where much less an effect of Reynolds number, as compared with a circular cylinder, is expected, and in the drag/inertia regime. The circular cylinder will also be studied, mainly as a basis for comparison. Flow reversal and its consequences, i.e. the return of the wake usually consisting of rather large vortices, and its interaction with the body was mentioned in the previous paragraph. This feature which is one of the more important characteristics of wave flows is always present in real situations, and will be examined by studying the relatively simpler case of planar oscillatory flow past various bluff bodies. Such a study, although not immediately useful to designers, will help to explain some features of the more complex real sea conditions. It also represents a simpler situation which can be treated mathematically, e.g. Stansby (1978) and therefore provides data for comparison with such computer models.

1.2 SOME PREVIOUS STUDIES IN THE DRAG/INERTIA REGIME

Probably the most singular significant contribution to the prediction of wave forces has been the proposal by Morison et al that the force may be represented by a summation of two independent components, the drag and the inertia.

In its usual form this equation is written as:

$$F = \tfrac{1}{2} \rho C_D D U / V + C_m \frac{\pi D^2}{4} \rho \frac{dU}{dt} \qquad (1.4)$$

where F = force per unit length acting normal to the axis of the body and in the direction of the incident wave, ρ = fluid

density, C_D = drag coefficient, D = diameter of the body, U = water particle velocity, dU/dt = particle acceleration, C_m = inertia coefficient. In their original work Morison and his co-workers measured the force on a vertical pile, and the wave profile; by solving equation (1.4) for zero water particle velocity C_m was obtained and at zero acceleration C_D was found. These coefficients were then assumed constant over a wave cycle and this input to equations 1.4 to predict the force. Values of C_m and C_D thus obtained by Morison et al showed no dependence on Reynolds number.

An alternative method of representing the force was proposed by Iversen and Balent (1951) who stated that the added mass should not be constant, but is a variable and depended on the state of the motion. Thus, they proposed that the force be represent by:

$$F = C \tfrac{1}{2} \rho U^2 S \qquad (1.5)$$

where F = total force, S = frontal area of body, and from similarity arguments they showed that:

$$C = \text{function (Reynolds No., Froude No., body geometry, } \dot{U} D/U^2) \qquad (1.6)$$

where the parameter $\dot{U} D/U^2$ is the acceleration modulus, sometimes referred to as Iversen's Modulus. They conducted experiments on flat disks at Reynolds number high enough so that this effect was secondary and in accelerated motion, and found good correlation between the coefficient C and the acceleration modulus; (see figure 1.3 taken from Crooke (1955)). However in estimating the added mass coefficient, they assumed C_D constant and independent of Iversen's modulus, an assumption which is strictly only justified at small values of the modulus where the force is likely to be drag dominated. Nevertheless they found that at large values of the modulus the added mass coefficient did approach the potential flow value and was fairly well correlated, however at smaller values of $\dot{U} D/U^2$ rather poor correlation was obtained. Iversen and Balent attributed this lack of correlation between the added mass coefficient and the acceleration modulus at small values of the latter, to wall interference effects, and that in their analysis technique at small $\dot{U} D/U^2$, the procedure involved taking the difference between two terms of the same order, i.e. the actual added mass or inertia force was very

small. The acceleration modulus can be regarded as a parameter which compares acceleration dependent forces, i.e. inertia, with velocity dependent forces, i.e. drag, and therefore implies some dependence between drag and inertia. It is thus very similar to the Keulegan and Carpenter number, and for a harmonically varying flow is related to NKC through the relation:-

$$\text{Iversen's modulus} = \frac{2\pi}{NKC}$$

This method of representing the force by a single coefficient was also used by Crooke (1955) who re-analysed some existing wave force data and found good correlation with the acceleration modulus. Keim (1956) used basically the same experimental arrangement as Iversen and Balent, but tested circular cylinders; his results expressed as a single coefficient also correlated well with Iversen's modulus and illustrated Reynolds number dependence. More recently Karanfilian and Kotas (1978), on experiments on spheres oscillating in still water noted that the force, again when expressed in terms of a single coefficient was a function of both Reynolds number and the acceleration modulus. It is worth noting that when the force was expressed in terms of a drag, an inertia and a history coefficient, a term included to represent the history of the motion; the inertia (C_m) and history coefficients (C_h) exhibited a certain amount of scatter, when plotted to show variation with the Reynolds number and acceleration modulus. In determining the two above mentioned coefficients, the drag coefficient was derived from available data; C_m and C_h were then obtained from points in the cycle where the inertia and history term respectively became zero. It is very interesting to note that in experiments on a sphere in harmonic flow, Sarpkaya (1975) did not find any Reynolds number dependence of the force coefficients C_m, and C_D obtained through the use of Morison's equation. However experiments on cylinders by Laird, Johnson and Walker (1959), led them to the conclusion that the resistance, or force coefficient did not correlate well with the acceleration modulus at small values of the parameter. As mentioned earlier, at small $\dot{U}\ D/U^2$, the force is likely to be drag dominated, and the force coefficient

will tend towards a constant quasi-steady flow value, thus independent of the acceleration modulus. This constant value will in general, however, be dependent on the flow conditions and in particular, for cylinders, a function of Reynolds number.

The variability of the added mass coefficient was noted by Keulegan and Carpenter (1958), but they used Morison's equation to represent the force and absorbed any variation of the added mass in the inertia coefficient. Here forces were measured on several flat plates and circular cylinders, placed at the node of a standing wave. By comparing Morison's equation with a Fourier series representation of the measured force, they obtained a series solution for C_m and C_D, thus time dependent values of these coefficients could be obtained. However they used only the first term of these series and obtained constant values averaged over the cycle for the drag and inertia coefficients, which they found, correlated well with the parameter now called the Keulegan and Carpenter number (NKC), defined earlier. Other measured quantities, namely the maximum force and the phase of the maximum force also correlated well with NKC. As mentioned previously, this parameter gives an indication of the flow development, which Keulegan and Carpenter established by noting that the growth and motion of the vortices were also related to NKC. The predicted force, obtained by substituting the calculated values of C_m and C_D in Morison's equation agreed fairly well with the measured force on the circular cylinder, except in the vicinity of NKC about 15. In general the agreement on plates was not as good. One of the most surprising results that was reported by Keulegan and Carpenter, is that no correlation with Reynolds number was obtained, neither for the flat plates nor the circular cylinders.

Subsequent replotting of Keulegan and Carpenter's data both by Sarpkaya (1976a) and by Garrison, Field and May (1977) showed some dependence of both drag and inertia coefficients on Reynolds number. This lack of Reynolds number dependence

was also overlooked earlier by Sarpkaya and Tuter (1974) and by Sarpkaya (1975). A probable reason for this was that the apparatus used both by Keulegan and Carpenter and by the above mentioned authors did not allow a systematic variation of Reynolds number, as changing NKC resulted in a corresponding change in Reynolds number. However, for any given body size at the same relative oscillation frequency, the ratio of the Reynolds number to NKC is constant. This constant, termed β by Sarpkaya is defined as D^2/ν T, where D = diameter of the body, ν = kinematic viscosity, T = period of oscillation. This parameter therefore gives a measure of the importance of Reynolds number and Yamamoto and Nath (1976) related it to the boundary layer thickness. It was by plotting Keulegan and Carpenter's data for different β values that Sarpkaya was able to observe trends with Reynolds number. Sarpkaya (1976a, 1976b) has carried out extensive measurements of both in-line and transverse forces on smooth and rough circular cylinders at high Reynolds numbers in a rather large U-tube water tunnel. These results show significant influence of Reynolds number on both the in-line and transverse force. Figures 1.4a, and 1.4b, taken from Sarpkaya (1976b) demonstrate the influence of Reynolds number, (by showing the results for different β values), on the drag and inertia coefficients. Sarpkaya (1976b) also reported that for Reynolds numbers less than 2×10^4 these coefficients do not vary appreciably with Reynolds number and that this explains why this dependence was overlooked in previous studies by Keulegan and Carpenter, Sarpkaya and Tuter (1974) and by Sarpkaya (1975). However the work of the last two authors covered a range of β values from 220 to 1380 approximately and Reynolds numbers as high as 5×10^4 were obtained; but the results presented did not reflect this variation of β and instead showed very little scatter when correlated with NKC. Further, the results of Sarpkaya (1976b), (figures 1.4a,1.4b) show significant difference in the C_m and C_D variation, for beta values of 497 and 1107.

Sarpkaya also observed that when Keulegan and Carpenter's data was replotted for different β values, C_m appeared to decrease with increasing β, whereas his showed opposite trends.

Further, Sarpkaya (1975) noted that for NKC greater than about 15, Keulegan and Carpenter's data exhibited a different trend. This anomaly may be explained if Keulegan and Carpenter's wave analysis is re-examined. In the theory for the water particle velocities at the node of the standing wave, (where the model was tested), they represent the horizontal velocity by:

$$U = -U_m \cos \omega t \tag{1.7}$$

and for the dimensions of the tank and under the conditions tested,

$$U_m = 3.43a \tag{1.8}$$

where U_m = maximum horizontal velocity, ω = cyclic wave frequency, and a = semiwave height. The vertical velocity at the same position then reduces to:

$$v = -0.0054\ U_m\ a \sin 2\omega t \tag{1.9}$$

replacing U_m by 3.43a then gives

$$v = -0.019\ a^2 \sin 2\omega t \tag{1.10}$$

The vertical velocity then increases rapidly as the wave height is increased, whereas the horizontal velocity increases linearly. At the instant when v becomes maximum, i.e. at $\omega t = \pi/4$

$$\left(\frac{v}{U}\right)_{\omega t = \pi/4} = \frac{v_{max}}{(U)_{\omega t = \pi/4}} = \frac{0.019\ a^2\sqrt{2}}{U_m} = 0.0076\ a \tag{1.11}$$

From Keulegan and Carpenter's tabulated values of U_m, using equation (1.8) results in values of the semi-wave height, which range from 2.9 to 21.4 cms. This gives values of $(v/U)_{\omega t = \pi/4}$ from 0.02 to 0.16. (note that the above equations are dimensionally correct, because the constants are not dimensionless, but were obtained for the dimensions of the tank used by Keulegan and Carpenter). Instantaneously therefore, the vertical velocity can be quite significant; further both v and U are functions of depth, and will therefore vary along the width of the body; this variation is in general small and will depend on wave height. The vertical velocity is in itself quite significant though, as the results of Maull and Norman (1978) show.

Maull and Norman (1978) examined the effect of different orbits, i.e. different v/U, on a horizontal circular cylinder

in waves. They noted that the primary effect of vertical velocity was to alter the trajectory of the vortices. By writing the force in terms of the vortex strengths and positions, using Blasius equation, this can be seen to affect both the in-line and transverse forces; the effect being more pronounced on the latter. Thus Keulegan and Carpenter's results probably represent a flow situation different from Sarpkaya's. The opposing trends between these two sets of results are then quite possibly due to the effect of the vertical velocity in modifying the vortex positions. However, at small enough wave heights and so at small NKC, the vertical velocity may be less significant, and the situation approximates to harmonic flow.

The effect of transverse or lift forces on circular cylinders, both in steady flow and in unsteady motion is well recognised. In a study of lift forces on vertical piles in waves, Bidde (1971) observed that these forces can sometimes be as much as 60% of the longitudinal force. Here, however there was a substantial gap between the end of the pile and the test bed, thus leading to some three dimensional end effects, which may reduce the lift. Isaacson and Maull (1976) also measured transverse forces on vertical cylinders in waves; this work was similar to Bidde's but root mean square and maximum values which showed a peak at NKC about 10 were presented. Spectral analysis showed that in this range of Keulegan and Carpenter number the dominant lift frequency was twice the wave frequency. They also explain the lift generation in terms of the vortex patterns. Sarpkaya and Tuter (1974) and Sarpkaya (1975) also measured lift on circular cylinders, but in a harmonically oscillating flow. They observed that the maximum lift force can sometimes even exceed the maximum in-line force. They found good correlation of the maximum lift force with NKC, as did Bidde, and Isaacson and Maull; however, the lift curve also showed peaks at NKC = 10 and 17 and a trough at about NKC = 15. These results also exhibited remarkably little scatter, except in the region of NKC between 20 and 25. These tests were conducted for Reynolds numbers up to about 5×10^4 and as previously mentioned no Reynolds number dependence

was observed. Sarpkaya (1976a,1976b) extended the Reynolds number range to about 10^6 and tested both smooth and rough cylinders in an oscillatory flow. Results presented show that the lift force on smooth cylinders was dependent on Reynolds number for $Re > 2 \times 10^4$, and on NKC, reaching a single peak at NKC between 10 and 15. As the Reynolds number increased the lift dropped, and at about $Re \approx 10^6$ it was almost constant at about 0.2. The lift frequency and Strouhal numbers were also dependent on NKC and Reynolds number.

Both in-line and transverse forces were also measured by Maull and Milliner (1978a) on a circular cylinder in a sinusoidal flow generated in a U-tube water tunnel. An alternative method of describing the in-line force, in terms of the root mean square (R.M.S) of the measured force, was presented. Good correlation between the R.M.S. force coefficient $C'_{F_{rms}}$, and NKC was achieved; where $C'_{F_{rms}}$ was defined as:

$$C'_{F_{rms}} = \sqrt{F^2} \cdot 2T^2/\rho D^3 \qquad (1.12)$$

Non-dimensionalising the force by $\rho D^3/2T^2$, has the advantage that for a particular body size in a given U-tube, this quantity is constant. Using Morison's equation to represent the force and non-dimensionalising by $\rho D^3/2T^2$, it can be shown (see for example Appendix:4) that the R.M.S. force coefficient is given by:

$$C'_{F_{rms}} = \left\{ \frac{NKC^2}{2} \left(\frac{3}{4} C_D^2 NKC^2 + \pi^4 C_m^2 \right) \right\}^{1/2} \qquad (1.13)$$

Maull and Milliner then showed that the force could be adequately predicted, using equation (1.13) with potential flow value of C_m and a fixed value for the drag coefficient. For their data, at a β value of 200, using $C_m = 2.0$ and $C_D = 1.45$ in equation (1.13) resulted in very good agreement with the measured force, in the range of $NKC \simeq 0$ to 30. Recently Maull (1978) showed that using an inertia coefficient of 2.0, and a fixed value of the drag coefficient which depended on the

Beta value, equation (1.13) obtained from Morison's equation could adequately predict the R.M.S. force for a range of Beta values. Further Maull and Milliner also used Blasius equation to obtain the force, again using the potential flow value of 2.0 for C_m, gives the in-line force as:

$$F = \sum \frac{d}{dt}(\Gamma\rho y) + \rho\frac{\pi D^2}{2}\frac{dU}{dt} \qquad (1.14)$$

and the transverse or lift force as:-

$$L = \sum \frac{d}{dt}(\Gamma\rho x) \qquad (1.15)$$

where Γ = vortex strength; y and x are the vertical and horizontal distances, respectively, between a vortex and its image, and the summation is taken over all vortices in the flow field. This method of representing the force, used also by Maull and Norman (1978), has the advantage that it enables a description of both in-line and transverse forces in terms of the motion and strength of the vortices. Maull and Milliner also found that lift generation was not constant, and traces of the lift force showed that lift generation occurs in uneven bursts his resulted in scatter of the R.M.S. and maximum lift force. Spectral analysis showed that the lift forces occured at multiples of the water oscillation frequency and were related to vortex shedding; the latter being related to the Keulegan and Carpenter number.

By considering a cylinder undergoing motion of the form $a = \sum_{m=1}^{3} a_m \sin(\omega_m t + \phi_m)$, where a = amplitude, Maull and Milliner (1978b) were able to extend their previous work to examine the effect of such a motion on the forces. Even relatively small deviations from a sinusoidal flow, produced noticeable changes both in the magnitude and frequency composition of the in-line force; the main effect being to amplify the harmonic that was introduced. At small values of a_2/a_1, spectra of the lift force revealed a frequency composition similar to that usually obtained for harmonic flow, with peaks occurring at the harmonics. As a_2/a_1, was increased and at moderate NKC, they observed that peaks in the spectra moved away from the harmonics, until at NKC = 32.2,

the peaks were at half-harmonis of the main oscillation frequency. Similar effects were also noticed when a third harmonic was introduced in the cylinder motion, but at a larger value of a_2/a_1, they observed that the peaks were once again occuring at harmonics of the oscillation frequency. Mercier (1973) in tests on circular cylinders which he oscillated, in still water, transverse to a stream and in-line with a stream, also noted that spectra of the transverse force obtained for oscillations in-line with the stream, showed peaks at half harmonics. The common feature in these two situations, i.e. oscillations in-line with a stream, and oscillations with harmonics is that the two halves of a cycle are almost unrelated. During one half of the cycle in Mercier's case, the cylinder is moving into a relatively undisturbed field as the stream has swept the vortices away, but on the next half it moves back into its wake. In Maull and Milliner's case, the situation is slightly different; during one part of the cycle the cylinder moves into a disturbed field due to the presence of vortices from the previous part of the motion, and as it moves the cylinder sheds more vortices. In the next part of the cycle the cylinder slows down, and approaches zero velocity at a rate depending on a_2/a_1, the vortices already shed move further away from the cylinder during this time. The velocity increases slowly at first and then quite rapidly, but during the time the vortices previously formed have moved further away and have diffused to some extent; the cylinder thus moves into a relatively less disturbed field. In both cases a situation arises where, during a part of the cylinder motion, it moves into a rather undisturbed fluid, and for another part the wake previously formed interacts with the cylinder. Bushnell (1977) has shown that for a pair of cylinders in tandem arrangement, in oscillating flow, at a spacing of three diameters, significant transverse force fluctuations arise only when the instrumented cylinder was in the wake of the dummy cylinder. This would suggest that the sweeping back of the vortices

plays an important part in lift generation. The frequency of transverse fluctuations may therefore be based, not only on the number of vortices shed during a cycle, but also on the number of vortices swept back against the cylinder and the time during which this happens. As vortex shedding is related to the Keulegan and Carpenter number, the frequency of the lift fluctuations will also depend on this parameter. Peaks in the lift spectrum, can therefore occur at half-harmonics, or intermediate frequencies, but will depend on the conditions of the motion and flow.

Other effects which have been studied in relative oscillatory flow includes the effect of cylinders close to a wall. This has been examined by Norman and Maull (1978), and for higher Reynolds numbers by Yamamoto and Nath (1976) and Sarpkaya (1977b). Significant effects on the in-line force coefficients, drag and inertia are obtained only when the gap ratio e/D is less than 1, (e = distance from the wall to cylinder). The transverse force is more sensitive to the gap ratio and may be affected for e/D slightly greater than 1. The most significant effect on the lift force, is that for small gap ratios, the cylinder experiences a non-zero time mean force, which increases as the gap decreases and is directed away from the wall.

Other recent studies in this field include the work of Dalton, Hunt and Hussain (1976) which is a follow up of the initial work of Hamman and Dalton (1971), and that of Matten *et al* (1978). Dalton et al did not use Morison's equation but instead plotted the instantaneous force variation with the corresponding Reynolds number for several values of the viscous parameter $D/\sqrt{\nu T} = \sqrt{\beta}$, and NKC. They showed that for increasing NKC, the force approached its equivalent steady flow value, as the instantaneous Reynolds number approached its maximum.

Matten, Hogben and Ashley (1978), measured the instantaneous pressure distribution around a circular cylinder oscillating in still water, at high Reynolds numbers. They noted that end effects can be important, and used end plates during their

study. Instantaneous pressure measurements are very useful in building up information on the flow development.

Most of the available studies in this field, some of which are mentioned here, are concerned strictly with circular cylinders. Besides the work of Keulegan and Carpenter, another more recent work on flat plates has been carried out by Shih and Buchanan (1977). This study was done in the very low Reynolds number range of 1.0 to 1.06 x 10^3, and the maximum force was assumed to be due to the drag only. This assumption is questionable especially as they were dealing with low NKC, where inertia is known to be important. Their results show, however that the drag coefficient, thus defined was independent of Reynolds number when Re >250.

1.3 AIMS OF PRESENT STUDY

In the foregoing discussion some of the problems associated with the prediction of loads on offshore structures, especially in the drag/inertia regime, and some relevant studies were mentioned. In this study an attempt will be made, not to repeat any of the previous work, where possible but rather to understand and explain some of the features present in the more complex situations.

Probably one of the more significant features in wave studies, is the formation and shedding of strong vortices which are swept back against the body as the flow reverses. This feature can be simply studied by considering relative harmonic motion past the test body. In view of the current problem of laboratory experiments, i.e. the lack of Reynolds number similarity, this problem will be minimised by concentrating on sharp-edged bodies. The main effect of Reynolds number on circular cylinders, both in steady flow and in waves, is due to changes in the development and separation of the boundary layer. It is appreciated that Reynolds number also affects the forces through the rate of diffusion of the shed vortices, however this effect is of less importance for flat plates, and Shih and Buchanan (1971)

showed that the force was more or less independent of Reynolds number for Reynolds number > 250. Thus, the above assumption that by considering sharp-edged, (fixed separation points) bodies, Reynolds number will have a lesser effect, is justified. Qualitative results of tests thus obtained will be applicable to higher Reynolds number flow situations. Furthermore, the circular cylinder has been studied extensively, so a detailed study of this will only be a repeat of work already done. Nevertheless, the circular cylinder will not be completely abandoned, and will be tested mainly as a basis for comparison with other workers, and to compare with results on other shapes, both in a qualitative and a quantitative manner.

Another question that often arises in laboratory experiments, is blockage; in oscillatory flow no systematic attempt has been made to examine this, as far as the author is aware. This will be examined here, using flat plates, geometrically similar, but of different sizes, and assuming little effect of Reynolds number.

Besides the work on circular cylinders, spheres and flat plates, very little has been done on the fluid loading on other bluff bodies in waves. Some work, however has been done on large square sections in waves, e.g. Isaacson (1978), Mogridge and Jamieson (1976), but these were of more relevance to the loading at very small values of NKC, i.e. in the inertia/diffraction regime.

The square section represents another sharp-edged body, with fixed separation points where, as with other high aspect ratio bluff bodies, the forces are associated with the formation and shedding of vortices. In a study of this nature, where the primary aim is to examine the effect of the vortices sweeping back against the body as the flow reverses; the square section therefore represents another body on which this effect could be studied. On square sections, as with flat plates, in steady flow, Reynolds number has little effect, e.g. Delany and Sorensen (1953). However square sections, especially at low incidence are sensitive to turbulence in

the free stream, e.g. Bearman (1978), Laneville et al (1975). Here turbulence results in a thickening of the shear layers and in an increase in the curvature, which can cause reattachment; the net effect is therefore to reduce the overall drag.

The bodies to be tested will therefore be three flat plates, a circular cylinder and a square at 0^{o} incidence, i.e. normal to the flow, and at 45^{o} incidence i.e. with a diagonal in-line with the flow (a diamond section). These tests will all be conducted in the drag/inertia regime, where measurements of the in-line and transverse force will be made.

Detailed flow visualisation studies will be made, partly with the help of cine films, to examine the flow development, especially the formation and shedding of vortices; their positions and their fate as the flow reverses will also be examined. By comparing the flow development on the various shapes, together with the results of force measurements, the effect of free and fixed separation points, and bluffness in oscillatory motion could be assessed. Although direct measurements of the vortex strengths and positions will not be made, rough estimates can be made from flow visualisation. These results coupled with force measurements will help to establish the effect of flow reversal.

Another major aim of this study is the assessment of Morison's equation, in this simpler case of harmonic flow. This will be achieved by representing the in-line force as suggested by this equation. On all shapes tested therefore inertia and drag coefficients will be obtained and predicted forces will be compared with those measured. For comparisons between measured and predicted force, the inertia and drag coefficients along with other relevant quantities such as root ream square (R.M.S.) force, maximum force, and the phase of the maximum force, will be obtained by averaging the measured force over several cycles. The variation of these quantities with the Keulegan and Carpenter will also be examined. The above mentioned coefficients will also be evaluated for individual cycles. By examining the variation of these coefficients from the cycle to cycle, the constancy

of the force coefficients can be assessed.

In light of the current knowledge of the importance of transverse forces, these will be measured on the square and diamond sections, and on the circular cylinder. Examinations and comparison of these results will also help to establish the significance of geometry of the body in oscillatory flow.

The other part of this study, discussed in Chapter: 2, is the initial phase, which was the design of suitable apparatus and equipment with which the above mentioned tests could be undertaken. The major part is the design of a tank to produce relative harmonic motion, together with associated drive and control mechanism which must be capable of sustaining stable amplitudes over long periods. A force measuring system, capable of detecting both in-line and transverse forces, together with a set of associated computer programs to assist data evolution, must also be devised. The tank must also allow adequate flow visualisation studies to be carried out.

CHAPTER: 2

EXPERIMENTAL EQUIPMENT AND TECHNIQUE

2.1 THE 'U' TUBE WATER TANK

2.1.1 PRELIMINARY CONSIDERATIONS

A survey of the available literature on fluid loading on offshore structures reveals that the types of rigs used in laboratory investigations fall into two main categories. these are:-

(1) those in which the body under test is made to move in some predetermined manner in a fluid otherwise at rest;

and (2) those where the body is kept stationary and the fluid is made to move.

Case (2) may further be classified into those where:

(a) the body is subjected to a train of waves, generated in a wave tank, e.g. Matten (1977), Maull and Norman (1978);

(b) the body is placed at the node of a standing wave, e.g. Keulegan and Carpenter (1958).

(c) the body is tested in a 'U' shaped tank, where the fluid is made to oscillate at its natural frequency, e.g. Sarpkaya and Tuter (1974), Sarpkaya (1976), Maull and Milliner (1978a).

Examples of the use of apparatus classified here as case(1) may be found in the works of Hamman and Dalton (1971), Garrison, Field and May (1977), Maull and Milliner (1978b). Case (2a), represents a situation where the incident flow is slightly more complex, with the velocity field being orbital. As mentioned earlier, this study is concerned with the more fundamental feature of flow reversal and its consequences in the simpler

case of planar relative harmonic motion. Case (2a) will therefore not be considered as,in waves another variable, the vertical velocity is present. It should be added however that qualitative results in planar oscillatory motion can be applied to the case of waves.

Kinematically, case (1) and case (2) for the same relative motion, with the exception of case (2a) are identical, but when measuring forces or pressures, expected and hence accountable differences arise. This difference is due to the fact that, when the fluid is moving relative to the body, the body experiences an additional force due to the pressure gradient that would exist in the fluid in the absence of the body. This pressure gradient is proportional to the fluid acceleration, and hence in this case the inertial part of the force is increased. This additional force is usually referred to as the Froude Krylov force and is equal to $\rho V \frac{dU}{dt}$, where V = volume of displaced fluid, $\frac{dU}{dt}$ = fluid acceleration.

In practical terms, substantial difference exist between these two cases, therefore the selection of experimental apparatus must be based on careful considerations which include the design requirements. Based on the aims of this study, these requirements are that the tank should be capable of producing relative harmonic flow with a wide range of stable amplitudes. Flow visualisation and force measurements must also be possible and other factors such as available space and construction time are also important.

The differences between these two cases, mentioned above, can be considered by examining the advantages and disadvantages of the two types of rig.

Case (1) : OSCILLATING THE BODY IN A FLUID OTHERWISE AT REST.

One of the main advantages of this system is that the amplitude and frequency may be varied independently. The implication of this is that the effect of Reynolds number (Re) can be studied separately, by fixing the Keulegan and Carpenter (NKC); or by fixing Re, the effect of NKC can be examined. Usually, also a higher Reynolds number can be achieved, compared to when the fluid is oscillated, e.g. in a U tube. This

increased Reynolds number can be achieved, quite simply by increasing the frequency of the oscillating body, and hence the velocity. In such a system also, by careful design, if desired, a more complex motion could be studied, e.g. Maull and Milliner (1978b). In this system however, the inertial force due to the mass of the oscillating body must be subtracted from the total force; this is usually achieved by mounting a second identical instrumented cylinder above the test body such that it performs the same motion in air; the aerodymanic forces on this image cylinder however are ignored as the forces on the test cylinder are about 1000 times greater. Alternatively, another method for correcting for the inertia due to the mass of the oscillating body, is to carry out tests, once in air and once in water. Further consequences of the use of this system is the inevitable vibration problem, leading to noise which may be of sufficiently low frequencies to interfere with the measuring signal. This noise is relatively common when water is used as the working fluid, as the added mass becomes important and thus lowers the overall frequency response, and shifts the noise to a lower frequency band. Such systems also usually employ open tanks where free surface effects, caused by surface waves induced by the oscillating model or support system may be important. When testing horizontal cylinders, the effect of a free surface is not so significant, provided the cylinder is tested well beneath the surface. However, for horizontal cylinders, the support system must be carefully designed, to minimise any disturbance that this might introduce. If struts are used, this can seriously affect the two dimensionality of the flow, by shedding vortices which will result in artificially reduced spanwise coherence. Vertical cylinders, on the other hand do not suffer from the support problems ; here however end effects and surface effects can be important. The cylinder must therefore either be of a length such that there is only a very small gap between itself and the floor, or have an end plate. Another way of eliminating any surface effects or end effects is to test only an element of the cylinder. Surface disturbances are also usually lessened by the introduction of a sheetover the surface which then damps out any irregularities.

Case (2): OSCILLATING THE FLUID PAST A STATIONARY BODY.

The main disadvantage of this system is that irrespective of whether the fluid is being oscillated in a 'U'-Tube or in a tank, the oscillations are usually at the natural frequency of the system. Forced oscillations, off the resonant frequency could be performed, but the power required to do so would be greater compared to where the fluid is oscillating at its natural frequency. It is also generally much more convenient and reliable to have the fluid oscillating at its natural frequency. Unfortunately, however this means that the only two variables are the body diameter and oscillation amplitude; the Reynolds number cannot therefore be varied independently of the Keulegan and Carpenter number. Even though the natural frequency of the system can be changed, substantial changes can be made only if large changes in the amount of fluid are made. However for a given body size, the viscous parameter, β , is constant and therefore a test on several bodies of different sizes can illustrate any Reynolds number effects. As in the previous system, if the fluid oscillations are generated through the use of a standing wave, in a wave tank, free surface effects will again be important. The main advantage is that in this system, there is likely to be less mechanically generated noise, as fewer moving parts are present. Based on these advantages and disadvantages, a 'U' tube type tank was chosen and designed to satisfy the present requirements. It should be noted that the main limitation of this apparatus, in that Re cannot be significantly varied independently of NKC, is not serious in this study, as emphasis is placed on sharp edged bodies where much less an effect of Reynolds number is expected compared with say circular cylinders.

2.1.2 DESIGN OF THE TANK

Although conceptually simple, careful considerations must be made before a final design of the 'U' tube shaped tank is produced. Important factors to be considered are, the geometry of the corners, the length of the working section and the height of the upright arms. The overall size of the

tank and in particular the size of the working section is also very important. From theoretical considerations of the liquid in a 'U' tube undergoing oscillations it can be shown that the natural frequency is given by:

$$f_m = \frac{1}{2\pi}\sqrt{\frac{2g}{L}} \qquad 2.1$$

where f_m = natural frequency in cycles/second, and L = overall length, g = gravitational acceleration. Therefore as the overall tank size is increased, so is L, and the frequency drops, and hence the stream velocity is decreased, resulting in a lower Reynolds number. Thus the corners, upright arms, and the working section (which make up the overall tank length) are important collectively as well as singularly. The corners are important, in that if they are too tight, flow separation can occur, which will introduce disturbances to the stream, and higher damping of the oscillations will result. If the corner is too gentle, the tank will be unnecessarily long, thus causing problems of length mentioned above, The upright arms are of interest as the length of these will also affect the natural frequency of the system. However the most important part of the tank is the working section. A wider working section enables a larger body to be tested, and hence a higher Reynolds number to be achieved.

There is not enough available information to make a confident decision on all of these parameters; a small scale model of a 'U' shaped tank was therefore built to test these parameters. This was made of perspex and in five modular sections, thus allowing either different corners, working section lengths or upright arms or combinations of these to be tested. As the effect of blockage and of aspect ratio in oscillatory flow is not known, the cross-section was made square. After testing various corners, it was decided to use one which had a mean radius of 1.5 times the cross-sectional height. This corner was tight enough to make the tank compact, but still gentle enough to avoid any flow separation. By injecting a filament of dye in to the working section, the effect of the corner on the uniformity of the flow was checked.

These observations, together with a rough idea of the desired maximum aplitude led to the criterion that a working section of length roughly 2.5 times the cross-sectional height was adequate. The height of the upright arms was based on the still water level and maximum amplitude, such that when the water was at its lowest operating level, it was still above the entry to the corners.

The final design is shown in plate (1) and with some later improvements in figure 2.1. For ease of construction and assembly, the tank was built in five modular sections, three of which were made of ⅜" thick aluminium alloy welded together and with 2" flanges. The upright arms however were made of ⅛" thick alumunium, but were reinforced using channel section stiffeners. The modules were assembled, using a rubber seal between adjacent flanges which were then bolted together using 2½" aluminium bolts, placed 2" apart. It should be noted that when assembled, no misalignment or discontinuity of more than about 1/32" of the inner surface of the tank was observed. The working section was 1.52 metres long, the cross-section uniform and of 0.61 metres square, and the corners had a mean radii of 0.91 metres. Finally, the upright arms were of length 1.22 metres.

Channel section stiffeners were later bolted on (three on each face) to the corners of the tank. This was done to stop these faces from flexing and thus to improve the fatigue life of the weld. When pressure measurements were attempted, low frequency fluctuations were observed in the signal, these were later traced to the walls of the corners; reinforcement thus also helped to reduce these fluctuations.

One of the upright arms had two small perspex windows one on either side of the mean water level; these were used to monitor the oscillations and also helped in calibrating the capacitance probe which was used to measure the water level.

The working section had a lid which fitted a 0.61 metre square opening, centrally located on the top surface. This lid was 0.76 metre square and was secured by a series of bolts placed roughly 2" apart; removal of this was necessary when

changing models or when cleaning the tank. A narrow slit, into which a perspex window fitted, was also cut into the lid; this gave a 0.41 m x 0.08 metre area through which the flow could be vertically illuminated for flow visualisation. On either side of the working section, again centrally located, there was a 0.61 m x 0.46 m opening into which windows could be fitted. When measuring forces, a ⅜" thick aluminium alloy plate, reinforced with 'T' sections stiffners was used as the window. For flow visualisation, however, ¾" thick perspex windows were used. Regardless of the windows used, construction was such that when correctly mounted, they were flush with the inside of the tank. Two types of windows were thought necessary because when measuring forces, flexure caused by less stiff windows could cause spurious force signals. Unfortunately , therefore flow visualisation and force measurements could not be undertaken simultaneously. Finally to prevent corrosion and so maintain a uniform inner surface texture, the inside of the tank was painted.

2.1.3 DRIVING MECHANISM AND WATER DISPLACEMENT GAUGE

A capacitance probe was used both to measure the instantaneous water level and to control the tunnel drive system. This was just over 1.22 metres long and consisted of a stainless steel rod which acted as one plate of a capacitance, and a long length of insulated wire doubled back on itself, as the second plate. A small fixed capacitor was connected in parallel with the probe so that when the water was oscillating at large amplitudes, the change in capacitance expressed as a fraction of the capacitance at still water level, was within the working range of the associated instrumentation. That is, the linearity of the probe output was maintained. Connected to the probe was a Disa oscillator, type 51EØ1, the output of which was fed into a Disa reactance converter type 51EØ1. The final output was noise free (R.M.S. of noise about 0.3 mv with water stationary) and the probe was sensitive enough to detect even small ripples on the water surface. This probe was fixed in the upright arm of the tank which has the small perspex windows (see fig.2.1) and with graduations at 1" intervals. The still water level was chosen to be coincident with one of these graduations,

located 0.61 metres above the corner. Calibration of the probe was then achieved by recording the water level signal and measuring the peak to peak amplitude. Because of the very low frequency of the oscillations, measurement of the amplitude was possible with a ruler, placed side-on in the inside of the tank for small amplitudes, and by measuring the position between the graduations (observed through the windows), for the larger amplitudes. This could be done to an accuracy of better than 1/16", however small errors could be introduced by surface tension. A typical calibration of the probe is given in figure 2.2, where the linearity of the output within the range may be observed.

In order to achieve continuous oscillations of the water in the tank with stable amplitudes, a fan mounted on the other upright arm of the tank and controlled by the following feedback system was used. The output from the probe via oscillator and reactance converter, hereafter referred to as the displacement signal, was fed first into a fixed gain amplifier (PHI (Patchable Hybrid Instruments) analogue module M19), set to have a gain of ten, and then into a voltage comparator (PHI Hybrid modale M21). The output from this was then used as input to a relay switch which controlled the switching on or off, of the fan. A variac connected in series with the fan was used to control the power to the fan and hence, the amplitude of oscillations. By suitable adjustment of the voltage comparator, the fan could be made to switch on and off at the 'best' time giving stable oscillations with a maximum amplitude of about 0.3 metres. The fan itself was of a very low power rating, and was mounted on a cover plate; when switched off therefore, air escapes through the blades of the fan, which incidentally was free to rotate in either direction. This method increases the damping considerably, but other methods which included a butterfly valve assembly did not produce very stable oscillations, and introduced spurious vibrations into the system.

2.1.4 CHARACTERISTICS OF THE TANK

In all the experiments, the still water level chosen was

0.61 metres above the top of the corner, at this level the oscillations had a period of 3.33 seconds. Theoretical calculations give the natural frequency of the system as in equation 2.1, from which a period of 3.36 seconds is obtained.

The damping of the oscillations of the water in the tank is shown in figure 2.3a, where the fan and cover plate is removed, (so that both ends are open); here it takes about 35 cycles for the amplitude to fall to half its maximum value. Obviously, the damping arises from the drag on the model and friction at the walls and is therefore not constant, but will be smaller at the lower amplitudes. With the cover plate and fan mounted, but with the fan switched off (so that one end is now closed), the damping is naturally much greater, (figure (2.3b)), and it takes just 15 cycles for the amplitude to fall to half its maximum value.

In order to examine the quality of the displacement signal several checks were carried out. The stability of the oscillations of the water, generated by the fan is illustrated in figure 2.4a, where a typical trace of the displacement signal over a number of cycles is presented. In figure 2.4b a sample of the unfiltered displacement signal is presented to show that this is noise free. The harmonic component of the signal is also analysed, firstly as in figure 2.5 where the displacement signal, averaged over about 50 cycles was compared with a sine wave. Two amplitude cases are presented and very slight deviations from a sine wave are observed in the region of $\theta = 270^{\circ}$; which corresponds to the water at its highest level. This deviation from a perfect sine wave could be due to non-linearity of the probe or be representative of the flow, but in any case it is very small. Another way of examining the frequency content of the displacement signal is to spectrally analyse the signal. In figures 2.6a and 2.6b, spectra of the displacement signal over two different frequency ranges are presented. Figure 2.6a shows that the displacement is primarily at the water oscillation frequency with a very small amount of energy at twice this frequency. The peak at about 2.5 Hz and the other peaks which

appear at higher frequencies, as in figure 2.6b were originally thought to be due to vibrations of the walls of the tank. However, it was later found that these peaks were introduced by the tape recorder during data recording. In figure 2.7a, a spectrum of the noise due to the tape recorder, (obtained by recording with the input shorted), is presented to show that the peaks at higher frequencies in the displacement signal were indeed introduced by the tape recorder. The vibrations of the tank, obtained from the output of an accelerometer placed on a side wall, was also spectrally analysed. This is presented in figure 2.7b, where it can be seen that any peaks in the vibration spectrum are due to the noise of the tape recorder; thus the walls of the tank are not expected to introduce any spurious signals. It should be noted that all the spectra presented were nondimensionalised by the mean square of the signal, and that the root mean square of the noise of the tape recorder was about 11 millivolts.

Finally, by introducing particles into the flow and observing the motion of these, the uniformity of the flow was examined. This was observed to be uniform and one-dimensional (in the absence of any test model) throughout the width and height of the observed part of the working section, except for very small regions close to the wall, i.e. the boundary layer. There was no direct way of measuring this; suffice to say that the influence of this appeared to be confined to a region of about a centimetre from the wall. A theoretical estimate of the influence of viscosity in periodic flow can be found from an exact solution of the equation of motion (Schlichting (1968)). The relevant parameter is the depth of penetration, and gives a measure of the extent to which the oscillating boundary layer will penetrate into the fluid, and is defined as $2\pi\sqrt{\frac{2\nu}{\omega}}$ where ν = kinematic viscosity and ω = frequency of oscillations. In the present case this corresponds to about 0.7 cm.

2.2 FORCE MEASURING SYSTEM

2.2.1 THE DESIGN.

In order to enable reliable measurement of the in-line and transverse forces, a complete force measuring system was

designed. This consisted of a pair of special windows for the working section, two pairs of strain gauged load cells and complementary models.

The design of the load cells must incorporate such features as, high enough natural frequency (with the model connected), linearity, sensitivity, and a maximum strength in excess of any expected loads. Because different sized bodies were to be tested in this study, the requirements of maximum load and sensitivity varied; this necessitated the construction of two pairs of load cells, the basic design of which was identical. The difference between the two pairs were such that one pair, used in conjunction with the largest model tested, a 3 inch diameter flat plate, had slightly stiffer measuring elements, resulting in a greater maximum strength. The remaining models were tested using the less stiff pair of load cells. Further, a pair of cells were necessary, one at either end of the model, so that the total force could be measured, independent of the point of application, by simply summing the outputs from the two cells.

The final design of one of the load cells is shown in figure 2.8, with the strain measuring elements of dimensions 1" x ⅛" x 1/16" ; the stiffer cells mentioned above were similar, but with the measuring elements of dimensions 1" x ⅛" x ⅛". These cells were machined from a ⅜" thick block of stainless steel, with two measuring elements per cell; strain gauges were mounted, one on each ⅛" face of the element, giving a total of four gauges per load cell. The two cells making up a pair were also slightly different in design, one as shown in figure 2.8, had a 3/16" hole centrally positioned; the other had instead a 5/16" clearance hole. This was chosen such that the model would be fixed to one load cell at one end, but free to move, in the axial direction only, at the other end connected to the other load cell. It was necessary to do this because, had the model been fixed at both ends to the load cells, when filling the tank the effect of the very large static pressure on the windows would set up lateral bending strains in the load cells which could

possibly cause damage to them. This system was therefore insensitive to axial loads on the model. Further, the sliding end of the model was such that no torque could be transmitted to the load cell at this end; in any case the gauges were connected as to be insensitive to torque.

The models were all constructed with similar end fittings, the end to be fixed had a 3/16" tapped hole through which a screw fixed the model to the cell; a boss prevented any axial movement of the model. The assembly of the other end, free to move in the axial direction is shown in figure 2.9, where the model is made with a 5/16" stud machined to a fine tolerance, which fits snugly into the clearance hole of the other cell.

As previously mentioned, when measuring forces, a different pair of windows, made of $\frac{3}{8}$" thick aluminium alloy and reinforced with 'T' section stiffeners were used. These windows also had a special housing for the load cells, and a 1" diameter clearance hole, through which the model was connected to the load cell; both the clearance hole and the load cell housing were centrally positioned. As can be seen in figure 2.9, the housing for the cell was outside the tank; during operation this was completely full of water, which totally covered the load cell. Any air was bled out through the cover plate which was then tightened to seal in the water. The wires for the strain gauges on the load cells passed through a sealed hole in the cover plate. When the models were connected to the load cells, the gap between the model and wall was usually not more than 1/16" on either side.

The models tested consisted of three geometrically similar flat plates of widths 3", 1.5" and 1" with a thickness to diameter ratio of 0.208, and an edge angle of 60^{o}, made of aluminium alloy, brass and stainless steel respectively. A circular cylinder made of perspex, thus very smooth, of 1 9/16" diameter was also tested. Finally, a square section, again of perspex with a diameter of 1.5" was tested at 0^{o} incidence (called a square normal) and at 45^{o} incidence (called a diamond section).

When measuring in-line forces, the cells were positioned such that the axes of the measuring elements were vertical; for measurement of transverse forces the cells were rotated until these axes were horizontal.

The strain gauges used were Techni Measure Limited type FLK6, with gauge dimensions 6mm x 1mm, and resistance of nominally 120 ohms. After bonding to their respective surfaces, using the appropriate adhesive, they were coated with a layer of microcrystalline wax and then overcoated with adhesive, to make them waterproof. The gauges were then connected to a Strainstall two channel strain conditioning unit, one channel per load cell, to form a full bridge. A later improvement was to add two external resistors in the form of 360 ohms rosette strain gauges, in series with the strain bridge to further reduce the effective bridge voltage, one rosette being used per bridge. This being necessary after initial tests showed that the gauge life was too short and probably due to too high operating currents. The Strainstall unit was modular in design and consisted primarily of a pair of amplifiers, one for each channel, a power supply, a switch selector, and a meter. By selecting the appropriate channel on the switch selector unit, the output from that channel can be displayed on the meter and then balanced if necessary. A continuous 0-1 volt output was also available for each channel, and this was then the'raw' load cell output. The two outputs corresponding to the two load cells were summed usuing an operational amplifier (PHI analogue module M16), this was then used in the calibration and in subsequent measurements.

Prior to a set of experiments on a model, the load cells were carefully aligned and then calibrated with the model connected. Calibration was achieved through the use of a simple pulley and weights system, which consisted of a near-frictionless pulley mounted on a small vertical traverse. By adjustment of the traverse a horizontal load was applied to the model and hence to the cells, when calibrating for in-line force measurement. Calibration was carried out for loads acting in both directions, i.e. from left to right, or from right to left, for in-line force measurements; these

were done in air, but initial tests showed that there was no difference when calibrated in water. For transverse force measurements, calibration was easier; loads acting vertically downwards were applied simply by hanging weights from the model, whereas for loads acting upwards, the pulley was again used. A typical calibration is shown in figure 2.10; similar calibration constants were obtained for all combinations of load cells and models (except for the large plate and stiffer cells) tested, even though this involved removal of the cells and re-aligning them, when a different model was fitted.

2.2.2 DYNAMIC RESPONSE OF LOAD CELLS AND MODELS

A dynamic calibration of the load cell and model was not undertaken, as this needed to be done with the model in the water and thus presented certain practical difficulties. The following is therefore a theoretical estimate of the responseof the various models and load cells.

The load cell and model used for force measurement may be represented diagramatically by the sketch below.

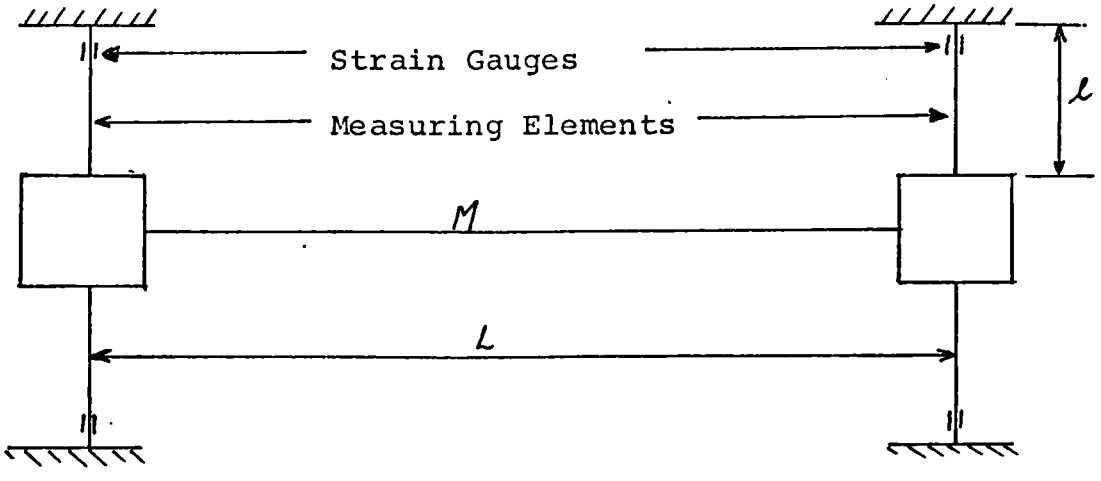

The mass M includes the actual mass of the model and the added mass, due to the unsteady flow past the model. This system may be idealised as a beam, clamped at both ends with a concentrated mass at the centre, as shown below.

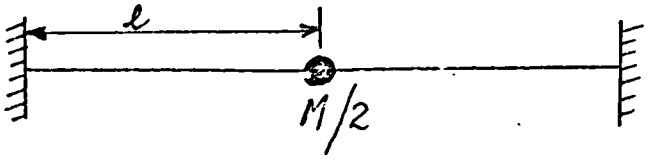

For this system the natural frequency is given by:

$$\omega = \sqrt{\frac{192\,EI}{(M/2)\cdot(2\ell)^3}} = \sqrt{\frac{48\,EI}{M\ell^3}} \qquad 2.2$$

where EI is the flexured stiffness of the beam, 2ℓ is the length of the beam, and $M/2$ is the concentrated mass.

In practice however, damping will be present thus modifying the system's response. Consider therefore a damped system whose motion may be represented by:

$$m\ddot{x} + c\dot{x} + kx = F \qquad 2.3$$

where m = mass of the model, c = structural damping, k = structural stiffness, F = forcing function, and x is the displacement of the model. In the present case, the forcing function F, may be obtained from Morison's equation, modified to take account of the assumed oscillating model (see e.g. Verley and Moe (1978)). Thus, F is given by:

$$\frac{F}{L} = \frac{1}{2}\rho C_D D(U-\dot{x})\left|(U-\dot{x})\right| + \frac{\pi D^2}{4}\rho C_m \dot{U} - \frac{\pi D^2}{4}\rho C_a \ddot{x} \qquad 2.4$$

where L is the length, and D is the diameter of the model, U and $\dot{U}$ are the velocity and acceleration, respectively of the incident flow, and C_a is the added mass coefficient. Substituting equation 2.4 into equation 2.3 and denoting the added mass by $m_a = \frac{\pi D^2}{4}\rho\, C_a$, and neglecting terms of order higher than $\dot{x}$, results in:

$$m\ddot{x} + c\dot{x} + kx = \frac{1}{2}\rho L C_D D\left(U|U| - 2\dot{x}|U|\right) + \frac{\pi D^2}{4} L\rho C_m \dot{U} - m_a\ddot{x}$$

re-arranging gives:

$$(m+m_a)\ddot{x} + (c + \rho L C_D|U|)\dot{x} + kx = \frac{1}{2}\rho L C_D U|U| + \frac{\pi D^2}{4} L\rho C_m \dot{U} \qquad 2.5$$

Equation 2.5, in its present form, is not easily solvable as it contains certain unknowns, the following assumptions will therefore be made. Assuming that the damping is mostly due to drag, then the structural damping C, can be neglected in comparison with $\rho\, L\, C_D\, D\, |U|$. Further, let the damping be constant over a cycle, then C_D can be the drag coefficient

averaged over a cycle, and $|U|$ can be replaced by U_m, the maximum velocity, thus giving the maximum fluid damping. Finally, the right hand side of equation 2.5 may be Fourier analysed into components of the form $P_0 \sin \nu t$. Therefore, for the purpose of determining the response of the system, different values of ν, the forcing frequency, can be substituted in to $P_0 \sin \nu t$, the term used to represent the R.H.S. of equation 2.5.

This analysis is obviously not exact, but it provides the worst possible response of the system, and at discrete values of the forcing frequency. Although it is interesting to determine the response over a wide frequency range, it should be noted that the inertia and drag coefficients, C_m and C_D as derived in the analysis by Keulegan and Carpenter (1958), are dependent only on the component of the force at the fundamental oscillation frequency.

Equation 2.5 may be written, after making the above assumptions, as:

$$\ddot{x} + \frac{\rho L C_D D U_m \dot{x}}{(m+m_a)} + \frac{k}{(m+m_a)} x = \frac{P_0 \sin \nu t}{(m+m_a)} \qquad 2.6$$

For the idealisation used, $m + m_a = m/2$, then by writing:

$$\left.\begin{aligned} \frac{\rho L C_D D U_m}{(m/2)} &= 2\gamma \\ \frac{k}{(m/2)} &= \omega^2 \\ \frac{P_0}{(m/2)} &= f_0 \end{aligned}\right\} \qquad 2.7$$

equation 2.6 becomes:

$$\ddot{x} + 2\gamma\dot{x} + \omega^2 x = f_0 \sin \nu t \qquad 2.8$$

The solution of equation 2.8 yields two parts; the complimentary solution which gives the transient response, and the particular. integral which gives the steady state response. In this analysis, the steady state response is of more relevance.

Rewriting equation 2.8 as:

$$(D^2 + 2\gamma D + \omega^2)x = f_0 \sin \nu t$$

where $D = \frac{d}{dt}$ then gives the steady state solution (X_p) as:

$$X_p = \frac{1}{(D^2 + 2\gamma D + \omega^2)} f_0 \sin \nu t = \frac{D^2 + \omega^2 - 2\gamma D}{(D^2 + \omega^2)^2 - 4\gamma^2 D^2} f_0 \sin \nu t$$

using the shift rule, this results in:

$$X_p = \frac{\omega^2 - \nu^2 - 2\gamma D}{(\omega^2 - \nu^2)^2 + 4\gamma^2\nu^2} f_0 \sin \nu t$$

$$= \frac{f_0}{(\omega^2 - \nu^2)^2 + 4\gamma^2\nu^2} \{(\omega^2 - \nu^2) \sin \nu t - 2\gamma\nu \cos \nu t\} \qquad 2.9$$

Equation 2.9 can also be written as:

$$X_p = A \sin (\nu t - \phi)$$

where $$A = \frac{f_0 \sqrt{(\omega^2 - \nu^2) + 4\gamma^2\nu^2}}{(\omega^2 - \nu^2)^2 + 4\gamma^2\nu^2}$$

but $$f_0 = \frac{P_0}{(m/2)} = \frac{P_0}{k} \omega^2$$

$$\therefore \quad A = \frac{P_0/k}{\sqrt{\left(1 - \frac{\nu^2}{\omega^2}\right)^2 + 4\left(\frac{\gamma}{\omega}\right)^2\left(\frac{\nu}{\omega}\right)^2}} \qquad 2.10$$

and $$\phi = \tan^{-1}\left(\frac{2\gamma\nu}{\omega^2 - \nu^2}\right) \qquad 2.11$$

Since $P_0/k = X_s$, the static deflection, then X_p may further be written as:

$$X_p = X_s \cdot \frac{1}{\sqrt{\left(1 - \frac{\nu^2}{\omega^2}\right)^2 + 4\left(\frac{\gamma}{\omega}\right)^2\left(\frac{\nu}{\omega}\right)^2}} \sin (\nu t - \phi) \qquad 2.12$$

The dynamic response of the system is therefore given by equation 2.12, where the quantity,

$$\frac{1}{\sqrt{\left(1-\frac{\nu^2}{\omega^2}\right)^2+4\left(\frac{\gamma}{\omega}\right)^2\left(\frac{\nu}{\omega}\right)^2}}$$

is the dynamic magnification factor (D.M.F.), and ϕ is the phase lag. Note that γ/ω is commonly written as c/c_o, the ratio of the damping of the system to the critical damping.

Before the response of the system can be determined, the natural frequency ω, and the damping coefficient γ must be found. In the design of the load cells, potential flow values for the inertia coefficient are used, from this the added mass is found. As the actual mass of the model, and the flexural stiffness of the load cell is also known, equation 2.2 is used to find ω. From equation 2.7, the damping coefficeint, γ is given as:

$$\gamma = \frac{\rho L C_D D U_m}{2(m/2)} = \frac{\rho L C_D D U_m}{M} = \left(\frac{\rho L D^2}{MT}\right) C_D \cdot NKC \qquad 2.13$$

where the quantity, $\frac{\rho L D^2}{MT}$ is fixed for a given model. For the tank being used, there is a maximum possible velocity, (and hence, a maximum value of NKC, depending on the size of the model) that could be achieved. Assuming quasi-steady flow at the maximum possible NKC, then the steady flow value for the drag coefficient, together with the maximum velocity is used in equation 2.13 to give the maximum damping coefficient. Having obtained the frequency ω, and the damping coefficient, γ, equation 2.11 and 2.12 are used to obtain the phase lag and the magnification factor, thus the response of the system is determined.

Obviously, choosing an added mass from potential flow, and a damping coefficient based on the steady flow drag coefficient, gives only a rough estimate of the response of the system. In order to check the response of the system, measured values of the inertia coefficient, (from which the added mass could be determined) were used to find the

frequency ω . Measured values of the drag coefficient were also used to find the damping coefficient γ . Using γ and ω, thus determined, the response of the system was again found, but now it was based on actual measured values.

The detailed calculations of the response of the various models, with the load cell connected are given in Appendix: 1. Here, calculations of the response based on potential flow C_m and steady flow C_D, are compared with those obtained using measured values of C_m and C_D. These results are given in figures 2.11a to 2.11f, and the responses obtained using the two methods are compared. As can be seen from the calculations in Appendix: 1 or in figures 2.11a - 2.11f, the response of all combination of models and load cells is more or less flat up to about 10 times the oscillation frequency, i.e. up to about 3 H_z . The phase lag, however drops very quickly as the frequency increases, and this is particularly noticeable for the 1½" diameter flat plate. Nevertheless, as stated before, in the calculations of C_m and C_D using the method derived by Keulegan and Carpenter (1958), these coefficients were related only to the component of the force at the fundamental frequency. At this frequency, for all the models and load cells used, the phase lag was less than 1^o. However, an analysis was carried out to examine the effect of a phase shift between the velocity and the force. This analysis is presented in Appendix: 2, where the effect of a phase shift, ϵ on the inertia and drag coefficients is shown to be given by:

$$C_{m_s} = \frac{8}{3} \frac{C_D\, NKC}{\pi^3} \sin\epsilon + C_m \cos\epsilon \qquad 2.14$$

and

$$C_{D_s} = C_D \cos\epsilon - \frac{3}{8} \frac{\pi^3 C_m}{NKC} \sin\epsilon \qquad 2.15$$

where subscript 's' refers to the shifted value of the coefficients. Thus for large values of NKC, i.e. as $NKC \longrightarrow \infty$, $C_{D_s} \longrightarrow C_D \cos\epsilon$, and in this region, substantial phase shift will be required to make a significant change in the drag coefficient.

Finally, in order to check the quality of the force signal, it was spectrally analysed. Some of these spectra are presented in figures 2.12a -2.12d; here it can be seen that no contribution to the force exists above about 3 H_z. The peaks above this frequency, all arise from spurious noise introduced by the tape recorder, as discussed earlier. In addition, figure 2.13 is presented to show, a typical force and displacement signal; both signals presented here were filtered at low pass 20 H_z and were obtained on tests on a flat plate.

2.3 DATA LOGGING

For the purposes of analysis , the force and displacement signals were simultaneously recorded on two channels of a fourteen track analogue tape using an Ampex analogue tape recorder, model FR 1300. This recorder had a flat frequency response up to $20/2^N$ KH_z at a speed of $60/2^N$ inches per second, where N = 0, 1,2.....5. Before recording both signals were filtered using a Rockland dual filter, set usually at low pass 10 H_z for NKC greater than about 15 and at low pass 5 H_z for the smaller values of NKC. From spectral analysis (see e.g. figures 2.12a-2.12d) it was observed that these filter settings were adequate, in that no significant component of the signal that would have been attenuated or cut off was present. From tests of the filter response, (figure 2.14), it was observed that at a setting of low pass 10 H_z only frequencies above about 6 H_z were attenuated; at low pass 5 H_z, only signals with frequencies above 3 H_z were affected. By passing signals of various frequencies through both parts of the dual filter, and comparing the outputs, the phase shift, between the two parts of the filter was examined, and found to be zero, i.e. the two halfs of the dual filter were closely matched. Thus, by passing both the force and the displacement signal through the dual filter, the component of the force at the water oscillation frequency was unaffected. It is however appreciated that the higher frequency components of the force signal, will be slightly shifted. Nevertheless, as mentioned earlier, the higher frequency components do not contribute to the inertia and drag coefficients as defined by

Keulegan and Carpenter. Finally, as the higher frequencies are only slightly shifted, and not attenuated, this will not affect the root mean square of the force.

After filtering both signals were then amplified using operational amplifiers to a value roughly $\pm$ 1 volt; this being necessary to improve the signal to noise ratio, as the tape recorder introduces some noise to the signal. By shorting the input and recording, the noise level of the tape recorder was found to be about 0.011 volts, r.m.s. The signal conditioning process is shown in figure 2.15. Recording was usually carried out for about 5-6 minutes, for in-line forces and for over 10 minutes for transverse forces; corresponding roughly to about 100 and 200 cycles respectively. For spectral analysis longer recordings were made. After each run, a sine wave of higher frequency obtained from a sine wave generator, was recorded, being input at position A of figure 2.15, and on both the displacement and force channels. This was used both as a calibration signal, from which the gain set on the operational amplifiers and any gain introduced by the recording or reproduction modules, could be calculated; it also served to distinguish individual runs.

This data was subsequently digitised, prior to analysis, on to digital magnetic tape using an analogue to digital convertor, controlled by a PDP-8 computer. When digitising the signals were again filtered, the setting corresponding to that at which they were recorded. The effective sampling rate was 250 samples/second/channel, which corresponded to about 835 points per cycle of data, however only half this amount was finally used; the choice of this will be discussed in Chapter:3. Suffice to say here that as unwanted higher frequency noise was filtered off before digitising, aliasing or folding could not occur, (Bendat & Piersol).

CHAPTER: 3

DATA ANALYSIS

3.1. DATA REDUCTION.

As the flow is harmonically varying, the horizontal velocity, U, can be represented by:

$$U = - U_m \cos\theta \qquad 3.1$$

where U_m = maximum velocity, $\theta = 2\pi t/T$, T being the period of oscillations. The force per unit length, acting on the body can be represented by:

$$F = f(t, T, U_m, D, \rho, \mu)$$

and dimensional reasoning results in C_F, the nondimensional force being given by:

$$C_F = \frac{F}{\frac{1}{2}\rho U_m^2 D} = f\left(\frac{t}{T}, \frac{U_m T}{D}, \frac{U_m D}{\nu}\right)$$

or

$$C_F = f\left(\theta, \frac{U_m T}{D}, \frac{U_m D}{\nu}\right) \qquad 3.2$$

where U_m T/D = Keulegan and Carpenter number (NKC) $= 2\pi A/D$ for sinusoidal oscillations in a U-Tube with amplitude A; U_m D/ν = Reynolds number. Morison's equation in its usual form is written as:

$$F = \frac{1}{2}\rho C_D D\, U|U| + C_m \frac{\pi D^2}{4}\frac{dU}{dt}\rho \qquad 3.3$$

and subsituting for U and $\frac{dU}{dt}$ from 3.1 into 3.3 results in

$$C_F = \frac{F}{\frac{1}{2}\rho U_m^2 D} = \pi^2 C_m \left(\frac{D}{U_m T}\right)\sin\theta - C_D \cos\theta\,|\cos\theta| \qquad 3.4$$

Representing the measured force by a Fourier series and comparing with equation 3.4 yields expressions for C_m and C_D, the inertia and drag coefficients. This analysis was first carried out by Keulegan and Carpenter (1958), but is repeated in Appendix:3, from which equations A3.12 and A3. 3 give :

$$C_m = \frac{1}{\pi^3}\left(\frac{U_m T}{D}\right)\int_0^{2\pi}\frac{F \sin\theta}{\frac{1}{2}\rho U_m^2 D}\, d\theta \qquad 3.5$$

$$\text{and } C_D = -\frac{3}{8}\int_0^{2\pi}\frac{F\cos\theta}{\frac{1}{2}\rho U_m^2 D}\, d\theta \qquad 3.6$$

The inertia and drag coefficients, C_m and C_D can therefore be obtained by direct substitution of the total measured force, F_{meas}, (= F x L, where L = length of cylinder) into equations 3.5 and 3.6 respectively, as the other quantities are known. This yields constant values, averaged over a cycle. However, equations 3.5 and 3.6 are obtained from the first term of series solutions for C_m and C_D respectively, (see equation A3.10 and A3.11), therefore time dependent values of C_m and C_D if needed could be obtained. In this study only constant averaged values will be presented.

In their original analysis used to derive the force coefficients, Keulegan and Carpenter (1958), assumed that since the incident flow is symmetric, the force will also be symmetric. This assumption isn't necessary, nor is it strictly true. If the force is assumed periodic but not necessarily symmetrical, equation A3.14 and A3.15 show that the solutions obtained for C_m and C_D are similar to those obtained assuming symmetry in the force. The only difference is that the even harmonics are now present; however the commonly used averaged values of C_m and C_D are exactly the same as those given in equations 3.5 and 3.6. Further any assumption that the force is symmetric is more likely to hold at very small values of NKC, say less than about 5, where the flow is almost potential. In this region vortices are just being symmetrically formed and the flow pattern is the same during each half cycle. Here also the growing vortices are very weak, and the force is therefore controlled by the symmetric incident flow. At larger values of NKC, strong vortices which are formed and shed are

subsequently swept back against the body. This wake reversal and subsequentinteraction with the body is not the same during each half cycle. Further, the actual paths of the vortices during each half cycle are not symmetrical. The force is therefore not quite symmetric, however the degree of asymmetry will in general not be substantial as the force is still dominated by the incident velocity field which is symmetric in the far field. The degree of asymmetry is not only small but variable, and since it is due to a random process, i.e. wake/body interaction as the flow reverses, must itself be random, with a small, if not zero mean over a number of cycles. Averaging theforce over a large number of cycles will therefore tend to make the signal symmetric.

Another method of obtaining C_m and C_D is by minimisation of the error between the measured force and that predicted by Morison's equation, i.e. a least squares method. Defining the error (E) between the measured force per unit length (F) and calculated force (F_c) as:

$$E = F - F_c \tag{3.7}$$

then C_m and C_D are calculated such that the quantity $\int_0^T E^2 dt$ is a minimum. This results in:

$$\int_0^T E \frac{\partial E}{\partial C_m} = 0 \tag{3.8}$$

which yields;

$$C_{m_{LS}} = \frac{1}{\pi^3}\left(\frac{U_m T}{D}\right)\int_0^{2\pi} \frac{F \sin\theta}{\frac{1}{2}\rho U_m^2 D} d\theta = C_m \tag{3.9}$$

The corresponding result for C_D is:

$$\int_0^T E \frac{\partial E}{\partial C_D} = 0 \tag{3.10}$$

which gives:

$$C_{D_{LS}} = -\frac{4}{3\pi}\int_0^{2\pi} \frac{F \cos\theta\,|\cos\theta|}{\frac{1}{2}\rho U_m^2 D} d\theta \tag{3.11}$$

where the subscript 'LS' refers to least squares. Thus the

Fourier series analysis and the method of least squares results in identical values for the inertia coefficient, and the results for the drag coefficients appear to be only slightly different. The Fourier analysis method is still more commonly used; of the available data therefore, more is obtained through the use of this method than by using the least squares method. In this study therefore, for easier comparison with other workers, and because of the small difference between the two methods, the Fourier analysis method was used.

Having obtained C_m and C_D through the use of equations 3.5 and 3.6, these can then be substituted in to Morison's equation (3.4) to give the nondimensionalised predicted force C_{Fc}. The error between the measured force and that predicted by Morison's equation, hereafter referred to as the remainder term is then:

$$C_{Frem} = C_F - C_{Fc} \qquad 3.12$$

By examining the variation of C_{Frem} over a cycle and for different Keulegan and Carpenter numbers, the accuracy of Morison's equation, in this simple case of planar oscillatory motion, can be assessed.

Another method of representing the force is in terms of its root mean square (r.m.s) value; which for the measured total force is given by:

$$C_{Frms} = \sqrt{\frac{1}{T}\int_0^{2\pi}\left(\frac{F_{meas}}{\frac{1}{2}\rho U_m^2 DL}\right)^2 dt} \qquad 3.13$$

This calculated r.m.s can be compared with that predicted by Morison's equation which can be shown (see Appendix: 4) to be given by:

$$C_{Frms_c} = \sqrt{\frac{1}{2NKC^2}\left(\frac{3}{4}C_D^2 NKC^2 + \pi^4 C_m^2\right)} \qquad 3.14$$

A similar approach was adopted by Maull and Milliner (1978a) who nondimensionalised the force by $\rho^3 D^3/2T^2$; the representative velocity being taken as D/T. Nondimensionalising in this manner, gives the r.m.s. of the predicted force as:

$$C'_{Frms_c} = \sqrt{\frac{NKC^2}{2}\left(\frac{3}{4} C_D^2 NKC^2 + \pi^4 C_m^2\right)} \qquad 3.15$$

thus $C'_{Frms_c} = NKC^2 \, C_{Frms_c}$. 3.16

However as can be seen from equation 3.15, nondimensionalising by $\rho D^3/2T^2$ results in: $C'_{Frms_c} \longrightarrow \infty$ as NKC $\longrightarrow \infty$, whereas equation 3.14 gives $C_{Frms_c} \longrightarrow$ 0.61 C_D as NKC $\longrightarrow \infty$, but now $C_{Frms_c} \longrightarrow \infty$ as NKC $\rightarrow$ 0.
In all results presented here, the forces were therefore always nondimensionalised by $\frac{1}{2}\rho U_m^2 D$. It should however be noted that nondimensionalising by $\rho D^3/2T^2$ has the advantage that for a given U-tube for a particular body size, this quantity is constant over all amplitudes.

Other quantities used to describe the in-line force are the maximum measured force, C_{Fmax} , defined as:

$$C_{Fmax} = \frac{\text{Maximum measured force during a cycle}}{\frac{1}{2}\rho U_m^2 D} \qquad 3.17$$

and the position where this occurs; i.e. the phase of the maximum force ϕ , defined here as:

$$\phi = 180^o - \text{position where maximum force occurs.} \qquad 3.18$$

These five coefficients, C_m, C_D, C_{Frms}, C_{Fmax}, and ϕ were then used to describe the in-line force on all the models. Here, these quantities were obtained both for an averaged cycle of force data (obtained by averaging the force over about 50 cycles) and for individual cycles. Evaluating these

coefficients for individual cycles and plotting the variation of these over a number of cycles, enabled the constancy of these quantities to be examined. However the comparison between the measured force and that obtained using Morison's equation was made using the averaged force data. Coefficients obtained from the averaged force data were also used to examine the variation of these with the Keulegan and Carpenter number, and to compare with similar results on other models.

The in-line force is in general regular, however, the transverse or lift force is not, and occurs in irregular bursts of uneven length. Thus the transverse force is non-stationary, and its description presents a problem. Nevertheless it is usual to present this data in the form of an r.m.s. of the entirerecord of data as:

$$C_{L_{rms}} = \sqrt{\frac{1}{T}\int_0^T \left(\frac{\text{measured total transverse force}}{\frac{1}{2}\rho U_m^2 DL}\right)^2 dt} \qquad 3.19$$

Another commonly used method of defining this force is in terms of its maximum value defined as:

$$C_{L_{max}} = \frac{\text{maximum total transverse force measured during a cycle}}{\frac{1}{2}\rho U_m^2 DL} \qquad 3.20$$

In addition, because of the greater asymmetry present in the transverse force, another useful quantity is the minimum transverse force defined in a similar manner to equation 3.20. However, because the data, at larger values of NKC is somewhat non-stationary these quantities defined above could be functions of the length of the data record. Another method of presenting this data is in terms of the distribution of these coefficients about their mean or maximum value; here however a very long record of data is needed for this distribution to be accurate. Further, because of the nature of the lift force, the question arises as to which is the best way to describe it. In this study, because of the

very low frequency of oscillations of the water, it was very time consuming to obtain a very long record of data with a large number of cycles. For this reason, only 10 minutes of data (corresponding to about 180 cycles) were recorded. Of this, because of the way in which the data was processed, only about 100 cycles were finally used, and this was not sufficient to give an accurate distribution plot of the coefficients. The transverse force was therefore described by equation 3.19 and 3.20. The r.m.s. force was obtained for the complete record of data used and for individual cycles, from which the variation of this coefficient from cycle to cycle was obtained. Also, the maximum r.m.s. force was found. The maximum transverse force was also obtained at individual cycles and its variation examined, here also the maximum value of this force instantaneously recorded was also determined.

Finally some spectral analysis was done on both the in-line and transverse forces, but more effort was concentrated on the latter, as the in-line force is rather regular and mostly concentrated at the fundamental frequency. Further some information on the frequency content of the in-line force could be determined from the remainder term. The transverse force on the other hand contains information over a wider frequency band, due to the shedding of vortices and the interaction between these and the body as the flow reverses. However, again because the transverse force is somewhat non-stationary, spectra thus obtained will also depend on the length of data record. These spectra are therefore only meant for a qualitative assessment. Finally, the dominant frequency of the transverse force (f_T) can also be obtained by visually inspecting the force trace and noting the zero crossings. This can be used to define a Strouhal number as:

$$St = \frac{f_T D}{U_m} = \frac{f_T}{f NKC} \qquad 3.21$$

where f = frequency of water oscillations.

3.2 BLOCKAGE CORRECTION

There are no established methods to correct for blockage in oscillatory flows; thus the results presented are in general uncorrected for blockage.

However, one of the aims of this study, as previously mentioned, is to examine the effect of blockage in oscillatory flow by testing three different sized flat plates. Differences in results from these experiments can then be attributed to either Reynolds number, aspect ratio or blockage effects. The results of Shih and Buchanan (1971) for flat plates in oscillatory flow show that for Reynolds numbers greater than about 250, this has little effect on the forces. Further, as the flow is closely two dimensional aspect ratio is not considered very important, thus any differences in results on different sized flat plates is expected to be due primarily to blockage. To test this assumption therefore a blockage correction ought to be applied to see whether any collapse of the results could be achieved.

In the absence of any known blockage correction methods, for oscillatory separated flow (i.e. for NKC not tending to zero), Maskell's (1963) method was used. It is appreciated that the use of this method is not justified, especially at low values of NKC. However, it is used only to test whether or not differences arising from results on different sized plates can be accounted for by taking into account the wake and tunnel dimensions.

The drag on a plate may be written as:

$$C_D = \overline{C_{p_F}} - C_{p_b} \qquad 3.22$$

where $\overline{C_{p_F}}$ = average pressure on the front face, and C_{p_b} = base pressure. The corrected drag coefficient is then:

$$C_{D_c} = \overline{C_{p_{F_c}}} - C_{p_{b_c}} = \overline{C_{p_{F_c}}} + k_c^2 - 1 \qquad 3.23$$

where suffix 'c' refers to corrected values and k is the base pressure parameter given by:

$$C_{P_b} = 1 - k^2 \qquad 3.24$$

Maskell's blockage correction analysis gives:

$$\frac{C_D}{C_{D_C}} = \frac{k^2}{k_c^2} = 1 + \frac{C_D}{k_c^2 - 1} \cdot \frac{S}{c} \qquad 3.25$$

where S = area of plate and c = area of tunnel.

Re-write equation 3.25 as:

$$C_D (k_c^2 - 1) = \left\{ (k_c^2 - 1) + C_D \frac{S}{c} \right\} C_{D_c}$$

then by substituting C_{D_C} from equation 3.23 and rearranging the result becomes:

$$k_c^4 + k_c^2 (\bar{C}_{P_{F_c}} + C_D \tfrac{S}{c} - C_D - 2) + (1 + C_D - \bar{C}_{P_{F_c}} - C_D \tfrac{S}{c} + C_D \tfrac{S}{c} \bar{C}_{P_{F_c}}) = 0 \qquad 3.26$$

It is known from steady flow results that over a wide range of base pressures, the average front face pressure on a flat plate remains remarkably constant, with very little variation. Choosing a mean value of 0.77 the average front face pressure, would therefore be reasonable for a wide range of base pressures. Equation 3.26 can then be solved to yield a value for k_c^2 which when substituted into equation 3.23 gives a 'corrected' drag coefficient.

The root mean square of the force can then be similarly corrected by first removing the inertial part, and correcting only the remaining drag part.

3.3 THE COMPUTER PROGRAMS

Several computer programs were written butthe bulk of the data analysis was done using only two of these. The first program was used to average the data over a number of cycles, usually about 50, and then store this for subsequent analysis, whereas the second program was used to evaluate the

force coefficients for individual cycles. In both programs, the data was analysed directly from the digital tape obtained from the analogue to digital converter, and the first step was to read and 'unpack' the data. Unpacking of the data was necessary to take account of the difference in word lengths between the PDP computer which controlled the digitising process, and the CDC 6500 on which the programs were compiled and executed. As two channels of information, (the force signal and the displacement signal), were simultaneously recorded, and so digitised, it was also necessary to recover, and sort out the information on the digital tape. Standard routines are available which performs these functions, and were incorporated into both programs.

These programs operated on blocks of data of about 1000 points each, and on two arrays, one representing the force and the other, the displacement signal. The number of points used to represent a cycle of data is controlled by the sampling rate when digitising, and in the programs, where a selection parameter (n) could be used to reduce the number of data points. Sampling was done usually at 250 samples/sec, which for a period of 3.33 seconds results in about 832 points per cycle. Initial tests using various values of the selection parameter (n) revealed that using 832 points was needlessly extravagant, and that for $n = 4$, i.e. using about 416 points, adequate results could be obtained. It should be added that for $n = 4$, i.e. using 208 points/cycle, results obtained were within 1% of those obtained using 416 points/cycle. Nevertheless results presented here were obtained using a representation of 416 points per cycle. As the data consists of fairly low frequency information, at first sight it would seem that using 416 points/cycle is an over representation and unnecessary. However, in both programs, a cycle of data must be located; this is done by scanning the displacement signal for zero crossings. As the data is digitally represented, this means that in practice, the true zero crossing will not be found, unless some interpolation between points on either side of the zero is performed. The location of a cycle in

this manner will therefore suffer from a random phase shift, the amount of which will depend on the number of points used to represent a cycle. In this study, representation of 416 points/cycle corresponds to a change of 0.87^{o} between adjacent data points. If there is some D.C offset in the displacement signal, location of zero points would not give the starting point of a cycle. Thus, in the routine used to locate a cycle, both positive going (i.e. positive gradients) and negative going crossings were found. The position of the first positive going and negative going crossings were then used to find the positive peak of the displacement signal; the positions of this and a knowledge of the cycle length (Obtained from the distance between sucessive positive going crossings), then made it possible to find the true starting point of the cycle. This routine which located a cycle also had several checks which included a test to determine whether the number of points in a cycle were within a small band centred on the expected value; any cycle of data outside this range was discarded.

The averaging program then worked by finding the useful cycles of data within every block; from the position of the start and end points of each cycle of displacement signal, the corresponding cycles of force data was obtained. Each cycle of data was then added to the previous ones, with great care being taken to ensure that corresponding points of a cycle are added, i.e. any mismatch is prevented. The data is then averaged over the total number of cycles used, and the averaged length of the cycle is also determined. From the averaged data (which contains more points than the average cycle length), an averaged cycle of data, of length equal to the average cycle length is extracted, and stored. This stored data is then analysed by a smaller subsidiary program, which reads in this data, together with the period and amplitude of oscillation, body diameter and length, gain factors and load cell calibration constant. The force signal is then corrected for gains and offsets and converted from volts to force by the calibration factor; inertia and drag coefficients are then calculated as in equations 3.5 and 3.6

respectively. C_m and C_D are subsituted into Morison's equation to yield the predicted force, and the remainder term is also evaluated. The root mean square force C_{Frms}, the maximum force C_{Fmax} and its phase, $\not\Phi$ are also evaluated. Finally the measured force, predicted force and the remainder term are plotted to show their variation over a cycle.

In the second program, the constants read in by the smaller program mentioned above are also read here. Having located the force cycle, (by first locating a cycle of displacement signal), the data is corrected as above and using a routine, which is a modified form of the smaller program mentioned, the quantities, C_m , C_D, C_{Frms}, C_{Fmax} and $\not\Phi$ are evaluated. These quantities are evaluated for every cycle of force data and are also stored; they are later plotted to show their variation from one cycle to another.

The transverse force data is analysed using a modification of the second program. Here only the coefficients C_{Lmax} , C_{Lmin}, and C_{Lrms} are evaluated, but as befo re this is done for every cycle of data. In analys:- ing this force the coefficients were first evaluated assuming there was no offset, but were stored into three arrays. By summing the force data over the complete data record, and dividing by the total number of points, the D.C offset was obtained, and was used to correct the previously evaluated coefficients. All the intergrations performed relied on a routine which used Simpson's rule.

CHAPTER: 4

FORCE MEASUREMENTS

4.1 IN-LINE FORCE

4.1.1 THE CIRCULAR CYLINDER

As mentioned earlier, there is a substantial amount of data available on force measurements on circular cylinders in waves and in oscillatory flow. However measurements of the forces on a circular cylinder were repeated for two reasons. Firstly, since the experimental facility was being used for the first time, a comparison with results obtained by other workers served as an ideal method of testing not only the apparatus, but also the experimental technique and data analysis programs. Secondly results of the forces on the circular cylinder were also needed to compare with results obtained on other sections.

The circular cylinder used was made of Perspex and thus was smooth; it had a diameter of 1 9/16" (0.0397 m) and measured just under 2' (0.61 m) in length. Forces were measured using the force measuring system as described in Chapter:2, and the data presented, unless otherwise specified was obtained for an averaged cycle of the in-line force. This averaged cycle, as described in Chapter:3, was obtained by averaging the force data, usually over about 50 cycles. Finally, both the displacement and force signals were low pass filtered at 10 H_z for NKC above about 15 and at 5Hz for smaller values of NKC. For an oscillation period of 3.33 seconds, the β value for this cylinder is 451 and the blockage (diameter of cylinder to width of tank) is 6.51%.

The results obtained are presented in table:1 of Appendix:5 and represent data from two sets of experiments, performed on separate days. It should be added that all the in-line force data presented for all sections tested represent data from at least two separate series of experiments; this being done to check the consistency of data. As with the circular

cylinder, the data on all the sections was found to be consistent, even though this involved re-aligning and recalibration of the model and load cells. These results for the circular cylinder are plotted in figures 4.1 to 4.9 to show the variation of the force coefficients with the Keulegan and Carpenter number and to compare with other workers in this field. The variation of the inertia and drag coefficients with NKC are plotted in figures 4.1 and 4.2 respectively and are compared with results of other workers using apparatus similar to that used in this study. For NKC less than about 10, where incidentally inertia is likely to be most important, the results for the inertia variation with NKC, as shown in figure 4.1 are in fairly good agreement. However beyond this value of NKC considerable scatter exists. The results of Milliner (1978) are much larger than those obtained here and do not even follow the trend which the present results and those of other workers exhibit. This difference cannot be accounted for, but it should be noted that Milliner's results were obtained for a β value of 200, i.e. a lower Reynolds number range. Further, as NKC increases the force becomes more drag dominated, so that the inertial part is smaller; thus, results for C_m at larger values of NKC are more likely to be in error. Figure 4.1 also shows that the present results are more or less in agreement with those of Sarpkaya (1976a) at a β value of 497, except in the region of NKC between 10 and 20, where Sarpkaya's results tend to be somewhat lower than those obtained here. Also plotted in figure 4.1, are the results of Sarpkaya and Tuter (1974) taken from the mean line through their data, which incidentally exhibited very little scatter even though their results covered a range of β values from about 250 to 1500. These results, which appear to be the same as those used by Sarpkaya (1975), are greater than those obtained in the present study, for NKC greater than about 15. In view of the fact that at larger values of NKC inertia is less important, this difference in results is not serious, and as mentioned above may be due to errors in determining C_m. This is quite possible in Sarpkaya and Tuter's case as their results were obtained by recording the force on a pen recorder, and using this trace in their analysis.

Further comparisons with other workers, in particular with those obtained by Mercier (1973) show even greater scatter in the variation of the inertia coefficient with NKC, as can be seen in figure 4.3. Mercier's results show that at NKC = 12.6, C_m varies from about 0.5 to 1.0. However, his results were obtained by oscillating the cylinder, and he reported certain difficulties in obtaining values for the inertia coefficient. Nevertheless, figure 4.3 shows that Mercier's results (which covered a β range from about 200-600) are in fairly good agreement with those of Milliner (1978), for NKC greater than about 20. The present results, when compared with those of Keulegan and Carpenter (1958) as in figure 4.4, are in good agreement for NKC less than about 20. Beyond this value of NKC, their results tend to be higher and show an increase in C_m with decreasing β; an effect which might help to explain why Milliner's (1978) results for C_m tend to be higher than the present ones. However, both Sarpkaya (1976a, 1976b) and Garrison, Field and May (1977), show that as β decreases C_m also decreases. Nevertheless, as stated in Chapter: 1, this difference in trends between the results of Keulegan and Carpenter and those mentioned above could quite possibly be due to the effect of a vertical velocity which was present in Keulegan and Carpenter's case.

The variation of the drag coefficient with NKC, when compared with other workers who also used 'U'-tube type apparatus as in figure 4.2, shows considerable disagreement. This lack of agreement is more noticeable between the present results and those of Sarpkaya (1976a), even though the β values were similar. Good agreement however, is found between the present results and those of Milliner (1978), even though his β value was lower, being equal to 200 as compared with 457 in the present case. This is not unexpected though, as Sarpkaya (1976a) reports that for Reynolds number less than 2×10^4 the effect of Reynolds number in planar oscillatory motion is small. However, this does not explain why the results of Sarpkaya and Tuter (1974) should exhibit such little scatter, (even though the values ranged from about 250 to 1500) because the Reynolds number range was about 2.5×10^3 to 5×10^4.

Further, Sarpkaya and Tuter's (1974) results are not in complete agreement with either those of Sarpkaya (1976a) or with those presented here, but do tend to agree with the present results at larger values of NKC. This scatter in the drag coefficient obtained by different workers is emphasised by further comparisons with other workers as in figures 4.5 and 4.6. In figure 4.5, it can be seen that of the recent available data on drag coefficients of circular cylinders in oscillatory flow, the results of Sarpkaya (1976a) represent an upper bound, whereas those obtained here and those of Milliner (1978) represent the lower bound. Figure 4.5 also shows that Mercier's results exhibit some scatter and at NKC = 12.6, several values for the drag coefficient are given; this could be due to difficulties associated with the apparatus used by Mercier. Here also, results of another recent work by Verley and Moe (1978) is shown. These results were obtained for decaying motion of a cylinder allowed to oscillate freely in still water; the drag was then calculated by recording the damping of the cylinder motion. Verley and Moe's results were for a limited NKC range, (less than 20) and in this range agree fairly well with the results of Sarpkaya and Tuter (1974), however such an indirect method of determining the drag force is more likely to lead to errors. Returning to the difference in results obtained by Sarpkaya and those obtained here, one possible reason could be due to differences in the data analysis techniques used. It is very interesting to note that the present results and those of Milliner (1978) were obtained by averaging the force over several cycles, and in this case good agreement was obtained. Sarpkaya's (1976a) results, on the other hand were obtained by analysing only a few cycles of data, obtained for decaying oscillations. He reported (1976a) that this data was treated in an analogue manner with data being read from a trace 'every 0.1 seconds which corresponded to every 6.8285 degrees in a cycle'. Further, it appears that some digital analysis of the data was also carried out 'to check the consistency of the data acquisition system'; however the digital sampling rate was set at either 10 samples/second/channel or at 20 samples/second/channel. Sampling at these rates implies that the distance

between adjacent data points corresponded to either 6.8285° or 3.414° respectively, for an oscillation period of 5.272 seconds. As mentioned in Chapter: 3, if Sarpkaya in his digital analysis located a cycle of data by noting zero crossings in the displacement signal, the use of such a small number of points to represent a cycle could lead to errors caused by the introduction of a phase shift, unless he interpolated between points either side of the zero crossing. Further, analysis of data by analogue methods which involves recording the data on a pen recorder is limited by the sensitivity of the recorder, the scale on which data is recorded, and to how precisely the data can be read. However these errors should only result in a random scatter, and not in the large consistent difference in results observed in figure 4.5.

Another possible reasons for this difference could be the use of filters in the present case, which could introduce a phase shift in the force signal. As mentioned before, both the force and displacement signals were low pass filtered usually at 10 Hz for NKC greater than 15 and at 5 Hz for smaller values of NKC. These settings were determined by examining spectra of the unfiltered force together with the filter response and were chosen such that no attenuation of the force was possible as this was concentrated mainly at the fundamental oscillation frequency. However, filtering does cause phase shifts, but because both the force and displacement signals were filtered simultaneously with matched filters at the same setting, only components of the force above the oscillation frequency are affected. It should be added that harmonics in the in-line force are always less than about 1/50 of the component at the fundamental frequency. Further, the method used in evaluating the drag and inertia coefficients rely on equations 3.5 and 3.6 which use only the component of the force at the oscillation frequency. Another possibility for the difference in results could lie in the response of the load cells. However the analysis given in Chapter: 2 showed that the response of the load cells was more than adequate with an extremely small phase lag occurring at the

oscillation frequency. The analysis in Appendix: 2 shows that although a shift in the phase of the force relative to the displacement results in some exchange between inertia and drag, such a shift must be considerable to result in the 20% difference in results seen in figure 4.5. As an example, at NKC $\approx$ 50, it would require a shift in phase about 25^{o} to explain the difference in results obtained by Sarpkaya (1976a) and those obtained here. However such a phase shift gives a value for the inertia coefficient which is clearly in error. Thus it is quite unlikely that the difference in results could have been caused by a phase shift. Finally, the present data was compared with the results of Keulegan and Carpenter (1958), as in figure 4.6. Although Keulegan and Carpenter's results may have been influenced by the presence of a vertical velocity, fairly good agreement is observed, except for NKC about 10 and 15.

Further comparisons with available data on other relevant coefficients are presented in figures 4.7 to 4.9. In figure 4.7, the variation of the r.m.s of the measured force with NKC, is compared with results from other workers. Good agreement between the present results and those of Milliner and Maull (1978a) is observed, but here again Sarpkaya's (1976a) results are about 10-15% greater. It should however be noted that, of the results shown in figure 4.7, only those obtained in this study and those of Milliner and Maull (1978a) are actual measured values of the r.m.s. of the force. The others were obtained from measured values of the inertia and drag coefficients, substituted into Morison's equation, as shown in Appendix: 4. Nevertheless the r.m.s. force calculated through the use of Morison's equation is generally in very good agreement with measured results, because as stated earlier, the in-line force is almost all at the water oscillation frequency. This difference in the results observed in figure 4.7 also discounts any possibility of a simple phase shift which would have resulted in an exchange between inertia and drag, but would have kept the r.m.s more or less constant.

In figure 4.8, the available data for the maximum in-line force during a cycle is compared with other available data. The present results, obtained on an averaged cycle are in agreement with the mean of the results obtained by Keulegan and Carpenter (1958) except in the region of NKC between 10 and 20. Here also there is disagreement between the present results and those of Sarpkaya (1976a); the latter again tend to be higher. Finally, the phase of the maximum force (i.e. the position of occurrence of the maximum force) was compared with available data. This comparison, presented in figure 4.9 show the results to be in fairly good agreement, and also suggests that the measuring system used here did not suffer from any gross phase lag.

The results and comparisons presented in figures 4.1 to 4.9 show that even when similar apparatus is used, the available data on in-line force coefficients on circular cylinders in oscillatory flow exhibit considerable scatter. This lack of agreement which is especially noticeable on the drag coefficient, is also reflected in the r.m.s. force and seems unaccountable for, as the likely errors cannot explain the large differences observed. However although similar apparatus were used, small differences in experimental and data analysis techniques still existed and may explain the variation in results. Both in the present case and in Milliner's work, the oscillations were forced and data obtained by averaging the force over many cycles, and here good agreement was obtained. However Sarpkaya (1976a) examined a case of free oscillations with the motion decaying, and analysed only a few cycles. Earlier though, Sarpkaya and Tuter (1974) did use forced oscillations, but examined only a few cycles, however more important was the fact that the cylinder was tested in an arm of the U-tube. Even though the model was well below the surface, when the oscillation was in its downward stroke the effect of the free surface could possibly have influenced the results. Thus it would seen that this range of expermental results for the drag coefficient on circular cylinders in planar oscillatory motion could be due to the fact that the experimental conditions and analysis techniques differed in each set of data.

The notion that small differences in experimental conditions can produce significant differences in results is supported by the fact that Sarpkaya (1976a) reports that in his case of free oscillations the in-line force is repeatable to a large extent, and results of coefficients evaluated on successive cycles agree very well. It would seem that as Sarpkaya (1976a) used oscillations which were decaying he could not have analysed many cycles, nevertheless it is remarkable that in the case of free oscillations the in-line force is as repeatable as reported. However, in the present case, where the oscillations were forced, the in-line force is not exactly repeatable, and figure 4.10 shows that although the displacement is regular, small variations do exist in the in-line force. Further when the coefficients are evaluated for individual cycles and for a number of cycles, considerable variation in the force coefficients are observed. This is amply demonstrated in figures 4.11 to 4.13, and exists throughout the range of NKC tested. As expected, these plots show that at small values of NKC, C_m exhibits less variation than C_D while at large values of NKC the reverse is true; the r.m.s. force coefficient however suffers from much less variation throughout the range of NKC. This variation in the force coefficients, evaluated for individual cycles, but for several cycles of data is summarised in the plots presented in figures 4.14 to 4.18. Here, the maximum and minimum values of the coefficients, obtained from analysis on many individual cycles are shown with the value obtained by averaging these coefficients. It should be noted that when results were obtained by evaluating the coefficients at individual cycles, and then averaging these coefficients over a number of cycles, they agreed to within 5% of those obtained by evaluating the coefficients on an averaged cycle of data. In figure 4.14 considerable variation is seen to exist in the inertia coefficient; however at the lower values of NKC such scatter is unexpected as the force is dominated by the potential flow inertia component. At large values of NKC, because the drag is now the dominant force, the determination of C_m is more likely to be in error and thus the scatter in the C_m value is expected. This suggests the possibility of noise in the force.

It is known that the unfiltered output of the load cells suffers from some spurious high frequency noise of about 10 mv r.m.s., however due to an oversight, the noise level at the filter settings used was not checked as the filtered signals appeared noise free when viewed on an oscilloscope. In addition, some noise was introduced by the tape recorder ($\approx$ 11 mv r.m.s), but because the signals were amplified to about $\pm$ 1 volt before recording, this was not considered a problem. One way of testing whether the scatter in these coefficients was due to noise or whether it was genuine, is to examine the magnitude of the scatter. Now, it would seem plausible that if the scatter was indeed due to noise alone, the amount of scatter, when converted in volts should be more or less constant. Such a test showed that this was definitely not the case, as the amount of scatter in the inertial part of the force ranged from about 2 mv at small values of NKC to about 25 mv at the largest values of NKC. Nevertheless, for NKC $<$ 15, as the scatter was equivalent to only about 5 mv, it is possible that in this range some of this may be due to noise. Figure 4.15 shows the variation of the drag coefficient with NKC, and there it can be seen that as NKC increases the scatter decreases. In this case, the scatter is equivalent to a variation of about 3 mv in the drag force at small values of NKC, and of about 30 mv at the larger values of NKC. Although this variation is larger at higher values of NKC, it does not appear so in figure 4.15 because the actual drag force is very large in this region, so the scatter represents only a small percentage of the total force. As a matter of fact the maximum variation in C_D is only about $\pm$ 6% of the average value at larger values of NKC. Variations in the r.m.s. force coefficient are also obtained and as figure 4.16 shows this variation also decreases with NKC. Here the scatter corresponds to a variation in the r.m.s. force of about 2 mv r.m.s. at small value of NKC and increasing to about 18 mv r.m.s at large values of NKC. The maximum force also exhibits some scatter which also decreases as NKC increases. This scatter shown in figure 4.17 corresponds to a variation in the maximum force of about 3 mv at small values of NKC increasing to about 58 mv at large values of NKC. These coefficients all

exhibit considerable variation, which is not due to noise, except possibly at small value of NKC where the force itself is very small and so small amounts of spurious noise can produce a significant signal to noise ratio. Nevertheless of all the coefficients the r.m.s of the force seems the most constant or repeatable. This is not really unexpected as small variations in the flow development from cycle to cycle can cause significant changes in the phase of the force and hence in the drag and inertia without signigicantly affecting the r.m.s. force. The fact that changes in the flow development can signigicantly affect the force coefficients is demonstrated in figure 4.18. Here the phase of the maximum force (i.e the position of occurence) is plotted and it can be inferred from this that for NKC between about 9 and 16 the flow development during every cycle is repeatable to a large extent. This repeatability in the flow development is reflected in the small variations in all the force coefficients during this range of NKC. On the other hand for NKC just less than 9, figure 4.18 shows that considerable scatter in the phase of the maximum force exists and implies that the flow pattern in this region is not constant during every cycle ; (this fact is verified in Chapter:5, where it can be seen that for NKC just less than 9 the flow is about to change from one regime to another). This changing of the flow pattern causes the large variation in the force coefficients in this region. However for very small values of NKC, say less than 5, as the variation in coefficients is only very small, some but not all of this scatter may quite possibly be due to noise. Most of this scatter is genuine even at NKC less than 5 because even here, as mentioned in Chapter: 5, during some cycles the flow development can be different to that of previous cycles. By plotting maximum and minimum values the possible band of values are shown; strictly a statistical description of the data would have been more revealing but for reasons mentioned in Chapter: 3 this was not presented. Nevertheless, thoughout the range of NKC, the percentage variation in the r.m.s. force about its average value rarely exceeded 6% except for NKC < 8 where some of this variation may have been caused by noise.

The other coefficients on the other hand, suffered from larger variations, being about 8% on average for C_D and about 18% on average for C_m. Thus contrary to the results of Sarpkaya (1976a), although the bulk of the incident flow is repetitive, neither the force nor the coefficients evaluated through the use of Morison's equation are similarly repetitive for the case of forced oscillations past a circular cylinder.

Next, the measured force, averaged over about 50 cycles was compared with that predicted by Morison's equation using values of C_m and C_D evaluated from the averaged measured force. These comparisons are presented in figures 4.19a to 4.19h, where it can be seen that except in the region of NKC between about 8 and 20, good agreement between the predicted and measured force is obtained. This agreement improves rapidly as NKC increases beyond about 20, and at NKC $\approx$ 48, figure 4.19h shows that Morison's equation predicts both the magnitude and the phase of the force well. For NKC between 8 and 20, the motion of the large vortices present results in a poorer prediction and neither the magnitude nor the phase of the force is well estimated. This results in an error term or remainder function which is quite large (as can be seen in figure 4.19d) and reaches a maximum at NKC between 14 and 15. In this range, the remainder function instantaneously attains a value of approximately 20% of the maximum force. At smaller values of NKC, the flow has just separated and only weak vortices are present, and here again Morison's equation predicts the force quite accurately as in figure 4.19a, where both the phase and magnitude of the force are accurately predicted.

Throughout the range of NKC tested, as can be seen in figures 4.19a to 4.19h, the remainder term is periodic, and for most of the range occurs at three times the oscillation frequency with a mixture of other frequencies superimposed. Although Morison's equation contains odd harmonics of the force because of the $\cos\theta/\cos\theta$/term, errors still occur at these harmonics because the values of C_m and C_D used were constant values averaged over the cycle. Had values of C_m and C_D

which included the higher odd harmonics, as in equations 10 and 11 of Appendix: 3, been calculated and used in Morison's equation the agreement would be vastly improved. This was verified by calculating values for C_m and C_D which contained up to the fifth harmonic of the force, i.e. the expression for the coefficients contained three terms (all odd harmonics). Using these values of C_m and C_D in Morison's equation the prediction was vastly improved, even in the region of NKC between 8 and 20; a typical comparison is shown in figure 4.20 for NKC$\approx$11. However this only proves that the force can be well represented by a Fourier Series containing three terms, and that in this case because the force has only a small component at even harmonics, these need not be represented. This also serves to illustrate the point that although Morison's equation contains only odd harmonics, these are not fully represented when constant, averaged values of C_m and C_D are used, and so results in a poorer prediction of the force during some ranges of NKC. Further, the force on the circular cylinder is concentrated at the fundamental frequency and significant components occur only at odd harmonics of the fundamental, thus for this case the assumption about the symmetry in the force made by Keulegan and Carpenter (1958) is more or less justified.

These results for the in-line force on the circular cylinder show that the apparatus and data analysis techniques used worked well, for although good agreement with results of other workers was not always obtained, this was due not to any fault in the present technique and apparatus but possibly to slightly different experimental conditions.

4.12 THE FLAT PLATES

A: THE 1.5"(3.81 cm) DIAMETER FLAT PLATE

This plate like the circular cylinder was about 2' (0.61m) long, and 5/16" (0.79 cm) thick with chamfered edges of internal angles 60°; the beta value was 427.5, and the blockage was 6.25%. These results, again obtained for averaged cycles of the force are presented in table: 2 of Appendix: 5.

The only known works on flat plates in oscillatory flow are those by Shih and Buchanan (1971) and by Keulegan and Carpenter (1958). However the work of Shih and Buchanan was at low Reynolds numbers and results were analysed in a different manner, and thus not suitable for comparison. The present results were therefore compared with those obtained by Keulegan and Carpenter (1958), in figures 4.21 to 4.25. Figure 4.21 shows the variation of the inertia coefficient with NKC, and also shows that the present results do not agree with those of Keulegan and Carpenter. This difference in results is considerable, and occurs throughout the range of NKC. Similarly, when results for the variation of the drag coefficient with NKC are compared with those of Keulegan and Carpenter as in figure 4.22 there is again considerable differences, with the present results being lower than those of Keulegan and Carpenter. Figures 4.23 and 4.24, also show differences in results for the r.m.s. and maximum force respectively when compared with Keulegan and Carpenter's results. It should be noted that Keulegan and Carpenter did not present r.m.s. measurements, and the r.m.s force used to compare with the present results was that obtained through the use of Morison's equation as shown in Appendix: 4. Figure 4.25, on the other hand shows fairly good agreement between the present results and those of Keulegan and Carpenter, for the phase of the maximum force. The lack of agreement, in general between the present results and those of Keulegan and Carpenter is surprising, at least on this scale particularly when for the circular cylinder fairly good agreement was observed. As stated before there are a number of possible reasons why good argeement between the present results and those of Keulegan and Carpenter is not expected. For instance, the effect of vertical velocity, or the effect of a free surface which may have influenced Keulegan and Carpenter's results. However these effects would have been present when they tested both the circular cylinders and the flat plates, and since fair agreement was obtained on the cylinder then a similar agreement would be expected on the plates. Further it is very doubtful whether such large difference observed in figures 4.21 to 4.24 could be due to the above mentioned effects, as

the vertical velocity was small, and the free surface was not close to the model. A more likely reason lies in the geometry of the plates; in the present case these had an internal edge angle of about 60^{o}, and were of a diameter to thickness ratio of 0.21. Although Keulegan and Carpenter did not specify the precise shape of their plates, flow visualisation photographs show that the plates they used were thinner and without sharp-pointed edges. This difference would certainly result in differences in the angle of the separating shear layers and would therefore influence the growth and strength of the vortices and hence the forces. Thus it is believed that the difference between the present results and thos obtained by Keulegan and Carpenter (1958) are due to slight differences in experimental conditions, including the differences in plate geometry. Finally it should be noted that Keulegan and Carpenter's results show no conclusive influence of Reynolds number on either the drag coefficient or the r.m.s force coefficient. The inertia coefficient does show some scatter when plotted for different values, but because enough data is not available, no concrete conclusions on the effect of Reynolds number on C_m can be made. However, since both the r.m.s. and drag force coefficients show no Reynolds number dependence, and since the r.m.s force is made up of both the inertial and drag parts, it seems unlikely that C_m on the flat plate will be Reynolds number dependent.

As with the circular cylinder, the in-line force coefficients on the flat plate were also evaluated for a number of individual cycles. These results, some of which are presented in figures 4.26 to 4.28, show that here again considerable cycle to cycle variation exists in the force coefficients, even though the incident flow is repetitive. This random variation in the coefficients exists throughout the range of NKC, but appears to be less at large values of NKC for C_D and C_{Frms}. These results, of analysis on individual cycles are also used to determine the maximum, minimum and average values, and so help to establish the degree of variation of these coefficients. This variation is summarised in figures 4.29 to 4.33. These plots all show substantial

variation in these coefficients; figure 4.29 for instance shows that the scatter in the inertia coefficient is large throughout the range of NKC. Figures 4.30, 4.31 and 4.32, on the other hand, shows that the scatter in C_D, C_{Frms} and C_{Fmax} decreases with increasing NKC. However, the variation in the phase of the maximum force appears to be quite large and random throughout the range of NKC. As with the circular cylinder, because of the large variation in these coefficients, particularly at small values of NKC, where the force is small, but is expected to be more repeatable than at higher values of NKC as only weak vortices are present, the question of noise in the signal again arises. Again, by relating this scatter to the actual force, in volts, it can be seen that the variation in inertia coefficient corresponds to about 6 mv variation in the inertial force at the lower range of NKC and increases to about 40 mv at larger values of NKC. Thus had this scatter been due to instrument noise, whether from the load cells or from the tape recorder, this noise would have been more or less constant throughout the range of NKC. Similarly the scatter in the drag coefficient corresponds to about 6 mv variation in the drag force at small values of NKC and increases to about 75 mv at the higher values of NKX. The corresponding variation in the r.m.s force is 3 mv r.m.s at small NKC and increasing to about 40 mv r.m.s at large values of NKC. It should be noted that although the variation corresponds to a large value in volts at the higher values of NKC the scatter in the drag and r.m.s force coefficients in this region is less (percentage wise) as these forces are quite large, whereas the inertia force is small and hence the scatter is greater. The scatter in the maximum force is also not constant but ranges from about 10 mv variation at low values of NKC to about 100 mv at larger values. Although it does not seem likely that this scatter is solely due to noise, because the amount of scatter is not constant, the very small variation (in volts) present in these coefficients at the smaller values of NKC suggests that some (but not all) of thisscatter might be due to noise. Of course it is possible that as this scatter (in volts) increases with NKC, it may be due to vibration of the tank or model. However spectra presented in

figures 2.7a, 2.7b and 2.12b, show that any peaks in the spectrum for the vibration of the side walls of the tank were introduced by the tape recorder noise. Similarly the spectrum of the force on the flat plate showed no evidence of vibration as here again all the peaks, with the exception of higher harmonics in the force arose from noise introduced by the tape recorder. It should also be noted that the level of the scatter is greater on the flat plate than on the circular cylinder. Further examination of figures 4.29 to 4.33 shows that the amount of variation is not just decreasing steadily with NKC, but changes non-uniformly during certain bands of NKC. This further suggests that the observed scatter is definitely not primarily due to noise. Finally it should be noted that of all the coefficients, C_{Frms} exhibited the least amount of scatter and rarely exceeded about $\pm$ 10% variation about its average value except at low values of NKC, where this was most likely caused by noise.

In figure 4.34a to 4.34h, the measured force, averaged over about 50 cycles is compared with that predicted by Morison's equation using values of C_m and C_D obtained from analysis on the averaged measured force. These results show that throughout the range of NKC, Morison's equation fails to predict the force accurately. Even at low values of NKC, the prediction, as shown in figure 4.34a is poor; even more remarkable is the fact that for NKC as low as 3.08, figure 4.35a shows that the prediction is still poor. This result was obtained on a larger plate and hence for a larger β, namely 1686. Returning to figure 4.34, it can be seen that as NKC increases the prediction becomes worse, as the remainder function increases and reaches a maximum at NKC approximately 15. Beyond this the prediction improves, but slowly, and at NKC $\approx$ 48, fairly good agreement is obtained. At even larger values of NKC as in figure 4.34h, taken from measurements on a smaller flat plate, with a beta value of 188, the agreement between the measured force and Morison's equation is still not very good, only improving slightly on the agreement at NKC $\approx$ 48. The remainder function instantaneously reaches a value of about 20% of the maximum force at NKC $\approx$ 3

and increases slowly to a maximum of about 30% of the maximum force at NKC $\approx$ 15. Thus, compared to the circular cylinder, the prediction of the force on the flat plate is very poor. Further it can be seen that throughout the range of NKC the remainder force is clearly periodic and at three times the fundamental oscillation frequency. Thus suggesting that this error was caused by the presence of a third harmonic in the force, which although present in the Cos θ/Cos θ/term is not well represented. The presence of the third harmonic in the force is evident in spectra of the in-line force and can be seen even at large values of NKC as in figure 2.12b. On the flat plate therefore Morison's equation fails to predict the force with any sufficient degree of accuracy.

B. BLOCKAGE

By measuring the forces on two other plates, similar in geometry to the 1.5" (3.81 cm) diameter plate, but of different sizes, the effect of blockage in oscillatory flow was examined. As the flow is two dimensional and because little effect of Reynolds number on these plates is expected, the primary effect obtained by testing plates of different sizes is that of blockage. The fact that Reynolds number has little effect on the forces on flat plates was confirmed by measurements of Shih and Buchanan (1971) who noted that for Reynolds numbers above about 250, this effect was secondary. This is also evidenced by the results of Keulegan and Carpenter (1958) which show no discernible effect of β as either the drag or r.m.s force coefficients as was seen in figures 4.22 and 4.23. Three plates were therefore used with diameters of 1.0"(2.54 cm), 1.5" (3.81 cm) and 3" (7.62 cm), thus having β values of 188.0, 421.5, and 1685.8, and blockage ratios of 4.17%, 6.25% and 12.5% respectively. The results obtained are tabulated and presented in tables: 2 to 4 of Appendix: 5, and were obtained from analysis on an averaged cycle of force data. In figure 4.36, the results of the inertia coefficients obtained on the three plates are compared; good agreement is obtained except for the results on the 1" (2.54 cm) diameter plate which tend to be larger for NKC greater than about 15. This effect is unlikely to

have been caused by blockage, because had this been the case, the large difference in blockage between the 1.5" (3.81 cm) and 3" (7.62 cm) plates would have resulted in differences in results between these two plates. The other possibility is that this difference could be due to the effect of Reynolds number, such that as β decreases C_m increases. This notion of Reynolds number having an effect on the inertia coefficient would seem to explain some of the scatter in Keulegan and Carpenter's results, as shown in figure 4.21, but as explained earlier this is highly unlikely. Further as the results of Keulegan and Carpenter (1958) and Shih and Buchanan (1971) both show little or at least no discernible effect of Reynolds number on the drag coefficient in this Reynolds number range; it is therefore odd that only the inertia coefficient would be affected. The effect of Reynolds number on the flow around the flat plates is primarily in the diffusion of the vortices, and this should also affect the drag forces. The data is however insufficient to be totally conclusive. Of course it is quite possible that the differences in results of the small plate could be due to the fact that in the region where the disagreement exists, inertia is not an important part of the force; it is therefore likely to represent a very small portion of the force and therefore be difficult to measure. However, as previously stated all results presented were obtained from two separate sets of experiments, carried out to check the consistency of the data. The data for the small plate do show a small amount of scatter and reflect the fact that because the forces are indeed smaller on this plate they are a bit more difficult to measure, but this does not explain the difference in results seen in figure 4.36. However figure 4.37 does show a definite effect of blockage on the drag coefficient. As was mentioned above, the work of others particularly that of Keulegan and Carpenter (1958) plotted in figure 4.22, show no effect of Reynolds number on C_D. Thus figure 4.37 does indeed demonstrate an effect of blockage in oscillatory flow; this effect is quite clear on the largest plate, with a blockage ratio of 12.5%. However, both because there is a small difference in blockage between the two

remaining plates and because of the scatter in the data for the small plate, differences between these results are obscured. Figure 4.37 also demonstrates that for a small values of NKC, say less than about 5, blockage is unimportant. A similar effect of blockage on the root mean square of the force is observed in figure 4.38, where results for the larger plate are clearly increased. Here again for NKC less than about 5 no effect is observed. The results for the maximum force, presented in figure 4.39 also show this effect of blockage. In this case however particularly at larger values of NKC, it can be seen that the results for the 1" plate do lie below those obtained on the 1.5" diameter plate. Figure 4.40, on the other hand shows that results for the phase of the maximum force on the three plates are more or less in agreement but with some scatter. Thus blockage seems to affect only the magnitude of the force and does not significantly alter the variation of the force during a cycle. This is evidenced in the plot of 4.35b which shows that the variation of the force on the 3" plate during a cycle is similar to that on the 1.5" diameter plate shown as in figure 4.34e.

Finally in order to ensure that the observed effect was indeed due to blockage, a correction method was used, not with a view to obtaining truly corrected results but to demonstrate that some collapse of data could be achieved if the blockage ratios were included. The correction method used was Maskell's, and details are given in Chapter:3. Both the drag and the r.m.s force were corrected, and these results presented in figures 4.41 and 4.42 respectively. Here it can be seen that some collapse of data is indeed achieved, thus demonstrating that the observed effect is one of blockage. It can therefore be concluded that blockage in oscillatory flow is just as important as in steady flow, except for very small values of NKC where this effect can be ignored. It should however be noted that although Maskell's blockage correction gives good collapse of data, there is no real justification for the use of this method in oscillatory flow, except perhaps at very large values of NKC where a quasi-steady flow is approached.

Incidentally great care must be taken if similar blockage experiments on circular cylinders are carried out, because a simple increase in size of the cylinder also increases the Reynolds number. Thus the effect of blockage and Reynolds number can be confused and at worst may cancel thus leading to erroneous results.

4.1.3 THE DIAMOND SECTION

This section is really a square section cylinder placed at 45^{o} incidence. It is therefore sometimes referred to as a square section with a diagonal in-line with the flow. The diagonal was 1.5" (3.81 cm) and this dimension was used to non-dimensionalise the force coefficients. The β value was 422.7 and the blockage was 6.25%. Results, again for analysis on the averaged cycle of force data are presented in table: 5 of Appendix: 5. As no other studies on this section were available no comparison could be made so the results of these measurements are presented on their own in figures 4.43 to 4.47. These results will be discussed later. Suffice to say here that as with the other sections the results presented were obtained from two sets of experiments which as can be seen are consistent.

Next, the variation of the coefficients from cycle to cycle was examined by evaluating the force coefficients for many individual cycles of data. Here again, as with the flat plate and circular cylinder considerable variation in the force coefficients is observed. This variation is random and quite large but with the exception of the inertia coefficient and phase of the maximum force, becomes less as NKC increases. Figures 4.48 to 4.51 demonstrate this cycle to cycle variation. Here also, these results of analysis on individual cycles are used to obtain the maximum, minimum and average values, which are plotted in figures 4.52 to 4.56 to show the degree of variation of these coefficients. In figure 4.52, large variations in the inertia coefficient are observed; this scatter seems to decrease for NKC between 15 and 24, but then increases again as NKC increases. The

large scatter at higher values of NKC is expected as the force is then drag dominated, however the scatter at small values of NKC is not really expected as the force in this region is inertia dominated, thus the question of noise again arises. As before, by converting this scatter into volts, the degree of variation can be examined. For the inertia coefficientthis variation corresponds to about 6 mv at small values of NKC and increases to about 20 mv at NKC about 50. The fact that the amount of scatter is not constant therefore suggests that this scatter is not all due to noise. Figure 4.53 also shows considerable variation in the drag coefficient; again this scatter decreases for NKC between about 15 and 24, and as NKC increases beyond about 24 this scatter first increases and then decreases. By converting this scatter in terms of an actual force variation, but expressing this in volts, the scatter is found to range from about 7 mv at small values of NKC and increasing to about 50 at the larger values of NKC. Thus here again it is very unlikely that the scatter is due to any noise. The r.m.s force coefficient showed in figure 4.54 suffers from much less scatter, and for NKC below about 10, less than about 10% variation about the average value is obtained. Here again the scatter reduces for NKC between about 15 and 24, and it is obvious that the scatter is not constant and thus unlikely to be due to noise. Incidentally this scatter ranged from about 3 mv r.m.s at small values of NKC to about 30 mv r.m.s at large NKC values. A similar behaviour is observed for the variation of the maximum force, shown in figure 4.55 where the scatter is particularly small at NKC about 20, and in general decreasing as NKC increases above this value. As with the other coefficients the large scatter at small values of NKC is probably not all genuine and may be influenced by noise. In this case the variation is equivalent to about 12 mv at small values of NKC and increasing to about 90 mv at NKC $\approx$ 50. It may be concluded therefore that for small values of NKC say less than about 10, the variation in the force coefficients may not all be genuine but may be influenced by some noise. However at larger values of NKC the variation is primarily a genuine consequence of the type of flow; i.e. the variation occurs because the flow development during every cycle is not

repetitive. This conculusion is founded on the supposition that noise alone would have resulted in a more or less constant variation in these coefficients. The fact that this variation is a genuine effect may be supported by examination of figure 4.56, which shows the variation in the phase of the maximum force. Here, the variation is clearly seen to decrease toa minimum at NKC$\approx$22, demonstrating that in this vicinity the flow is extremely regular. The regularity of the flow in this region of NKC is reflected in the variation of the coefficients, which all show a smaller amount of scatter in this region.

Finally, the measured force, averaged over about 50 cycles was compared with that predicted by Morison's equation. These comparisons, presented in figures 4.57a to 4.57h, show that as NKC increases beyond about 25, the predicted force agrees fairly well with the measured force but the agreement is still not as good as that obtained on the circular cylinder. Figure 4.57a shows that even for NKC as low as 4.8, the agreement between the measured force and that predicted by Morison's equation is not good, with neither the maximum force nor the phase of the maximum force being well predicted. Here, the remainder function is at three times the oscillation frequency and instantaneouslyattains a value of about 20% of the maximum measured force. As NKC increases the prediction gets worse and for NKC between about 7 and 10, the remainder function instantaneously attains a value of almost 30% of the maximum force. Here also the remainder function begins to show evidence of other harmonics besides the third. For NKC above about 10 the agreement between Morison's equation and the measured force begins to improve and by NKC$\approx$15, the agreement is good. This can be seen in figure 4.57d for NKC =15.7. Here also harmonics higher than the third can be observed in the remainder function. As NKC increases beyond about 15 the agreement once again deteriorates and the remainder function can then instantaneously attain a value of about 20% of the maximum measured force. However as NKC increases beyond about 25, the predicted force once again agrees quite well with the measured force and by NKC$\approx$50, figure 4.57h shows good

agreement. On the whole however the agreement is not as good as that obtained on the circular cylinder except in the vicinity of NKC approximately 15 where the agreement on the diamond is very good, whereas on the circular cylinder the prediction is poor.

4.1.4 THE SQUARE SECTION

The model was the same as the diamond section but now placed at zero degrees incidence. The characteristic dimension used to non-dimensionalise the forces was the length of a face, which for a diagonal of 1.5", measured 1.06" (2.69 cm). Thus the β value based on this dimension was 208 and the blockage ratio equal to 4.42%. The results obtained, again for averaged cycles of force data are presented in table: 6 of Appendix: 5. As with the diamond section, no other data is available on this section; the results are therefore presented on their own in figures 4.58 to 4.62. These will not be discussed here, except to say that here again these were obtained from two separate experiments and figures 4.58 to 4.62 show that the data is consistent.

Results obtained by analysing individual cycles of data show that throughout the range of NKC, the coefficients exhibit considerable scatter. This scatter, as demonstrated in figures 4.63 to 4.65 is quite large and random, but with the exception of the inertia coefficient and phase of the maximum force decreases as NKC increases. This is more clearly evident in figures 4.66 to 4.70, where these results for individual cycles were used to obtain maximum, minimum and average values of the coefficients and these then presented. These plots show that C_D, C_{Frms} and C_{Fmax} exhibit much less variation for NKC greater than about 20; this is especially so for C_{Frms} as can be seen in figure 4.68. The inertia coefficient, on the other hand, exhibits a large scatter throughout the range of NKC as can be seen in figure 4.66. This figure also clearly shows that the amount of variation in C_m increases as NKC decreases, a fact which is not expected as inertia dominance is expected at low values of NKC. Thus the question of noise again arises. This section presents a

smaller face to the flow, than any of the other sections tested, and the overall forces were smaller; thus it is more likely that results on this section at small NKC values would be affected by noise. By converting this scatter to a force, but expressed as a voltage, it was found that for the inertia coefficient, the scatter was equivalent to about 4 mv variation in the force at low NKC and increased to about 12 mv at NKC 70. Similarly the scatter in C_D ranged from about 5 mv to about 16 mv, whereas that in C_{Frms} ranged from about 3 mv r.m.s at low values of NKC to about 10 mv r.m.s at the larger NKC values. It seems therefore that some of the scatter for NKC less than about 20 may have been influenced by noise. However it should be noted that although the scatter in these coefficients appears to be large, the average values agree to within less than 5% of those obtained when the force itself was averaged. As stated earlier, presentation of the results of analysis on individual cycles in terms of the maximum and minimum reflects the worst situation and gives a possible band of values. Finally, for NKC $>$ 20 the variation in the r.m.s. and drag coefficients is less than 10% of the average value and by NKC $\approx$ 70, it decreases to about 5%; the corresponding variation in C_m is about 20% of the average value.

Next, the averaged measured force is compared with that predicted by Morison's equation. This comparison is presented in figures 4.71a to 4.71h. It should be noted that although it was concluded above that for NKC $<$ 20, the results were possibly influenced by noise, figures 4.71a to 4.71h show that the averaged force is unaffected as any random noise is removed by averaging. Thus, the results for the average cycle of force on this and all the other models are not influenced by noise. Returning to the comparison between the measured force and that predicted by Morison's equation, it can be seen (figure 4.71a) that at NKC $\approx$ 8 and also for smaller NKC values, the prediction is quite good. Here also, and throughout most of the range of NKC the remainder function occurs at three times the oscillation frequency. As NKC increases beyond 8 the prediction becomes increasingly poor, and for NKC between

about 10 and 30, the remainder function instantaneously attains a value of about 20-30% of the maximum measured force. The agreement between the measured force and Morison's equation is particularly poor for NKC between 20 and 25. Again throughout this range the remainder function is periodic and at three times the oscillation frequency. As NKC increases beyond 30 the prediction slowly improves, but by NKC $\approx$ 71, figure 4.71h shows good agreement, with both the magnitude and phase of the force being fairly accurately predicted.

4.2 TRANSVERSE FORCE

4.2.1 THE CIRCULAR CYLINDER

By rotating the load cells through 90^{o}, such that the measuring elements were in a horizontal plane, the lift force on the circular cylinder, the diamond section and the square section was measured. Incidentally, calibration of the load cells in this position yielded calibration constants similar to those obtained when the cells were positioned to measure the in-line force. This was the same circular cylinder as that used in the measurement of the in-line force and so the β value was again 451.

Measurement of the transverse force on the circular cylinder revealed that this force was non-stationary, with periods of very little lift followed by bursts of high lift. The length of the bursts was uneven and occurred throughout the range of NKC, except forNKC equal to 14.20, where the lift appeared to be regular. This non-stationarity of the transverse force data, which incidentally was also observed by Maull and Milliner (1978a), makes it difficult to describe quantitites such as r.m.s, spectral content, and any others obtained by an averaging process since they will be a function of the length of data used. In the analysis of the lift force on these models, the force data was therefore not averaged (as was done for the in-line force); instead the data was analysed for individual cycles to yield such quantities as r.m.s force and maximum force. As would be expected from such a'cycle by cycle' analysis the force coefficients exhibited

considerable scatter as the data was not regular. These were not presented as they only serve to demonstrate the now established fact that the lift force is not regular. Therefore only the maximum measured transverse force and the r.m.s of the total block of data are presented. These results were obtained on analysis of 100 cycles of data but tests showed that results obtained for many more cycles (≈ 200) were in close agreement, usually within 5% of those obtained from analysis on 100 cycles.

The irregularity of the transverse force on the circular cylinder is clearly demonstrated in figures 4.72a to 4.72h, where it can be seen that with the exception of figure 4.72c, for NKC $=14.20$, lift occurs in uneven bursts even though the displacement is regular. This non-stationarity in the transverse force data probably explains the large scatter in results observed when similar data from other workers also using 'U-tube' type apparatus are compared, as in figure 4.73. Here the results for the variation of the maximum transverse force with NKC are compared with those of other workers. With the exception of the results of Sarpkaya and Tuter (1974), these results, including the present ones show considerable scatter, but the general trend is the same. Sarpkaya and Tuter's results were obtained for a range of β values (250-1500), but these results showed very little scatter except in the range of NKC between 20 and 25; their results are therefore presented as a mean line with a branch at NKC between 20 and 25. Figure 4.73 also shows that all the results presented do tend towards a peak at NKC ≈ 18, and a trough at NKC ≈ 15, as the results of Sarpkaya and Tuter (1974) clearly show. However, Sarpkaya and Tuter's results show another peak at NKC ≈ 10 and for NKC < 10 their results are shown decreasing to zero. This behaviour is not repeated by any of the remaining results in figure 4.73; instead they show C_{Lmax} increasing as NKC decreases. This is surprising as C_{Lmax} must eventually $\rightarrow 0$ as NKC $\rightarrow 0$, but because the force was non-dimensionalised by $\frac{1}{2}\rho U_m^2$ DL if $U_m \rightarrow 0$ faster than the measured transverse force then C_{Lmax} would become very large as NKC decreases.

In figure 4.74, the variation of the root mean square of the lift force with NKC, is compared with the results of Milliner and Maull (1978a). Because of the nature of the lift force, the results show considerable scatter and reflect the difficulty in describing this force. However figure 4.74 shows that the present results follow the trend indicated by those of Maull and Milliner. Figure 4.74 also shows that $C_{Lr.m.s}$ tends towards a constant at large values of NKC.

Unlike the in-line force, the transverse force does not occur mainly at the water oscillation frequency; instead, it occurs at multiples of the fundamental frequency which is related to the vortex shedding frequency which in turn is dependent on NKC. However when speaking of the frequency of the transverse force, some ambiguity arises as the transverse force contains information at different frequencies, caused by the number of vortices shed, and the number of distinct vortices swept back past the body. In figure 4.75a to 4.75j, the variation of the lift force during two cycles of water oscillation are shown; here it can be clearly seen that as NKC increases the transverse force occurs at higher frequencies. Further, figures 4.75g to 4.75i also shows very clearly that this force occurs at a mixture of frequencies. It should be noted that in these figures, 4.75e and 4.75j show the corresponding variation of the water displacement; these figures therefore show where the lift is developed during each cycle. However a single frequency of the transverse force could be defined by counting the number of zero crossings; such a frequency is not a true frequency but does take into account peaks in the lift force caused both by vortex shedding and by the passage of vortices past the cylinder. Because more vortices may be shed during certain cycles, particularly at large values of NKC, and also because the interaction between the vortices and the body may not be the same during each cycle, such a frequency can sometimes adopt more than one value for the same NKC. Nevertheless, defining the frequency of the transverse force (f_T) by the number of zero crossings during a cycle of oscillation, enables a Strouhal number to be defined as in equation 3.21, where

$St = f_T / f_{NKC}$, where f = frequency of water oscillation. It is appreciated that it is usual to define the Strouhal number based on the vortex shedding frequency, but in this case where lift is developed both by the shedding of vortices and by their interaction with the body it seemed reasonable to include this. This Strouhal number, defined thus, then gives an indication of the frequency content of the transverse force, in a suitable non-dimensional form. Figure 4.76 shows the variation of this Strouhal number, and the frequency of the transverse force, with NKC. Here as expected, because the number of vortices increases with NKC, f_T also increases, however the Strouhal appears to approach a constant value of approximately 0.15. More data at larger values of NKC is needed to justify any certain conclusion about this tendency to a constant value as NKC increases. Figures 4.75a to 4.75j also show the form of the lift variation changes with the flow pattern. The flow past the circular cylinder was observed to adopt certain flow patterns as described in Chapter: 5, and for the different patterns lift on the cylinder was developed in different ways. For NKC greater than about 25 the form of the lift variation was similar except that the frequency content was higher for the larger values of NKC. In these larger ranges of NKC the flow approaches a quasi-steady situation, and lift is then primarily due to the shedding of vortices which causes a wake oscillation. For NKC between about 15 and 25 figures 4.75d and 4.75f show that lift variation during a cycle is similar, now being caused both by vortex shedding and by their passage past the cylinder as the flow reverses. Figure 4.75c shows that for NKC between about 10 to 15, the lift variation adopts another form as here another flow pattern is set up. For NKC between about 5 and 10, yet another form of lift generation is observed corresponding to another flow pattern. In this region vortices are rarely shed; lift is then due to the asymmetry in the flow development and by the passage of the forming vortices back over the cylinder as the flow reverses.

Finally, the transverse force was spectrally analysed to examine the frequency content in a qualitative manner. Some

of these spectra, presented in figures 4.77a to 4.77h show that the transverse force does indeed occur at a number of frequencies, all of which are multiples of the water oscillation frequency. Even at NKC = 14.20, where the lift was observed to be the most regular, figure 4.77c shows that the lift force occurred at several discrete frequencies. More interesting is the fact that as NKC increases, the lift force occurs over a wider band of frequencies, but still all multiples of the water oscillation frequency.

4.2.2 THE DIAMOND SECTION

This section was also the same as that on which the in-line force was measured, and as the conditions were more or less the same the β value was again 422.7. Data was measured and analysed in exactly the same manner as on the circular cylinder. Here however, measurements of the transverse force revealed that unlike the circular cylinder, for NKC less than about 20, the lift was much more regular. Beyond this the lift force did show a behaviour similar to that obtained on the circular cylinder. This fact is demonstrated in figures 4.78a to 4.78h; here it can be seen that for NKC < 20, although some cycle to cycle variation is observed, this is much less than that observed on the circular cylinder. For NKC > 20, figures 4.78f and 4.78g show that here again lift generation occurs in uneven bursts. It should also be noted that figures 4.78d and 4.78h show the corresponding displacement signal recorded at the same speed (as the lift force) and matched to give the correct phase. Here again the maximum force observed in 100 cycles of data and the root mean square of this record were evaluated. In view of the fact that no other data was available for comparison, the results were compared with those obtained on the other models. In figure 4.79 the results for the maximum force are compared; here it can be seen that the force on this, the diamond section is smaller than that obtained on the circular cylinder throughout the range of NKC. Careful inspection of figure 4.79 reveals that as with the circular cylinder the results tend to form a peak at NKC between 15 and 20. A similar comparison for the r.m.s of the

force, as presented in figure 4.80 shows that here again for NKC > 20 the diamond section experiences a smaller force than the other sections. However for NKC < 20 the root mean square force on the diamond section appears to be greater than that on the cylinder. This is probably due to the fact that in this range the force on the diamond section is more regular than that on the circular cylinder. Figures 4.79 and 4.80 also show that both C_{Lmax} and $C_{Lr.m.s}$ tends to very large values as NKC becomes smaller. As mentioned before however, this could be a consequence of the manner in which the force was non-dimensionalised. Another possibility is that for small values of NKC the signal is more likely to be influenced by noise, as the magnitude of lift generated is only very small.

As with the circular cylinder, figures 4.81a to 4.81i show that the lift force on the diamond section also occurs at several frequencies which increase with NKC. Using traces similar to these, to determine the frequency (f_T) of the transverse force as defined earlier, enabled a Strouhal number to be calculated. The variation of this Strouhal number and the frequency of the transverse force with NKC is as shown in figure 4.82. Here again the results presented show that the Strouhal number appears to tend towards a constant at large values of NKC, but more results at higher values of NKC are needed to establish this observation as a fact. Figures 4.81a to 4.81i also show that the form of the lift variation during a cycle varies during certain bands of NKC. For NKC above 25, the flow approaches a quasi-steady situation and the lift generation is similar to that observed in steady flow where lift is due primarily to vortex shedding which results in a wake oscillation. For NKC about 15 to 25 a different flow pattern is observed and this is reflected in the lift variation during a cycle as shown in figures 4.81d and 4.81f. Figures 4.81a to 4.81c are however similar to each other but different to the others and again reflect another change in flow pattern. These flow patterns are described in some detail in Chapter 5, but it should be mentioned that there are no rigid boundaries of NKC which

separate the types of flow pattern. As a matter of fact during one value of NKC two flow patterns may be adopted and this can result in different forms of the lift variation during a cycle.

Finally, spectra presented in figures 4.83a to 4.83f, show that on the diamond section also lift occurs over a band of frequencies, again all multiples of the water oscillation frequency. Here it can be seen that during some values of NKC the dominant part of the transverse force occurs at odd multiples of the oscillation frequency, whereas at other values it occurs at even multiples of the oscillation frequency. At values of NKC between these, the transverse force occurs over a wide band of frequencies, both odd and even multiples of the oscillation frequency. As an example, figure 4.83a shows the force to occur mainly at 2,4,6 and 8 times the oscillation frequency, with minor contributions at 1,3, and 5 times. Figure 4.83c, on the other hand, clearly shows that the transverse force in this case occurs mostly at the odd harmonics namely at 1,3,5,7, 9 and 11 times the oscillation frequency. However figure 4.83b shows that here the force occurs both at odd and even harmonics of the fundamental frequency. The question as to whether the lift frequency will be at odd or even harmonics of the fundamental depends on the flow pattern; further if the flow pattern is repeatable to a large extent then spectra shows that either odd or even harmonics will dominate. If on the other hand the flow pattern changes during the record of data analysed the spectra will tend to be more broad band with contributions at even and odd harmonics of the fundamental frequency.

4.2.3 THE SQUARE SECTION

The β value for this section was again 208, and the results were processed as for the cylinder and diamond sections. On this section, the lift again occurred in bursts throughout the range of NKC as shown in figures 4.84a to 4.84i. Figure 4.84a also shows that at smaller values of NKC, the mean lift is not constant but varies irregularly, but here the actual

amount of lift force generated is small. For NKC above about 25, figures 4.84d to 4.84h show that lift generation on this section was similar to that observed on the other sections.

The results for the maximum and r.m.s force were presented in figures 4.79 and 4.80 respectively, where they were compared with results on other sections. This comparison, for the variation of the maximum force with NKC, presented in figure 4.79, reveals that the square section experiences a greater lift force than on the cylinder or diamond sections for most of the range of NKC. A similar comparison, presented in figure 4.80, reveals that the root mean square lift force on the square section is also greater than that experienced by the other two sections. In both these plots, for NKC less than about 20, the results on the square section are shown increasing rapidly as NKC decreases. As mentioned before this is most likely due to the fact that non-dimensionalising by $\frac{1}{2}\rho U_m^2$ DL results in the coefficients becoming very large as NKC tends to zero, if the force tends to zero slower than U_m^2. Of course, in this region the forces could also be influenced by spurious noise which could result in errors. For this reason lift results for values of NKC less than about 15 are not presented as these were thought to have contained some noise.

In figure 4.85a to 4.85i the variation of the lift force over two cycles is presented. Here it can be seen that for NKC above about 30 lift is generated in a manner similar to that observed on the other two sections. This is not due to a coincidence but instead, because here the flow also approaches a quasi-steady situation with a number of vortices being shed which result in the lift variation shown. For NKC less than 30, no definite differences in the form of the lift variation is observed and this is due to the fact that in this region the flow pattern is more or less the same as described in Chapter: 5.

Again using traces similar to those in figure 4.85, a frequency of the transverse force was estimated and this used to form a Strouhal number. Figure 4.86 shows the variation of this Strouhal number and the frequency of the transverse

force with NKC. As with the cylinder and diamond section these results tend to show the Strouhal number approaching a constant value of about 0.1, but this might be a slow variation instead and more results are needed to justify a conclusion.

Finally, the transverse force was spectrally analysed and these results are presented in figures 4.87a to 4.87f. These results show that at NKC greater than about 25, lift occurs over a number of frequencies, both odd and even harmonics of the fundamental. Here also it can be seen that as NKC increases the band of frequencies increases. At the smaller values of NKC, figures 4.87a and 4.87b show that the transverse force occurs at singular discrete frequencies. These results agree with visual observations of the flow which show that for NKC less than about 25 no distinct changes of the flow pattern occurs. As mentioned earlier only when definite changes in the flow pattern take place, do the spectra become more broad band. It should however be noted that although no definite changes in the flow pattern occur minor changes do take place and these result in irregularity of the lift.

CHAPTER: 5

FLOW VISUALISATION

5.1 INTRODUCTION

The following is an account of detailed, but mainly qualitative, flow visualisation studies carried out on all the models tested during this program of research. As stated earlier, the models include flat plates, a circular cylinder, and a square section at 0^{o} incidence and at 45^{o} incidence, i.e a diamond section. Visualisation studies were undertaken to examine the structure of the wake and the interaction between this and the body as the flow reversed, and revealed some very interesting and previously unreported flow patterns.

The flow about circular cylinders in relative oscillatory motion has been visualised and studied by several workers, e.g Grass and Kemp (1978), and Maull and Milliner (1978). Similar studies have been made by Zdravkovich and Namork (1977) and by Isaacson and Maull (1976) for cylinders in waves. Keulegan and Carpenter (1958) also did flow visualisation on circular cylinders and on flat plates, placed at the node of a standing wave. Unfortunately however, most of these studies tend to be either brief or were limited to a small Keulegan and Carpenter number range. In this study therefore the flow over a wide range of NKC, (up to about 70 for the square section and up to about 50 for the other sections) was visualised and examined.

5.2 VISUALISATION TECHNIQUE

The flow around the model and indeed in the entire tank was made visible by the introduction of white polystyrene particles into the water. These particles were of diameters ranging from 0.1 mm to 0.3 mm, and of density only very slightly greater than that of the water. In flow visualisation studies, the choise of particle size and density is very important for a number of reasons. Obviously if the particle is of

different density to the ambient fluid, buoyancy forces will act on the particle and it will tend to sink or float. Size of the particle also creates additional problems as pressure differences across the particle can cause forces on the particle which could result in particle trajectories which do not follow the flow. This is especially important in regions of high velocity gradients and hence pressure gradients, such as in the vicinity of vortices and separated regions. Selection of particle type and the problems associated with using particles to track the flow are adequately discussed by Merzkirch (1974). In this study only a qualitative analysis of the results of flow visualisation studies were attempted, thus the particle size and density chosen was considered adequate, especially as they were small enough and more or less neutrally buoyant.

Smaller particles, namely aluminium powder were also tried during inital tests, however these particles when in suspension tended to coagulate resulting in a very patchy or non-uniform distribution of particles. Polystyrene particles on the other hand seemed to be much more uniformly distributed. It should however be added that in order to obtain a uniform distribution of polystyrene particles these were first mixed with a little soap solution; this prevented the particles from clinging together, though the same technique applied to the aluminium powder was not very successful.

The flow was illuminated from above through a slit in the top of the working section of the tank. Thus, only a narrow vertical plane, perpendicular to the axis of the model was illuminated. Only a section of the flow was illuminated and results for this were analysed. However, because the flow was nominally two dimensional, the flow in any one perpendicular plane was typical of the flow field anywhere along the span of the model. The two dimensionality of the flow was verified by illuminating horizontal planes of the flow field and viewing this from above; in all the cases looked at, the upstream (or incident flow) and the wake was well correlated along the span. There was however some evidence of three dimensionality in the

wake of the square section during some parts of the cycle at large values of NKC. Illumination was achieved by means of two light sources, each containing a 1000 watt bulb and a lens arrangement to produce a parallel beam of light. A reflector strip placed on the floor of the working section (i.e. inside the tank), and directly below the light sources helped to intensify the illumination. Unfortunately however, the finite thickness of the models resulted in small shadows on the lower portion of the flow. Finally, the inside of the working section was painted black, thus giving good contrast between the illuminatedparticles and the black background.

For all the models studied, the flow patterns, i.e. the growth and formation of vortices and their subsequent motion occurred fairly quickly. Direct visual observations of the flow past these models was therefore limited to examining the large scale motion of the vortices or to the flow at very small values of NKC, where the events occur at a much slower pace. Still photography, using a 35 mm camera, and ciné films of the flow around the models over a wide range of NKC were therefore necessary for detailed analysis. Here again, still photographs of the flow are of limited use, unless the position during a cycle is known, however they serve to illustrate or highlight certain features of the flow. Thus, the bulk of the analysis was made with the aid of ciné films.

Photography of oscillatory flows is not straight forward, as the velocity is not constant, but varies sinusoidally from zero to a maximum value. Great care must therefore be taken with the exposure time, if adequate particle streak lengths are to be obtained. Too long an exposure time results in very long streak lengths, which give rise to a confusing picture and are difficult to interpret. On the other hand, a short exposure time results in particles which appear stationary, i.e. frozen, so that a single shot or a single frame of a ciné film is meaningless. The ideal exposure time should really be different for different parts of a cycle and also be dependent on NKC, because as NKC increases, (for the same model) the velocity increases. Further problems arise because

the amount of light reaching the camera, depends on the number of particles present (to reflect the incident light) and also on the exposure time; the longer the exposure time the more light will reach the film. In order to establish the 'best' exposure times and particle density, intial tests using still photography were conducted. These tests revealed the optimum exposure settings and the variation of this with the incident velocity. The exposure time was kept constant throughout a cycle, for the still shots; this had the advantage that by comparing different photographs during a cycle and examining the streak lengths immediate comparisons of the velocities could be made. It should be noted that the 'best' exposure time also depended on the nature of the wake. When large vortices are present, ie. with strong circulation and hence high velocities, a shorter exposure time was used, as compared with cases where, for the same incident velocity weaker vortices were present. The ciné films were shot at 12 frames per second and this obviously set a limit on the longest exposure time. After carrying out initial tests with the ciné film also, it was decided from the exposure range limitation and other factors mentioned above to 'shoot' the films for all the models and at all values of NKC with a fixed exposure setting. In a typical sequence therefore, at higher velocities streaks are present, and the lengths of these are proportional to the velocity, whereas at lower velocities the particles appear as dots. Analysis was possible by projecting the ciné film slowly or by examining each frame individually. By finding the frame in which the particles far from the model appeared stationary, the zero velocity position in each cycle was found; this was used to determine the number of frames per cycle and the position of each frame during a cycle. In all the films about 43 frames repesented a cycle. Frame by frame analysis was also used to determine the movement of the vortices during a cycle; some of the positions are tabulated in tables 1-5 of Appendix: 6, and should be particular interest to mathematical modellers. The positions thus tabulated are not extremely accurate; one of the main inaccuracies resulting from difficulties in determining the exact centres of the

vortices, especially when the vortices become weak or when they are swept back against the body. Further, in order to get as much detail as possible of the wake interaction, the field of view of the camera was chosen so as to concentrate on the region close to the model, and therefore, occasionally the vortices moved out of view. Nevertheless the positions tabulated in Appendix: 6 are fairly accurate and certain comments are also presented to inform likely users of any inaccuracies or any peculiarities observed.

Throughout this thesis, the velocity of the fluid in the tank is defined by: $U = -U_m \cos\theta$, where U_m = maximum velocity, $\theta = 2\pi t/_T$, and T is the period of oscillations. Thus in order to get from the zero velocity position, observed on the ciné film to the start of the cycle as defined above a simple correction was necessary. Defining the zero velocity position as that position when the flow was about to go from the left to the right, and denoting velocity in this direction as positive, this means that the zero velocity position corresponds to $t/_T = 0.25$. Successive frames therefore corresponded to $t/_T = 0.25 + (n/43)$, where n is the number of frames after the zero velocity frame and 43 is the number of frames per cycle. In figure 5.1 the notation is specified and a sketch of the velocity variation, together with the frame number at certain positions is presented. The relation between the frame number and $t/_T$ is given in the tables presented in Appendix: 6.

5.3 THE CIRCULAR CYLINDER

The circular cylinder used during flow visualisation was the same as that used for force measurements, i.e. made of perspex, thus smooth and with a diameter of 1.56" (3.96 cm) giving a β value of 451. The flow was observed to follow certain distinct patterns, which were dependent on the Keulegan and Carpenter number. These patterns were not defined by any strict values of NKC, however between certain ranges of NKC one particular pattern was most likely to develop.

SYMMETRICAL REGION: NKC < 4

In this region the flow around the cylinder is just beginning to develop; the velocity and the Reynolds number are both very low (the maximum Re No. $\approx$ 1800) and the boundary layer appears laminar. The exact separation point and its movement throughout a cycle could not accurately be determined but for most of the cycle, in particular when the velocity approaches maximum, the flow separates approximately in the 90^{o} region. A pair of weak vortices are formed symmetrically, one on either side of the cylinder; as the flow decelerates they remain very close to the cylinder, then just as the flow reverses they begin to move back over the cylinder. The recirculating flow within the vortices moves fairly rapidly over the cylinder generating vorticity of opposite sign which then goes into the formation of another pair of weak vortices on the other side of the cylinder. Throughout this region no interaction between the vortices was observed. This process is sketched in figure 5.2a. Although a symmetrical pair of vortices were observed in this region, it is possible to have some asymmetry at NKC say about 3.0, or on the other hand, a symmetric pair of growing vortices at NKC say of 5 is possible though not very likely and depends on the history of the motion.

ASYMMETRICAL REGION: 8 > NKC > 4

Now the separated shear layers begin to interact and one vortex begins to grow quicker and stronger than the other, but no shedding occurs. The history of the motion determines which vortex grows larger, but if the top one grows on the left hand side of the cylinder, then as the flow reverses the bottom vortex will dominate. A typical sequence of events during this region is sketched in figure 5.2b, where at $t/_{T} \approx 0$, L1 is the dominant vortex. As the flow reverses L2 moves back over the top of the cylinder, creating as it does vorticity of opposite sign which first cancels out L2 and then goes into the formation of new vortex R1. In the meantime L1 is squashed against the cylinder and high velocities are generated in this region. Most of the vorticity in L1 is lost through cancellation by vorticity of opposite sign created by the

passage of L1 very close to the cylinder. This vorticity (of sign opposite to that contained in L1), not only cancels some of L1 but also goes into the formation of a weak secondary vortex, which together with L1 convect away quite rapidly due to the velocity they induce on each other. However while moving away they also cancel out each other and very soon both decay. As the flow develops further R1 grows quite large and another smaller vortex R2 also begins to grow from the lower surface. As the flow reverses R1 (like L1 in the half cycle before) is squashed against the top of the cylinder and loses some of its vorticity again by cancellation with opposite signed vorticity created by the high velocity fluid moving back over the top of the cylinder. As before, this opposite signed vorticity also forms a weak secondary vortex, which together with a much weaker R1 convect away quite rapidly, decaying as the do.R2 on the other hand moves under the cylinder, losing all of its vorticity, and as the flow develops further another vortex L1'forms and grows quite rapidly. A weaker vortex L2' is also formed at the top of the cylinder and the pattern then repeats itself. During this region the separation positions varies almost constantly throughout the cycle. Towards the upper limit of this ranges, i.e. as NKC approaches a value of about 8, the larger vortices formed during each half cycle are almost shed. When these vortices are shed a different flow pattern is set up.

SIDEWAYS VORTEX STREET: 15>NKC > 8

This pattern is very unusual, with a series of vortices alternating in sign going off more or less vertically above or below the model; for this reason this regime has been termed the sideways vortex street. Strictly, a vortex street is not formed, but instead during each half cycle a vortex of different sign is formed and convects away from the cylinder. Whether the vortices go off to the top or the bottom depends on the history of the motion. However when this pattern is set up, one is quite likely to observe a switching from vortices going to the top to vortices going to thebottom or vice versa. On this, the circular cylinder the ability of the flow pattern to switch undoubtedlylinks in with the arbitrariness of the separation points. A

typical sequence during a cycle is sketched in figure 5.2c, where the vortices are shown moving off to the top of the cylinder. At about $t/_T \neq 0$, two previously shed vortices, A (shed a half cycle earlier) and B (just shed) together with two growing vortices L1 and L2 are present. B remains fairly close to the cylinder and induces the shear layer from the lower surface to curve upwards, thus assisting in thegrowth of L1 while inhibiting L2. As the flow is about to reverse, B starts moving to the right and L1 is pressed against the cylinder, but the high velocities induced by the presence of B, moves most of L1 around to the top of the cylinder. The movement of L1 over the top of the cylinder creates more vorticity of the same sign of L1, thus this vortex is strengthened and as the flow progresses L1 is soon shed. During this time L2 also moves back over the cylinder but is cancelled out by vorticity of opposite sign caused by this movement over the cylinder. Part of L1 also goes under the cylinder but this too is cancelled out. In the meanwhile A and B, being of opposite sign are interacting and slowly diffusing moving more or less slowly away from the cylinder. After L1 is shed, it remains close to the cylinder and again the shear layer from the lower surface of the cylinder is pulled across resulting in some assistance to the growth of R1 while R2 is again inhibited. As the flow reverses at $t/_T \approx 0.75$ most of R1 is pulled over the top of the cylinder, where its growth is accelerated and it is soon shed. Thus the development during each half cycle is similar with one vortex being shed soon after it goes over the top of the cylinder. In each half cycle therefore a vortex of different sign is shed and slowly goes off to the top. However only the last two vortices shed are of any signigicant strength as others previously shed soon lose their circulation by cancellation with others of opposite sign and by slowly diffusing. In figure 5.3a a still photograph, at $t/_T \approx 0.7$ for NKC = 11.0 is presented to show this behaviour. Here the vortices are again moving off to the top; note that there is little activity on the lower half of the picture. Here again, as can be seen in figure 5.3a the separation points are different on the upper and lower surfaces and definitely not at the 90^o point. It is probably

the fixing of the separation position at 90^{o} which result in Stansby (1977, 1978) predicting vortex positions that are totally different to those observed here.

CYCLIC REGION: $25 > NKC > 15$

In this region the vortices appear to rotate about the body, with the direction of rotation again depending on the history of the motion. Figure 5.2d shows a sequence of sketches illustrating this effect; here the rotation is shown anti-clockwise. Between $t/_{T} \approx 0.0$ and 0.1, vortex L1 is shed and remains in the lower half of the flow; this vortex encourages L2 to grow very close to the cylinder. At about $t/_{T} \approx 0.25$, the velocity of L1 induced on L2 causes the latter to become squashed against the cylinder, with some of the vorticity from L2 going under the cylinder. As the flow reverses, most of L2 and L1 goes under the cylinder and as the flow progresses they move rapidly away from the cylinder. The rest of L2 moves back over the top of the cylinder and is cancelled out in the process. A new vortex, R1 is formed on the top surface as L1 and L2 move away from the cylinder and decays, L2 decaying before L1. R1 is soon shed and remains in the upper half of the flow, where it induces a velocity on the growing vortex R2 and pulls it slightly upwards and close to the cylinder. As the flow reverses R2 is first squashed against the cylinder then as the flow develops, both R2 and R1 go over the top of the cylinder and again depart rapidly. As they depart a new vortex L1' forms at the lower half of the cylinder, this is soon shed and the process is repeated. This behaviour is shown in figure 5.3b, where for $NKC \approx 17$, and at $t/_{T} \approx 0.75$, a pair of vortices is about to go under the cylinder; here the rotation is clockwise. For anti-clockwise rotation, as in the sketches in figure 5.2d, the vortex positions, for $NKC = 20.42$, are presented in table: 1 of Appendix:6. These positions are also plotted in figure 5.4, with the appropriate notation in figure 5.1. Here again it would be unwise to use fixed separation points to model this behaviour, as the separation points vary substantially during a cycle.

PSEUDO - KARMAN STREET: NKC > 25

As the amplitude of oscillation, and hence for the same body, the Keulegan and Carpenter number increases, the wake becomes more fully developed with a number of vortices being shed during each half cycle. The actual number of vortices shed depends on the value of NKC, and increases with it. In this region of NKC the wake therefore bears some resemblance to a Karman vortex street with vortices of opposite signs being shed alternately from the top and bottom of the cylinder. As the flow is about to reverse, the vortices are squashed together and become distorted; they also interact with each other, thus as the flow reverses the incident flow contains vorticity in the form of small eddies. Here however there is only little evidence of any three dimensional motion. The last vortex shed and the dominant growing one during each half cycle are usually swept back past the cylinder as distinct vortices but these soon interact and decay. Figure 5.3c shows the wake of the cylinder at $t/_T \approx 0.7$ for NKC = 52.9, to be composed of several distinct vortices, which are just starting to get squashed together. At this stage these vortices still retain most of their circulation but as mentioned above, the definite vortex structure soon breaks down into smaller eddies as the flow is about to reverse.

5.4 THE FLAT PLATES

As with the circular cylinder, flat plates in oscillatory flow tend to exhibit certain flow patterns which varied with the Keulegan and Carpenter number. Here, however, for most of the range of NKC, the flow was dominated by larger vortices, than those observed on the circular cylinder. These patterns again fall into several regimes classified below.

SYMMETRIC REGION: NKC < 3

At these very low values of NKC, the flow is barely developed; the separating shear layers roll up symmetrically at both edges to form very weak vortices. No interaction between the opposing shear layers takes place, thus each edge

acts independently. As the flow reverses, the fluid in the recirculating region darts over to the other side where it again separates and rolls up weakly to form another pair of vortices. This process is sketched in figure 5.5a. Here again the boundaries defining these regions are not strict, so it is possible to have a symmetric pair of vortices forming at say NKC $\approx$ 4.

ASYMMETRIC REGION: $7 > NKC > 4$

In this region the separated shear layers emanating from the opposite edges of the plate begin to interact, resulting in one vortex growing quicker and larger than the other, but is not shed. This process is sketched in figure 5.5b, where the top vortex is shown as the larger; as before the history of the motion determines which vortex dominates. At $t/_T \approx 0$, two vortices L1 and L2 are present, L1 being the larger and occupies more than half of the plate at about NKC say of 6. As the flow reverses direction some of L1 and L2 goes under the plate and as the velocity increases they emerge in the form of a disturbance which appears as a weak jet. The remainder of L1 goes over the top and appears to be cancelled out, and a new vortex R1 begins to form at the top edge. As the flow develops further, the disturbance produced by L1 and L2 going under the plate dies out, and a new vortex R2 starts to form at the lower edge. The flow reverses again and part of R1 together with R2 moves under the plate and one more emerges as a weak jet of fluid. The remaining part of R1 goes over the top and is cancelled out by vorticity of opposite sign which concentrates in a new vortex L1'. This pattern then repeats itself as L1' grows larger and another smaller vortex L2' begins to form. Thus, in this regime a disturbance is produced in the lower half of the flow everytime the flow reverses.

CYCLIC REGION: $25 > NKC > 7$

For NKC just greater than about 7, a cyclic region, similar to that observed on the circular cylinder is set up. This pattern is extremely stable and once set up will continue for hours. As with the circular cylinder the vortices tend to

rotate around the plate, with the direction of rotation depending on the starting conditions. Unlike the circular cylinder, however, very strong vortices, sometime occupying the width of the plate, are formed. It appears that a necessary prerequisite for this motion to develop is that at least one vortex must be fully developed or shed during each half cycle. At the upper limit of this region two vortices are shed during each half cycle, and the pattern begins to break down. A typical sequence, say at NKC of about 15, with one vortex shed during each half cycle is sketched in figure 5.5c; here the rotation is clockwise. This region is a natural extension of the asymmetric region where at $t/_T \approx 0$, the vortex L1 is shed. This vortex induces a velocity on the growing vortex L2 which moves slightly upwards and close to the plate; L1 also moves slightly upwards, but to the left after being shed. As the flow comes to rest at $t/_T \approx 0.25$, L1 moves slightly upwards and to the right; the very large velocities induced by this on L2 results in it being squashed against the plate with some of it going over the top. As the flow develops further, between $t/_T \approx 0.25$, and 0.3, L2 is squashed even closer to the plate and more of it goes over the top where it is enhanced by vorticity of the same sign. This vorticity seems to concentrate in a secondary vortex RO which is quickly shed and together with L1, they depart rapidly away from the plate. Vortex RO, appears to be formed by some of the vorticity from L2, and also by the separating shear layer at the top edge which results from the high velocities caused by the presence of L1. As L1 and RO move away towards the top right hand segment of the flow, a new vortex R1 forms at the lower edge. By about $t/_T \approx 0.5$ R1 is just shed and another vortex R2 grows quite close to the plate under the influence of R1; at this time L1 and RO have almost decayed. Between $t/_T \approx 0.6$ and 0.7, the shed vortex R1 moves slightly to the right and downwards, pulling R2 slightly downwards as it does so; R2 remains in this position until about $t/_T \approx 0.75$. At this time R1 moves further downwards and slightly to the left, and R2 is squashed against the plate. As in the previous half cycle some transfer of vorticity from R2 to LO takes place, and the latter is quickly shed, and pairs off with R1 to move quickly away from the plate as the flow

develops. Further development leads to the formation of two new vortices L1' and L2', with the former being shed and the pattern repeated. In figures 5.6a to 5.6e a sequence of photographs are presented to demonstrate this behaviour, with the rotation clockwise and at NKC = 14.8. Rotation in the anti-clockwise direction and at NKC = 8.0, is shown in figures 5.7a and 5.7b. Figures 5.6 and 5.7 were obtained for the larger flat plate, (β = 1685.8) because the larger vortices were easier to photograph; similar patterns were observed for the smaller plate (β = 421.5). By analysing each frame of the ciné film, the vortex positions during this cyclic region were obtained for a few values of NKC, these positions are presented in tables 2-4 of Appendix: 6. Figures 5.8a and 5.8b show plots of these vortex positions for the larger flat plate (β = 1685.8) at NKC = 15.13, rotating anti-clockwise and for the 1.5" diameter plate (β = 421.5), at NKC = 15.2, rotating clockwise.

Although the flow pattern throughout the range of NKC in this region is basically the same, small differences do occur at the upper and lower limits. At smaller values of NKC say about 7 or 8, vortex L1 is just shed or about to be shed, and L2 is not quite so strong. As the flow reverses, some of L2 besides going over the top, goes under the plate and is cancelled out; the vortex RO is then usually much weaker. A similar behaviour occurs in the next half cycle, so the 'pairing off', of the vortices are much weaker. Towards the upper limit of this region, NKC say about 22, L2 is very strong and a third vortex starts to form at the top edge. As the flow reverses L1 and RO 'pairs off' and moves away, except that now they are quickly followed by another weaker vortex of the same sign as RO. A similar behaviour is observed during the next half cycle. Finally, as NKC increases the angle at which the pair of vortices depart becomes less steep and approaches the horizontal plane. As NKC approaches a value of about 25, L2 and R2 almost shed; when L2 and R2 are shed the rotation continues for a little while longer, then the pattern becomes unstable.

PSEUDO - KARMAN STREET: NKC > 25

As with the circular cylinder, at the higher values of NKC the wake is much more fully developed, with vortices of opposite signs being shed alternately from the top and bottom edges. The wake again resembles a Karman vortex street, however as the flow reverses the vortices are squashed together and the strain field makes them become elliptical before finally breaking down into smaller still two dimensional eddies. Thus the incident flow in the subsequent half cycle initially contains some vorticity of the previous half cycle. It should however be noted that during each half cycle, usually the last vortex shed and the dominant growing one retain most of their vorticity just as the flow reverses, but as the flow reverses and develops these soon decay.

5.5 THE DIAMOND SECTION

The flow about this section also exhibited certain distinct flow patterns with fairly stong vortices being formed. These patterns were very stable once set up and here again depended on the Keulegan and Carpenter number. These results were obtained for a β value of 423.

SYMMETRIC REGION NKC < 4

At very low values of NKC, a pair of vortices were observed to grow symmetrically from the edges B and D of the model, as sketched in figure 5.9a. The flow remains attached on the faces BC and CD, but separates from the edges B and D to form rather weak vortices. As the flow reverses, the fluid in the circulating region moves back over the model and again separates from the edges B and D, forming a new pair of weak vortices. The shear layers from the opposite edges of the model do not interact at this stage.

ASYMMETRIC REGION: 8 > NKC > 4

In this region, the shear layers from the opposite edges of the model interact and a pair of vortices grow asymmetrically from the edges, as sketched in figure 5.9b. At $t/_T \approx 0$, vortex L1 is the larger of the two vortices, but at this stage is not

yet shed. As the flow reverses, both vortices move back over the edges from which they were formed; the recirculating flow in the smaller vortex L2 moves rapidly over the edge D and a new vortex R1 begins to grow. During this time, the larger vortex L1 moves quickly over the face AB, and the passage of this results in the formation of a weak secondary vortex RO, of sign opposite to L1. RO and L1, now much weaker due to cancellation by vorticity of opposite sign created as it moved over the face AB, then depart rapidly away from the model as a weak vortex pair, and soon decays. Note that it is some of the vorticity formed as L1 moves over AB that also goes into the formation of RO. As the flow develops further R1 grows larger and a new vortex R2 forms at edge B. When the flow reverses R2 goes over the top and a new vortex L1' starts to form. Meanwhile R1 moves back along the face CD, losing some of its vorticity as it does so, but inducing high enough velocites along CD to result in the creation of enough vorticity which goes into the formation of another weak secondary vortex LO. These two vortices LO, and a much weaker R1 then convect away under the velocity they induce on each other quite rapidly, but soon decay. Further development of the flow leads to the growth of L1' and the formation of L2' at D which then behave as before. Towards the upper limit of this region, L2 and R2 become larger; as the flow reverses these vortices then move back over their respective edges and secondary vortices are formed at both edges.

'SIDEWAYS' VORTEX STREET: $17 > NKC > 8$

The 'sideways' vortex street observed on the circular cylinder was also observed here, except that the vortices were stronger. This pattern was the most stable pattern observed on this section and unlike the circular cylinder, once set up, it remained in this configuration. Here again, whether the vortices go off towards the top or the bottom of the model, depends on the starting condition. This process is sketched in figure 5.9c, where the vortices are shown moving off to the top of the model. The flow development in this region is much the same as that described for the similar region on the circular cylinder. Here however the larger of the growing

vortices during each half cylce interact with the edges A and C. At $t/_T \approx 0$ two previously shed vortices, R (shed during the previous half cycle) and LO (just shed), together with the growing vortices L1 and L2 are present. Some of the recirculating flow in L1 is incident on A as the flow decelerates. As the flow decelerates to about $t/_T \approx 0.2$, LO pulls L1 across, and L2 moves back over the edge B where it is cancelled out. Further development of the flow leads to the transfer of vorticity from L1 to RO which grows rapidly and is soon shed. At this time L1 is pressed close to the model and the fluid that was incident on edge A moves along AD to form a new vortex R1. During this time LO moves more or less in a direction parallel to AB and R moves slightly upwards, but R is rather weak by about $t/_T \approx 0.5$. At this stage RO is still very close to the body and pulls up the shear layer from D, thus R1 moves slightly upwards. As the flow develops further RO moves more to the right and slightly upwards, pulling R1 upwards as it does so; at this time also a new vortex R2 begins to form at edge B. As the flow reverses most of R1 goes over the top resulting in the formation of LO' and RO moves upwards and to the left. The reciruclating flow in R1, that was incident on C as R1 was pressed against the model, then travels along the edge CD to form a new vortex L1'. As the flow progresses LO' is shed and L1' grows quite large, and the patternis repeated. Figure 5.10a demonstrates this behaviour, again with the vortices moving off to the top of the model, at $t/_T \approx 0.68$ for a value of NKC = 13.61. In table 5 of Appendix: 6, the vortex positions during a cycle of motion, in this region are presented for NKC = 15.18; these positions are also plotted in figure 5.11. It should be added that in this region, when the shed vortices move they appear to roll on each other, thus interacting and cancelling out eventually; the dominant vortices are therefore the growing ones and the last two shed.

CYCLIC REGION: $25 > NKC > 17$

In this region the rotation of the vortices around the body similar to that found with the plates and the circular

cylinders was observed. Here however the vortices were weaker than those formed on the plate, and again some interaction between the vortices and edges A and C was observed. A typical sequence of events is as sketched in figure 5.9d where at $t/_T \approx 0.1$, L1 is shed and the growing vortex L2 interacts with edge A. As the flow reverses L1 pulls most of L2 under the model and these rapidly depart; in the meantime the remaining part of L2 goes over the top and is cancelled out. A new vortex R1 forms at edge B and by about $t/_T \approx 0.5$, L1 and L2 have moved some distance from the model; at this time also another vortex R2 forms at edge D. Further development of the flow leads to the shedding of R1 and the interaction between edge C and R2. As the flow reverses R1 and R2 then go over the top of the model and move quickly away. The pattern repeats itself as a new pair of vortices L1' and L2' forms. As with the flat plates, towards the upper limit of this regime as L1 and L2 move away from the cylinder, they are quickly followed by a weaker vortex formed by the higher velocities at edge D caused by the passage of L1 and L2. A similar effect occurs during the subsequent half cycle.

PSEUDO - KARMAN STREET: NKC > 25

As NKC approaches a value of about 25, two vortices are shed during each half cycle and the cyclic rotation breaks down. For larger values of NKC more vortices are shed alternately from either side of the model; the wake then resembles a Karman vortex street. In figure 5.10b, for NKC = 52.1 at $t/_T \approx 0.25$, the wake is shown to be composed of several distinct vortices. These vortices, as with the flat plates and circular cylinder are squashed together as the flow is about to reverse and so become very distorted before finally breaking down into smaller eddies. As the flow reverses, the model is therefore exposed to an incident flow containing vorticity from the previous half cycle. It should be noted that this initial incident flow appears turbulent, but in fact there is very little evidence of three-dimensionality. Thus as the flow reverses only the last shed vortex and the dominant growing ones retain most of their vorticity, but these quickly decay as the flow develops.

5.6 THE SQUARE SECTION

The flow about this section did not exhibit any distinct pattern, and the vortices formed were in general quite weak. Photography of the flow around this section was not very successful as the weak vortices had very little circulation, leading to very low velocities in the vortex core. Thus adequate steak lines could only be achieved with long exposure times. The patterns observed were a symmetric region for NKC < 5, an asymmetric region for 25 > NKC > 5, and a pseudo-Karman street for NKC > 25. The asymmetric region can however be subdivided into smaller regions where slight differences appeared.

SYMMETRIC REGION: NKC < 5

The flow development around the model in this region is as sketched in figure 5.12a, where at about $t/_T \approx 0$, the flow has separated from edges B and C, resulting in recirculating fluid on the upper and lower surfaces. As the flow reverses the recirculating fluid on the upper and lower surfaces moves back along these faces, creating new vorticity of opposite sign. This results in weak local disturbances, as the flow between the recirculating region and the growing vortex along the upper and lower surfaces departs rapidly (compared with the ambient velocity, which is almost zero) away from the model. As the flow develops further, separation occurs at the edges A and D as shown; no reattachment of the separated shear layers takes place, but some interaction between these and the edges B and C occurs. The flow then develops as in the previous half cycle.

ASYMMETRIC REGION 25 > NKC > 5

REGION(1) 12 > NKC > 5

In the lower end of the asymmetric region, sketched as in figure 5.11b, the flow is separated at edges B and C, at about $t/_T \approx 0$. Here, the shear layers roll up behind the face AD; a little interaction takes place and results in asymmetrical

growth of a pair of vortices. As the flow reverses the vortices move back over the model and lose most of their vorticity, because this movement results in vorticity of opposite sign being created. These weaker vortices, together with the recirculating flow on the upper and lower surfaces, results in quite large velocities in the vicinity of AB and CD which appears to 'shoot' off just as the flow has reversed. As the flow develops further, shear layers from the edges A and D grow slowly and eventually interact behind the face BC, resulting in the asymmetrical growth of another pair of vortices. By this time the disturbance caused earlier by the return of vorticity across the model has died out. The flow then behaves in a manner similar to that described for the previous half cycle. It should be noted that, if during one half cycle the top vortex grows larger than the bottom, then during the next half cycle the reverse is true.

REGION (2) : 17 > NKC > 12

Within this region (sketched in figure 5.12c), greater interaction between the shear layers takes place and the vortices though not completely shed during each half cycle, are stronger than those formed in the previous region. This pattern is more or less the same as before except that now, some of the vorticity contained in the opposite shear layer is pulled across by the stronger vortex as the flow reverses. In figure 5.12c, L1 pulls some of L2 across and over the top of the model and these two vortices convect away quite rapidly from the model, but soon break down into smaller scale eddies which decay shortly. On the lower surface, a similar behaviour is observed with the remaining part of L2 pairing of with a weaker vortex formed by the passage of L2 under the model. The following half cycle is similar except that the vortex formed at the lower edge, R1, is now the stronger of the two growing vortices.

REGION (3) : 25 > NKC > 17

This region is the obvious extension to region 2, where the wake is more developed and at least one vortex is completely

shed during each half cycle. This pattern is much the same as that described above, as can be seen in figure 5.12d. The main difference is that now, as the flow reverses the pairing of vortices is more clearly evident, but here again these also very soon lose their distinct structure and break down into smaller eddies. The flow is thus more locally disturbed than before. This behaviour occurs on both the upper and lower surfaces, but as figure 5.12d shows, the surface with the larger vortex results in a more disturbed flow near that surface. Towards the upper NKC limit of this region a second vortex is about to shed during each half cycle, and the interaction between the model and the wake as the flow reverses is stronger leading to flow which is even more disturbed locally. In other words there is more evidence of smaller scale eddies in the vicinity of the model; in addition at the upper limit of this region there is also some evidence of three dimensionality in the wake. This appears in the form of a few weak eddies, i.e. the wake is becoming turbulent but with very low intensity in the spanwise direction of the model.

PSEUDO - KARMAN STREET: NKC > 25

As NKC increases beyond about 25, the wake becomes more developed and a number of vortices of different sign are shed alternately from opposite edges of the model during each half cycle. The wake then resembles the usual Karman vortex street. Here again, the number of vortices formed and shed depends on the Keulegan and Carpenter number, and increases with it. As the flow is about to reverse, the velocity field induced by the vortices on each other causes them to be squashed together resulting in considerable distortion of these vortices. As the flow reverses most of the vortices break down under this unfavourable strain field resulting in smaller eddies. The flow is very disturbed during the initial motion in the reversed flow direction and there is evidence of some three dimensional motion. Thus in this region of NKC, the wake interaction with the body results in an initially turbulent incident flow, with apparently high intensities in the vertical plane, but a somewhat weaker intensity in the

horizontal plane (i.e. in the spanwise or axial direction of the model). A typical flow pattern at large NKC is presented in figure 5.13, with figure 5.13a representing the flow at $t/_T \approx 0.15$, while figure 5.13b shows the pattern at $t/_T \approx 0.3$, the Keulegan and Carpenter number was 60.72.

5.7 CONCLUSIONS

These flow visualisation studies revealed the presence of large discrete vortices throughout most of the range of NKC, except on the square section. The square section proved to be a unique body, as here the presence of an afterbody delayed the separated shear layers from interacting and the vortices formed were therefore weaker. On the remaining sections much larger vortices were formed, particularly on the flat plate. These vortices set up certain distinct motions which are in general similar on these three models. On all the models for NKC less than about 4, the pattern is very similar with the flow being more or less symmetric. At larger values of NKC, say above about 25, the pattern on all the sections are again similar; here the wake has had time to develop during each half cycle and a series of vortices of opposite signs are formed, thus resembling a Karman vortex street. For NKC between about 4 and 8 the flow past the three sections, namely the circular cylinder, flat plate and diamond are similar with large vortices being formed but not shed; instead they remain close to the sections. For NKC between about 8 and 15, the flow past the circular cylinder and diamond section are similar and set up a pattern termed a sideways vortex street. In this regime the vortices tend to go either above or below the body, but this pattern was observed only on these two sections. For NKC above about 15, the pattern on all three sections are again similar, and the vortices set up a cyclic motion about the sections. This regime is the most dominant on the flat plate and occurs for a wide range of NKC, from about 8 to 25. Finally, on all the sections the strongest vortices were formed during the cyclic region; in other words, for a given section (except on the square), when the strongest vortices are formed they set up a cyclic motion around the section.

CHAPTER: 6

DISCUSSION

6.1 IN-LINE FORCE

In Chapter: 4 results of measurements of the in-line force on the four sections tested, i.e. a circular cylinder, flat plate, diamond section and square section, were presented using three different methods of describing the force. Of these methods of representing the in-line force, namely:- in terms of a drag and an inertia coefficient obtained through the use of Morison's equation, in terms of the root mean square of the force, and lastly in terms of the maximum force and its phase, the first method is the most widely used and thus results obtained using this method are discussed first.

Using Morison's equation therefore to represent the in-line force, results in values of the inertia coefficient (C_m), which tend to the potential or attached flow value as NKC tends to zero, for all the sections tested. This is demonstrated in figure 6.1, where the variation of C_m with NKC is shown for the four sections tested. It should however be noted that the potential flow value of C_m for the flat plate was taken as 1.2 instead of the usual value of 1.0. This was done to take account of the finite thickness of the plate used in these experiments; i.e. in this case the flat plate was assumed to experience an additional force, the Froude Krylov force due to the pressure gradient that existed in the fluid in the absence of the body. Further, the forces on all the sections were nondimensionalised using the maximum transverse dimension of these bodies, and the inertia coefficents were based on the volume of a hypothetical circular cylinder of diameter equal to this transverse dimension. Thus, the relevant dimension for the square section was the length of a face, whereas the length of the diagonal was used for the diamond section. This then resulted in the

potential flow value of the inertia coefficent for the square section (2.78) being twice that on the diamond section (1.39).

As figure 6.1 shows, by about NKC $\approx$ 5, the inertia coefficients on all the sections tested, gradually approach their corresponding potential flow values. This is expected for the circular cylinder and square section because flow visualisation reveals the tendency towards an attached flow situation as NKC is decreased beyond about 5. On the flat plates and diamond section however at NKC $\approx$ 5, and at lower values of NKC large areas of separated flow are visible together with weak symmetrical vortices, i.e. the flow does not appear to approach towards an attached flow situation. It is therefore surprising that figure 6.1 shows that at NKC $\approx$ 5, the inertia coefficients should closely approach the potential flow values, on these two sections. Obviously as NKC becomes extremely small, the vortex strengths must tend to zero and the potential flow result will be obtained. Evidently therefore for NKC $\approx$ 5, on the flat plates and diamond section the large area of separated flow and the weak vortices do not significantly contribute towards the acceleration dependent forces. On these two sections however the vortices present and the large separated flow do give rise to a drag which as figure 6.2 shows results in very large drag coefficients, whereas on the square section and circular cylinder the tendency towards attached flow leads to a much smaller drag force.

Returning to the variation of the inertia coefficient with NKC for the sections tested, figure 6.1 shows that on all these sections good correlation with NKC is obtained. Further with the exception of the square section, the result on all the sections show similar trends with NKC; in particular for NKC between 10 and 20 they all experience a minimum in C_m. The results for the square section on the other hand are almost constant at the potential flow value for NKC less than about 25, and then gradually decreases as NKC increases beyond this. This difference between results obtained on the square section and those obtained on the remaining sections are associated with differences in flow patterns as described in Chapter: 5.

For the cylinder, flat plates, and diamond section, throughout the entire range of NKC, (with the exception of small values of NKC, say < 5), the wake is composed of rather large distinct vortices, and in particular for NKC in the region of 15, these vortices are very strong and set up clearly defined motions around the body. The considerable vortex activity, associated with the growth and motion of these vortices results in the flow pattern, and particularly the wake, varying considerably during a cycle as described in Chapter: 5. This variation in wake characteristics, for values of NKC in the region of 15 results in the minima in inertia coefficients observed on the circular cylinder, diamond section and flat plate. The square section, on the other hand doesnot produce any distinct vortex structure for NKC less than about 25. Vortices do form, but as described in Chapter: 5 they are weak and do not go into any clearly defined motions about the body; instead they interact with each other and with the body and soon decay. On the square section therefore, dramatic changes in the wake do not take place, as the long afterbody (i.e. the upper and lower surfaces) cause some delay in interaction between the separated shear layers, (often with some partial reattachment or at least interference by the rear edges) and produces only weak vortices. The result is therefore to produce an inertia coefficient which is almost constant at its potential flow value even for NKC of up to about 25.

The minima in the inertia coefficients of the other three sections are such that in some cases they represent values of the added mass coefficient on these sections which are negative. The concept of an added mass arises from the fact that when a body is immersed in an unsteady flow, it locally disturbs the flow and results in increased fluid accelerations which causes the body to experience an extra force. This extra force is then conveniently expressed as being equivalent to an extra or added mass, which experiences the undisturbed fluid acceleration. The notion of negative added mass is therefore not a physical reality, and arises because the growth and motion of the vortices in this region alter the phase of the force. The fact that a shift in the phase of the force could

result in an exchange between inertia and drag is demonstrated in Appendix: 2. In this region where negative added masses were obtained, the strong vortex activity results in rapid changes in the velocity and accelerations in the vicinity of the body during a cycle, thus the added mass strictly as defined should be a time dependent quantity. This fact that the added mass from a strict interpretation of the definition, should vary during a cycle was noted by Keulegan and Carpenter (1958), but was absorbed into the variation of C_m. However although they derived time dependent solutions for C_m, constant averaged values were presented and here again for NKC in the region of 15, some of these represent negative added masses. Time varying added masses were also proposed by McNown and Keulegan (1959) and more recently by McNown and Learned (1978). In the latter study, it was suggested that for cases where vortex activity was particularly strong, representation of the added mass coefficient by a single fixed quantity can be misleading; and negative values may be obtained. These results seem to support this fact, except here the vortex activity is viewed as causing a shift in the phase.

The behaviour of the inertia coefficients with NKC, for the circular cylinder, flat plate and diamond section are therefore associated with changes in the flow pattern, and as these are similar on the three sections, similar behaviour in the C_m variation is obtained. On the square section however, as mentioned briefly above, no distinct vortex patterns are observed and as such no dramatic behaviour in the C_m variation is obtained. The vortices that do form are so weak that their influence on the in-line force is not very important. This lack of any distinct vortex structure for values of NKC less than about 20 is due to the effect of an afterbody; a consequence of the geometry of this section. As described in Chapter: 5, the flow separates on the front face of the square; interaction between the shear layers is therefore prevented by the presence of the afterbody, and must take place downstream of the rear face, thus the vortices eventually formed are weaker than those that would have formed say on a flat plate. This effect on afterbody in delaying the interaction between

the separated shear layers has been studied in steady flow by using splitter plates. Several authors, including Bearman (1965), Gerrard (1966) and Roshko (1954) have shown that by delaying the interaction between the separated shear layers, vortex formation can be inhibited leading to a reduced base suction and hence to a lower drag. The vortex shedding frequency also drops.

This fact that by delaying the shear layer interaction results in weaker vortices being formed and a lower drag being felt is demonstrated in figure 6.2, for the drag on the square section. Here again by using Morison's equation, the drag on the four sections was obtained and its variation with NKC compared in figure 6.2. This plot shows that for NKC between about 8 and 20, the drag on the square section is lower than that obtained on any of the other sections, but for NKC above 20 the smaller wake width on the circular cylinder results in this section experiencing the lowest drag. The smaller wake width present on the circular cylinder throughout the range of NKC, should have resulted in this section experiencing the smallest drag throughout the range of NKC. However for NKC between 10 and 20, the large vortices formed on this section remain close to the cylinder and results in very low base presures and hence a large drag. It should also be noticed that for the circular cylinder, the orientation of the vortices is such that the largest drag is experienced in this region of NKC, i.e. between about 8 and 15, Figure 6.2 also shows that for NKC greater than about 10, the results on the three sections, i.e. the circular cylinder, flat plate and diamond, are similar, with the plate experiencing the highest drag and the cylinder, the lowest. Further, as is evident in this figure and as shown also by Bearman, Graham and Singh (1978), besides behaving in a similar manner, the drag on these three sections all tend towards their steady flow value as NKC is increased, and at NKC $\approx$ 50, the C_D's are only slightly above their steady flow value at the corresponding Reynolds number value (subcritical in this case). However the results for the square section are different to those observed on the other sections, being more or less constant for NKC less than

about 20 and increasing slowly but gradually with NKC. Further, unlike the other sections, at large values of NKC the drag coefficient on the square is well below its steady, smooth flow value. As mentioned in Chapter: 5, the wake of the square section cylinder was noticeably turbulent, (but with a weaker spanwise intensity than in the other two directions); this is the most likely reason for the lower drag at high NKC, as it is well known that in steady flow turbulence in the free stream reduces the drag on square section cylinders. It should be noted that as described in Chapter: 5, at high values of NKC (in excess of about 30) where a Karman vortex street was observed, the break down of the large two dimensional vortices as the flow reversed and interacted with the body led generally to very little or no three dimensionality, except for the square section. On the square also, in general the scale of turbulence generated seemed smaller, apparently due to the fact that the vortices formed were actually smaller, and that considerable small scale motion was introduced from the recirculating flow on the upper and lower surfaces. Note also that of the sections tested, the square section presented the smallest face to the flow, thus this is also a reason for producing smaller vortices.

Results of studies in steady flow, especially those of Vickery (1966), and Laneville, Gartshore and Parkinson (1975), show quite clearly that the square section is very sensitive to turbulence in the free stream. The presence of free stream turbulence seems to accelerate the growth of the separated shear layers, to such an extent that some reattachment, or at least some interference between the shear layers and the rear edges takes place, and thus results in a drag coefficient smaller than that for smooth flow. The other sections are much less sensitive to free stream turbulence, as discussed by Bearman (1978), with very little if any effect on the flat plate. On the diamond section, i.e. a square section at 45° incidence, results again of Vickery (1966) show very little effect of turbulence. The circular cylinder, on the other hand is sensitive to free stream turbulence, but as the early results of Fage and Warsap (1929) show this is only noticable

for values of the Reynolds number approaching the critical, as here the main effect is to promote earlier transition in the shear layers. Returning to figure 6.2, as stated earlier for NKC above 10 the drag on all the sections with the exception of the square are all similar, however for NKC < 10, the drag on the circular cylinder drops and decreases further as NKC is reduced. This effect is again associated with the presence of vortices; for NKC greater than about 10 these vortices are quite large and do exert considerable influence on the in-line force on the cylinder, diamond and plate. As NKC is decreased below 10, the effect of vortices on the circular cylinder is much less, as now they are not very strong, and do not produce as great a disturbance to the flow. The force on the cylinder is therefore more inertia dominated for NKC less than about 10, whereas on the square section inertia plays an important part throughout a large range of NKC. This fact may be evidenced in figure 6.5 which shows that as the force becomes more inertia dominated, the phase of the maximum force approaches 90^{o}. On the circular cylinder this is observed as quite a rapid variation in phase for NKC between about 8 and 10. For the square the results are quite different and show a slow tendency towards inertia dominance as NKC is decreased. The results for the drag coefficient of the flat plate and diamond section, however show an increase in C_D as NKC decreases and suggests that for these sections even at these low values of NKC, the drag part of the force is still very important. Examination of figure 6.5 also reveals that the phase of the maximum force on these sections, even at small values of NKC show no signs of tending towards 90^{o}. Thus body geometry clearly has an effect on the drag coefficient. This effect is associated with the formation of vortices, which play an important part even at low values of NKC on the diamond section and flat plate; on the square and circular cylinder at the low values of NKC no discernible vortices are formed and the force is then almost all inertial. The importance of vortex formation on sharp edged bodies at low values of NKC was also recognised by Graham (1978) who noted that thiseffect might be important even in the diffraction regime.

Using the second method of representing the in-line force, i.e. in terms of root mean square force coefficient, results in values of C_{Frms} which correlate well with NKC for all the sections tested, as shown in figure 6.3. Here it can be seen that throughout the range of NKC the circular cylinder experiences the lowest force. These results also show that as NKC increases, C_{Frms} on all the sections tends towards a constant value, but as NKC tends to zero C_{Frms} becomes very large. This is an unfortunate consequence of nondimensionalising by $\frac{1}{2}\rho U_m^2 D$, where the presence of a finite force at small values of NKC leads to very large values of the coefficient. Figure 6.3 also shows that as NKC decreases below about 20, C_{Frms} on the square section increases rapidly and for NKC less than about 10, the root mean square force on the square is comparable with that on the flat plate. This happens because the inertial force is very large on the square section, so that although the drag is small the r.m.s force, composed of the drag and inertia is still quite large.

Using the third method of describing the in-line force i.e in terms of its maximum value and phase, results in values of C_{Fmax} and ϕ which are plotted in figures 6.4 and 6.5 respectively. This method of description of the force much favoured by designers, is also very useful in gaining an insight to the more important features of the flow. The results for C_{Fmax} and ϕ are in agreement in principle with the results of other coefficients. Figure 6.4 shows that throughout the range of NKC, the flat plate experiences the largest force, and the cylinder, the lowest. Here again the results for the square section disagree with the trends observed by the results on the other sections. For NKC $<$ 20 where inertial forces are large on the square section, it experiences a large maximum force, second only to that on the flat plate. At larger values of NKC where drag becomes more important, the maximum force on the square section is only just greater than that on the cylinder, and this drop in force is related to the decrease in drag caused by turbulence, as mentioned above. It is also worth noting that

figure 6.4 also shows the strong effect of the vortices on the cylinder and diamond section in the region of NKC between about 10 and 15 where the flow pattern changes from one flow regime to another. On the flat plate no change in flow regime takes place, hence the curve is smooth. Note also that although the change in flow pattern was clearly reflected in C_{Fmax}, figure 6.3 shows that the r.m.s. is almost unaffected.

Changes in the flow pattern are also clearly reflected in the phase of the maximum force as figure 6.5 shows. Also as mentioned early such a plot gives a clear idea of the importance of drag and inertia on the various sections and how this varies with NKC. This figure shows that at about NKC $\approx$ 50, the flow past all the sections is drag dominated. Forthe diamond section, flat plate and circular cylinder, figure 6.5 shows that inertia is relatively unimportant for NKC greater than about 20. This figure also shows that although the flow past the cylinder and square section is inertia dominated by about NKC $\approx$ 5, the flat plate and diamond section are not. Here also it can be seen that for NKC less than about 25 inertia is the dominant force on the square section.

In the foregoing sections the results presented and discussed were those obtained from data evaluated on average cycles of the force. However results were presented in Chapter 4 to show that the in-line force on all the sections, when described by any of the three methods discussed above, is not constant from cycle to cycle. These results show that, although when recorded on a pen recorder or on an oscilloscope the force shows only a little variation from cycle to cycle (figure 4.10 being a typical example), when the force is represented by coefficients substantial variation from cycle to cycle is observed. As mentioned in Chapter: 4, some of this variation particularly at low values of NKC and on the square section may be due to noise. It should however be stressed that this variation is definitely not all due to noise, and at higher values of NKC the signal to noise ratio was high enough to discount noise as a contributing factor. These results show that of all the coefficients used to describe the

force, and on all the sections the variation in the r.m.s is the least being always less than about ± 10% of the average except for very small values of NKC where some of this variation is probably due to noise. It is also noticeable that on all the sections tested the variation is neither the same for every section, nor is it constant and independent of NKC. Further, the variation changes with NKC and not always in an orderly manner, so that during certain ranges of NKC the variation may be definitely smaller than that observed at other values of NKC. The most striking example of this is shown in figure 4.52 to 4.56 for the coefficients on the diamond section. Here it is quite clear that for NKC between 20 and 25 the variation in all the coefficients is markedly less; figure 4.56 also shows clearly that the phase of the maximum force is also quite repeatable and exhibits the least variation in this range of NKC. This without doubt shows that this variation is not all due to noise but instead reflects a genuine behaviour of the force, i.e that it is not as repeatable as was first thought. Such variation in the in-line force from cycle to cycle is not at first thought plausible because the incident flow is extermely repetitive. However during a cycle vortices formed and possibly shed (depending on the value of NKC) are swept back against the body where some cancellation with vorticity of opposite sign takes place. In any case a complex interaction between the vortices and the body occurs, and this interaction also affects the strength and later the motion of the vortices subsequently formed. Thus in order for the force to be exactly repeatable these processes, i.e. interaction between the vortices and the body, interaction between vortices of opposite sign, the strength and the motion of the vortices, must all be precisely the same from cycle to cycle. It is the differences in these processes, mainly in vortex strength and motion, which result in changes in the in-line force from cycle to cycle. First experiments, on the circular cylinder led to the possibility that a contributing factor may have been the arbitrariness of the separation point. Though this in another factor, for the circular cylinder, it is not the important fact as later experiments revealed that the force on sharp-edged bodies also

varied from cycle to cycle. Further, of all the sections the variation was most on the flat plate, where the largest and most dominant vortices were observed. On this section also during flow reversal the most dramatic interaction with the body took place, and resulted in vortex paths differing noticeably from cycle to cycle. These vortex paths some of which are presented in Chapter: 5 were obtained from studies of ciné film. Visual observations cannot reveal the small variation in the vortex paths. These variation in the vortex strengths and positions, result in changes of the force which then causes substantial changes in the force coefficients obtained from Morison's equation, i.e. C_m and C_D. However, only much smaller variations occur in C_{Frms} as this is more or less independent of phase changes. This therefore suggests that the r.m.s. method of representing the in-line force as proposed by Maull and Milliner (1978a) is possibly a suitable alternative to Morison's equation.

6.2 MORISON'S EQUATION

The equation proposed by Morison et al (1950) now known as Morison's equation is widely used in the field of offshore engineering. However some controversy and doubts still exist on its applicability and reliability. This equation was therefore examined by applying it to several body shapes. On the circular cylinder the work of Sarpkaya (1976) suggests that Morison's equation does indeed work admirably well except in the range of NKC between about 10 to 20. On flat plates however, the early work of Keulegan and Carpenter (1958) suggests that when applied to such sharp-edged sections Morison's equation fails to predict the force with any acceptable degree of accuracy. In this study Morison's equation was applied to the measured in-line force not only on a cylinder and plate but also on a square and on a diamond section. This application led to values of C_m and C_D which were then used to predict the force as given by Morison's equation. The bulk of these results were presented in Chapter: 4, however in figures 6.1 and 6.2 values of the inertia and drag coefficients obtained on the various sections

are compared. These coefficients, obtained through the use of Morison's equation are very sensitive to changes in the flow pattern. Apparently, the presence of large vortices which remain close to the body and interact with it as the flow reverses, results in noticeable changes in the variation of the force coefficients with NKC. This is especially noticeable for the C_m variation with NKC, where the presence of these vortices close to the body result in values of C_m which can correspond to negative added masses. As discussed above this is not physically possible, and therefore suggests a failing of Morison's equation when applied in this manner. With the absence of any clearly defined vortex structure, as on the square section, the coefficients then show a gradual variation with NKC. Representing the force by means of an inertial and a drag component as determined by Morison's equation also suffers from the drawback that these coefficients are very sensitive to changes in the phase of the force, as shown in Appendix: 2. It has also been shown that even in this relatively simpler case of planar oscillatory motion, where the incident flow is without doubt extremely regular and two dimensional in the far field, the interaction between vortices and the body and/or with others of opposite sign results in a slight random variation in the in-line force. This small variation, shows up quite clearly in C_m and C_D as these are phase sensitive but only a small variation in C_{Frms} is observed, thus suggesting that this might be a better method of describing the force.

Using measured values of the inertia and drag coefficients in Morison's equation, also yielded the predicted force variation during a cycle. These results, presented in Chapter: 4 shows that, as was previously found by Sarpkaya (1976), Morison's equation does indeed predict the force on the circular cylinder remarkably well for values of NKC outside the range $10 < NKC < 20$. In the range of NKC between 10 and 20, the strong vortices present remain in motion close to the body as described in Chapter: 5. At low values of NKC, however the flow is almost attached, no vortices of any significance are formed and the force is almost all inertial,

with the maximum force occuring at around 90^{o}, and here figure 4.19a shows that Morison's equation works quite well. As NKC increases the flow is now asymmetric with vortices being formed but not shed, the pattern being as shown in figure 5.2b. In this region during each half cycle, one vortex grows quite large which results in a second maximum in the force which occurs at about 180^{o}; the real maximum in the force still occurs at about 90^{o} as shown in figure 4.19b. However the growth of this vortex results in the predicted force being wrong at the peaks. As NKC increases further the vortices grow stronger and the flow pattern changes. The pattern is now as shown as in figure 5.2c for NKC about 10, and here these stronger vortices result in a shift of the maximum force from about 90^{o} to around 180^{o} (note that the phase of maximum force (Φ) is defined as 180^{o} - position of maximum force) which corresponds to a change in Φ from about 90^{o} to approximately 0^{o} as can be seen in figure 6.5 for NKC just below 10. This pattern exists for NKC up to about 15 and during this regime Morison's equation fails to predict the force accurately because the effect of the voritices is not propertly accounted for. This behaviour of the vorticies in this region also accounts for the peak in C_{Fmax} and in C_{D}, as the dramatic change in phase results in an increase in the drag part of the force and a decrease in the inertial part. The variation of the measured and predicted force during this region is given in figures 4.19c and 4.19d; in this region as can be seen the prediction by Morison's equation is the poorest being especially bad at NKC $\approx$ 15. As NKC increases beyond this a different flow patternis observed, with the vortices now tending to rotate around the cylinder as shown in figure 5.2d. Here the agreement between the predicted force and Morison's equation begins to improve and by NKC $\approx$ 20, quite a good prediction is obtained from Morison's equation. Apparently, although quite large vortices are present, because of the configuration and motion about the cylinder no dramatic instantaneous effects are produced and Morison's equation therefore works fairly well. As NKC increases beyond about 20 more vortices are formed, and by about NKC $\approx$ 25 some semblance of a vortex street is observed. Here however, and for

larger values of NKC, Morison's equation predicts the force very accurately.

On the flat plate however results presented in figures 4.34 and 4.35 show that the force predicted by Morison's equation is in poor agreement with the measured force for most of the range of NKC. Figure 4.35a shows that even for NKC as low as 3 the force predicted by Morison's equation is not very accurate. However for NKC greater than about 20 the agreement between the measured force and Morison's equation improves, slowly. By NKC $\approx$ 50, the agreement is fair but not as good as that obtained for the cylinder. This lack of agreement between the predicted force and that measured on the flat plate, is directly attributable to the influence of the stronger vortices formed on this section on the force, even at low values of NKC where they result in a large drag. The greatest influence of these vortices is possibly during flow reversal, where strong interactions between them and the plate occurs. For larger values of NKC, say above 20, a number of vortices are formed and shed (depending on the value of NKC) and the overall effect on the force is not as dramatic resulting in a better agreement between the predicted and measured force.

On the diamond section results presented in figure 4.47a to 4.47h show that here also the predicted force is not very accurate for NKC less than about 2 5. Even for NKC as low as 4.8, figure 4.57 shows that the presence of growing vortices results in a poor prediction. As NKC increases the prediction first becomes worse, but between NKC = 13 to 16, the prediction is quite good; beyond this the prediction again depreciates and then slowly improves so that by about NKC $\approx$ 25 and for larger values of NKC the prediction is fairly good. Throughout the range of NKC vortices are formed, but for NKC between about 20 and 10 these are particularly strong and set up clearly defined motions close to the body. The fact that for NKC $\approx$ 15, fairly good agreement is obtained between the measured and predicted forces is therefore surprising. However this is just coincidental and occurs because in this region the force is influenced by a series of vortices, with the pattern as shown in figures 5.9c and 5.10a. As with the other sections,

it appears that if the cumulative effect of the vortices is such that a gradual change in the force occurs throughout a cycle, then Morison's equation works well.

For the square section, results presented in figure 5.71a to 5.71h show that for NKC less than 8 the prediction starts to improve, but for NKC between about 10 and 30 the prediction is poor. As NKC increases above about 30 the prediction gradually improves and by NKC $\approx$ 50, the predicted force is in fair agreement with the measured force. In the range of NKC between 10 and 30, although strong dominant vortices are not present, nevertheless it appears that the interaction between the body and these vortices are enough to result in the poor prediction observed.

Thus, it seems that of all the sections, Morison's equation is more suitbale to the prediction of the force on the circular cylinder except for value of NKC between about 10 and 20. The reason for this failure has been suggested by other workers, e.g. Sarpkaya (1976a) as due to the fact that Morison's equation contains only odd harmonics and therefore assumes symmetry in the in-line force. This poor prediction it is claimed, then results because in this region ($10 < NKC < 20$) the presence of large vortices close to the body results in a force which is not symmetrical; the large error then reflects this asymmetry in the force which is absent in Morison's equation. It should be noted that since the values of C_m and C_D, commonly used are constant averaged values, (i.e. obtained from the first term of equation A3.10 and A3.11), assumption about the symmetry of the in-line force does not affect these values. However it has been shown in Chapter: 4 the poor agreement between Morison's equation and the measured force is not due to the assumption of symmetry implied by Morison's equation. This was proved by showing that the agreement between the predicted and measured forces could be vastly improved by using values of C_m and C_D in Morison's equation which were not constant, but instead were time dependent, i.e. varied during a cycle. The expresions for C_m and C_D were therefore modified to include the third and

fifth harmonics of the force, (i.e only odd harmonics, so that the assumption of symmetry was still implied). Using these value of C_m and C_D in Morison's equation resulted in extremely good agreement between the predicted and measured force, as seen in figure 4.20. This improvement in prediction was obtained throughout the range of NKC, on the cylinder though at larger values of NKC it appeared that better agreement could be obtained if higher odd harmonics were included. Therefore, without doubt this shows that the poor prediction by Morison's equation is not primarily due to the fact that it assumes that the force is symmetrical. This is not really surprising as the measured force, at least when averaged over a number of cycles shows no signs of gross asymmetry. One way of looking at the failure of Morison's equation to predict the force accurately on the circular cylinder for NKC between about 10 and 20, is that even though it does contain odd harmonics of the force, these are not adequately modelled.

On the sharp-edged sections the prediction by Morison's equation is notably worse with the remainder function instantaneously attaining values of between 20 - 30% of the maximum measured force for NKC less than about 25. This is especially evident on results obtained for the flat plate. On the circular cylinder, however poor agreement between Morison's equation and the measured force was obtained only for a limited range of NKC, say between 10 and 20, and it was shown that the error was due to incorrect modelling of the higher odd harmonics in the force. The presence of odd harmonics is also evident in the remainder function obtained on the sharp-edged sections, and it would seem that here again the reason for the poor prediction is due to these not being properly represented by Morison's equation. Thus, on all the sections tested poor agreement was not primarily due to the assumption of symmetry implied in Morison's equation. However two important questions remain unanswered; firstly, why are the odd harmonics not properly modelled and secondly why should the agreement be better on the cylinder. Before these questions can be answered, Morison's equation must be closely

examined. Morison's equation was not founded on any firm theoretical evidence, but instead was a result of empiricism, where the force was assumed to be equal to the linear summation of two terms, one in phase with the acceleration and the other in phase with the velocity. It should be noted that for the simpler case of uni-directional accelerated flow, Sarpkaya and Garrison (1963) showed that, in this case the force could indeed be represented as suggested by Morison's equation, i.e. by the summation of an inertia and a drag term. No evidence however is available which suggests that for the relatively more complex case of planar oscillatory flow, where the acceleration is not just variable but periodic, Morison's equation might still be applicable. Morison's equation takes no account of the history of the motion, which must play an important part as the flow development is definitely influenced by the previous half cycle. Further this equation uses constant coefficients averaged over a cycle and then uses these to artifically introduce some time dependence into the force. It is therefore remarkable that Morison's equation should work at all. From the reason above it would seem that Morison's equation would tend to work better when the assumptions it makes becomes valid or at least justified. These assumptions, the most important being that the inertia and drag coefficients are constant during a cycle, and that the history effect of the flow can be ignored, would in practice never be fully valid. However when the form of the wake is not varying dramatically during a cycle, i.e. when the wake width and the flow pattern around the body does not change by large amounts, and when the effect of the previous half cycle is also not expected to be of primary importance, these assumptions can be made. Thus, for values of NKC where large vortices are present which interact strongly with the body, these assumptions will not hold and this explains the poor prediction by Morison's equation. Strong vortices close to the body have the effect of producing large variations in the wake, thus constant values of C_m and C_D will produce errors in the predicted force. These vortices, as they are swept back against the body, also directly affect the growth of the

vortices and subsequent flow development. Therefore both assumptions are totally invalid. At low values of NKC, if the flow tends towards attached flow, as on the circular cylinder these assumptions are more likely to be plausible, and therefore explains the fair prediction by Morison's equation of the force on the cylinder in this region. For the sharp-edged bodies however attached flow is not present even at low values of NKC, instead vortices though weak are present, and the interaction as the flow reverses is enough to render the assumptions invalid and result in poor prediction. The presence of the sharp edges always causes a more sudden or violent interaction between the vortices and the body, but on the circular cylinder the interaction is more gentle with the vortices allowed to move more easily across the surface as the flow reverses. It should be remembered that Morison's equation predicts a force which gives an average variation during a cycle, and rapid changes in the force cannot therefore be modelled and result in an error. On the cylinder therefore the prediction by Morison's equation is always better than on the sharp-edged sections. At large values of NKC, a number of vortices are formed and shed, however although the wake changes rapidly, these variations are not large, here also the effect of the vortices sweeping back past the cylinder is limited to only a very small portion of the cycle. Therefore for very large values of NKC these assumptions seem to be justified and Morison's equation again works fairly well. The reason for the poor prediction by Morison's equation can therefore be summarised by noting that this equation tries to predict the force which varies during a cycle, using constant averaged force coefficients which do not take account of the history of the motion or the rapid changes in the flow which produce components at higher frequencies, mainly at odd harmonics of the basic. Another way of viewing this, is in terms of the frequency content of the force. Thus, for situations where the form of the vortices and the manner in which they interact with the body are such that higher harmonics of notable energy are produced, Morisons's equation would not hold.

6.3 TRANSVERSE FORCE

Following the work of Isaacson and Maull (1976), Maull and Milliner (1978a) and Sarpkaya (1975,1976a,1976b), on circular cylinders, it is now well recognised that the lift force or transverse force is very important on circular cylinders in waves and oscillatory flow. With this knowledge in hand, the transverse forces on three of the sections namely, the cylinder, diamond and square section, were measured. These measurements revealed that on all the sections, for most of the range of NKC lift generation was not the same for every cycle, but instead occurred in uneven or irregular bursts. This irregularity in the transverse force data was especially noticeable for values of NKC above 25, for all the sections. For lower values of NKC (< 25), certain regions exist where the irregularity may cease, and the lift is then more 'well-behaved', but still varying from cycle to cycle though by only smaller amounts. This is clearly seen in figure 4.72c for NKC = 14.20 on the circular cylinders, where lift is generated almost regularly every cycle. On the diamond section, for NKC less than about 20, the lift is generally much more regular than on the cylinder, however at certain values of NKC irregular lift generation is observed on this section. The square section also experiences a lift force which is irregular; here however this irregularity is observed throughout the entire range of NKC. The reason for this irregularity in the lift force can be best understood if the mechanism responsible for lift generation is examined.

Lift forces result from asymmetry in the flow which is produced by the growth and motion of vortices. However in oscillating flow, the return of vortices against the body also plays an important role in lift generation. This is particularly important at values of NKC less than about 20, where large growing vortices generate substantial lift as they move back over the body when the flow reverses. At larger values of NKC, greater than about 25, the flow then becomes quasi-steady and here lift generation is maily due to the shedding of a series of vortices which result in the oscillation of the wake. Irregularity of the lift force

therefore results because of a number of reasons depending on the Keulegan and Carpenter number range. At low values of NKC say less than about 8, only weak vortices are formed and at even lower values of NKC (< 5) sometimes no distinct vortex pattern is observed. In this region therefore irregularity in the lift force occurs because during some cycles little or no vortex structure is formed and therefore little or no lift is produced. This is especially noticable on the circular cylinder and square section, however on the diamond section, because of the sharp edges distinct vortices are formed even at low values of NKC. On this section therefore any irregularity in the lift at low values of NKC is due to the fact that sometimes the vortices may form almost symmetrically thus creating little lift. At other times, the vortex from one edge may dominate with more lift being generated. At the intermediate range of NKC, between about 10 and 20, irregularity in the lift is produced because, the strengths, positions, and the manner in which these stronger vortices now interact with the body is not the same during every cycle. It is worth noting that in this range the strongest vortices appear to be formed, and the interaction between these and the body is therefore the strongest during this region. However the lift in this region, on the diamond section is generally much more regular because the sharp edges, tended to dictate the motion of the vortices as the flow reversed. These sharp edges were responsible also for flow patterns which were repeatable (in general) over long periods. On the circular cylinder, the arbitrary nature of the separation point resulted in flow patterns which generally were not very regular, though the overall motion was more or less the same. On this section, as the flow reversed the vortices were free to move either above or below the cylinder and this produced very irregular lift. At certain values of NKC however, the position and strengths of the vortices were such that a more regular pattern was produced, as was the case for NKC = 14.20 as figure 4.72c shows. At this value of NKC, the vortices induce strong enough velocities on each other to make the paths of each other more or less fixed.

On the square section during the intermediate range of NKC, as described in Chapter: 5, no distinct vortex pattern was produced, instead vortices formed were weak and even then the amount of vorticity seemed to vary considerably from cycle to cycle, thus leading to very irregular lift generation. At the larger values of NKC where lift is now caused by the regular shedding of vortices, lift is produced every cycle but the amount of lift produced varies considerably and irregularly as figure 4.72, 4.78, and 4.84 shows. Visual examination of the flow in this region, reveals that precisely the same conditions do not exist during every cycle. The way in which the vortices interact with the body as the flow reverses is not the same during every cycle, and since this interaction determines how the flow develops then the flow development is not the same. Further, during certain cycles noticeably weaker vortices are formed, whereas in some cycles more vortices may be formed than in others (though the difference is usually by 1). Therefore a considerable number of variables are present, and it appears that differences in these processes result in the cycle to cycle variation in the lift. In addition, during certain cycles the growth and motion of the vortices are such as to favour lift generation (i.e. stronger vortices with a much smaller cancellation), and the lift is noticeably large. During other cycles however, weaker vortices interacting with each other result in a much lower lift. It should be remembered that since the sole mechanism responsible for lift generation is the growth and motion of the vortices, and since these are very sensitive to changes in the flow conditions, then the lift will be very sensitive to small variations in the flow pattern. The in-line force on the other hand is not all due to the effect of the vortices, and although it does vary from cycle to cycle this variation is small compared with that on the transverse force.

This irregulatity in lift generation results in the data being non-stationary. Description of this force was therefore a problem, as quantities such as r.m.s and maximum force would be a function of the length of data recorded. It would seem more suitable to describe the data in a statistical

manner, however such a description requires a considerable quantity of data to give fairly accurate results. In this case, since the data obtained was not applicable, at least not in a quantitative manner, to any real situation and because of the large amount of data needed, the time and effort involved was enormous, the statistical approach was not used. Instead, using a 100 cycles of data, the root mean square and the maximum lift force were obtained and these used to describe the magnitude of this force. Results obtained in this manner were presented in figures 4.79 and 4.80.

For NKC above about 25, figure 4.80 shows that the root mean square lift force on all three sections appears to tend towards constant values. In this region also the results exhibit very little scatter even though the lift appeared to be highly irregular; this therefore suggests that the amount of data used in the analysis (100 cycles) was a representative sample. In this region also it appears that the square section experiences the largest r.m.s force, and the diamond section the lowest. At first sight this seems odd because the vortices formed on the square section are the weakest while those on the diamond are the strongest (of those formed on these three sections), especially since the growth and motion of vortices are responsible for the lift. However no contradiction arises; it is just that the asymmetry caused by the vortices acts over a greater area on the square section than on the diamond section. In other words a greater portion of the square is in the wake, where the pressure differences between the lower and upper surfaces caused by the vortices give rise to large lift forces. On the diamond section however a smaller portion of the body is subjected to the pressure differences. The circular cylinder as can be seen in figure 4.80, from a combination of the area of separated flow and strength of vortices experiences only a slightly larger r.m.s force than the diamond section. As NKC is decreased to less than 25 the data on all the sections exhibit considerable scatter, with the square section behaving the most erratic and the diamond, the least. Also for NKC less than about 20 the results on the diamond section are now noticeably greater than those on the circular cylinder. This

jump in the results on the diamond section and the wide scatter observed in this region of NKC occurs because of the regularity or irregularity of the lift force. On the diamond section because of the general regularity in the lift data for NKC less than about 20, a higher root mean square force is obtained, whereas on the circular cylinder lower and generally more scattered results are obtained. This fact that the increase in regularity of the lift force causes an increase in the r.m.s is clearly demonstrated for NKC = 14.20 on the circular cylinder, where a large r.m.s value is obtained for a fairly regular lift signal (figure 4.72c). On the square section the large scatter in C_{Lrms} is also due to the irregularity or regularity in the lift signal. However here also at certain values of NKC some mean lift is also generated, but the direction in which this mean acts is arbitrary, therefore for more or less the same value of NKC largely differences in results may be obtained as for NKC $\approx$ 15, in figure 4.80. This scatter in data resulting from the peculiar nature of lift generation is clearly demonstrated in figure 4.74. Here, comparison with other data for the r.m.s lift force on the circular cylinder reveals that for NKC $<$ 25, the force can adopt a range of values, for the same value of NKC. The upper bound represents regular lift generation, as for NKC = 14.20, and the lower bound to very uneven or irregular liftgeneration. This plot (figure 4.74) also shows that the present data on its own could be misleading because insufficient measurements were made, and not at low enough values of NKC to give the complete picture. The present data, for the results on the three sections tested, as presented in figure 4.80 appears to show C_{Lrms} increasing rapidly at low values of NKC, however for the circular cylinder figure 4.74 shows that as expected $C_{Lrms} \longrightarrow 0$ as NKC $\rightarrow$ 0. Thus the present results quite simply do not show measurements at low enough values of NKC where C_{Lrms} will tend to zero, and therefore should not be extrapolated. Measurements were not made at very small values of NKC because of the difficulty associated with measuring such small quantities. It is probably noticeable that on the square section, measurements for NKC below about 12 were

not presented, because this section experienced very small forces up to this value of NKC. Ideally because the transverse force is smaller than the in-line force, a more sensitive pair of load cells should have been designed to measure this force. Further, because of the wide range of NKC tested, two pairs of load cells, one more sensitive than the other would have been better, however time and cost did not permit this.

Data for the maximum lift force in general shows much more scatter, and throughout the entire range of NKC. This is demonstrated in figure 4.73, where results for the maximum lift force on the circular cylinder is compared with data obtained by other workers also using 'U-tube' shaped water tanks. With the exception of data obtained by Sarpkaya and Tuter (1974), figure 4.73 exhibits considerable scatter. In this figure, the mean line through Sarpkaya and Tuter's data is shown. However in their paper, results presented showed very little scatter except in the range of NKC between 20 and 25; this is represented in figure 4.73 by a branch in the mean line. Sarpkaya and Tuter's data also show the maximum lift tending to zero with NKC as would be expected, but this fact is not shown by any of the other data including the present results. Obviously, had these experiments been conducted at low enough values of NKC the results would show C_{Lmax} tending to zero with NKC. However the fact that Sarpkaya and Tuter's results show tend to zero earlier together with the small overall scatter suggests that in their case lift generation was probably more orderly and regular, and with the flow becoming symmetric at earlier values of NKC. However they did not present root mean square values so no definite conclusions about the difference in behaviour of their results, can be made. Nevertheless it is interesting to note that in their experiments, the cylinders were placed in an upright arm of the tank, whereas all the other data were obtained with the cylinder in the horizontal sections of the tanks. It is possible therefore that positioning the cylinder in the arm of the tank results in more repeatable flow patterns and hence more regular lift generation. It

should be remembered that the maximum lift force is a very sensitive quantity, and it requires strong lift generation only for a few cycles, to give a large maximum lift force, and this may explain why the present results and those of other workers (with the exception of Sarpkaya and Tuter) show large values of C_{Lmax} at fairly small values of NKC. Similar behaviour of the maximum lift on the other two sections were observed as shown in figure 4.79 where the results for the square and diamond sections are shown compared with those on the circular cylinder. Here again as with the r.m.s force, for NKC $>$ 25 the square section again experiences the greatest force, and the diamond section, the smallest, for reasons already mentioned. Figure 4.79 also shows that the scatter in the data is the greatest on the square section and again for similar reasons as for the scatter on the r.m.s force. This figure also shows that for NKC between about 15 and 20, the maximum lift on the diamond section is lower than that on the circular cylinder, but as was mentioned earlier in this region the r.m.s on the diamond is greater than that on the circular cylinder. This point thus validates the claim that it is the regularity of the lift that is responsible for large r.m.s forces.

Both figures 4.79 and 4.80 show some similarity in the behaviour of the lift forces on all three sections for NKC greater than about 25. This similarity, in trends is a direct result of the similarity in the flow. As described in Chapter: 5, for NKC greater than about 25, the flow past all these sections approach a quasi-steady situation with a series of vortices being shed. This causes an oscillation of the wake and a lift generation, which is similar on these sections, as demonstrated in figures 4.75, 4.81 and 4.85, for the larger values of NKC. However for NKC $<$ 25, figure 4.75 and 4.81 show that the lift on the circular cylinder and diamond section are very much alike whereas figure 4.85 shows that in this region lift generated on the square section is of a different form. This behaviour is again due to the fact that on the diamond section and circular cylinder similar patterns are

produced, where lift is produced both by the growth of the vortices and their motion, especially as they are swept back against the body. On the square section however, the growth and motion of the vortices are completely different, with only weak vortices being formed and the motion being ill-defined. The fact that the similar flow patterns produce similar lift generation can be seen in figures 4.75a, 4.75b and 4.81a where on both sections the flow pattern was similar with a pair of asymmetric growing vortices being formed during each half cycle. By examining the sketches in figures 5.2b and 5.9b the variation in lift during a cycle can be predicted from the motion of these vortices. On the circular cylinder and diamond section, figures 5.2c and 5.9c show that during certain ranges of NKC a 'sideways vortex street' is produced; this pattern produces lift as shown in figure 4.75c (for the circular cylinder), and in figures 4.81b and 4.81c for the diamond section. This distribution in lift over a cycle during the 'sideways vortex street' can be verified by examining the position of the vortices as sketched in figure 5.2c and 5.9c. For slightly higher values of NKC, figures 5.2d and 5.9d show that similar patterns are again produced; the pattern now being a cyclic rotation of the vortices about the body. In this region the lift generation over a cycle is as shown in figures 4.75d, 4.75f, 4.81d and 4.81f, and can be verified by examining the position of the vortices as sketched in figures 5.2d and 5.9d. Thus on the circular cylinder and diamond section similar lift is generated throughout the entire range of NKC; here also lift is generated both by the formation of vortices and the passage of these over or under the body as the flow reverses. On the square section however, lift variation over a cycle for NKC < 25 is different because the flow pattern is different. Here, although strong vortices are not formed considerable lift is generated because a large area of the body is in the wake and is therefore subjected to large pressure differences arising from the presence of the weak vortices, On this section therefore lift is generated more through the formation and shedding of vortices, than by the return of vortices past the body as the flow reverses.

This happens because as mentioned in Chapter: 5, the weak vortices formed, quickly break down as the flow reverses, so no definite vortex structure is swept back past the body. Instead, an apparently turbulent (with weak spanwise intensity) flow is incident on the model as the flow reverses and this itself does not produce much lift.

Figures 4.75, 4.81 and 4.85 also show that throughout the range of NKC, lift is not generated at a constant frequency; this is easily verified by examining spectra of the lift force presented in figures 4.77, 4.83 and 4.87. Here it can be seen that lift is generated over a band of frequencies, all multiples of the water oscillation frequency, and the range of frequencies increases with NKC. This fact that the transverse force occurs over a band of frequencies makes it difficult to define a dominant frequency of the transverse force. As vortex shedding plays an important part in lift generation, the vortex shedding frequency would seem a useful parameter in the description of the transverse force. However for some regions, although considerable lift is generated, no vortex is completely shed, and lift is generated from the growth and movement of the growing vortices as the flow reverses. Further, even at larger values of NKC the vortex shedding frequency is not constant, as the first vortex shed is usually influenced by other vortices interacting with the body. In addition, as considerable lift is generated by the interaction between previously formed vortices and the body, a vortex shedding frequency to describe the transverse force was therefore not used. Instead a more representative but not precise frequency description of the force was based on a frequency obtained by checking the number of zero crossings. This frequency is thus a sort of averaged frequency, and was used to define a Strouhal number. These results presented in figures 4.76, 4.82 and 4.86, show this Strouhal number appearing to tend towards a constant value as NKC increases. Here also it can be seen that for NKC less than about 25, similar results are obtained on the circular cylinder and diamond section, whereas the square section again show a

different behaviour. Further,as expected the Strouhal number on the square section is also the lowest, due to the fact that the afterbody in delaying the interaction between the separated shear layers also reduce the number of vortices shed. A fact which is evident in steady flow.

As mentioned above, spectra presented in figures 4.77, 4.83 and 4.87 clearly reveal that the transverse force occurs at several frequencies all multiples of the fundamental frequency. It should be noted that the peak shown in these spectra at just over 3 Hz is not genuine but instead due to noise introduced by the tape recorder. For NKC > 25, these plots show that lift is produced over a wide band of frequencies, which increases with NKC. The wide band nature of the lift force occurs because the vortex shedding frequency is not constant, and also because lift produced by the return of vortices is not the same for every cycle. At smaller values of NKC (< 25), the lift spectra is generally not so broad band and lift tends to occur at discrete frequencies, either odd or even multiples of the oscillation frequency. The nature of the spectrum however depends on the flow pattern, and changes with it.

These results demonstrate that as on the circular cylinder, the transverse force on the two other bluff sections are also very important, both in magnitude and frequency. For NKC greater than about 25, results presented show that lift on all the sections occurs in uneven bursts of significant notable magnitude and over a wide range of frequencies increasing with NKC. For NKC < 25 lift forces can adopt a range of values depending on the regularity of the flow, here the frequency content is less broad band depending on the nature of the flow pattern. It also appears that the maximum lift force, root mean square force and the Strouhal number appear to tend towards constant values. Finally it appears that, as would be expected, the range of frequencies over which the transverse force acts, at larger values of NKC, is centred on the Strouhal frequency.

6.4 SOME IMPORTANT EFFECTS

6.4.1 BODY GEOMETRY

These results show that the singularly most important feature in oscillatory flow is the production and interaction of vortices. Providing the formation process is not inhibited, vortices are formed which set up similar motions around all the sections. The similar behaviour of these vortices result in similar variation of the forces, both in-line and transverse. The primary effect of the body shape is therefore in the production of vortices. However the angle of the separating shear layers is also very important as this generally determines the strength of the vortices formed, which in turn determines the magnitude of the drag. This incidentally is one explanation for the larger forces experienced by Keulegan and Carpenter (1958), during their experiments on thin untapered flat plates, where the angle of the separating shear layers was higher than in the present case where the flat plates were tapered to give an internal edge angle of 60°. Bodies with free separation points, usually have weaker vortices and hence a smaller drag. In an oscillating flow also the separation points on such a body vary considerably during a cycle, particularly at intermediate values of NKC. This variation in separation point during a cycle results in a more gradual development of the flow. However the most important consequence of free separation points, is that the interaction process between vortices and the body is usually more gentle, with the vortex free to move either above or below the body. Further, unlike sharp edged bodies less stretching of the previously shed vortices occurs. This gentler process of interaction and formation of vortices leads to less randomness in the in-line force, but more in the transverse force (as paths of vortices are not dictated). Body geometry also plays an important role in determing the nature of the force at small values of NKC. On the sharp-edged bodies, even at low values of NKC vortices are formed and the force is still influenced by drag. On bodies where reattachment is possible however, this effect

may cause the force to be considerably influenced by inertia even at substantially large values of NKC. The larger wake and the wider variation in wake characteristics, together with the more complicated interaction between vortices and body result in a poorer prediction by Morison's equation of the in-line force on sharp-edged bodies. Lift forces or transverse forces, being related to the vortex growth and movement is also affected by geometry. The magnitude of the lift besides being affected by the strength of vortices, also depends on the area of body in the separated region, thus on the square, even though weaker vortices are formed larger lift forces are obtained.

6.4.2 BLOCKAGE

By examining the force on different sized flat plates blockage in oscillatory flow was examined. Results presented in figures 4.37, 4.38 and 4.39, show distinct effects of blockage on the drag, r.m.s and maximum force on flat plates. These effects are primarily due to blockage because as mentioned in Chapter: 4 Reynolds number is not expected to have much an effect, (a fact demonstrated by the works of Keulegan and Carpenter (1958) and Shih and Buchanan (1971)). Aspect ratio is not considered very important as the flow is more or less two dimensional, with L/D large enough so as not to be influenced by the very small gap flow, that must exist at the ends of the models. In any event, figures 4.41 and 4.42 show that good collapse of results can be achieved if Maskell's blockage correction method is used. This correction method was not strictly applicable and was used only to show that collapse of results could be achieved by taking the blockage ratio into account. These results clearly indicate that blockage is important in steady flow for blockage ratios more than about 5%. However it should be noted that the importance of blockage decreases as NKC decreases, and for NKC less than about 5 blockage is not very important. These conclusions are definitely in disagreement with those of Sarpkaya (1976a) where his experiments on the blockage on circular cylinders

in oscillating flow led him to the conclusion that 'blockage effect in harmonic flows is negligible at least for D/W ratios less than 0.18.' Sarpkaya's method of examining blockage was by means of pressure tappings on the surface of the tank, where he compared the acceleration in the vicinity of the model with that elswhere in the tank. The fact that he found little difference is therefore is disagreement with the present results which showed a definite effect of blockage. However his study was on circular cylinders whereas the present experiments were on flat plates. The present experiments were based on force measurements on a series of plates, however a similar set of experiments on circular Cylinders could have been misleading as a simple increase in dimension also increases the Reynolds number. This was not a problem on the flat plates where as already mentioned Reynolds number has little effect. On the circular cylinder however an increase in Reynolds number causes a decrease in drag, whereas blockage is expected to increase the drag. Nevertheless these experiments reveal that blockage is important in oscillatory flows, at least on flat plates, and possibly bodies where the angle of the separating shear layers is large, i.e. with large wake widths, for values of NKC in excess of about 5. The fact that Sarpkaya (1976a) did not notice any measurable change in the acceleration, as observed in his surface pressure measurements is probably due to the wake width being much smaller on the circular cylinder.

6.5. REPRESENTATION OF THE FORCES

The results and discussion presented above show that even in this relatively simpler case of planar oscillatory flow, representing the in-line force by Morison's equation is not very accurate, except at large values of NKC where fairly good agreement is generally achieved. Of course on the circular cylinder the agreement between the force predicted by Morison's equation and the measured force is better than on the other sections. The main disadvantage of using Morison's equation is that the coefficients used with it are averaged values, which are then used to represent forces which vary considerably during a cycle; time dependence being introduced by multiplying

these coefficients by the appropriate velocities or accelerations. Such coefficients tend to be misleading and for the inertia coefficient can represent values which are not physically possible. The Morison coefficients are also extremely sensitive to changes in the phase of the force which can result from changes in the flow pattern. This causes noticable variations in these coefficients from cycle to cycle even though the incident flow is repetitive. In a real situation the use of Morison's equation to derive coefficients is very suspect as a wide variation of results is expected since the incident flow is not regular.

A suitable alternative approach was suggested by Maull and Milliner (1978a), where a single coefficient, the r.m.s was used to describe the force. Such a method of describing the force is attractive, because although substantial cycle to cycle variations were observed in the Morison coefficients, much less variation was observed in C_{Frms}. In addition the behaviour of C_{Frms} is not as sensitive as the other coefficients, tochanges in the flow pattern. The variation of this coefficient with NKC is therefore more orderly and gently tends towards a constant value at large values of NKC. The idea of a single coefficient to represent the force was earlier used very successfully for the case of uni-directional accelerated motion by Iversen and Balent (1951) and by Keim (1956). More recently, Karanfilian and Kotas (1978), showed that the force on a sphere oscillating in still water can also be adequately described by a single coefficient. Further, Maull (1978), showed that the force on a circular cylinder can be well represented using constant values of C_m and C_D in Morison's equation to give C_{Frms} (see Appendix: 4), for a range of β values provided the appropriate C_D's are used. Thus it seems that the in-line force can be adequately described in terms of a single r.m.s force coefficient which may be predicted using constant values of C_m and C_D in Morison's equation. Using this approach Morison's equation was used to predict the r.m.s of the in-line force on the four sections tested, again using constant values of C_m and C_D. The inertia coefficient used was the appropriate potential flow value,

and the drag coefficient was the steady, smooth flow value in the corresponding Reynolds number range. These results presented in figures 6.6 to 6.9 show that on all the sections except the square section the predicted value is in good agreement with themeasured values at large values of NKC. On the square section this behaviour is due to the fact that the flow about this section is somewhat turbulent, thus the drag experienced and the r.m.s force is lower than that for smooth flow. Obviously such a prediction, i.e. using potential flow value C_m and steady flow C_D, is only really justified at the extreme ranges of NKC, i.e. at small or large values. However on the circular cylinder the prediction is good throughout most of the range of NKC. On the other sections the prediction is not so good. Nevertheless figures 6.6 to 6.9 show that on all the sections the in-line force data can be represented by a single r.m.s force coefficient. Prediction of this coefficient on all but the circular cylinder, using constant values of C_m and C_D in Morison's equation is however not very accurate. A family of such curves could however be presented which would be valid in certain ranges of NKC and under certain conditions, but this idea needs to be supported by further study. It should be noted though that although presentation of the force in this manner is attractive for the reasons mentioned above, Morison's equation has the advantage that the force distribution could be predicted, and this information is usually needed by designers.

Measurements of the transverse force, reveal that on all the sections this force is generated in irregular bursts leading to a large band of values for NKC < 25. In a real situation, the more complex incident flow is likely to result in even more irregularity in the transverse force, however in this case the correlation along the span of the body would most probably be less than in the corresponding two-dimensional flow. Therefore in the 2-D case, the higher correlation together with the flow being more regular would lead to a higher lift force. Relevant experiments i.e. at the appropriate conditons but in two dimensional flow could be used

to obtain an upper bound of data for design purposes. This irregularity in the lift force, even for the simpler case of planar oscillatory motion is due to changes in the vortex growth, motion and interaction; lift forces are therefore very difficult to predict, and at this stage impossible for the more complex real situations. However research is being done, to model oscillatory flow using discrete vortices, and then to use Blasius equation as in equation 1.14 and 1.15 to yield both the in-line and transverse forces. Some of these studies are currently being carried out at Imperial College, and some attempts have been made in the past, e.g Stansby (1978) but these are still in the initial stages. The other important point as regards the transverse force is its frequency composition; again prediction of this is not possible from any present theoretical knowledge and data must be obtained from experiments. These experiments suggest that the transverse force occurs over a wide band of frequencies, centred on a Strouhal frequency as defined earlier, with the lowest component at the main water oscillation frequency. Obviously the situation is more complex in real life and the data presented here is to be treated only in a qualitative manner.

CHAPTER: 7

CONCLUSIONS

A 'U-tube' type water tank and associated drive mechanism were designed which produced stable sinusoidal oscillations; these oscillations attained a maximum amplitude of about 12". A force measuring system was also designed and both in-line and transverse forces on four bluff sections were measured. The flow past these sections was also visualised. The following conclusions were drawn from these results.

(1) Comparison of the in-line force data on the circular cylinder with similar data obtained by other workers also using U-tube type apparatus reveals a considerable amount of disagreement. No obvious explanation for this large difference exists but it appears that it might be due to different data analysis techniques and to the manner in which the oscillations are produced.

(2) Flow visualisation reveals that with the exception of the square section, similar flow patterns are observed on all the models. For NKC between about 10 and 25, (with the exception of the square section) large vortices are formed which set up clearly defined motions around the sections. On these sections the strongest vortices are formed during this region. For NKC above 25, the flow pattern on all sections is similar; here quasi- steady flow is approached as a series of vortices are shed. At small values of NKC, below about 5, the pattern on all the sections is more or less symmetrical, but on the flat plate and diamond section weak vortices are clearly observed. On the circular cylinder the flow remains attached over most of its surface, and on the square section the flow separates on the front face and weak recirculation is evident on the upper and lower surfaces.

(3) The similarity in flow patterns observed on the diamond section, flat plate and circular cylinder results in the

in-line force being similar on these sections. The behaviour of the force is directly related to the growth and motion of the vortices, and it is because these are similar on the three sections, that the behaviour of forces is similar. These results also show that on all the sections, as NKC decreases the inertia coefficients all approach their attached flow values, even though attached flow is not observedon all these sections, notably on the flat plate and diamond section. This therefore suggests that the weak vortices present at low values of NKC do not signigicantly influence acceleration dependent forces. However the presence of weak vortices at low values of NKC on the flat plate and diamond section result in a drag force which is still important even at these small values of NKC. At large values of NKC, the drag on all these sections approach their steady flow values at the appropriate Reynolds number; on the square section though,the presence of turbulence in the flow (caused by the wake/body interaction) results in a drag coefficient lower than the steady flow value. The behaviour of the square section throughout the range of NKC is different because the afterbody results in weaker vortices being formed, and these do not set up any clearly defined motions. These weak vortices present on this section result in a very low drag (the lowest of all the sections tested) for NKC less than about 25, and at the same time the inertia coefficient is almost constant at its attached flow value.. The more dominant vortices present on the other sections result in considerable variation in the Morison coefficients particularly in C_m. However the r.m.s of the in-line force is not noticeably affected by changes in the flow pattern. These results show that C_{Frms} is largest on the flat plate and lowest on the circular cylinder; the same results was obtained for the maximum force. For NKC less than about 20, on the square section, although the drag coefficient was small, quite large values of C_{Frms} and C_{Fmax} were obtained, as the square then experienced forces lower than the flat plate only; the reason for this being the large contribution from inertia. For NKC above 20, the forces on the

diamond section were larger than those on the square.

(4) Unlike previously reported conclusions, results presented here clearly show that blockage is important in oscillatory flows, at least on flat plates where blockage ratios larger than about 5% result in increased forces. This effect increases with NKC, but for NKC less than about 5, little effect of blockage is observed. It also appears that the importance of blockage varies with the body geometry, and that bodies with larger wake widths, resulting from large angles of the separating shear layers may be more affected by blockage.

(5) These results also show that even though the incident flow is repetitive, the in-line force is not, and substantial cycle to cycle variations are observed in the force coefficients. This variation in the in-line force occurs because the strengths and positions of the vortices are not the same during each cycle; another reason is that the interaction process is not the same during every cycle. Because C_m and C_D, the Morison coefficients are very sensitive to slight changes in phase, the slight variation in the form of the in-line force, results in quite large random variation in these coefficients from cycle to cycle. However the r.m.s force varies by a smaller amount. The Morison coefficients, C_m and C_D, are also very sensitive to changes in the flow pattern, and C_m in particular varies noticeably with NKC. This variation in C_m, is such that for certain values of NKC, a minimum is produced which corresponds to negative added mass, and is a direct result of changes in the phase of the force brought about by the motion of vortices close to the body.

(6) The use of averaged values for C_m and C_D in Morison's equation also results in a poor prediction of the force on the sharp-edged bodies and on the circular cylinder during certain ranges of NKC where large vortices are formed and remain in motion close to the body. This poor prediction results because Morison's equation tries

to represent a time varying force with constant averaged coefficients; time dependence being introduced by multiplication by the velocity or acceleration, both functions of time. At times where the flow pattern changes rapidly and by large amounts, due to the presence of large vortices close to the body and/or to their interaction with the body, Morison's equation therefore fails to predict the force accurately. The problems associated with using Morison's equation both to predict the force and to derive values of C_m and C_D suggests the need for an alternative approach to the description and prediction of the in-line force. Such an alternative method exists. This method is based on the use of a single r.m.s force coefficient and is attrative because of its relative insensitivity to slight phase changes and therefore to changes in the flow pattern. This method however suffers from the drawback that the complete force history cannot be predicted, though the r.m.s force may be predicted using constant values of C_m and C_D in Morison's equation. The value of C_D however ought to be chosen to be representative of the conditions.

(7) The transverse force on all the sections tested show considerable irregularity with lift being generated in bursts of irregular lengths. This irregularity in the lift force occurs because lift is produced solely by the growth and motion of vortices and it is therefore very sensitive to changes in the strengths and positions of these. The interaction mechanism also produces lift and as this is not always the same during every cycle, it adds to the irregularity of the lift. Similar vortex patterns on the circular cylinder and diamond section results in similar formation of lift throughout the range of NKC; obviously the detailed variation of the lift during a cycle depends on the precise flow pattern, so similar patterns produce similar lift variation. At larger values of NKC ($>$ 25) the flow pattern is similar so on all the sections at these values of NKC the formation of lift is similar, due primarily to the wake oscillation caused by

the shedding of vortices.

This irregularity of the lift results in a band of values both for the r.m.s and maximum forces for NKC less than about 25, the scatter being larger for C_{Lmax}. The more regular the lift generation, the higher the r.m.s, such that at the same value of NKC, several values of the r.m.s may be obtained, the largest corresponding to extremely regular lift generation. The maximum force also exhibits a band of values, again related to the flow pattern; during certain periods the body may experience a mean lift, and this mean lift varies with the flow pattern. The frequency of the transverse force in this case of planar oscillatory motion, is not a constant, but varies with NKC. At any particular value of NKC lift is not produced at a single frequency but at a number of discrete frequencies all multiples of the water oscillation frequency. The nature of the frequency distribution is such that for NKC above about 25, the spectrum is more wide band and centred on a Strouhal frequency. This Strouhal frequency, as defined earlier appears to approach a constant value as NKC increases. Finally of the three sections on which lift was measured, for NKC greater than about 20 the square experienced the largest lift and the diamond the lowest. This occurred because on the square section a larger area of the body was in the wake and subjected to the pressure differences.

(8) Of the four sections, tested therefore, the flat plates experienced the larges forces as would be expected. These experiments also show that for the purposes of design the circular cylinder is the best shape as it experiences the smallest overall in-line forces. Although the diamond section experienced smaller transverse forces than the circular cylinder over certain band of NKC, such a section will be very sensitive to angle of incidence and for some angles of incidence (such that it appears as a square) forces larger than those on the cylinder will be experienced.

REFERENCES

Achenbach, E. 1971. The influence of surface roughness on the cross-flow around a circular cylinder. Jnl. of Fluid Mechs., Vol. 46, pp 321-335.

Ball, D.J. and Cox, N.J. 1978. Hydrodynamic drag forces on groups of flat plates. Jnl. of the Waterway, Port, Coastal and Ocean Div., Proc. A.S.C.E., No. WW2, May 1978.

Bearman, P.W. 1965. Investigation of the flow behind a two-dimensional model with a blunt trailing edge and fitted with splitter plates. Jnl. of Fluid Mech., Vol. 21, pp 241-255.

Bearman, P.W. 1978. Turbulence effects on bluff body mean flow. 3RD, U.S. National Conf. on Wind Engineering Research., University of Florida.

Bearman, P.W., Graham, J.M.R., and Singh, S. 1978. Forces on cylinders in harmonically oscillating flow. Symp. on Mech. of Wave-Induced forces on cylinders., Vol. 1, paper A3. Bristol., U.K. 1978.

Bendat, J.S., and Piersol, A.G. 1966. Measurement and Analysis of random data. John Wiley and Sons Inc., New York.

Bidde, D.D. 1971. Laboratory study of lift forces on circular piles. Jnl. of the Waterways, Harbors and Coastal Eng. Div. Proc. A.S.C.E., Vol. 97, No.WW4, Nov. 1971.

Borgman, L.E. 1967. Spectral Analysis of ocean wave forces on piling. Jnl. of the Waterways and Harbors Div., Proc. A.S.C.E. Vol. 93, No.WW2, May 1967.

Bushnell, M.J. 1977. Forces on cylinder arrays in oscillating flow. Proc. Offshore Technology Conference, Paper No. OTC 2903.

Crooke, R.C. 1955. Re-analysis of existing wave force data on model piles. U.S. Army, Corps of Engineers, Beach Erosion Board Tech. Memo., No. 71, April 1955.

Dalton, C., Hunt, J.P., and Hussain, A.K.M.F. 1976. The forces on a cylinder oscillating sinusoidally in water: II, Further experiments. Proc. Offshore Technology Conference. 1976. Paper No. OTC 2538.

Dean, R.G. 1970. Relative validites of water wave theories. Jnl. of the Waterways and Harbors Division., Proc. A.S.C.E., Vol. 96, No. WW1, Feb. 1970.

Dean, R.G. 1976. Methodology for evaluating suitability of wave and force data for determining drag and inertia forces. Proc., Behaviour of Offshore Structures, (BOS '76), Trondheim, August 1976.

Delany, N.K., and Sorensen, N.E. 1953. Low speed drag of cylinders of various shapes. U.S. National Advisory Committee for Aeronautics, TN 3038, Nov. 1953.

Fage, A. and Warsap, J.H. 1929. The effects of turbulence and surface roughness on the drag of a circular cylinder. A.R.C. R and M 1283., 1929.

Garrison, C.J., Field, J.B. and May, M.D. 1977. Drag and Inertia forces on a cylinder in periodic flow. Jnl. of Waterway, Port Coastal and Ocean Division., Proc. A.S.C.E., Vol. 103, No. WW2, May 1977.

Garrison, C.J. and Chow, P.Y. 1972. Wave forces on Submerged bodies. Jnl. of the Waterways, Harbors and Coastal Engineering Div., Proc. A.S.C.E., Vol. 98, No. WW3, Aug. 1972.

Gerrard, J.H. 1966. The mechanics of the formation region of vortices behind bluff bodies. Jnl. Fluid Mech., Vol. 25, Part 2, pp 401-413, 1966.

Graham, J.M.R. 1978. Forces on Cylindrical Bodies in Oscillatory flow at low Keulegan Carpenter Numbers. Symp. On Mech. of Wave-Induced forces on cylinders. Paper B1, Vol. 1, Bristol, U.K. 1978.

Grass, A.J. and Kemp, P.H. 1978. Flow Visualisation Studies on Oscillatory flow past smooth and rough circular cylinders. Symp. On Mech. of Wave-Induced forces on cylinders. Paper B2, Vol. 1, Bristol, U.K. 1978.

Hamann, F.H. and Dalton, C. 1971. The forces on a cylinder oscillating sinusoidally in water. Jnl. of Engineering for Industry, TRANS. A.S.M.E., Vol. 93, Series B, No. 4, pp 1197-1202. 1971.

Hogben, N. 1974. Fluid loading on offshore structures, a state of art appraisal; wave loads. Maritime Technology Monograph No. 1, published by the Royal Institution of Naval Architects, Nov. 1974.

Hogben, N. 1976. Wave loading on structures. Proc. Behaviour of Offshore Structures Conf. (BOS '76), Trondheim, August, 1976.

Hogben, N., Miller, B.L, Searle, J.W., and Ward, G. 1977. Estimation of Fluid loading on offshore structures National Maritime Institute. Report No. R11, April 1977.

Hogben, N., Osborne, J. and Standing, R.G. 1974. Wave loading on Offshore Structures - theory and experiment. Proc. Symp. on Ocean Engineering. Royal Institution of Naval Architects., Nov. 1974.

Hogben, N., and Standing, R.G. 1974. Wave loads on large bodies. Proc. International Symposium on Dynamics of Marine Vehicles and Structures in waves., published by Instn. of Mech. Engineers, 1974.

Isaacson, M. de St. Q. 1978. Wave forces on large Square cylinders. Symp. on Mech. of Wave - Induced forces on cylinder. Paper H1, Vol. 2, Bristol, U.K, 1978.

Isaacson, M. de St. Q. and Maull, D.J. 1976. Transverse forces on Vertical Cylinders in waves. Jnl. of the Waterways Harbors and Coastal Eng. Div., Proc. A.S.C.E., No. WW1, Feb. 1976.

Iversen, H.W. and Balent, R. 1951. A correlating modulus for Fluid resistance in accelerated motion. Jnl. of Applied Physics., Vol. 22, No.3, March 1951.

Karanfilian, S.K. and Kotas, T.J. 1978. Drag on a sphere in unsteady motion in a liquid at rest. Jnl. of Fluid Mechanics, Vol. 87, Part 1, pp 85-96, 1978.

Keim, S.R. 1956. Fluid resistance to cylinders in accelerated motion. Jnl. of Hydraulics Div., Proc. A.S.C.E., Vol. 82, No. HY6, December 1956.

Keulegan, G.H. and Carpenter, L.H. 1958. Forces on cylinders and plates in an oscillating fluid. Jnl. of Res. of the National Bureau of Standards, Vol. 60, No.5, May 1958, pp 423-440.

Laird, A.D.K,, Johnson, C.A. and Walker, R.W. 1959. Water forces on accelerated cylinders. Jnl. of the Waterways and Harbors Div., Proc. A.S.C.E., No. WW1, March 1959.

Laird, A.D.K, Johnson, C.A. and Walker, R.W. 1960. Water Eddy forces on oscillating cylinders. Jnl. of the Hydraulics Div., Proc. A.S.C.E., No. HY9. Nov.1960.

Laird, A.D.K and Warren, R.P. 1963. Groups of vertical cylinders oscillating in water. Jnl. of the Eng. Mech., Proc. A.S.C.E., No. EM1, Feb. 1963.

Laneville, A., Gartshore, I.S. and Parkinson, G.V. 1975. An explanation of some effects of turbulence on bluff bodies. Proc. 4th International Conf. on Wind Effects on Buildings and Structures. 1975.

Maskell, E.C. 1963. A theory of blockage effect on bluff bodies and stalled wings in a closed wind tunnel. ARC R and M 3400, 1963.

Matten, R.B. 1977. The influence of roughness on the drag of circular cylinders in waves. Proc. Offshore Technology Conference. Houston, Texas. Paper No. OTC 2902, 1977.

Matten, R.B., Hogben, N. and Ashley,R.M. 1978. A circular cylinder oscillating in still water, in waves and in currents. Proc. Symp. on Mechanics of Wave Induced forces on cylinders. Vol. 1, Paper C5, Bristol, U.K. 1978.

Maull, D.J. 1978. Wave loading in the drag/inertia regime with particular reference to horizontal cylinders. Position paper presented at Symp. on Mech. of Wave Induced Forces on Cylinders, Bristol, U.K. 1978.

Maull, D.J. and Milliner, M.G. 1978 (a). Sinusoidal flow past a circular cylinder. COASTAL ENG. Vol:2, No.2, Oct'78.

Maull, D.J. and Milliner, M.G. 1978 (b). The forces on a cylinder having a complex periodic motion. Symp. on Mech. of Wave - Induced forces on cylinders., Vol. 1, Paper B3, Bristol, U.K. 1978.

Maull, D.J. and Norman, S.J. 1978. A Horizontal circular cylinder under waves. Symp. on Mech. of Wave - Induced forces on cylinders., Vol. 1, Paper A1, Bristol, U.K. 1978.

McNown, J.S. and Keulegan, G.H. 1959. Vortex formation and resistance in periodic motion. Jnl. of Eng. Mech. Div., Proc. A.S.C.E., Vol. 85, No. EM1, January 1959.

McNown, J.S. and Learned, A.P. 1978. Discussion on 'Drag and Inertia forces on a cylinder in periodic flow' Proc. A.S.C.E., No. WW2, May 1978.

Mercier, J.A. 1973. Large amplitude oscillations of a circular cylinder in a low-speed stream. Ph.D. dissertation, Stevens Institute of Technology, Dept. of Mechanical Engineering, 1973.

Merzkirch, W. 1974. Flow visualisation. Published by Academic Press Inc.

Milgram, J.H. 1976. Wave and wave forces. Proc. Behaviour of offshore structures, (BOS '76), Trondheim August 1976.

Milliner, M.G. 1978. Private communication.

Mogridge, G.R. and Jamieson, W.W. 1976. Wave forces on square caissons. Proc. 15th Conf. on Coastal Engineering., Vol. 3, 1976.

Morison, J.R., O'Brien, M.P., Johnson, J.W. and Schaaf, S.A. 1950. The force exerted by surface waves on piles. Petroleum Trans., A.I.M.E., Vol. 189, 1950.

Roshko, A. 1954. On the drag and shedding frequency of two-dimensional bluff bodies. U.S. National Advisory Committee for Aeronautics, TN 3169, 1954.

Sarpkaya, T. 1975. Forces on cylinders and spheres in a sinusoidally oscillating fluid. Jnl. of Applied Mech., Vol. 42, No.1, pp 32-37, March 1975.

Sarpkaya, T. 1976 (a). Vortex shedding and resistance in harmonic flow about smooth and rough circular cylinders at high Reynolds Numbers. Naval Postgraduate School, Monterey, California, NPS - 59SL 76021, Feb 1976.

Sarpkaya, T. 1976 (b). In-line and transverse forces on smooth and sand roughened cylinders in oscillatory flow at high Reynolds numbers. Naval Postgraduate School, Monterey, California, NPS 69SL 76062, June 1976.

Sarpkaya, T. 1977(a). The hydrodynamic resistance of roughened cylinders in harmonic flow. Paper presented at the 1977 Spring Meetings of the Royal Institution of Naval Architects.

Sarpkaya, T. 1977(b) In-line and transverse forces on cylinders near a wall at high Reynolds numbers. Proc. offshore Technology Conference, Houston, Texas, 1977. Paper No.OTC 2898.

Sarpkaya, T. 1978. Wave loading in the drag/inertia regime with particular reference to groups of cylinders. Symposium on Mechanics of Wave - induced forces on cylinders, Bristol, U.K. 1978.

Sarpkaya, T. and Garrison, C.J. 1963. Vortex formation and resistance in unsteady flow. Jnl. of applied Mechs. Trans. A.S.M.E. Vol. 30, Series E, No.1, March 1963.

Sarpkaya, T. and Tuter, O. 1974. Periodic flow about bluff bodies. Part: 1, Forces on cylinders and spheres in a sinuoidally oscillating fluid. Naval Postgraduate School, Monterey, California, Report No. NPS - 59SL 74091 Sept. 1974.

Schlichting, H. 1968. Boundary layer theory, 6th Edition, McGraw Hill, New York 1968.

Shih, C.C. and Buchanan, H.J. 1971. The drag on oscillating plates at low Reynolds numbers. Jnl. of Fluid Mech. Vol. 48, Part. 2, 1971.

Standing, R.G. 1978. Applications of wave diffraction theory. N.M.I report No. R32. Jan 1978.

Stansby, P.K. 1977. An inviscid model of vortex shedding from a circular cylinder in steady and oscillatory far flows. Proc. Instn. of Civil Engrs., Part 2, Vol. 63, Dec. 1977.

Stansby, P.K. 1978. Mathematical modelling of vortex shedding from circular cylinders in Planar oscillatory flows, including the effects of harmonics and response. Symp. on Mech. of wave- induced forces on cylinders. Vol. 1, Bristol U.K. 1978.

Ver ley, R.L.P. and Moe, G. 1978. The effect of cylinder vibration on the drag force and the resultant hydrodynamic damping. Proc. Symp. on Mech. of Wave- induced forces on cylinders., Vol. 2, Bristol, U.K. 1978.

Vickery, B.J. 1966. Fluctuating lift and drag on a long cylinder of square cross-section in a smooth and in a turbulent stream. Jnl. of Fluid Mech., Vol. 25, 1966.

Weigel, R.L. 1964. Oceanographical Engineering. Prentice Hall. 1964.

Weigel, R.L., Beeb, K.E. and Moon, J. 1957. Ocean wave forces on circular cylindrical piles. Proc. A.S.C.E. Vol. 83, No. HY2, 1957.

Yamamoto, T. and Nath, J.H. 1976. High Reynolds numbers oscillating flow by cylinders. Proc. 15th Coastal Eng. Conf. 1976. Vol. 3, Ch.136.

Zdravkovich, M.M. 1977. Review of flow interference between two cylinders in various arrangements. Jnl. of Fluids Engineering, Trans. A.S.M.E. Vol. 99, pp 618-633.

Zdravkovich, M.M. and Namork, J.E. 1977. Formation and reversal of vortices around circular cylinders subjected to water waves. Proc. A.S.C.E. No.WW3 August 1977.

APPENDIX : 1

RESPONSE OF LOAD CELLS AND MODELS

In Section 2.2.2. the equations governing the response of the load cell and model are given. These are :-

the frequency $$\omega = \sqrt{\frac{48 EI}{M \ell^3}} \qquad \text{Al.1}$$

the damping $$\gamma = \frac{\rho L C_D D U_m}{M} = \left(\frac{\rho L D^2}{MT}\right) C_D \cdot NKC \qquad \text{Al.2}$$

the dynamic magnification factor,

$$D.M.F = \frac{1}{\sqrt{\left(1-\frac{\nu^2}{\omega^2}\right)^2 + 4\left(\frac{\gamma}{\omega}\right)^2\left(\frac{\nu}{\omega}\right)^2}} \qquad \text{Al.3}$$

and the phase lag,

$$\phi = \tan^{-1}\left(\frac{2\gamma\nu}{\omega^2-\nu^2}\right) \qquad \text{Al.4}$$

where M = mass of the model and added mass, EI = flexural stiffness, L = length of the model.

THE CIRCULAR CYLINDER

Potential flow gives an added mass coefficient of 1.0; therefore the added mass = $1.0 \times \rho \times \frac{\pi D^2}{4} \times L$. The circular cylinder used had a diameter of 1-9/16" and was made of perspex,

∴ mass of cylinder = 0.58 lbs.

and added mass = 1.66 lbs.

∴ Total mass = 2.24 lbs.

The flexural stiffness of the load cell used with the circular cylinder is 0.53 lbf ft², and the length, l, of the measuring element is 1.0".

Equation Al.1 therefore gives :

ω = 140.09 rads/sec, or f = 22.3 Hz.

The steady flow drag coefficient, C_D , for a circular cylinder is 1.2, and the maximum velocity in the tank is about 1.96 f.p.s. Using these values in equation Al.2 gives a damping coefficient γ = 17.06; ∴ γ/ω = 0.12 The response of the circular cylinder and load cell, using the potential flow for C_m , and the steady state drag coefficient is therefore found from equations Al.3, and Al.4, and is as tabulated below.

ν (Hz)	0.3	1	2	3	4	5	6	7	8	9	10
D.M.F	1.0	1.002	1.008	1.02	1.03	1.05	1.08	1.11	1.14	1.19	1.24
$\phi°$	0.19	0.63	1.26	1.91	2.58	3.29	4.04	4.85	5.73	6.70	7.79

Experiments at a Keulegan and Carpenter number of 50.4, gives the measured inertia coefficient, C_m = 1.04, and the drag coefficient, C_D = 1.32. Thus the added mass coefficient = 0.04, ∴ the added mass = 0.07 lbs; as before, the actual mass of the cylinder is 0.58 lbs.

∴ Total mass, M = 0.65 lbs.

∴ the frequency, ω, using equation A1.1 is

ω = 260.06 rads/sec, or f = 41.39 Hz.

The damping coefficient, γ, from equation A1.2, with NKC = 50.4, C_D = 1.32 is :

$$\gamma = 65.03, \qquad \therefore \ \gamma/\omega = 0.25$$

The response of the circular cylinder and load cell, using measured results for C_m and C_D, to determine, the added mass and damping respectively is therefore as tabulated below :-

ν(Hz)	0.3	1	2	3	4	5	6	7	8	9	10
D.M.F	1.0	1.001	1.002	1.005	1.008	1.01	1.02	1.026	1.034	1.043	1.053
$\phi°$	0.21	0.69	1.39	2.09	2.79	3.51	4.23	4.98	5.73	6.51	7.31

In figure 2.11 a, these responses are plotted.

THE 3" DIAMETER FLAT PLATE

From potential flow, the inertia coefficient for a flat plate, C_m is 1.0. Defining C_m as :

$$C_m = C_a + r \qquad \text{A1.5}$$

where C_a = added mass coefficient, and r the volume ratio given by :

$$r = \frac{\text{volume of plate}}{\text{volume of circular cylinder based on the same diameter,}} \qquad \text{A1.6}$$

then, for the flat plates used, r = 0.22

C_a = 0.78

the added mass = $C_a \rho L \pi D^2/4$ = 4.78 lbs.

The actual mass of the plate, which is made of Aluminium alloy is, 3.63 lbs;

∴ the total mass, M = 8.41 lbs.

This model was used in conjunction with the stiffer load cell, where the flexural stiffness is 4.24 lbf ft², thus equation A1.1 gives :

ω = 204.49 rads/sec ; or f = 32.55 Hz.

In this case, using a steady flow value for the drag coefficient is not quite justifiable, because the size of the plate is such that the Keulegan and Carpenter number is too low. Further, the maximum velocity in the tank

would be less, because of the greater resistance offered by the large plate. Nevertheless, using a steady state value for the drag coefficient of 2.1 and a maximum value, still of 1.96 f.p.s. gives, γ = 15.27.

$$\therefore \gamma/\omega = 0.075$$

Therefore the response of the 3" diameter plate and load cell, using potential flow to derive C_m, and a steady flow value for the drag coefficient is as tabulated below :-

ν (Hz)	·3	1	2	3	4	5	6	7	8	9	10
D.M.F	1·00	1·001	1·004	1·008	1·015	1·024	1·035	1·048	1·064	1·082	1·103
$\phi°$	0·079	0·26	0·53	0·80	1·07	1·35	1·63	1·93	2·24	2·56	2·9

Experimental results at NKC = 20.7, give an inertia coefficient, C_m = 0.46, and a drag coefficient, C_D of 3.17. The added mass is therefore = 1.47 lbs, and thus the total mass is 5.1 lbs. This gives, ω = 262.6 rads/sec, or f = 41.79 Hz. Using a drag coefficient of 3.17 at NKC = 20.7 gives a damping coefficient, γ = 30.14: $\therefore \gamma/\omega = 0.11$. The response of this plate and the load cell, using measured values for the inertia and drag coefficients, to determine the frequency and the damping respectively is therefore as tabulated below :-

ν (Hz)	·3	1	2	3	4	5	6	7	8	9	10
D.M.F	1·0	1·001	1·002	1·005	1·009	1·014	1·02	1·03	1·04	1·05	1·06
$\phi°$	0·094	0·31	0·63	0·95	1·27	1·60	1·93	2·27	2·61	2·97	3·33

These results are plotted in figure 2.11 b.

THE 1.5" DIAMETER FLAT PLATE

As in equation Al.5, and Al.6, for the 3" diameter flat plate, the added mass coefficient, from potential flow is 0.78.

The added mass = 0.78 x $\rho \times \pi D^2/4 \times L$ = 1.2 lbs.

Total mass, M = 4.0 lbs.

This plate was used with the load cell of flexural stiffness, EI = 0.53 lbf ft^2, therefore equation Al.1 gives :

ω = 104.83 rads/sec or f = 16.68 Hz.

The steady flow drag coefficient of a flat plate is 2.1, using this and a maximum velocity of 1.96 f.p.s. in equation Al.2 gives the damping coefficient as :

$$\gamma = 16.05, \quad \therefore \gamma/\omega = 0.15$$

Therefore the response of the 1.5" diamter flat plate and load cell, using

potential value C_m and steady flow C_D is as tabulated.

ν(Hz)	·3	1	2	3	4	5	6	7	8	9	10
D.M.F	1·0	1·003	1·014	1·03	1·06	1·09	1·14	1·20	1·28	1·37	1·5
ϕ°	0·31	1·05	2·13	3·26	4·45	5·76	7·20	8·86	10·80	13·11	15·98

Experimental results give $C_m = 1.49$, and $C_D = 2.18$ at NKC = 48.04. Using this value for the inertia coefficient gives an added mass coefficient = 1.49 - 0.22 = 1.27.

∴ The added mass = 1.95 lbs; the actual mass of the model, as above, is 2.8 lbs, ∴ The total mass, M = 4.75 lbs.

This gives, ω_r = 96.2 rads/sec, or f = 15.31 Hz.

Using the drag coefficient of 2.18, at NKC = 48.04, in equation A1.2 gives,

γ = 12.91; ∴ γ/ω = 0.13.

The response of this plate and load cell, using measured values of C_m and C to determine the frequency and damping respectively is as tabulated :-

ν(Hz)	·3	1	2	3	4	5	6	7	8	9	10
D.M.F	1.0	1·004	1·02	1·04	1·07	1·11	1·17	1·25	1·35	1·49	1·67
ϕ°	0·3	1·008	2·04	3·13	4·30	5·60	7·08	8·82	10·92	13·55	17·0

These results are plotted in figure 2.11 c.

THE 1" DIAMETER FLAT PLATE

As with the other two plates above, potential flow gives an inertia coefficient of 1.0, and for the geometry of this plate, the volume ratio r, as defined in equation A1.6 is again 0.22.

The added mass coefficient = 0.78.

∴ the added mass = 0.53 lbs;

the actual mass of this plate, made of stainless steel is 1.16 lbs.

∴ Total mass, M = 1.69 lbs.

Equation A1.1 then gives the natural frequency of this plate and the load cell, of flexural stiffness, 0.53 lbf ft² as :

ω_r = 161.28 rads/sec or f = 25.67 Hz.

As before, the steady state value for the drag coefficient is 2.1, using this and a maximum velocity of 1.96 f.p.s. in equation A1.2 gives :

γ = 25.33, ∴ γ/ω = 0.16

The response of this plate and load cell, with potential flow used to determine the added mass, and hence frequency, and with the damping coefficient obtained

from the steady flow drag coefficient is therefore as tabulated :

ν (Hz)	0·3	1	2	3	4	5	6	7	8	9	10
D.M.F	1·0	1·001	1·006	1·01	1·02	1·04	1·05	1·08	1·1	1·13	1·17
ϕ°	0·21	0·70	1·41	2·13	2·87	3·64	4·44	5·29	6·19	7·16	8·21

Experimental results at NKC = 73, give C_m = 1.98, and C_D = 2.1. Using this measured value of the inertia coefficient, gives an added mass coefficient of 1.98 - 0.22 = 1.76, and hence the added mass = 1.2 lbs. Thus the total mass = 2.36 lbs.

Equation A1.1 gives, ω = 136.48 rads/sec; or f = 21.72 Hz. Using a measured C_D of 2.1 at NKC = 73 in equation A1.2 gives the damping coefficient

γ = 16.91 ; $\therefore$ γ/ω = 0.12.

The response of this plate and load cell, using measured values of C_m and C_D is therefore as tabulated.

ν (Hz)	0·3	1	2	3	4	5	6	7	8	9	10
D.M.F	1·0	1·002	1·008	1·02	1·03	1·05	1·08	1·11	1·15	1·20	1·26
ϕ°	0·2	0·65	1·32	2·00	2·70	3·45	4·23	5·09	6·03	7·07	8·24

These results are plotted in figure 2.11d.

THE SQUARE SECTION NORMAL TO THE FLOW

This model is made of perspex with each face 1.0607", thus, the mass of the model is 0.81 lbs. From potential flow, the inertia coefficient, Cm is 2.78, whereas in equation A1.5, $C_m = C_a + r$, and r is as defined in equation A1.6. Thus in this case, r = 1.27,

$\therefore$ C_a = 2.78 - 1.27 = 1.51 ; $\therefore$ the added mass = 1.16 lbs;

the total mass, M = 1.97 lbs.

The frequency, ω, of this model and the load cell is therefore given by :

ω = 149.38 rads/sec, or f = 23.77.

Using the steady flow value for the drag coefficient, C_D = 2.2 and at the maximum velocity of the tank of 1.96 f.p.s., equation A1.2 gives, γ = 24.14, $\therefore$ γ/ω = 0.16.

The response of this system, using these values, is therefore as tabulated.

ν (Hz)	0·3	1	2	3	4	5	6	7	8	9	10
D.M.F	1·0	1·002	1·007	1·02	1·03	1·04	1·06	1·09	1·12	1·16	1·2
ϕ°	0·23	0·78	1·57	2·37	3·20	4·07	4·97	5·95	6·99	8·13	9·38

Experiments on this section at NKC = 70.5, give an inertia coefficient, C_m

= 1.63, and a drag coefficient, C_D = 1.74. Using this value for C_m gives $C_a = C_m - r$, where r is the same as above, $\therefore C_a = 0.36$.

The added mass = 0.28 lbs.

As before the mass of the model is 0.81 lbs, thus giving the total mass as : M = 1.09 lbs.

This gives the frequency of the system, ω, as

ω = 200.82 rads/sec or f = 31.96 Hz.

Using the measured value of 1.74 for the drag coefficient at NKC = 70.5, in equation A1.2 gives :

γ = 32.95 rads/sec, $\therefore \gamma/\omega = 0.16$

The response of this model and load cell, using measured values of C_m and C_D is therefore as tabulated.

ν (Hz)	0·3	1	2	3	4	5	6	7	8	9	10
D·M·F	1·0	1·001	1·004	1·008	1·015	1·024	1·034	1·047	1·063	1·081	1·101
ϕ°	0·18	0·59	1·18	1·78	2·39	3·01	3·65	4·32	5·01	5·73	6·49

These results are plotted in figure 2.11e.

THE DIAMOND SECTION

This is the same model that was used above for the square section, but now it is at 45° incidence, the actual mass of the model is thus still 0.81 lbs. The potential flow value for the inertia coefficient is now 1.39; here the volume of fluid is based on a circular cylinder of diameter equal to the length of a diagonal. Thus r, as defined in equation A1.6 is 0.64, and the added mass coefficient, C_a = 0.75 giving :

added mass = 1.15 lbs.

Total mass, M = 1.96 lbs.

Thus the frequency of the model and load cell combination, as given by equation A1.1 is : ω = 149.76 rads/sec, or f = 23.84 Hz. Using the steady flow value for the drag coefficient, C_D = 1.71, and the maximum value of 1.96 f.p.s. for the velocity in the tank gives,

γ = 26.68; $\therefore \gamma/\omega = 0.18$

The response of this system, using potential flow to find C_m and a steady flow value for the drag coefficient is therefore as tabulated.

ν (Hz)	0·3	1	2	3	4	5	6	7	8	9	10
D·M·F	1·0	1·002	1·007	1·015	1·027	1·043	1·063	1·087	1·12	1·15	1·19
ϕ°	0·26	0·86	1·73	2·61	3·52	4·47	5·47	6·53	7·68	8·92	10·28

Experiments on this section at NKC = 50.3, give an inertia coefficient, C_m of 1.26, and a drag coefficient, C_D = 1.86. Using this value for C_m and a value of r = 0.64 as above, gives :

$C_a = C_m - r = 0.62$

Thus the added mass = 0.95 lbs, and the total mass, M = 1.76 lbs.

and $\therefore$ the frequency ω = 158.04 rads/sec, or f = 25.15 Hz.

Using a drag coefficient of 1.86, at NKC = 50.3 in equation A1.2, gives the damping coefficient, γ = 31.13, $\therefore \gamma/\omega = 0.2$.

The response of this system, using measured values of C_m and C_D to derive the frequency and damping respectively is therefore as tabulated.

ν (Hz)	0.3	1	2	3	4	5	6	7	8	9	10
D.M.F	1.0	1.001	1.006	1.013	1.024	1.038	1.055	1.076	1.102	1.132	1.168
$\phi°$	0.27	0.9	1.81	2.73	3.68	4.66	5.69	6.78	7.94	9.18	10.54

These results are plotted in figure 2.11f.

APPENDIX : 2

PHASE SHIFT ANALYSIS

Using Morison's equation, the force may be written as :

$$\frac{F_T}{L} = \frac{1}{2}\rho C_D U|U| D + \pi D^2/4 \rho C_m \frac{dU}{dt} \qquad \text{A2.1}$$

where F_T is now the total force.

Let the velocity be given by $U = -U_m \cos\theta$, where $\theta = 2\pi t/T$, and T is the period of oscillations, then equation A2.1 becomes :

$$F_T = -\frac{1}{2}\rho C_D D L U_m^2 \cos\theta|\cos\theta| + \frac{\pi D^2}{4}\rho C_m L \cdot \frac{2\pi}{T} U_m \sin\theta \qquad \text{A2.2}$$

From Keulegan and Carpenter's analysis :

$$C_m = \frac{1}{\pi^3}\frac{U_m T}{D}\int_0^{2\pi}\frac{F_T}{\frac{1}{2}\rho U_m^2 D L}\sin\theta\, d\theta \qquad \text{A2.3}$$

and $$C_d = -\frac{3}{8}\int_0^{2\pi}\frac{F_T\cos\theta}{\frac{1}{2}\rho U_m^2 D L}\, d\theta \qquad \text{A2.4}$$

Now let a phase shift occur between the velocity and the force, such that $\theta \longrightarrow \theta+\epsilon$, so U is now given by :

$$U = -U_m \cos(\theta+\epsilon) \qquad \text{A2.5}$$

Substituting equation A2.5 into equation A2.1 results in an equation similar to equation A2.2, but now with θ replaced by $(\theta+\epsilon)$. Denoting, this new total force shifted in relation to the velocity, by F_s, then this is given by :

$$\frac{F_s}{\frac{1}{2}\rho U_m^2 D L} = -C_D\cos(\theta+\epsilon)|\cos(\theta+\epsilon)| + \pi^2\left(\frac{D}{U_m T}\right)C_m\sin(\theta+\epsilon) \qquad \text{A2.6}$$

Then, by substituting for the force but now using equation A2.6, into equations A2.3, and A2.4, the effect of a phase shift on the inertia and drag coefficients, respectively, may be assessed.

Thus, for the inertia coefficient :

$$C_{m_s} = \frac{1}{\pi^3}\cdot NKC\int_0^{2\pi}\left[-C_D\cos(\theta+\epsilon)|\cos(\theta+\epsilon)| + \frac{\pi^2}{NKC}C_m\sin(\theta+\epsilon)\right]\sin\theta\, d\theta \qquad \text{A2.7}$$

where C_{m_s} refers to the inertia coefficient obtained when the force

is shifted in relation to the velocity, and C_m is the inertia coefficient with no phase shift.

The integration in equation A2.7 can be carried out by considering the two separate parts. Therefore, let :

$$I = \int_0^{2\pi} \cos(\theta+\varepsilon) \left|\cos(\theta+\varepsilon)\right| \sin\theta \, d\theta \qquad \text{A2.8}$$

and $$J = \int_0^{2\pi} \sin(\theta+\varepsilon) \sin\theta \, d\theta \qquad \text{A2.9}$$

Equation A2.8 may further be written as :

$$I = \int_0^{\alpha} g(\theta)\, d\theta - \int_{\alpha}^{\pi+\alpha} g(\theta)\, d\theta + \int_{\pi+\alpha}^{2\pi} g(\theta)\, d\theta = a - b + c \qquad \text{A2.10}$$

where α is given by $\cos(\alpha+\varepsilon) = 0$; or $\alpha = \frac{\pi}{2} - \varepsilon$

and $g(\theta) = \cos^2(\theta+\varepsilon)\sin\theta$

$$= \frac{\sin\theta}{2}\left(1 + \cos 2(\theta+\varepsilon)\right)$$

$$= \frac{1}{2}\left(\sin\theta + \frac{\sin(3\theta+2\varepsilon) - \sin(\theta+2\varepsilon)}{2}\right)$$

Therefore, $a = \int_0^{\alpha} g(\theta)\, d\theta = \frac{1}{4}\left[-2\cos\theta - \frac{1}{3}\cos(3\theta+2\varepsilon) + \cos(\theta+2\varepsilon)\right]_0^{\alpha}$

$$a = \frac{1}{2} - \frac{\cos\alpha}{2} - \frac{1}{12}\cos(3\alpha+2\varepsilon) + \frac{1}{4}\cos(\alpha+2\varepsilon) - \frac{1}{6}\cos 2\varepsilon$$

and $$b = \frac{1}{4}\left[-2\cos(\pi+\alpha) - \frac{1}{3}\cos(3\pi+3\alpha+2\varepsilon) + \cos(\pi+\alpha+2\varepsilon)\right]$$

$$+ \frac{\cos\alpha}{2} + \frac{1}{12}\cos(3\alpha+2\varepsilon) - \frac{\cos(\alpha+2\varepsilon)}{4}$$

and $$c = -\frac{1}{2} - \frac{1}{12}\cos(6\pi+2\varepsilon) + \frac{1}{4}\cos(2\pi+2\varepsilon)$$

$$+ \frac{1}{2}\cos(\pi+\alpha) + \frac{1}{12}\cos(3\pi+3\alpha+2\varepsilon) - \frac{1}{4}\cos(\pi+\alpha+2\varepsilon$$

Thus, $I = a - b + c$

$$= -2\cos\left(\frac{\pi}{2} - \varepsilon\right) - \frac{1}{3}\cos\left(\frac{3\pi}{2} - \varepsilon\right) + \cos\left(\frac{\pi}{2} + \varepsilon\right)$$

$$I = -\frac{8}{3}\sin\varepsilon \qquad \text{A2.11}$$

From equation A2.9, $J = \int_0^{2\pi} \text{Sin}(\theta+\epsilon)\ \text{Sin}\theta\ d\theta$

$$J = -\frac{1}{2}\int_0^{2\pi} (\text{Cos}(2\theta+\epsilon) - \text{Cos}\ )\ d\theta$$

$$J = \pi\ \text{Cos}\ \epsilon \qquad \text{A2.12}$$

Substituting for I, and J in equation A2.7 gives

$$C_{m_s} = \frac{NKC}{\pi^3}\left\{ C_d \times \frac{8}{3}\ \text{Sin}\epsilon + \frac{\pi^2}{NKC}\ C_m \cdot \pi\ \text{Cos}\ \epsilon \right\}$$

$$\therefore\ C_{m_s} = \frac{8}{3}\ \frac{C_d\ NKC}{\pi^3}\ \text{Sin}\ \epsilon\ + C_m\ \text{Cos}\ \epsilon \qquad \text{A2.13}$$

Similarly for the drag coefficient the effect of a phase shift results in :

$$C_{d_s} = -\frac{3}{8}\int_0^{2\pi} \left[- C_d\ \text{Cos}(\theta+\epsilon\ )\ \left|\text{Cos}\ (\theta+\epsilon\ )\right| + \frac{\pi^2}{NKC}\ C_m\ \text{Sin}(\theta+\epsilon)\ \text{Cos}\theta\ d\theta \qquad \text{A2.14}$$

As before, let $I = \int_0^{2\pi} \text{Cos}\ (\theta+\epsilon\ )\ \left|\text{Cos}\ (\theta+\epsilon)\right|\ \text{Cos}\theta\ d\theta$

and $J = \int_0^{2\pi} \text{Sin}\ (\theta+\epsilon\ )\ \text{Cos}\theta\ d\theta.$

However, by writing ϵ as $\epsilon' - \pi/2$, I and J can be easily solved, being related to I and J as defined earlier.

Thus $I = 8/3\ \text{Cos}\ \epsilon$ and $J = \pi\ \text{Sin}\ \epsilon$.

Substituting for I and J into equation A2.14 gives :

$$C_{d_s} = -\frac{3}{8}\left\{ - C_d \times \frac{8}{3}\ \text{Cos}\ \epsilon\ + \frac{\pi^2}{NKC}\ C_m\ \pi\ \text{Sin}\ \epsilon \right\}$$

$$C_{d_s} = C_d\ \text{Cos}\ \epsilon\ - \frac{3}{8}\ \frac{\pi^3\ C_m}{NKC}\ \text{Sin}\ \epsilon \qquad \text{A2.15}$$

Further, as can be seen in equation A2.15, as $NKC \longrightarrow \infty$

$$C_{d_s} \longrightarrow C_d\ \text{Cos}\ \epsilon$$

APPENDIX : 3

IN LINE FORCE COEFFICIENTS

Representing the horizontal velocity by :

$$U = -U_m \quad \text{Cos } \theta \qquad \text{A3.1}$$

where $\theta = 2\pi t/T$, and substituting into Morison's equation results in :

$$\frac{F}{\frac{1}{2}\rho U_m^2 D} = \pi^2 C_m \left(\frac{D}{U_m T}\right) \text{Sin } \theta \quad - C_D \quad \text{Cos} \quad |\text{Cos } \theta| \qquad \text{A3.2}$$

where F = force per unit length acting on the body. In the analysis by Keulegan and Carpenter (1958), they assumed that since the force is periodic and the incident flow is symmetric, then $F(\theta) = -F(\theta + \pi)$; an assumption that is not quite true or necessary. If this assumption is not made, the results for C_m and C_D as can be seen later are only slightly different. Nevertheless, whether or not this assumption is made, the analysis is basically the same, however assuming for the time being $F(\theta) = -F(\theta + \pi)$ slightly simplifies the algebra, and F can then be represented by :

$$C_F = \frac{F}{\frac{1}{2}\rho U_m^2 D} = A_1 \text{Sin } \theta + A_3 \text{ Sin } 3\theta + A_5 \text{ Sin } 5\theta + \ldots\ldots$$
$$+ B_1 \text{ Cos } \theta + B_3 \text{ Cos } 3\theta + B_5 \text{ Cos } 5\theta + \ldots\ldots \qquad \text{A3.3}$$

The coefficients A_n and B_n are then given by :

$$A_n = \frac{1}{\pi} \int_0^{2\pi} \frac{F \text{ Sin } n\theta \quad d\theta}{\frac{1}{2}\rho U_m^2 D}$$
$$B_n = \frac{1}{\pi} \int_0^{2\pi} \frac{F \text{ Cos } n\theta \quad d\theta}{\frac{1}{2}\rho U_m^2 D} \qquad \text{A3.4}$$

Since the drag term, $\text{Cos } \theta \, |\text{Cos } \theta|$ in equation A3.2 is an even function of θ, this may also be represented by a Fourier Series as : A3.5

$$\text{Cos } \theta \, |\text{Cos } \theta| = a_0 + a_1 \text{ Cos } \theta + a_2 \text{ Cos } 2\theta + a_3 \text{ Cos } 3\theta + \ldots$$

where the coefficients a_n are given by :

$$a_n = \sum_{n=0}^{\infty} \frac{\int_0^{2\pi} \text{Cos } \theta \, |\text{Cos } \theta| \text{ Cos } n\theta \, d\theta}{\int_0^{2\pi} \text{Cos}^2 n\theta \, d\theta} \qquad \text{A3.6}$$

Equation A3.6 reduces to : $a_n = 0$ for n even

$$a_n = \frac{(-1)^{\frac{n+1}{2}} \, 8}{n(n^2-4)\pi} \qquad \text{for } n \text{ odd,}$$

thus equation A3.5 may be written as :

$$\cos\theta\,|\cos\theta| = a_1 \cos\theta + a_3 \cos 3\theta + a_5 \cos 5\theta + \ldots\ldots \qquad \text{A3.7}$$

Equation A3.3 may be re-written as :

$$C_F = A_1 \sin\theta + A_3 \sin 3\theta + A_5 \sin 5\theta + \ldots\ldots$$

$$+ \frac{B_1}{a_1}\,(a_1 \cos\theta + a_3 \cos 3\theta + a_5 \cos 5\theta + \ldots\ldots)$$

$$- \frac{B_1}{a_1}\,a_3 \cos 3\theta - \frac{B_1\,a_5}{a_1} \cos 5\theta - \ldots\ldots\ldots$$

$$+ B_3 \cos 3\theta + B_5 \cos 5\theta + \ldots\ldots$$

$$= \sin\theta\,\left(A_1 + \frac{A_3 \sin 3\theta}{\sin\theta} + \frac{A_5 \sin 5\theta}{\sin\theta} + \ldots\ldots\ldots\right)$$

$$+ \frac{B_1}{a_1} \cos\theta\,|\cos\theta| + \left(B_3 - \frac{B_1\,a_3}{a_1}\right) \cos 3\theta + \left(B_5 - \frac{B_1\,a_5}{a_1}\right) \cos 5$$

$$+ \ldots\ldots\ldots \qquad \text{A3.8}$$

Let $\frac{B_1}{a_1} = B_1'$, $\quad B_3 - \frac{B_1\,a_3}{a_1} = B_3'$

and $B_5 - \frac{B_1\,a_5}{a_1} = B_5'$ etc.,

then equation A3.8 becomes :

$$C_F = \sin\theta \left(A_1 + \frac{A_3 \sin 3\theta}{\sin\theta} + \frac{A_5 \sin 5\theta}{\sin\theta} + \ldots\ldots\ldots \right)$$

$$+ B_1' \cos\theta\,|\cos\theta| + B_3' \cos 3\theta + B_5' \cos 5\theta + \ldots\ldots \qquad \text{A3.9}$$

Comparing equation A3.9 with A3.2 results in :

$$\pi^2 C_m \left(\frac{D}{U_m T}\right) = A_1 + \frac{A_3 \sin 3\theta}{\sin\theta} + \frac{A_5 \sin 5\theta}{\sin\theta} + \ldots\ldots \qquad \text{A3.10}$$

and

$$C_D = -B_1' - \frac{B_3' \cos 3\theta}{\cos\theta\,|\cos\theta|} - \frac{B_5' \cos 5\theta}{\cos\theta\,|\cos\theta|} - \ldots\ldots \qquad \text{A3.11}$$

Equations A3.10 and A3.11 are the basis for calculation of the drag and inertia coefficients, but in general only the first term of these series are used, resulting in :

$$C_m = \left(\frac{U_m T}{D}\right) \frac{A_1}{\pi^2} = \frac{1}{\pi^3} \left(\frac{U_m T}{D}\right) \int_0^{2\pi} \frac{F \sin\theta}{\frac{1}{2}\rho\, U_m^2\, D}\, d\theta \qquad \text{A3.12}$$

and $$C_D = -B_1' = -\frac{B_1}{a_1} = \frac{-3}{8}\int_0^{2\pi} \frac{F\cos\theta}{\frac{1}{2}\rho U_m^2 D}\, d\theta \qquad \text{A3.13}$$

Thus C_m and C_D calculated in this manner, represents the weighted averages over a cycle.

Had the assumption that $F(\theta) = -F(\theta+\pi)$, not been made then equations A3.10 and A3.11 would have become respectively :

$$\pi^2 C_m \left(\frac{D}{U_m T}\right) = A_1 + \frac{A_2 \sin 2\theta}{\sin\theta} + \frac{A_3 \sin 3\theta}{\sin\theta} + \frac{A_4 \sin 4\theta}{\sin\theta} + \ldots \qquad \text{A3.14}$$

and $$C_D = -B_1' - \frac{B_2 \cos 2\theta}{\cos\theta|\cos\theta|} - \frac{B_3' \cos 3\theta}{\cos\theta|\cos\theta|} - \frac{B_4 \cos 4\theta}{\cos\theta|\cos\theta|} - \frac{B_5' \cos 5\theta}{\cos\theta|\cos\theta|} \qquad \text{A3.15}$$

Thus the commonly used expressions for C_m and C_D , i.e. the first term of the series as in equations A3.12 and A3.13 remain unchanged.

APPENDIX : 4

R.M.S. FORCE FROM MORISON'S EQUATION

Substituting $U = U_m \cos\theta$ into Morison's equation, where $\theta = 2\pi t/T$ results in :

$$F = -C_D \times \frac{1}{2}\rho \, D \, U_m^2 \cos\theta |\cos\theta| + C_m \frac{\pi D^2}{4} \rho \frac{2\pi}{T} U_m \sin\theta \qquad \text{A4.1}$$

$$= P \cos\theta |\cos\theta| + Q \sin\theta$$

where $P = -C_D \times \frac{1}{2}\rho D U_m^2$, $Q = C_m \frac{\pi^2 D^2 \rho U_m}{2T}$

The means square of equation A4.1 is :

$$\overline{F^2} = \frac{1}{T}\int_0^T \left(P^2 \cos^2\theta |\cos\theta|^2 + Q^2 \sin^2\theta + 2PQ \sin\theta \cos\theta |\cos\theta| \right) dt \qquad \text{A4.2}$$

Now ; $\cos^2\theta |\cos\theta|^2 = \cos^4\theta = \frac{1}{8}(\cos 4\theta + 1 + 4\cos 2\theta + 2)$

$$\therefore \int_0^{2\pi} \cos^4\theta = \frac{3}{4}\pi$$

$$\sin^2 2\theta = \frac{1 - \cos 2\theta}{2}$$

$$\therefore \int_0^{2\pi} \sin^2 2\theta = \pi$$

and $2 \sin\theta \cos\theta |\cos\theta| = \sin 2\theta |\cos\theta|$

$$\int_0^{2\pi} \sin 2\theta |\cos\theta| = 0$$

Therefore Equation A4.2 may be re-written as :

$$\overline{F^2} = \frac{1}{T}\int_0^{2\pi} (P^2 \cos^4\theta + Q^2 \sin^2\theta + PQ \sin 2\theta |\cos\theta|) \frac{T}{2\pi} \, dt$$

$$= \frac{1}{2\pi}(P^2 \frac{3}{4}\pi + \pi Q^2)$$

$$= \frac{3}{8} P^2 + \frac{Q^2}{2} \qquad \text{A4.3}$$

Substituting for P^2 and Q^2 gives :

$$\overline{F^2} = \frac{3}{8} C_D^2 \times \frac{1}{4}\rho^2 D^2 U_m^4 + \frac{1}{2} C_m^2 \frac{\pi^4 D^4 \rho^2 U_m^2}{4T^2}$$

$$= \frac{\rho^2 U_m^4 D^2}{8} \left(\frac{3}{4} C_D^2 + \pi^4 C_m^2 \left(\frac{D}{U_m T} \right)^2 \right)$$

$$= \frac{\rho^2 U_m^4 D^2}{8} \left(\frac{3}{4} C_D^2 + \pi^4 C_m^2 / NKC^2 \right)$$

$$= \rho^2 \frac{U_m^4 D^2}{8\, NKC^2} \left(\frac{3}{4} C_D^2\, NKC^2 + \pi^4 C_m^2 \right) \qquad \text{A4.4}$$

Non-dimensionalising by $\frac{1}{2} \rho U_m^2 D$ then gives :

$$\frac{\overline{F^2}}{\left(\frac{1}{2} \rho U_m^2 D \right)^2} = \left(C_{F_{RMS}} \right)^2 = \frac{1}{2\, NKC^2} \left\{ \frac{3}{4} C_D^2\, NKC^2 + \pi^4 C_m^2 \right)$$

$$C_{F_{RMS}} = \sqrt{\frac{\overline{F^2}}{\left(\frac{1}{2} \rho U_m^2 D \right)^2}} = \sqrt{\frac{1}{2\, NKC^2}} \left(\frac{3}{4} C_D^2\, NKC^2 + \pi^4 C_m^2 \right)^{1/2} \qquad \text{A4.5}$$

Non-dimensionalising by $\frac{1}{2} \rho \frac{D^3}{T^2}$ results in :

$$\left(C'_{F_{RMS}} \right)^2 = \frac{\overline{F^2}}{\left(\frac{1}{2} \rho D^3 / T^2 \right)^2} = \frac{NKC^2}{2} \left(\frac{3}{4} C_D^2\, NKC^2 + \pi^4 C_m^2 \right) \qquad \text{A4.6}$$

Thus $C_{F_{RMS}} = C_{F_{RMS}} NKC^2 \qquad \text{A4.7}$

APPENDIX : 5

IN - LINE FORCE COEFFICIENTS - DATA

TABLE : 1 CIRCULAR CYLINDER

β = 451 : D = 1.5625" : D/W = 6.51%

NKC	RE No.x 10^{-3}	C_M	C_D	$C_{F\ RMS}$	$C_{F\ MAX}$	ϕ°
4.78	2.13	1.72	1.42	2.65	3.74	65.1
6.79	3.03	1.58	1.53	1.87	2.55	70.8
7.67	3.42	1.41	1.72	1.66	2.18	71.7
8.55	3.82	1.28	1.75	1.50	1.94	9.4
8.92	3.98	1.12	1.93	1.49	2.15	0.4
9.17	4.10	1.13	2.01	1.52	2.15	- 0.4
10.05	4.49	1.03	1.89	1.36	2.01	4.3
10.05	4.49	1.08	1.99	1.44	2.21	0.2
10.43	4.66	1.03	2.02	1.43	2.20	1.3
11.06	4.94	0.98	2.02	1.39	2.17	0.2
11.18	4.99	0.90	1.92	1.32	2.04	0.4
11.44	5.11	0.89	2.00	1.35	2.15	1.3
12.32	5.50	0.97	1.91	1.30	1.99	1.3
12.57	5.61	0.81	1.97	1.30	2.12	0.4
13.19	5.89	0.89	1.90	1.27	2.04	1.3
14.07	6.29	0.99	1.81	1.22	1.93	1.3
14.33	6.40	0.84	1.78	1.18	1.90	- 1.3
14.83	6.62	0.99	1.70	1.15	1.82	2.2
14.95	6.68	0.85	1.80	1.19	1.97	- 2.2
16.46	7.35	0.93	1.63	1.07	1.63	2.2
16.71	7.46	0.90	1.58	1.04	1.64	- 1.3
19.35	8.64	0.97	1.67	1.08	1.65	20.2
19.98	8.92	0.97	1.62	1.05	1.66	17.6
20.11	8.98	1.09	1.57	1.03	1.61	20.2
25.89	11.56	1.06	1.49	0.95	1.51	8.2
26.64	11.90	1.03	1.48	0.94	1.48	7.7
31.92	14.26	1.09	1.40	0.89	1.39	3.7
32.42	14.48	1.11	1.43	0.91	1.41	7.8
32.92	14.70	1.10	1.39	0.88	1.36	2.2
37.82	16.89	1.02	1.41	0.88	1.36	5.6
38.45	17.17	1.03	1.38	0.86	1.33	8.2

NKC	Re No. x 10^{-3}	C_m	C_D	$C_{F_{RMS}}$	$C_{F_{MAX}}$	ϕ^0
43.73	19.53	0.98	1.36	0.85	1.31	6.4
43.86	19.59	1.07	1.34	0.84	1.71	4.7
44.61	19.92	0.97	1.33	0.83	1.27	- 0.4
47.12	21.05	1.07	1.35	0.84	1.33	2.2
47.88	21.38	0.99	1.35	0.84	1.30	1.7
50.39	22.51	1.04	1.32	0.82	1.26	0.0

TABLE : 2 1.5"D FLAT PLATE

β = 421.5 : D/W = 6.25%

NKC	Re No x 10^{-3}	C_m	C_D	$C_{F_{RMS}}$	$C_{F_{MAX}}$	ϕ^0
3.80	1.60	1.46	5.19	4.20	7.23	30.0
6.02	2.50	1.35	3.77	2.80	4.58	28.7
6.15	2.59	1.35	3.91	2.84	4.66	35.7
7.33	3.09	1.43	3.86	2.73	4.78	27.4
7.98	3.37	1.41	3.62	2.56	4.14	40.0
9.03	3.81	1.28	3.23	2.22	3.50	37.7
9.16	3.86	1.36	3.22	2.23	3.83	28.3
9.69	4.08	1.29	3.19	2.17	3.59	39.1
10.08	4.25	1.24	3.07	2.06	3.41	31.4
10.47	4.41	1.26	3.04	2.05	3.51	34.3
10.60	4.47	1.31	3.11	2.10	3.62	37.9
11.26	4.74	1.16	3.03	1.99	3.27	32.2
11.52	4.85	1.17	3.00	1.98	3.17	39.4
11.91	5.02	1.08	2.92	1.91	3.32	33.1
12.70	5.35	0.91	2.83	1.82	2.83	39.1
12.83	5.41	0.92	2.98	1.90	3.06	35.7
14.40	6.07	0.69	2.74	1.72	2.72	35.7
14.66	6.18	0.70	2.82	1.76	2.84	33.1
14.79	6.23	0.62	2.86	1.78	2.84	31.4
16.89	7.12	0.51	2.79	1.72	2.75	29.6
17.15	7.23	0.48	2.66	1.64	2.65	28.8
21.07	8.88	0.48	2.70	1.65	2.64	20.2
21.34	8.99	0.57	2.62	1.61	2.56	23.6
23.95	10.09	0.72	2.54	1.56	2.43	18.5
26.05	10.98	1.05	2.62	1.61	2.43	5.6
28.27	11.92	1.29	2.42	1.50	2.28	9.9
32.07	13.52	1.34	2.48	1.52	2.31	12.9

NKC	Re No. x 10^{-3}	C_m	C_D	$C_{F_{RMS}}$	$C_{F_{MAX}}$	ϕ°
32.72	13.79	1.39	2.41	1.49	2.24	13.3
34.82	14.67	1.41	2.36	1.45	2.21	12.9
37.83	15.95	1.40	2.35	1.45	2.20	0.4
38.48	16.22	1.45	2.26	1.39	2.10	9.0
41.23	17.38	1.49	2.23	1.37	2.07	6.0
42.94	18.10	1.49	2.30	1.41	2.13	3.9
43.33	18.26	1.43	2.22	1.36	2.07	4.7
44.77	18.87	1.52	2.22	1.36	2.05	6.0
46.21	19.48	1.58	2.19	1.34	2.04	6.9
46.47	19.59	1.45	2.21	1.35	2.03	2.6
46.60	19.64	1.47	2.23	1.36	2.09	3.9
48.04	20.25	1.49	2.18	1.33	2.02	3.4
48.43	20.41	1.71	2.16	1.33	2.01	3.0

TABLE : 3 3" D FLAT PLATE

β = 1685.8 : D/W = 12.5%

NKC	Re No.x 10^{-3}	C_m	C_D	$C_{F_{RMS}}$	$C_{F_{MAX}}$	ϕ°
3.08	5.19	1.46	6.52	5.25	8.76	24.4
3.34	5.63	1.46	5.85	4.75	7.96	27.1
3.80	6.40	1.50	5.41	4.35	7.54	28.3
3.86	6.51	1.53	5.38	4.35	7.66	32.2
4.19	7.06	1.51	5.03	4.01	7.00	28.8
4.39	7.39	1.47	4.97	3.86	6.63	32.2
4.45	7.50	1.55	5.06	3.96	6.72	28.3
4.65	7.83	1.60	4.87	3.86	6.74	34.8
4.91	8.28	1.64	4.90	3.82	6.46	32.2
4.97	8.39	1.56	4.87	3.72	6.34	31.7
5.17	8.72	1.65	4.74	3.68	6.24	33.9
5.50	9.27	1.61	4.66	3.52	5.91	33.6
5.56	9.38	1.59	4.56	3.44	5.70	34.3
5.83	9.82	1.64	4.39	3.34	5.63	34.8
6.28	10.58	1.63	4.34	3.22	5.33	38.2
6.28	10.58	1.67	4.40	3.27	5.45	33.1
6.81	11.48	1.59	4.14	3.02	5.13	33.1
7.33	12.36	1.69	4.11	2.99	5.10	33.6
7.40	12.47	1.59	4.08	2.93	5.20	29.1
8.12	13.69	1.57	3.91	2.76	4.52	38.5
8.97	15.12	1.55	3.81	2.63	4.37	36.9
9.23	15.56	1.48	3.77	2.58	4.60	27.0

NKC	Re No x 10^{-3}	C_m	C_D	$C_{F_{RMS}}$	$C_{F_{MAX}}$	ϕ^o
11.52	19.42	1.26	3.52	2.30	3.81	34.3
11.52	19.42	1.45	3.45	2.30	3.88	34.8
12.89	21.73	0.92	3.39	2.16	3.62	31.5
13.16	22.19	0.93	3.45	2.18	3.59	33.1
14.20	23.94	0.82	3.31	2.07	3.57	22.4
14.27	24.06	0.77	3.38	2.11	3.49	30.5
16.23	27.36	0.60	3.30	2.03	3.37	29.3
16.95	28.57	0.47	3.30	2.03	3.37	25.4
17.28	29.13	0.48	3.23	1.98	3.31	19.0
17.93	30.23	0.53	3.24	1.99	3.28	16.4
18.85	31.78	0.40	3.23	1.97	3.22	21.5
18.98	32.00	0.41	3.18	1.94	3.17	19.8
19.90	33.55	0.41	3.30	2.01	3.25	19.0
19.96	33.65	0.49	3.24	1.97	3.14	16.8
20.68	34.86	0.46	3.17	1.93	3.13	14.0

TABLE : 4 1" D FLAT PLATE : $\beta = 188.0$: $D/w = 4.17$

NKC	Re No x 10^{-3}	C_m	C_D	$C_{F_{RMS}}$	$C_{F_{MAX}}$	ϕ^o
5.50	1.04	1.51	4.61	3.42	5.76	30.0
8.84	1.67	1.28	3.26	2.24	3.76	31.7
9.42	1.79	1.28	3.38	2.27	3.79	30.9
9.72	1.84	1.24	3.14	2.13	3.56	37.7
10.80	2.04	1.20	2.96	1.97	3.11	30.0
11.78	2.24	1.13	3.15	2.04	3.41	32.9
11.88	2.25	1.23	2.89	1.91	3.19	36.9
13.35	2.52	0.94	2.74	1.75	2.87	32.2
14.14	2.67	0.87	2.81	1.77	2.94	31.4
14.14	2.68	0.90	2.97	1.88	3.17	30.0
15.12	2.86	0.74	2.73	1.70	2.75	25.4
16.10	3.04	0.78	2.68	1.67	2.74	29.6
16.30	3.09	0.73	2.78	1.73	2.89	27.4
16.89	3.19	0.85	2.64	1.65	2.62	27.9
17.87	3.38	0.70	2.57	1.59	2.56	26.2
18.26	3.47	0.78	2.76	1.71	2.81	25.7
18.65	3.52	0.73	2.63	1.63	2.57	17.6
20.22	3.82	0.73	2.51	1.55	2.52	21.9
20.42	3.86	0.87	2.52	1.56	2.46	21.1

NKC	Re.No. $\times 10^{-3}$	C_m	C_D	$C_{F_{RMS}}$	$C_{F_{MAX}}$	ϕ°
20.42	3.88	0.83	2.65	1.64	2.60	18.0
21.40	4.05	0.95	2.45	1.52	2.38	20.2
22.78	4.32	0.98	2.57	1.59	2.48	20.2
22.97	4.34	0.95	2.47	1.52	2.35	21.9
24.45	4.62	1.11	2.48	1.54	2.28	9.9
25.72	4.88	1.36	2.59	1.61	2.42	15.9
26.51	5.01	1.21	2.43	1.51	2.25	12.5
29.45	5.57	1.46	2.26	1.41	2.13	13.3
32.01	6.08	1.58	2.46	1.53	2.30	13.3
33.38	6.31	1.47	2.23	1.39	2.08	11.6
37.21	7.03	1.58	2.19	1.36	2.01	11.6
39.47	7.49	1.65	2.30	1.42	2.09	9.0
42.80	8.09	1.45	2.09	1.28	1.92	5.6
46.53	8.80	1.55	2.08	1.28	1.88	5.6
49.68	9.43	1.86	2.21	1.36	1.98	9.0
52.62	9.95	1.60	2.04	1.26	1.84	- 1.3
57.92	11.00	1.73	2.12	1.30	1.93	6.4
59.89	11.30	1.65	1.96	1.20	1.79	5.6
66.17	12.60	1.78	2.10	1.28	1.93	8.2
73.43	13.90	1.98	2.04	1.25	1.86	3.0

TABLE : 5 DIAMOND SECTION

β = 422.7 : D = 1.5" : $D/_W$ = 6.25%

NKC	Re.No. $\times 10^{-3}$	C_m	C_D	$C_{F_{RMS}}$	$C_{F_{MAX}}$	ϕ°
4.84	2.05	1.18	3.65	2.81	4.51	35.1
6.15	2.60	1.08	3.24	2.32	3.64	32.0
6.54	2.77	1.04	3.21	2.25	3.62	24.9
7.46	3.15	0.99	3.21	2.18	3.54	38.2
7.85	3.32	1.02	2.88	1.99	3.28	41.1
8.25	3.49	0.98	2.99	2.01	3.26	36.5
8.90	3.76	0.89	2.99	1.96	3.22	36.5
9.69	4.09	0.88	2.89	1.88	3.06	35.7
10.21	4.32	0.77	2.81	1.80	2.82	27.9
10.47	4.43	0.73	2.79	1.78	2.78	30.5
10.86	4.59	0.71	2.73	1.74	2.59	25.4
11.52	4.87	0.64	2.69	1.70	2.39	23.7
11.91	5.04	0.62	2.60	1.65	2.37	15.0
12.17	5.15	0.66	2.59	1.64	2.31	24.5

NKC	Re.No. x 10^{-3}	C_m	C_D	$C_{F_{RMS}}$	$C_{F_{MAX}}$	ϕ^o
13.09	5.53	0.54	2.46	1.55	2.23	6.9
13.09	5.53	0.55	2.51	1.58	2.31	3.9
13.74	5.81	0.68	2.46	1.56	2.25	12.1
14.79	6.25	0.81	2.32	1.47	2.21	25.8
15.18	6.42	0.75	2.25	1.43	2.12	15.0
15.71	6.64	0.85	2.37	1.50	2.53	6.0
17.28	7.30	0.88	2.31	1.46	2.40	12.1
17.80	7.53	0.75	2.34	1.46	2.47	16.8
18.98	8.02	0.72	2.30	1.44	2.46	15.5
21.86	9.24	0.80	2.23	1.39	2.47	15.9
23.95	10.13	0.94	2.11	1.32	2.22	17.6
26.83	11.34	1.01	2.12	1.32	2.08	14.6
27.10	11.45	1.04	2.18	1.35	2.11	17.1
27.88	11.79	1.01	2.20	1.36	2.25	20.2
28.14	11.90	1.10	2.10	1.31	2.04	18.5
29.45	12.45	1.20	2.16	1.34	2.15	24.1
32.46	13.72	1.25	1.99	1.24	1.89	5.2
33.25	14.05	1.23	2.06	1.27	1.92	5.2
35.74	15.11	1.20	2.03	1.25	1.93	8.5
39.01	16.49	1.14	1.98	1.21	1.82	8.6
39.14	16.54	1.18	2.02	1.24	1.84	7.3
41.76	17.65	1.24	1.95	1.21	1.87	2.9
43.85	18.53	1.29	1.91	1.17	1.77	0.9
45.81	19.37	1.21	1.98	1.22	1.94	2.1
47.39	20.03	1.16	1.89	1.16	1.75	0.9
47.78	20.20	1.36	1.94	1.19	1.79	1.7
50.27	21.25	1.26	1.86	1.14	1.75	2.6

TABLE : 6 SQUARE SECTION

β = 208.6 : D = 1.061" : $D/_W$ = 4.42%

NKC	Re.No. x 10^{-3}	C_m	C_D	$C_{F_{RMS}}$	$C_{F_{MAX}}$	ϕ^o
5.92	1.22	2.51	1.68	3.14	4.48	55.7
7.59	1.60	2.75	1.45	2.68	4.00	63.4
8.15	1.68	2.70	1.86	2.57	3.69	60.6
9.44	2.00	2.64	1.51	2.16	3.22	61.7
9.81	2.02	2.65	1.67	2.14	3.20	53.7
10.18	2.10	2.56	1.60	2.01	2.93	55.4
10.92	2.25	2.50	1.60	1.87	2.74	64.6
11.11	2.35	2.63	1.55	1.90	2.97	64.9

NKC	Re.No. $\times 10^{-3}$	C_m	C_D	$C_{F_{RMS}}$	$C_{F_{MAX}}$	ϕ^c
11.85	2.44	2.57	1.59	1.80	2.71	59.4
12.03	2.54	2.63	1.46	1.76	2.66	54.6
12.77	2.63	2.65	1.59	1.74	2.61	56.0
12.96	2.67	2.71	1.51	1.72	2.50	62.3
13.33	2.74	2.71	1.55	1.70	2.61	58.6
15.18	3.12	2.80	1.57	1.60	2.34	66.6
16.11	3.40	2.62	1.41	1.42	2.07	62.3
16.48	3.39	2.75	1.54	1.49	2.18	66.0
17.03	3.60	2.62	1.38	1.36	1.99	55.1
17.59	3.62	2.77	1.58	1.45	2.20	63.5
17.77	3.76	2.72	1.47	1.39	2.03	58.5
18.98	3.91	2.71	1.57	1.37	1.99	64.0
19.99	4.23	2.56	1.42	1.24	1.81	59.7
20.55	4.23	2.73	1.51	1.30	1.87	59.4
22.40	4.61	2.66	1.47	1.21	1.71	48.7
22.96	4.85	2.65	1.43	1.18	1.65	41.3
23.23	4.78	2.72	1.49	1.21	1.74	50.0
25.55	5.26	2.56	1.48	1.13	1.59	54.3
26.47	5.60	2.69	1.49	1.14	1.58	47.4
27.95	5.75	2.54	1.52	1.11	1.54	43.9
29.99	6.17	2.56	1.53	1.10	1.53	43.1
32.40	6.85	2.51	1.56	1.09	1.49	37.4
37.02	7.62	2.19	1.57	1.03	1.44	27.5
38.88	8.22	2.25	1.64	1.07	1.50	20.2
40.73	8.38	2.25	1.60	1.04	1.42	19.8
45.35	9.33	2.07	1.65	1.05	1.48	10.3
50.35	10.36	2.00	1.65	1.03	1.51	6.0
55.17	11.35	1.75	1.69	1.04	1.58	4.3
58.13	11.96	1.83	1.69	1.05	1.59	3.4
58.31	12.32	1.99	1.70	1.06	1.59	3.4
62.02	12.76	1.61	1.70	1.04	1.62	3.4
64.98	13.37	1.68	1.74	1.07	1.68	- 1.7
68.12	14.02	1.53	1.73	1.06	1.69	1.7
69.61	14.71	1.79	1.73	1.07	1.68	1.7
70.53	14.52	1.63	1.74	1.07	1.72	2.6

APPENDIX : 6

VORTEX POSITIONS DURING A CYCLE

TABLE : 1 THE CIRCULAR CYLINDER, BETA (β) = 451

CYCLIC REGION, NKC = 20.42 ROTATION ANTI-CLOCKWISE.

D = DIAMETER OF CYLINDER.

FRAME No.	TIME t/T	VORTEX POSITION x/D	y/D	SIGN	EDGE	COMMENTS
1	0.99	- 1.90	0.80	- ve	Top LH	(This vortex is now very weak)
1	0.99	- 1.10	0.15	+ ve	Bottom LH	
1	0.99	- 0.40	0.50	- ve	Top LH	(This vortex is just starting to grow)
2	0.02	- 0.50	0.40	- ve	Top LH	
2	0.02	- 1.10	0.15	+ ve	Bottom LH	(This is shed about now)
3	0.04	- 1.40	- 0.25	+ ve	Bottom LH	
3	0.04	- 0.60	0.30	- ve	Top LH	
4	0.06	- 1.65	- 0.30	+ ve	Bottom LH	
4	0.06	- 0.65	0.10	- ve	Top LH	
5	0.09	- 1.90	- 0.35	+ ve	Bottom LH	
5	0.09	- 0.75	0.0	- ve	Top LH	
6	0.11	- 2.05	- 0.55	+ ve	Bottom LH	
6	0.11	- 0.85	- 0.05	- ve	Top LH	
7	0.13	- 2.25	- 0.75	+ ve	Bottom LH	
7	0.13	- 0.70	- 0.10	- ve	Top LH	
8	0.16	- 2.40	- 0.80	+ ve	Bottom LH	
8	0.16	- 0.80	0.15	- ve	Top LH	
9	0.18	- 2.35	- 0.95	+ ve	Bottom LH	
9	0.18	- 0.70	0.35	- ve	Top LH	
10	0.20	- 2.55	- 0.90	+ ve	Bottom LH	
10	0.20	- 0.70	0.40	- ve	Top LH	(Starts to split up and goes
11	0.23	- 2.30	- 1.1	+ ve	Bottom LH	(underneath the cylinder to th (bottom R.H.)
11	0.23	Vortex from Top LH now squashed against cylinder.				
12	0.25	- 2.05	- 0.8	+ ve	Bottom LH	(The top R.H. vortex still
12	0.25					(squashed against the cylinder (as flow about to reverse. (Position on other side of (cylinder indeterminate)
13	0.27	- 1.95	- 0.90	+ ve	Bottom LH	
14	0.30	- 1.60	- 1.05	+ ve	Bottom LH	
15	0.32	- 1.45	- 1.50	+ ve	Bottom LH	
16	0.34	- 1.20	- 1.35	+ ve	Bottom LH	
17	0.37	- 0.85	- 2.05	+ ve	Bottom LH	

TABLE : 1, Continued..

FRAME No.	TIME (t/T)	VORTEX POSITION x/D	y/D	SIGN	EDGE	COMMENTS
18	0.39	- 0.45	- 2.35	+ ve	Bottom LH	
19	0.41	0.00	- 2.80	+ ve	Bottom LH	(This vortex started growing (some time before, but only
19	0.41	0.70	0.15	+ ve	Top RH	(now is its position clear)
20	0.44	0.75	0.25	+ ve	Top RH	
20	0.44	(This vortex from the			Bottom RH now goes	out of view, but exists up to t/T ≈ 0.5)
21	0.46	0.85	0.20	+ ve	Top RH	
22	0.48	0.95	0.10	+ ve	Top RH	
23	0.51	1.15	0.20	+ ve	Top RH	(This vortex is now shed)
24	0.53	1.50	0.20	+ ve	Top RH	
24	0.53	0.60	- 0.10	- ve	Bottom RH	(Just beginning to grow)
25	0.55	1.70	0.20	+ ve	Top RH	
25	0.55	0.75	0.00	- ve	Bottom RH	
26	0.58	2.10	0.50	+ ve	Top RH	
26	0.58	0.95	0.50	- ve	Bottom RH	
27	0.60	2.55	0.50	+ ve	Top RH	
27	0.60	0.75	0.50	- ve	Bottom RH	
28	0.52	2.70	0.75	+ ve	Top RH	
28	0.62	1.05	0.40	- ve	Bottom RH	
29	0.65	2.90	0.85	+ ve	Top RH	
29	0.65	1.15	0.35	- ve	Bottom RH	
30	0.67	2.85	1.05	+ ve	Top RH	
30	0.67	0.95	0.25	- ve	Bottom RH	
31	0.69	3.05	1.00	+ ve	Top RH	
31	0.69	0.90	0.40	- ve	Bottom RH	(This is the same vortex which
31	0.69	0.35	0.75	- ve	Bottom RH	(appears to split up)
32	0.72	2.90	0.95	+ ve	Top RH	
32	0.72	0.35	0.80	- ve	Bottom RH	
32	0.72	1.05	- 0.20	- ve	Top LH	(Some of this vorticity came (from the Bottom RH.)
33	0.74	- 0.10	0.90	- ve	Top LH	
33	0.74	3.00	1.20	+ ve	Top RH	
34	0.76	3.05	1.50	+ ve	Top RH	
34	0.76	- 0.30	0.80	- ve	Top LH	
35	0.78	2.70	1.65	+ ve	Top RH	
35	0.78	The vortex from the top LH is no longer distinct, it is very weak.				

TABLE : 1, Continued...

FRAME No.	TIME (t/T)	VORTEX POSITION x/D	y/D	SIGN	EDGE	COMMENTS
36	0.81	2.95	1.75	+ ve	Top RH	
37	0.83	2.20	2.00	+ ve	Top RH	
38	0.85	1.95	2.25	+ ve	Top RH	
39	0.88	1.40	2.60	+ ve	Top RH	(This vortex then disappears from view)
40	0.90	- 0.65	0.15	+ ve	Bottom LH	(New vortex forming)
41	0.92	- 0.80	0.10	+ ve	Bottom LH	
41	0.92	- 0.85	0.70	- ve	Top LH	
42	0.95	- 1.30	0.80	- ve	Top LH	
42	0.95	- 0.80	0.10	+ ve	Bottom LH	
43	0.97	- 1.75	0.90	- ve	Top LH	
43	0.97	- 0.90	0.15	+ ve	Bottom LH	

TABLE : 2 THE 3" DIAMETER FLAT PLATE, β = 1685.8
CYCLIC REGION - NKC = 15.13,
ROTATION ANTI-CLOCKWISE
D = DIAMETER OF PLATE

FRAME No.	TIME (t/T)	VORTEX POSITION x/D	y/D	SIGN	EDGE	COMMENTS
1	0.99	- 0.75	- 0.18	+ ve	Bottom LH	
2	0.02	- 0.84	- 0.31	+ ve	Bottom LH	
3	0.04	- 1.06	- 0.22	+ ve	Bottom LH	This vortex is now shed
3	0.04	- 0.49	0.40	- ve	Top LH	New vortex growing
4	0.06	- 1.15	- 0.35	+ ve	Bottom LH	
4	0.06	- 0.58	0.31	- ve	Top LH	
5	0.09	- 1.33	- 0.44	+ ve	Bottom LH	
5	0.09	- 0.62	- 0.40	- ve	Top LH	
6	0.11	- 1.15	- 0.58	+ ve	Bottom LH	
6	0.11	- 0.62	0.13	- ve	Top LH	
7	0.13	- 1.15	- 0.80	+ ve	Bottom LH	
7	0.13	- 0.58	0.04	- ve	Top LH	
8	0.16	- 1.33	- 0.84	+ ve	Bottom LH	
8	0.16	- 0.66	0.00	- ve	Top LH	
9	0.18	- 1.46	- 0.89	+ ve	Bottom LH	
9	0.18	- 0.58	- 0.09	- ve	Top LH	
10	0.20	- 1.64	- 0.89	+ ve	Bottom LH	
10	0.20	- 0.40	0.13	- ve	Top LH	
11	0.23	- 1.55	- 1.33	+ ve	Bottom LH	
11	0.23	- 0.66	- 0.09	- ve	Top LH	
12	0.25	- 1.37	- 1.33	+ ve	Bottom LH	
12	0.25	- 0.53	0.00	- ve	Top LH	
13	0.27	- 1.68	- 1.29	+ ve	Bottom LH	
13	0.27	- 0.53	- 0.18	- ve	Top LH	
14	0.30	- 1.42	- 1.42	+ ve	Bottom LH	
14	0.30	- 0.40	- 0.18	- ve	Top LH	
15	0.32	- 1.29	- 1.51	+ ve	Bottom LH	
15	0.32	- 0.27	- 0.35	- ve	Top LH	
16	0.34	- 1.02	- 1.73	+ ve	Bottom LH	
16	0.34	The vortex from the top LH edge is now squashed against the pl				
17	0.37	- 0.66	- 1.91	+ ve	Bottom LH	(and its position is not
18	0.39	- 0.40	- 2.08	+ ve	Bottom LH	(identifiable)

TABLE : 2, Continued..

FRAME No.	TIME (t/T)	VORTEX POSITION x/D	y/D	SIGN	EDGE	COMMENTS
18	0.39	- 0.44	- 0.66	- ve	Bottom RH	(This vortex appears to
18	0.39	0.18	0.35	+ ve	Top RH (New vortex growing here)	(contain some vorticity (from the top LH edge.)
19	0.41	- 0.31	- 2.22	+ ve	Bottom LH	
19	0.41	0.58	- 0.58	- ve	Bottom RH	
19	0.41	0.31	0.27	+ ve	Top RH	
20	0.44	0.18	- 2.26	+ ve	Bottom LH	
20	0.44	Vortex from Bottom RH edge is weak and its position is not clear)				
20	0.44	0.44	0.22	+ ve	Top RH	
21	0.46	0.71	- 2.35	+ ve	Bottom LH	(This vortex now goes out c (view but decays by about (t/T ≈ 0.55)
21	0.46	1.55	- 0.62	- ve	Bottom RH	(Weak vortex - position approximate)
21	0.46	0.58	0.18	+ ve	Top RH	
22	0.48	0.71	0.09	+ ve	Top RH	(Vortex about to be shed)
22	0.48	1.68	- 0.62	- ve	Bottom RH	(Approximate position)
23	0.51	0.89	0.13	+ ve	Top RH	
23	0.51	1.86	0.53	- ve	Bottom RH	(Vortex almost totally diffused)
24	0.53	0.98	0.18	+ ve	Top RH	
24	0.53	0.31	- 0.40	- ve	Bottom RH	(New vortex growing here)
25	0.55	1.06	0.22	+ ve	Top RH	
25	0.55	0.31	- 0.18	- ve	Bottom RH	
26	0.58	1.11	0.40	+ ve	Top RH	
26	0.58	0.27	- 0.22	- ve	Bottom RH	
27	0.60	1.24	0.49	+ ve	Top RH	
27	0.60	0.44	- 0.18	- ve	Bottom RH	
28	0.62	1.33	0.53	+ ve	Top RH	
28	0.62	0.40	- 0.13	- ve	Bottom RH	
29	0.65	1.46	0.62	+ ve	Top RH	
29	0.65	0.44	- 0.04	- ve	Bottom RH	
30	0.67	1.64	0.66	+ ve	Top RH	
30	0.67	0.53	0.09	- ve	Bottom RH	
31	0.69	1.51	0.89	+ ve	Top RH	
31	0.69	0.58	- 0.04	- ve	Bottom RH	
32	0.72	1.68	0.93	+ ve	Top RH	
32	0.72	0.53	0.00	- ve	Bottom RH	
33	0.74	1.86	1.02	+ ve	Top RH	
33	0.74	0.40	0.09	- ve	Bottom RH	
34	0.76	1.64	0.98	+ ve	Top RH	
34	0.76	0.49	- 0.13	- ve	Bottom RH	

TABLE : 2, Continued..

FRAME No.	TIME (t/T)	VORTEX POSITION x/D	y/D	SIGN	EDGE	COMMENTS
35	0.78	1.68	1.06	+ ve	Top RH	
35	0.78	0.31	0.00	- ve	Bottom RH	(About to go over the top L.H. edge)
36	0.81	1.42	1.06	+ ve	Top RH	
36	0.81	- 0.22	0.44	- ve	Top LH	(This vortex contains (vorticity from the vortex (at the Bottom RH edge)
37	0.83	1.15	1.24	+ ve	Top RH	
37	0.83	- 0.35	0.53	- ve	Top LH	
38	0.85	0.84	1.51	+ ve	Top RH	
38	0.85	- 0.62	0.49	- ve	Top LH	
39	0.88	0.62	1.73	+ ve	Top RH	
39	0.88	- 0.84	0.53	- ve	Top LH	
40	0,90	0.22	1.95	+ ve	Top RH	(This vortex then moves out (of view but decays by t/T ($\approx$1.0)
40	0.90	- 1.02	0.66	- ve	Top LH	(This vortex almost complet (ly diffused)
40	0.90	- 0.18	- 0.35	+ ve	Bottom LH	(New vortex forming)
41	0.92	- 0.35	- 0.09	+ ve	Bottom LH	
42	0.95	- 0.44	- 0.22	+ ve	Bottom LH	
43	0.97	- 0.53	- 0.27	+ ve	Bottom LH	

TABLE : 3 THE 1.5" DIAMETER FLAT PLATE, β = 421.5

CYCLIC REGION - NKC = 15.18

ROTATION CLOCKWISE

D = DIAMETER OF PLATE

FRAME No.	TIME (t/T	VORTEX POSITION x/D	y/D	SIGN	EDGE	COMMENTS
1	0.99	- 0.71	0.22	- ve	Top LH	
1	0.99	- 1.90	- 0.69	+ ve	Top RH	(Vortex now very weak, position approximate)
2	0.22	- 0.51	- 0.54	+ ve	Bottom LH	(New vortex forming)
2	0.22	- 0.83	0.20	- ve	Top LH	
3	0.04	- 0.97	0.14	- ve	Top LH	
3	0.04	- 0.49	- 0.41	+ ve	Bottom LH	
4	0.06	- 0.43	- 0.43	+ ve	Bottom LH	
4	0.06	- 0.94	0.31	- ve	Top LH	
5	0.09	- 1.05	0.32	- ve	Top LH	
5	0.09	- 0.43	- 0.30	+ ve	Bottom LH	
6	0.11	- 0.43	- 0.35	+ ve	Bottom LH	
6	0.11	- 1.08	0.43	- ve	Top LH	
7	0.13	- 1.16	0.57	- ve	Top LH	
7	0.13	- 0.49	- 0.20	+ ve	Bottom LH	
8	0.16	- 0.45	- 0.24	+ ve	Bottom LH	
8	0.16	- 1.17	0.69	- ve	Top LH	
9	0.18	- 1.20	0.80	- ve	Top LH	
9	0.18	- 0.45	- 0.04	+ ve	Bottom LH	
10	0.20	- 0.45	- 0.09	+ ve	Bottom LH	
10	0.20	- 1.12	0.86	- ve	Top LH	
11	0.23	- 1.13	0.94	- ve	Top LH	
11	The vortex now starts to go over to the					top R.H. edge of the plate. Position unclear.
12	0.25	- 0.68	- 0.43	+ ve	Bottom LH	
12	0.25	0.30	0.46	+ ve	Top RH	(This vortex contains vorticity (from the Bottom LH edge)
12	0.25	- 1.19	0.91	- ve	Top LH	
13	0.27	- 1.08	0.97	- ve	Top LH	
14	0.30	- 0.94	1.15	- ve	Top LH	
15	0.32	- 0.73	1.31	- ve	Top LH	
15	0.32	0.38	0.66	+ ve	Top RH	(The position of this vortex (was not clear in frames 13 & 1
16	0.34	0.66	0.74	+ ve	Top RH	
16	0.34	- 0.56	1.47	- ve	Top LH	
17	0.37	- 0.29	1.79	- ve	Top LH	

TABLE : 3, Continued..

FRAME No.	TIME (t/T)	VORTEX POSITION x/D	y/D	SIGN	EDGE	COMMENTS
17	0.37	0.83	0.74	+ ve	Top RH	
18	0.39	1.07	0.80	+ ve	Top RH	
18	0.39	0.04	2.03	- ve	Top LH	
18	0.39	0.35	- 0.35	- ve	Bottom RH	New Vortex growing here.
19	0.41	0.52	- 0.32	- ve	Bottom RH	
19	0.41	0.44	2.14	- ve	Top LH	
19	0.41	1.46	0.85	+ ve	Top RH	
20	0.44	1.70	0.86	+ ve	Top RH	
20	0.44	1.01	2.33	- ve	Top LH	
20	0.44	0.58	- 0.26	- ve	Bottom RH	
21	0.46	0.68	- 0.30	- ve	Bottom RH	
21	0.46	1.24	2.35	- ve	Top LH	
21	0.46	2.32	1.24	+ ve	Top RH	(This vortex is now weak and i
22	0.48	2.47	1.01	+ ve	Top RH	(position unclear, after frame
22	0.48	1.74	2.50	- ve	Top LH	(22 it becomes insignificant).
22	0.48	0.89	- 0.31	- ve	Bottom RH	(This vortex then goes out of (view but by t/T≈0.5 is almos (diffused)
22	0.48	0.61	0.43	+ ve	Top RH	New vortex forming.
23	0.51	1.01	- 0.38	- ve	Bottom RH	
23	0.51	0.63	0.35	+ ve	Top RH	
24	0.53	0.67	0.22	+ ve	Top RH	
24	0.53	1.12	- 0.46	- ve	Bottom RH	
25	0.55	1.16	- 0.61	- ve	Bottom RH	
25	0.55	0.71	0.14	+ ve	Top RH	
26	0.58	0.69	0.04	+ ve	Top RH	
26	0.58	1.31	- 0.68	- ve	Bottom RH	
27	0.60	1.45	- 0.87	- ve	Bottom RH	
27	0.60	0.72	0.00	+ ve	Top RH	
28	0.62	0.64	- 0.05	+ ve	Top RH	
28	0.62	1.55	- 0.90	- ve	Bottom RH	
29	0.65	1.60	- 1.04	- ve	Bottom RH	
29	0.65	0.76	- 0.20	+ ve	Top RH	
30	0.67	0.76	- 0.20	+ ve	Top RH	
30	0.67	1.70	- 1.10	- ve	Bottom RH	
31	0.69	1.84	- 1.19	- ve	Bottom RH	
31	0.69	0.76	- 0.20	+ ve	Top RH	
32	0.72	0.76	0.02	+ ve	Top RH	
32	0.72	1.89	- 1.30	- ve	Bottom RH	

TABLE: 3, Continued..

FRAME No.	TIME (t/T)	VORTEX POSITION x/D	y/D	SIGN	EDGE	COMMENTS
33	0.74	1.82	- 1.42	- ve	Bottom RH	
33	0.74	0.79	- 0.02	+ ve	Top RH	
34	0.76	0.69	- 0.04	+ ve	Top RH	
34	0.76	1.66	- 1.47	- ve	Bottom RH	
35	0.78	1.59	- 1.64	- ve	Bottom RH	
35	0.78	0.57	- 0.09	+ ve	Top RH	(This vortex then goes under (the plate and is enhanced by (vorticity from the bottom LH
36	0.81	1.41	- 1.83	- ve	Bottom RH	(edge)
37	0.83	1.07	- 1.96	- ve	Bottom RH	
38	0.85	0.79	- 2.06	- ve	Bottom RH	
38	0.85	- 0.38	- 0.36	+ ve	Bottom LH	(This vortex contains some
39	0.88	- 0.51	- 0.39	+ ve	Bottom LH	(vorticity from the top RH edge
39	0.88	0.49	- 2.11	- ve	Bottom RH	
40	0.90	0.30	- 2.20	- ve	Bottom RH	
40	0.90	- 0.21	0.44	- ve	Top LH	New vortex forming here.
40	0.90	- 0.58	- 0.44	+ ve	Bottom LH	
41	0.92	- 1.00	- 0.60	+ ve	Bottom LH	
41	0.92	- 0.02	- 2.27	- ve	Bottom RH	
41	0.92	- 0.36	0.34	- ve	Top LH	
42	0.95	- 0.48	0.30	- ve	Top LH	
42	0.95	- 0.46	- 2.27	- ve	Bottom RH	
42	0.95	- 1.33	- 0.57	+ ve	Top RH	
43	0.97	- 1.42	- 0.60	+ ve	Top RH	
43	0.97	- 0.58	0.26	- ve	Top LH	
43	0.97	- 0.86	- 2.30	- ve	Bottom RH	

TABLE : 4 THE 1.5" DIAMETER FLAT PLATE, β = 421.5

CYCLIC REGION : NKC = 18.6 : ROTATION ANTI-CLOCKWISE

FRAME No.	TIME (t/T)	VORTEX POSITION x/D	y/D	SIGN	EDGE	COMMENTS
1	0.99	- 0.59	0.47	- ve	Top LH	
1	0.99	- 0.99	- 0.37	+ ve	Bottom LH	
2	0.02	- 1.14	- 0.43	+ ve	Bottom LH	
2	0.02	- 0.59	0.33	- ve	Top LH	
3	0.04	- 0.65	0.17	- ve	Top LH	
3	0.04	- 1.34	- 0.56	+ ve	Bottom LH	
4	0.06	- 1.46	- 0.71	+ ve	Bottom LH	
4	0.06	- 0.69	0.13	- ve	Top LH	
5	0.09	- 0.80	0.00	- ve	Top LH	
5	0.09	- 1.68	- 0.89	+ ve	Bottom LH	
6	0.11	- 1.91	- 1.04	+ ve	Bottom LH	
6	0.11	- 0.89	- 0.09	- ve	Top LH	
7	0.13	- 0.93	- 0.04	- ve	Top LH	
7	0.13	- 2.13	- 1.07	+ ve	Bottom LH	
8	0.16	- 2.25	- 1.32	+ ve	Bottom LH	
8	0.16	- 1.04	- 0.14	- ve	Top LH	
9	0.18	- 1.17	- 0.18	- ve	Top LH	
9	0.18	- 2.39	- 1.33	+ ve	Bottom LH	
10	0.20	- 2.41	- 1.46	+ ve	Bottom LH	
10	0.20	- 1.24	- 0.17	- ve	Top LH	
11	0.23	- 1.20	- 0.32	- ve	Top LH	
11	0.23	- 2.30	- 1.42	+ ve	Bottom LH	
12	0.25	- 1.09	0.03	- ve	Top LH	
12	0.25	- 2.36	- 1.37	+ ve	Bottom LH	
13	0.27	- 2.21	- 1.67	+ ve	Bottom LH	
13	0.27	- 1.02	0.03	- ve	Top LH	
14	0.30	- 0.76	- 0.11	- ve	Top LH	
14	0.30	- 1.65	- 1.71	+ ve	Bottom LH	
15	0.32	- 1.54	- 1.70	+ ve	Bottom LH	
15	0.32	- 0.54	- 0.32	- ve	Top LH	
16	0.34	The vortex from the Top LH edge is now squashed against the plate and some of it starts to go under the plate.				
16	0.34	- 0.90	- 1.76	+ ve	Bottom LH	
17	0.37	- 0.69	- 1.78	+ ve	Bottom LH	

TABLE : 4, Continued..

FRAME No.	TIME (t/T)	VORTEX POSITION x/D	y/D	SIGN	EDGE	COMMENTS
17	0.37	0.44	- 0.45	- ve	Bottom RH	(This vortex contains most of (the vorticity from the vortex (that was at the top LH edge, (but which transferred to the
18	0.39	0.60	- 0.43	- ve	Bottom RH	(Bottom RH edge)
18	0.39	- 0.30	- 1.81	+ ve	Bottom LH	
18	0.39	0.36	0.41	+ ve	Top RH	New vortex forming here.
19	0.41	0.41	0.37	+ ve	Top RH	
19	0.41	- 0.14	- 1.87	+ ve	Bottom LH	
19	0.41	0.85	- 0.51	- ve	Bottom RH	
20	0.44	1.13	- 0.66	- ve	Bottom RH	
20	0.44	———	———	+ ve	Bottom LH	Position not clear.
20	0.44	0.47	0.23	+ ve	Top RH	
21	0.46	0.54	0.19	+ ve	Top RH	
21	0.46	1.26	- 1.91	+ ve	Bottom LH	This vortex then moves out of view.
21	0.46	1.57	- 0.52	- ve	Bottom RH	(This vortex is now very (weak and insignificant)
22	0.48	0.75	0.17	+ ve	Top RH	
22	0.48	0.40	- 0.63	- ve	Bottom RH	New vortex forming here.
23	0.51	0.89	0.17	+ ve	Top RH	
23	0.51	0.50	- 0.62	- ve	Bottom RH	
24	0.53	0.54	- 0.48	- ve	Bottom RH	
24	0.53	0.92	0.23	+ ve	Top RH	
25	0.55	1.12	0.31	+ ve	Top RH	
25	0.55	0.52	- 0.39	- ve	Bottom RH	
26	0.58	0.44	- 0.22	- ve	Bottom RH	
26	0.58	1.26	0.39	+ ve	Top RH	
27	0.60	1.45	0.52	+ ve	Top RH	
27	0.60	0.55	- 0.13	- ve	Bottom RH	
28	0.62	0.56	- 0.09	- ve	Bottom RH.	
28	0.62	1.68	0.61	+ ve	Top RH	
29	0.65	1.80	0.80	+ ve	Top RH	
29	0.65	0.63	- 0.03	- ve	Bottom RH	
30	0.67	0.64	0.03	- ve	Bottom RH	
30	0.67	2.02	0.82	+ ve	Top RH	
31	0.69	2.10	0.89	+ ve	Top RH	
31	0.69	0.68	0.10	- ve	Bottom RH	
32	0.72	0.63	- 0.10	- ve	Bottom RH	
32	0.72	2.02	1.00	+ ve	Top RH.	

TABLE : 4, Continued..

FRAME No.	TIME (t/T)	VORTEX POSITION x/D	y/D	SIGN	EDGE	COMMENTS
33	0.74	1.97	1.13	+ ve	Top RH	
33	0.74	0.59	0.12	- ve	Bottom RH	
34	0.76	0.61	0.09	- ve	Bottom RH	
34	0.76	1.88	1.30	+ ve	Top RH	
35	0.78	1.68	1.56	+ ve	Top RH	
35	0.78	0.45	0.13	- ve	Bottom RH	
36	0.81	Vortex from the Bottom R.H. edge goes over the top of the plate,but its position is not clear)				
36	0.81	1.36	1.70	+ ve	Top RH	
37	0.83	0.92	1.89	+ ve	Top RH	
37	0.83	- 0.44	0.71	- ve	Top LH	(This vortex contains vorticit (from the bottom RH vortex (which went over the top of th (plate)
38	0.85	- 0.72	0.69	- ve	Top LH	(Position unclear, and uncerta (after this frame)
38	0.85	0.68	1.94	+ ve	Top RH	
39	0.88	0.20	2.05	+ ve	Top RH	(This vortex then moves out of view)
39	0.88	- 0.30	- 0.34	+ ve	Bottom LH	(New vortex forming)
40	0.90	- 0.37	- 0.35	+ ve	Bottom LH	
41	0.92	- 0.52	- 0.38	+ ve	Bottom LH	
42	0.95	- 0.69	- 0.30	+ ve	Bottom LH	
43	0.97	- 0.85	- 0.35	+ ve	Bottom LH	
43	0.97	- 0.48	0.56	- ve	Top LH	(New vortex forming)

TABLE : 5 THE DIAMOND SECTION (β = 422.7)

SIDEWAY VORTEX STREET. NKC = 15.18

FRAME No.	TIME	VORTEX POSITION x/D	y/D	SIGN	EDGE	COMMENTS
1	0.99	- 1.21	0.71	- ve	Top LH	
1	0.99	0.36	2.64	+ ve	Top RH	
2	0.02	0.07	2.86	+ ve	Top RH	
2	0.02	- 1.50	0.64	- ve	Top LH	
3	0.04	- 1.79	0.79	- ve	Top LH	
3	0.04	- 0.50	2.93	+ ve	Top RH	
4	0.06	- 1.00	3.07	+ ve	Top RH	
4	0.06	- 2.14	0.93	- ve	Top LH	
4	0.06	- 0.71	0.00	+ ve	Bottom LH	(This vortex began growing (sooner, at about t/T≈0, but (only now is its position clea
5	0.09	- 0.86	0.00	+ ve	Bottom LH	
5	0.09	- 2.43	0.93	- ve	Top LH	
5	0.09	- 1.36	3.50	+ ve	Top RH	(This vortex then goes out of (view, but it is quite weak)
6	0.11	- 2.79	1.07	- ve	Top LH	
6	0.11	- 0.86	0.00	+ ve	Bottom LH	
7	0.13	- 1.00	0.00	+ ve	Bottom LH	
7	0.13	- 3.07	1.14	- ve	Top LH	
8	0.16	- 3.21	1.29	- ve	Top LH	
8	0.16	- 1.14	0.14	+ ve	Bottom LH	
9	0.18	- 1.07	- 0.07	+ ve	Bottom LH	
9	0.18	- 3.29	1.71	- ve	Top LH	
10	0.20	- 3.50	2.00	- ve	Top LH	
10	0.20	- 1.14	- 0.21	+ ve	Bottom LH	
11	0.23	- 1.29	- 0.21	+ ve	Bottom LH	
11	0.23	- 3.57	2.14	- ve	Top LH	
12	0.25	- 1.14	- 0.21	+ ve	Bottom LH	
12	0.25	- 3.79	2.14	- ve	Top LH	
13	0.27	- 1.07	- 0.07	+ ve	Bottom LH	
13	0.27	- 3.71	2.36	- ve	Top LH	
14	0.30	- 1.00	- 0.21	+ ve	Bottom LH	(This vortex starts to split u
14	0.30	0.29	0.50	+ ve	Top RH	(This vortex contains some of (the vorticity from the botton (LH)
14	0.30	- 3.50	2.43	- ve	Top LH	

TABLE : 5, Continued..

FRAME No.	TIME (t/T)	VORTEX POSITION x/D	y/D	SIGN	EDGE	COMMENTS
15	0.32	- 1.00	- 0.43	+ ve	Bottom LH	
15	0.32	0.57	0.36	+ ve	Top RH	
15	0.32	- 3.57	2.57	- ve	Top LH	
16	0.34	- 3.43	2.79	- ve	Top LH	
16	0.34	- 0.86	- 0.43	+ ve	Bottom LH	
16	0.34	0.43	0.36	+ ve	Top RH	
17	0.37	0.71	0.36	+ ve	Top RH	
17	0.37	- 0.57	- 0.43	+ ve	Bottom LH	(This vortex then goes under (the model and is cancelled ou
17	0.37	- 3.21	3.00	- ve	Top LH	
18	0.39	- 3.07	2.86	- ve	Top LH	
18	0.39	0.79	0.14	+ ve	Top RH	(This vortex is now shed)
19	0.41	0.86	0.29	+ ve	Top RH	
19	0.41	- 2.86	3.14	- ve	Top LH	
20	0.44	- 2.64	3.21	- ve	Top LH	
20	0.44	0.93	0.14	+ ve	Top RH	
21	0.46	1.14	0.14	+ ve	Top RH	
21	0.46	0.64	- 0.43	- ve	Bottom RH	(Vortex growing here)
21	0.46	- 2.43	3.29	- ve	Top LH	
22	0.48	- 2.14	3.07	- ve	Top LH	
22	0.48	0.64	- 0.21	- ve	Bottom RH	
22	0.48	1.36	0.21	+ ve	Top RH	
23	0.51	1.43	0.21	+ ve	Top RH	
23	0.51	0.71	- 0.14	- ve	Bottom RH	
23	0.51	- 1.86	3.21	- ve	Top LH	
24	0.53	- 1.64	3.21	- ve	Top LH	
24	0.53	1.64	0.29	+ ve	Top RH	
24	0.53	0.71	0.00	- ve	Bottom RH	
25	0.55	0.86	- 0.14	- ve	Bottom RH	
25	0.55	1.93	0.36	+ ve	Top RH	
25	0.55	- 1.29	3.21	- ve	Top LH	
26	0.58	- 0.86	3.21	- ve	Top LH	
26	0.58	2.14	0.29	+ ve	Top RH	
26	0.58	0.86	0.00	- ve	Bottom RH	
27	0.60	1.00	- 0.14	- ve	Bottom RH	
27	0.60	2.14	0.64	+ ve	Top RH	
27	0.60	- 0.36	3.29	- ve	Top LH	(This vortex then goes out of view)
28	0.62	2.36	0.57	+ ve	Top RH	

TABLE : 5, Continued...

FRAME No.	TIME (t/T)	VORTEX POSITION x/D	y/D	SIGN	EDGE	COMMENTS
28	0.62	1.00	0.07	- ve	Bottom RH	
29	0.65	1.00	- 0.14	- ve	Bottom RH	
29	0.65	2.36	0.79	+ ve	Top RH	
30	0.67	2.57	0.79	+ ve	Top RH	
30	0.67	1.14	0.14	- ve	Bottom RH	
31	0.69	1.29	0.00	- ve	Bottom RH	
31	0.69	2.79	0.86	+ ve	Top RH	
32	0.72	2.93	1.07	+ ve	Top RH	
32	0.72	1.14	- 0.07	- ve	Bottom RH	
33	0.74	1.14	- 0.07	- ve	Bottom RH	
33	0.74	3.00	1.21	+ ve	Top RH	
34	0.76	2.79	1.36	+ ve	Top RH	
34	0.76	1.14	- 0.07	- ve	Bottom RH	
35	0.78	3.00	1.43	+ ve	Top RH	
35	0.78	1.00	0.07	- ve	Bottom RH	
36	0.81	0.79	0.14	- ve	Bottom RH	
36	0.81	2.64	1.57	+ ve	Top RH	
37	0.83	2.43	1.79	+ ve	Top RH	
37	0.83	0.50	0.14	- ve	Bottom RH	(This vortex then goes over th (top and a new vortex begins (to form at Top LH)
38	0.85	Vortex from Bottom RH squashed as it goes over the top.				
38	0.85	2.29	1.93	+ ve	Top RH	
39	0.88	2.00	2.07	+ ve	Top RH	
39	0.88	- 0.29	0.43	- ve	Top LH	
40	0.90	- 0.43	0.43	- ve	Top LH	
40	0.90	1.64	2.14	+ ve	Top RH	
41	0.92	1.36	2.36	+ ve	Top RH	
41	0.92	- 0.50	0.21	- ve	Top LH	
42	0.95	- 0.71	0.50	- ve	Top LH	
42	0.95	1.07	2.43	+ ve	Top RH	
43	0.97	0.64	2.50	+ ve	Top RH	
43	0.97	- 1.00	0.57	- ve	Top LH	

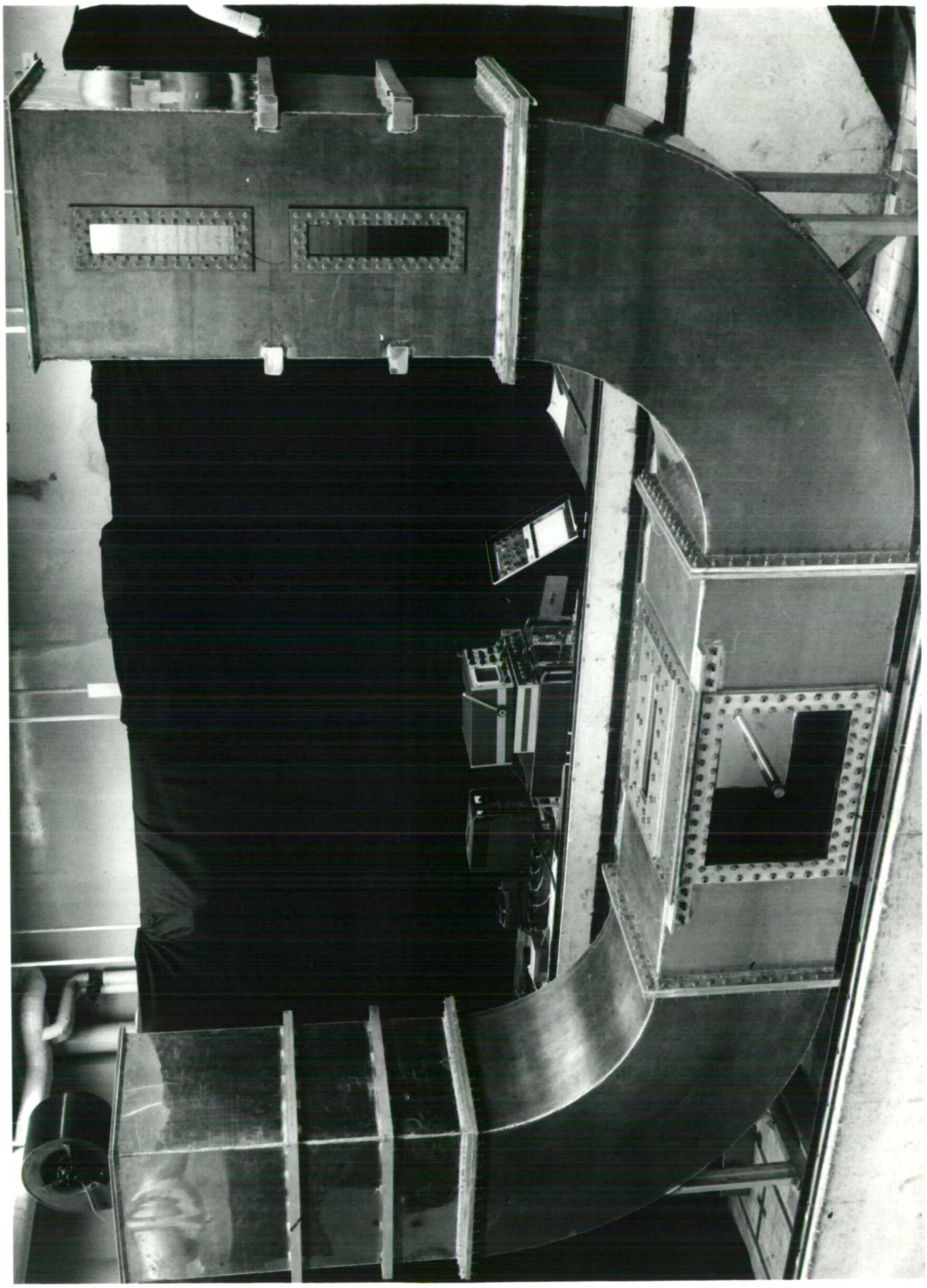

THE U-TUBE WATER TANK

PLATE : 1

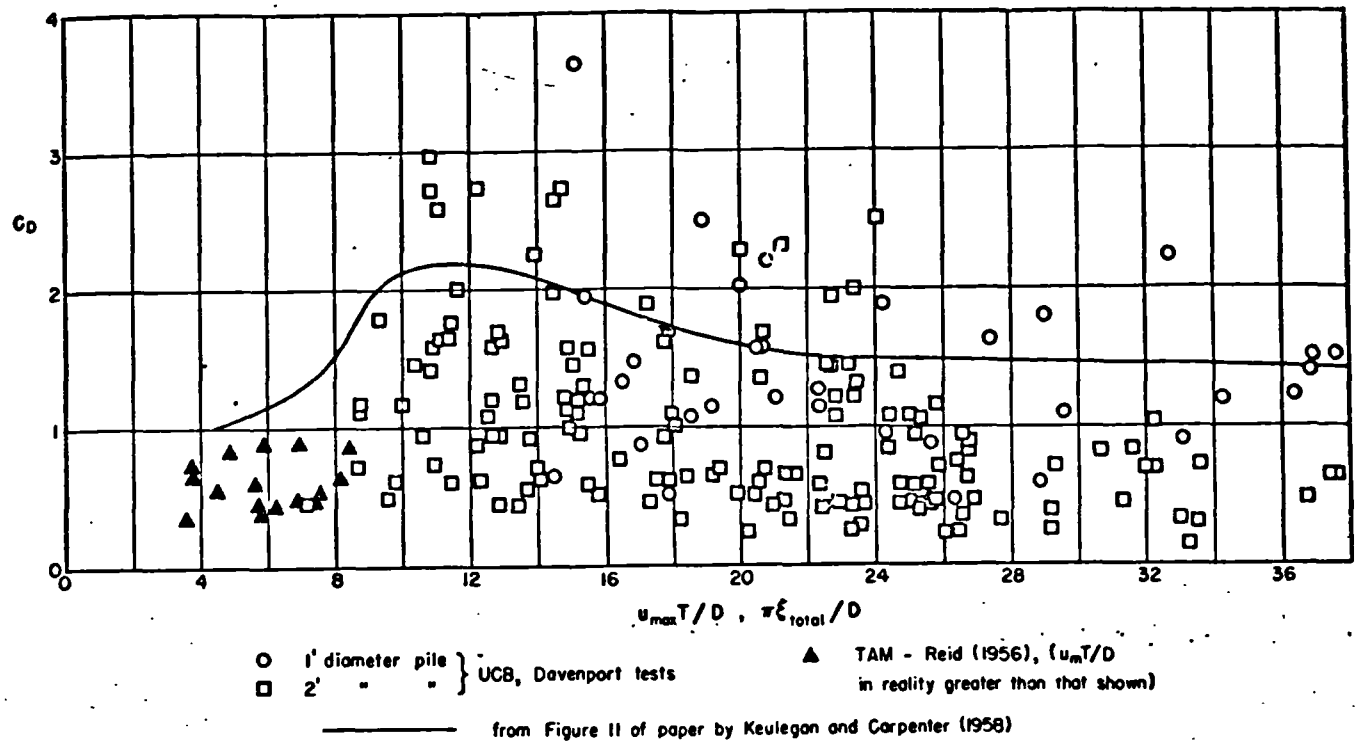

Fig. 1/a Comparison of C_D with the Keulegan-Carpenter modulus

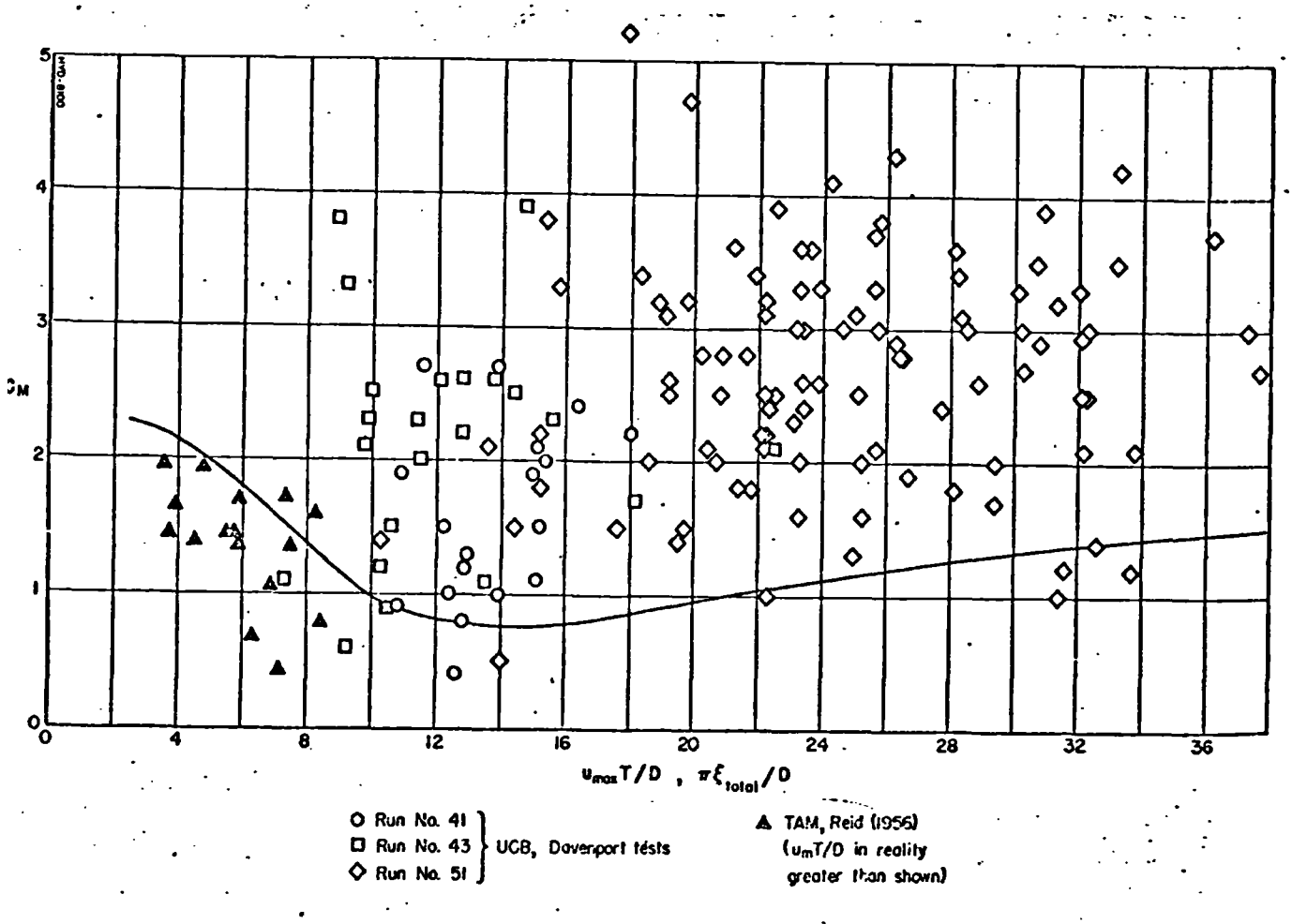

Fig. 1/b Comparison of C_M with the Keulegan-Carpenter modulus

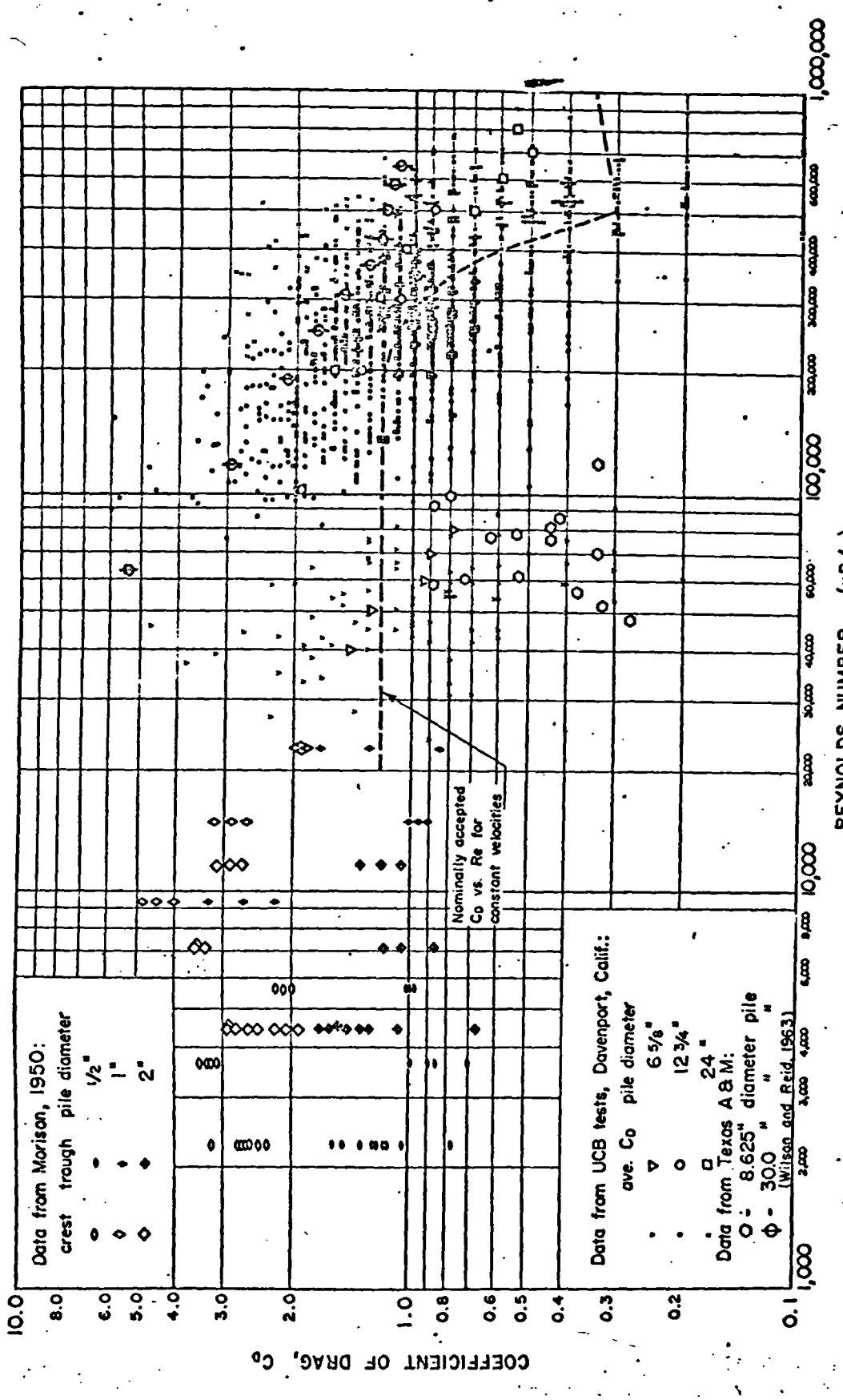

Fig. 12. Coefficient of drag for circular cylindrical piles of various diameters (from Wiegel, Beebe, and Moon, 1957)

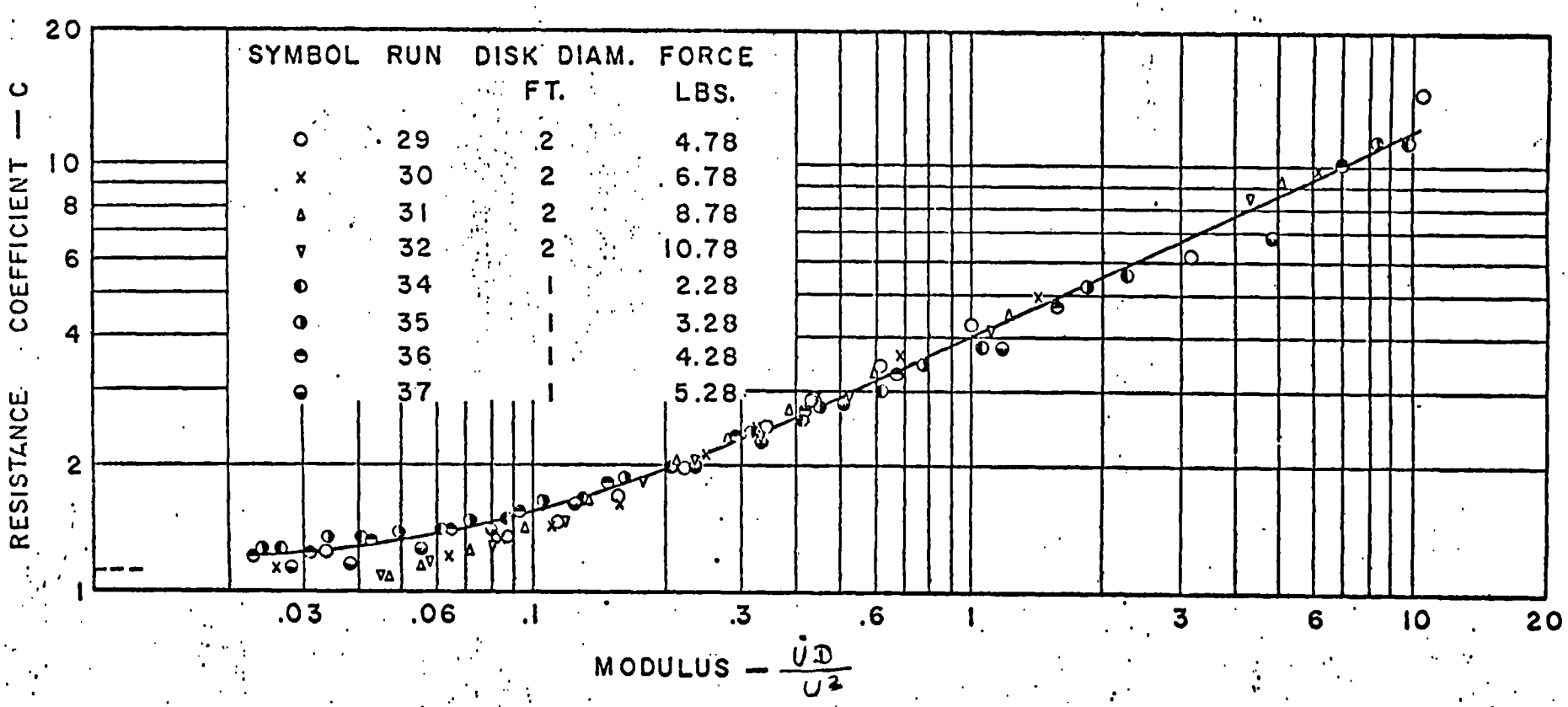

FIGURE 1-3 "C" vs. $\frac{\dot{U}D}{U^2}$ FOR DISKS AS MEASURED BY IVERSEN

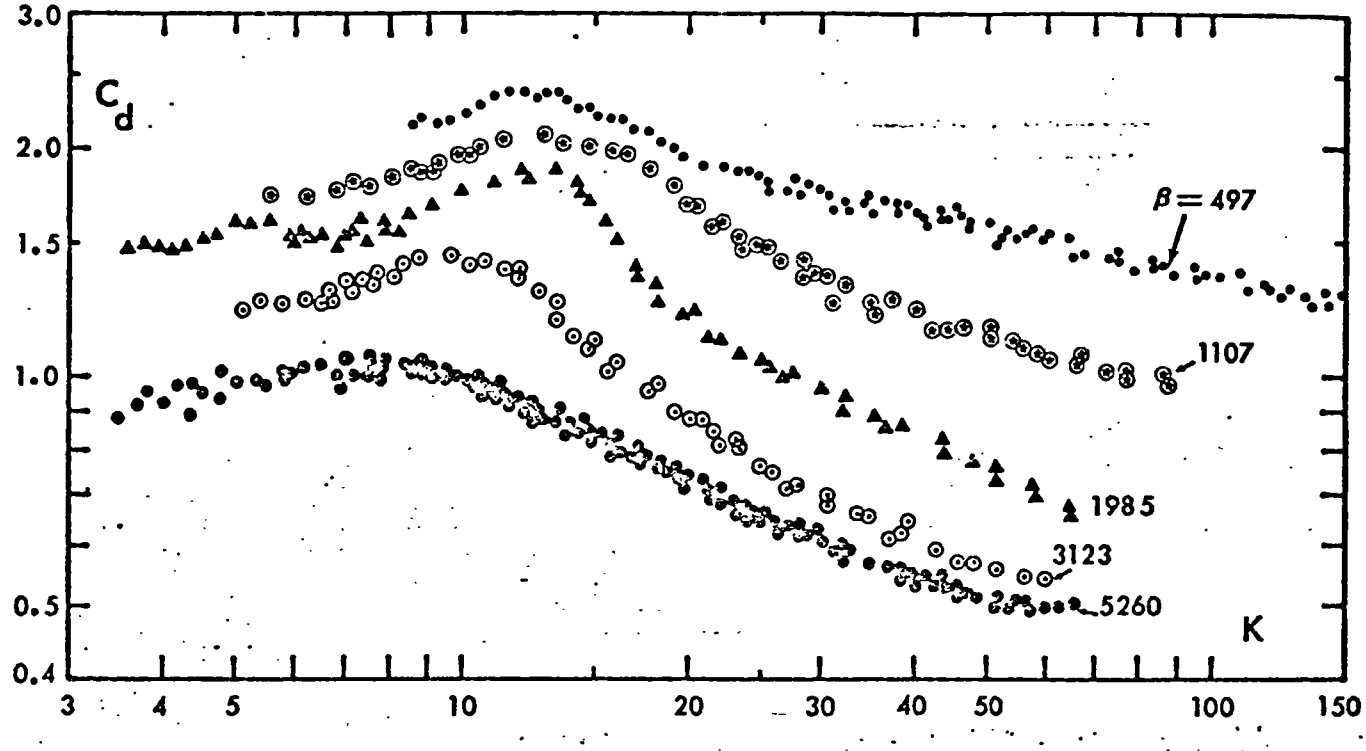

Fig.1.4a C_d versus K for various values of β, (Sarpkaya's Data)

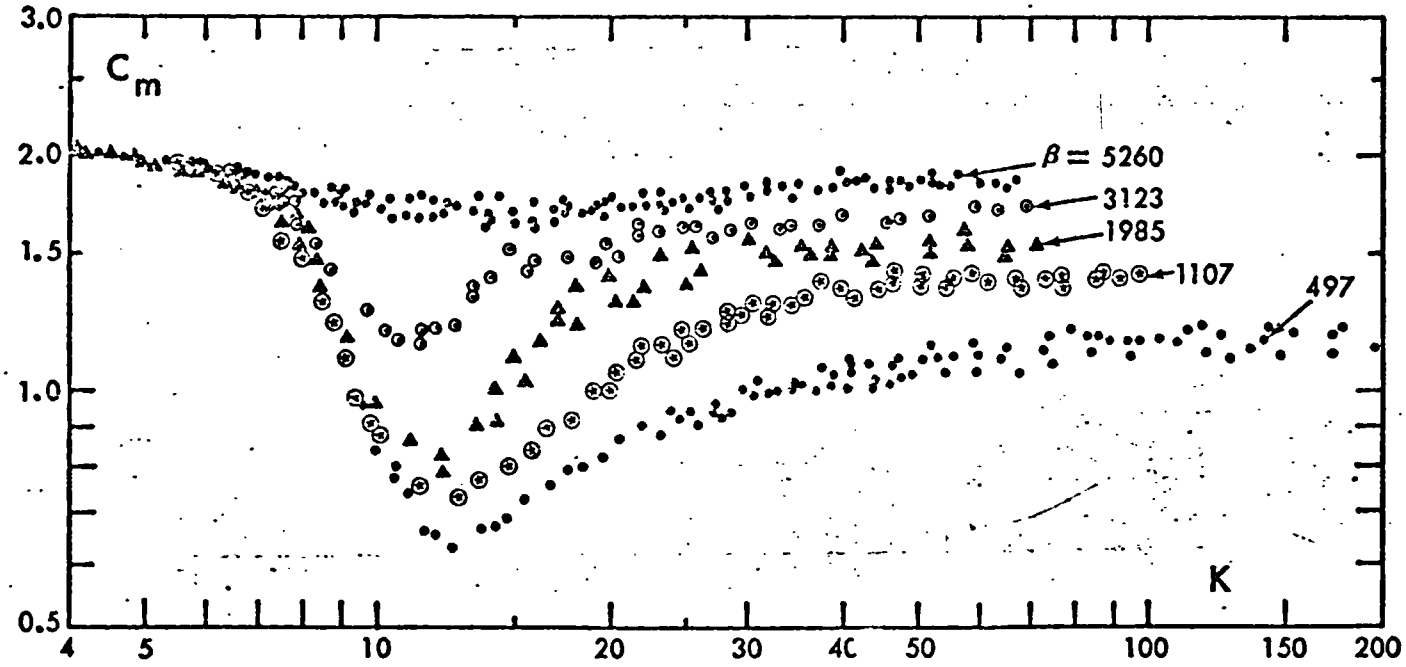

Fig 1.4b C_m versus K for various values of β, (Sarpkaya's Data)

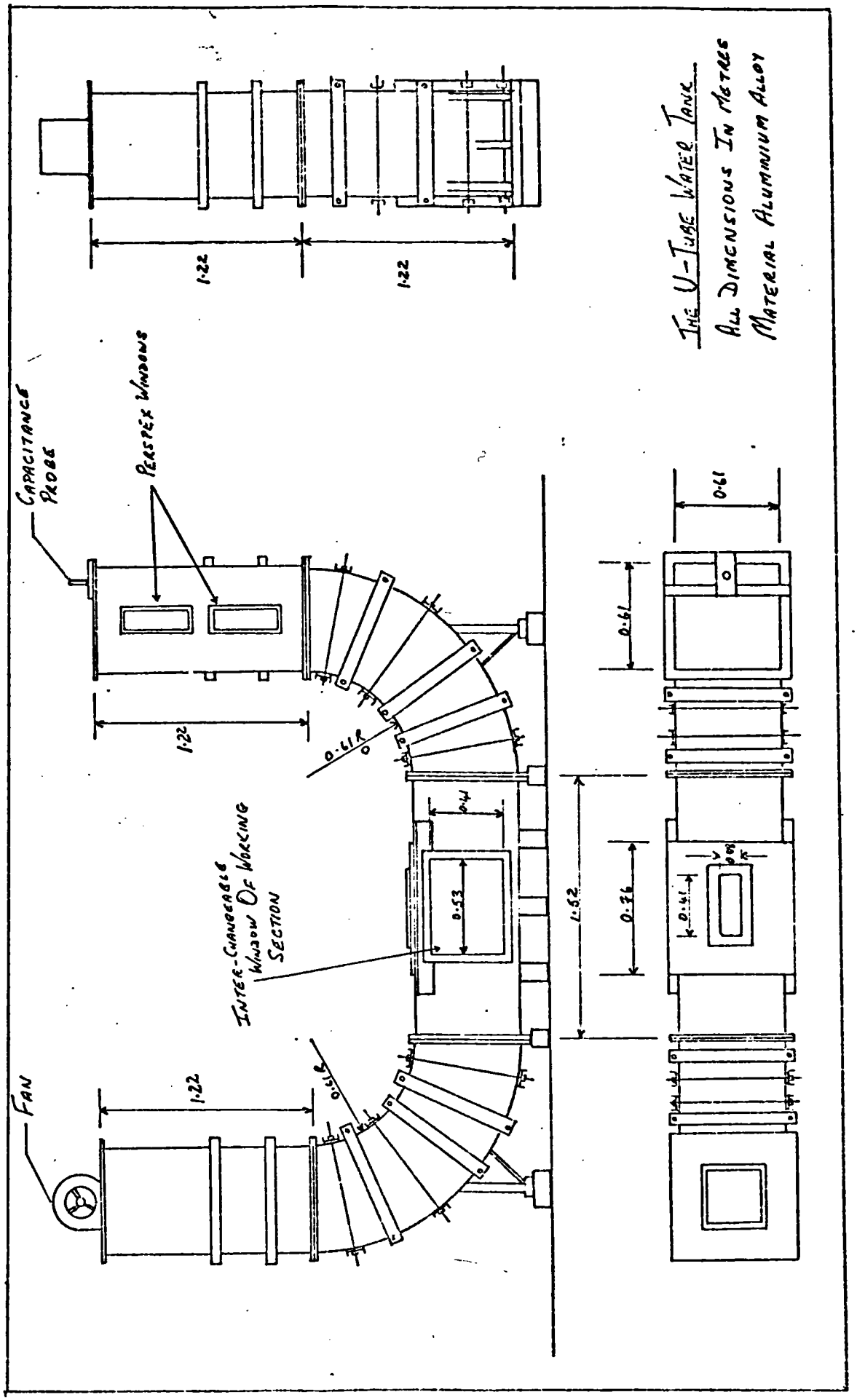
THE U-TUBE WATER TANK
ALL DIMENSIONS IN METRES
MATERIAL ALUMINIUM ALLOY
CAPACITANCE PROBE
PERSPEX WINDOWS
FAN
INTER-CHANGEABLE WINDOW OF WORKING SECTION
1.22
1.22
1.22
0.61R
0.61
0.61
0.41
0.53
1.52
0.76
0.41
0.08R

FIG : 2·1

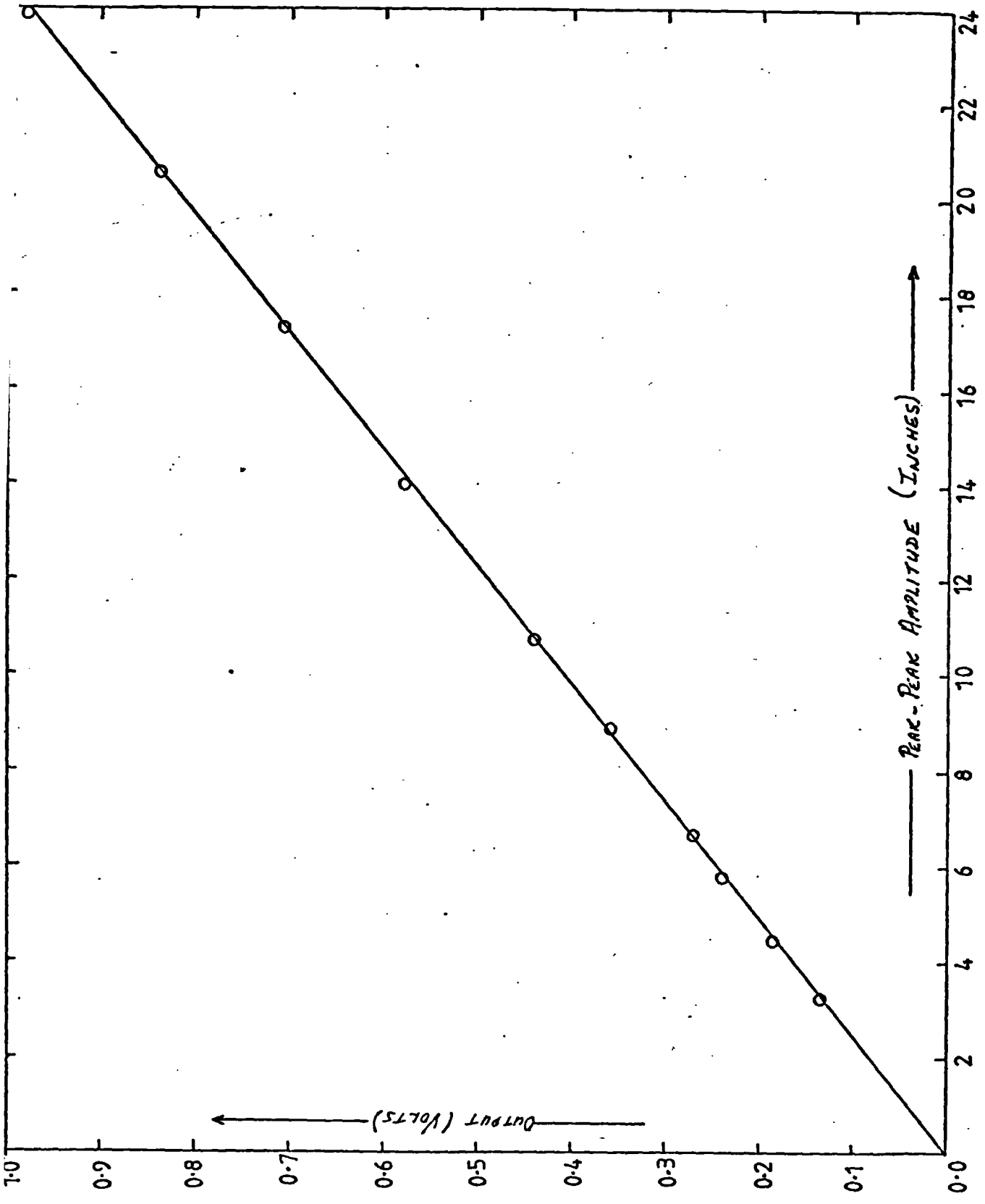

FIG: 2·2 STATIC CALIBRATION OF CAPACITANCE PROBE

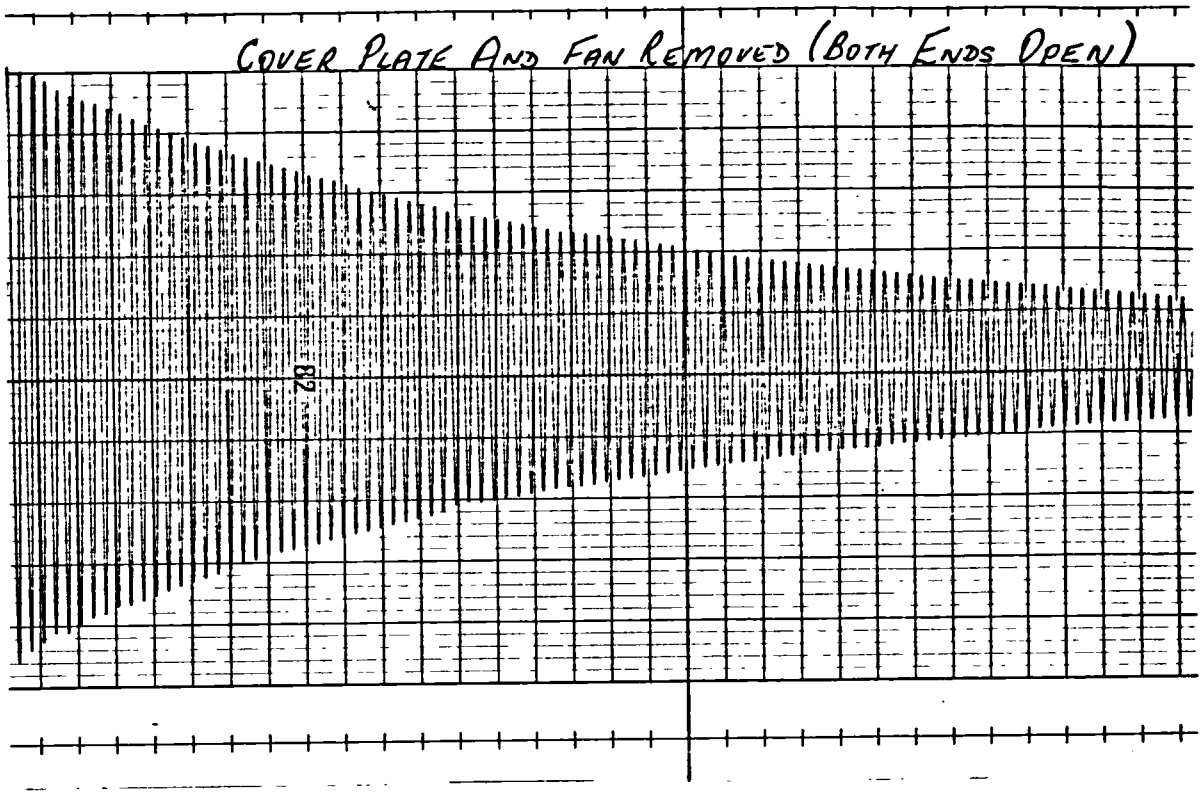

FIG : 2·3(a)

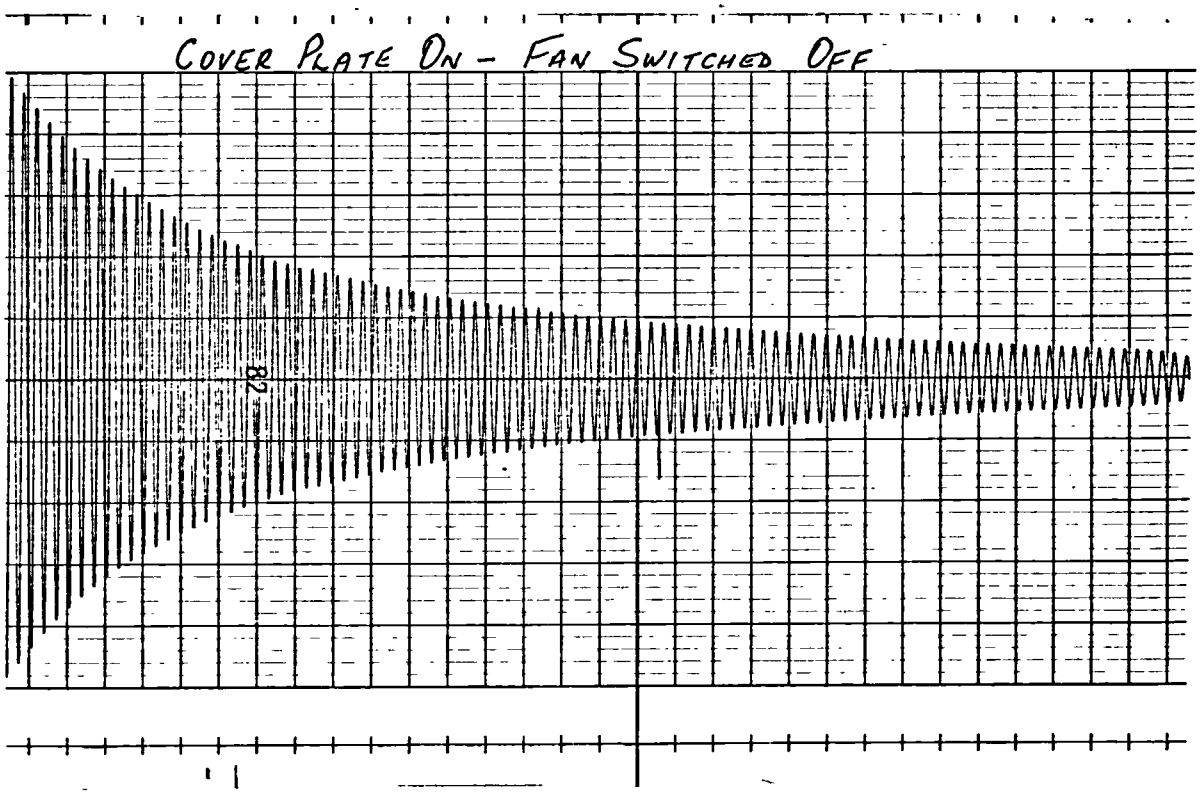

FIG : 2·3(b)

DAMPING OF OSCILLATIONS - WITH AND WITHOUT COVER PLATE

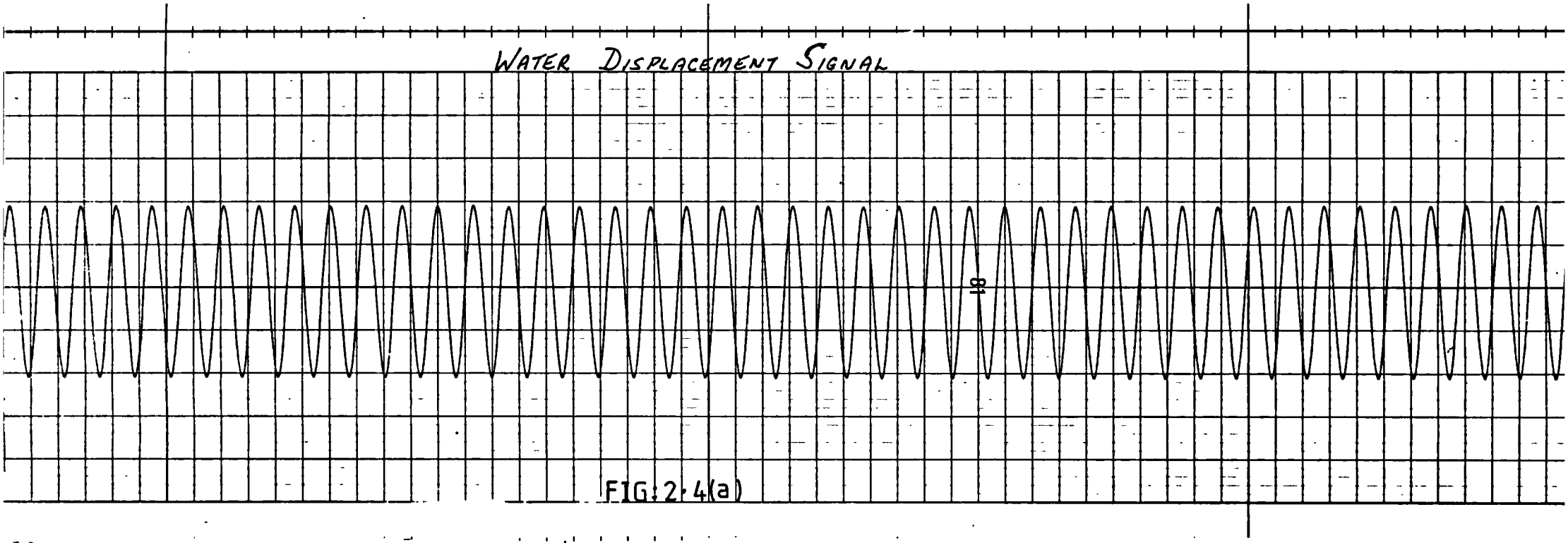

FIG: 2·4(a)

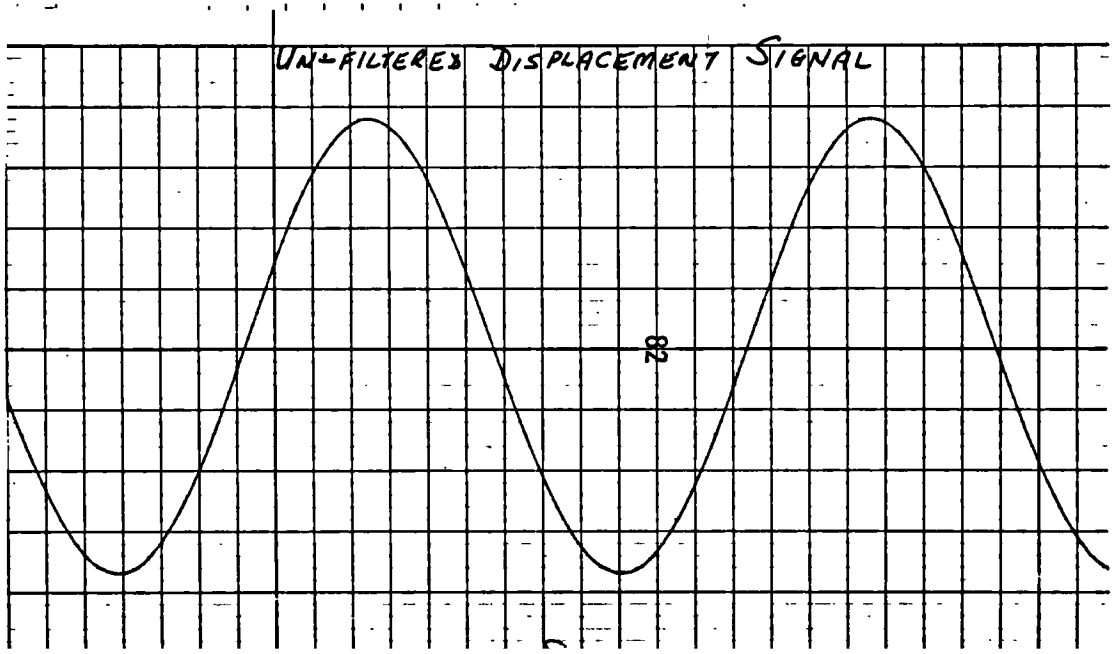

FIG:2·4(b)

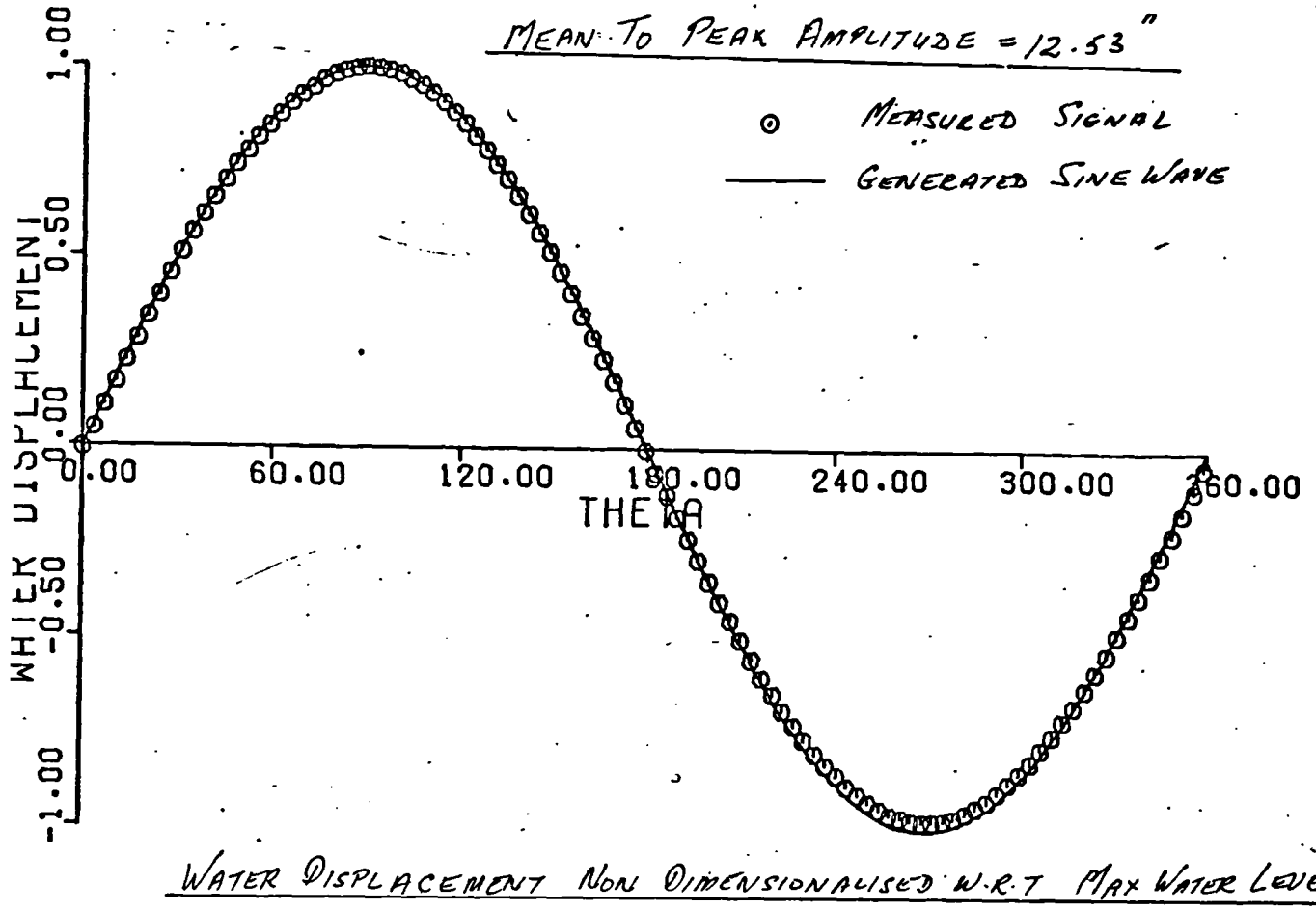

WATER DISPLACEMENT NON DIMENSIONALISED W.R.T MAX WATER LEVEL

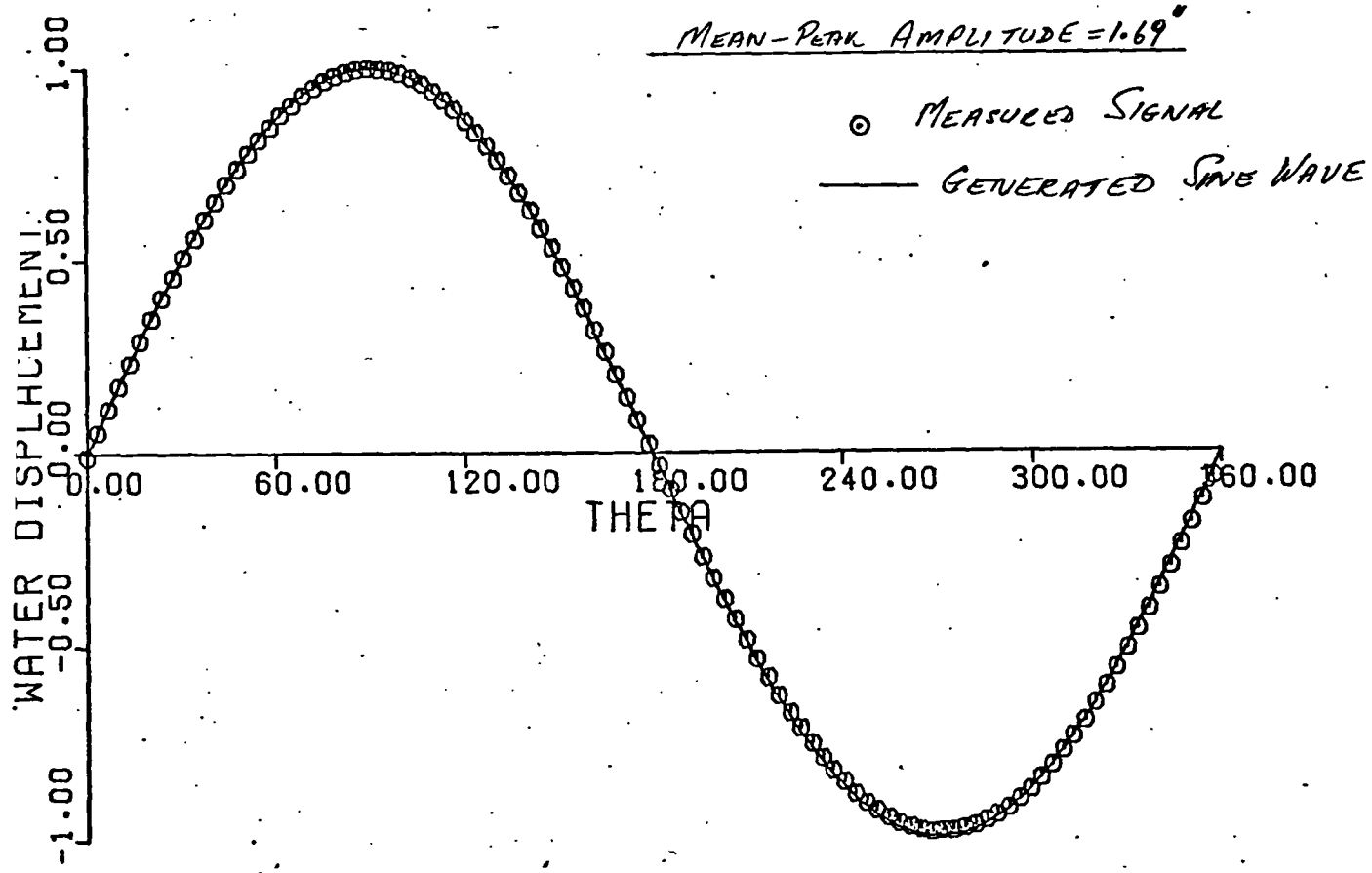

FIG: 2.5

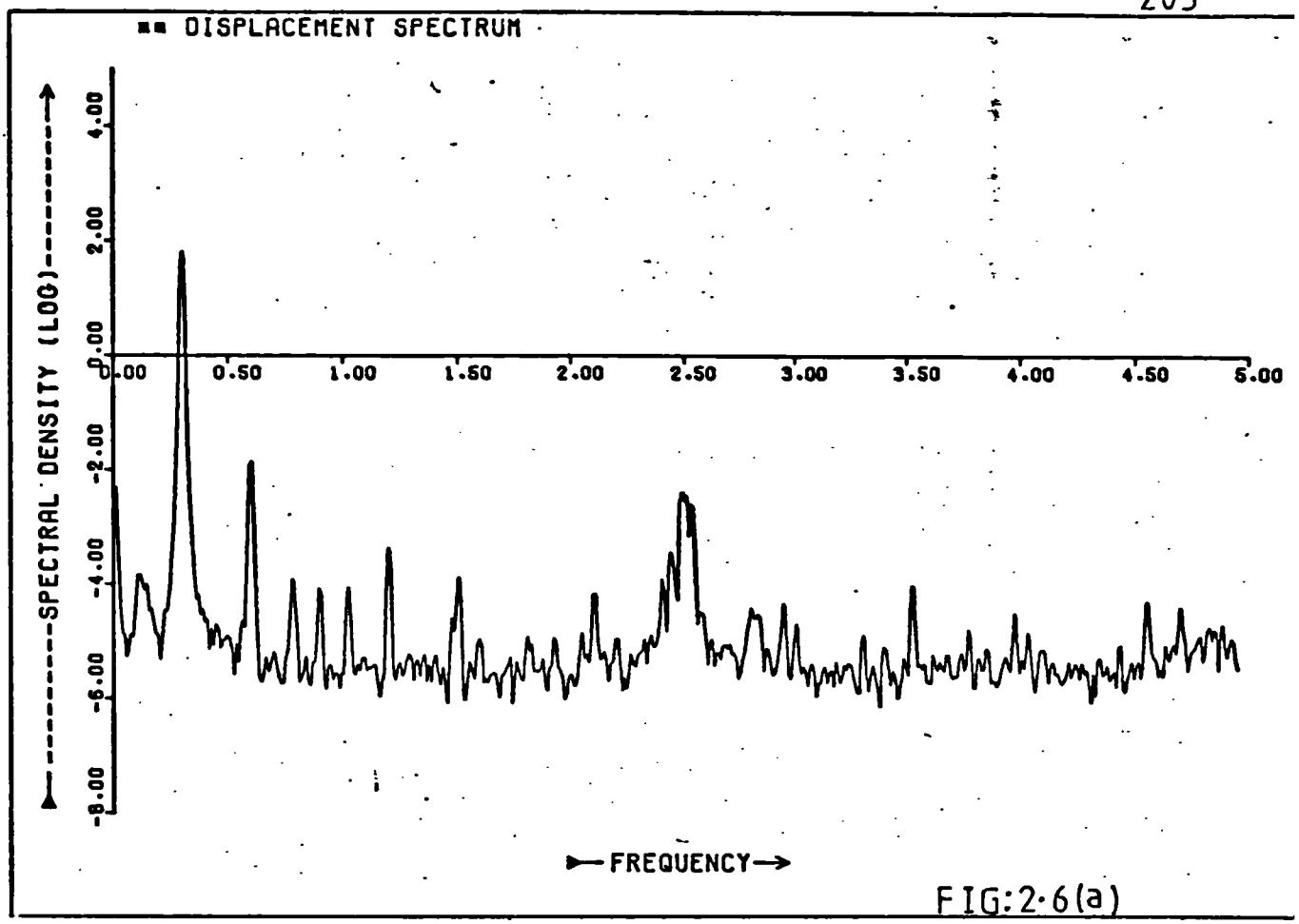

FIG:2·6(a)

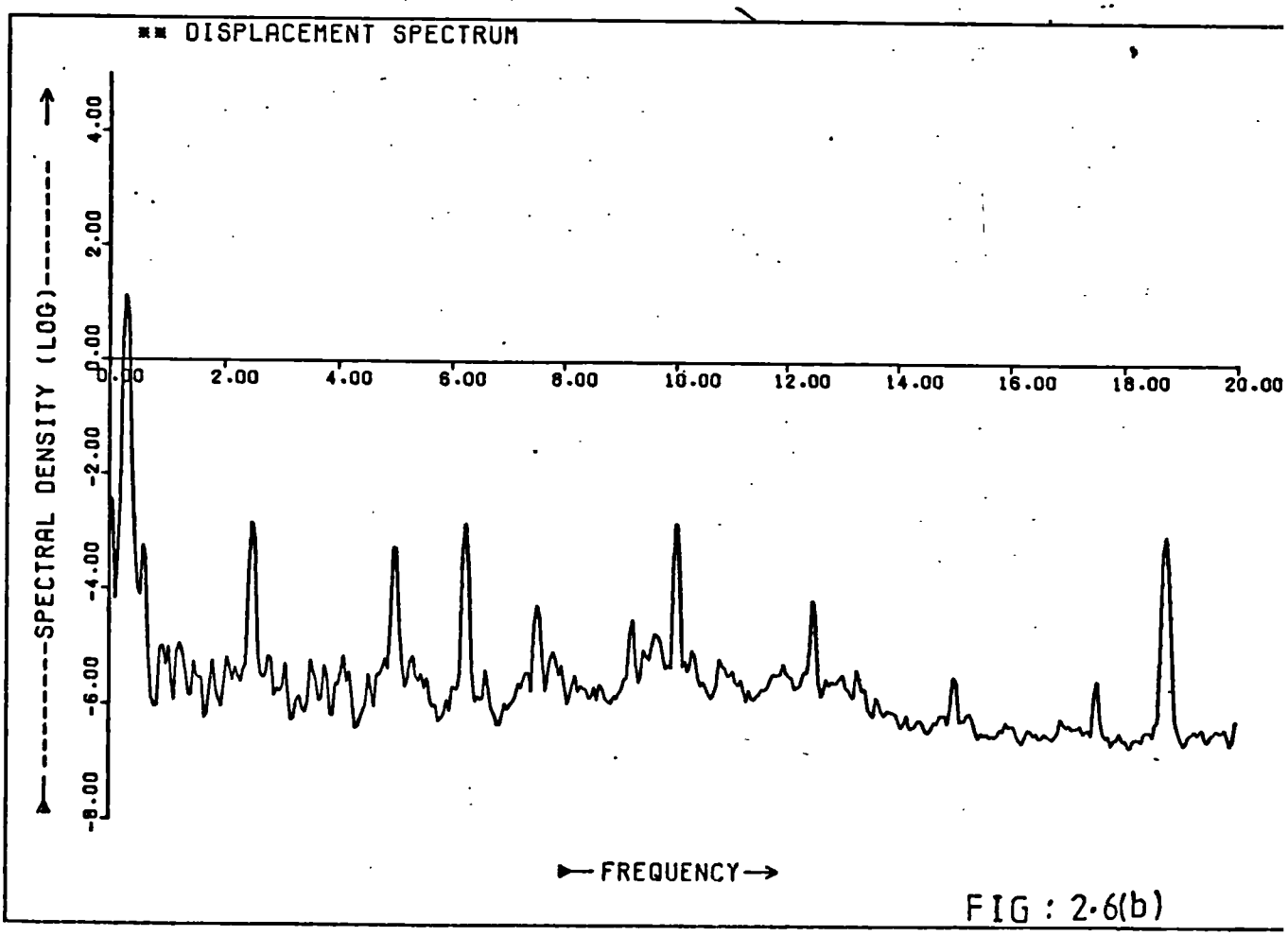

FIG : 2·6(b)

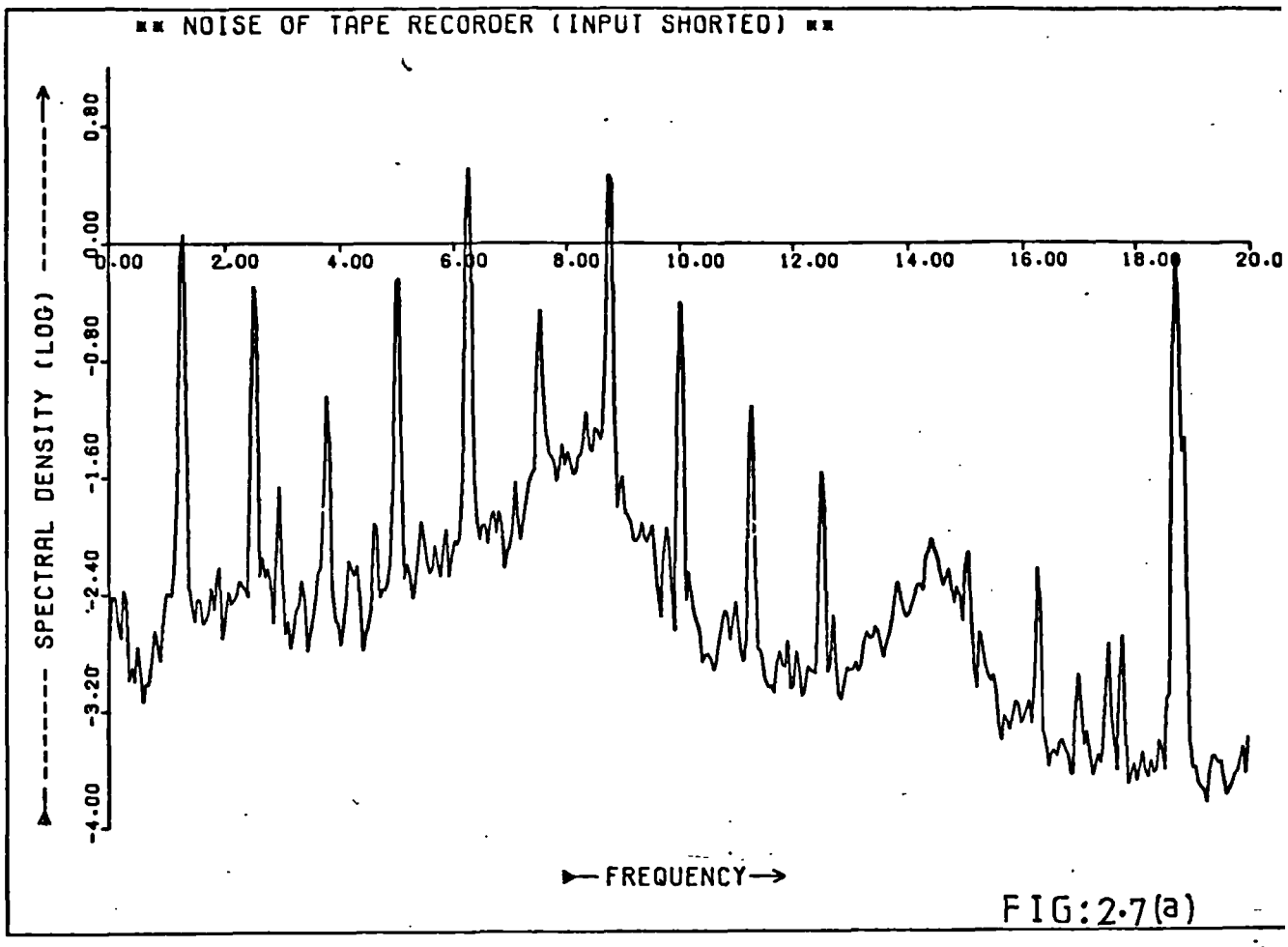

FIG: 2·7(a)

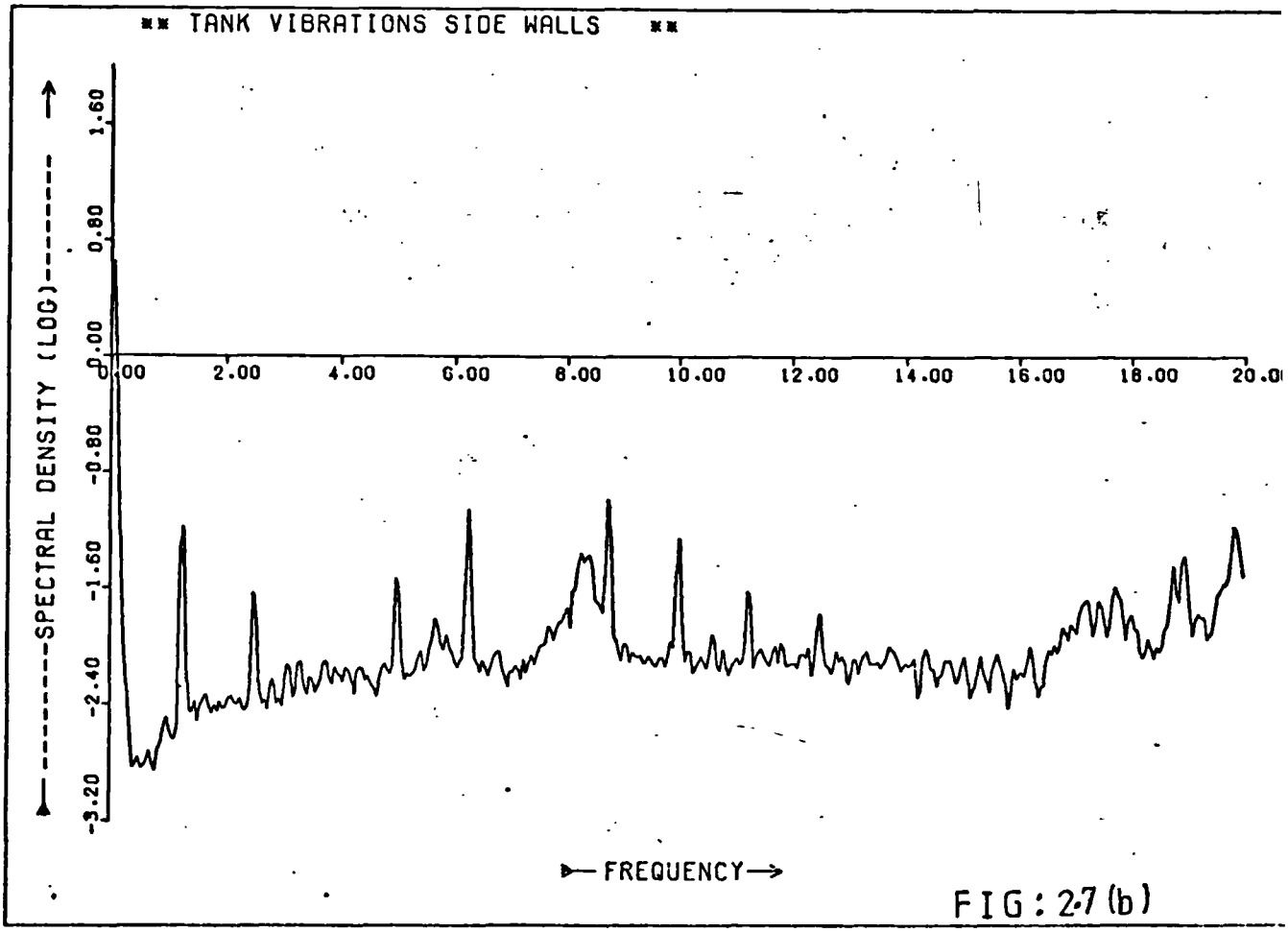

FIG: 2·7 (b)

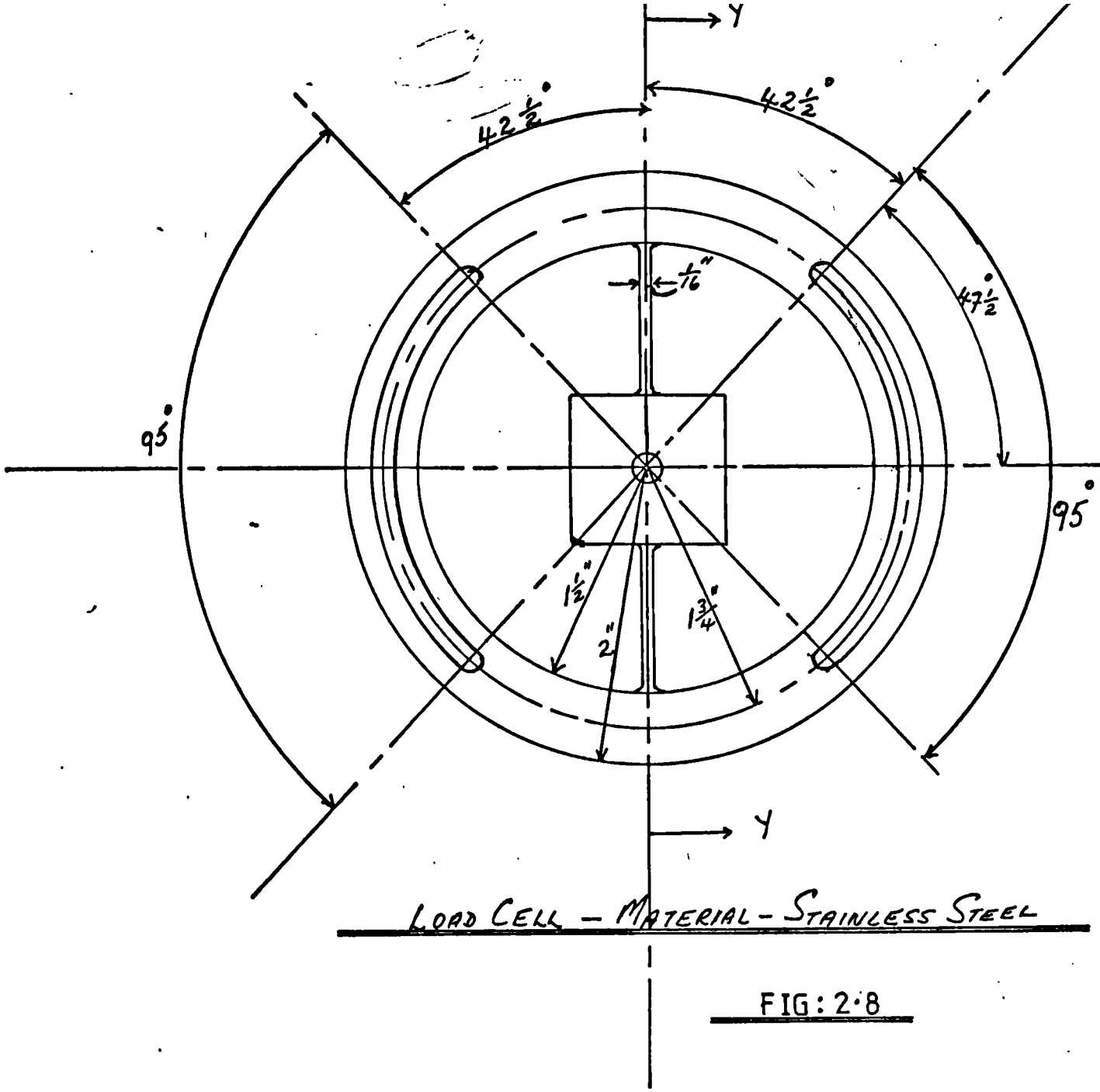

LOAD CELL – MATERIAL – STAINLESS STEEL

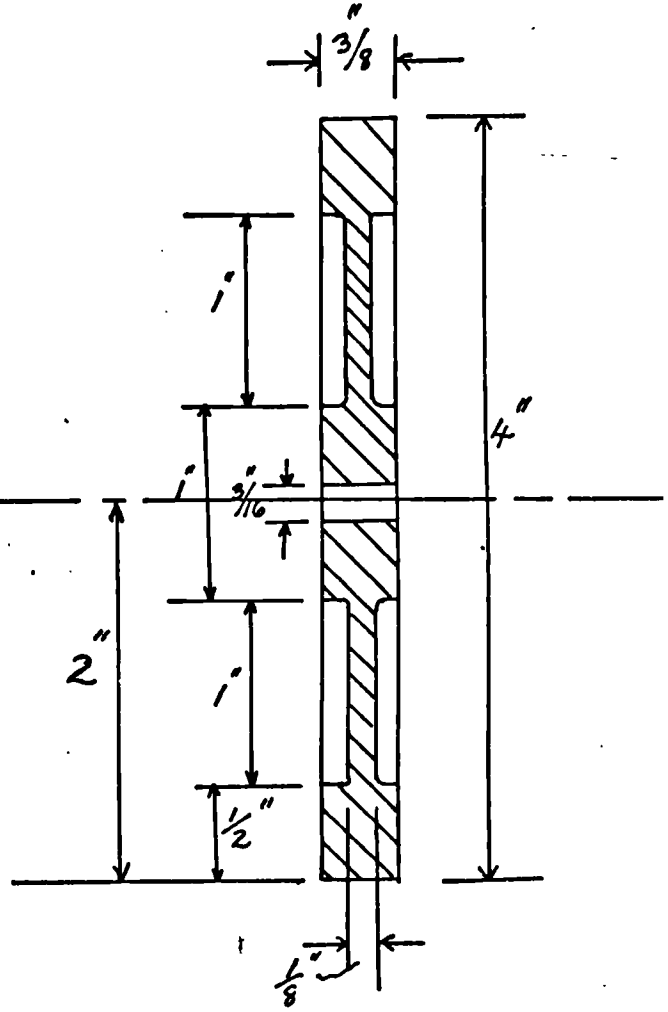

SECTION THROUGH Y-Y

FIG: 2·8

SKETCH SHOWING LOAD CELL AND FREE END OF TEST SECTION
AS USED WHEN MEASURING FORCES

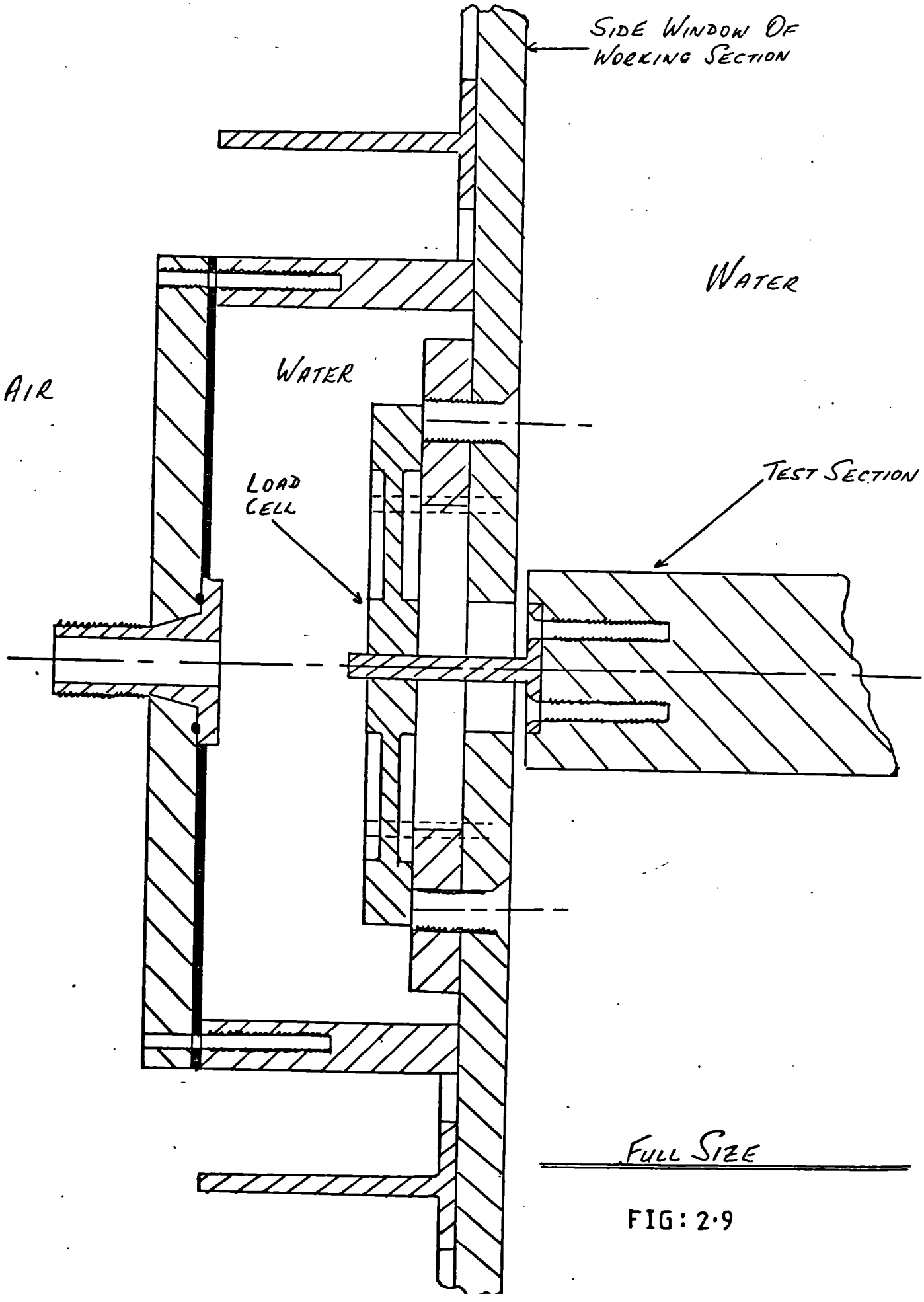

FULL SIZE

FIG: 2·9

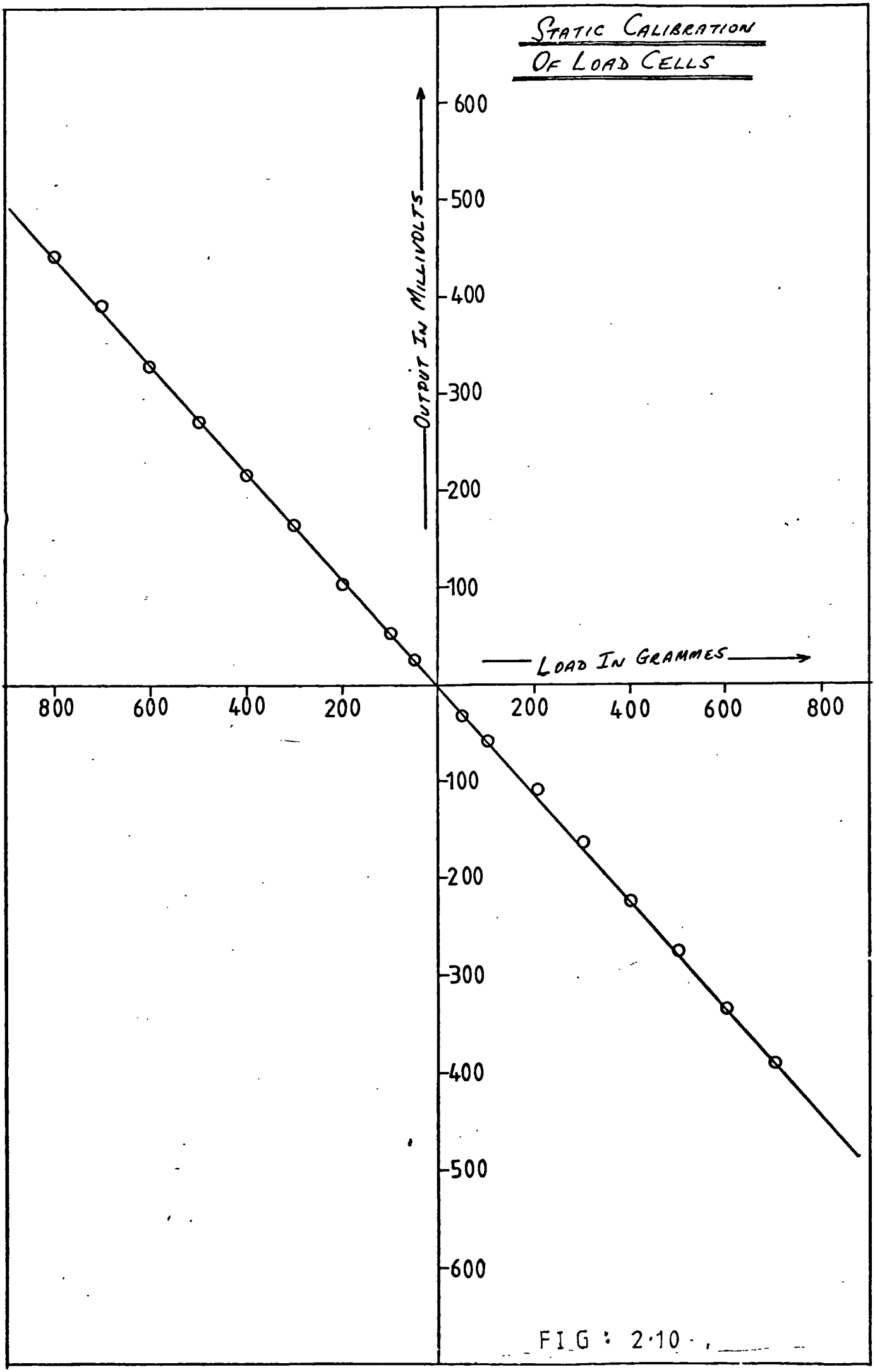
STATIC CALIBRATION
OF LOAD CELLS
OUTPUT IN MILLIVOLTS
600
500
400
300
200
100
LOAD IN GRAMMES
800
600
400
200
200
400
600
800
100
200
300
400
500
600

FIG : 2·10

DYNAMIC RESPONSE OF LOAD CELLS AND MODELS

THE CIRCULAR CYLINDER

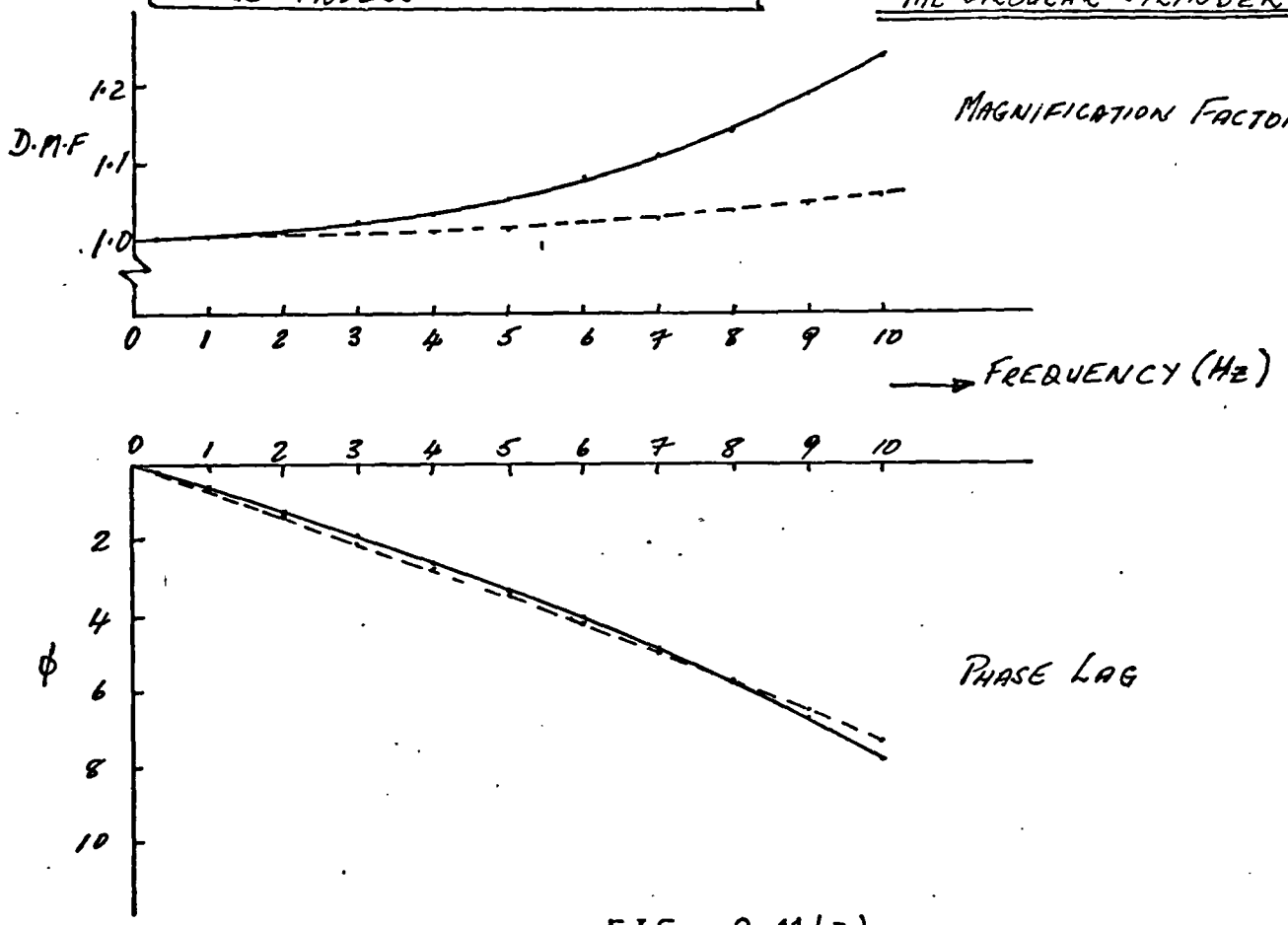

FIG : 2·11(a)

THE 3" DIAMETER FLAT PLATE

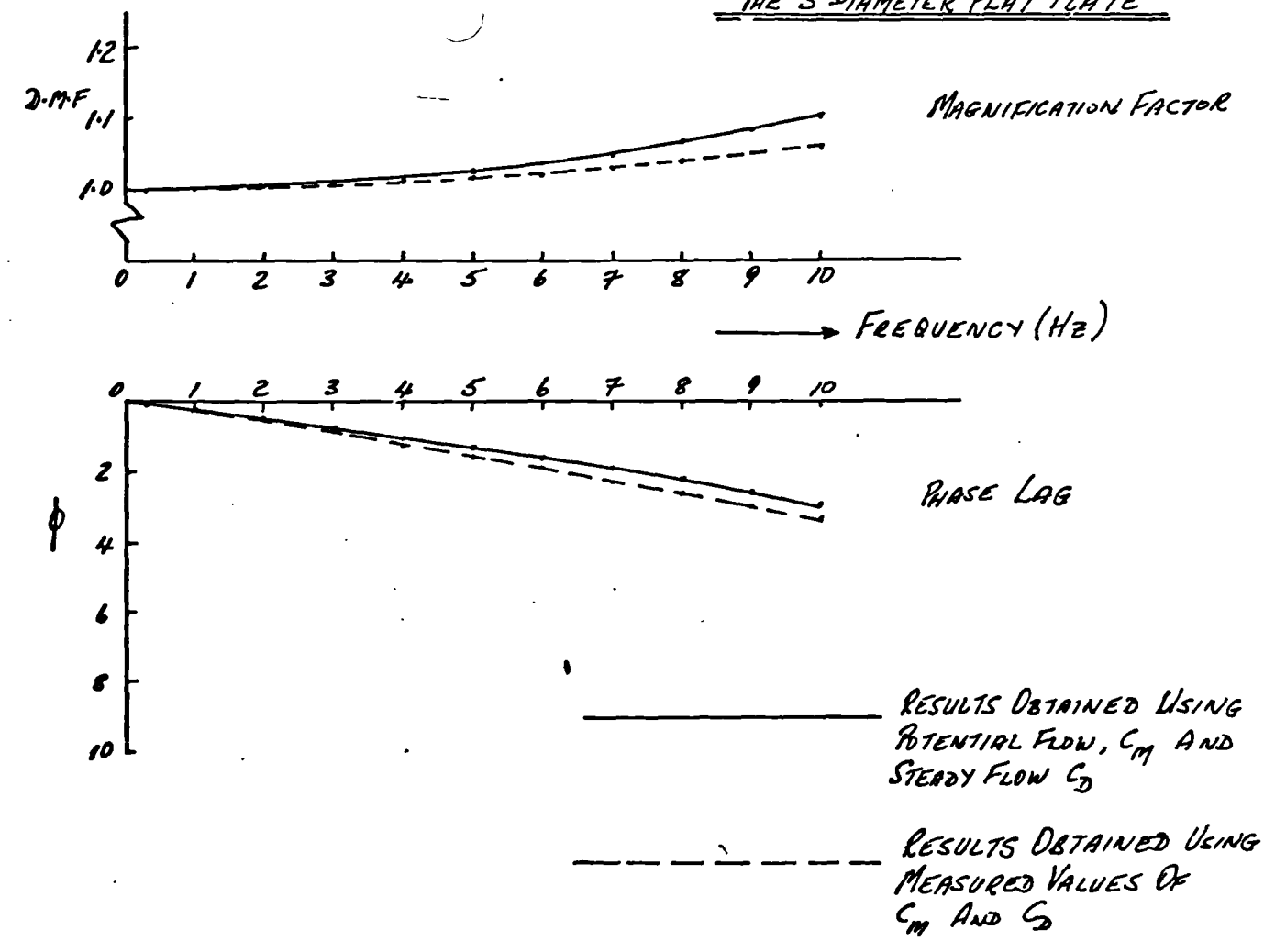

FIG : 2·11(b)

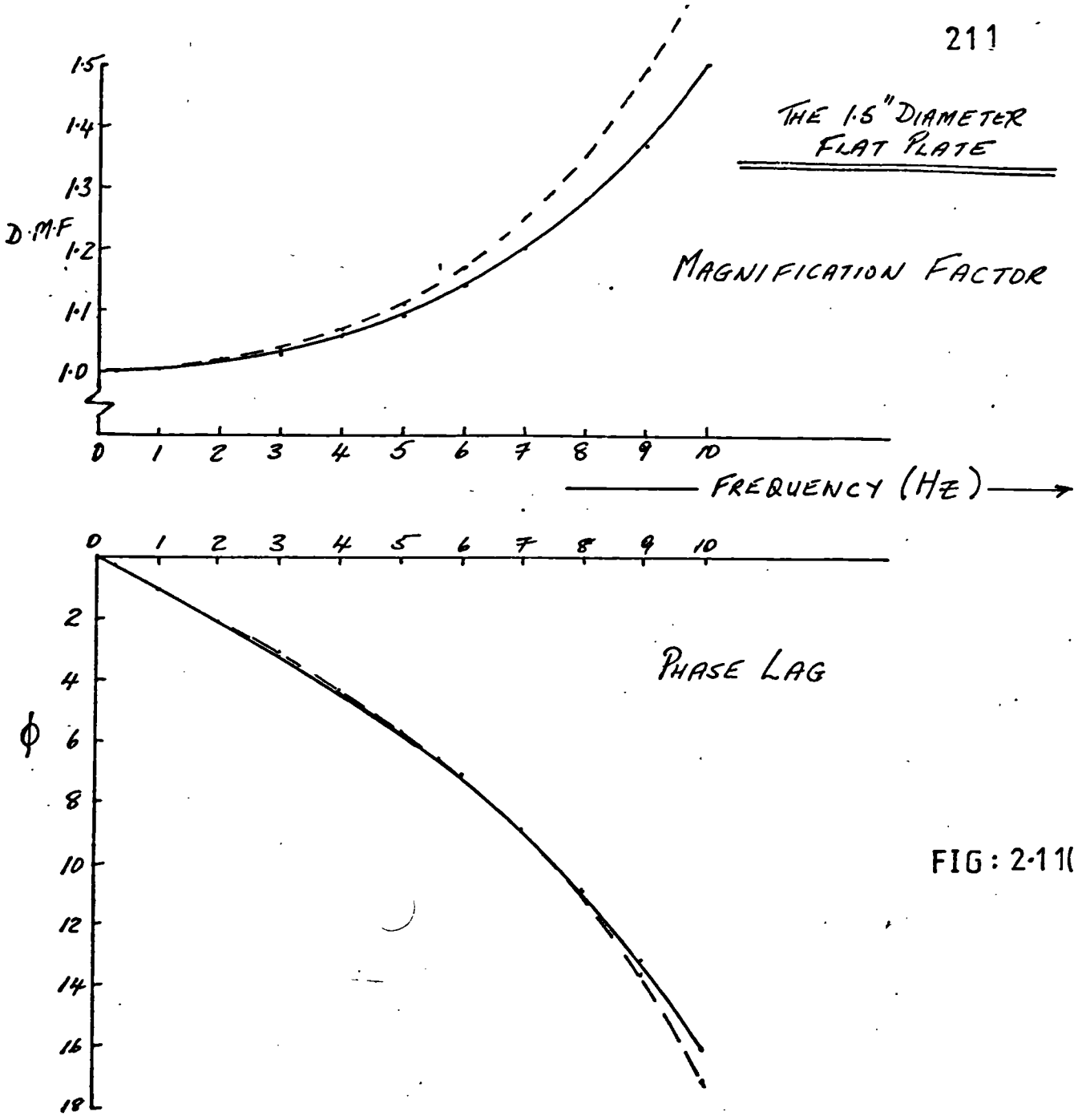

FIG: 2·11(c)

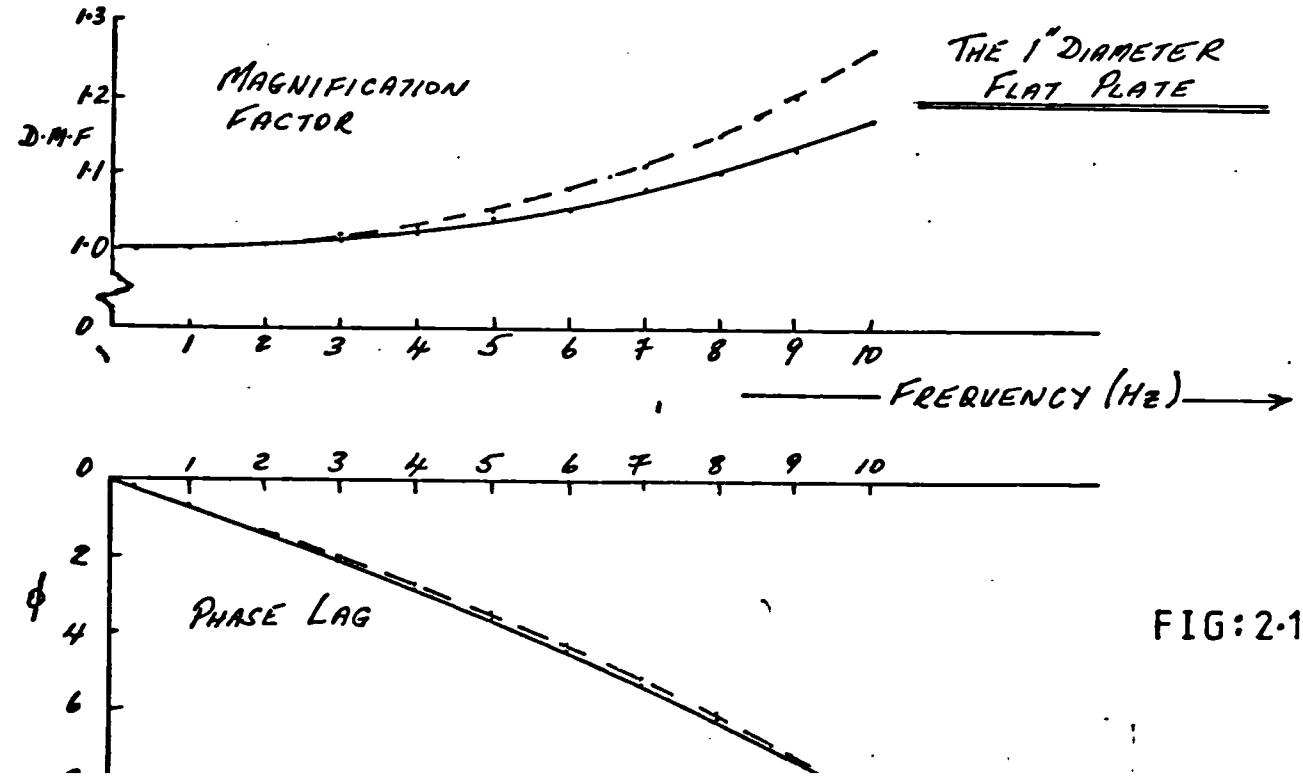

FIG: 2·11(d)

THE SQUARE NORMAL

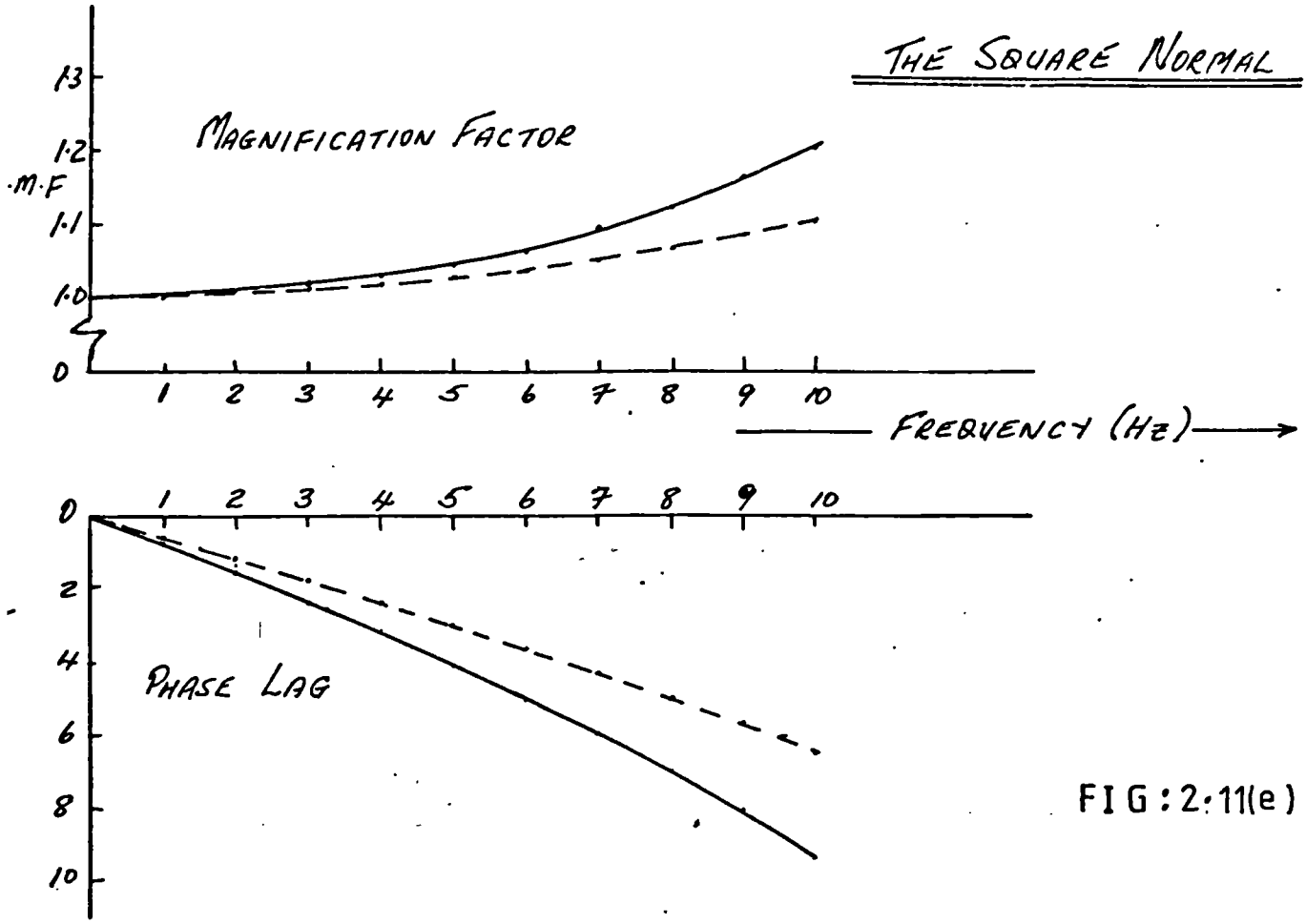

FIG: 2·11(e)

THE DIAMOND SECTION

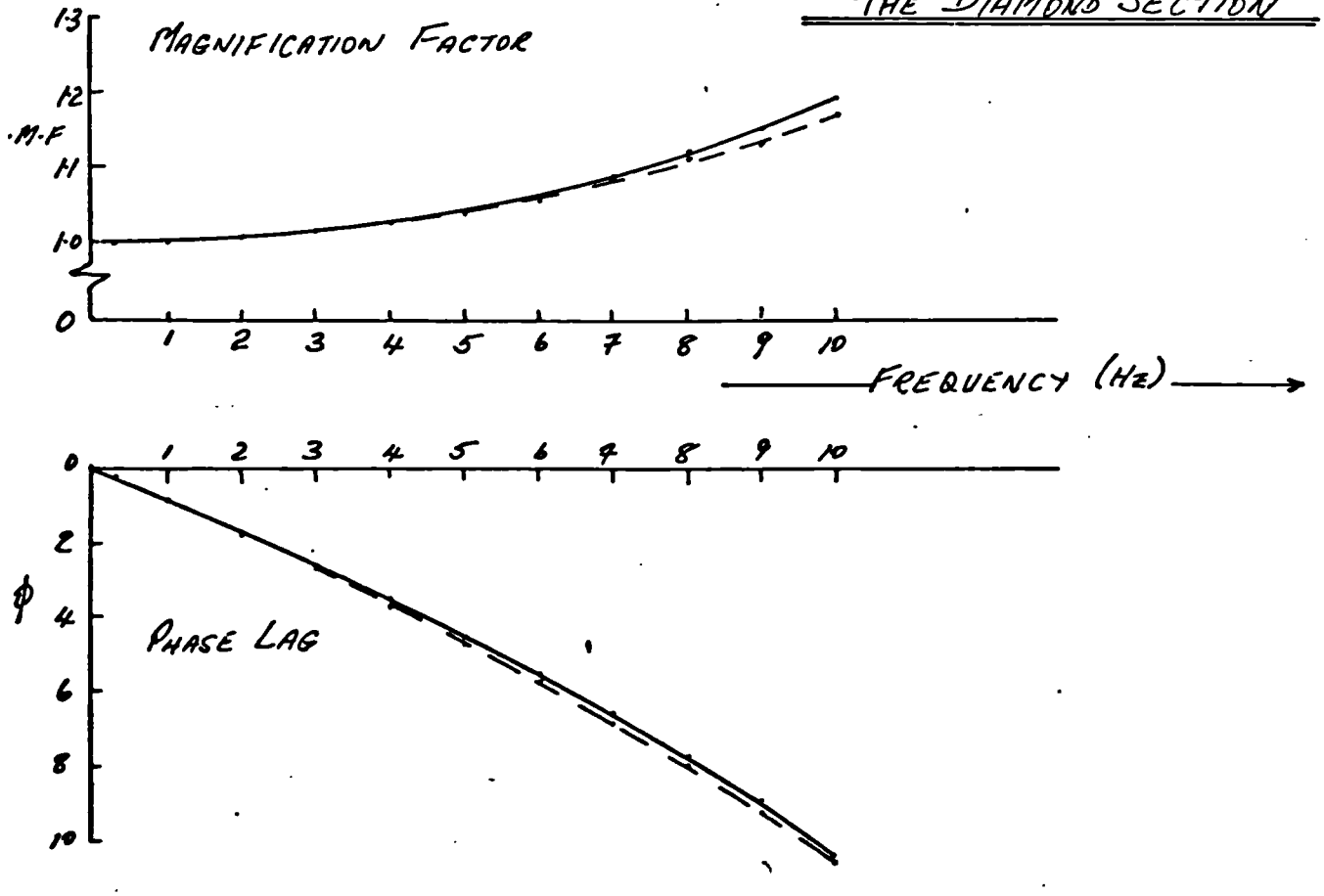

FIG: 2·11(f)

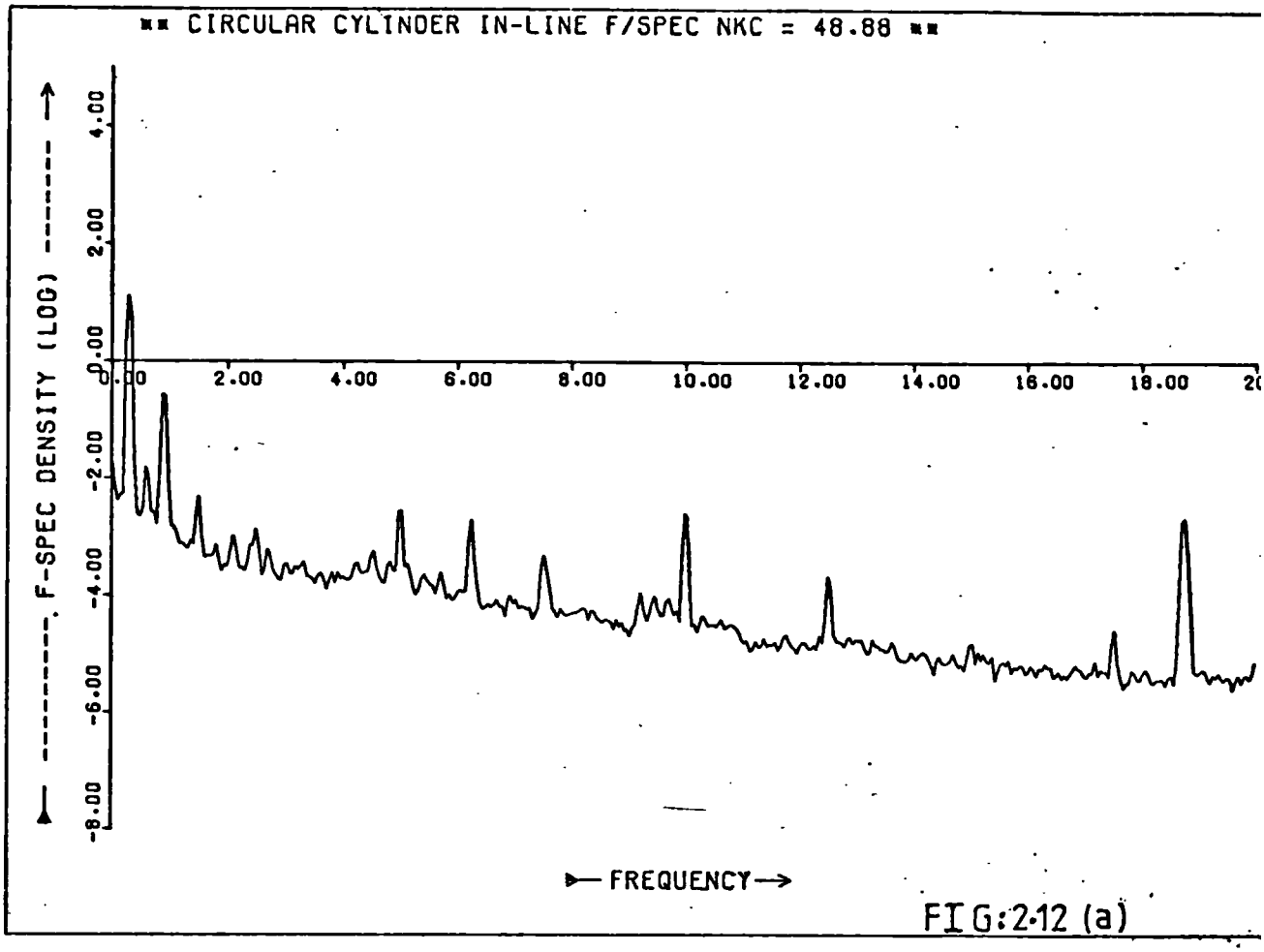

FIG:2·12 (a)

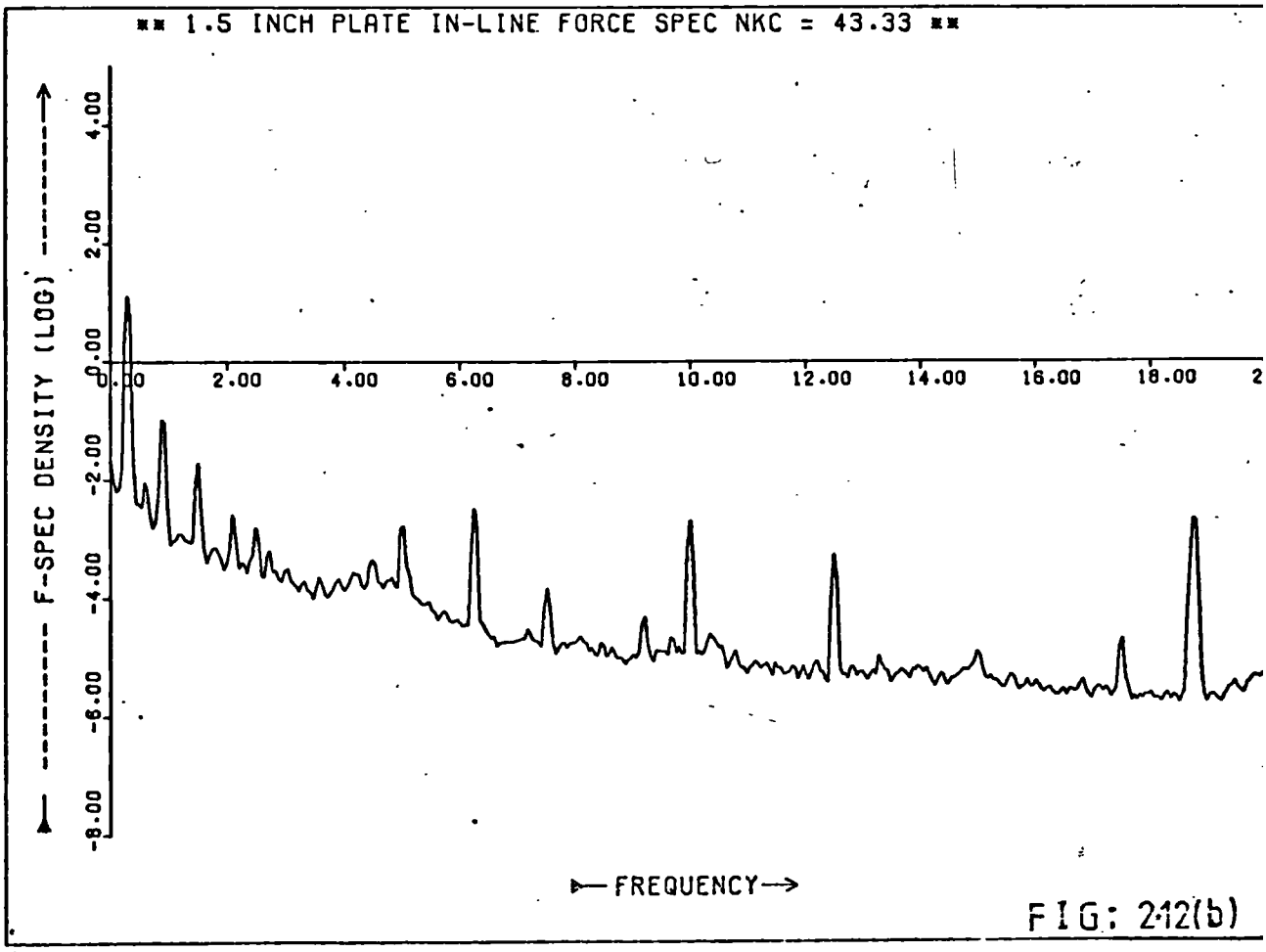

FIG: 2·12(b)

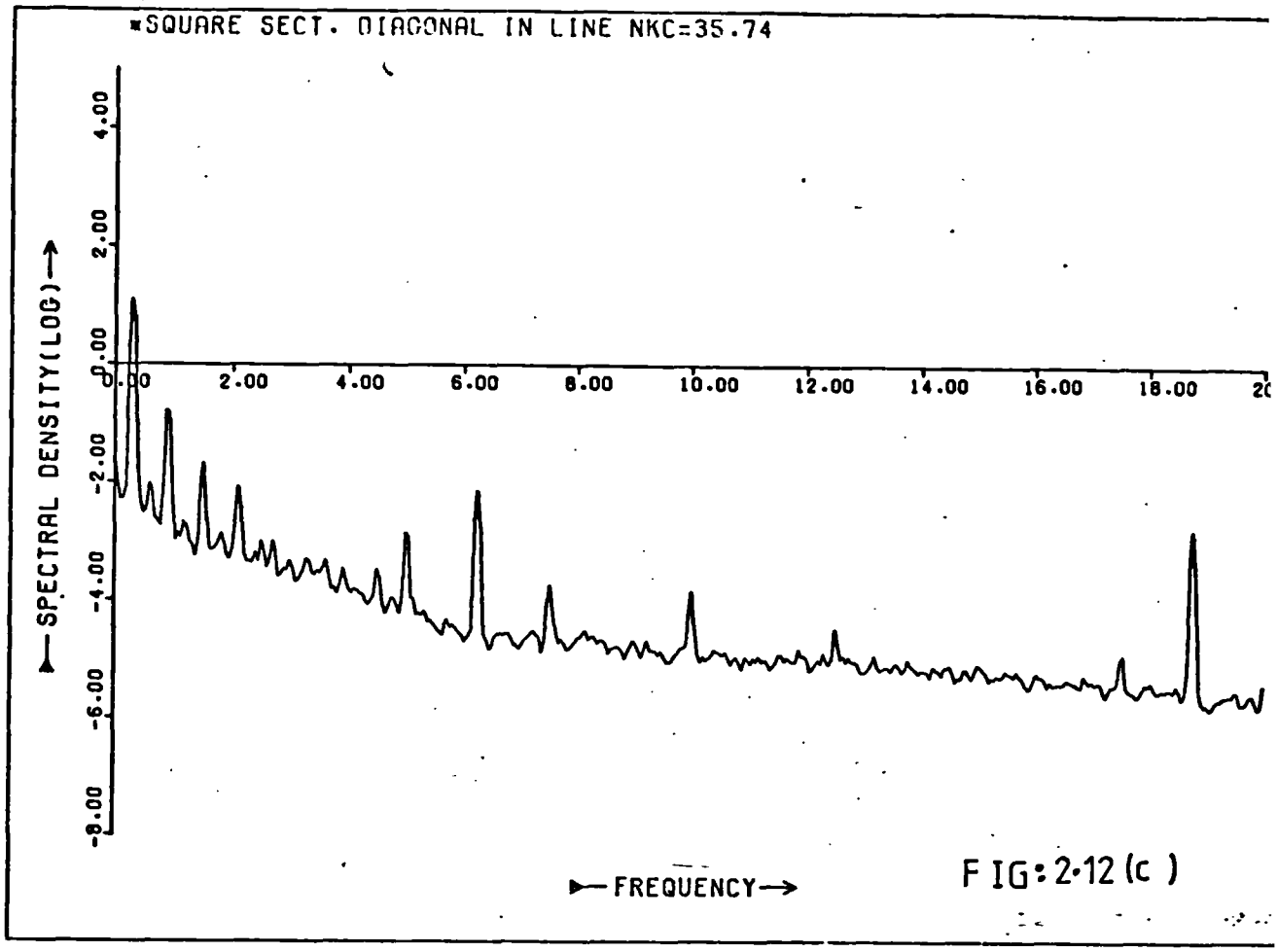

FIG: 2·12 (c)

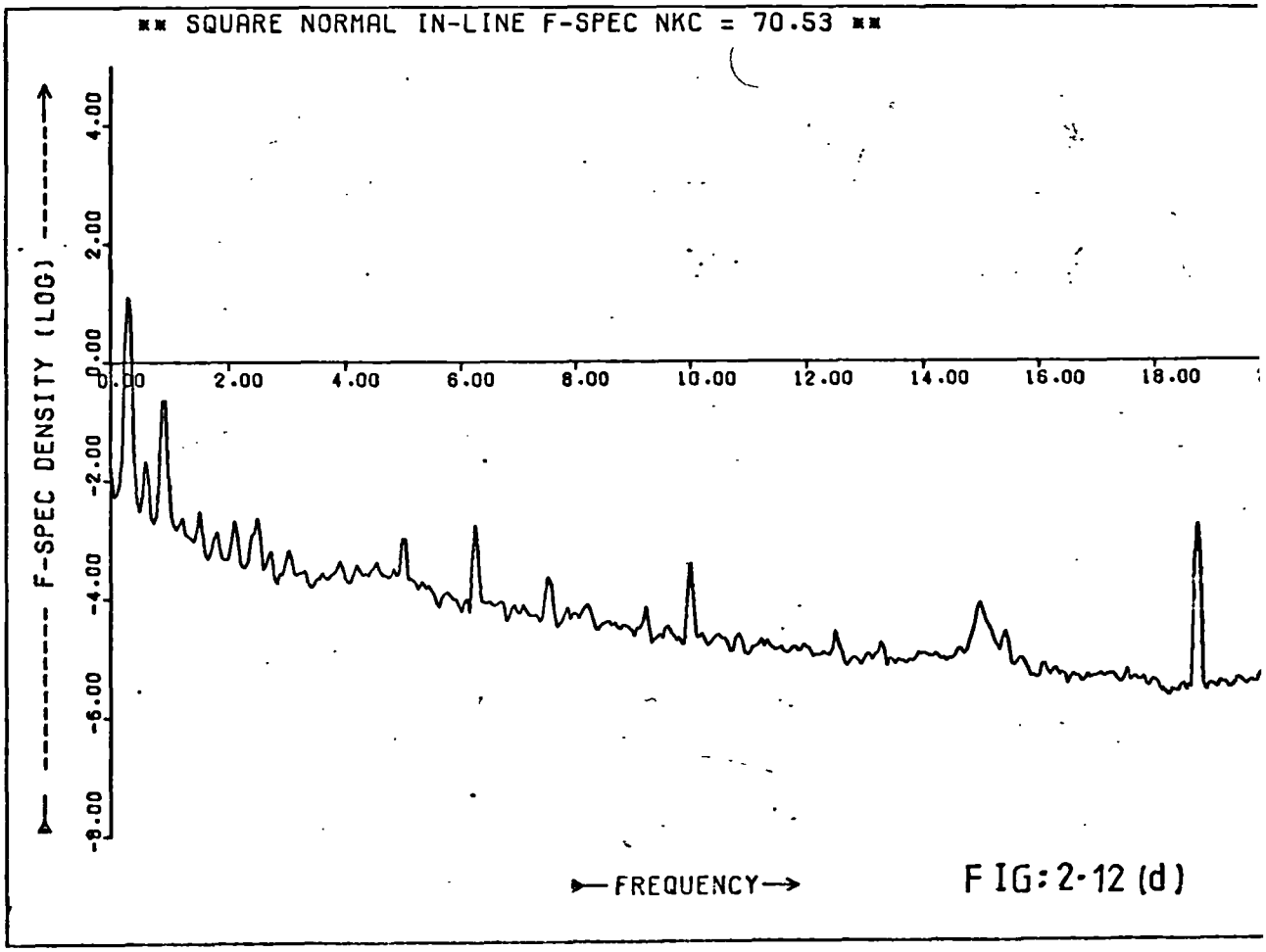

FIG: 2·12 (d)

IN-LINE FORCE AND DISPLACEMENT TRACES

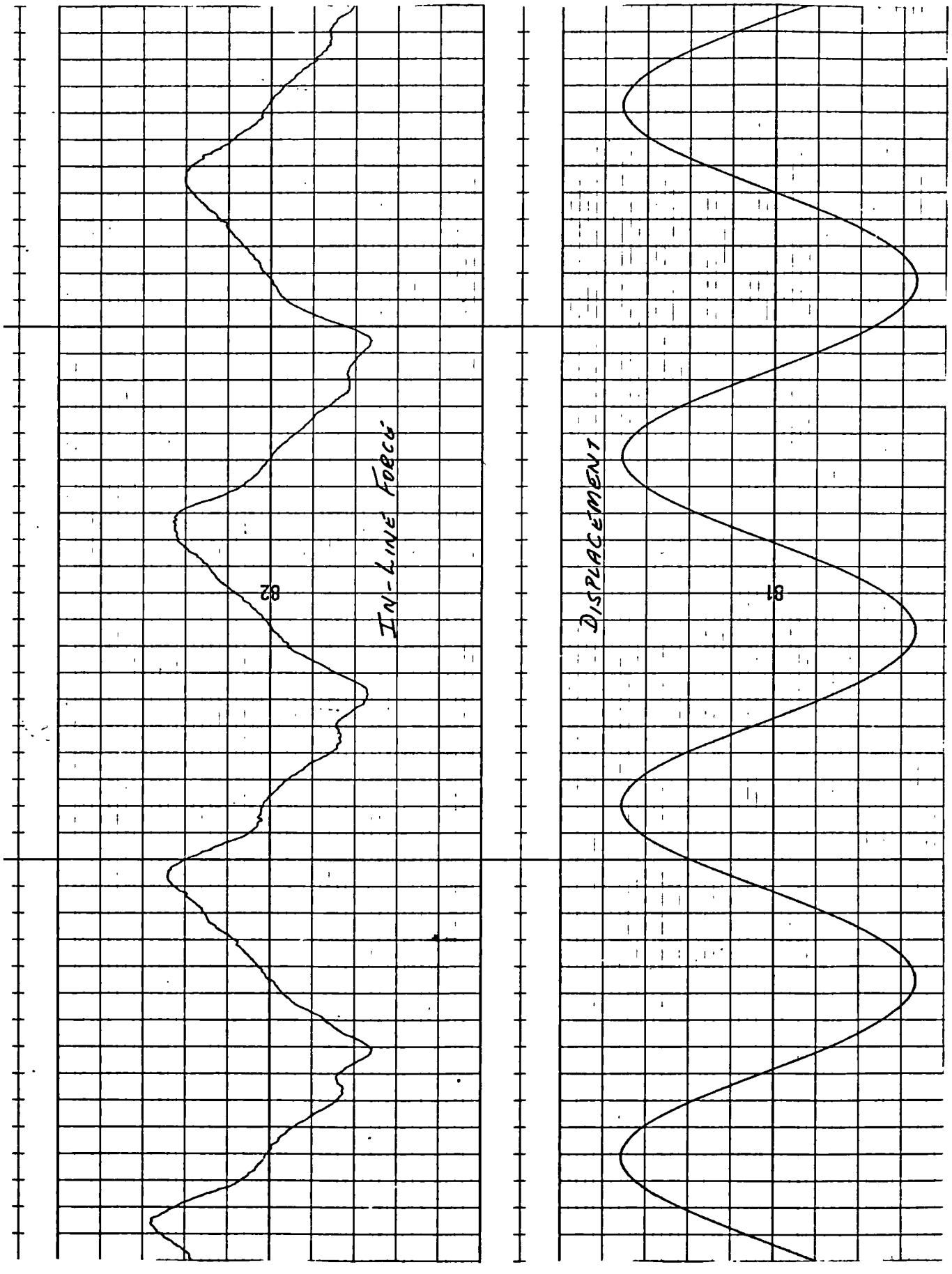

FIG: 2·13

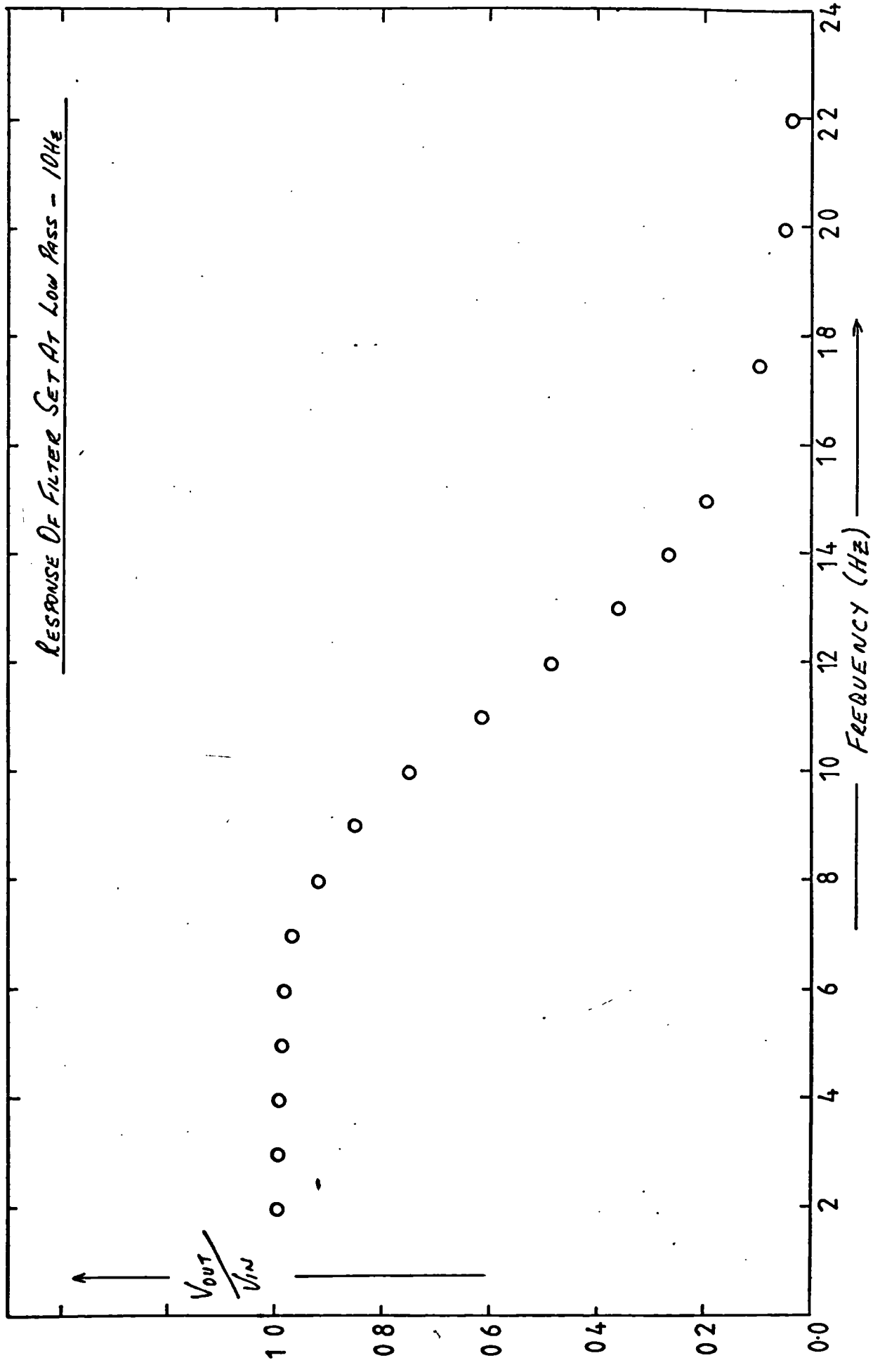
RESPONSE OF FILTER SET AT LOW PASS - 10Hz
V_{out}/V_{in}
1·0
0·8
0·6
0·4
0·2
0·0
2
4
6
8
10
12
14
16
18
20
22
24
FREQUENCY (Hz)

FIG : 2·14

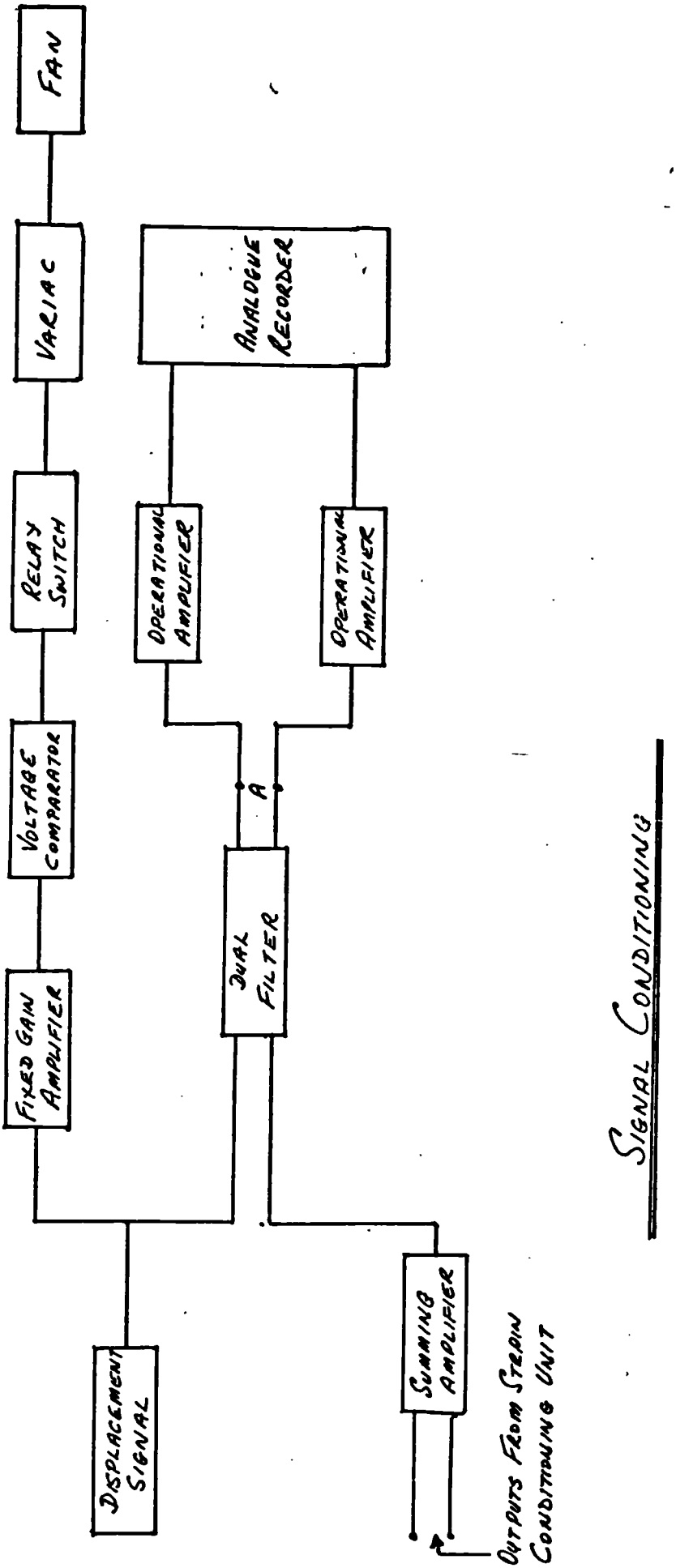
FAN
VARIAC
RELAY SWITCH
VOLTAGE COMPARATOR
FIXED GAIN AMPLIFIER
ANALOGUE RECORDER
OPERATIONAL AMPLIFIER
OPERATIONAL AMPLIFIER
A
DUAL FILTER
DISPLACEMENT SIGNAL
SUMMING AMPLIFIER
OUTPUTS FROM STRAIN CONDITIONING UNIT
SIGNAL CONDITIONING

FIG: 2·15

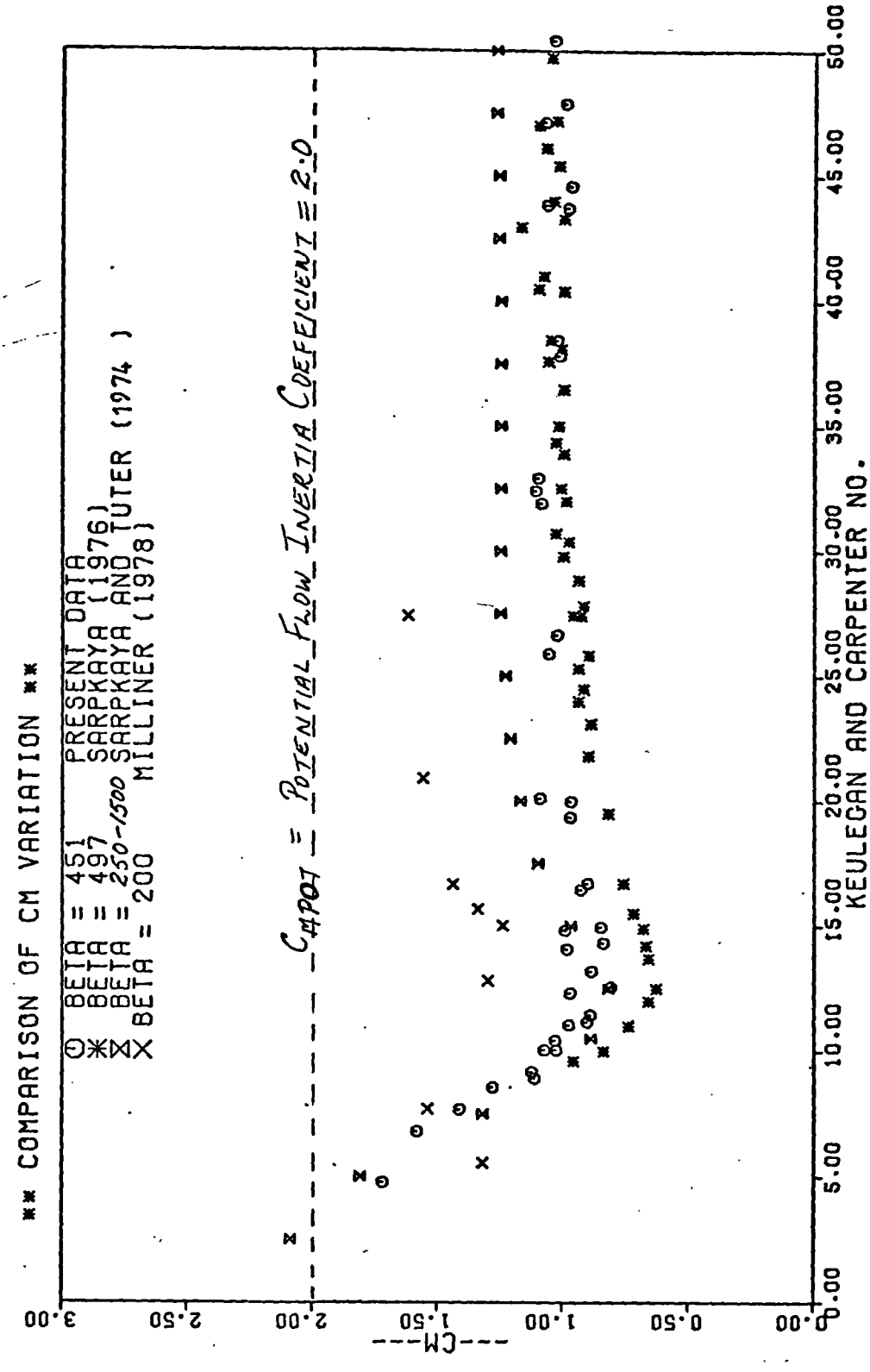
** COMPARISON OF CM VARIATION **
BETA = 451 PRESENT DATA
BETA = 497 SARPKAYA (1976)
BETA = 250-1500 SARPKAYA AND TUTER (1974)
BETA = 200 MILLINER (1978)
CAPOT = POTENTIAL FLOW INERTIA COEFFICIENT = 2.0
---CM---
KEULEGAN AND CARPENTER NO.
0.00
0.50
1.00
1.50
2.00
2.50
3.00
0.00
5.00
10.00
15.00
20.00
25.00
30.00
35.00
40.00
45.00
50.00

FIG : 4.1

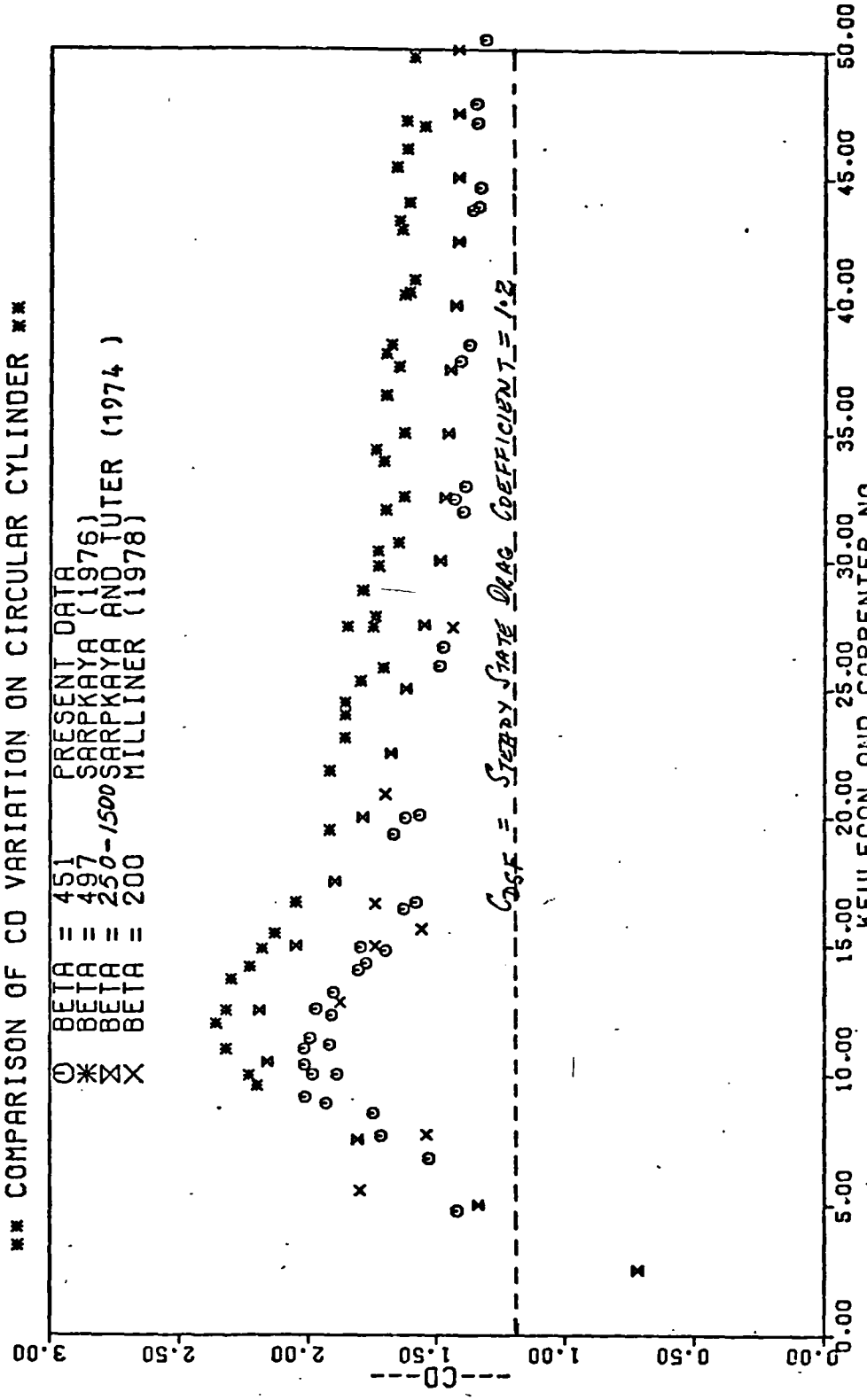
** COMPARISON OF CD VARIATION ON CIRCULAR CYLINDER **
O BETA = 451 PRESENT DATA
* BETA = 497 SARPKAYA (1976)
⊠ BETA = 250-1500 SARPKAYA AND TUTER (1974)
X BETA = 200 MILLINER (1978)
CDSS = STEADY STATE DRAG COEFFICIENT = 1.2
---CD---
KEULEGAN AND CARPENTER NO.
0.00
0.50
1.00
1.50
2.00
2.50
3.00
5.00
10.00
15.00
20.00
25.00
30.00
35.00
40.00
45.00
50.00

FIG:4.2

** COMPARISON OF CM ON CIRCULAR CYLINDER **
BETA = 421.5 PRESENT DATA
BETA = 497 250-1500 SARPKAYA (1976)
BETA = 200 SARPKAYA AND TUTER (1974)
BETA = 200-600 MILLINER (1973)
MERCIER (1973)
---CM---
KEULEGAN AND CARPENTER NO.
0.00
0.50
1.00
1.50
2.00
2.50
3.00
5.00
10.00
15.00
20.00
25.00
30.00
35.00
40.00
45.00
50.00

FIG:4.3

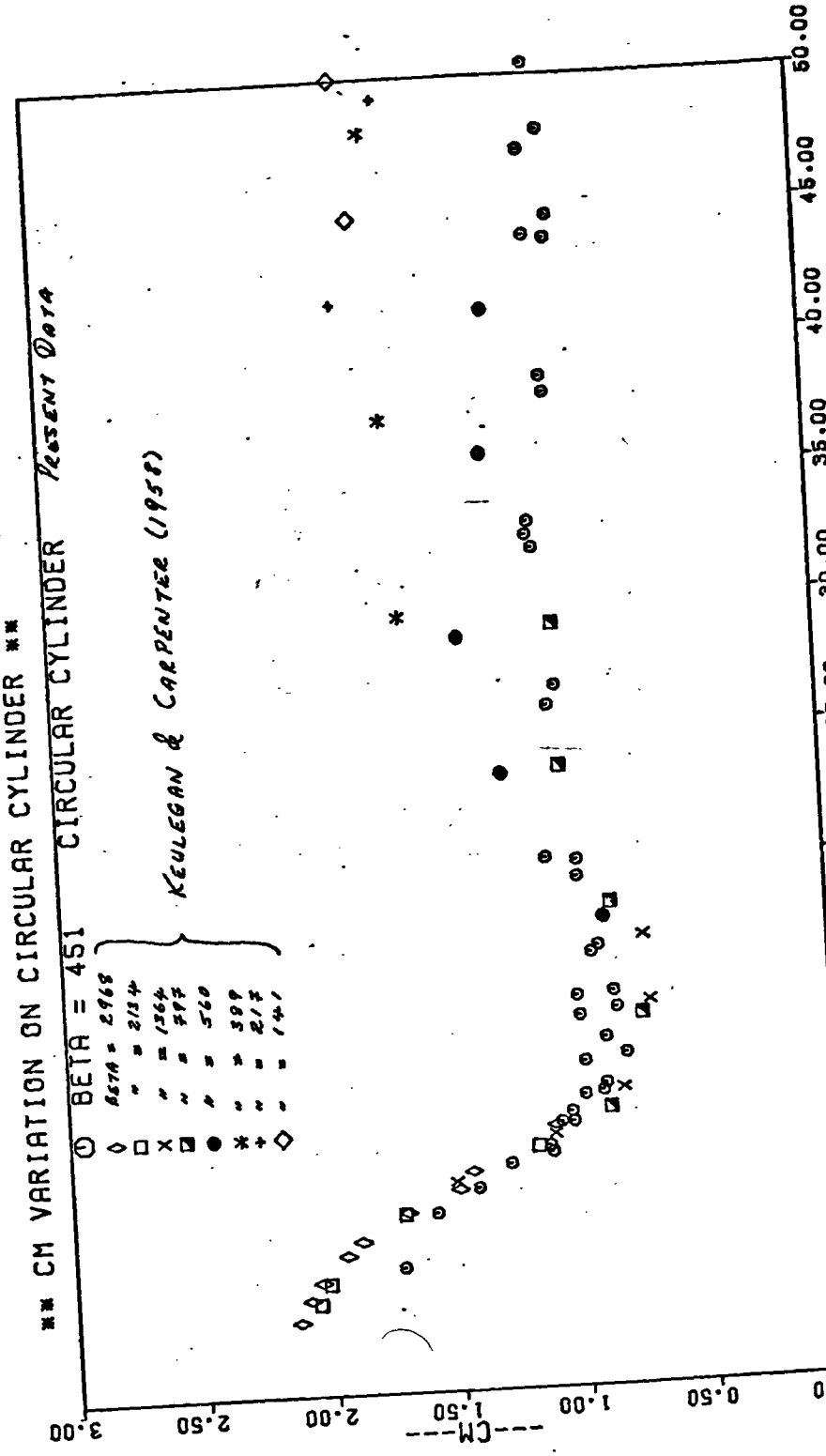
** CM VARIATION ON CIRCULAR CYLINDER **
CIRCULAR CYLINDER
PRESENT DATA
BETA = 451
KEULEGAN & CARPENTER (1958)
BETA = 2968
" = 2134
" = 1364
" = 955
" = 510
" = 389
" = 273
" = 141
---CM---
KEULEGAN AND CARPENTER NO.
0.00
0.50
1.00
1.50
2.00
2.50
3.00
5.00
10.00
15.00
20.00
25.00
30.00
35.00
40.00
45.00
50.00

FIG:4.4

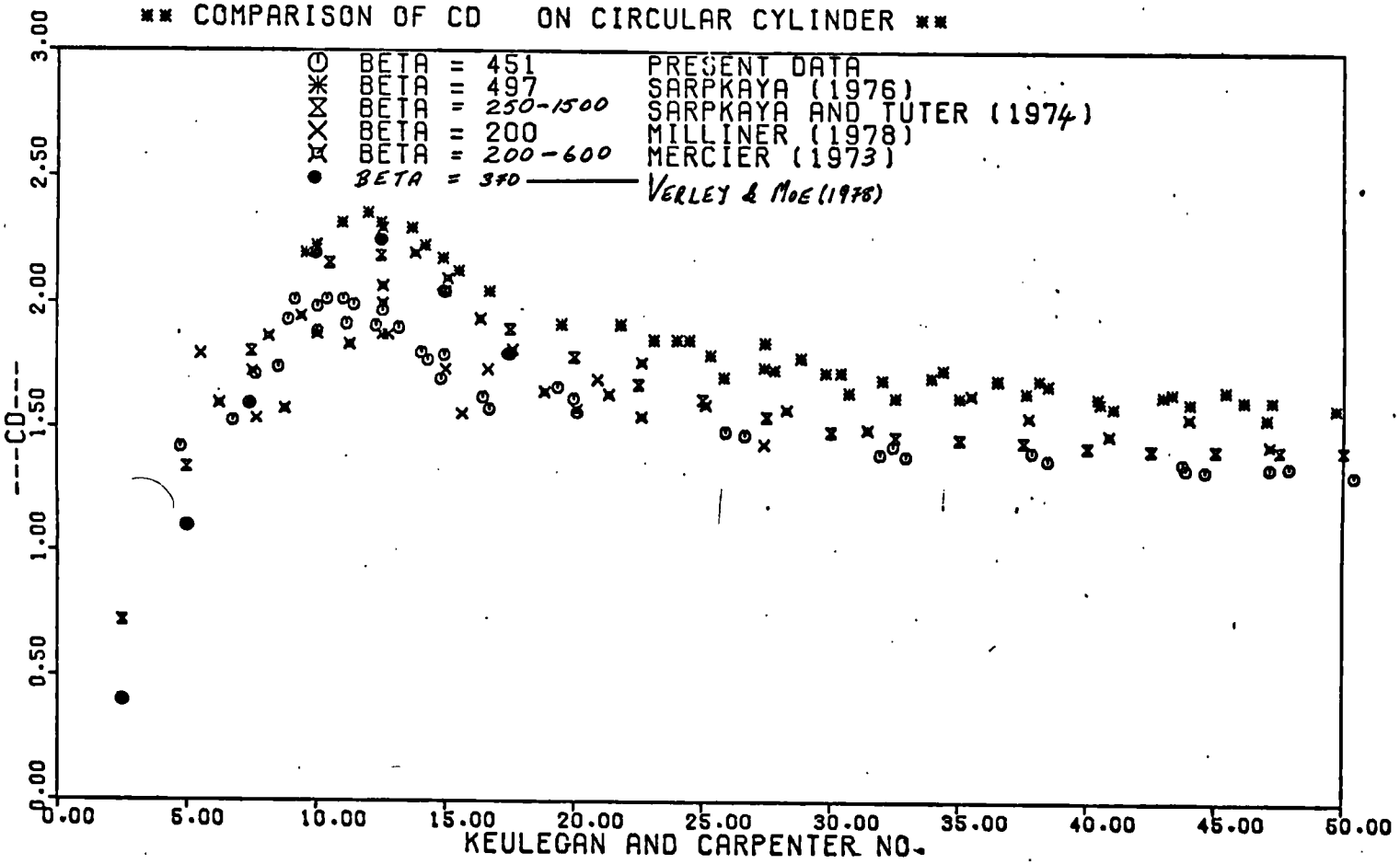
** COMPARISON OF CD ON CIRCULAR CYLINDER **
BETA = 451 PRESENT DATA
BETA = 497 SARPKAYA (1976)
BETA = 250-1500 SARPKAYA AND TUTER (1974)
BETA = 200 MILLINER (1978)
BETA = 200-600 MERCIER (1973)
BETA = 370 VERLEY & MOE (1978)
---CD---
0.00
0.50
1.00
1.50
2.00
2.50
3.00
0.00
5.00
10.00
15.00
20.00
25.00
30.00
35.00
40.00
45.00
50.00
KEULEGAN AND CARPENTER NO.

FIG:4.5

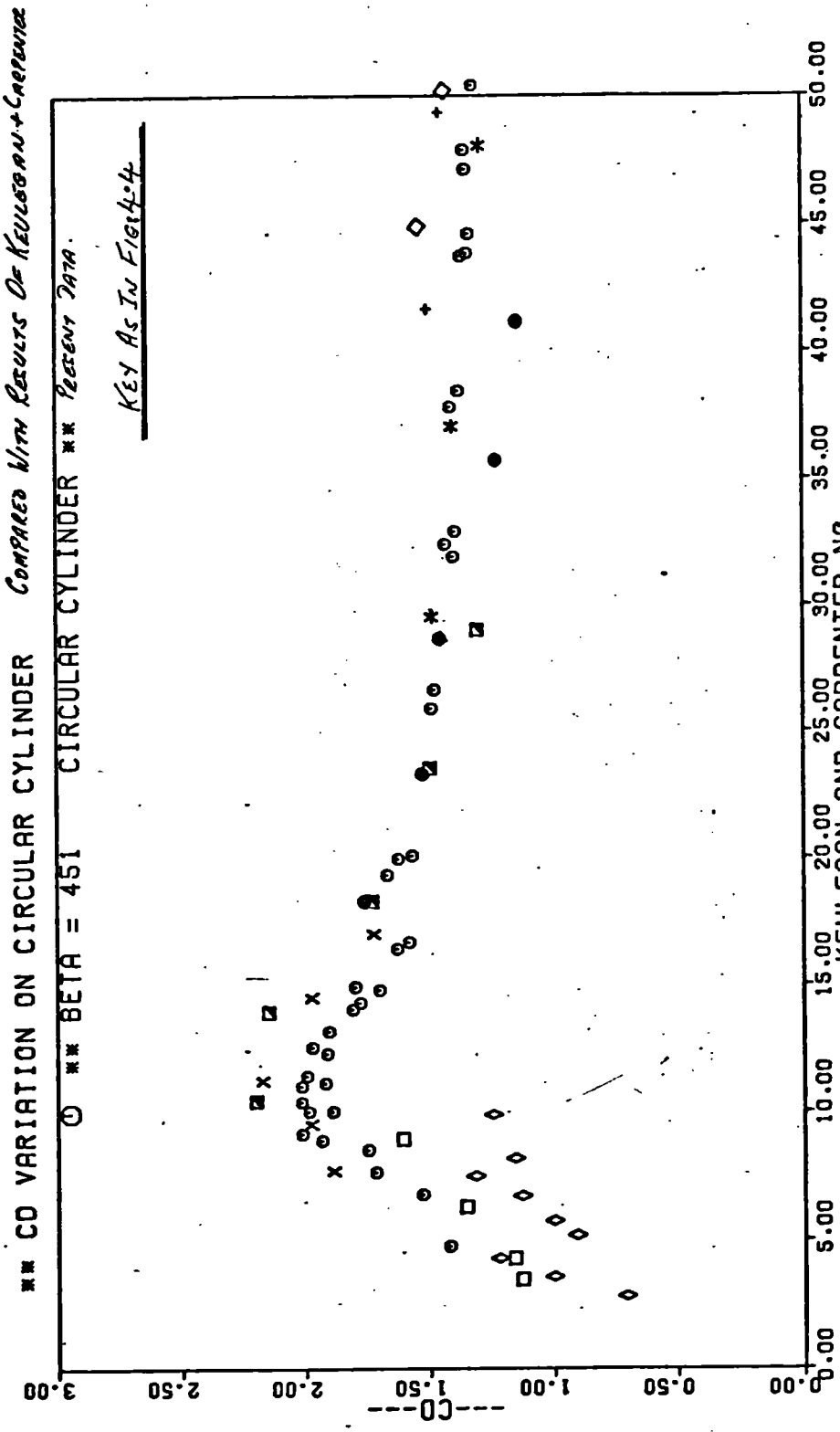
** CD VARIATION ON CIRCULAR CYLINDER COMPARED WITH RESULTS OF KEULEGAN+CARPENTER
O ** BETA = 451 CIRCULAR CYLINDER ** PRESENT DATA.
KEY AS IN FIG4.4
---CD---
KEULEGAN AND CARPENTER NO.
0.00
0.50
1.00
1.50
2.00
2.50
3.00
0.00
5.00
10.00
15.00
20.00
25.00
30.00
35.00
40.00
45.00
50.00

FIG:4.6

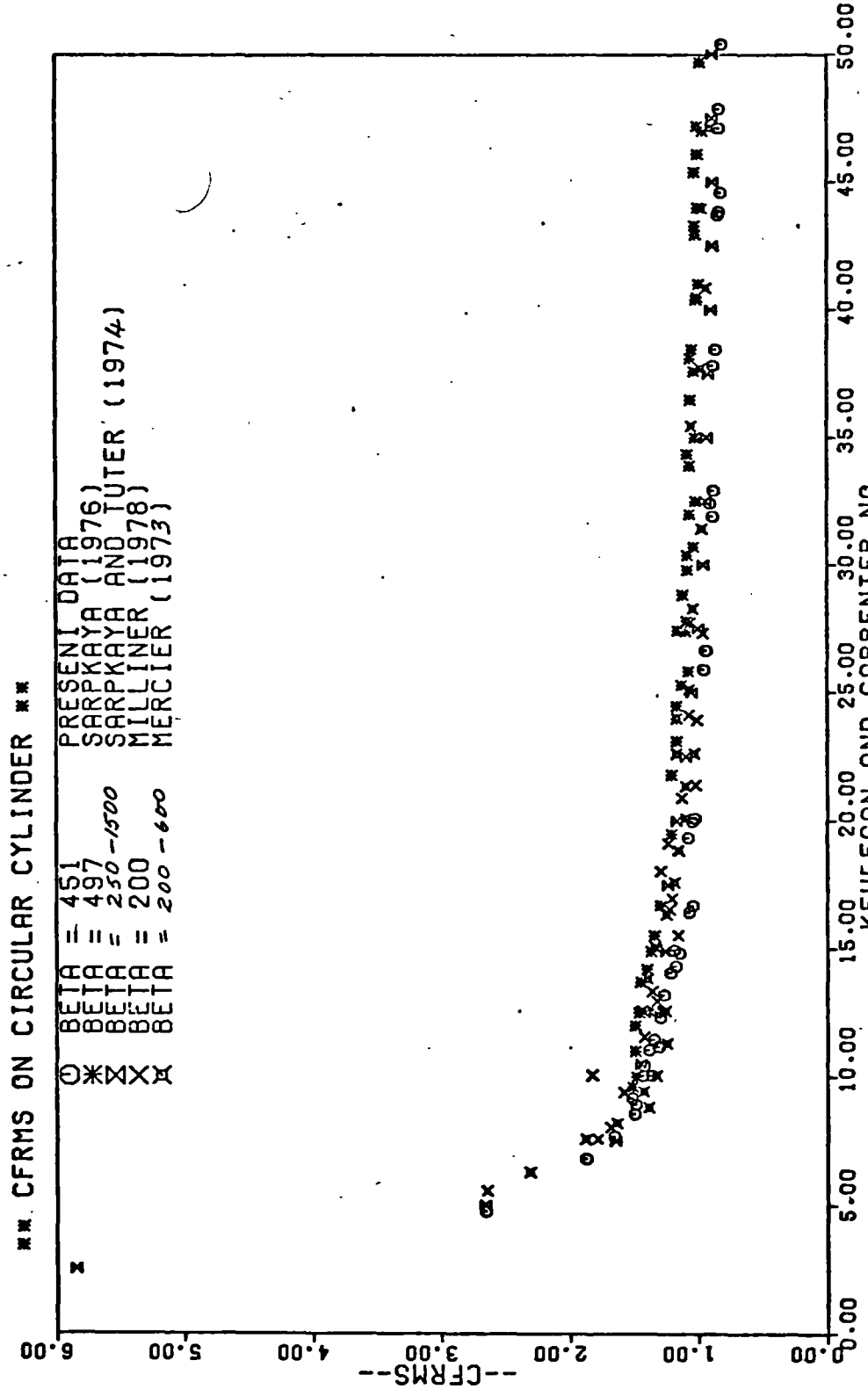
** CFRMS ON CIRCULAR CYLINDER **
BETA = 451 PRESENT DATA
BETA = 497 SARPKAYA (1976)
BETA = 250-1500 SARPKAYA AND TUTER (1974)
BETA = 200 MILLINER (1978)
BETA = 200-600 MERCIER (1973)
--CFRMS--
KEULEGAN AND CARPENTER NO.
0.00
1.00
2.00
3.00
4.00
5.00
6.00
0.00
5.00
10.00
15.00
20.00
25.00
30.00
35.00
40.00
45.00
50.00

FIG : 4.7

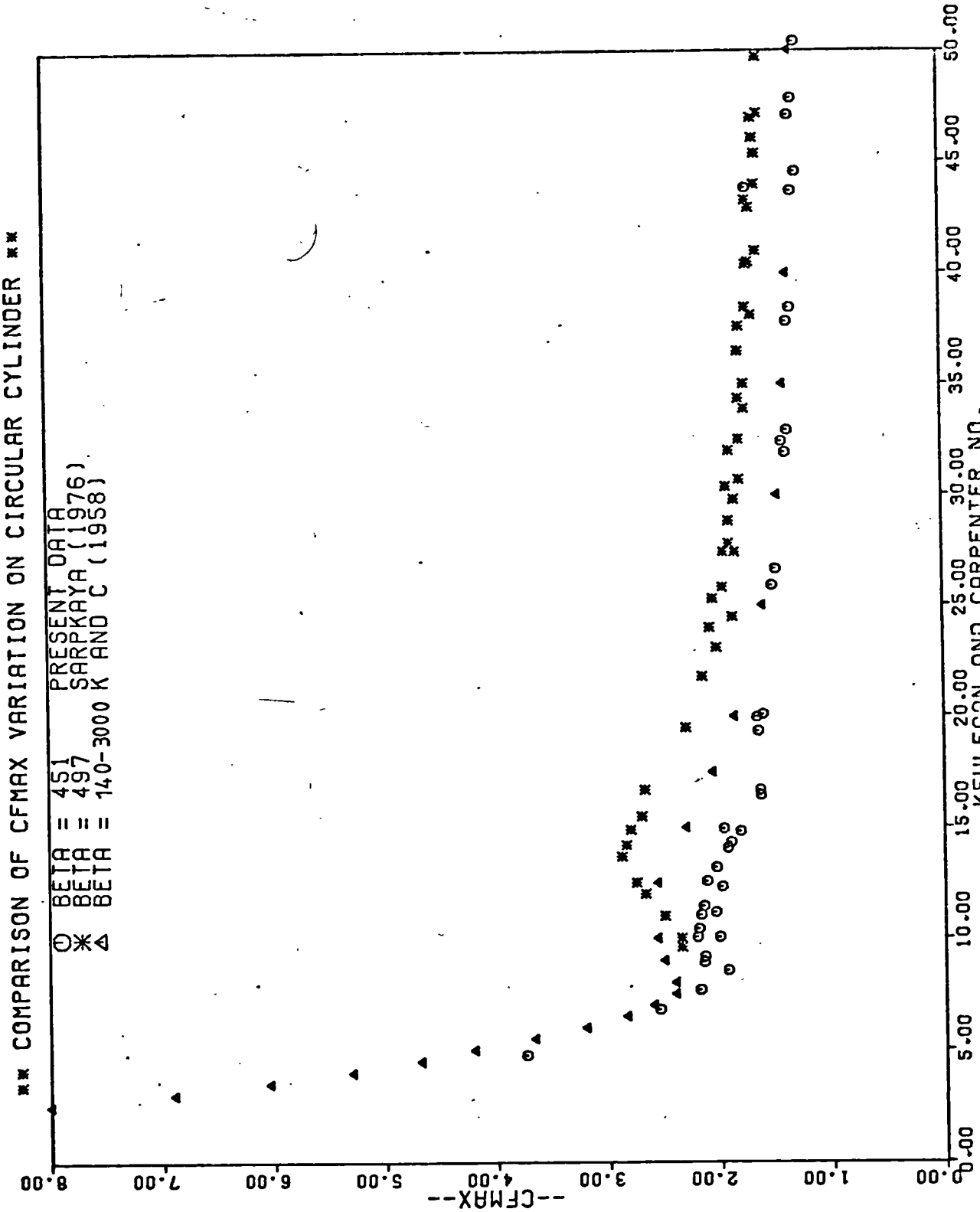
** COMPARISON OF CFMAX VARIATION ON CIRCULAR CYLINDER **
PRESENT DATA
SARPKAYA (1976)
K AND C (1958)
BETA = 451
BETA = 497
BETA = 140-3000
--CFMAX--
KEULEGAN AND CARPENTER NO.
0.00
1.00
2.00
3.00
4.00
5.00
6.00
7.00
8.00
0.00
5.00
10.00
15.00
20.00
25.00
30.00
35.00
40.00
45.00
50.00

FIG: 4.8

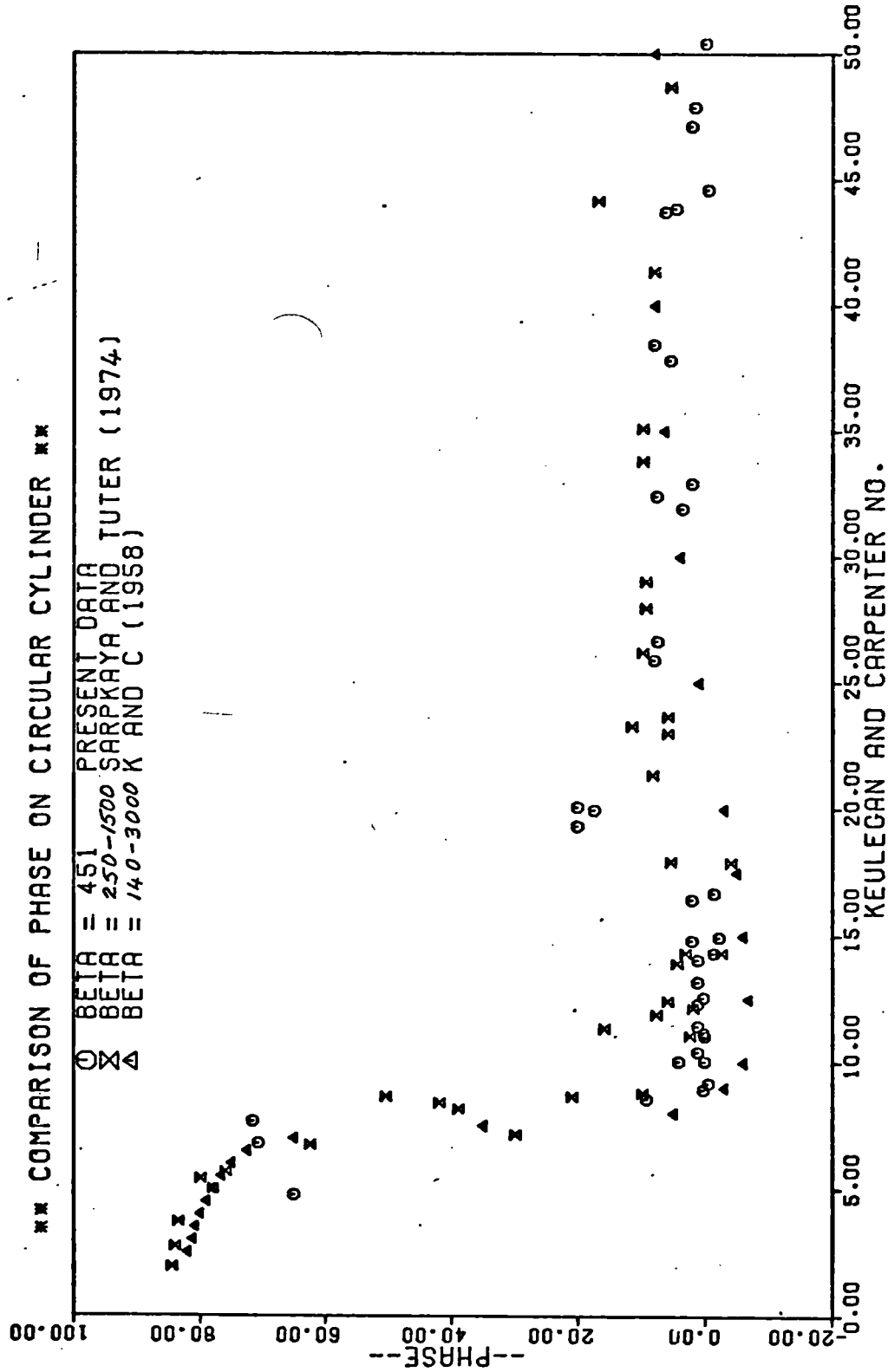
** COMPARISON OF PHASE ON CIRCULAR CYLINDER **
BETA = 451 PRESENT DATA
BETA = 250-1500 SARPKAYA AND TUTER (1974)
BETA = 140-3000 K AND C (1958)
--PHASE--
KEULEGAN AND CARPENTER NO.
100.00
80.00
60.00
40.00
20.00
0.00
-20.00
0.00
5.00
10.00
15.00
20.00
25.00
30.00
35.00
40.00
45.00
50.00

FIG : 4·9

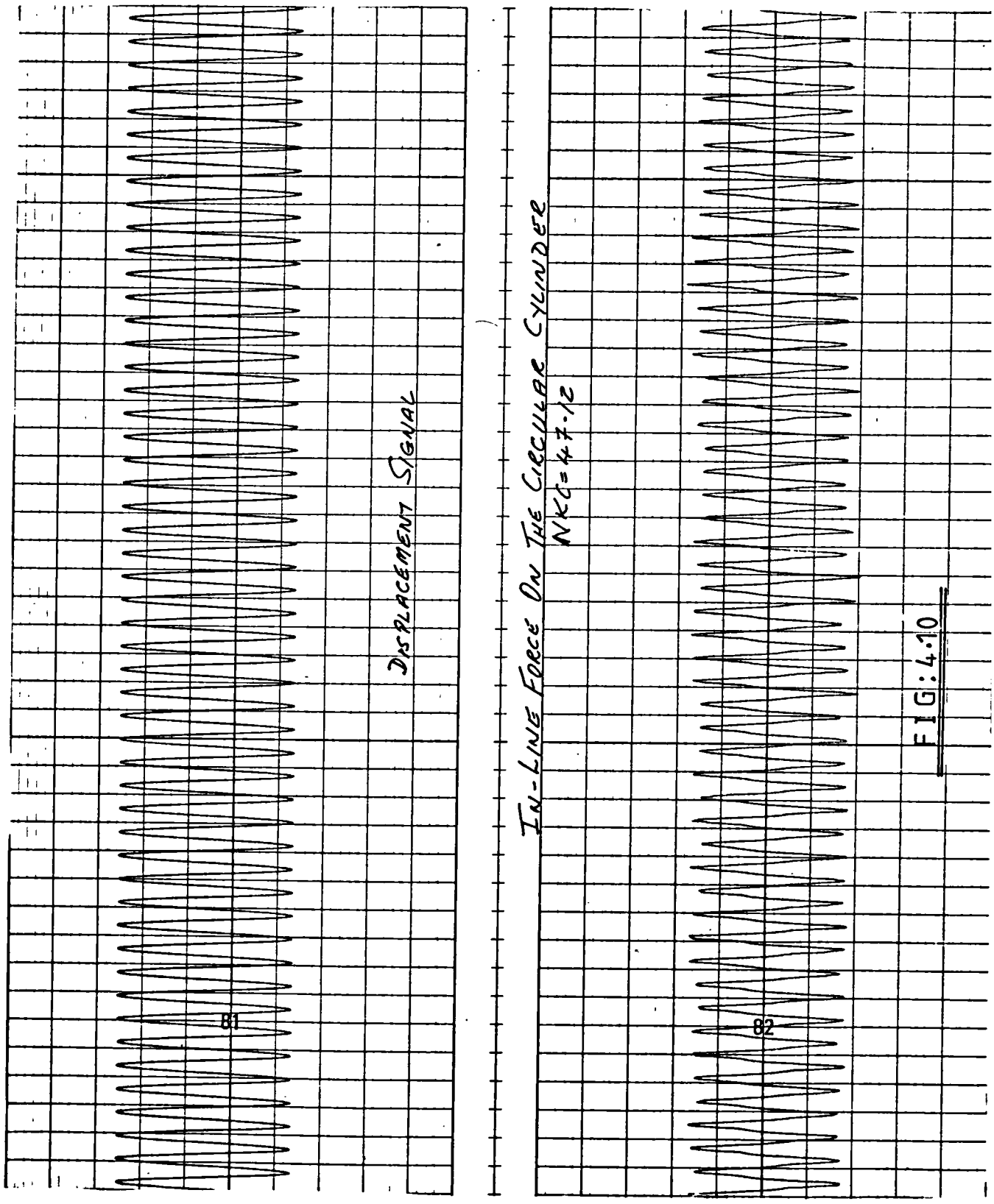
DISPLACEMENT SIGNAL
81
IN-LINE FORCE ON THE CIRCULAR CYLINDER
NKC=47.12
82

FIG: 4.10

***NKC=7.67 CIRCULAR CYLINDER BETA=451

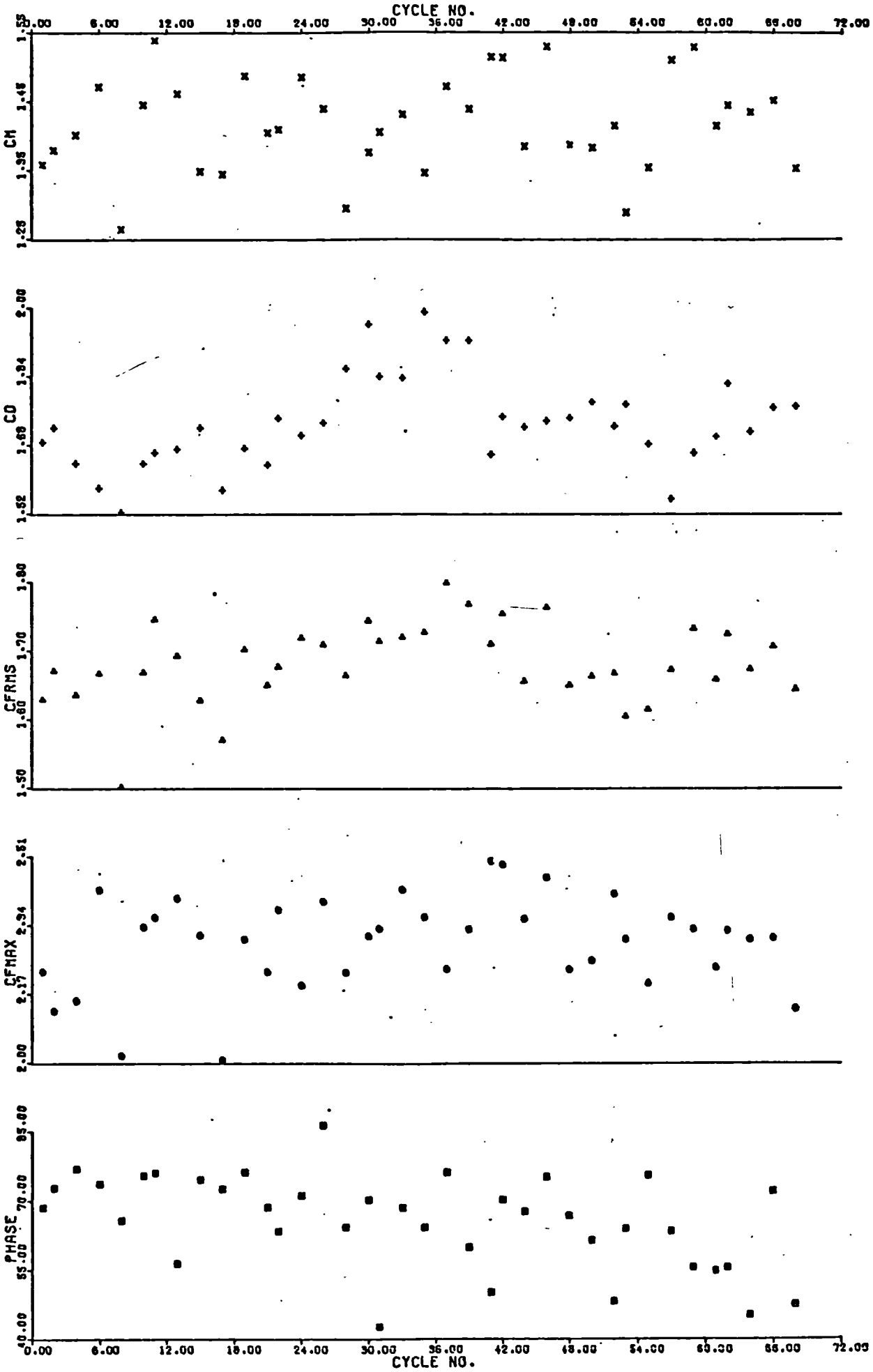

FIG: 4.11

**NKC=19.98 CIRCULAR CYLINDER BETA=451 **

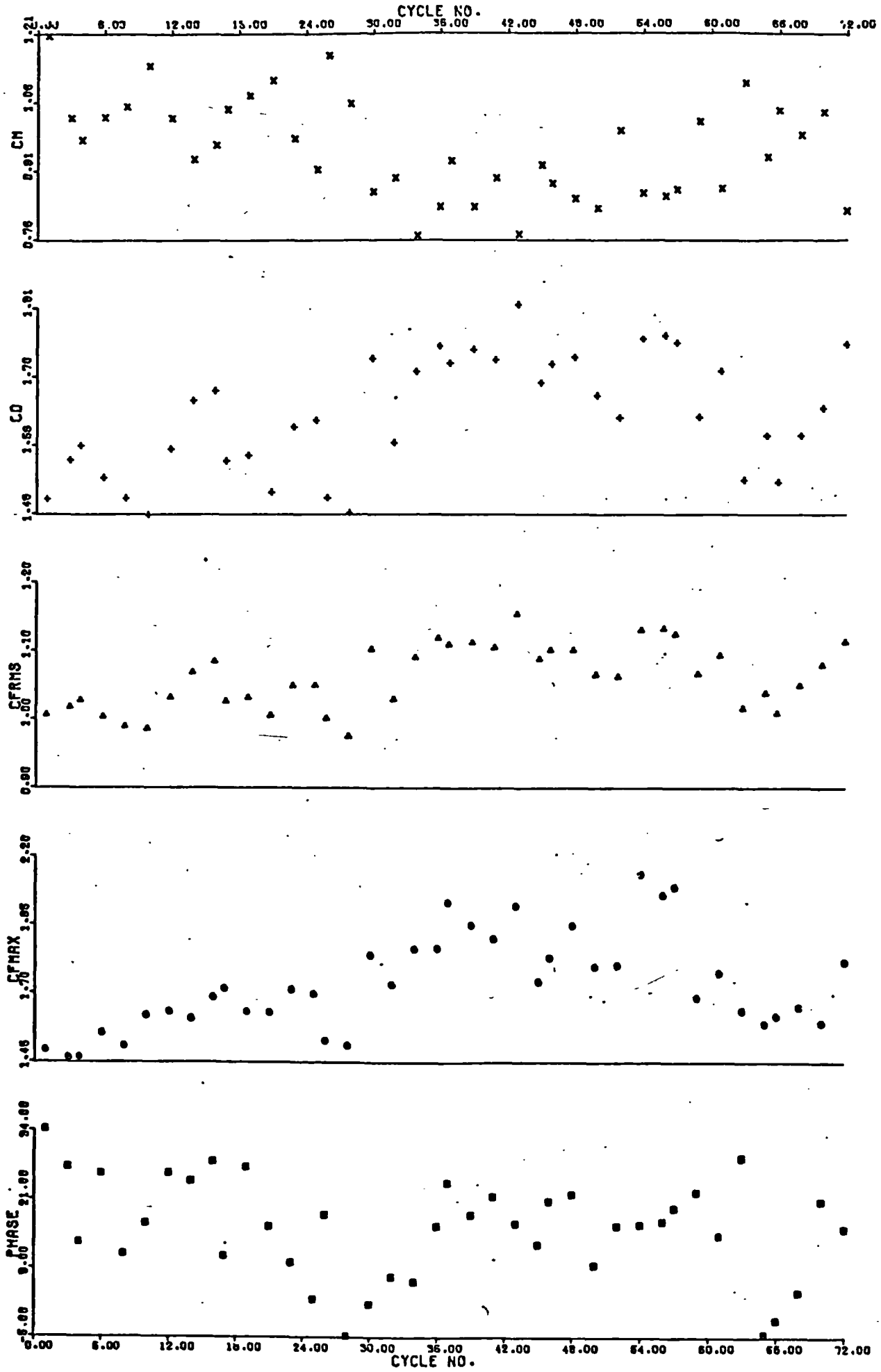

FIG:4.12

** NKC=50.39 CIRCULAR CYLINDER BETA=451

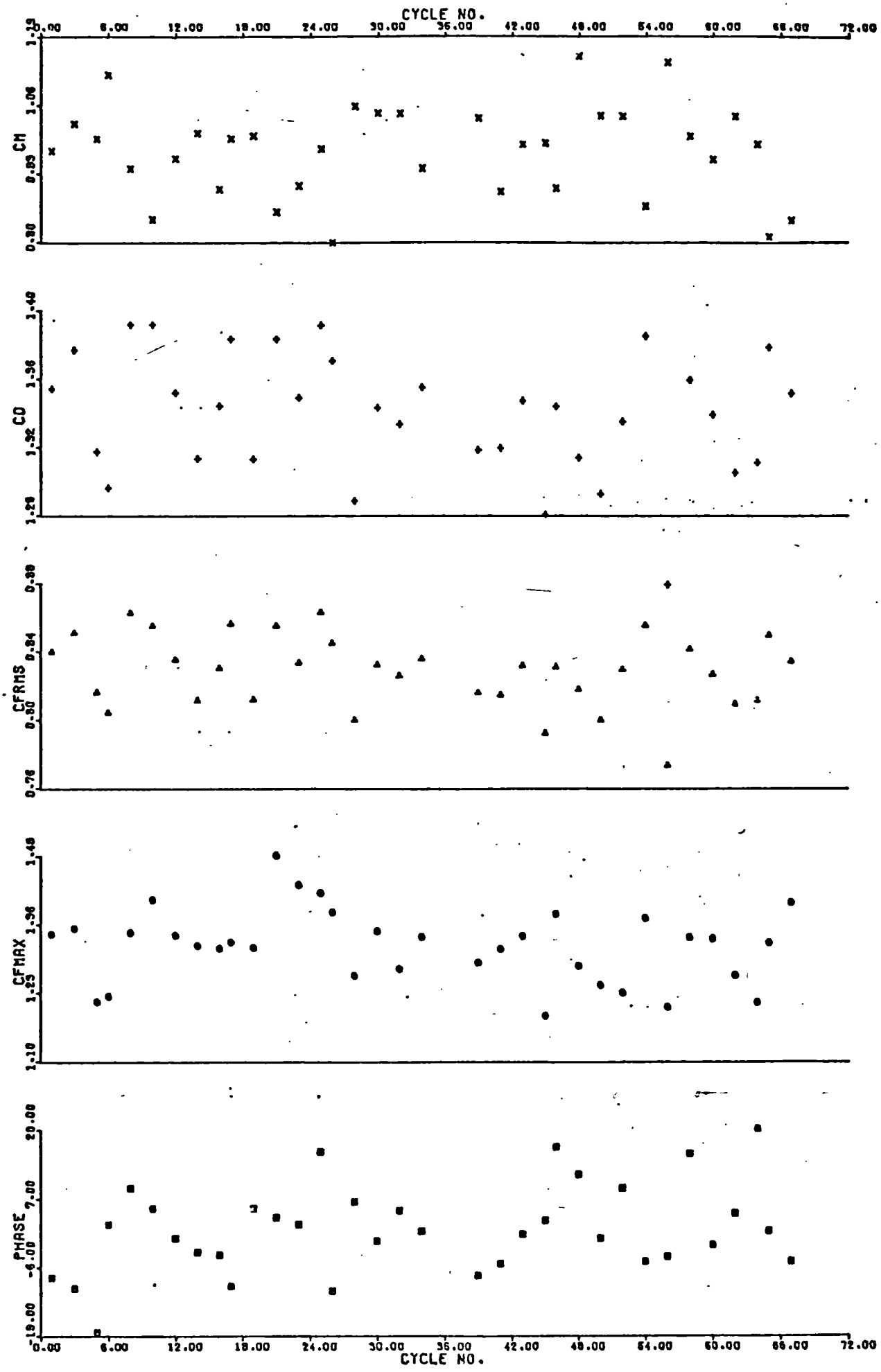

FIG:4·13

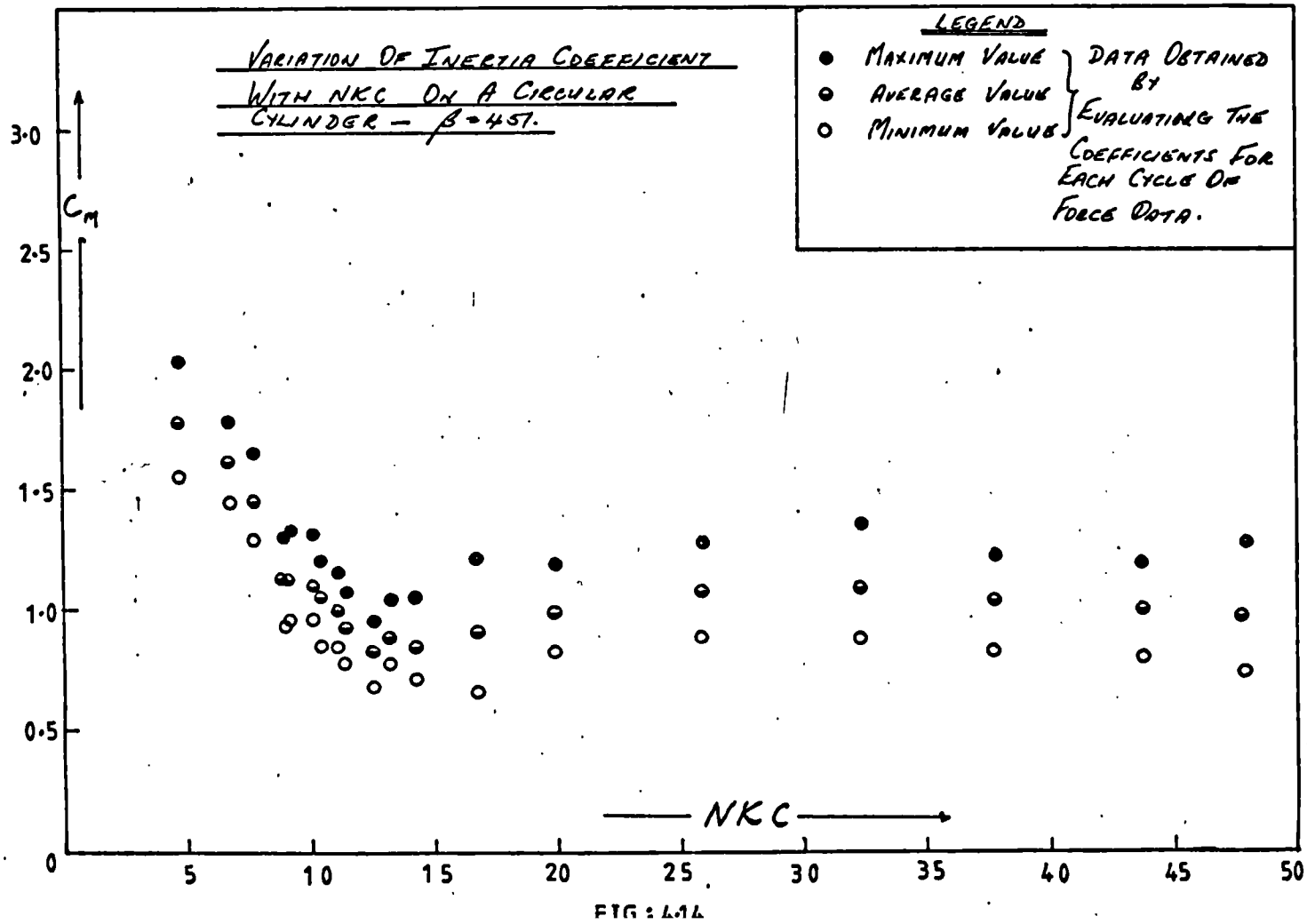
VARIATION OF INERTIA COEFFICIENT WITH NKC ON A CIRCULAR CYLINDER — β=45°.
LEGEND
MAXIMUM VALUE
AVERAGE VALUE
MINIMUM VALUE
DATA OBTAINED BY EVALUATING THE COEFFICIENTS FOR EACH CYCLE OF FORCE DATA.
C_M
3·0
2·5
2·0
1·5
1·0
0·5
0
5
10
15
20
25
30
35
40
45
50
NKC

FIG : 4.14

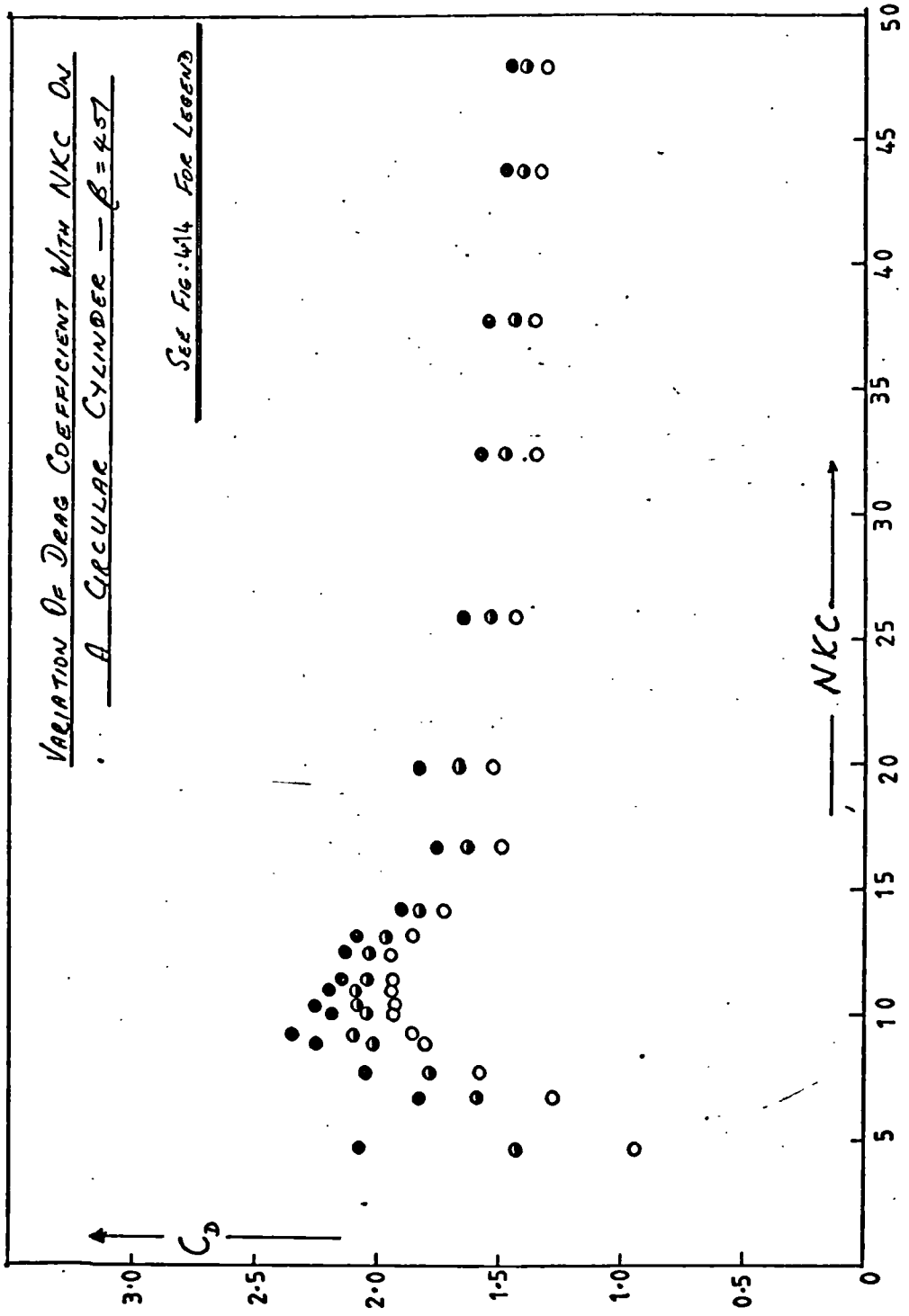
VARIATION OF DRAG COEFFICIENT WITH NKC ON A CIRCULAR CYLINDER — β = 457
SEE FIG: 4·14 FOR LEGEND
C_D
NKC
3·0
2·5
2·0
1·5
1·0
0·5
0
5
10
15
20
25
30
35
40
45
50

FIG: 4·15

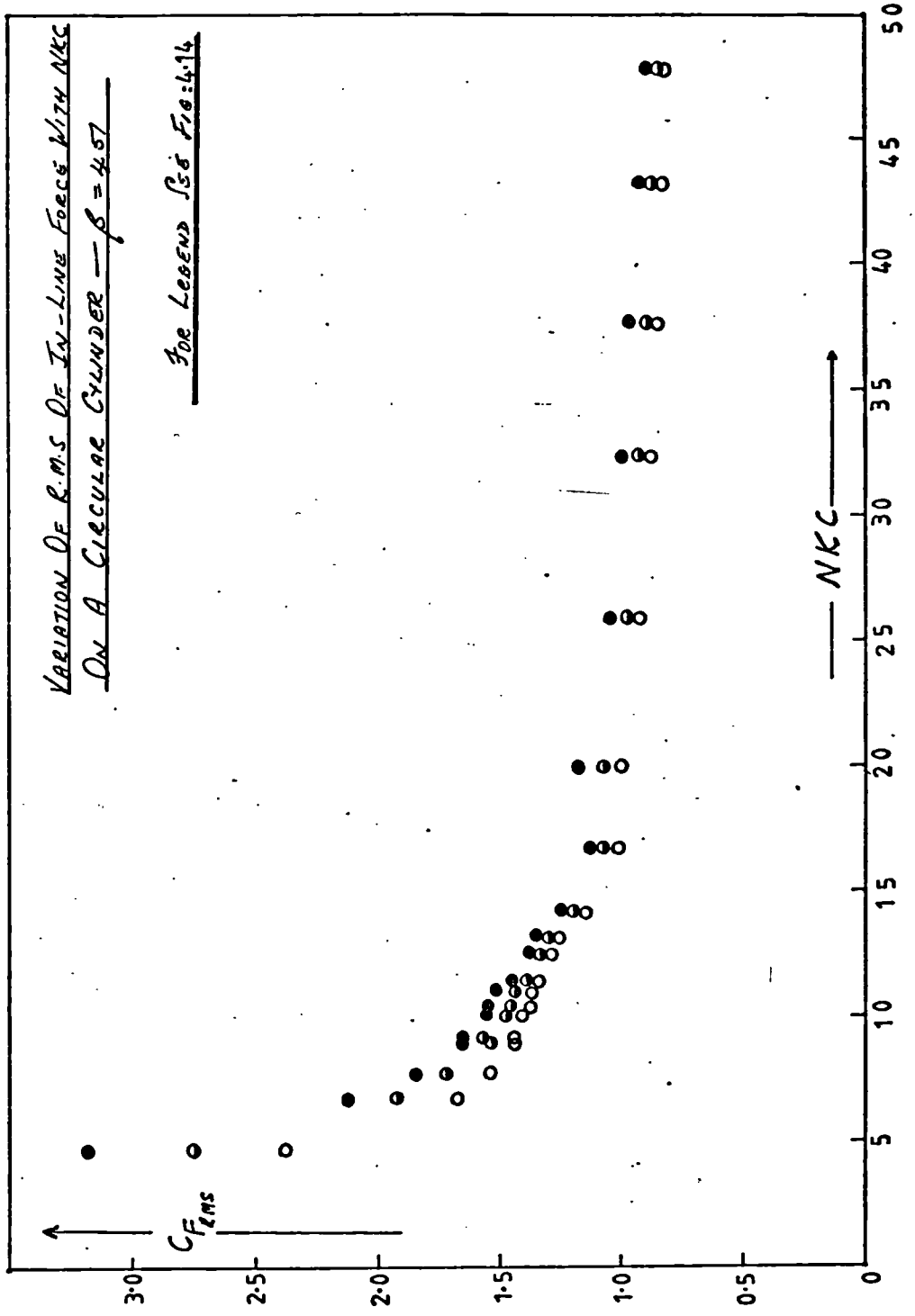
VARIATION OF R.M.S OF IN-LINE FORCE WITH NKC
ON A CIRCULAR CYLINDER — β = 457
FOR LEGEND SEE FIG:4.14
$C_{F_{RMS}}$
NKC
3·0
2·5
2·0
1·5
1·0
0·5
0
5
10
15
20
25
30
35
40
45
50

FIG:4.16

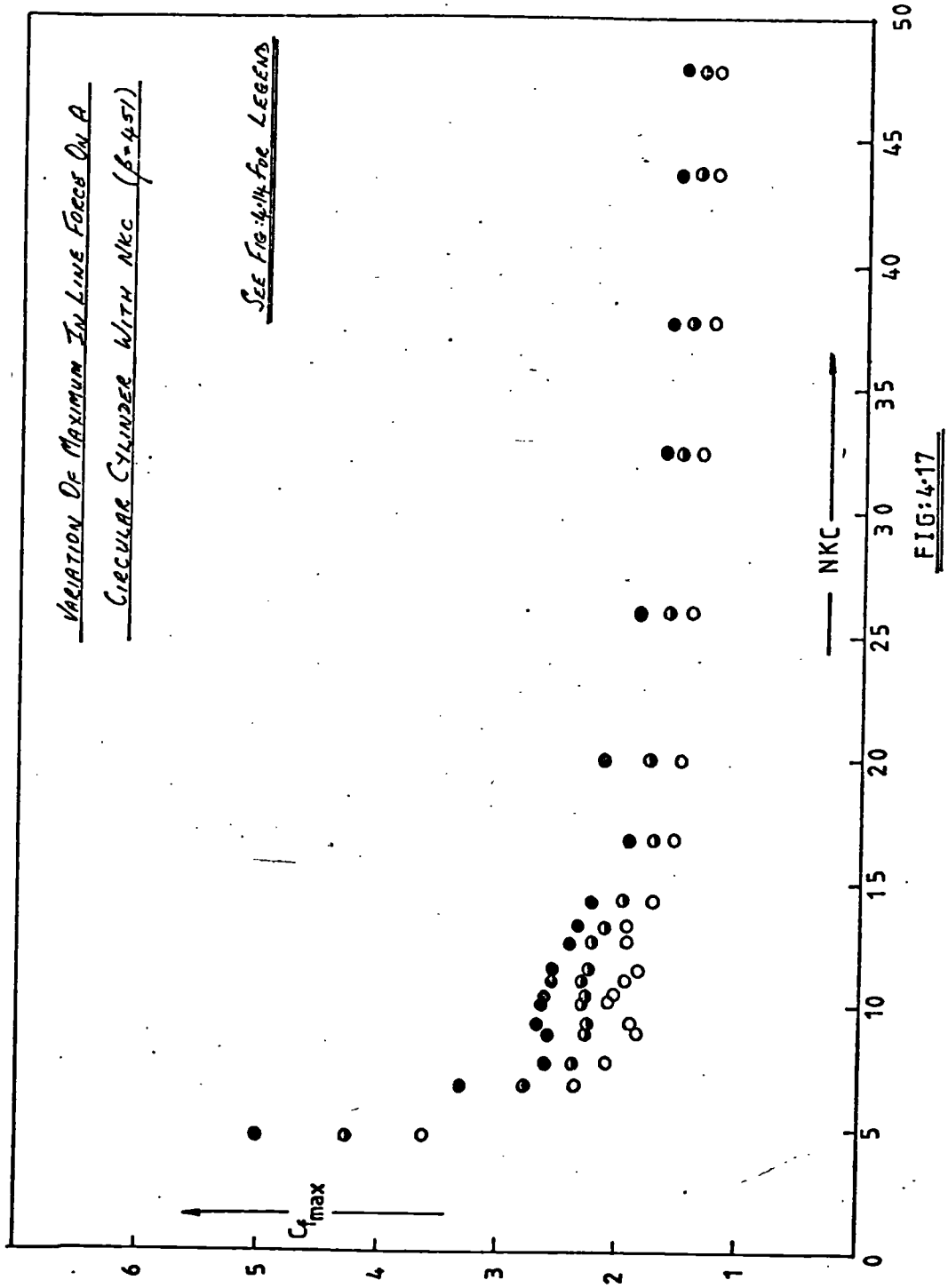
VARIATION OF MAXIMUM IN LINE FORCE ON A
CIRCULAR CYLINDER WITH NKC (β=45°)
SEE FIG:4·14 FOR LEGEND
$C_{f_{max}}$
NKC
0
5
10
15
20
25
30
35
40
45
50
1
2
3
4
5
6

FIG:4·17

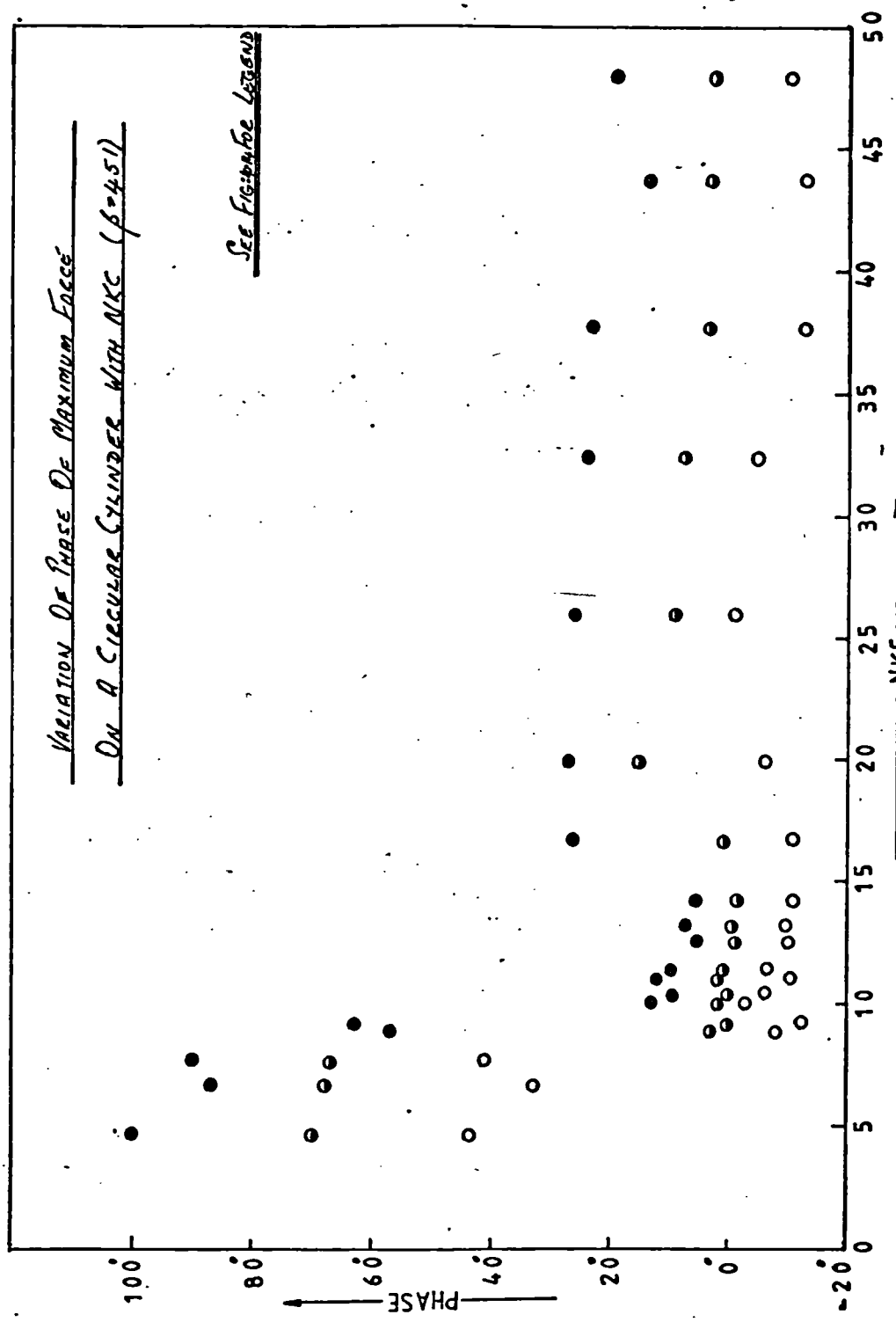
VARIATION OF PHASE OF MAXIMUM FORCE
ON A CIRCULAR CYLINDER WITH NKC (β=45°)
SEE FIG:4.16 FOR LEGEND
PHASE
NKC
100°
80°
60°
40°
20°
0°
-20°
0
5
10
15
20
25
30
35
40
45
50

FIG : 4.18

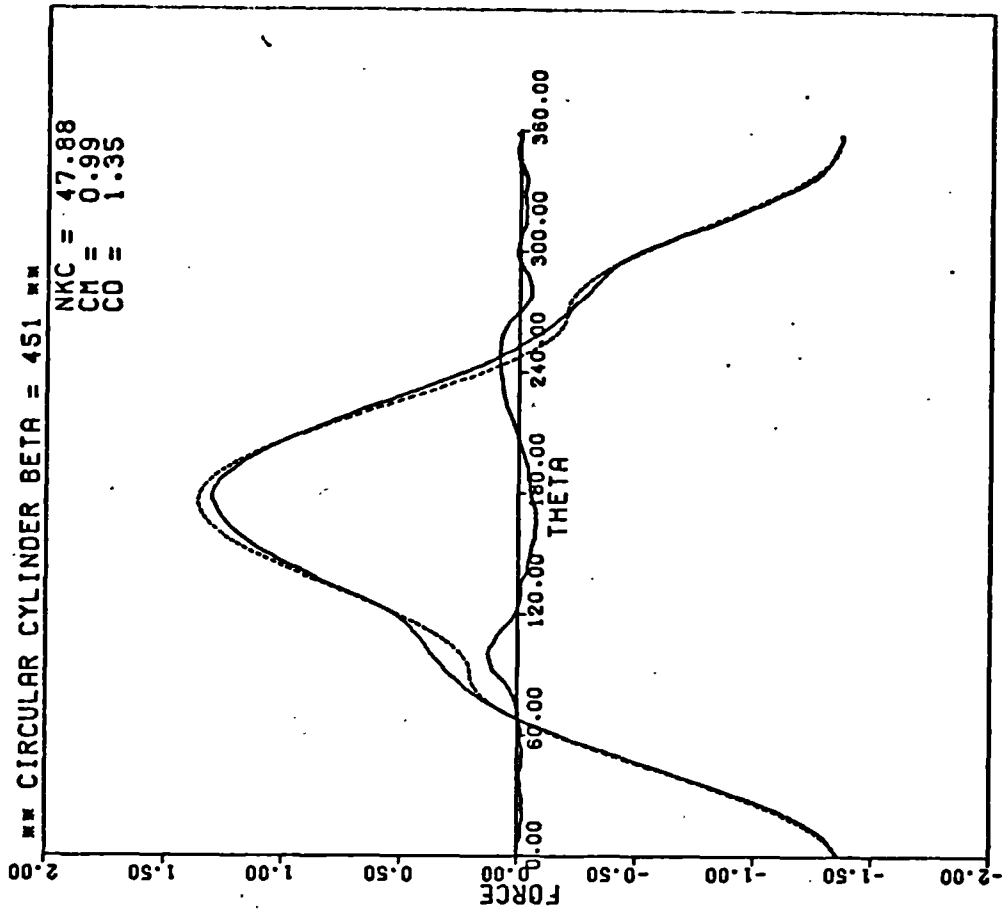

FIG: 4.19 (h)

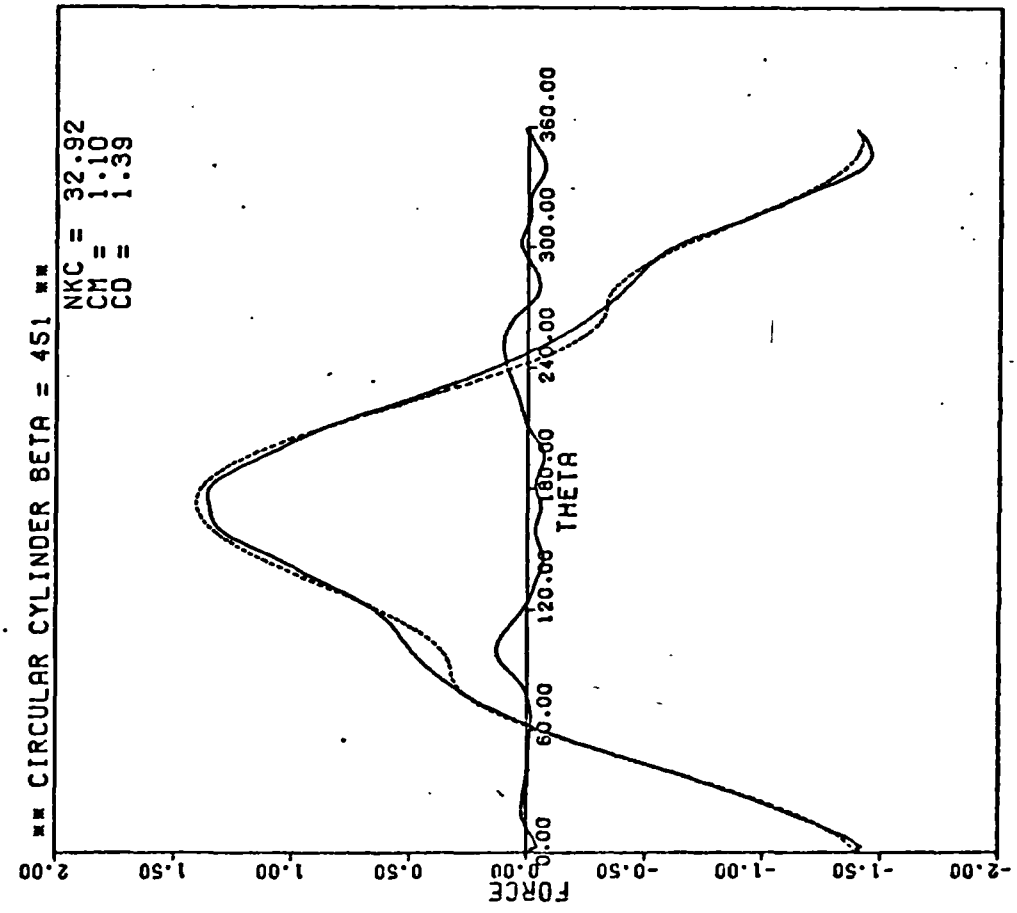

FIG: 4.19 (g)

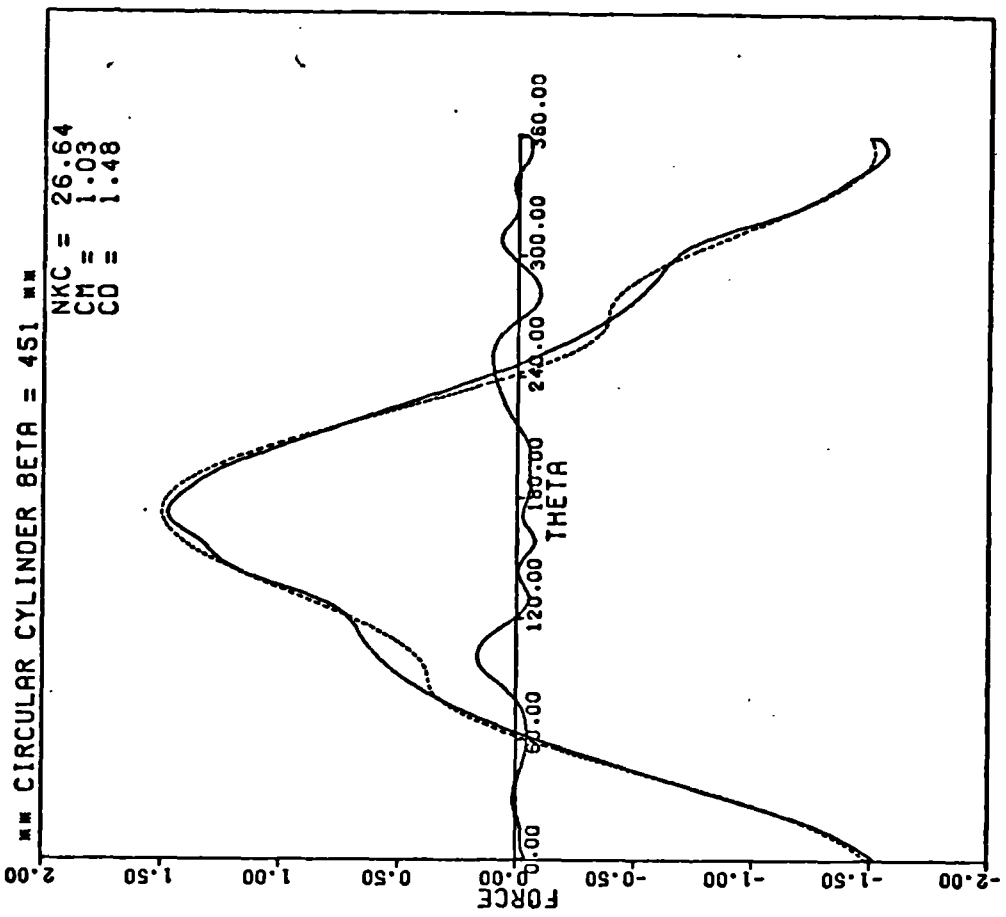

FIG: 4.19 (f)

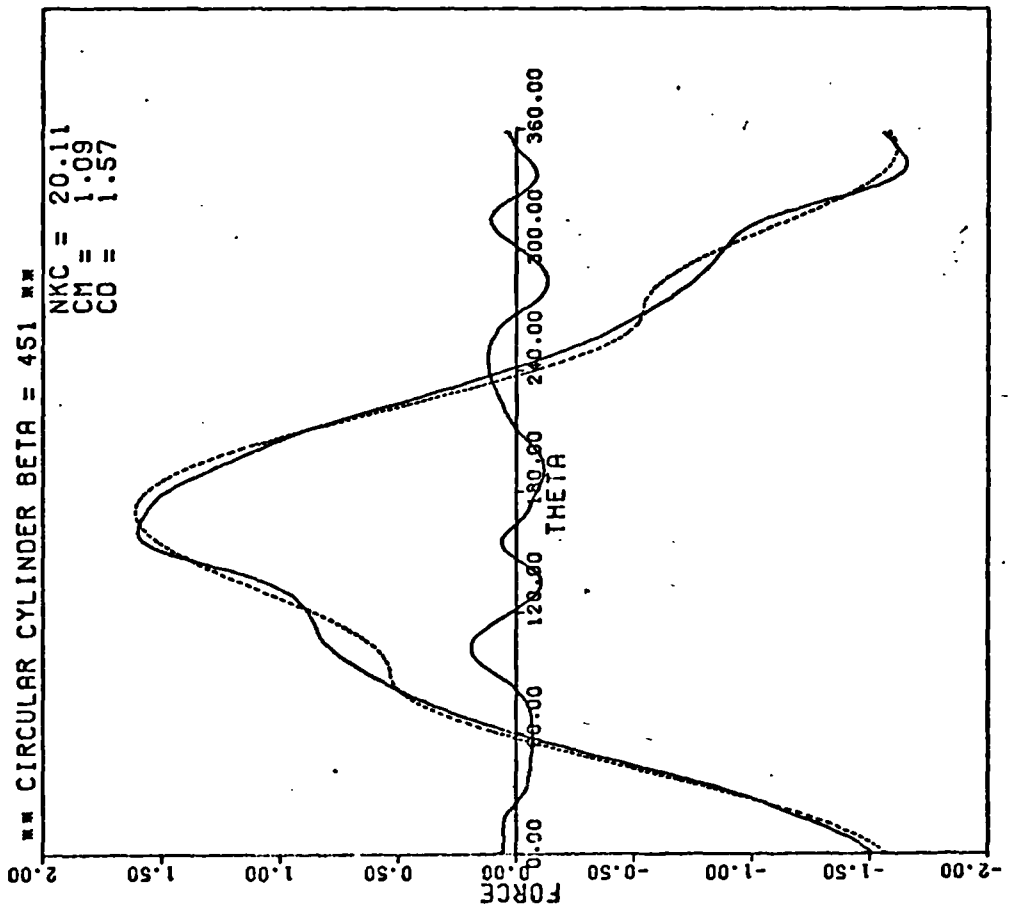

FIG: 4.19 (e)

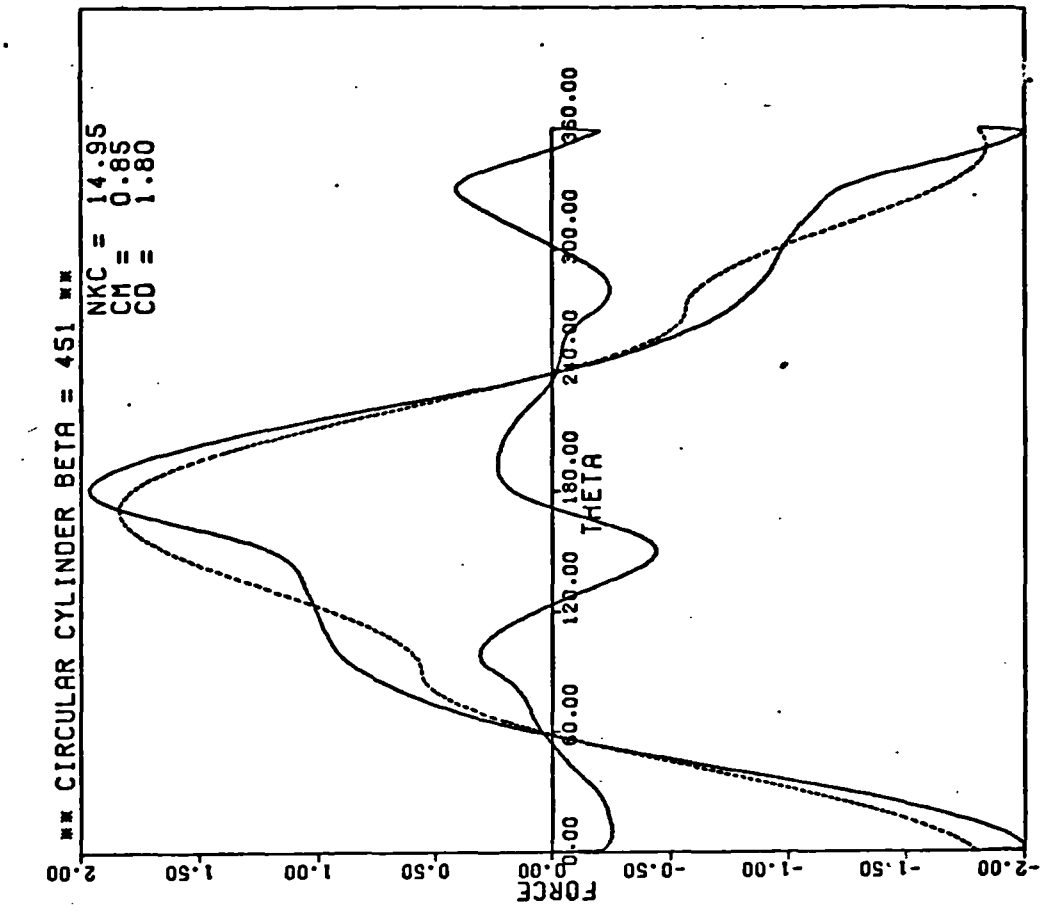

FIG: 4.19 (d)

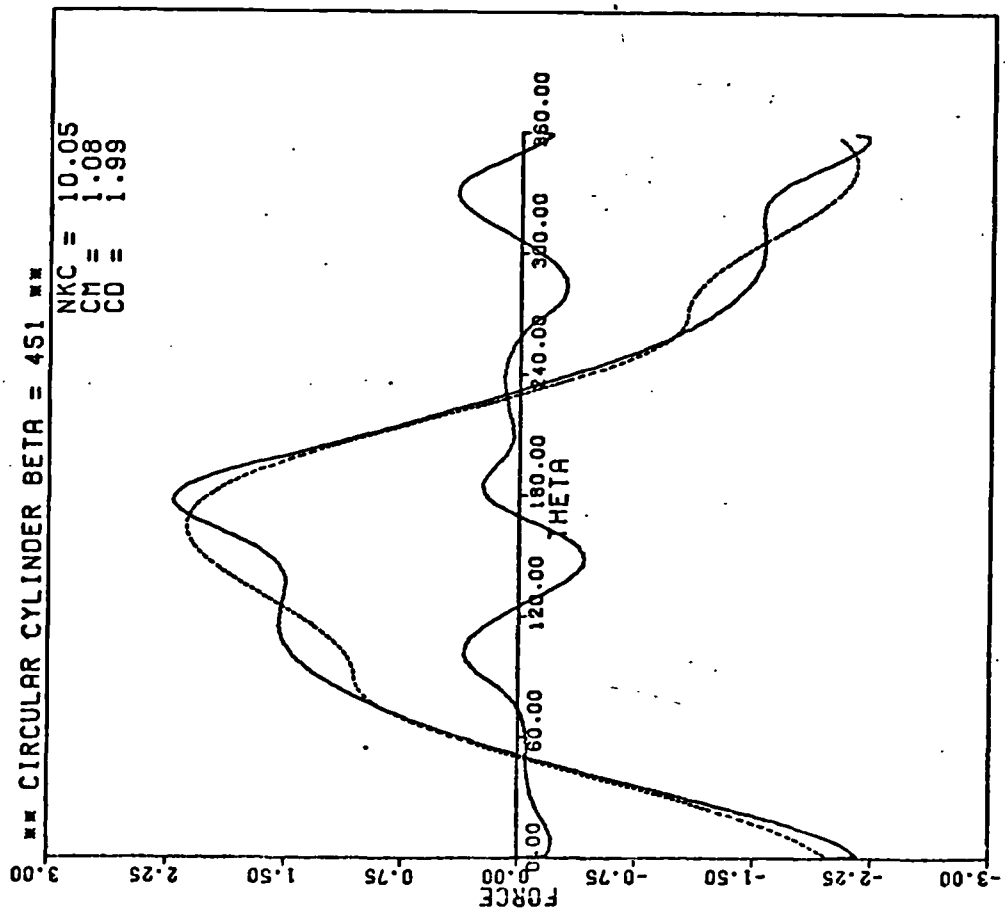

FIG: 4.19 (c)

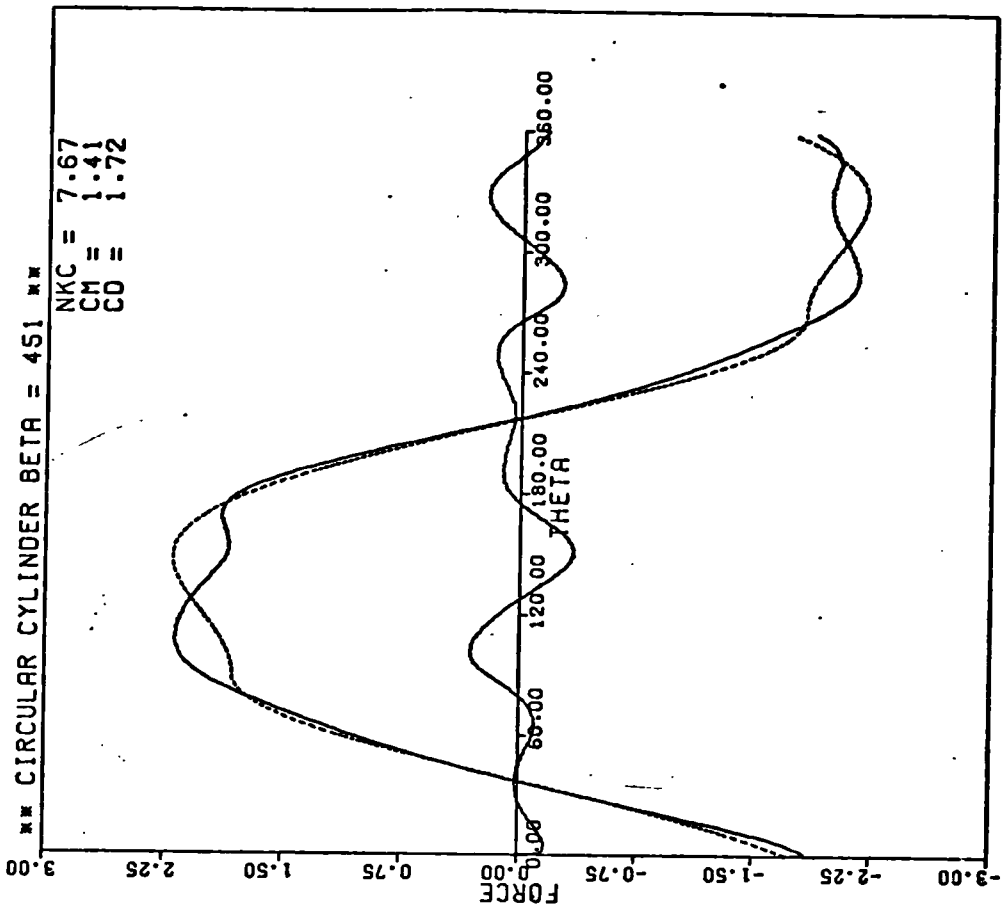

FIG: 4.19 (b)

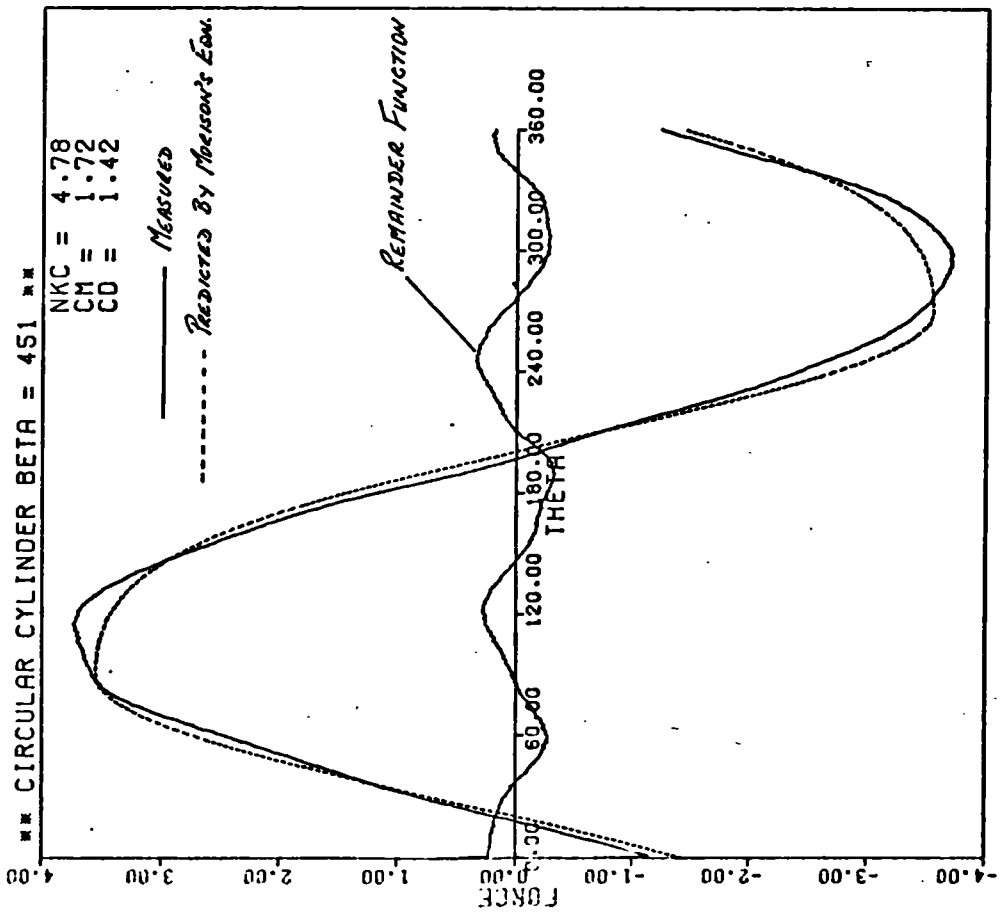

FIG: 4.19 (a)

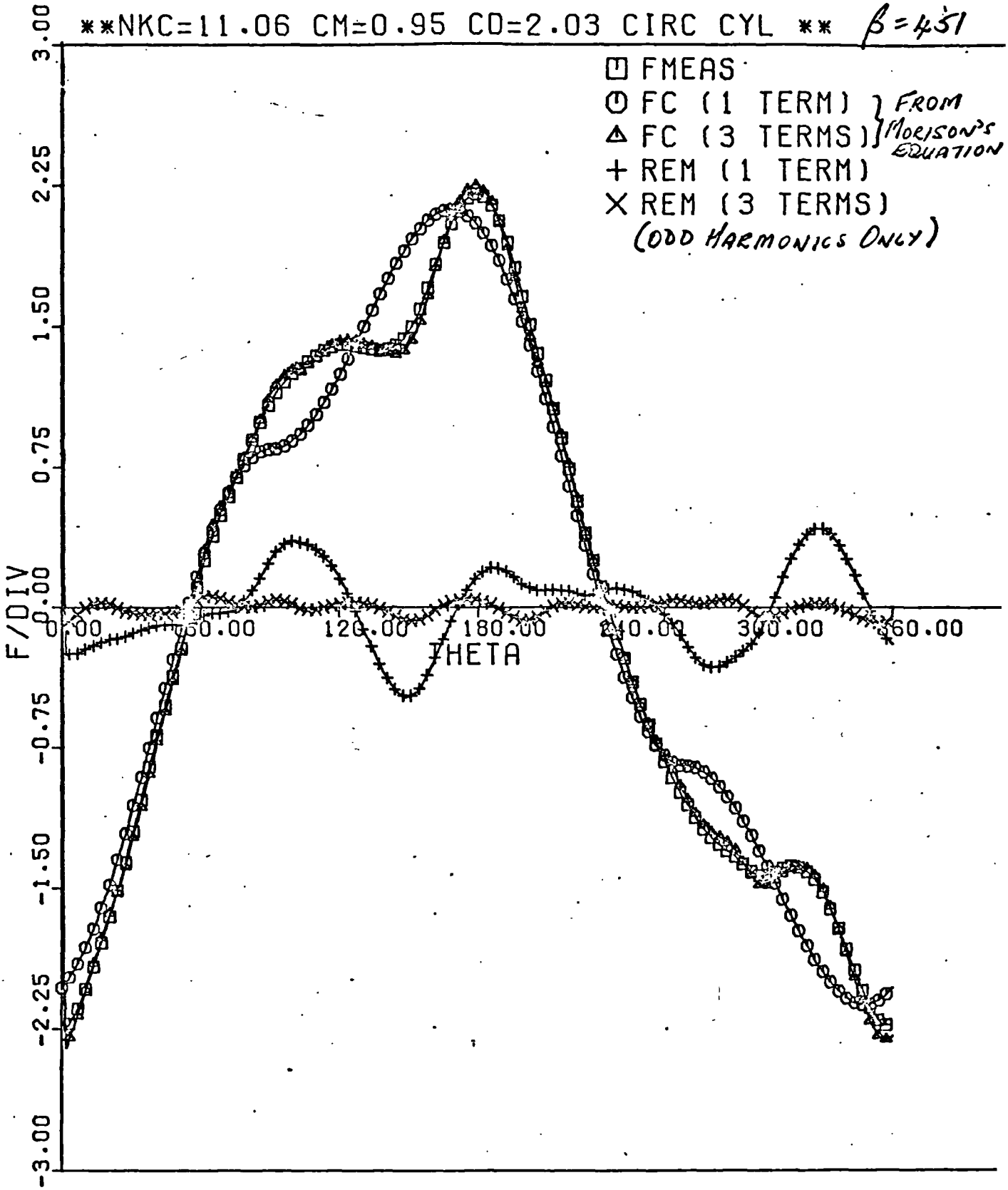
**NKC=11.06 CM=0.95 CD=2.03 CIRC CYL **
β=451
FMEAS
FC (1 TERM)
FC (3 TERMS)
FROM MORISON'S EQUATION
REM (1 TERM)
REM (3 TERMS)
(ODD HARMONICS ONLY)
F/DIV
3.00
2.25
1.50
0.75
0.00
-0.75
-1.50
-2.25
-3.00
0.00
60.00
120.00
180.00
240.00
300.00
360.00
THETA

FIG: 4.20

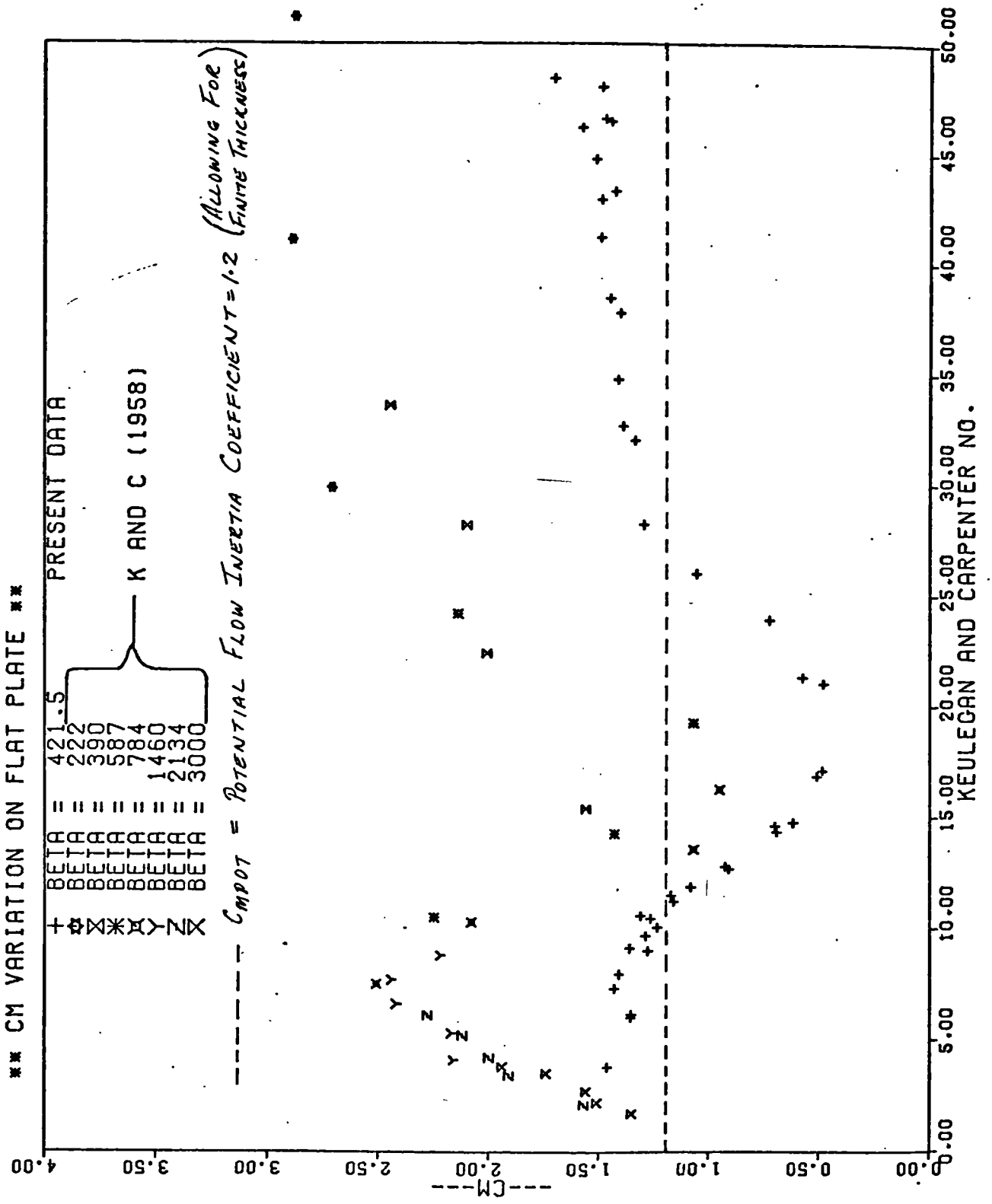
** CM VARIATION ON FLAT PLATE **
PRESENT DATA
BETA = 421.5
BETA = 222
BETA = 3390
BETA = 5587
BETA = 7784
BETA = 14600
BETA = 21340
BETA = 30000
K AND C (1958)
CMDOT = POTENTIAL FLOW INERTIA COEFFICIENT = 1.2 (ALLOWING FOR FINITE THICKNESS)
---CM---
KEULEGAN AND CARPENTER NO.
0.00
5.00
10.00
15.00
20.00
25.00
30.00
35.00
40.00
45.00
50.00
0.00
0.50
1.00
1.50
2.00
2.50
3.00
3.50
4.00

FIG:4·21

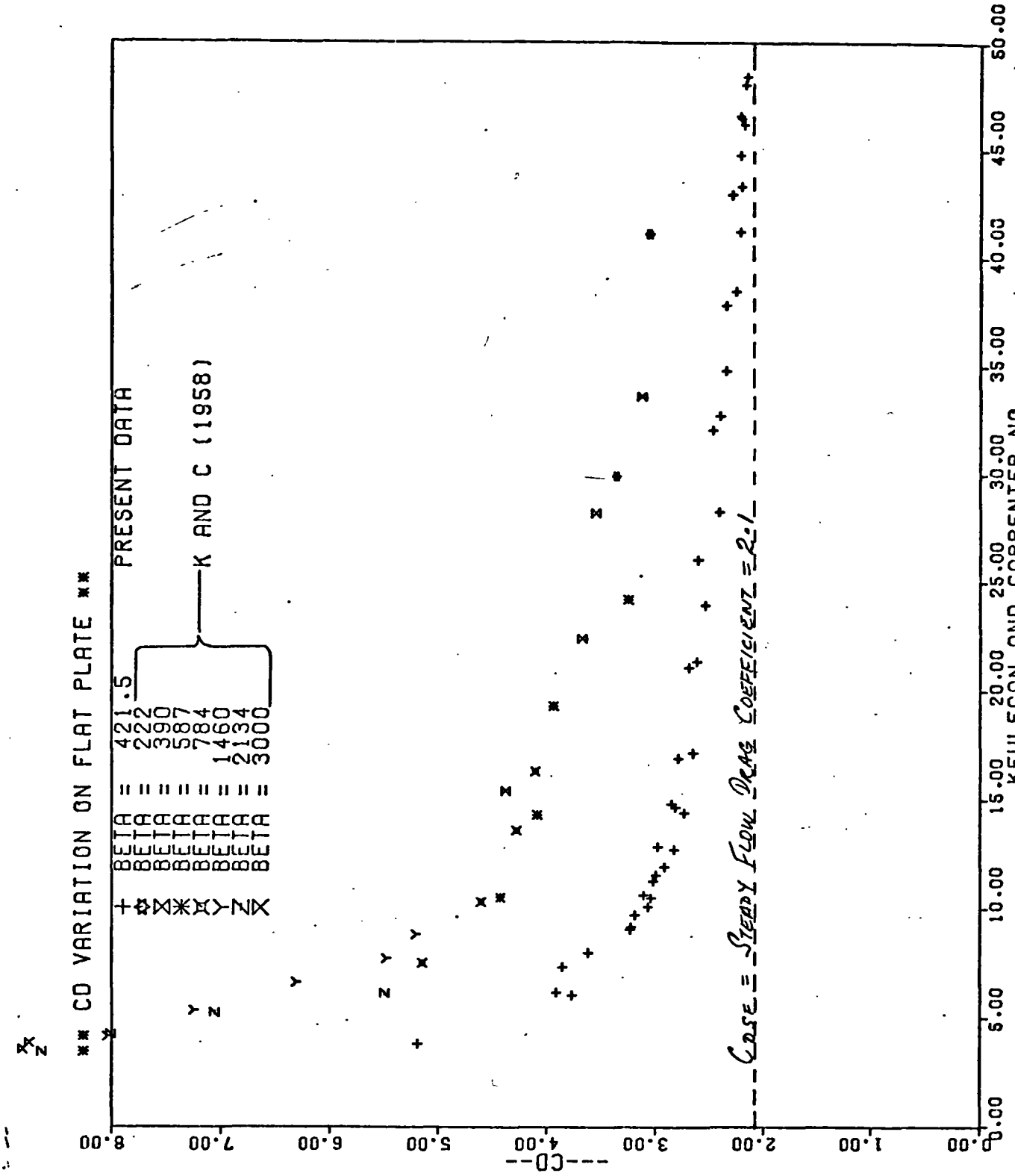
** CD VARIATION ON FLAT PLATE **
PRESENT DATA
BETA = 421.5
BETA = 222
BETA = 390
BETA = 587
BETA = 784
BETA = 1460
BETA = 2134
BETA = 3000
K AND C (1958)
CASE = STEADY FLOW DRAG COEFFICIENT = 2.1
--CD--
KEULEGAN AND CARPENTER NO.
0.00
5.00
10.00
15.00
20.00
25.00
30.00
35.00
40.00
45.00
50.00
1.00
2.00
3.00
4.00
6.00
7.00
8.00

FIG: 4.22

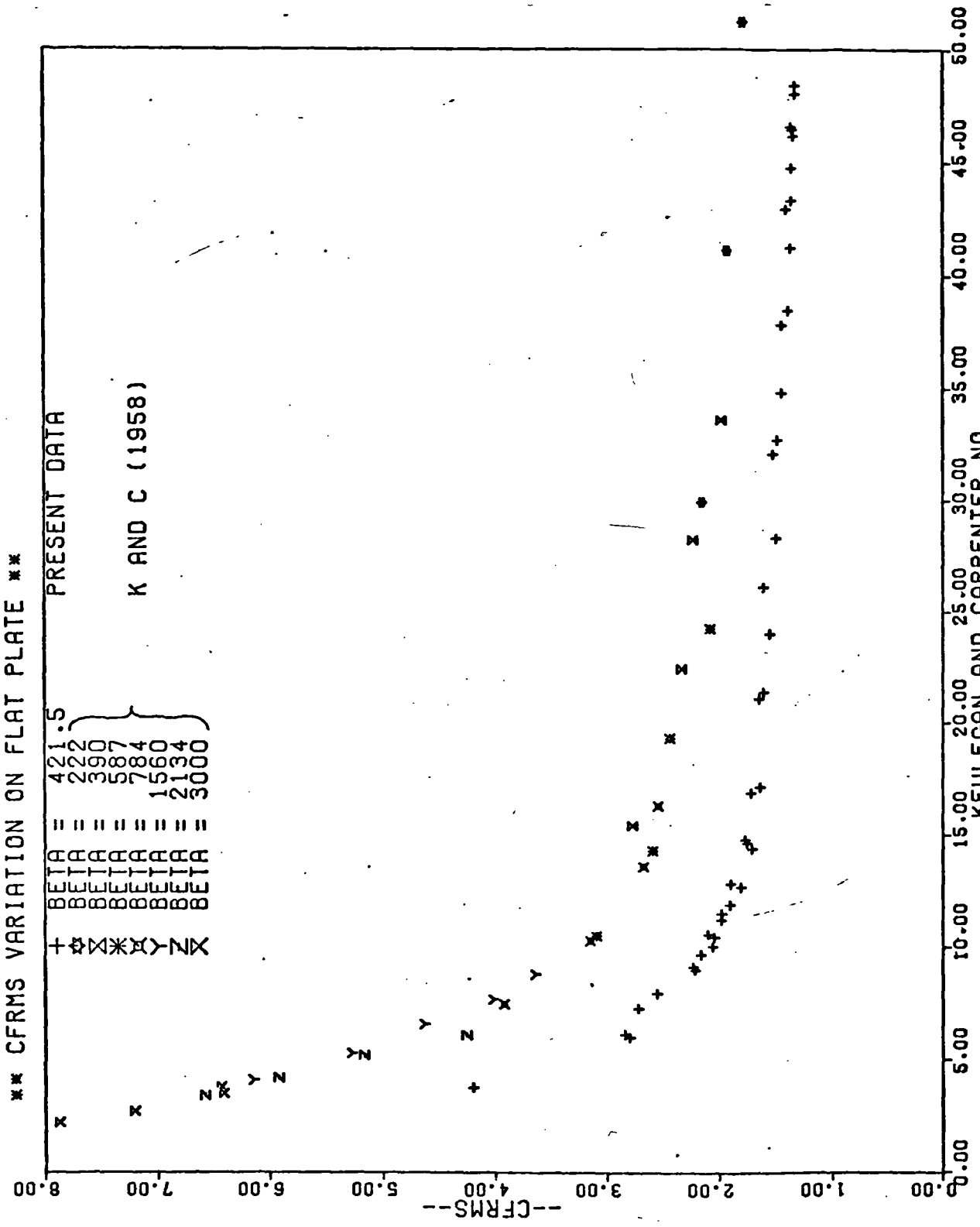
** CFRMS VARIATION ON FLAT PLATE **
PRESENT DATA
K AND C (1958)
BETA = 421.5
BETA = 2222
BETA = 3990
BETA = 5587
BETA = 7784
BETA = 15560
BETA = 21134
BETA = 30000
--CFRMS--
KEULEGAN AND CARPENTER NO-
0.00
1.00
2.00
3.00
4.00
5.00
6.00
7.00
8.00
0.00
5.00
10.00
15.00
20.00
25.00
30.00
35.00
40.00
45.00
50.00

FIG:4.23

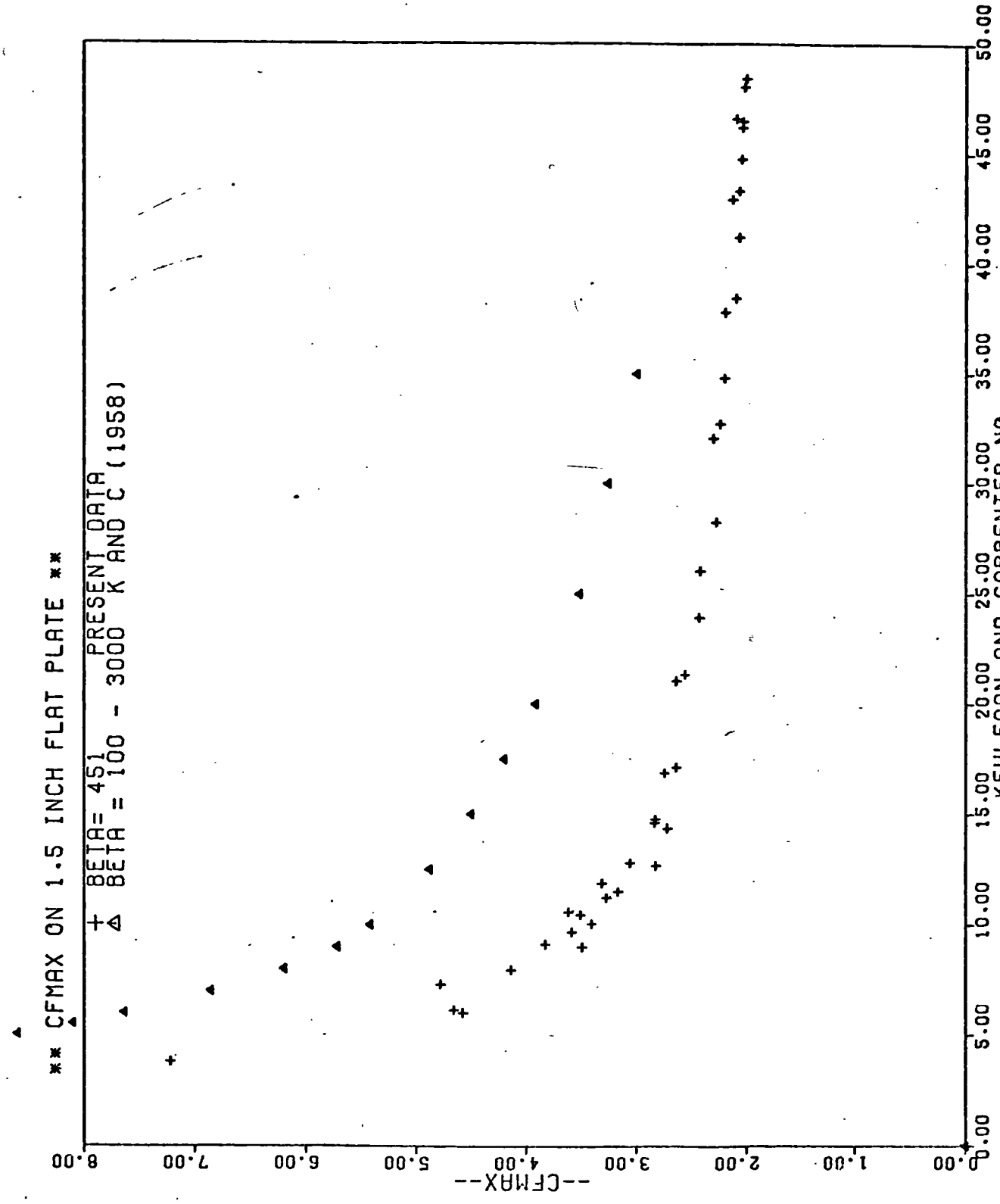
** CFMAX ON 1.5 INCH FLAT PLATE **
+ BETA= 45 PRESENT DATA
Δ BETA = 100 - 3000 K AND C (1958)
--CFMAX--
KEULEGAN AND CARPENTER NO.
0.00
1.00
2.00
3.00
4.00
5.00
6.00
7.00
8.00
0.00
5.00
10.00
15.00
20.00
25.00
30.00
35.00
40.00
45.00
50.00

FIG: 4·24

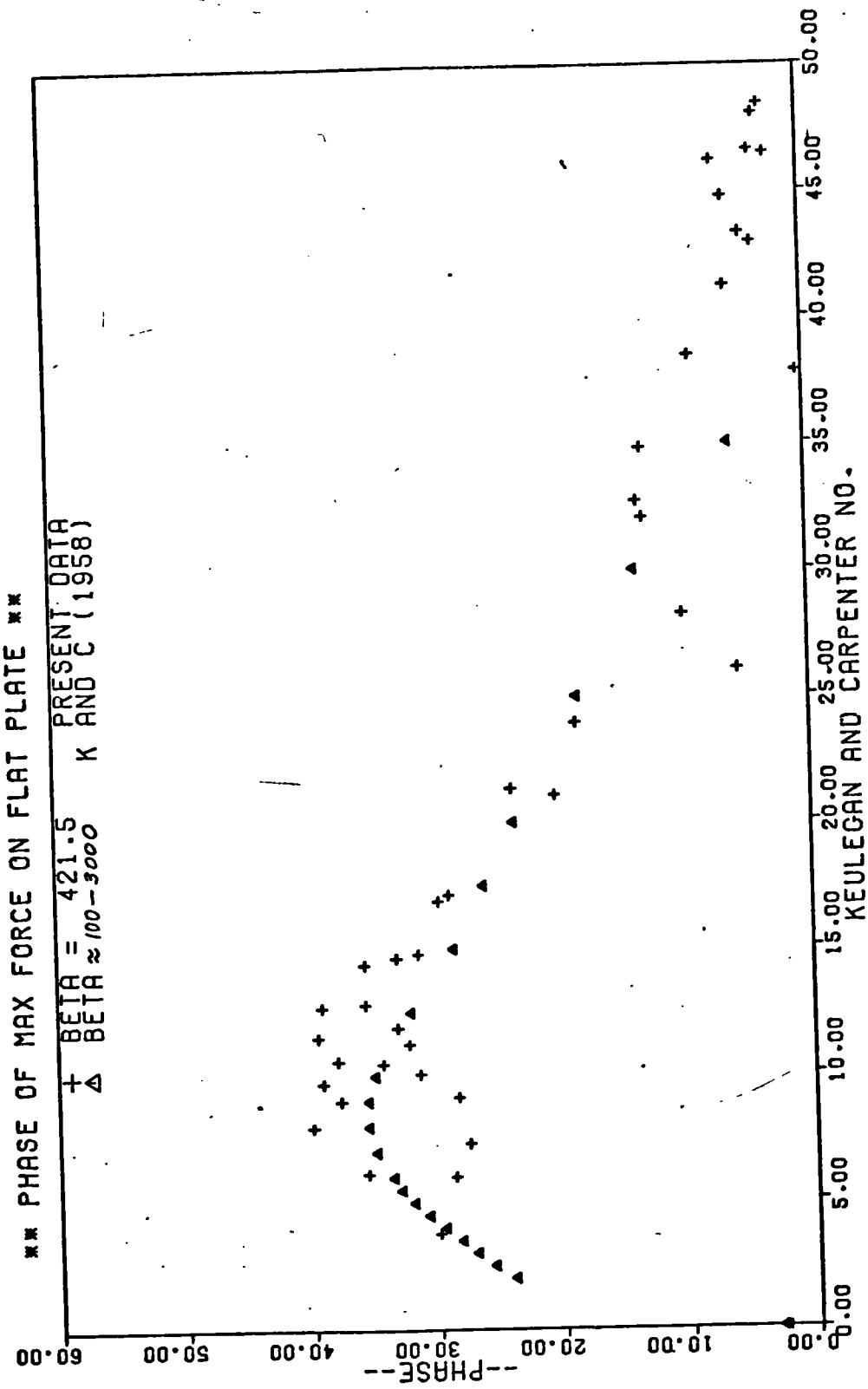
** PHASE OF MAX FORCE ON FLAT PLATE **
+ BETA = 421.5 PRESENT DATA
Δ BETA ≈ 100-3000 K AND C (1958)
--PHASE--
KEULEGAN AND CARPENTER NO.
0.00
5.00
10.00
15.00
20.00
25.00
30.00
35.00
40.00
45.00
50.00
10.00
20.00
30.00
40.00
50.00
60.00

FIG:4·25

RUN 39 NKC =6.15 1.5 IN DIAMETER FLAT PLATE $\beta = 421.5$

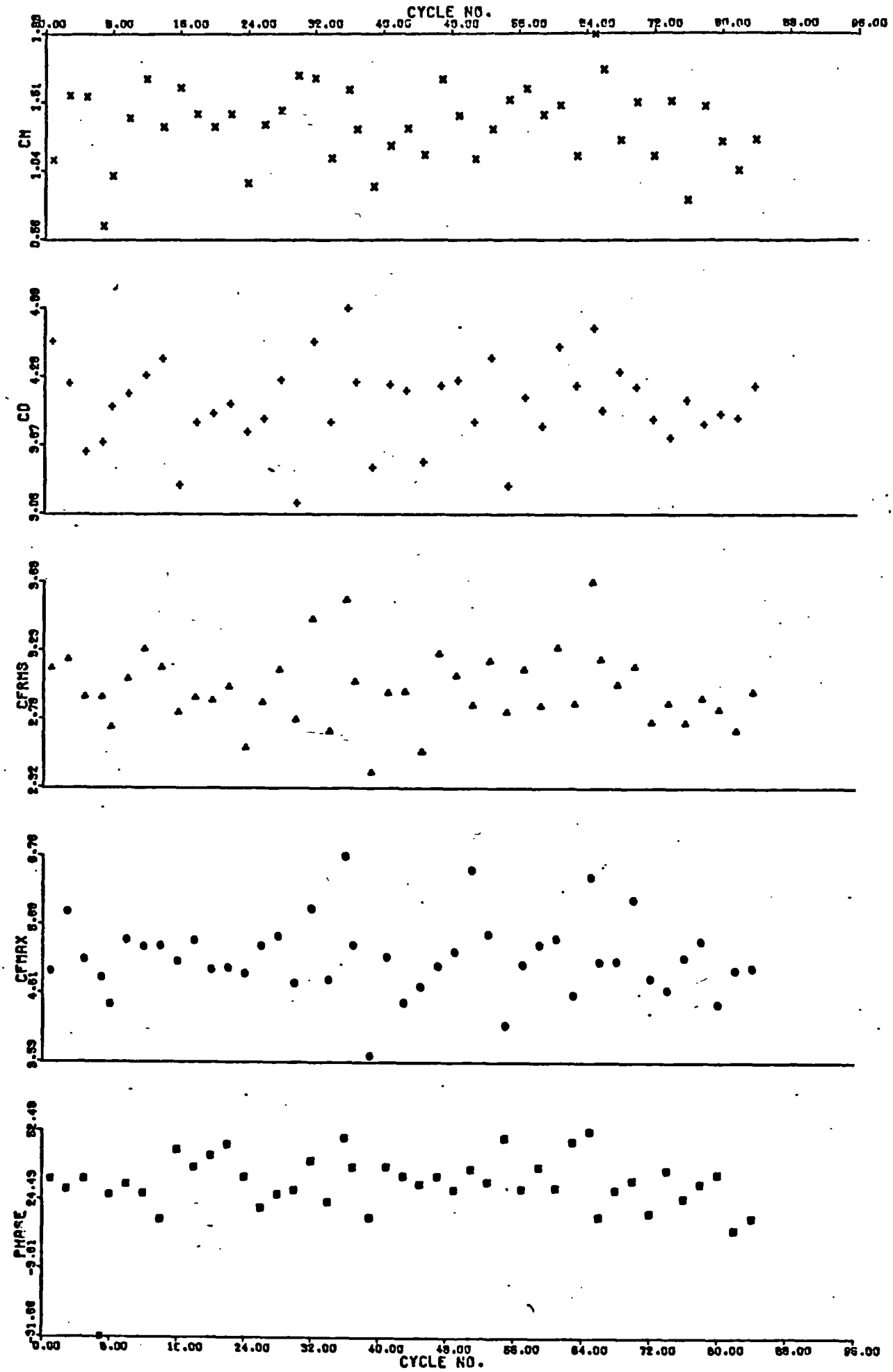

FIG: 4·26

** 1.5 IN FLAT PLATE NKC = 14.79 ** $\beta = 421.5$

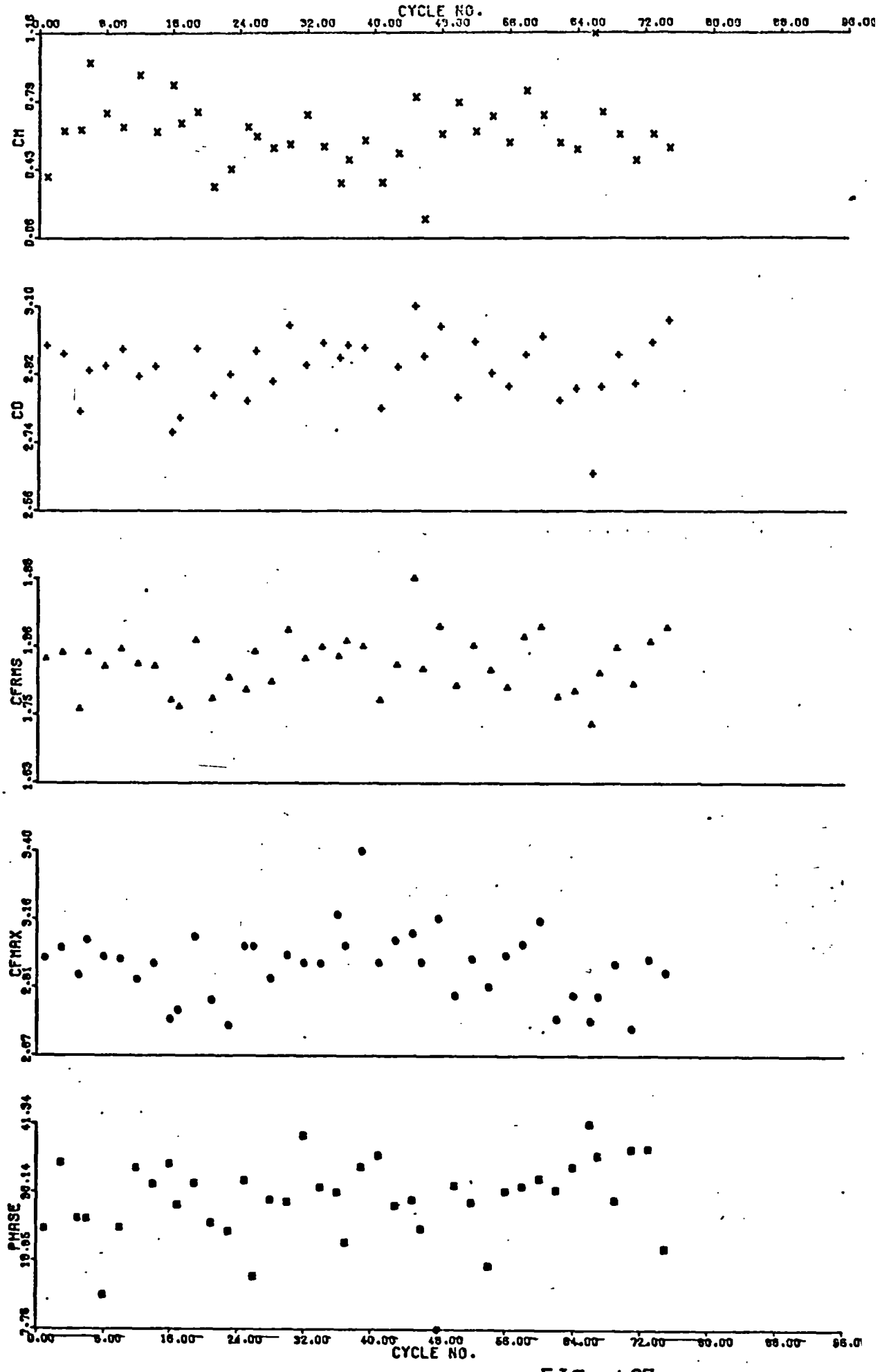

FIG : 4.27

RUN 29 NKC =43.33 1.5 IN DIAMETER FLAT PLATE $\beta = 421.5$

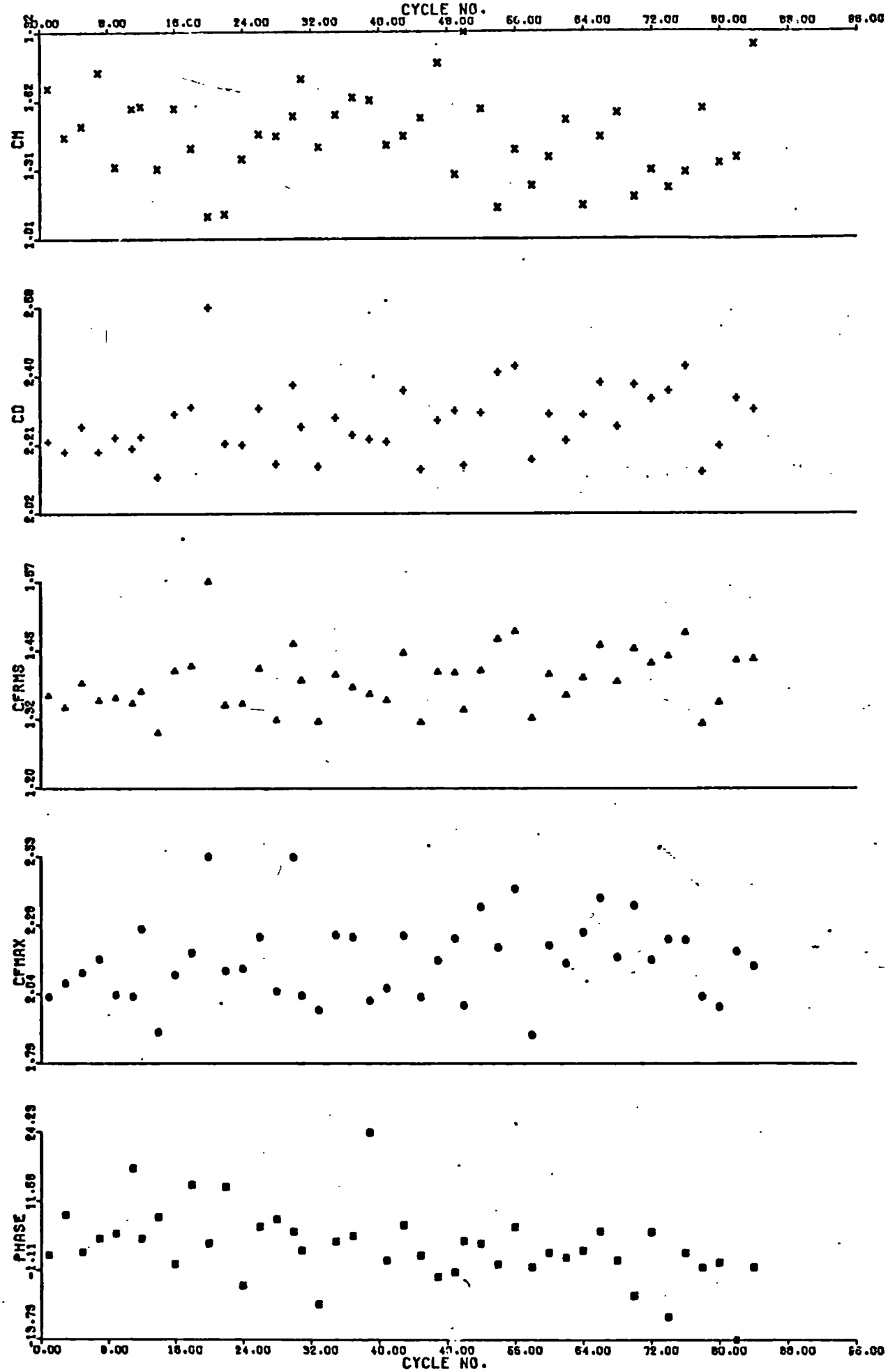

FIG : 4·28

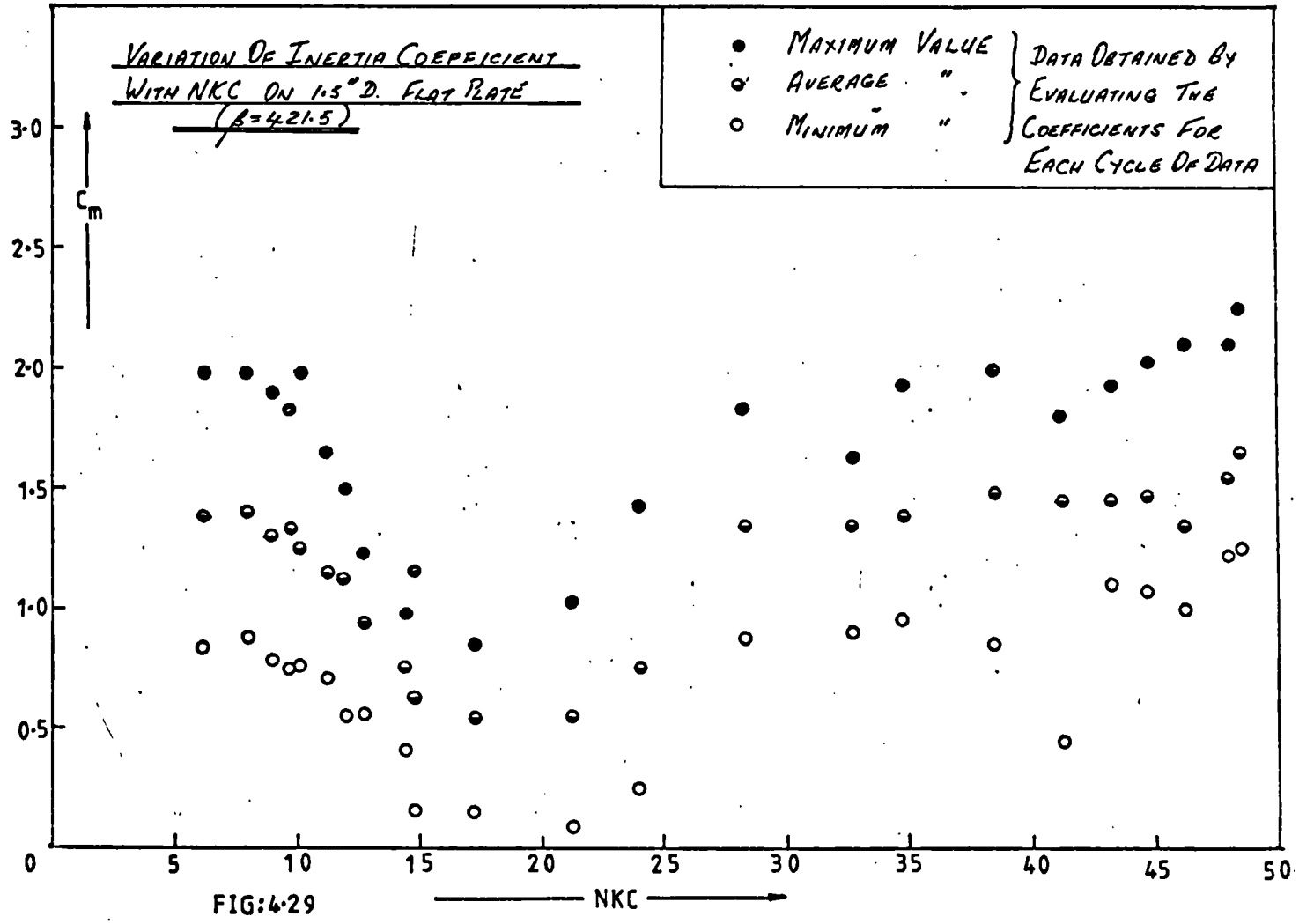
VARIATION OF INERTIA COEFFICIENT
WITH NKC ON 1.5" D. FLAT PLATE
(β=421.5)
MAXIMUM VALUE
AVERAGE "
MINIMUM "
DATA OBTAINED BY EVALUATING THE COEFFICIENTS FOR EACH CYCLE OF DATA
C_m
3·0
2·5
2·0
1·5
1·0
0·5
0
5
10
15
20
25
30
35
40
45
50
NKC

FIG:4·29

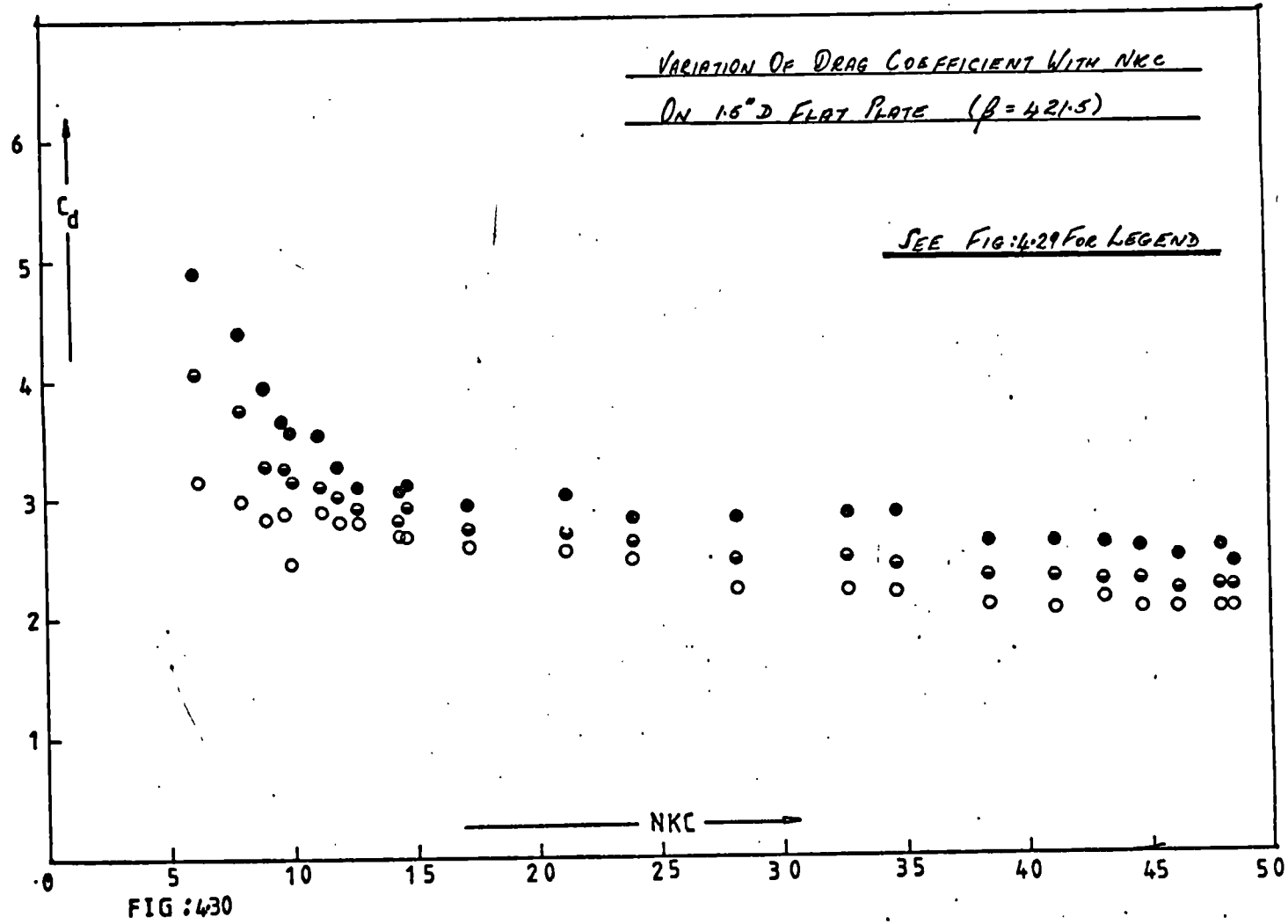
VARIATION OF DRAG COEFFICIENT WITH NKC
ON 1.6"D FLAT PLATE (β = 421.5)
SEE FIG:4.29 FOR LEGEND
C_d
NKC
0
1
2
3
4
5
6
5
10
15
20
25
30
35
40
45
50

FIG :4.30

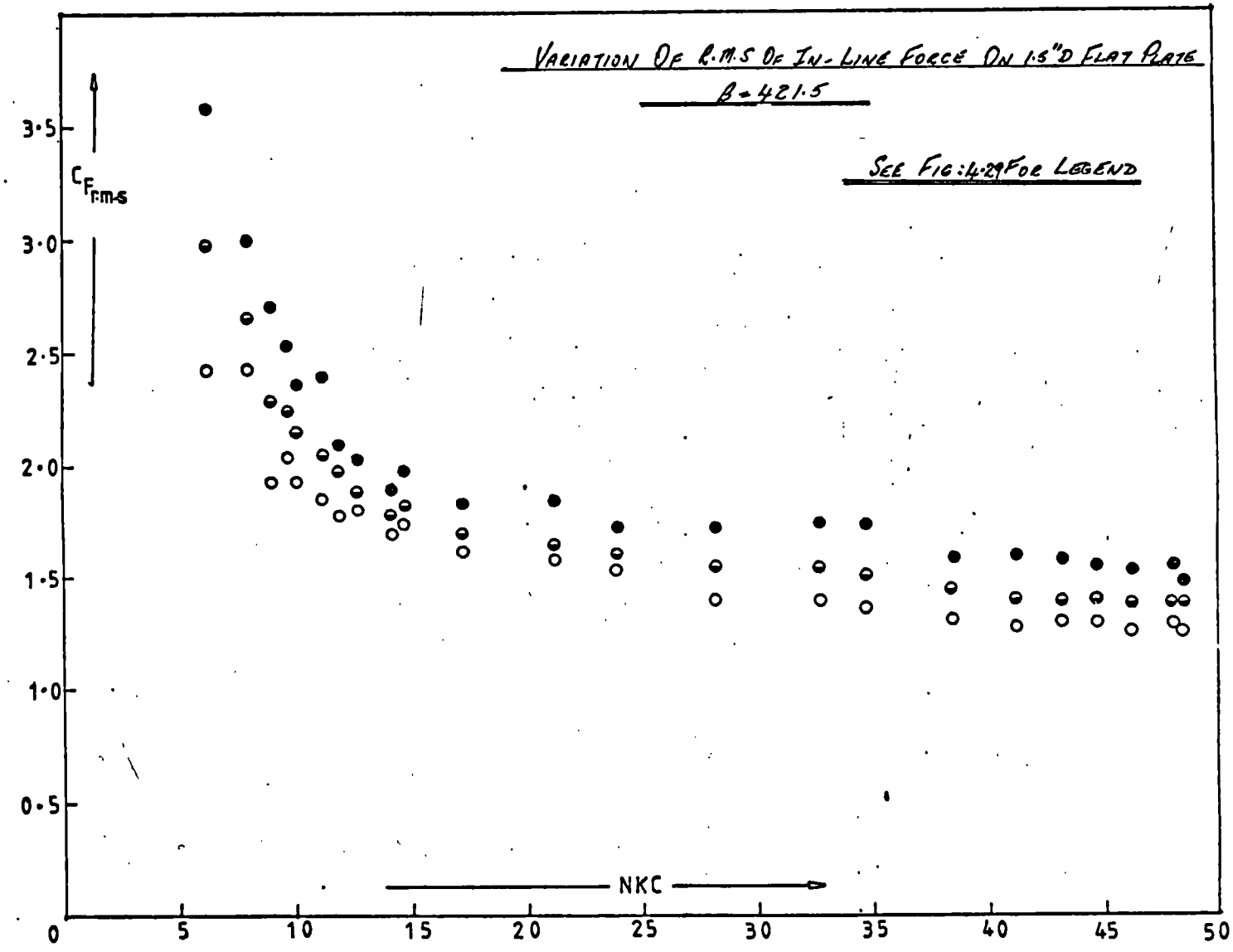
VARIATION OF R.M.S OF IN-LINE FORCE ON 1.5"D FLAT PLATE
B=421.5
SEE FIG:4.29 FOR LEGEND
$C_{F_{r.m.s}}$
3·5
3·0
2·5
2·0
1·5
1·0
0·5
0
5
10
15
20
25
30
35
40
45
50
NKC

FIG: 4.31

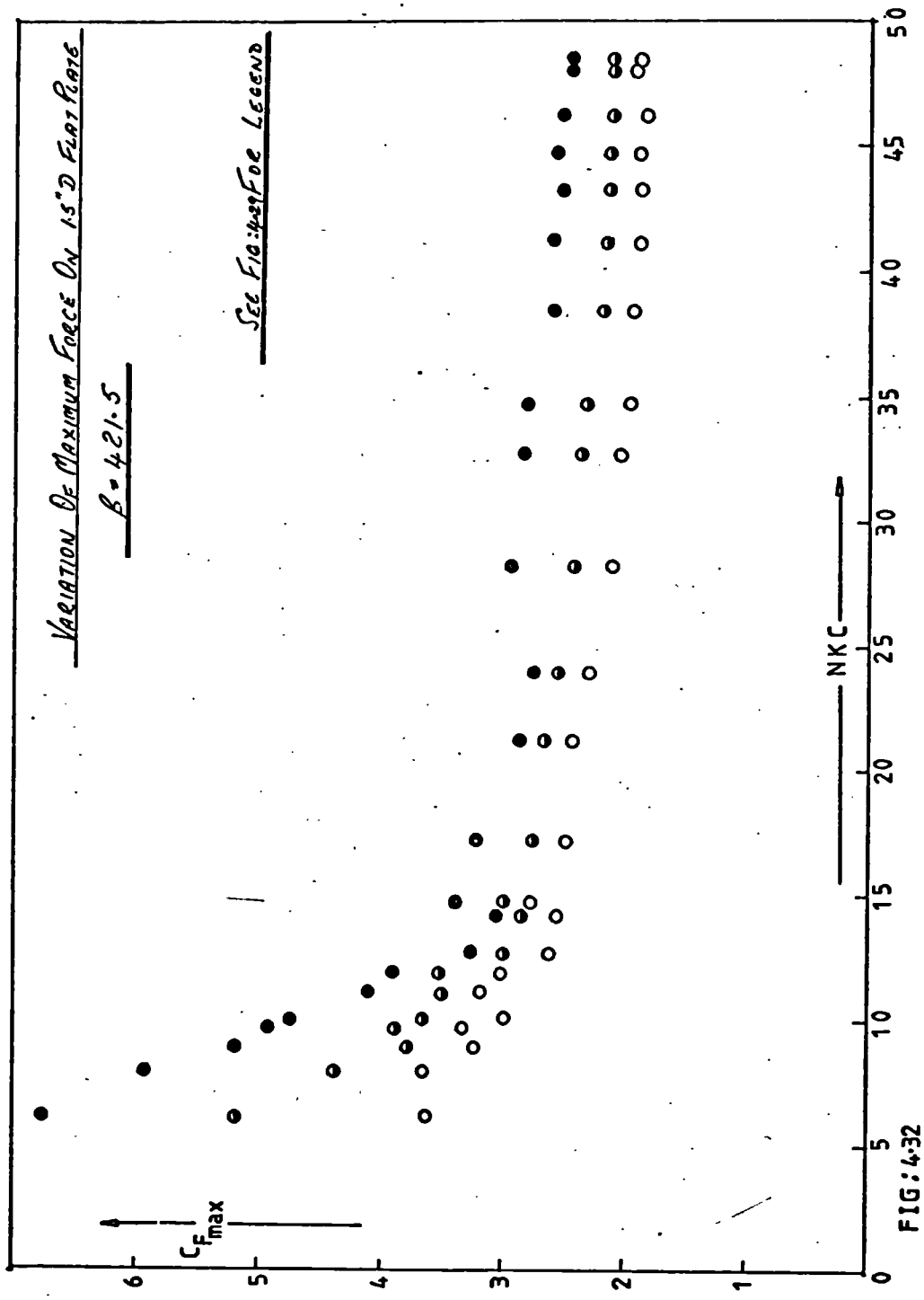
VARIATION OF MAXIMUM FORCE ON 15°D FLAT PLATE
β = 421.5
SEE FIG: 4.28 FOR LEGEND
$C_{F_{max}}$
NKC
0
1
2
3
4
5
6
10
15
20
25
30
35
40
45
50

FIG: 4.32

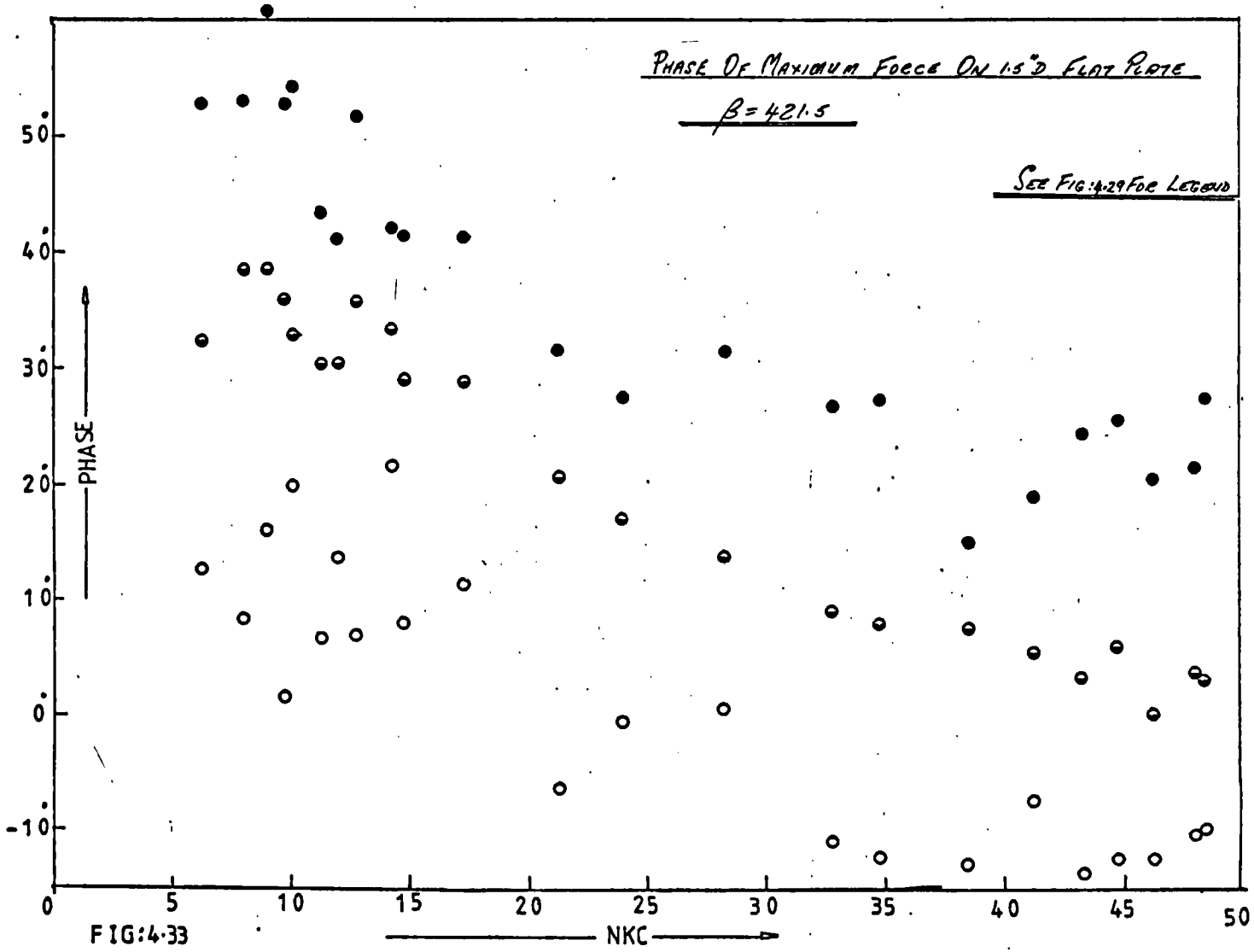
PHASE OF MAXIMUM FORCE ON 1.5"D FLAT PLATE
β=421.5
SEE FIG:4.29 FOR LEGEND
PHASE
50
40
30
20
10
0
-10
0
5
10
15
20
25
30
35
40
45
50
NKC

FIG:4.33

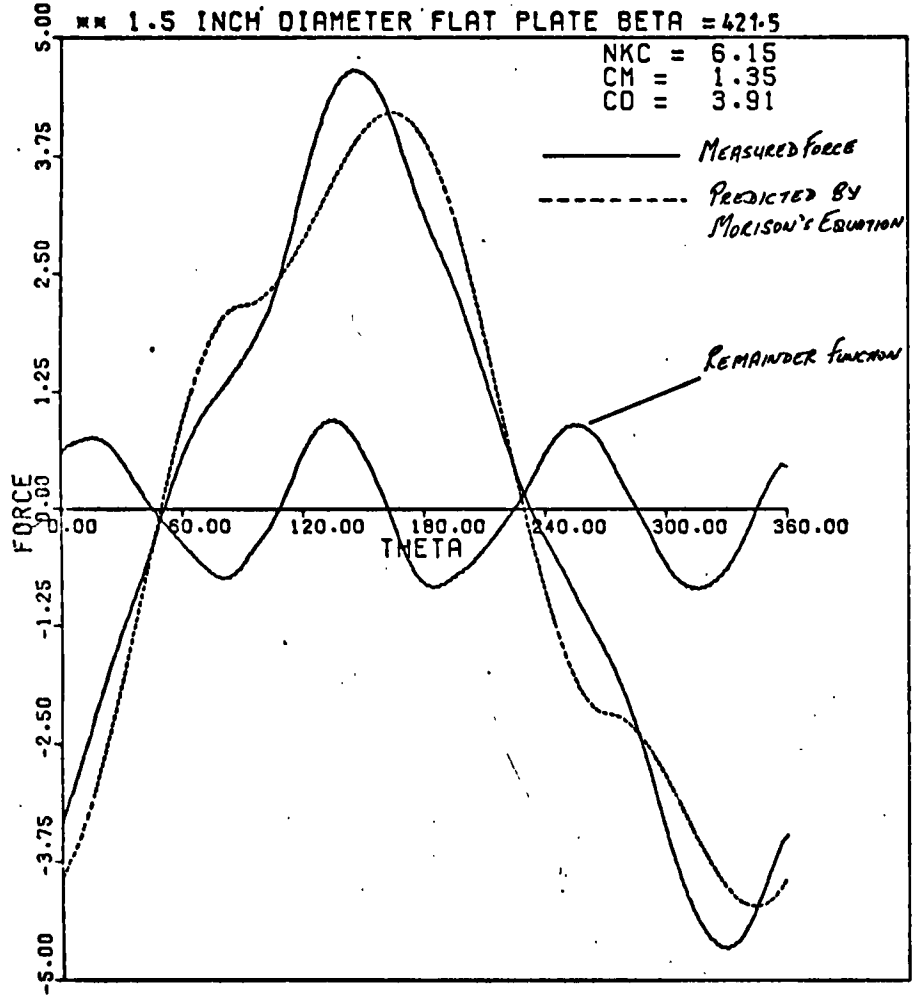

FIG: 4.34 (a)

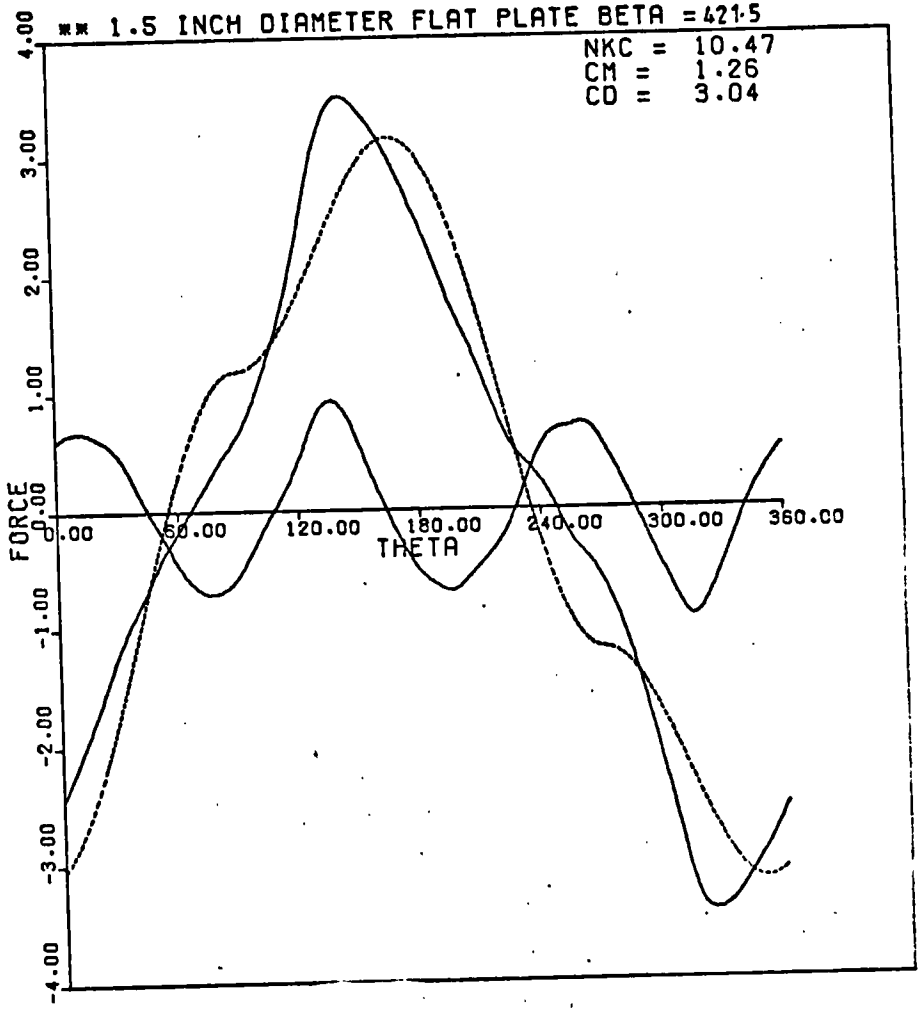

FIG: 4.34 (b)

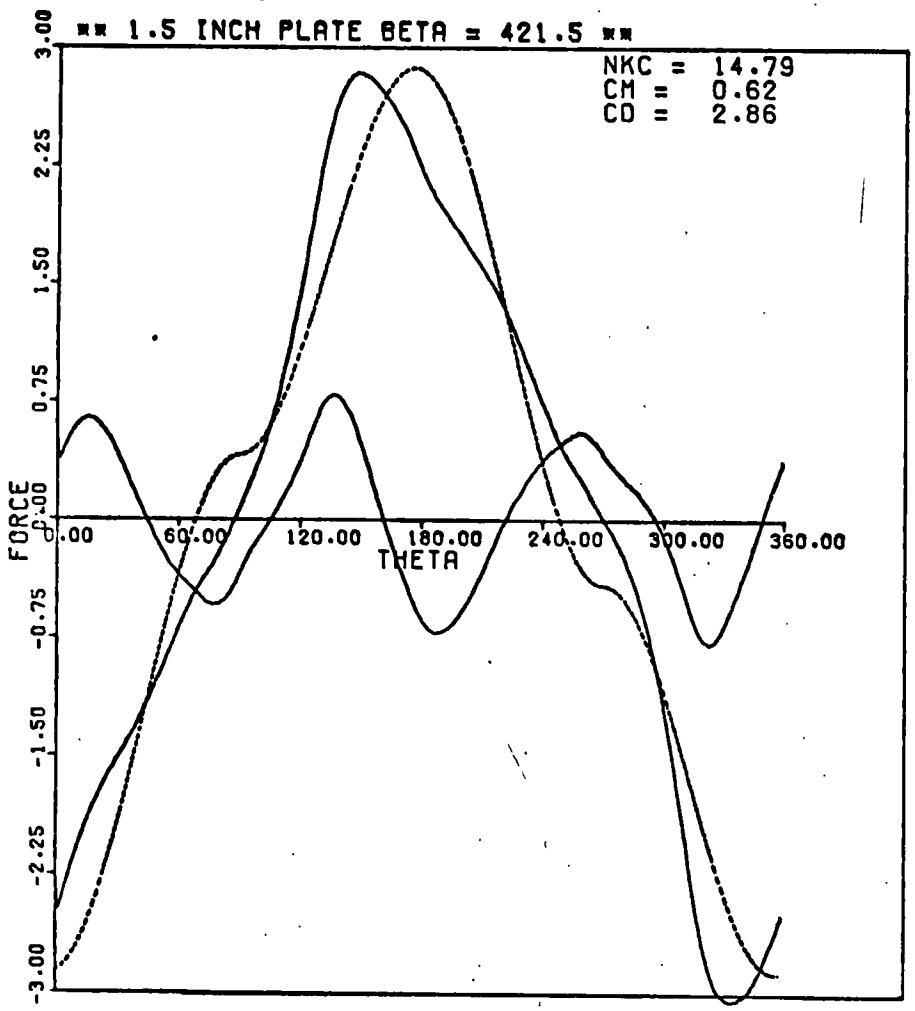

FIG: 4.34 (c)

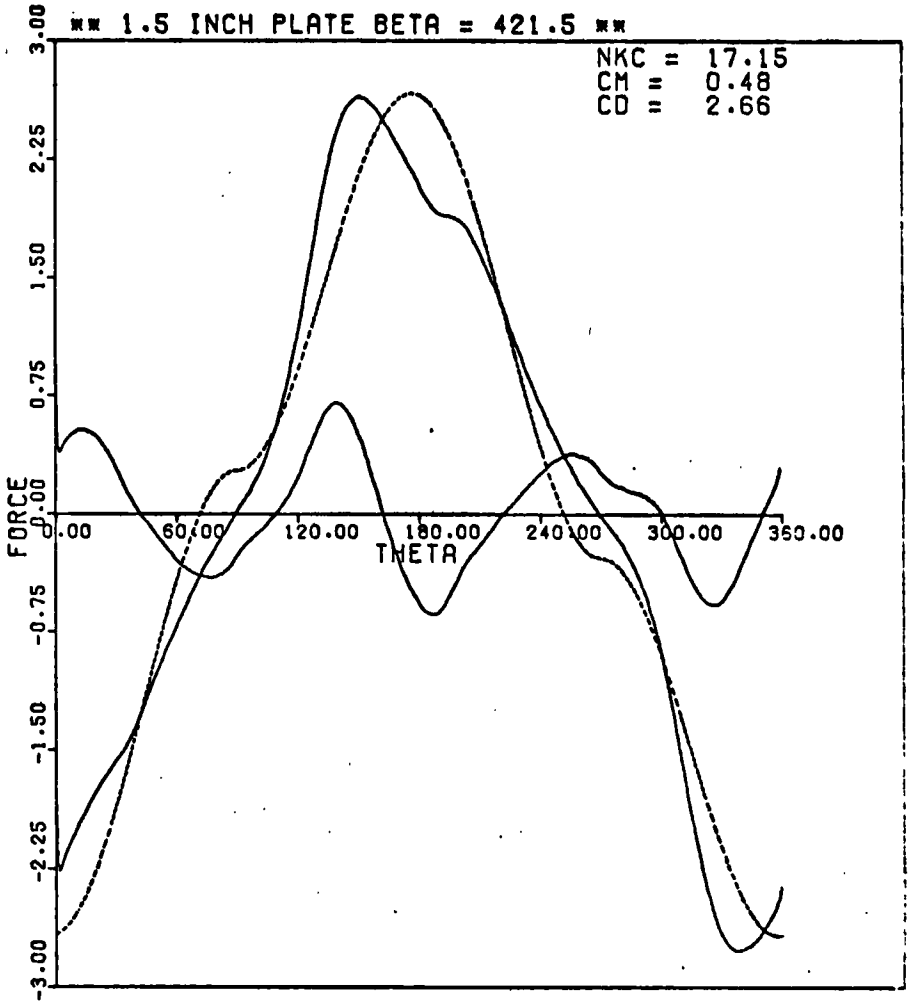

FIG: 4.34 (d)

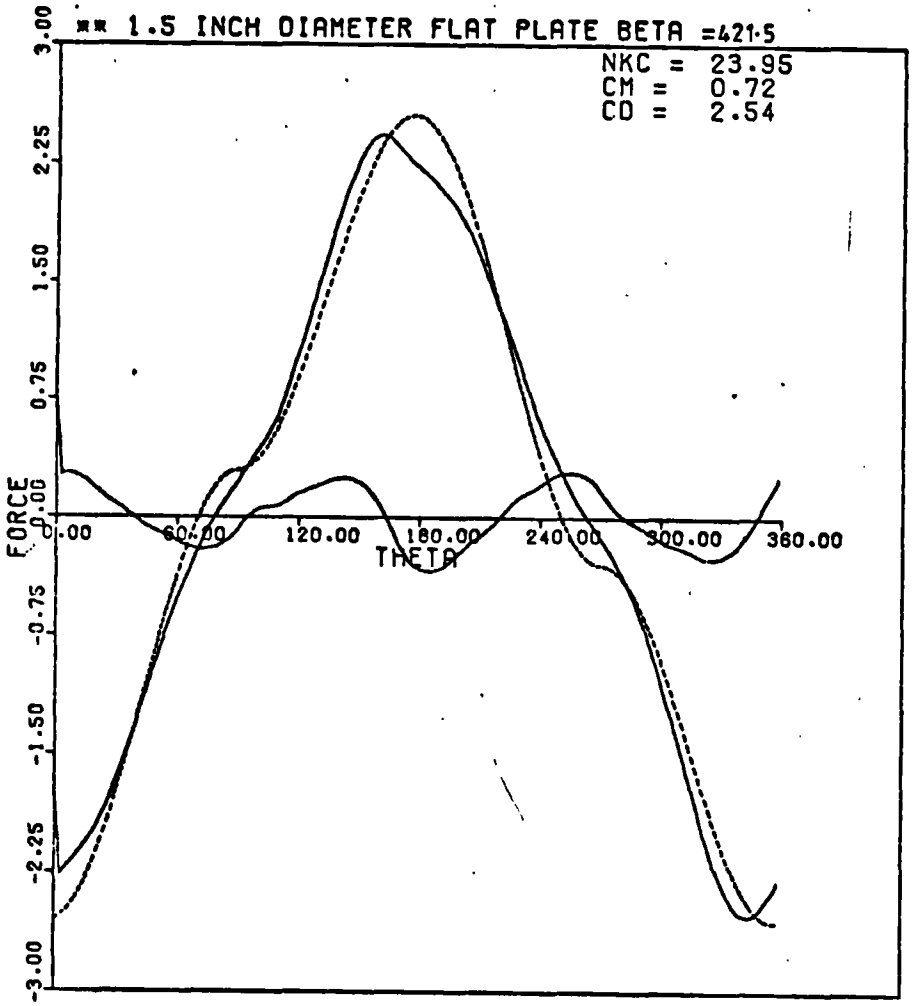

FIG: 4.34 (e)

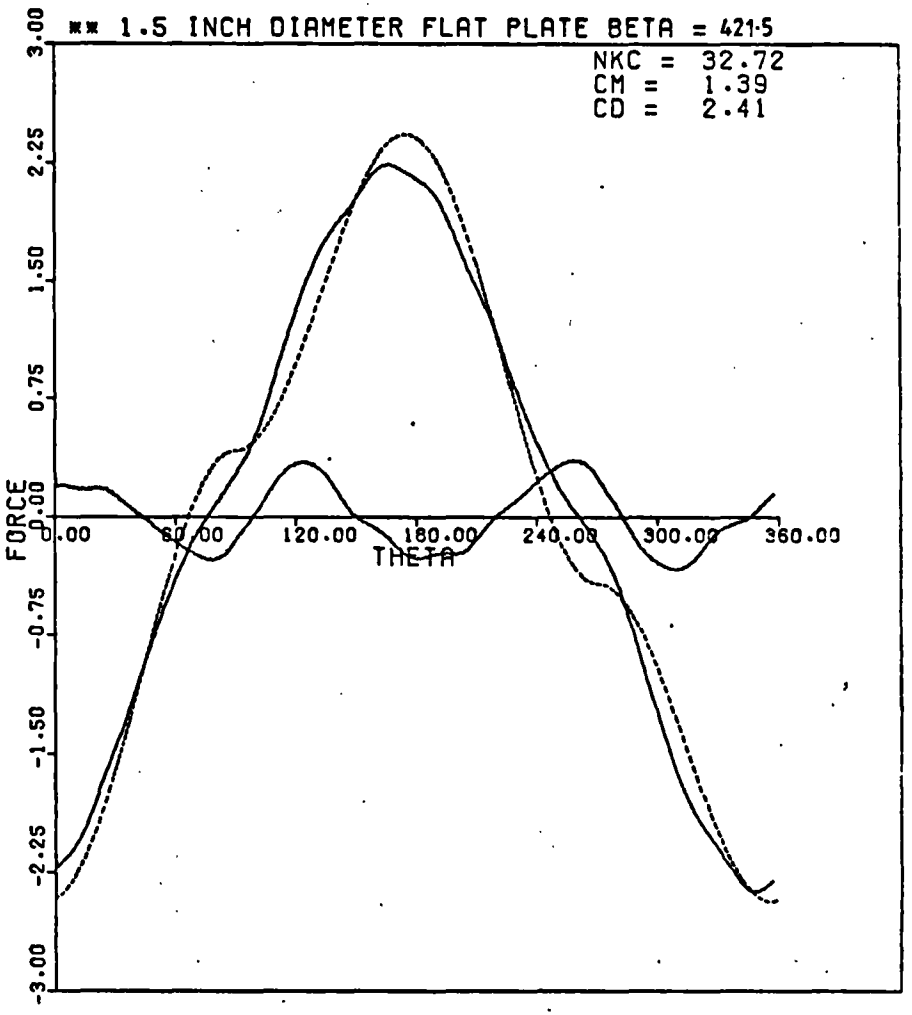

FIG: 4.34 (f)

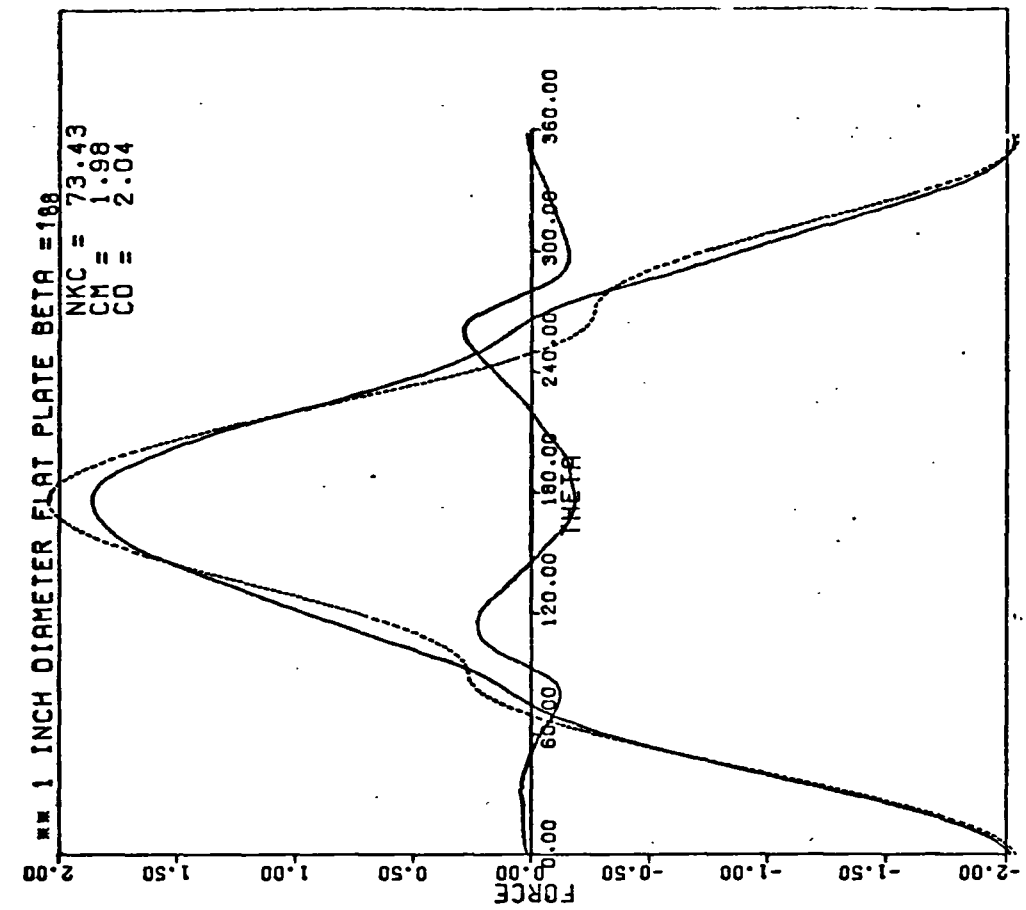

FIG: 4.34 (h)

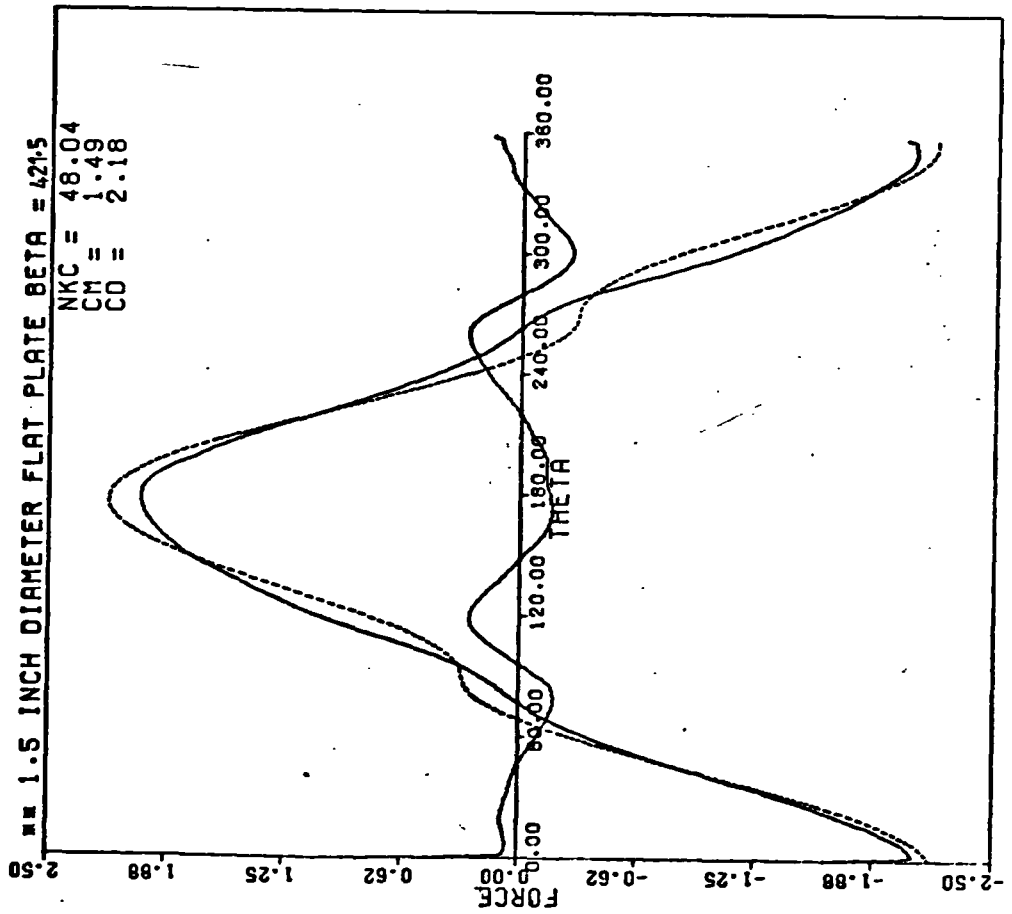

FIG: 4.34(g)

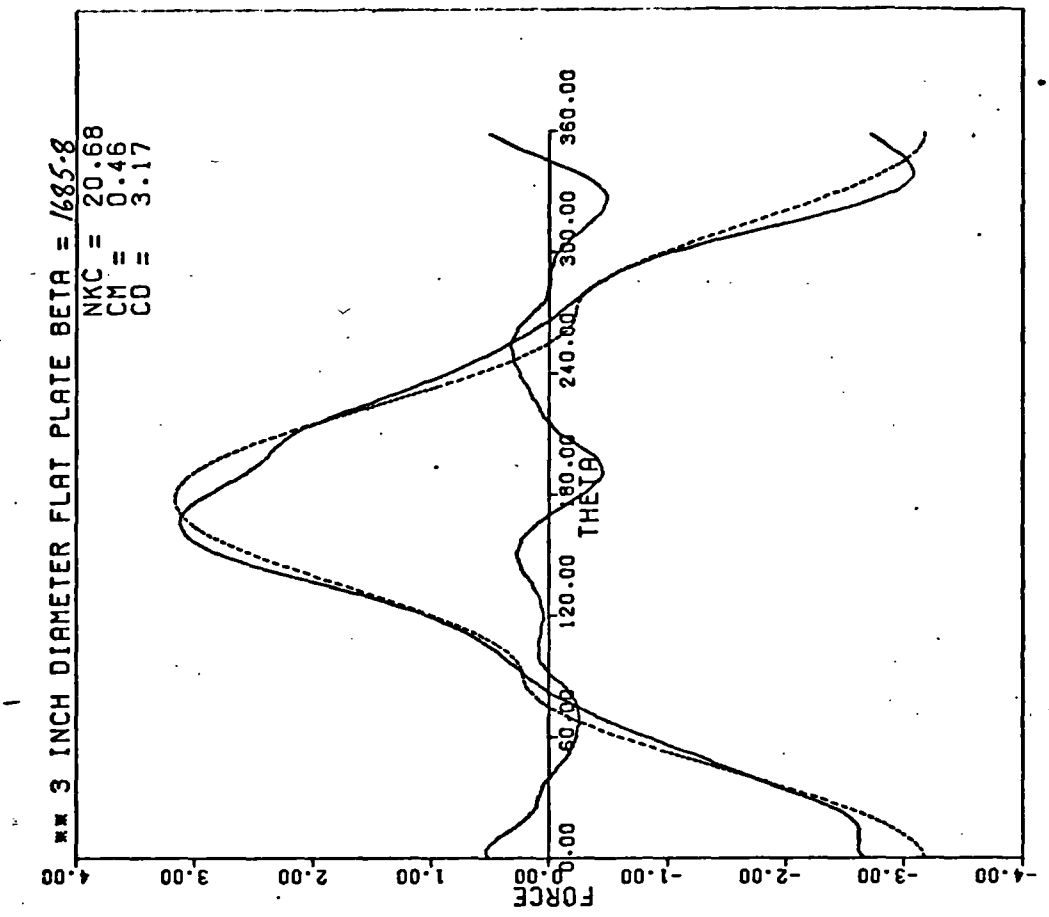

FIG: 4.35 (b)

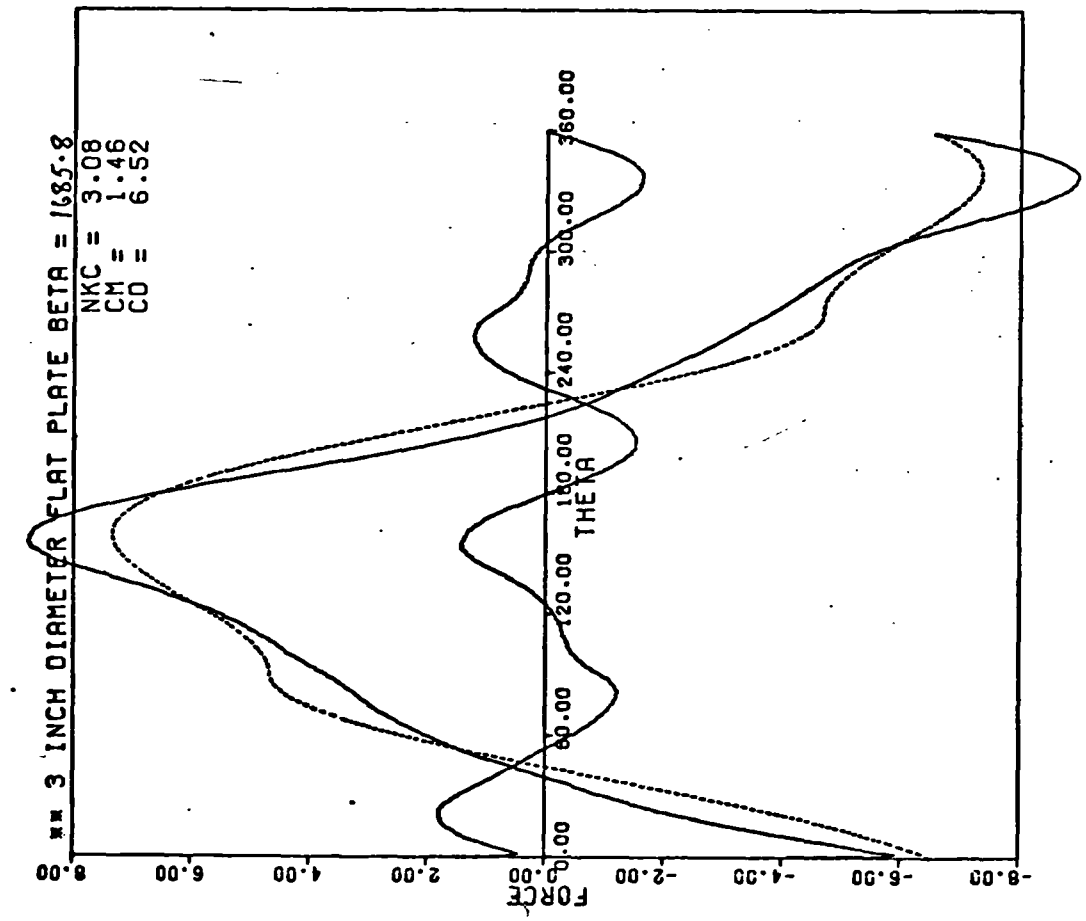

FIG: 4.35 (a)

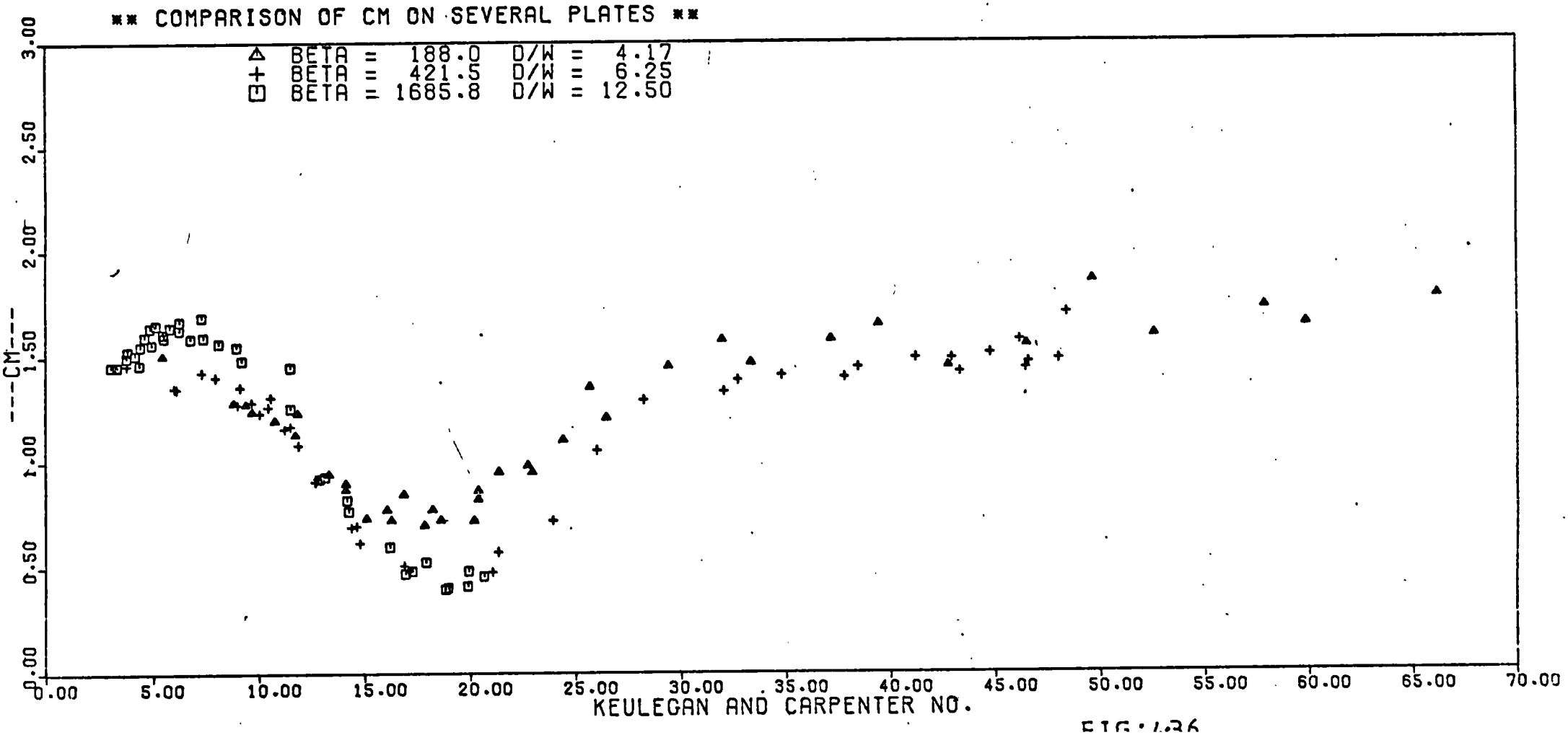
** COMPARISON OF CM ON SEVERAL PLATES **
△ BETA = 188.0 D/W = 4.17
+ BETA = 421.5 D/W = 6.25
□ BETA = 1685.8 D/W = 12.50
---CM---
0.00
0.50
1.00
1.50
2.00
2.50
3.00
0.00
5.00
10.00
15.00
20.00
25.00
30.00
35.00
40.00
45.00
50.00
55.00
60.00
65.00
70.00
KEULEGAN AND CARPENTER NO.

FIG. 4.36

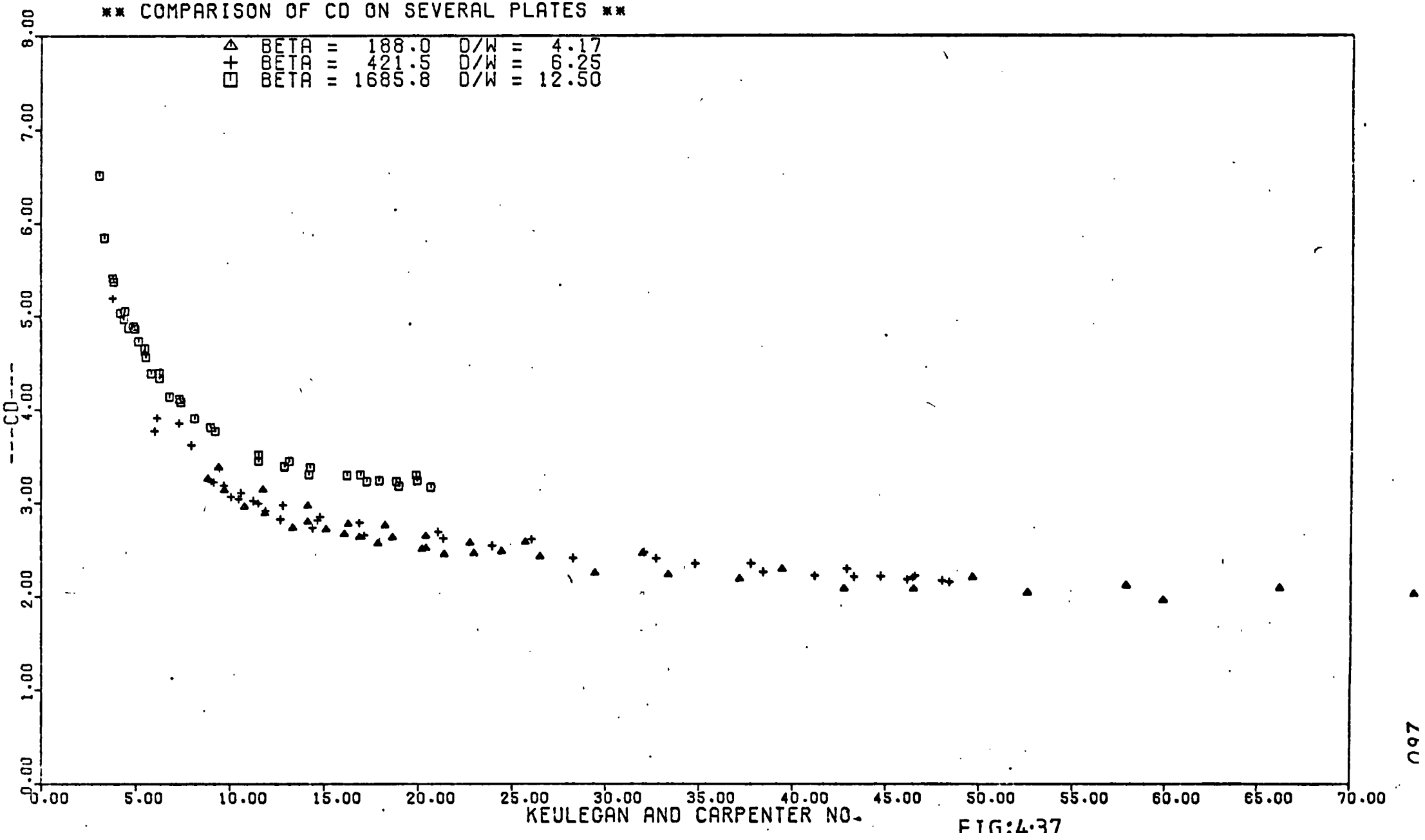
** COMPARISON OF CD ON SEVERAL PLATES **
BETA = 188.0 D/W = 4.17
BETA = 421.5 D/W = 6.25
BETA = 1685.8 D/W = 12.50
---CD---
0.00
1.00
2.00
3.00
4.00
5.00
6.00
7.00
8.00
0.00
5.00
10.00
15.00
20.00
25.00
30.00
35.00
40.00
45.00
50.00
55.00
60.00
65.00
70.00
KEULEGAN AND CARPENTER NO.

FIG:4.37

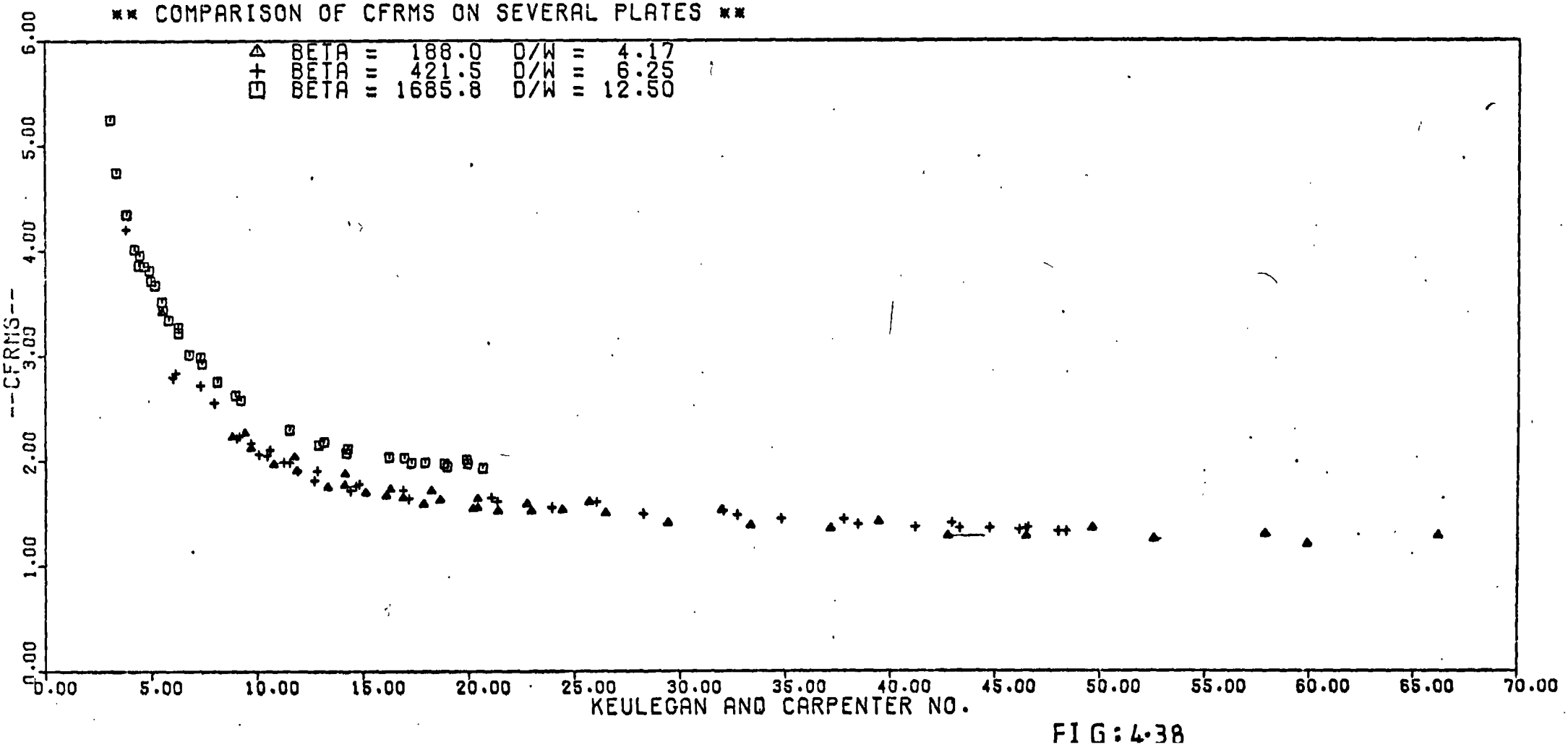
** COMPARISON OF CFRMS ON SEVERAL PLATES **
BETA = 188.0 D/W = 4.17
BETA = 421.5 D/W = 6.25
BETA = 1685.8 D/W = 12.50
--CFRMS--
0.00
1.00
2.00
3.00
4.00
5.00
6.00
0.00
5.00
10.00
15.00
20.00
25.00
30.00
35.00
40.00
45.00
50.00
55.00
60.00
65.00
70.00
KEULEGAN AND CARPENTER NO.

FIG:4.38

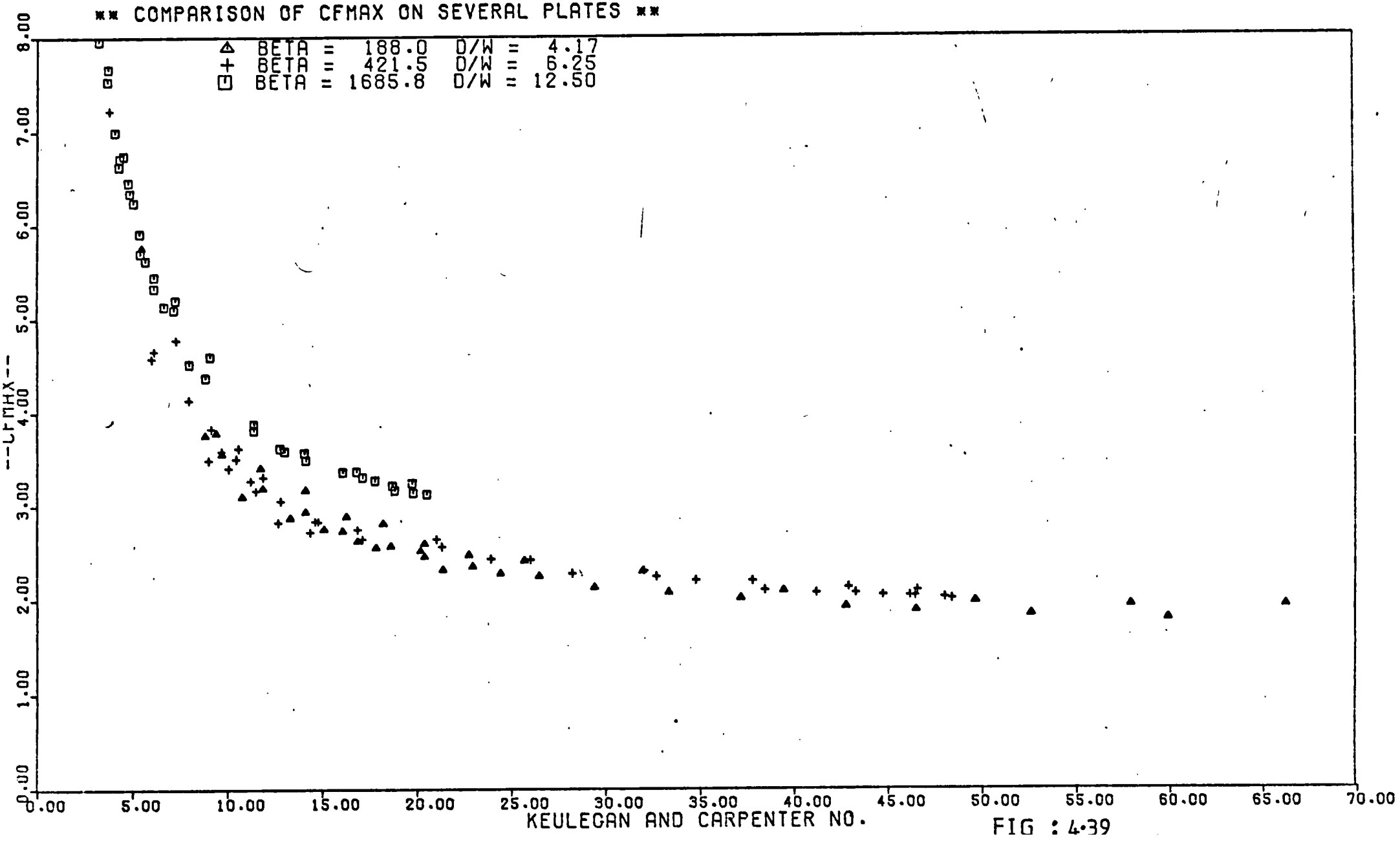
** COMPARISON OF CFMAX ON SEVERAL PLATES **
△ BETA = 188.0 D/W = 4.17
+ BETA = 421.5 D/W = 6.25
□ BETA = 1685.8 D/W = 12.50
--CFMAX--
0.00
1.00
2.00
3.00
4.00
5.00
6.00
7.00
8.00
0.00
5.00
10.00
15.00
20.00
25.00
30.00
35.00
40.00
45.00
50.00
55.00
60.00
65.00
70.00
KEULEGAN AND CARPENTER NO.

FIG : 4·39

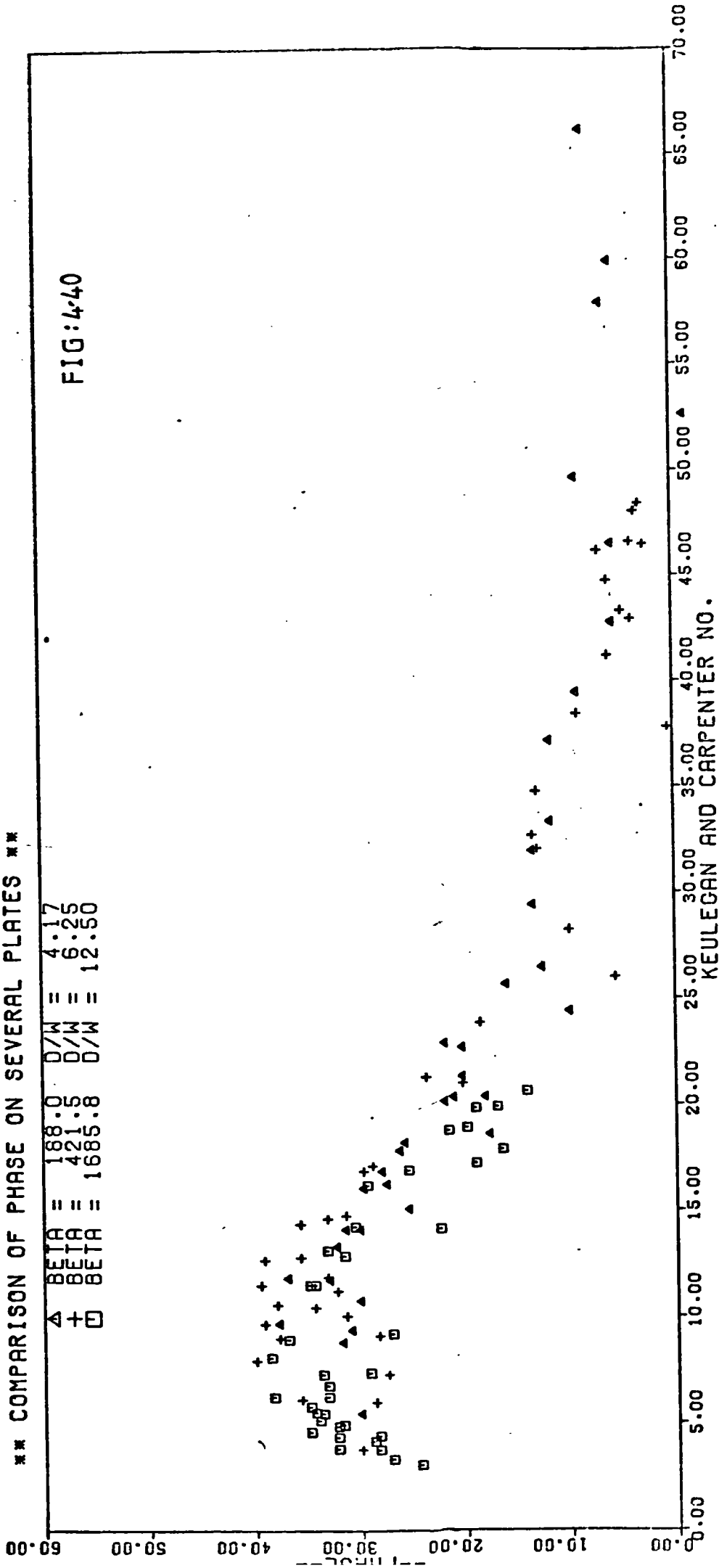
** COMPARISON OF PHASE ON SEVERAL PLATES **
BETA = 188.0 D/W = 4.17
BETA = 421.5 D/W = 6.25
BETA = 1685.8 D/W = 12.50
KEULEGAN AND CARPENTER NO.
0.00
5.00
10.00
15.00
20.00
25.00
30.00
35.00
40.00
45.00
50.00
55.00
60.00
65.00
70.00
10.00
20.00
30.00
40.00
50.00
60.00

FIG:4.40

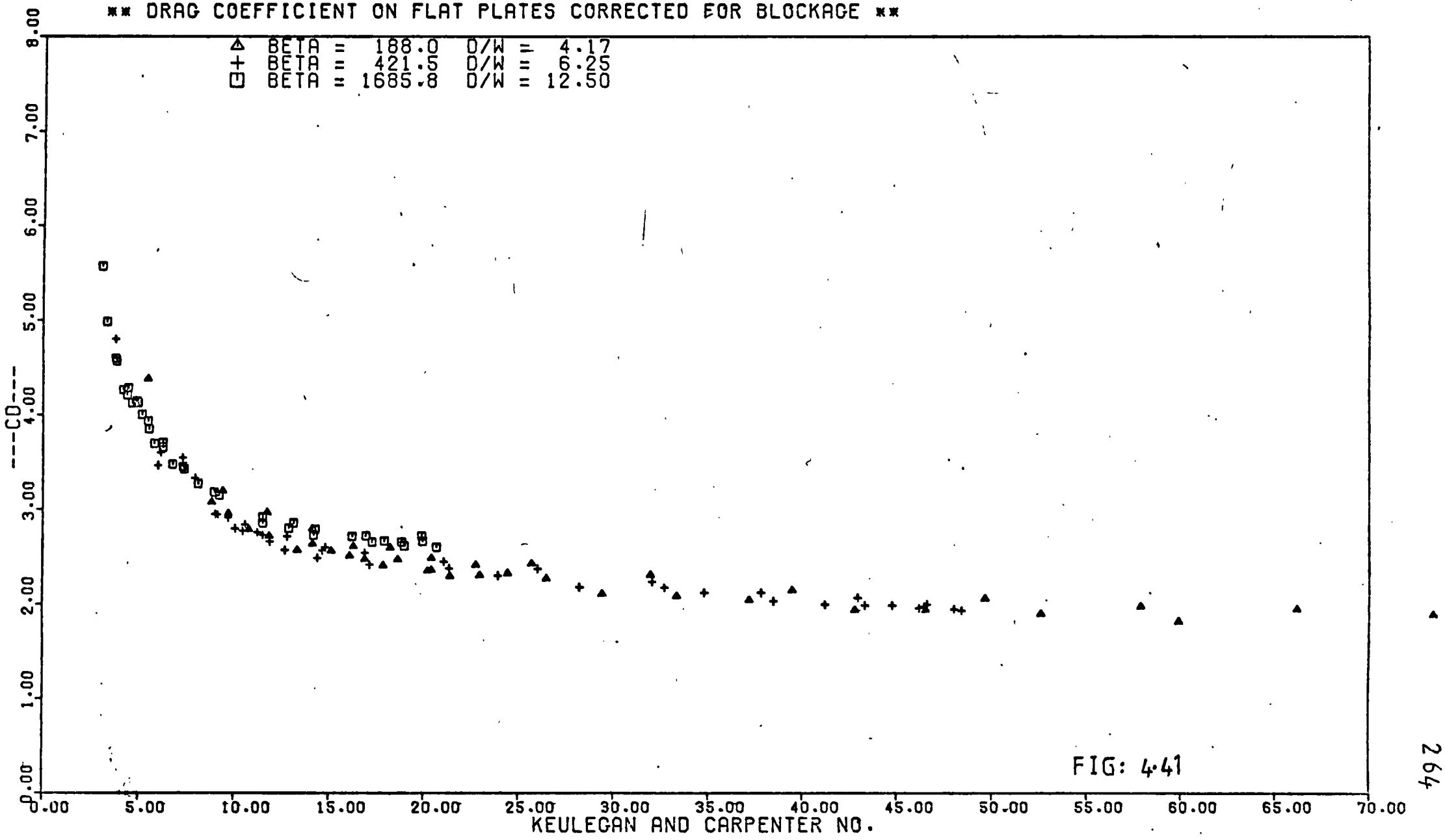
** DRAG COEFFICIENT ON FLAT PLATES CORRECTED FOR BLOCKAGE **
BETA = 188.0 D/W = 4.17
BETA = 421.5 D/W = 6.25
BETA = 1685.8 D/W = 12.50
---CD---
0.00
1.00
2.00
3.00
4.00
5.00
6.00
7.00
8.00
0.00
5.00
10.00
15.00
20.00
25.00
30.00
35.00
40.00
45.00
50.00
55.00
60.00
65.00
70.00
KEULEGAN AND CARPENTER NO.

FIG: 4.41

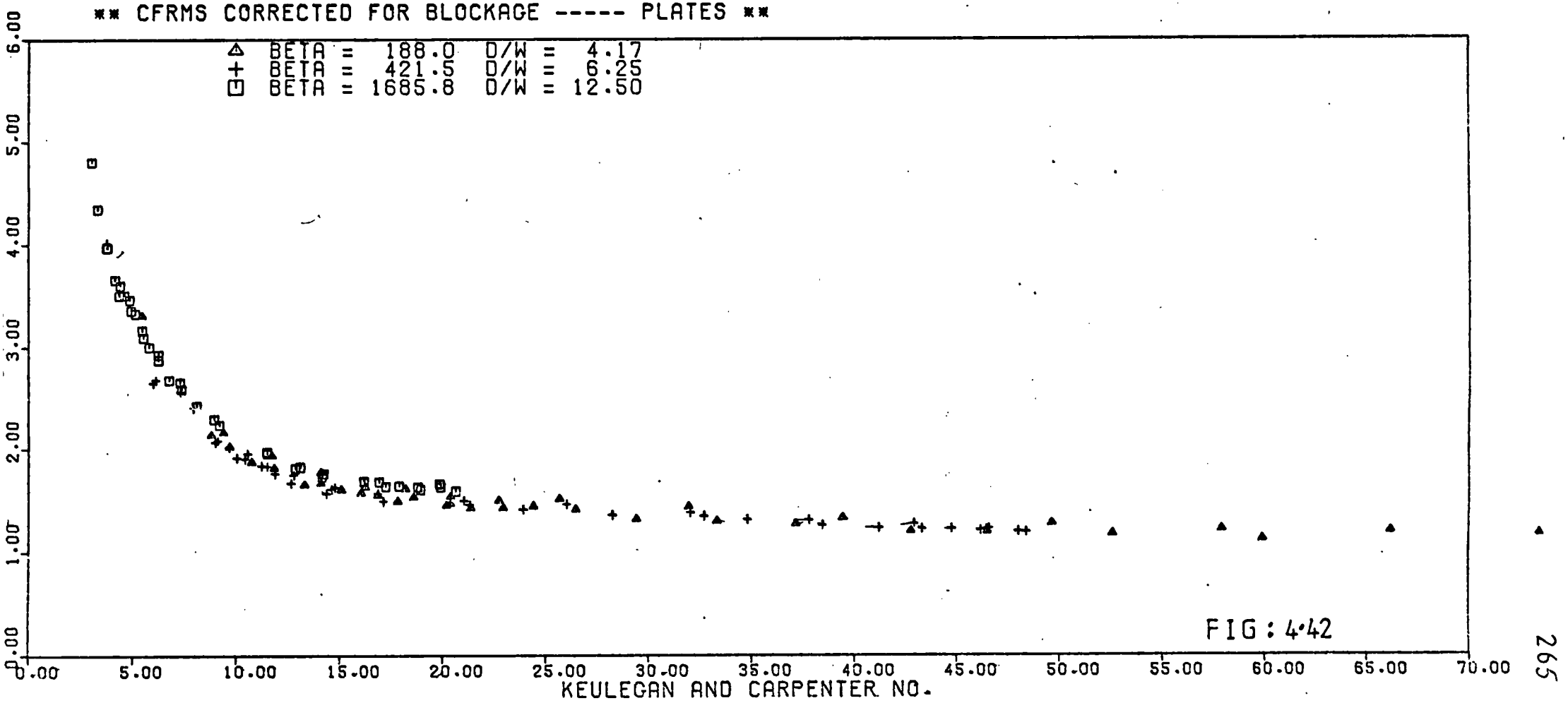
** CFRMS CORRECTED FOR BLOCKAGE ----- PLATES **
△ BETA = 188.0 D/W = 4.17
+ BETA = 421.5 D/W = 6.25
□ BETA = 1685.8 D/W = 12.50
6.00
5.00
4.00
3.00
2.00
1.00
0.00
0.00
5.00
10.00
15.00
20.00
25.00
30.00
35.00
40.00
45.00
50.00
55.00
60.00
65.00
70.00
KEULEGAN AND CARPENTER NO.

FIG : 4·42

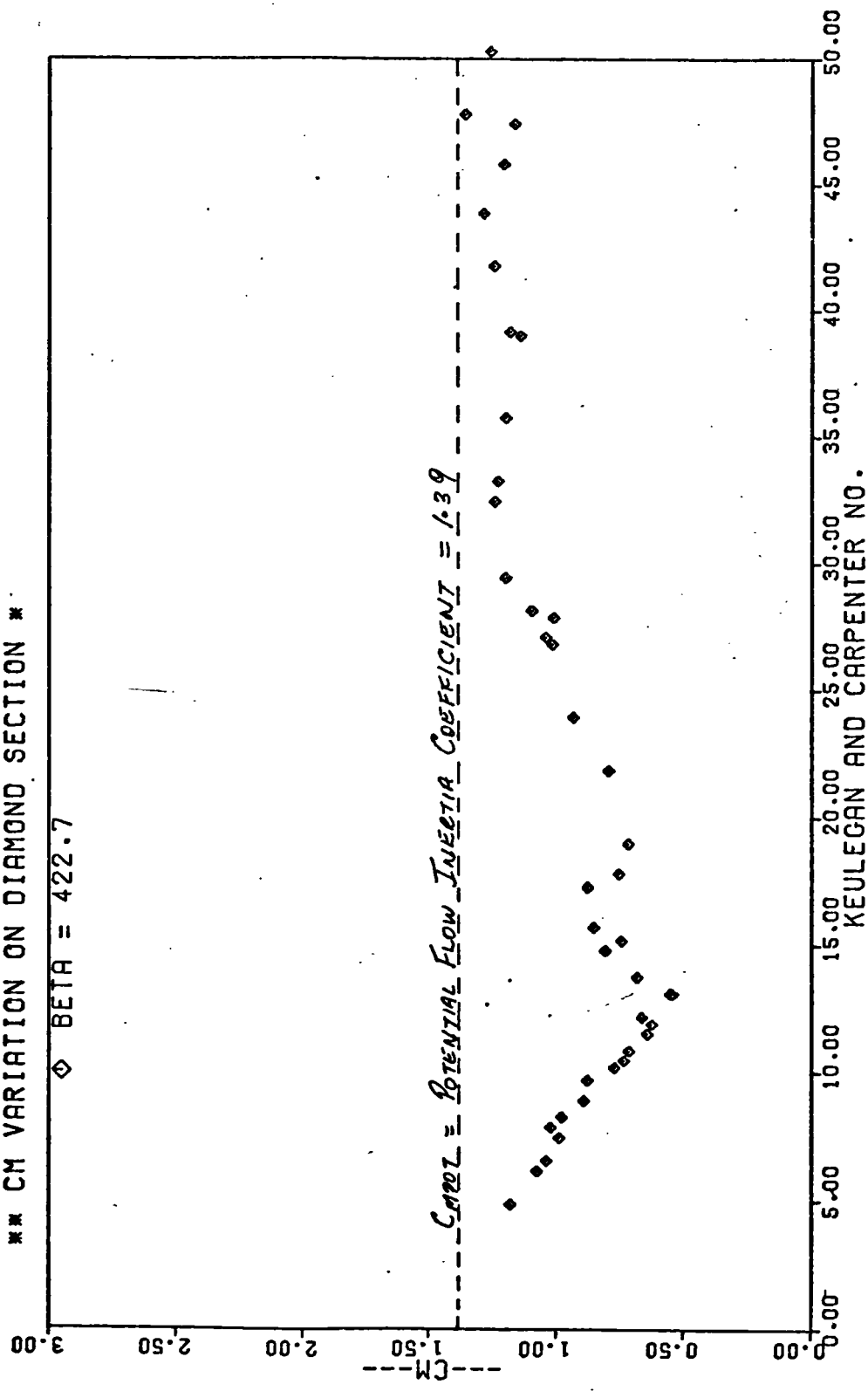
** CM VARIATION ON DIAMOND SECTION **
◇ BETA = 422.7
CMDOT = POTENTIAL FLOW INERTIA COEFFICIENT = 1.39
---CM---
3.00
2.50
2.00
1.50
1.00
0.50
0.00
0.00
5.00
10.00
15.00
20.00
25.00
30.00
35.00
40.00
45.00
50.00
KEULEGAN AND CARPENTER NO.

FIG: 4.43

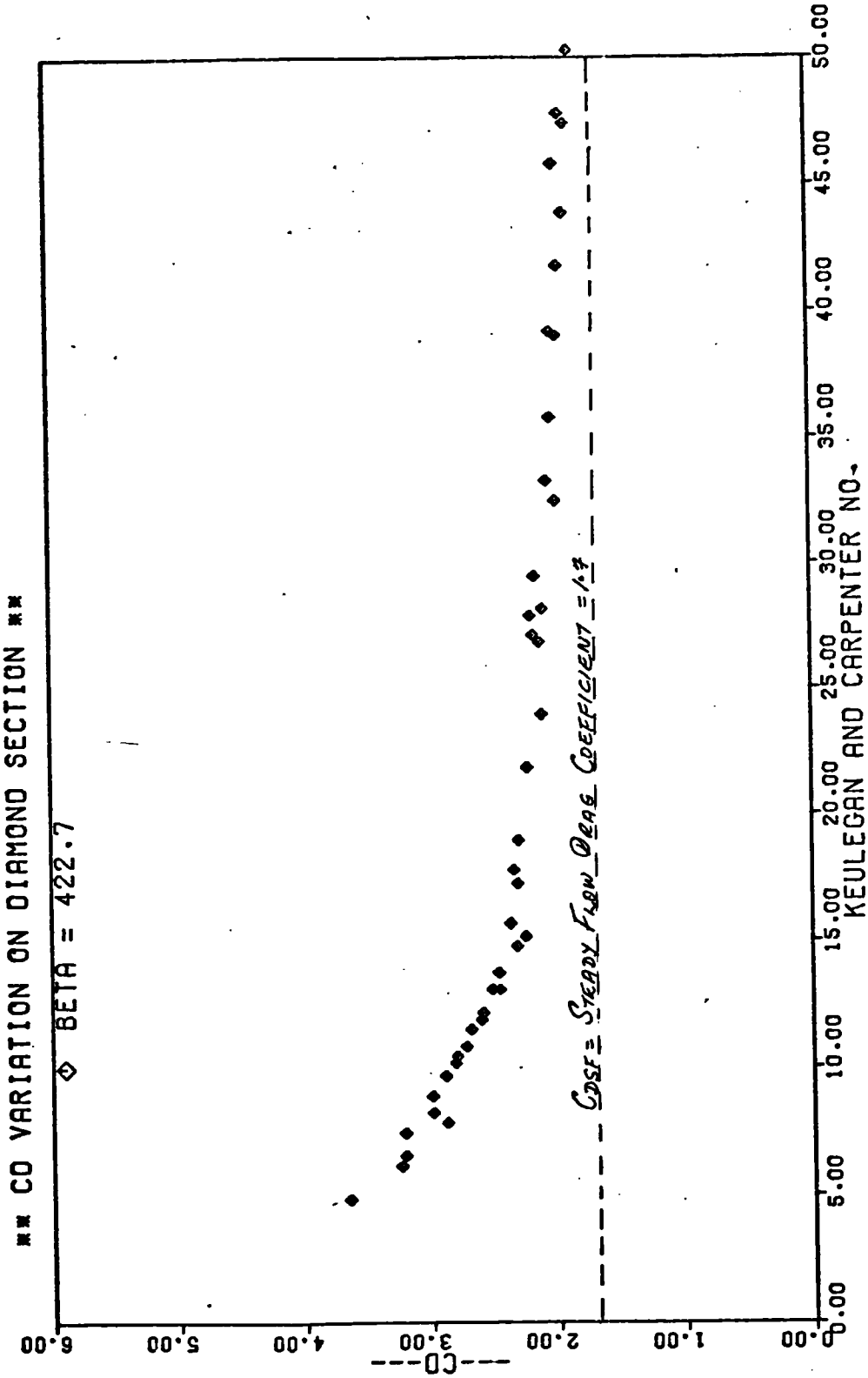
** CD VARIATION ON DIAMOND SECTION **
◇ BETA = 422.7
CDSF = STEADY FLOW DRAG COEFFICIENT = 1.2
---CD---
KEULEGAN AND CARPENTER NO.
0.00
1.00
2.00
3.00
4.00
5.00
6.00
0.00
5.00
10.00
15.00
20.00
25.00
30.00
35.00
40.00
45.00
50.00

FIG: 4·44

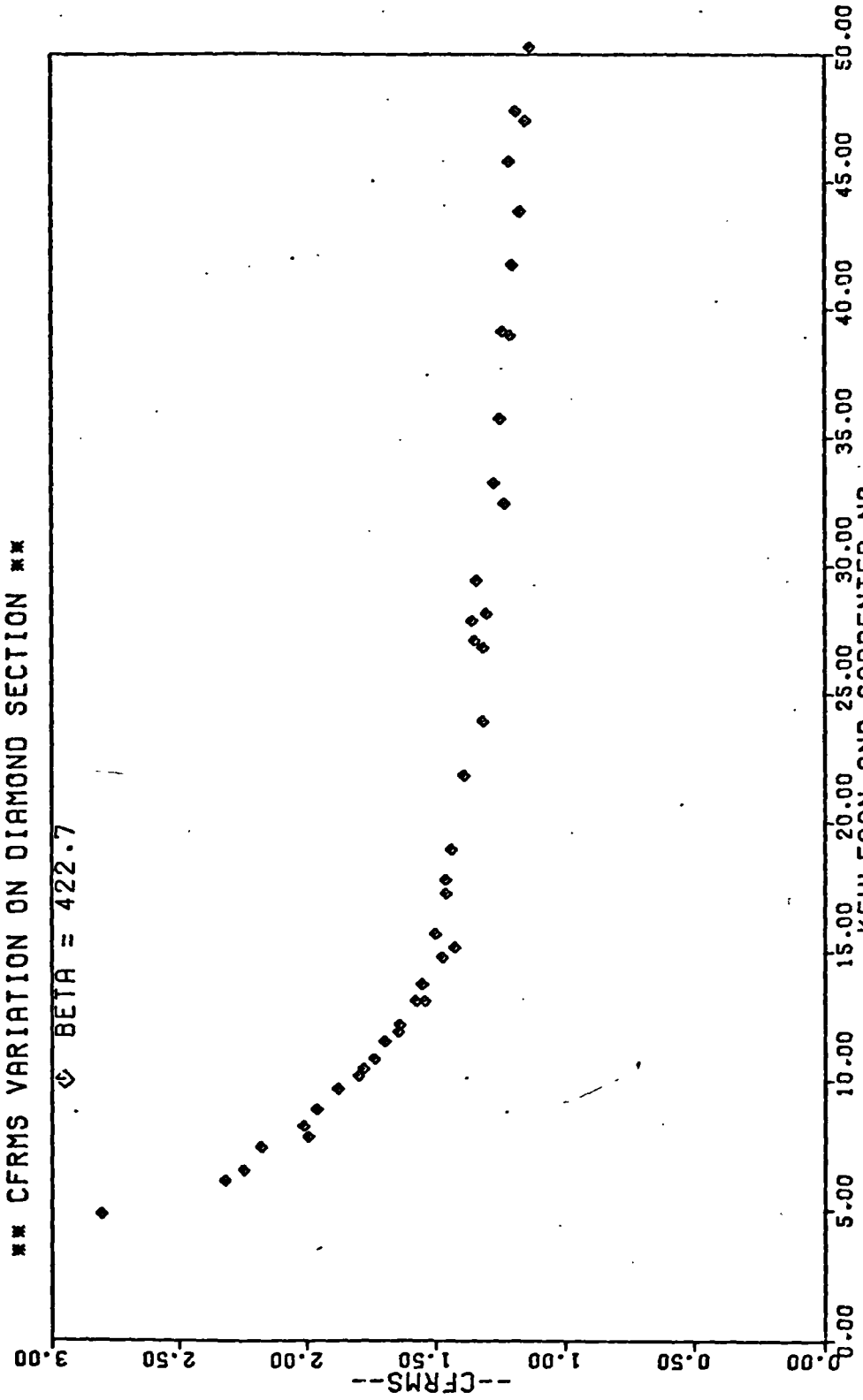
** CFRMS VARIATION ON DIAMOND SECTION **
BETA = 422.7
--CFRMS--
0.00
0.50
1.00
1.50
2.00
2.50
3.00
0.00
5.00
10.00
15.00
20.00
25.00
30.00
35.00
40.00
45.00
50.00
KEULEGAN AND CARPENTER NO.

FIG : 4·45

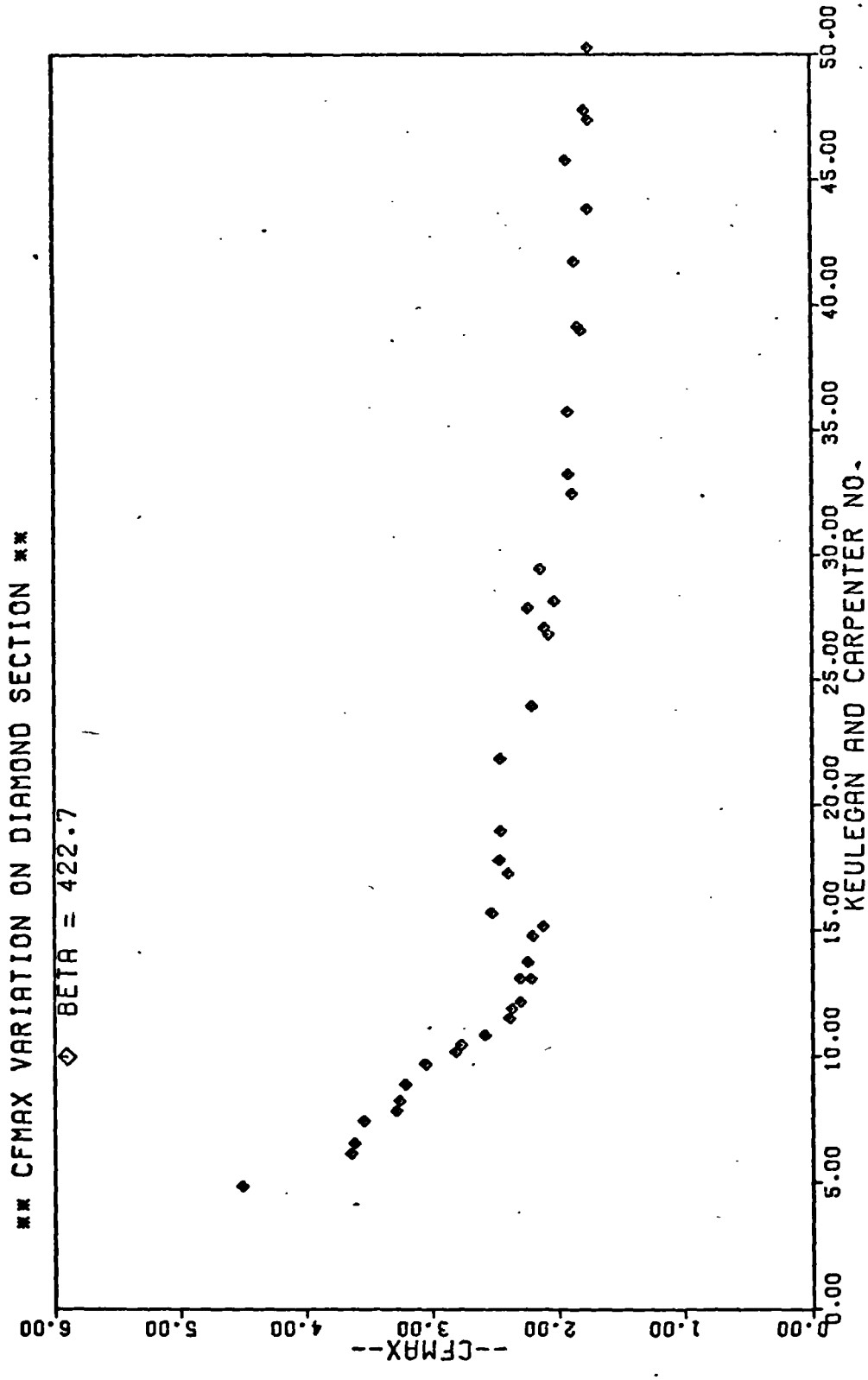
** CFMAX VARIATION ON DIAMOND SECTION **
◇ BETA = 422.7
--CFMAX--
KEULEGAN AND CARPENTER NO.
0.00
1.00
2.00
3.00
4.00
5.00
6.00
0.00
5.00
10.00
15.00
20.00
25.00
30.00
35.00
40.00
45.00
50.00

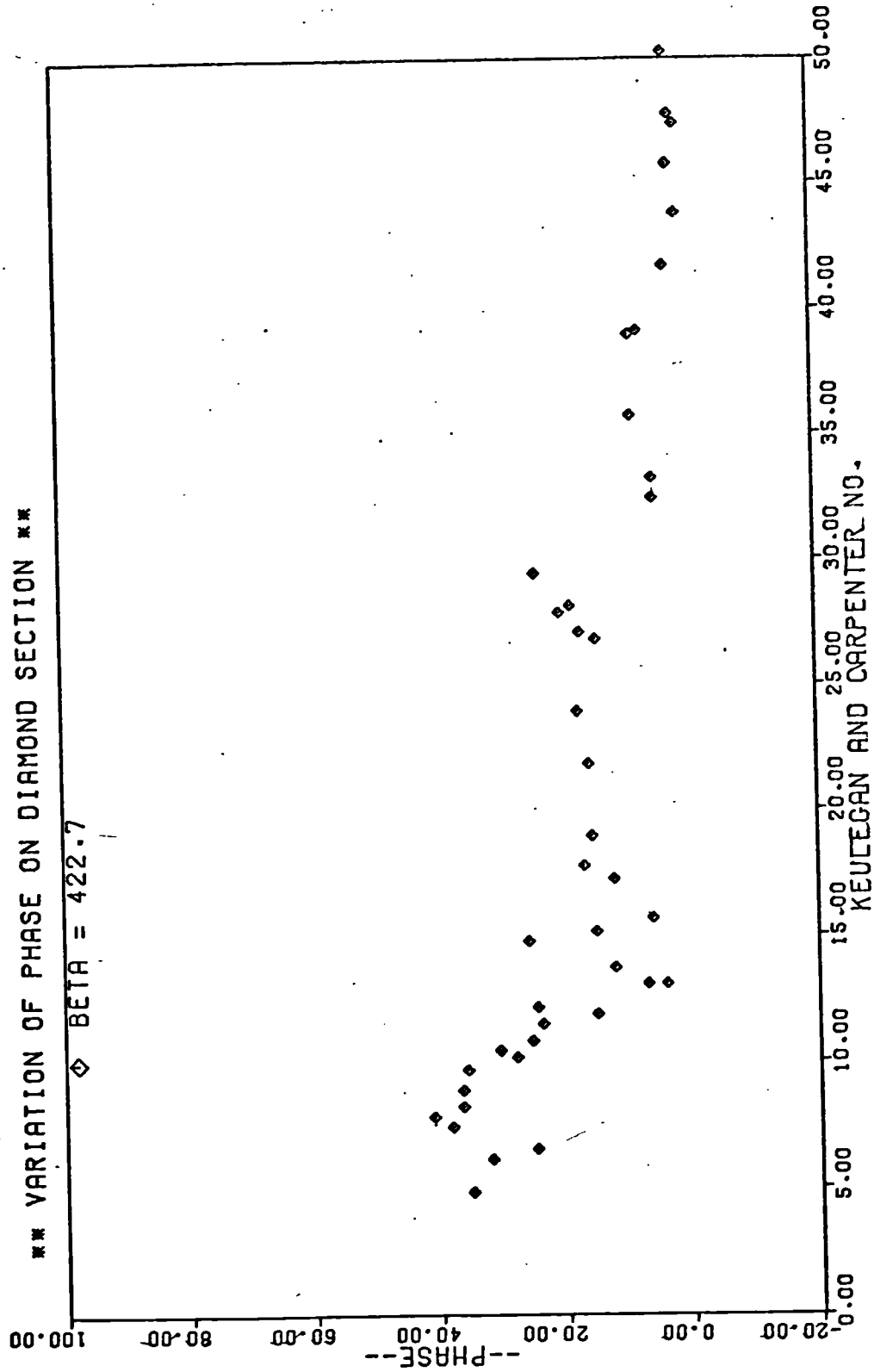
** VARIATION OF PHASE ON DIAMOND SECTION **
◇ BETA = 422.7
--PHASE--
100.00
80.00
60.00
40.00
20.00
0.00
-20.00
0.00
5.00
10.00
15.00
20.00
25.00
30.00
35.00
40.00
45.00
50.00
KEULEGAN AND CARPENTER NO.

FIG. 4.4.7

RUN 7 $\beta = 422.7$ NKC= 8.25 SQUARE (DIAGONAL IN LINE

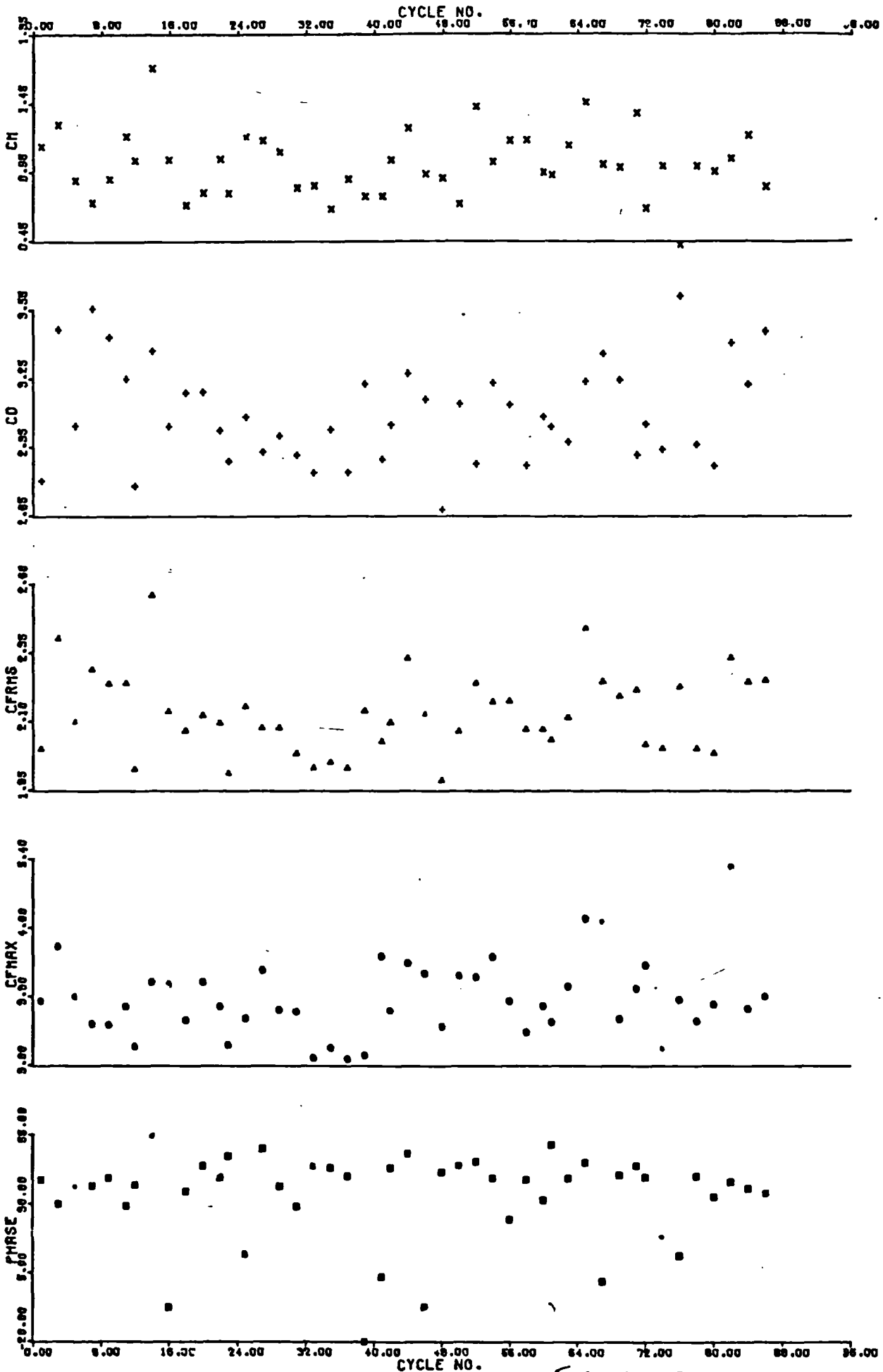

FIG : 4.48

RUN 25 . $\beta = 422.7$ NKC=14.79 IN SQUARE (DIAGONAL IN LINE

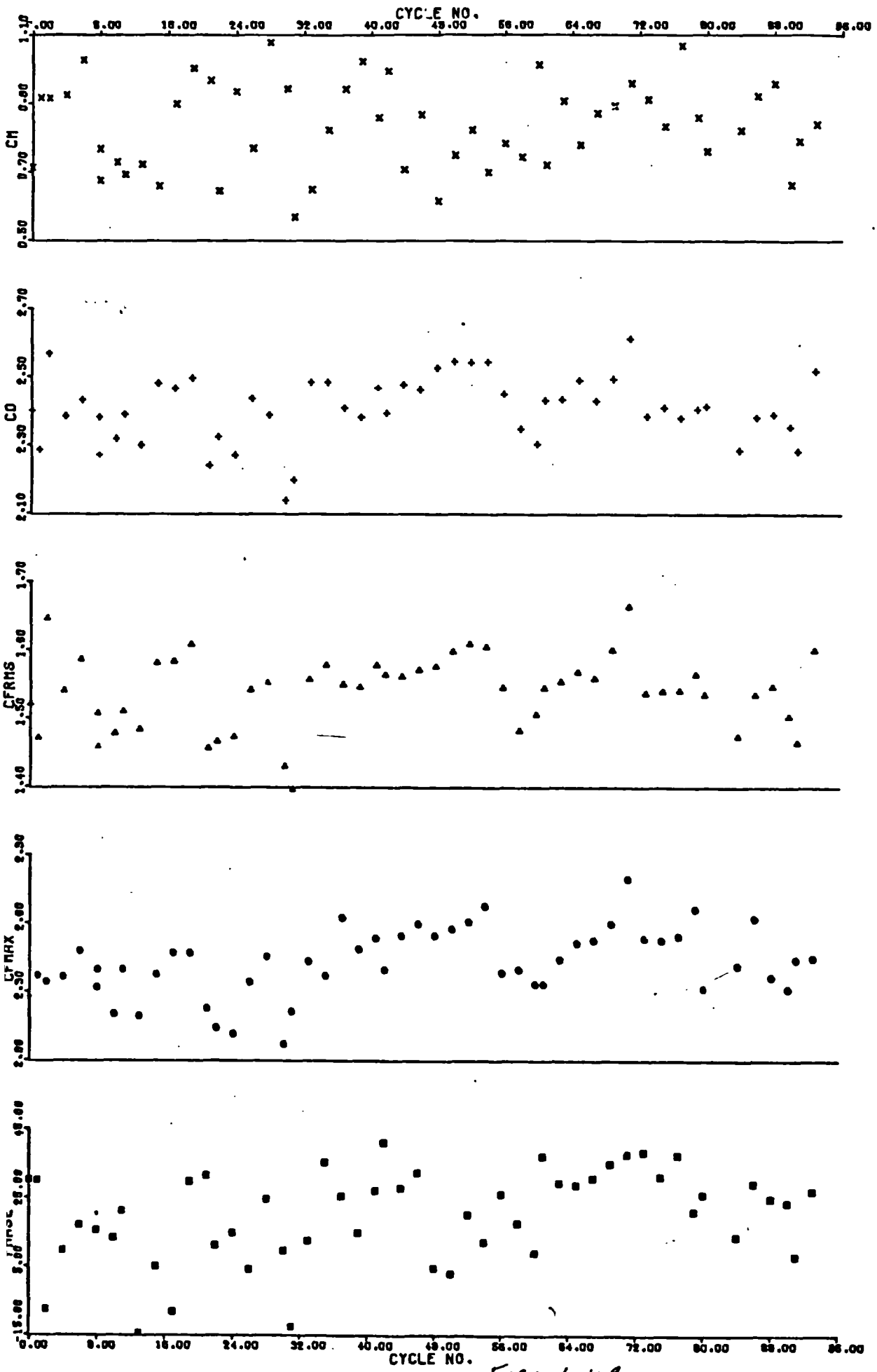

FIG: 4.49

RUN 33 $\beta = 422.7$ NKC=21.86 IN SQUARE (DIAGONAL IN LINE

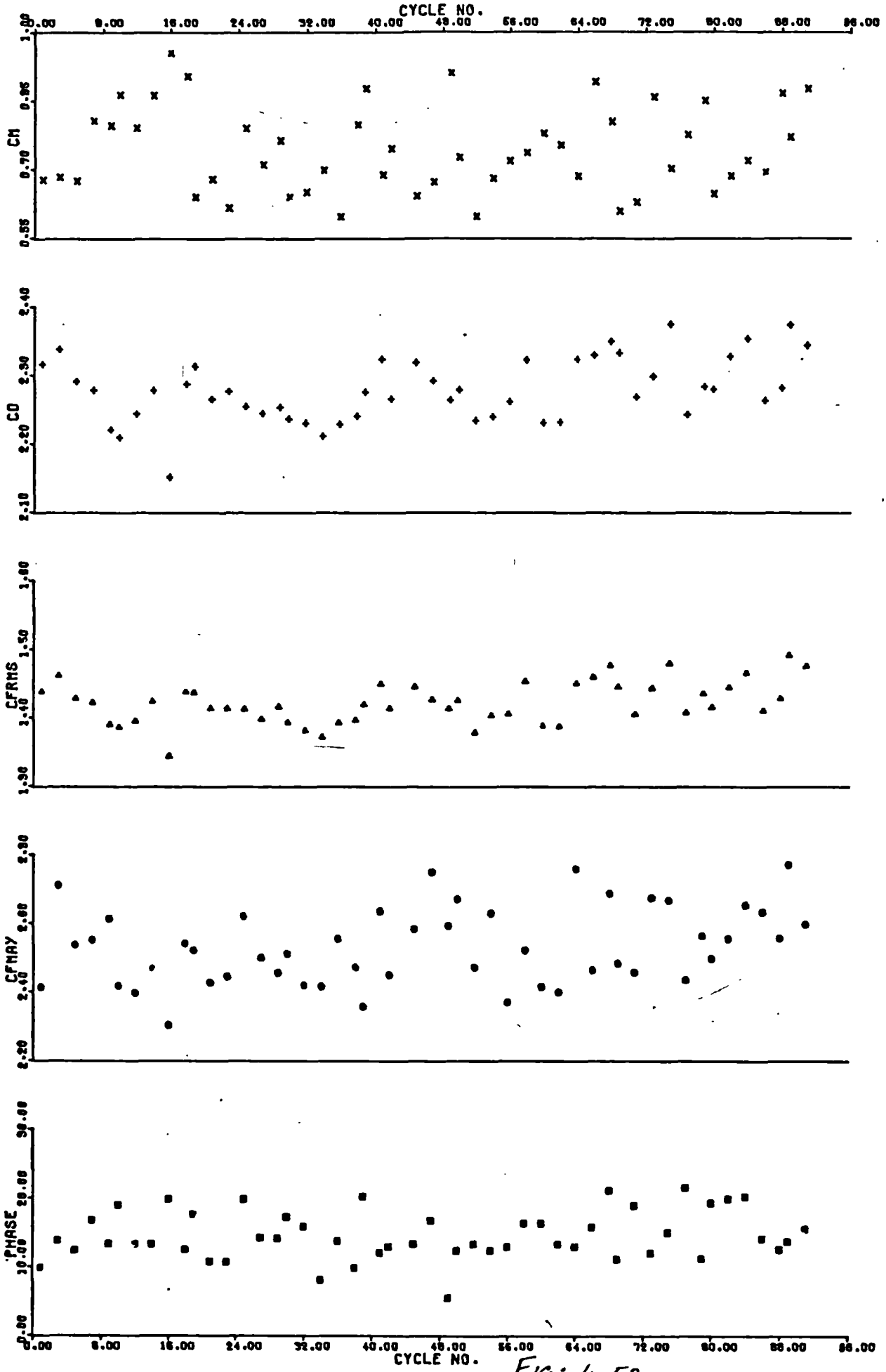

FIG: 4.50

RUN 3 $\beta = 422.7$ NKC=47.39 IN SQUARE (DIAGONAL IN LIN

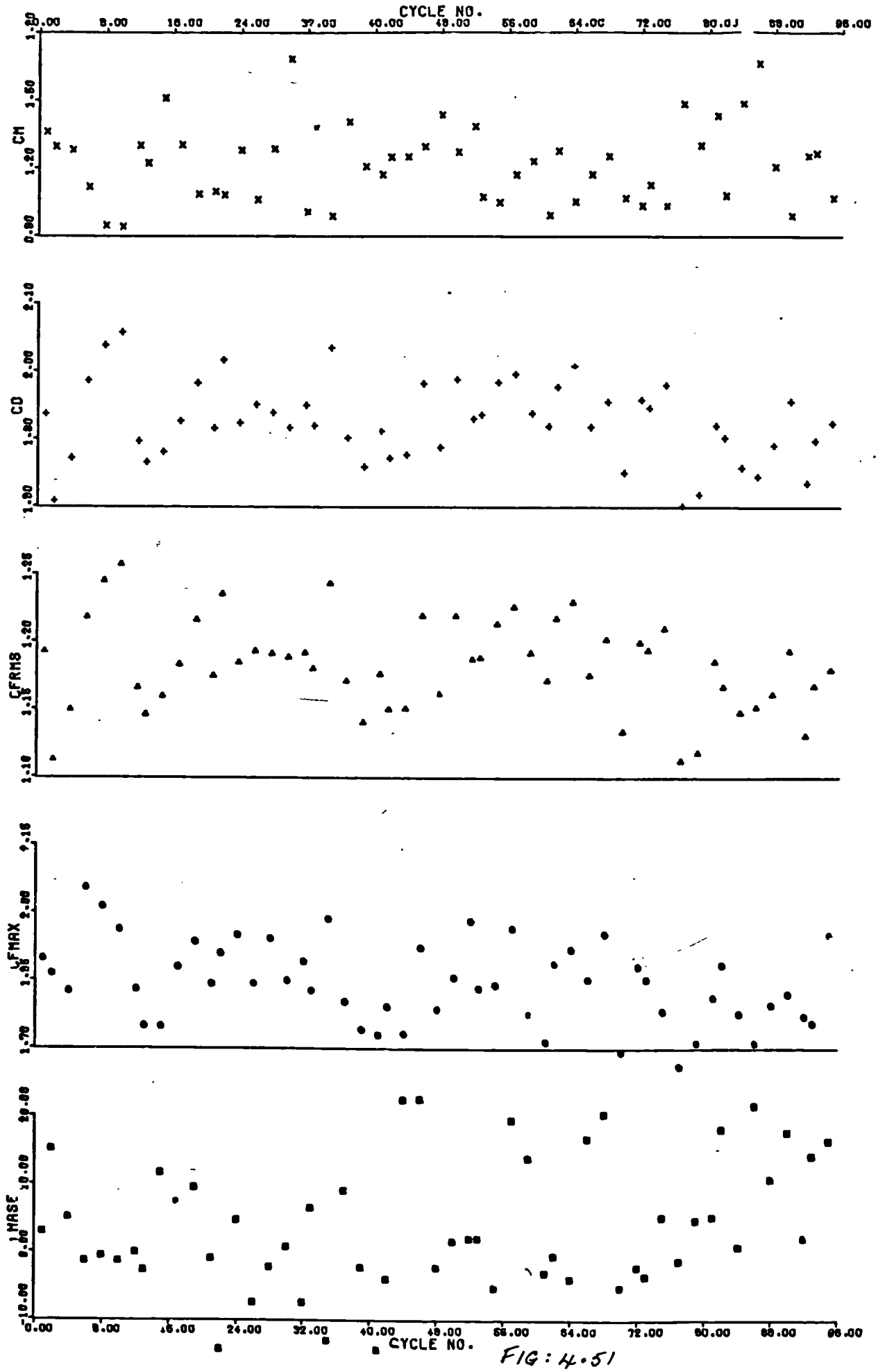

FIG: 4.51

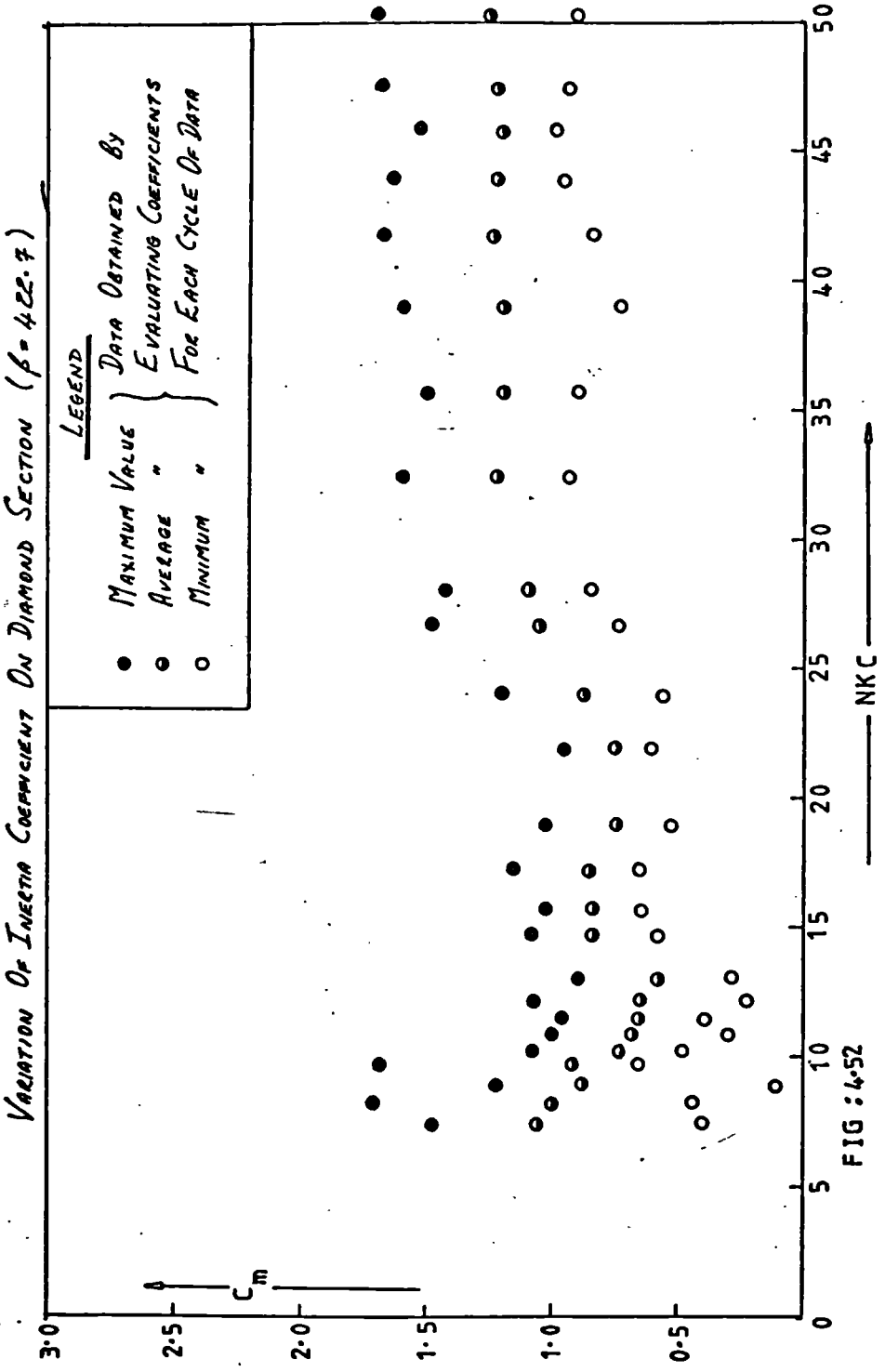
VARIATION OF INERTIA COEFFICIENT ON DIAMOND SECTION (β = 422.7)
LEGEND
MAXIMUM VALUE
AVERAGE "
MINIMUM "
DATA OBTAINED BY EVALUATING COEFFICIENTS FOR EACH CYCLE OF DATA
Cm
NKC
3·0
2·5
2·0
1·5
1·0
0·5
0
5
10
15
20
25
30
35
40
45
50

FIG : 4.52

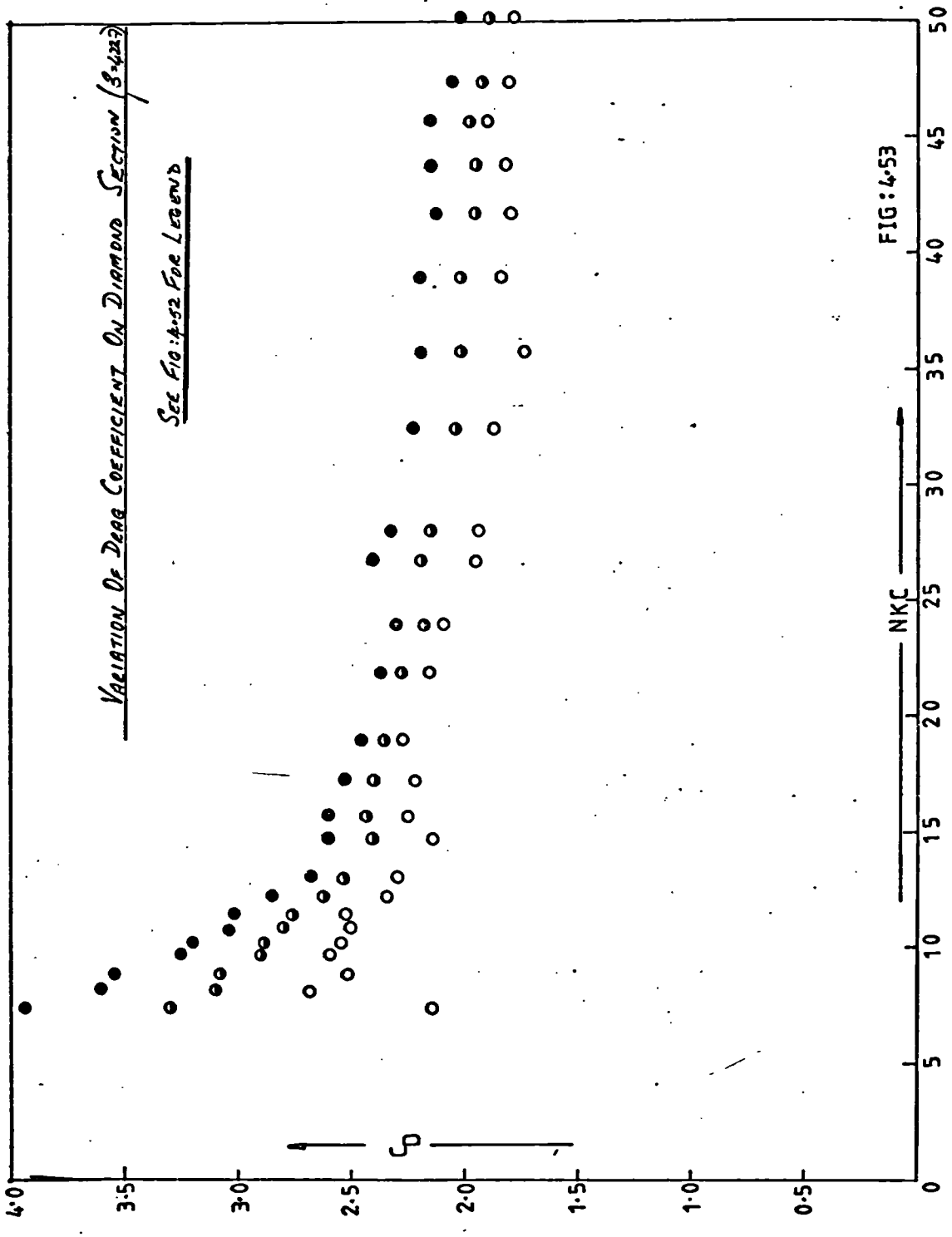
VARIATION OF DRAG COEFFICIENT ON DIAMOND SECTION (8=42°)
SEE FIG:4·52 FOR LEGENDS
CD
NKC
4·0
3·5
3·0
2·5
2·0
1·5
1·0
0·5
0
5
10
15
20
25
30
35
40
45
50

FIG:4·53

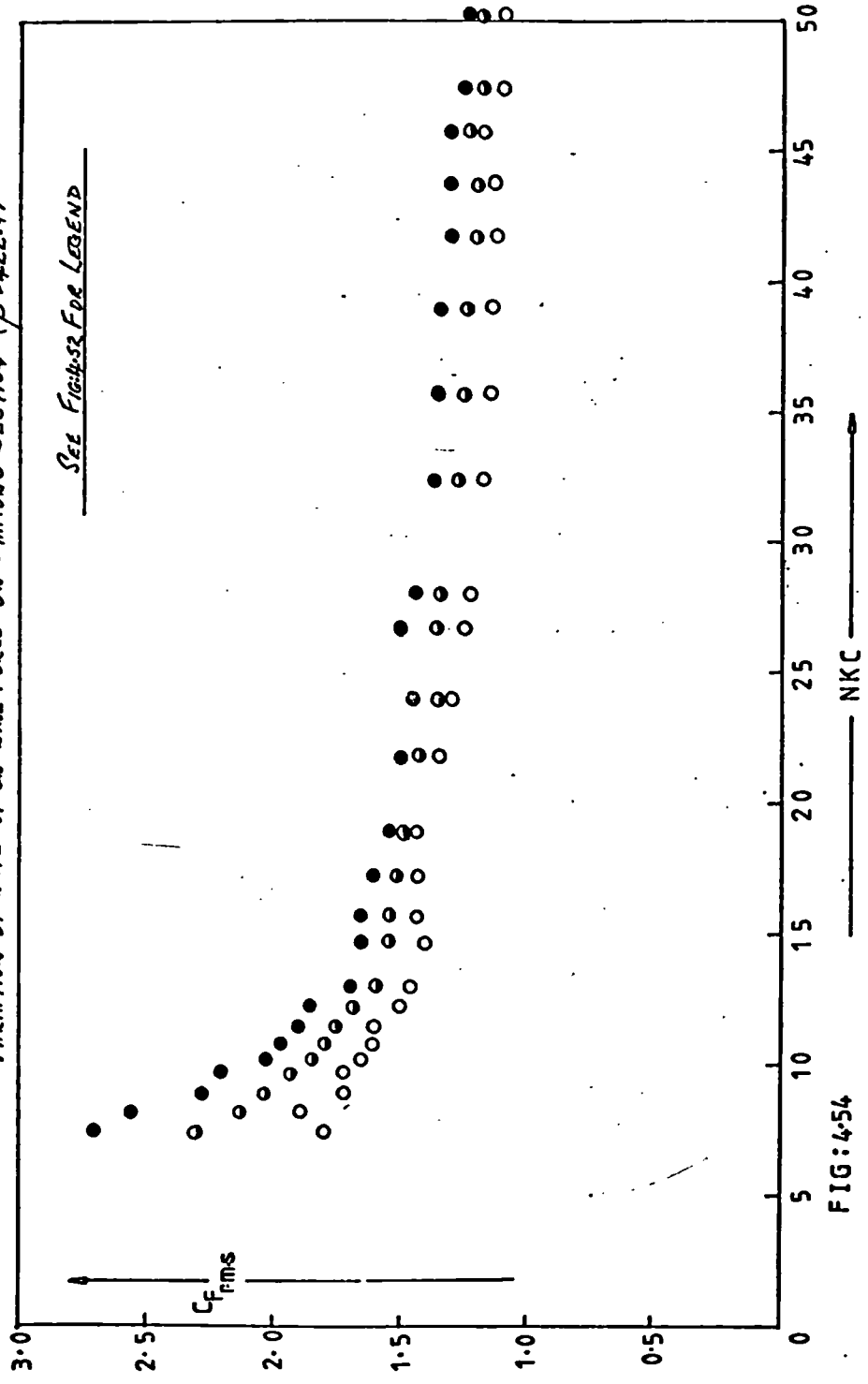
VARIATION OF R.M.S OF IN-LINE FORCE ON DIAMOND SECTION (β=422.5)
SEE FIGURE FOR LEGEND
$C_{F_{r.m.s}}$
3·0
2·5
2·0
1·5
1·0
0·5
0
5
10
15
20
25
30
35
40
45
50
NKC

FIG:4.54

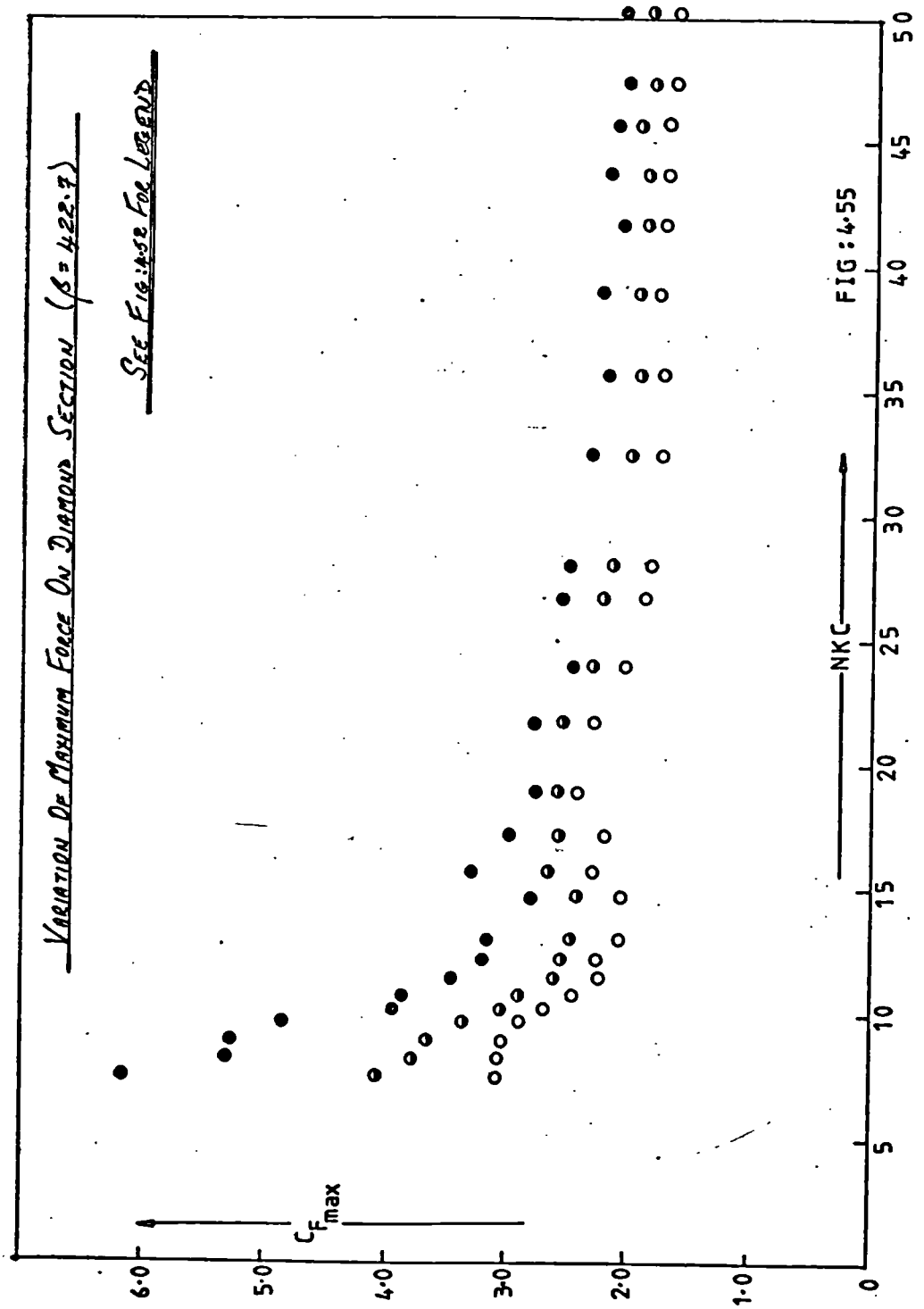
VARIATION OF MAXIMUM FORCE ON DIAMOND SECTION (β = 42.2°)
SEE FIG:4.58 FOR LEGEND
$C_{F_{max}}$
NKC
6·0
5·0
4·0
3·0
2·0
1·0
0
5
10
15
20
25
30
35
40
45
50

FIG:4.55

VARIATION OF PHASE OF MAXIMUM IN-LINE FORCE ON DIAMOND SECTION (β=422.7)

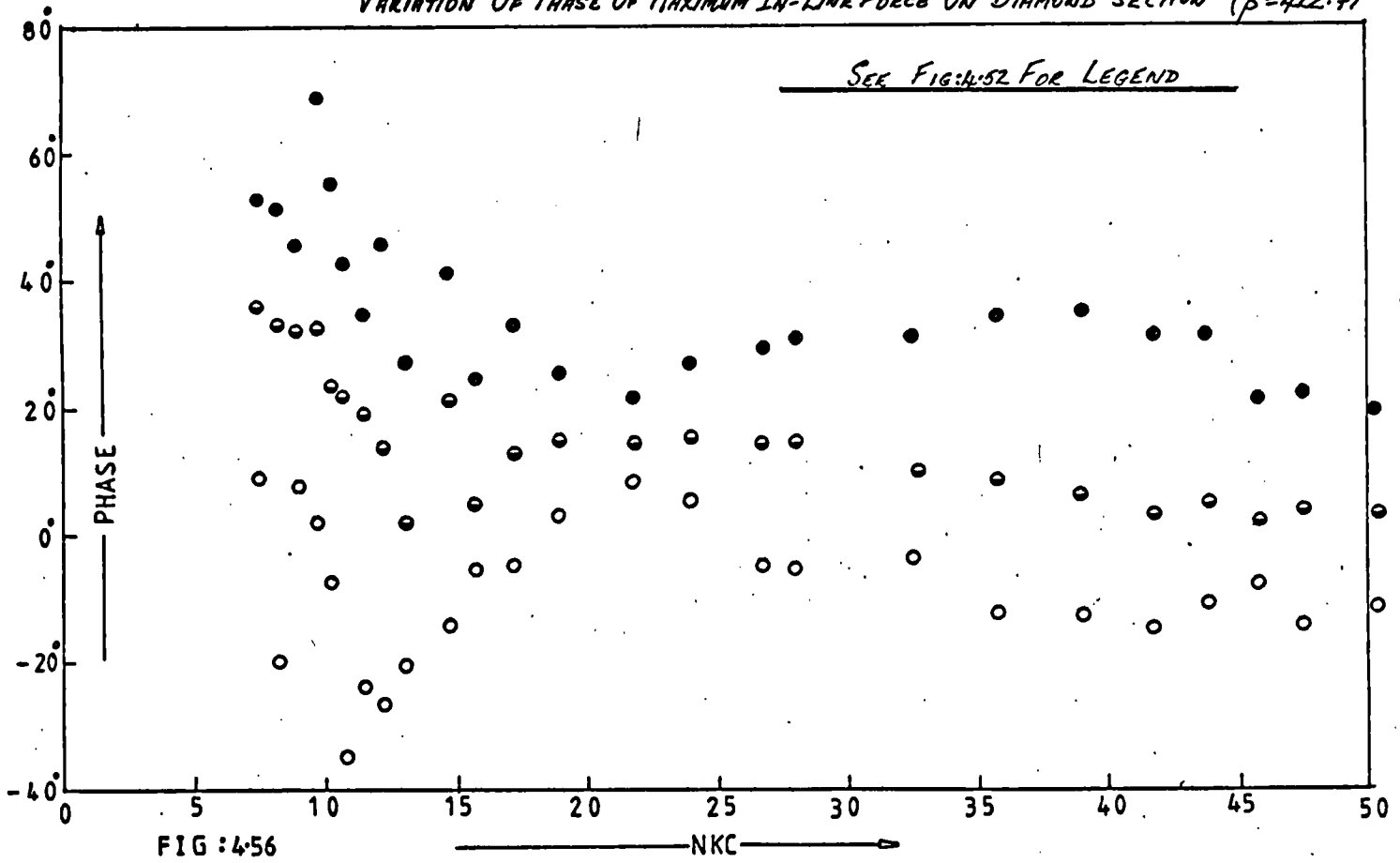

FIG : 4·56

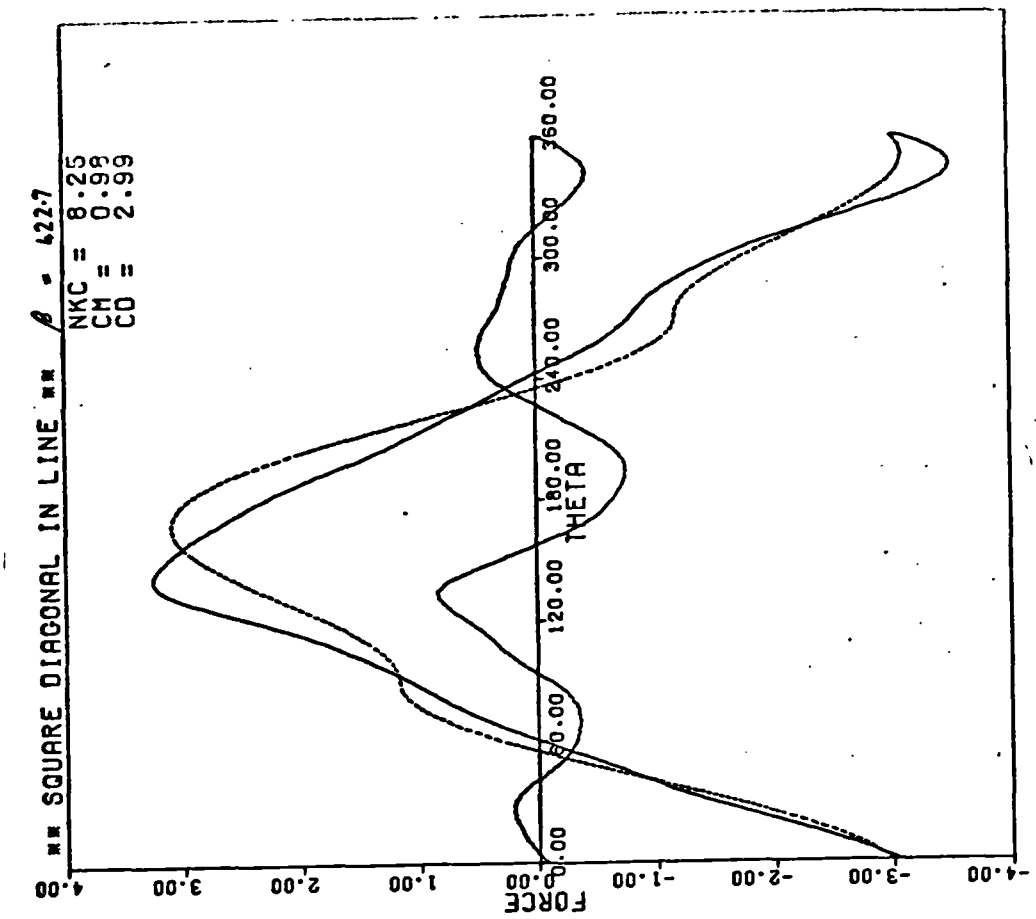

FIG: 4.57 (b)

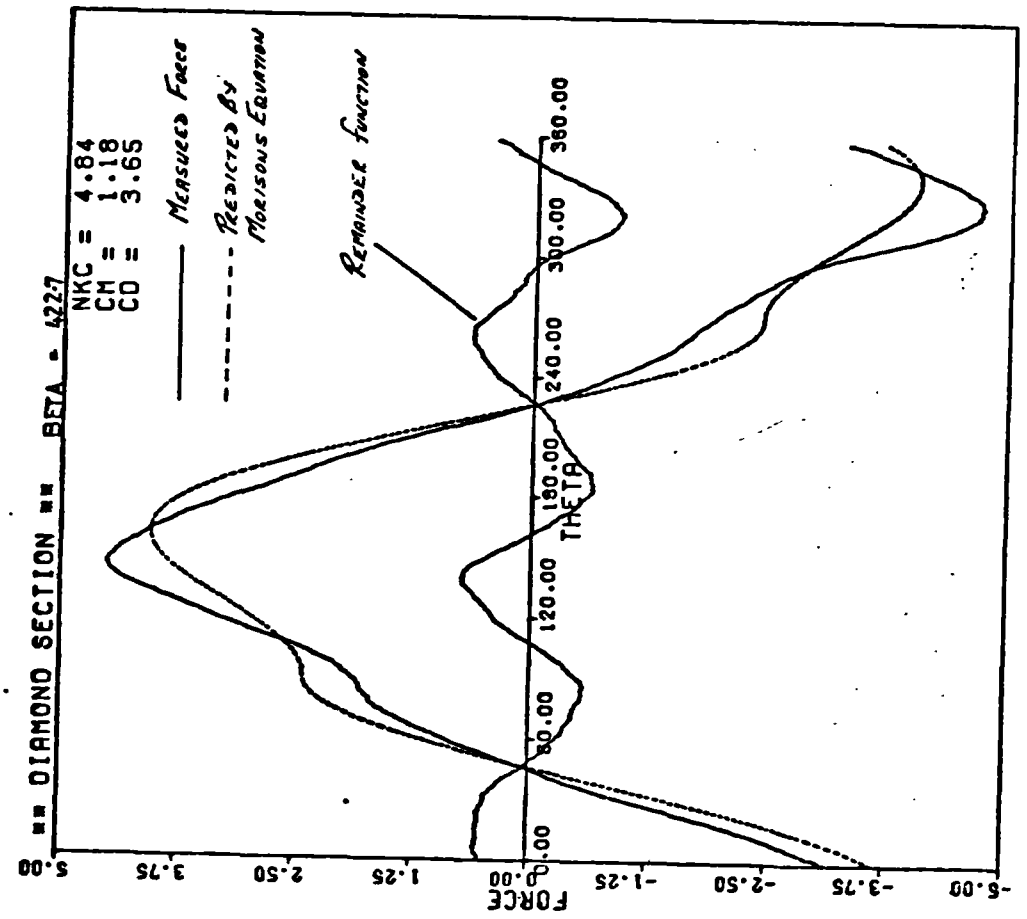

FIG: 4.57 (a)

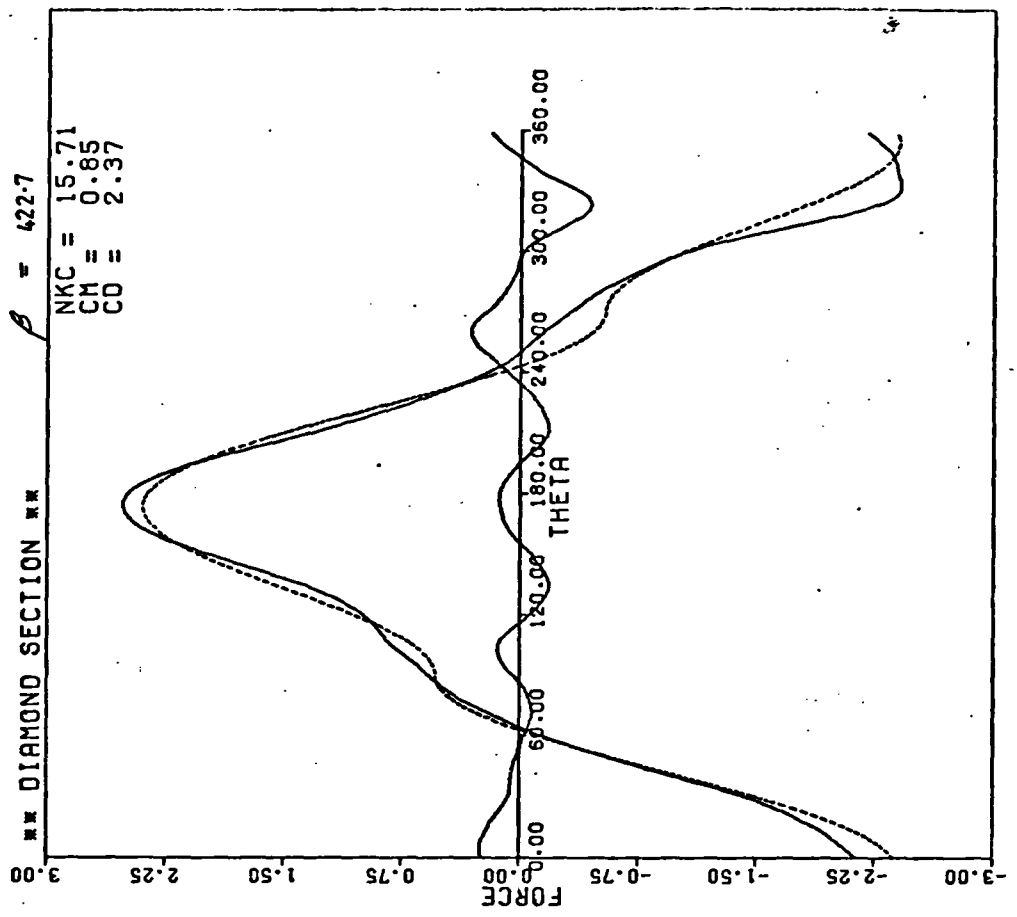

FIG: 4.57 (d)

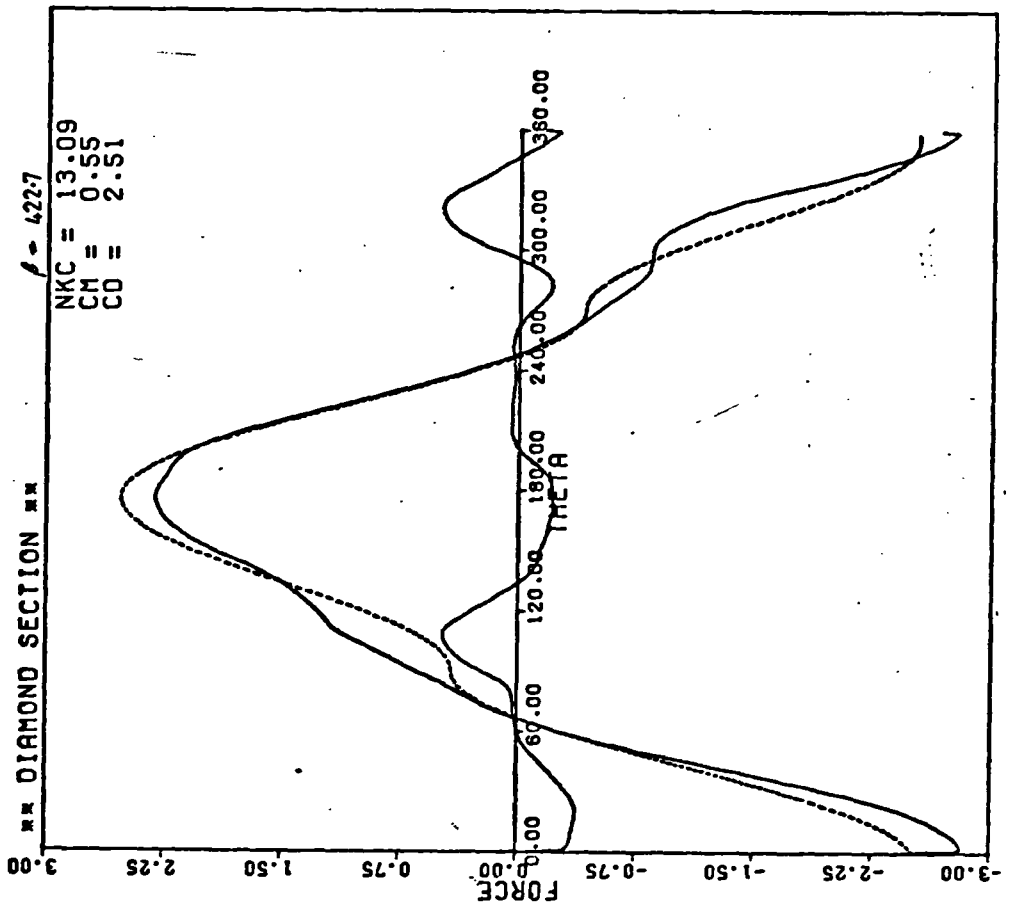

FIG: 4.57 (c)

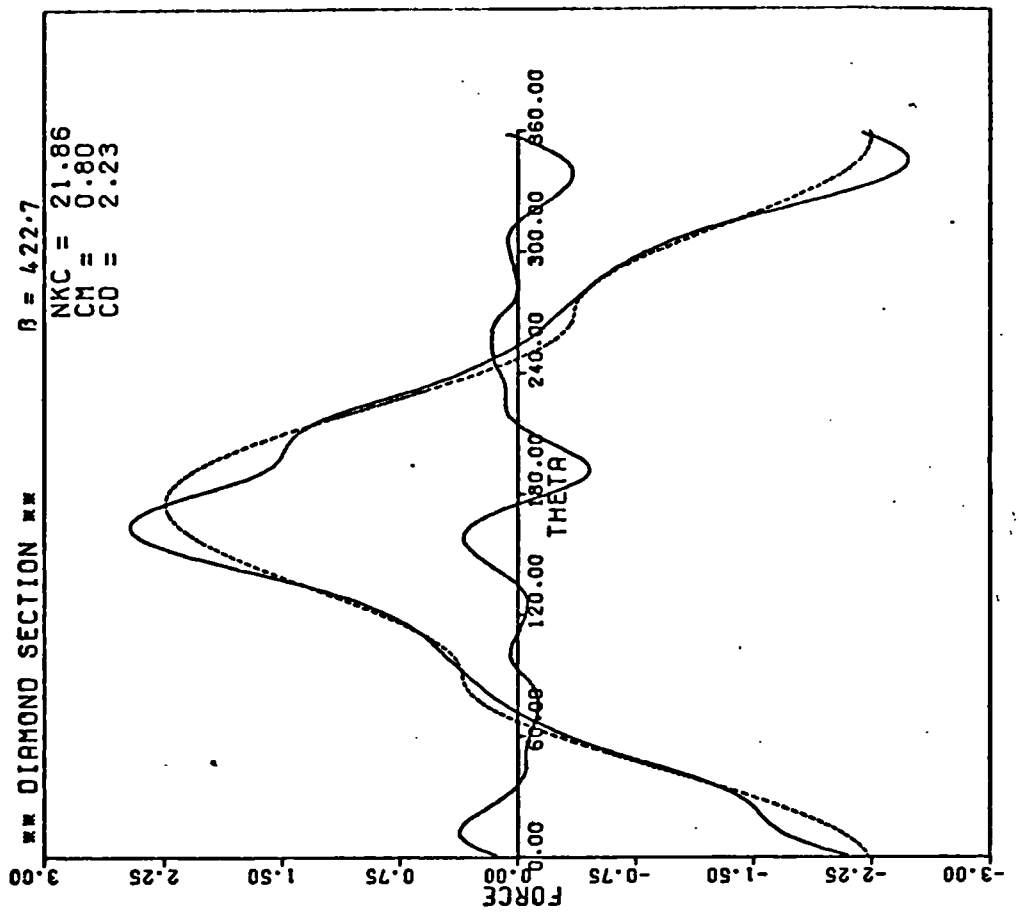

FIG: 4.57 (f)

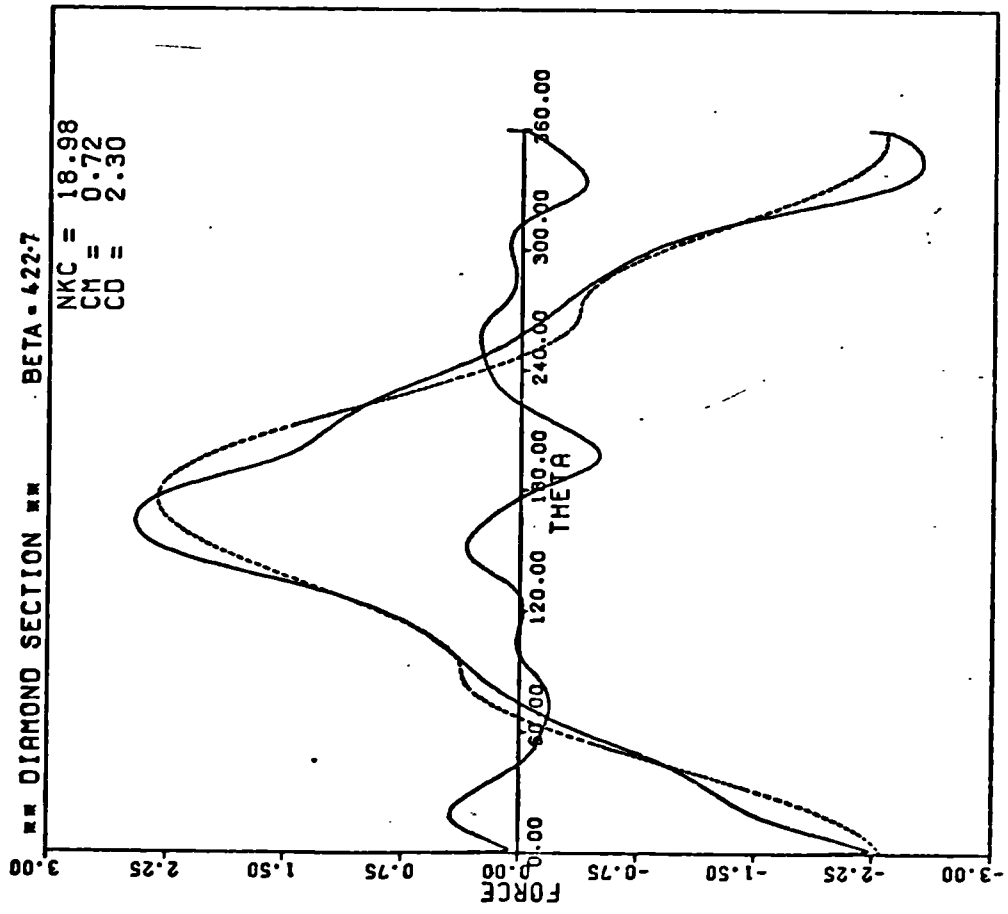

FIG: 4.57 (e)

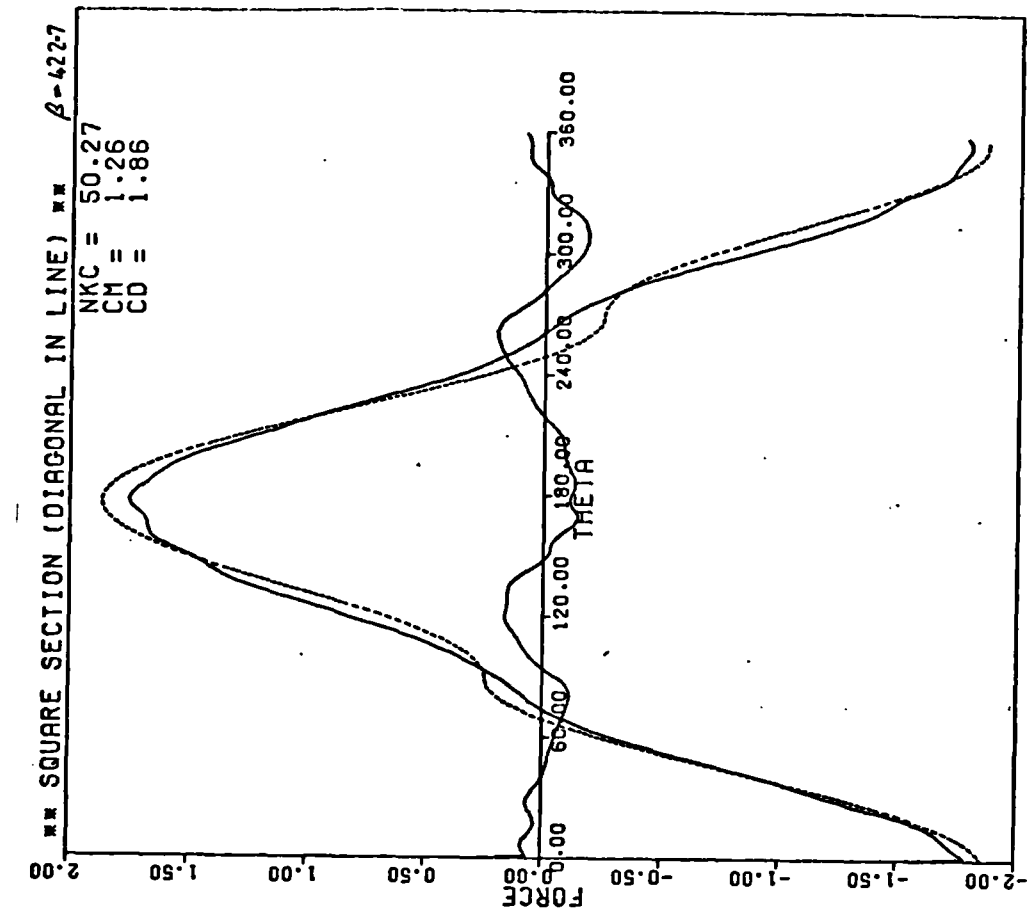

FIG: 4.57 (h)

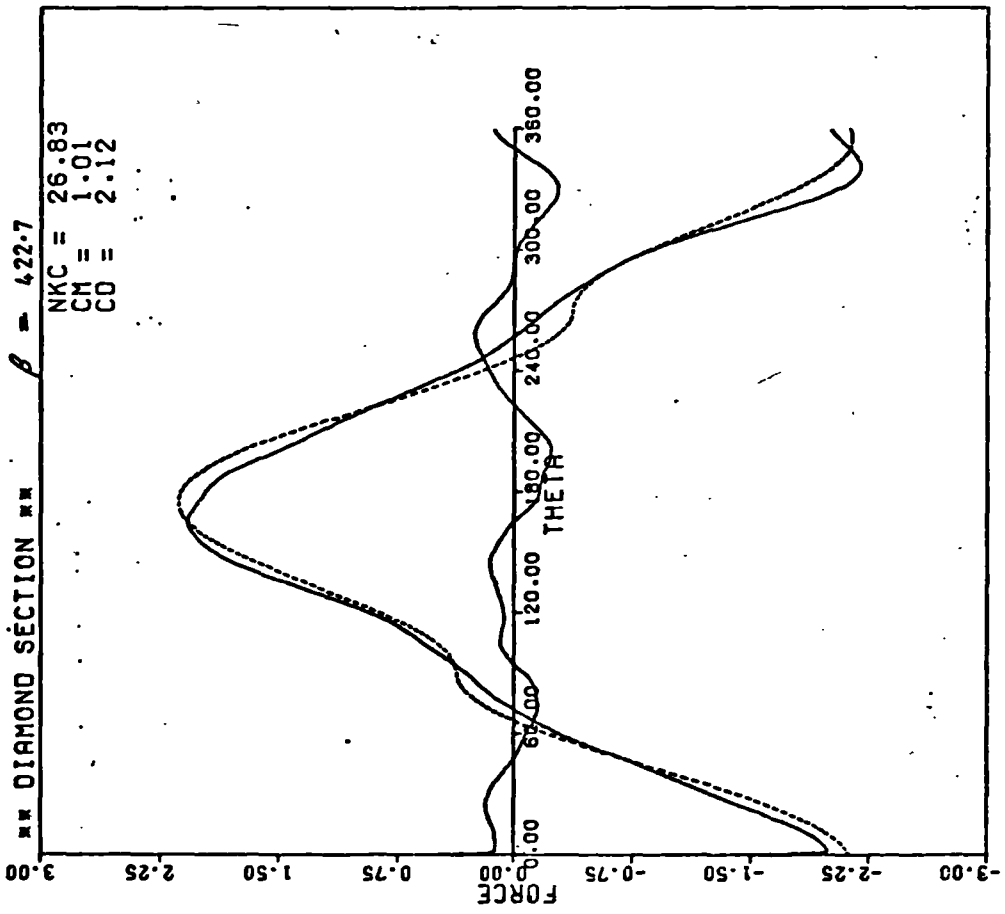

FIG: 4.57 (g)

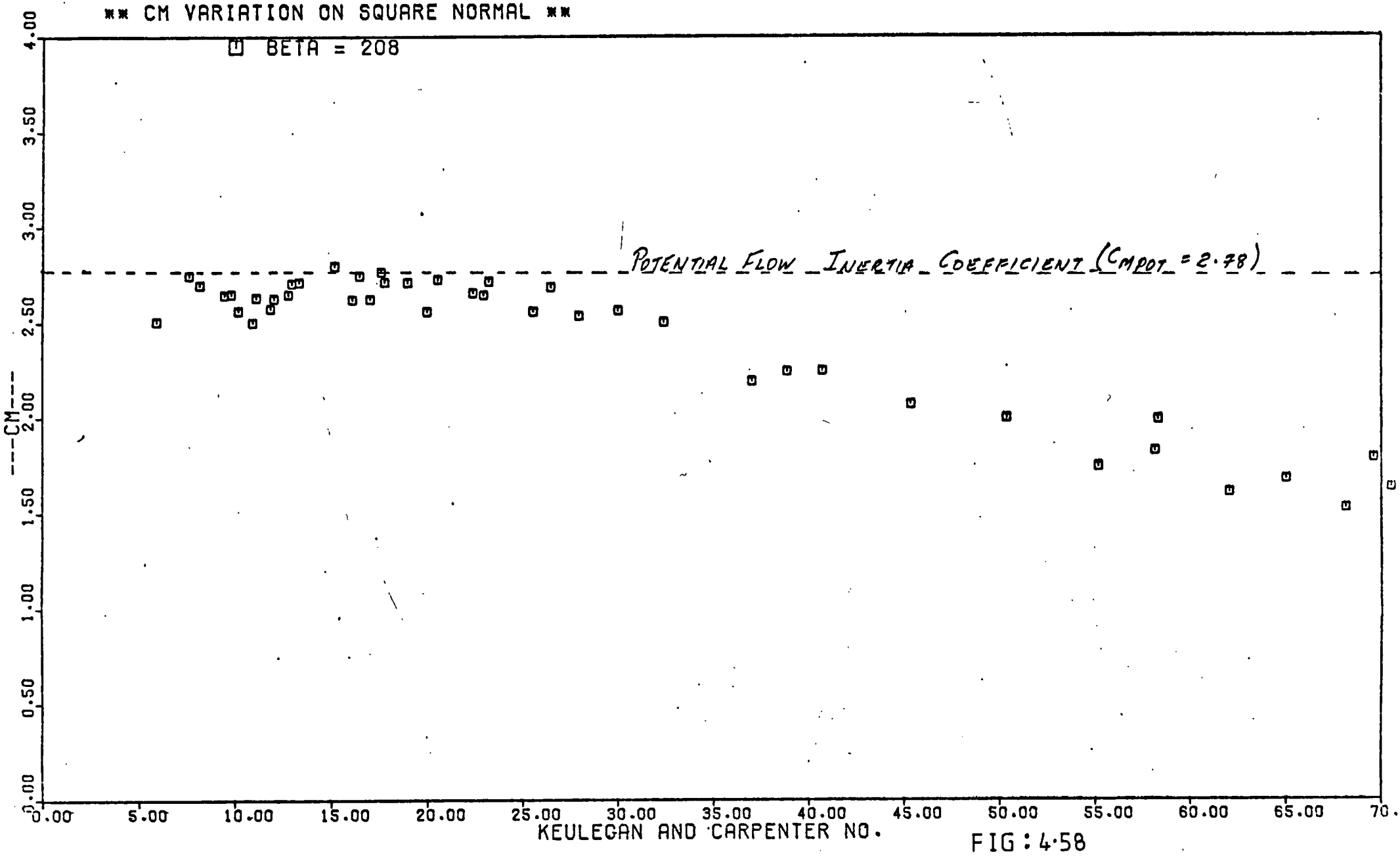
** CM VARIATION ON SQUARE NORMAL **
BETA = 208
POTENTIAL FLOW INERTIA COEFFICIENT (CMPOT = 2.78)
---CM---
4.00
3.50
3.00
2.50
2.00
1.50
1.00
0.50
0.00
0.00
5.00
10.00
15.00
20.00
25.00
30.00
35.00
40.00
45.00
50.00
55.00
60.00
65.00
70.00
KEULEGAN AND CARPENTER NO.

FIG : 4·58

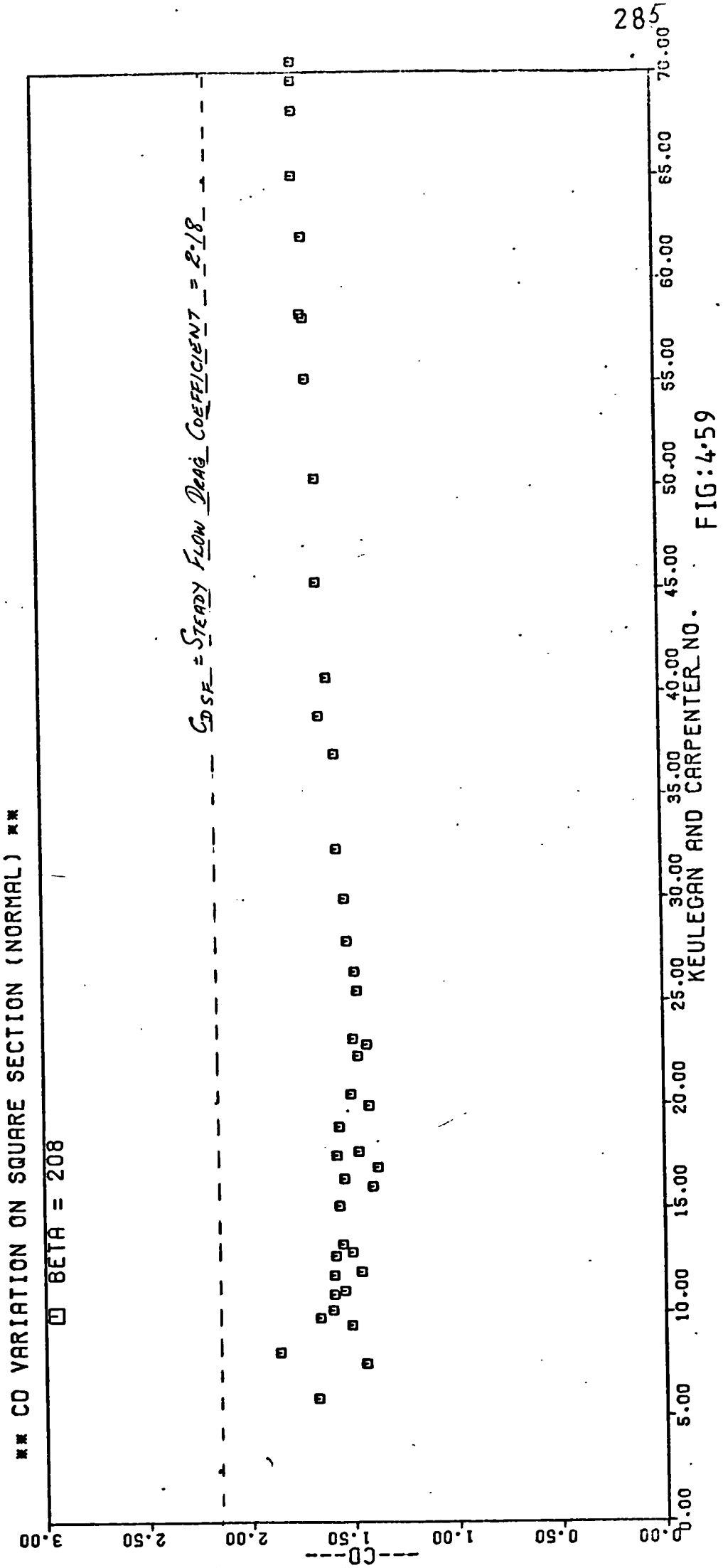
** CD VARIATION ON SQUARE SECTION (NORMAL) **
BETA = 208
CDSE = STEADY FLOW DRAG COEFFICIENT = 2.18
---CD---
0.00
0.50
1.00
1.50
2.00
2.50
3.00
0.00
5.00
10.00
15.00
20.00
25.00
30.00
35.00
40.00
45.00
50.00
55.00
60.00
65.00
70.00
KEULEGAN AND CARPENTER NO.

FIG:4·59

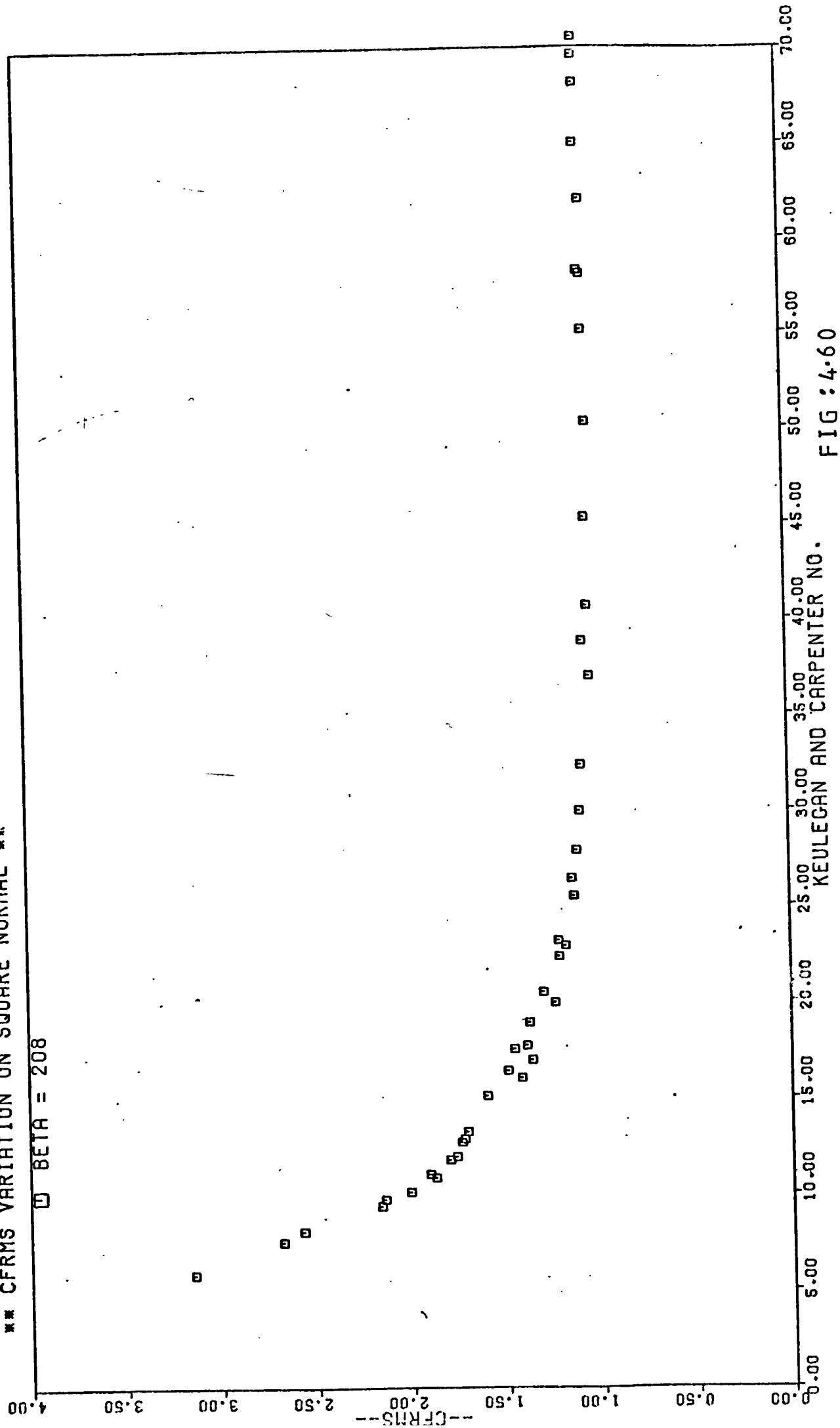
** CFRMS VARIATION ON SQUARE NORMAL **
BETA = 208
--CFRMS--
0.00
0.50
1.00
1.50
2.00
2.50
3.00
3.50
4.00
5.00
10.00
15.00
20.00
25.00
30.00
35.00
40.00
45.00
50.00
55.00
60.00
65.00
70.00
KEULEGAN AND CARPENTER NO.

FIG : 4·60

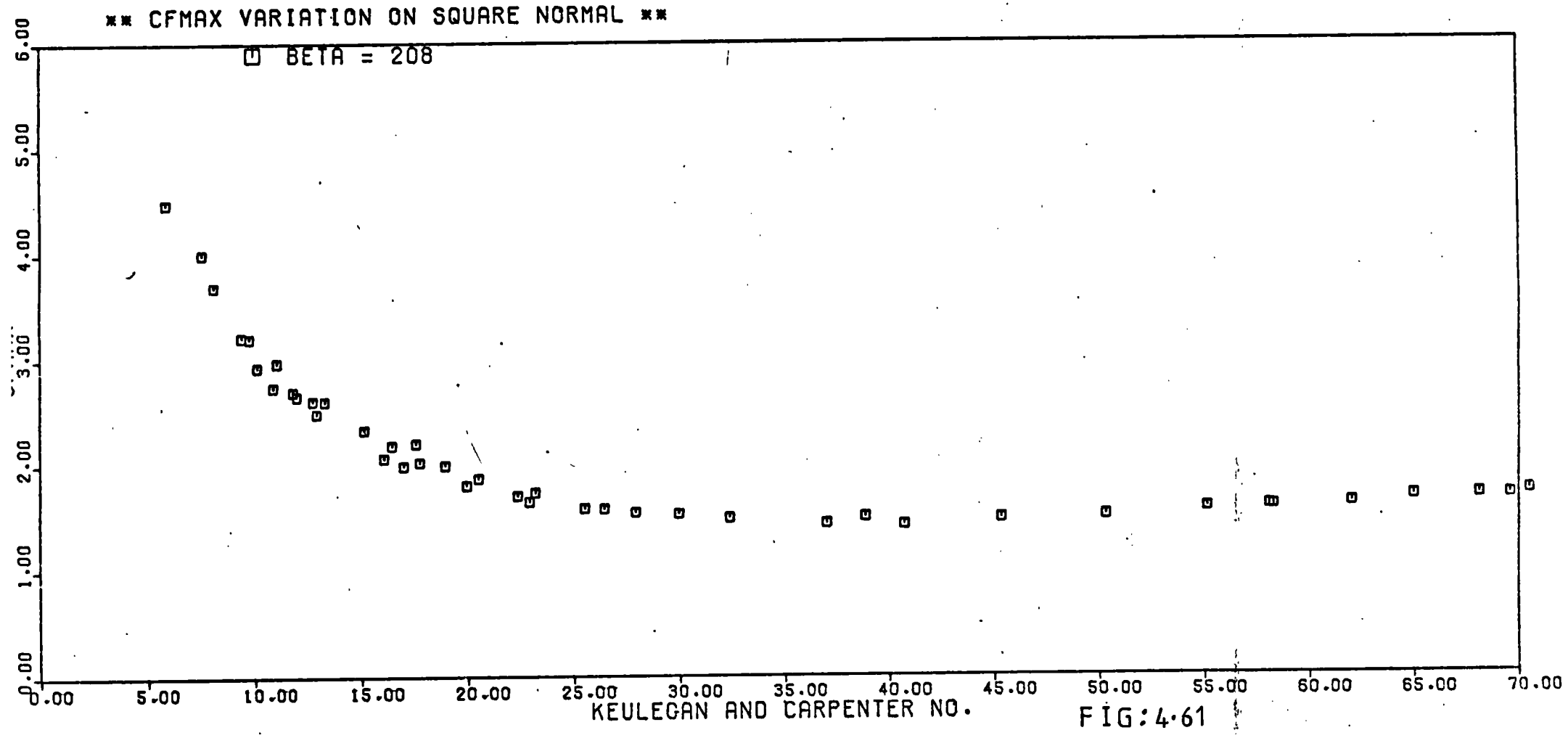
** CFMAX VARIATION ON SQUARE NORMAL **
BETA = 208
6.00
5.00
4.00
3.00
2.00
1.00
0.00
0.00
5.00
10.00
15.00
20.00
25.00
30.00
35.00
40.00
45.00
50.00
55.00
60.00
65.00
70.00
KEULEGAN AND CARPENTER NO.

FIG: 4·61

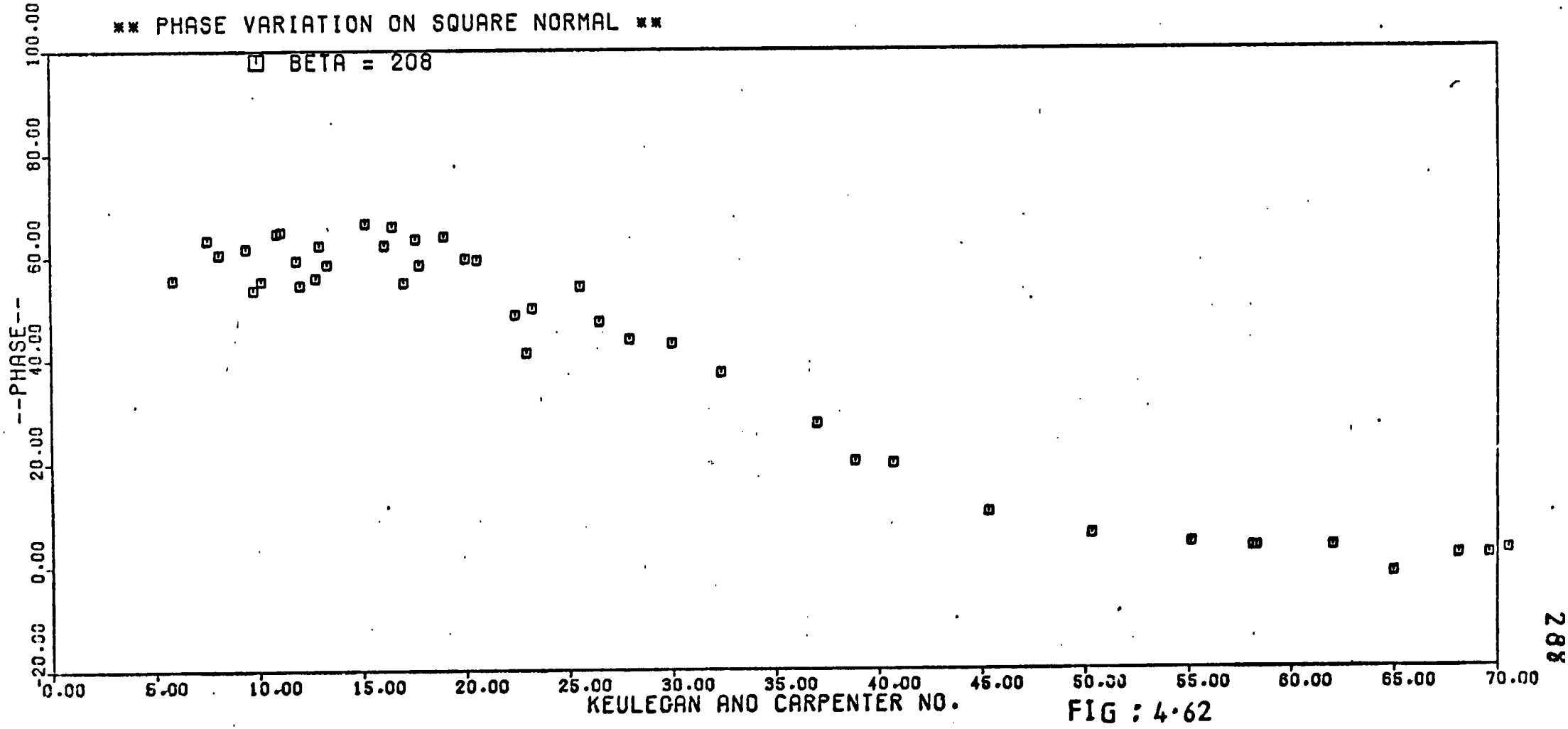
** PHASE VARIATION ON SQUARE NORMAL **
BETA = 208
--PHASE--
100.00
80.00
60.00
40.00
20.00
0.00
-20.00
0.00
5.00
10.00
15.00
20.00
25.00
30.00
35.00
40.00
45.00
50.00
55.00
60.00
65.00
70.00
KEULEGAN AND CARPENTER NO.

FIG : 4·62

RUN 53 NKC = 9.81 **SQUARE NORMAL SET ONE *** $\beta = 208$

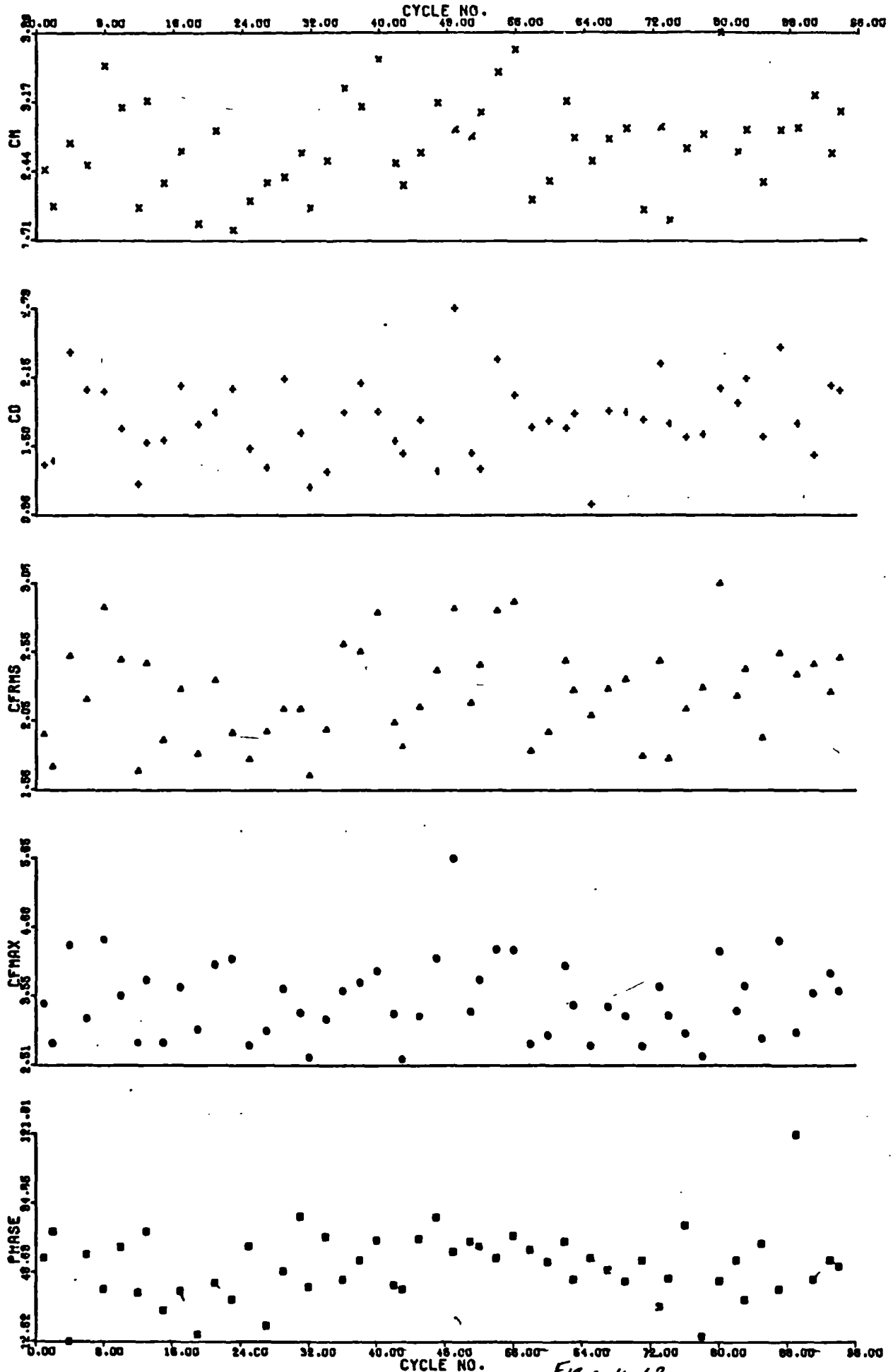

FIG: 4.63

RUN 21 NKC=29.999 : β= 208 SQUARE SECTION NORMAL TO FLOW

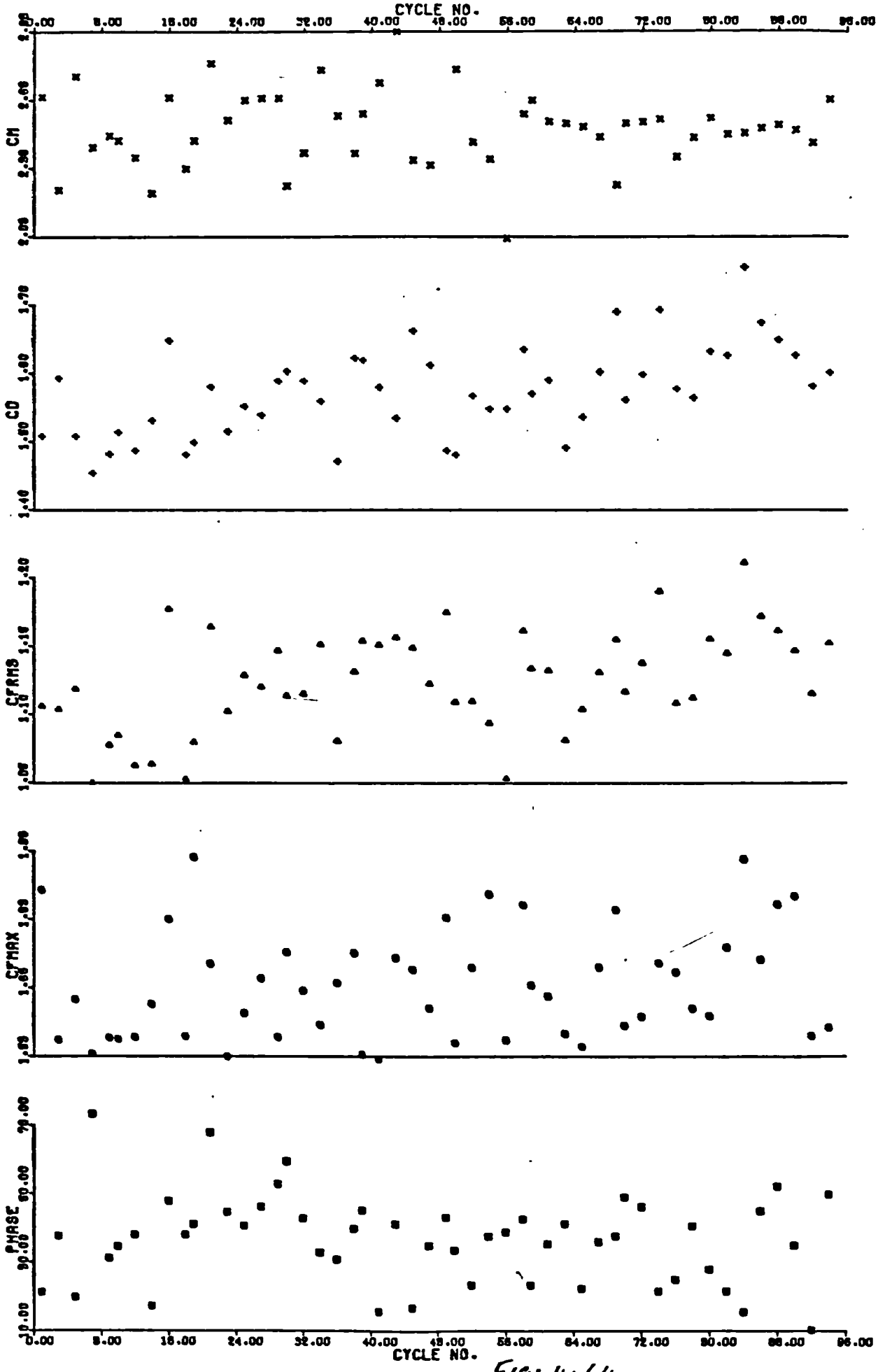

Fig: 4.64

RUN 3 NKC=68.12 β = 208 SQUARE SECTION NORMAL TO FLOW

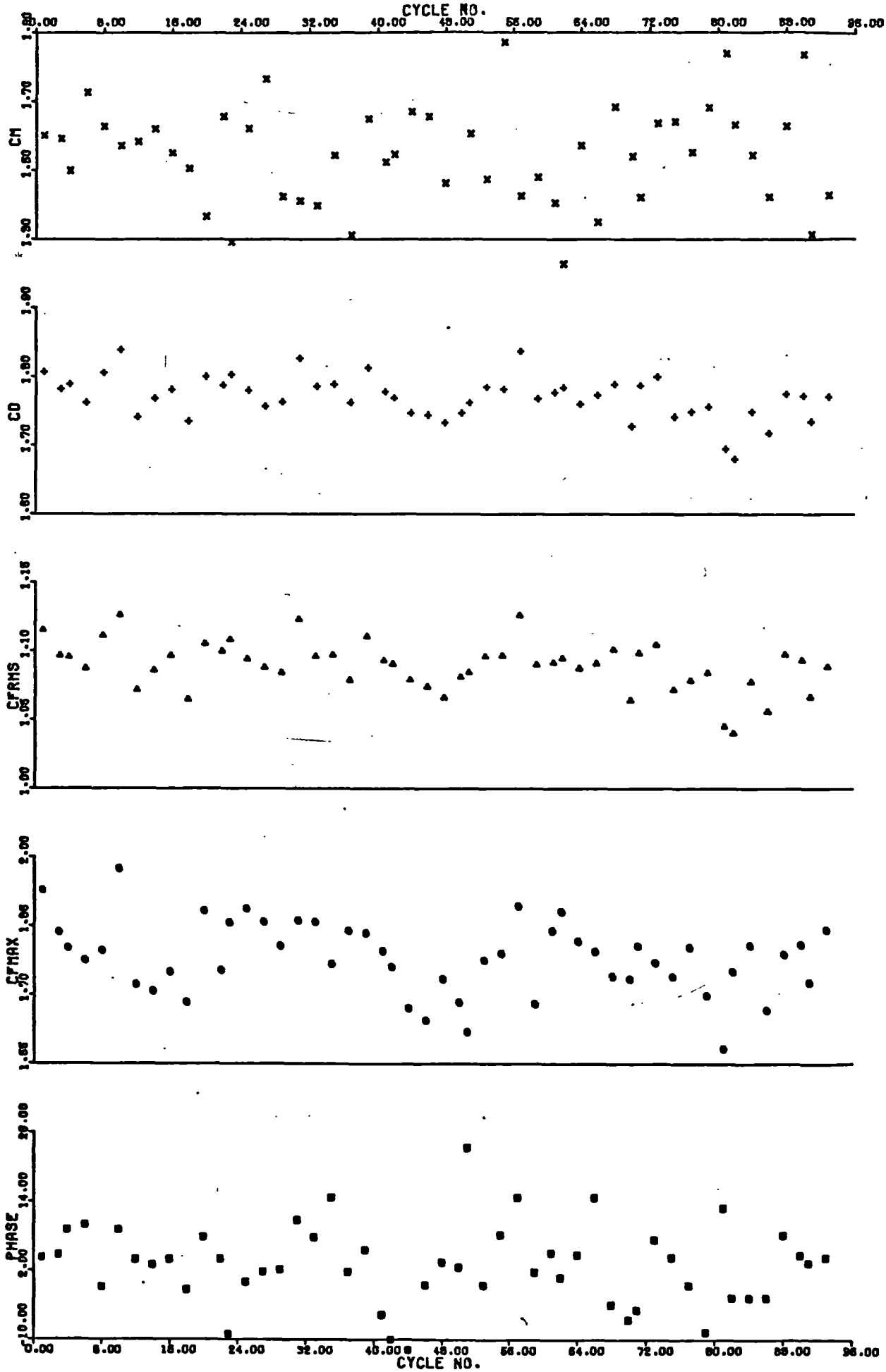

FIG: 4.65

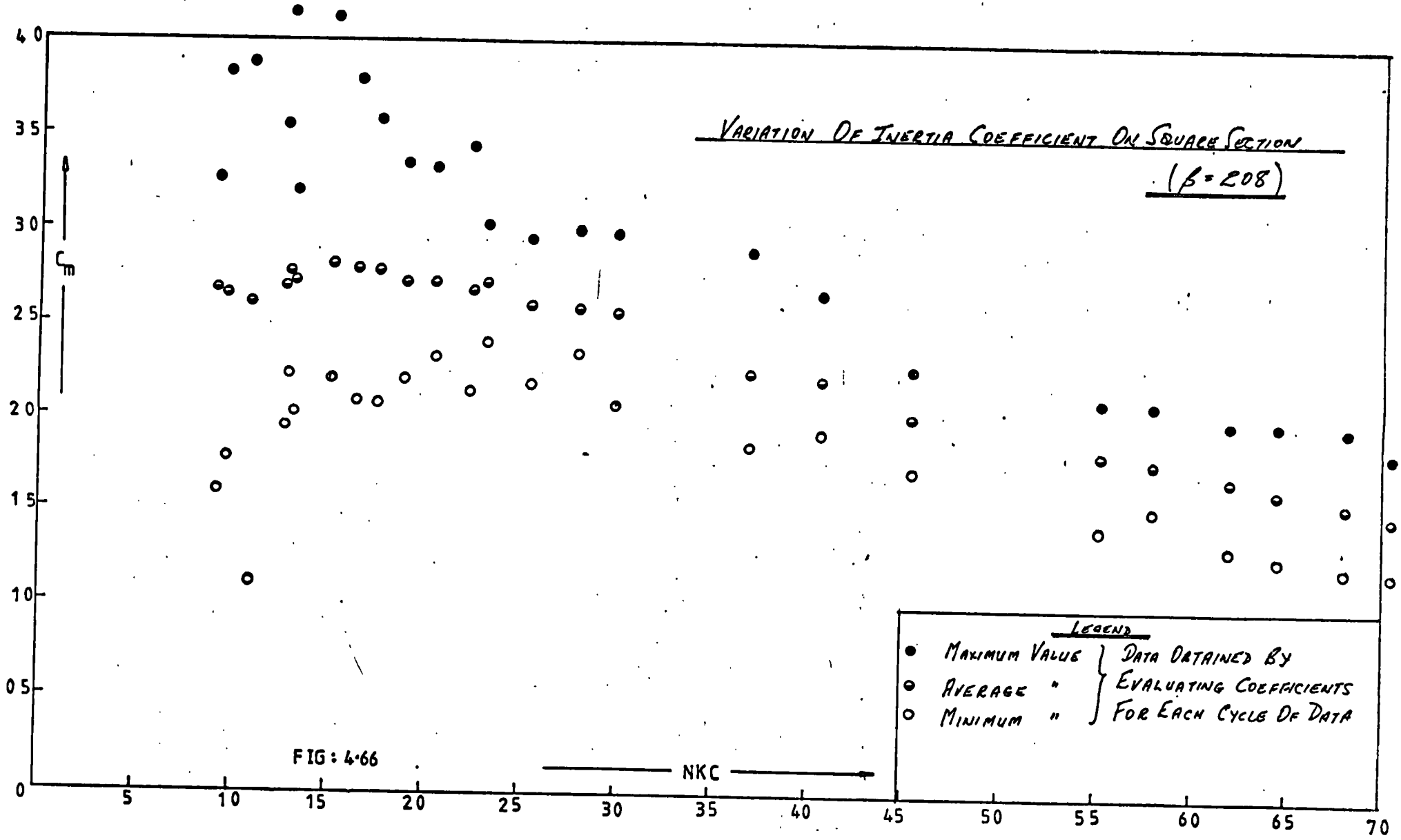
VARIATION OF INERTIA COEFFICIENT ON SQUARE SECTION
(β = 208)
C_m
NKC
LEGEND
Maximum Value
Average "
Minimum "
Data Obtained By Evaluating Coefficients For Each Cycle Of Data
0
0·5
1·0
1·5
2·0
2·5
3·0
3·5
4·0
5
10
15
20
25
30
35
40
45
50
55
60
65
70

FIG : 4·66

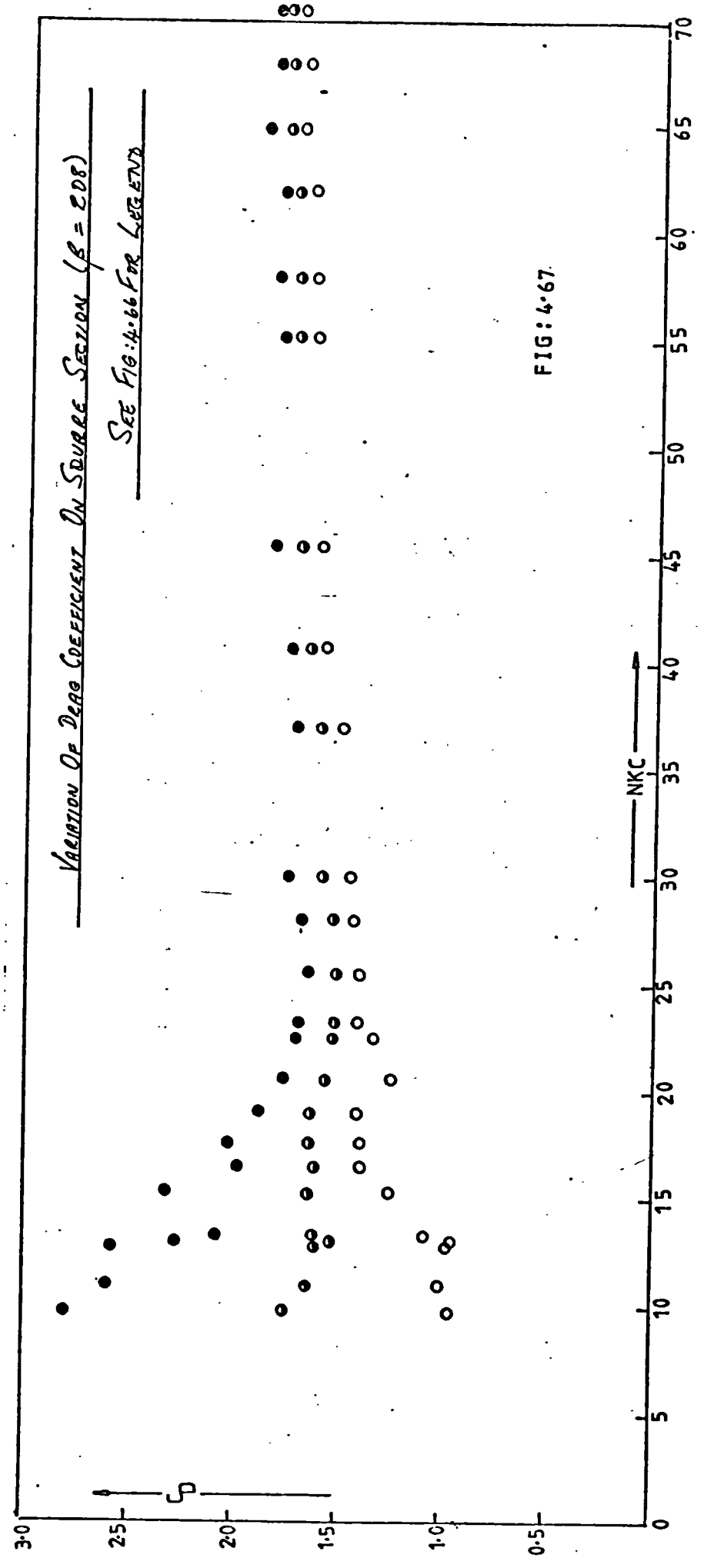
VARIATION OF DRAG COEFFICIENT ON SQUARE SECTION (β = 2·05)
SEE FIG: 4·66 FOR LEGEND
CD
NKC
3·0
2·5
2·0
1·5
1·0
0·5
0
5
10
15
20
25
30
35
40
45
50
55
60
65
70

FIG: 4·67

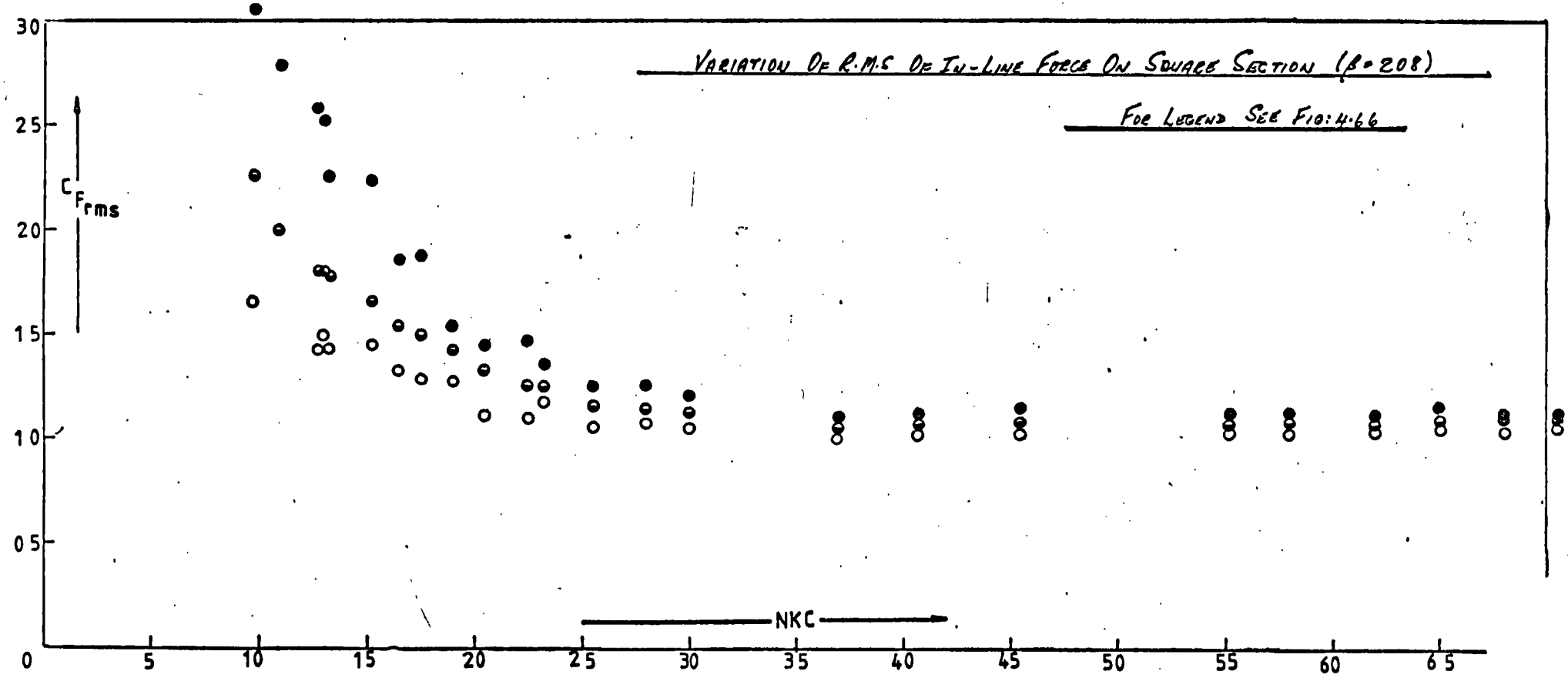
VARIATION OF R.M.S OF IN-LINE FORCE ON SQUARE SECTION (β=208)
FOR LEGEND SEE FIG:4.66
$C_{F_{rms}}$
NKC
30
25
20
15
10
05
0
5
10
15
20
25
30
35
40
45
50
55
60
65

FIG:4·68

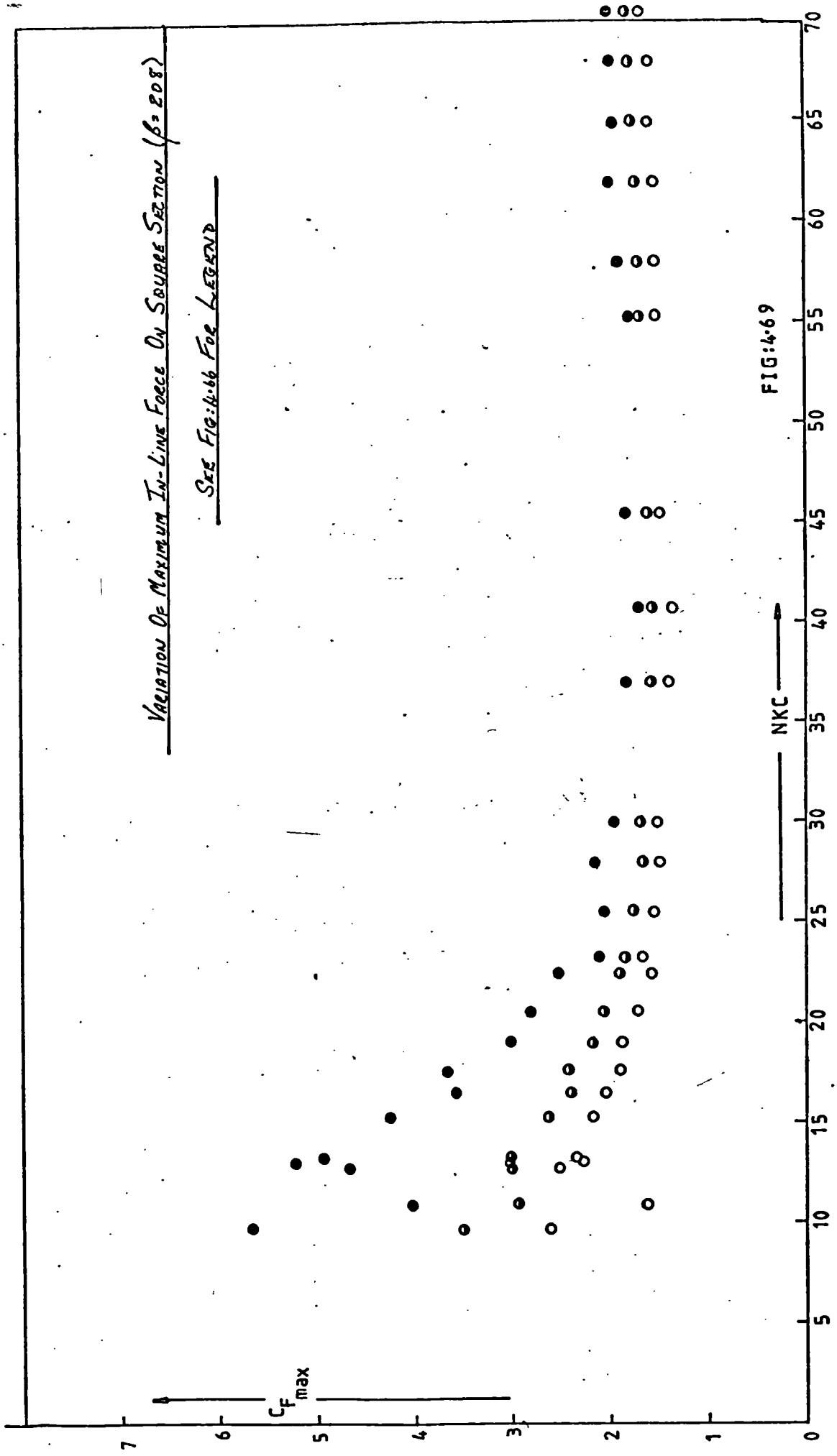
VARIATION OF MAXIMUM IN-LINE FORCE ON SQUARE SECTION (β= 208)
SEE FIG:4.66 FOR LEGEND
$C_{F_{max}}$
NKC
0
1
2
3
4
5
6
7
5
10
15
20
25
30
35
40
45
50
55
60
65
70

FIG:4.69

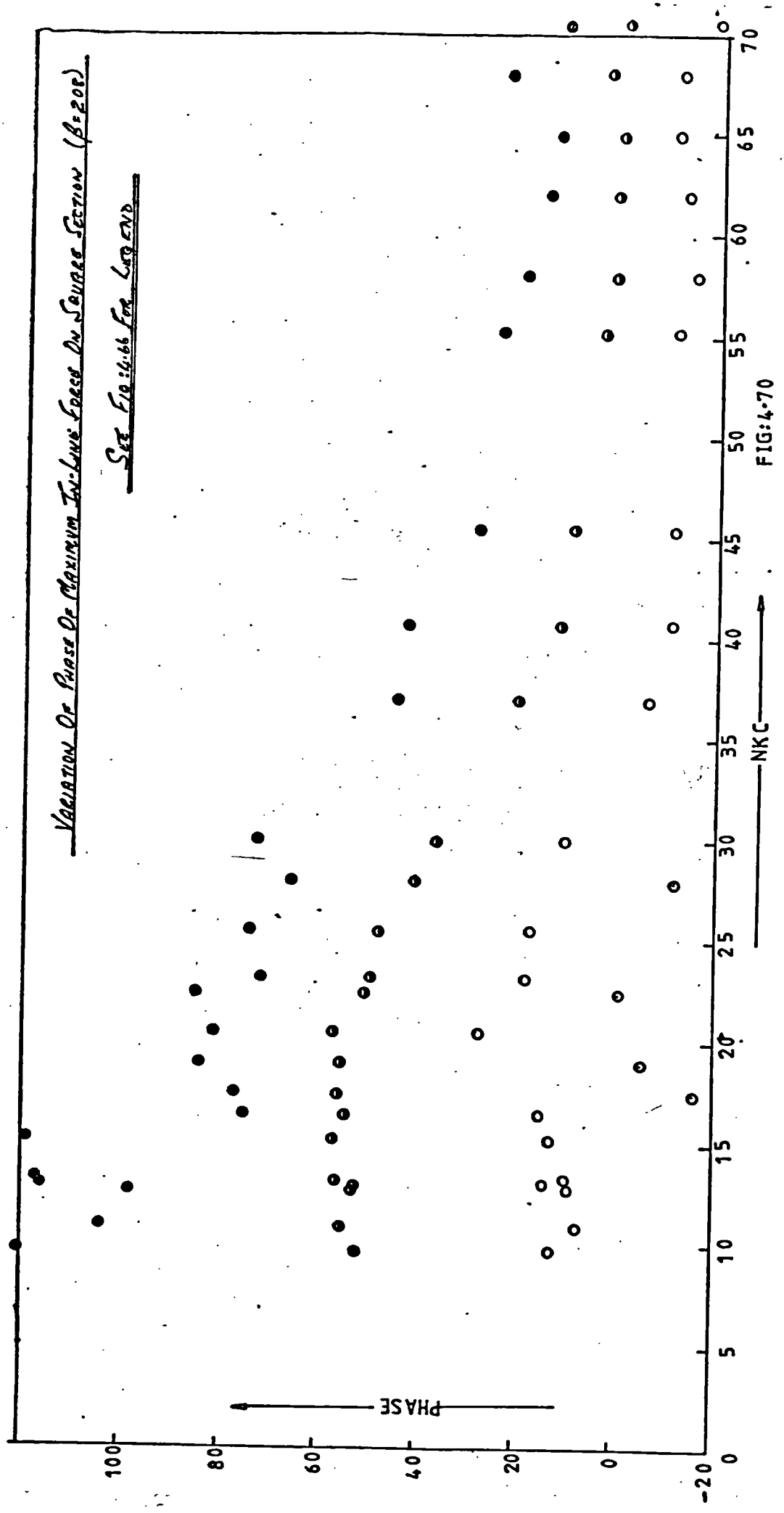
VARIATION OF PHASE OF MAXIMUM FLUX LINE FORCE ON SQUARE SECTION (β=20°)
SEE FIG:4.66 FOR LEGEND
PHASE
NKC
-20
0
20
40
60
80
100
0
5
10
15
20
25
30
35
40
45
50
55
60
65
70

FIG:4.70

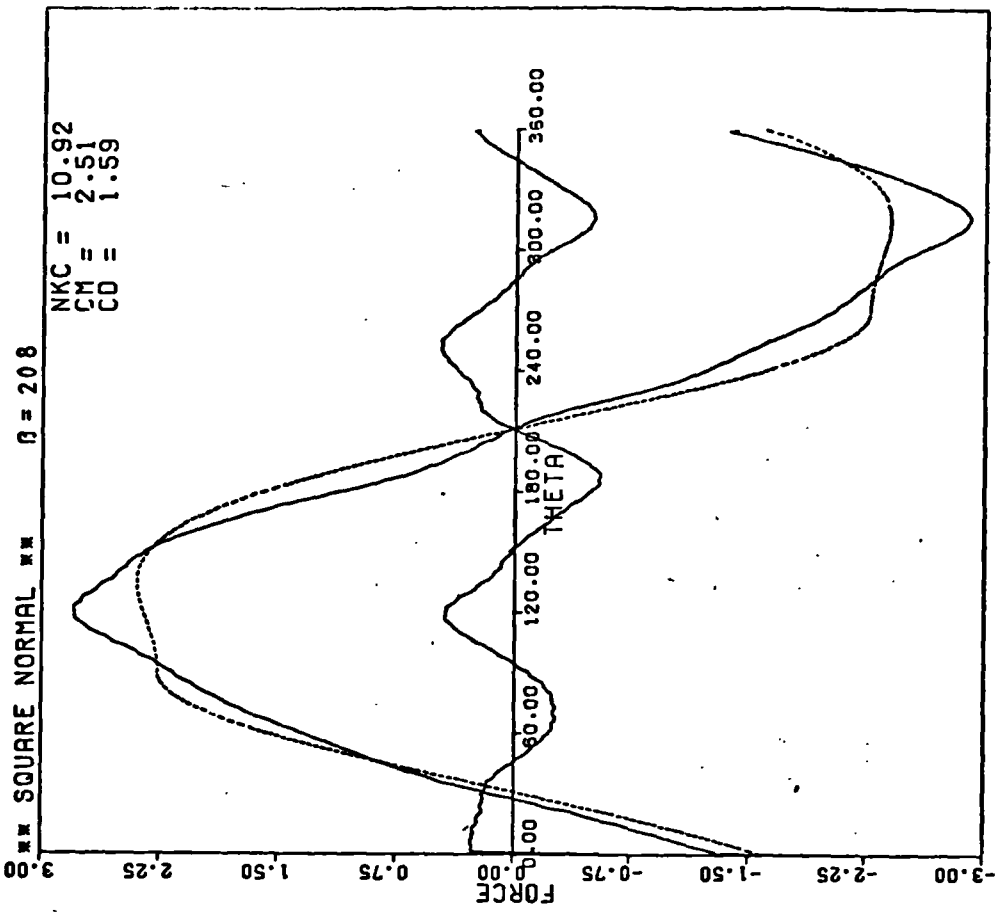

FIG: 4.71 (b)

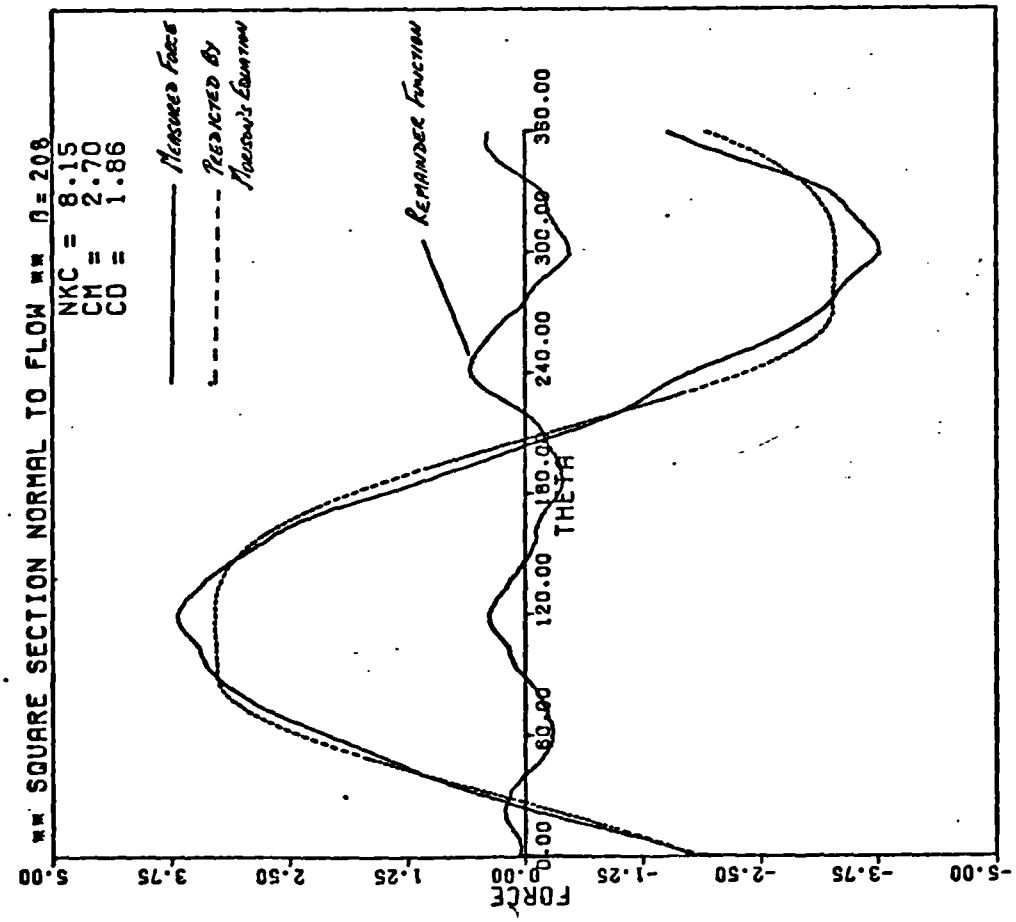

FIG: 4.71 (a)

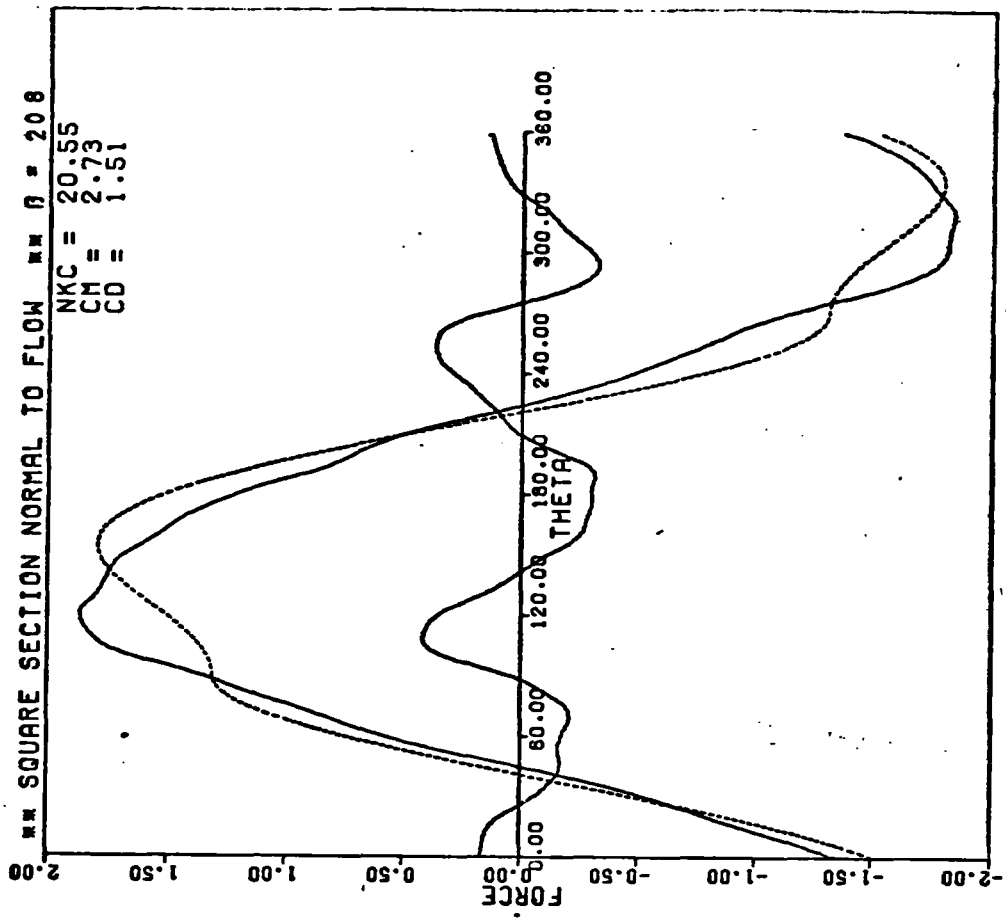

FIG: 4.71 (d)

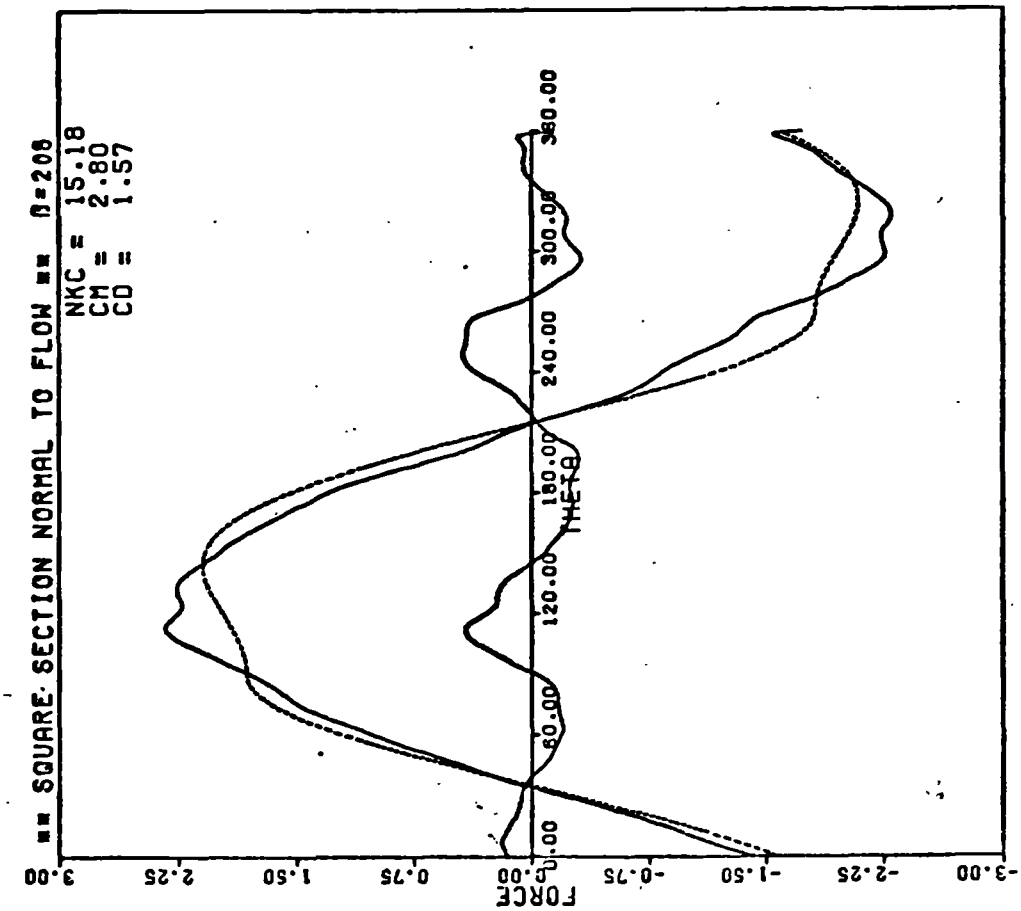

FIG: 4.71 (c)

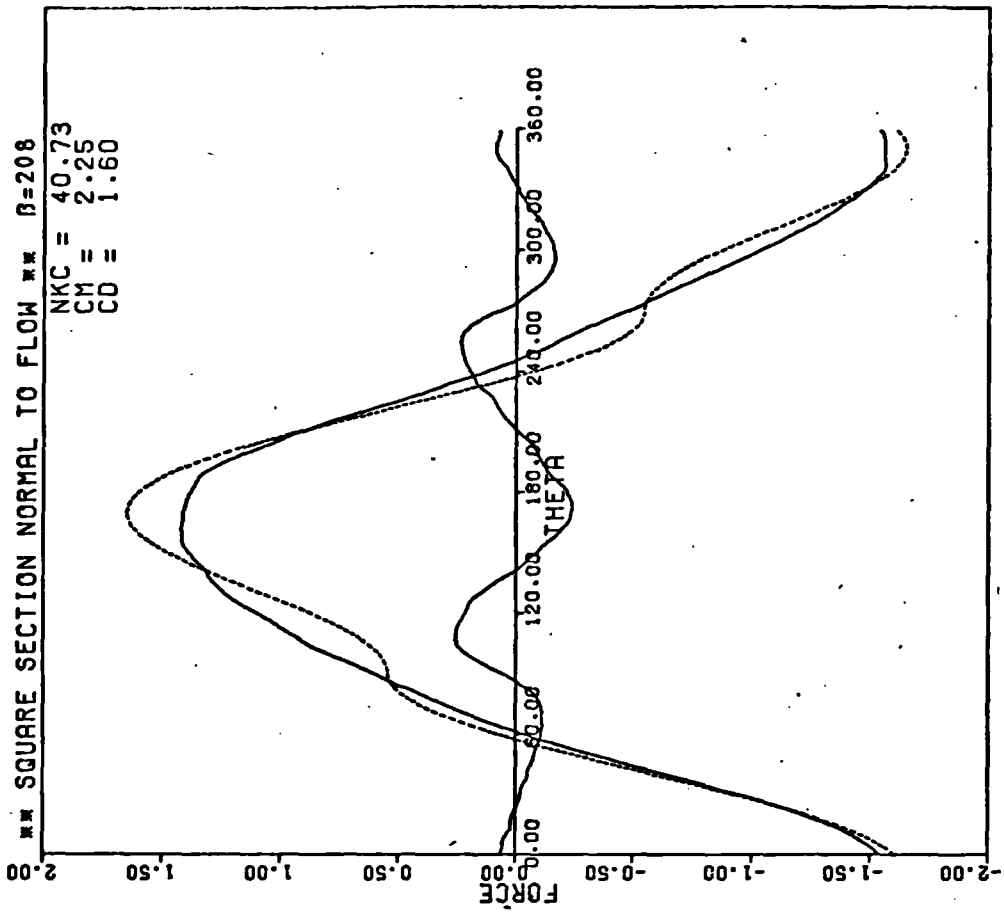

FIG: 4.71 (f)

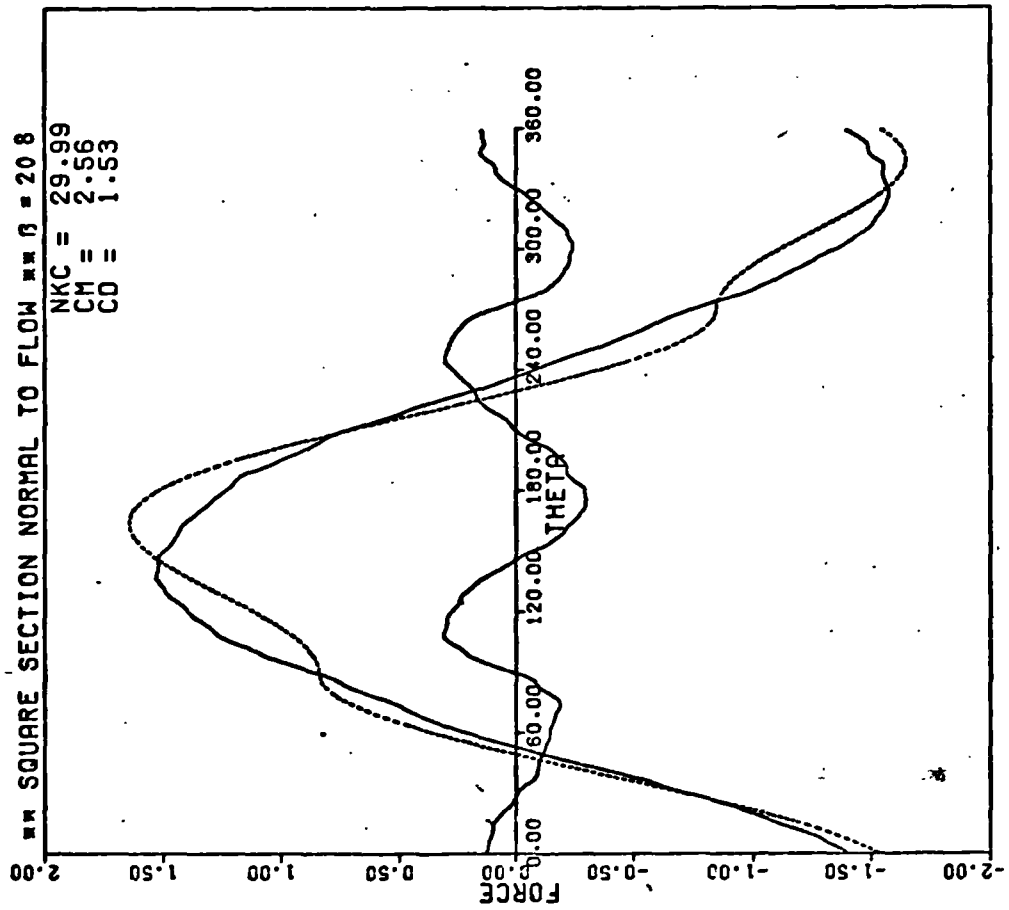

FIG: 4.71 (e)

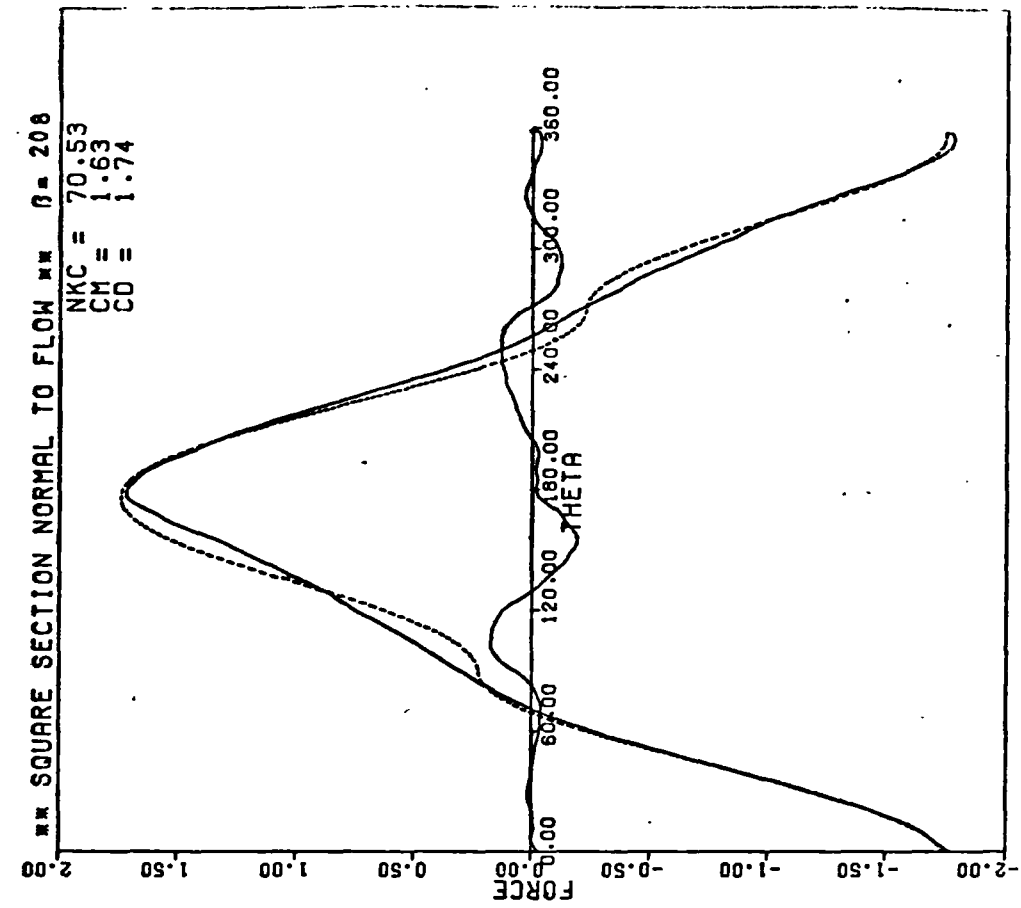

FIG: 4.71 (h)

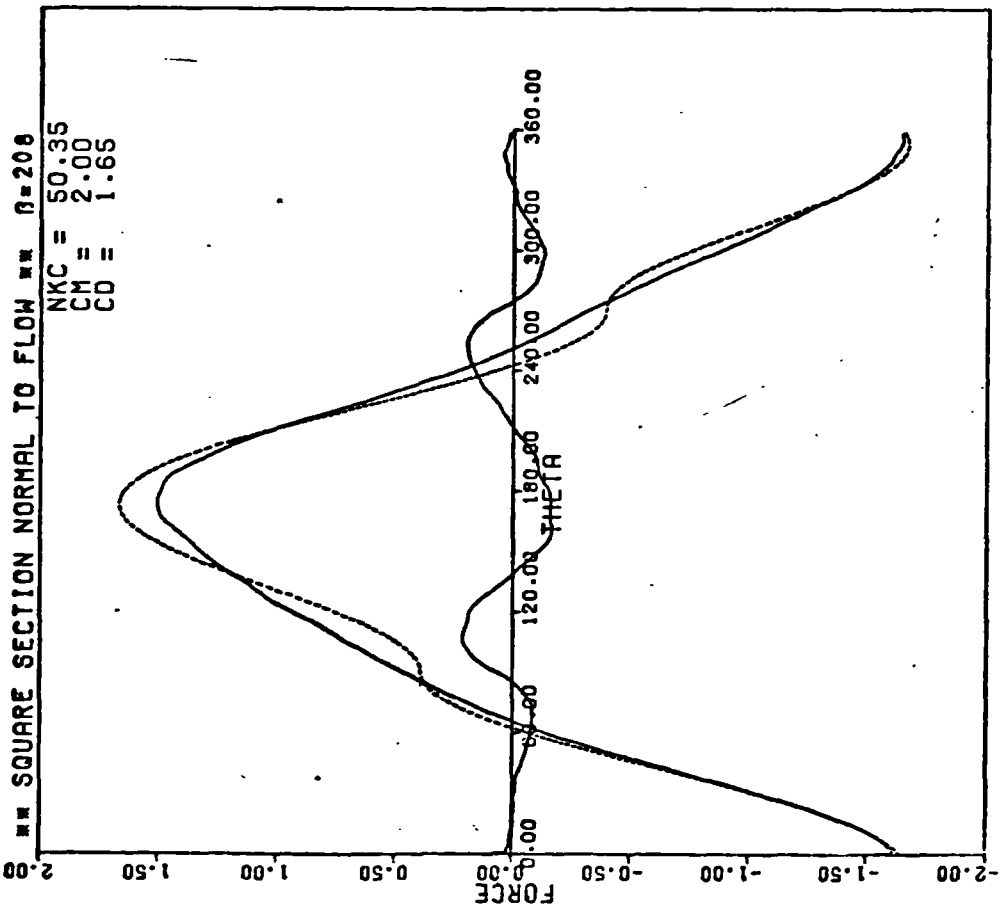

FIG: 4.71 (g)

FIG: 4·72 VARIATION OF LIFT ON THE CIRCULAR CYLINDER

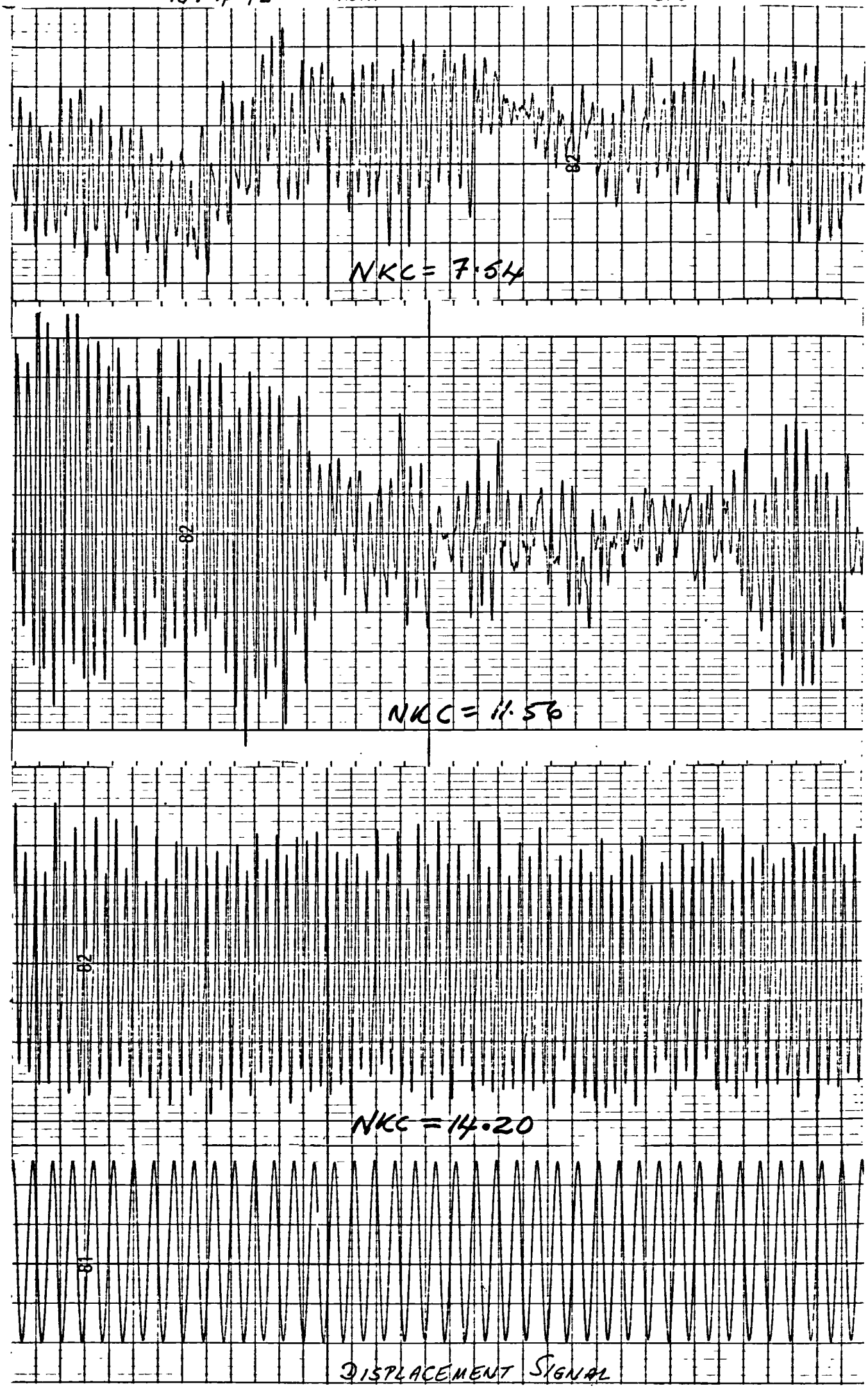

FIG: 4·72

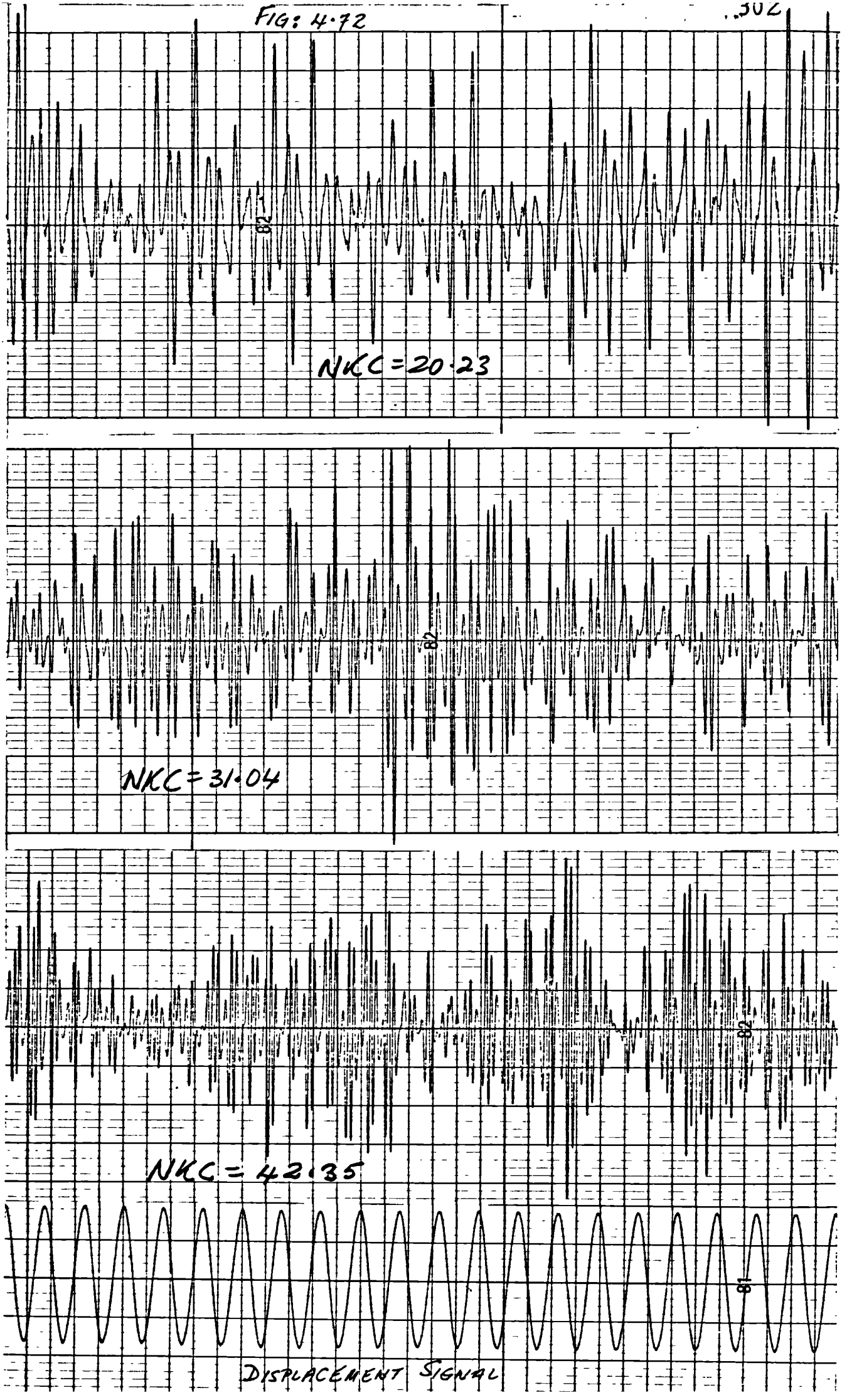

(e.

(f.

(g)

(h)

DISPLACEMENT SIGNAL

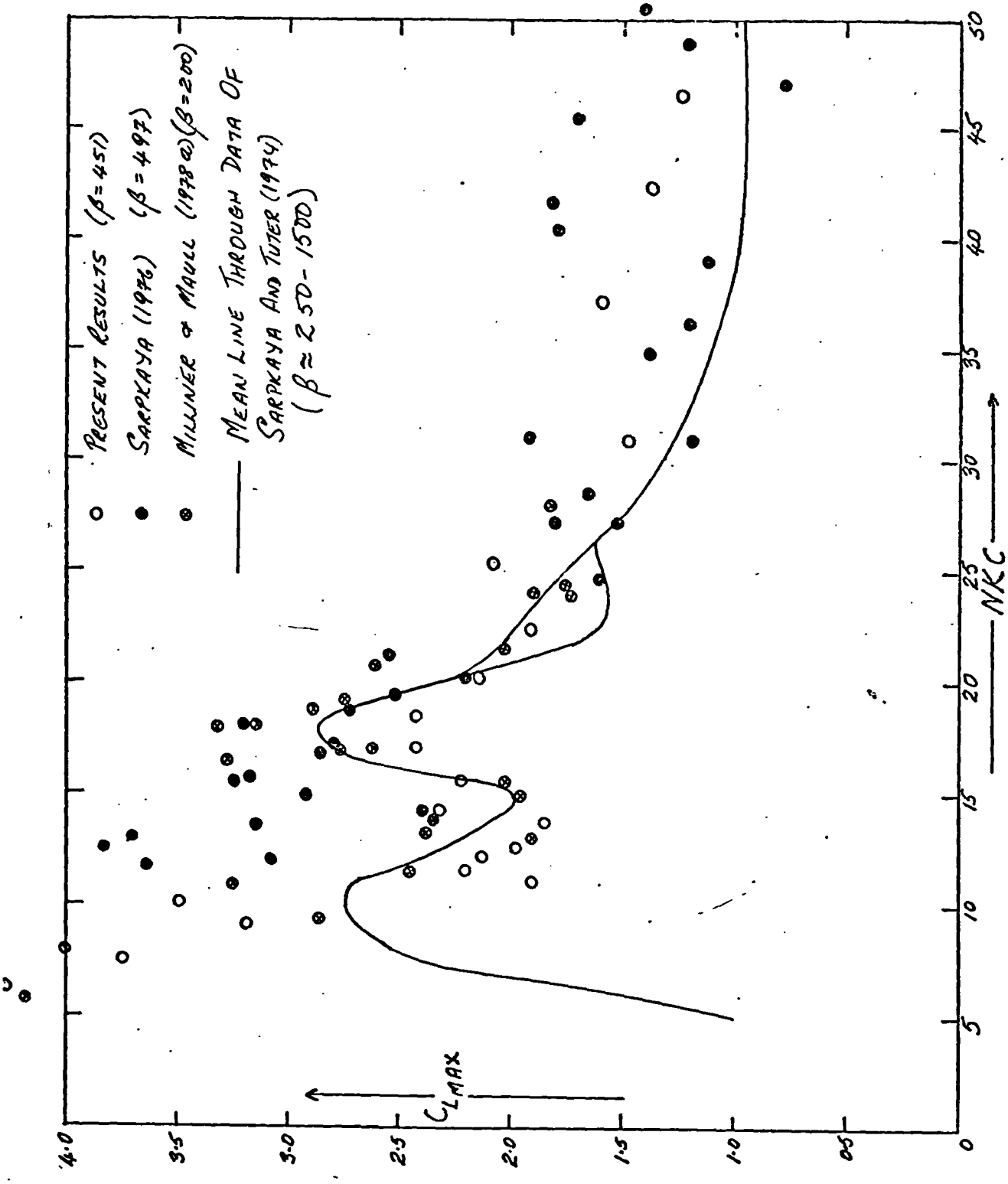
PRESENT RESULTS (β=451)
SARPKAYA (1976) (β=497)
MILLINER & MAULL (1978@)(β=200)
MEAN LINE THROUGH DATA OF SARPKAYA AND TUTER (1974) (β≈250-1500)
CLMAX
NKC
4.0
3.5
3.0
2.5
2.0
1.5
1.0
0.5
0
5
10
15
20
25
30
35
40
45
50

FIG:4·73

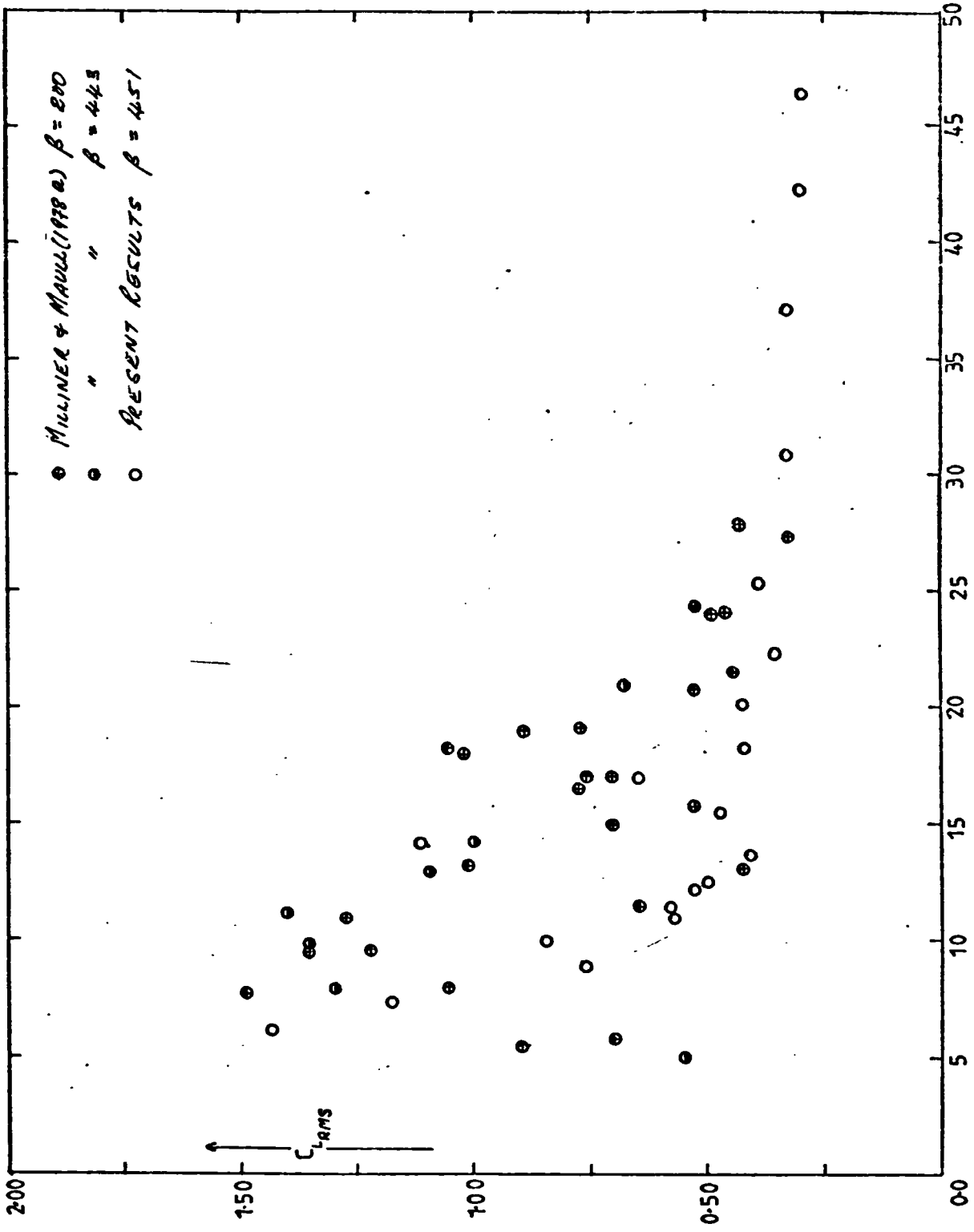
MILLINER & MAULL (1978 a) β = 0·80
" β = 4·43
PRESENT RESULTS β = 4·51
$C_{L_{RMS}}$
2·00
1·50
1·00
0·50
0·0
0·0
5
10
15
20
25
30
35
40
45
50

FIG: 4·74

FIG: 4·75 VARIATION OF LIFT ON A CIRCULAR CYLINDER DURING 2 CYCLES

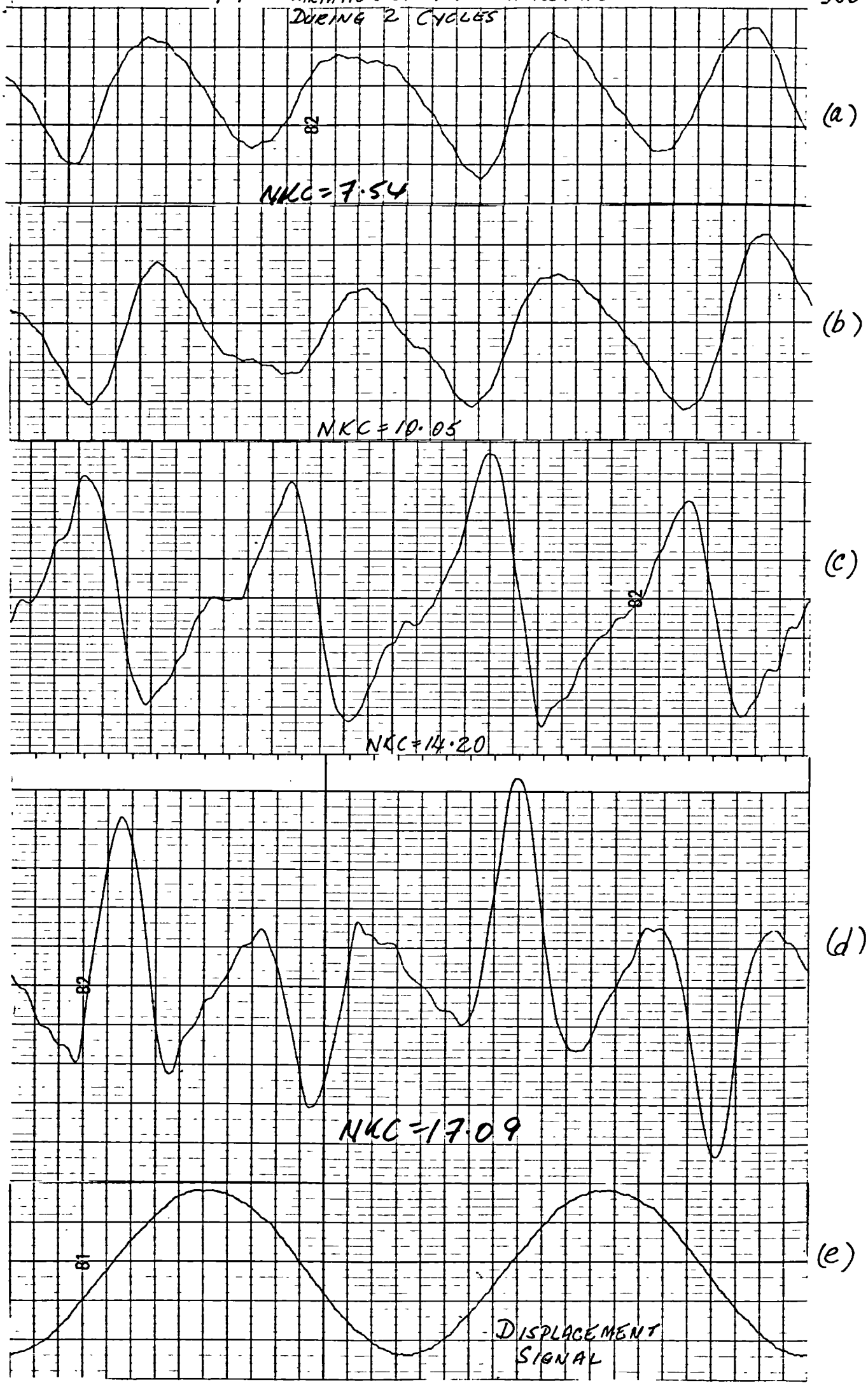

FIG:4·75

VARIATION OF LIFT ON A CIRCULAR CYLINDER DURING 2 CYCLES

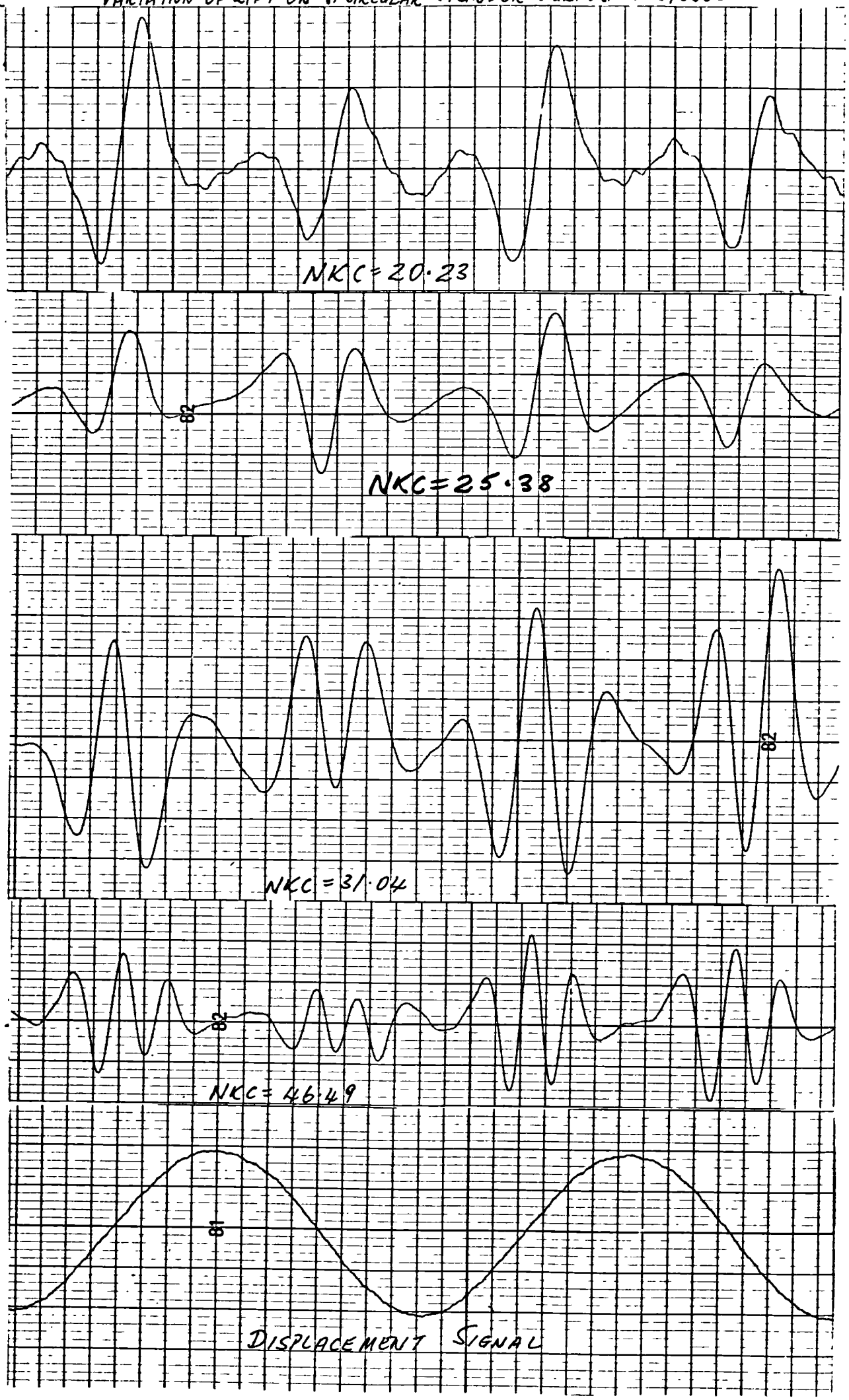

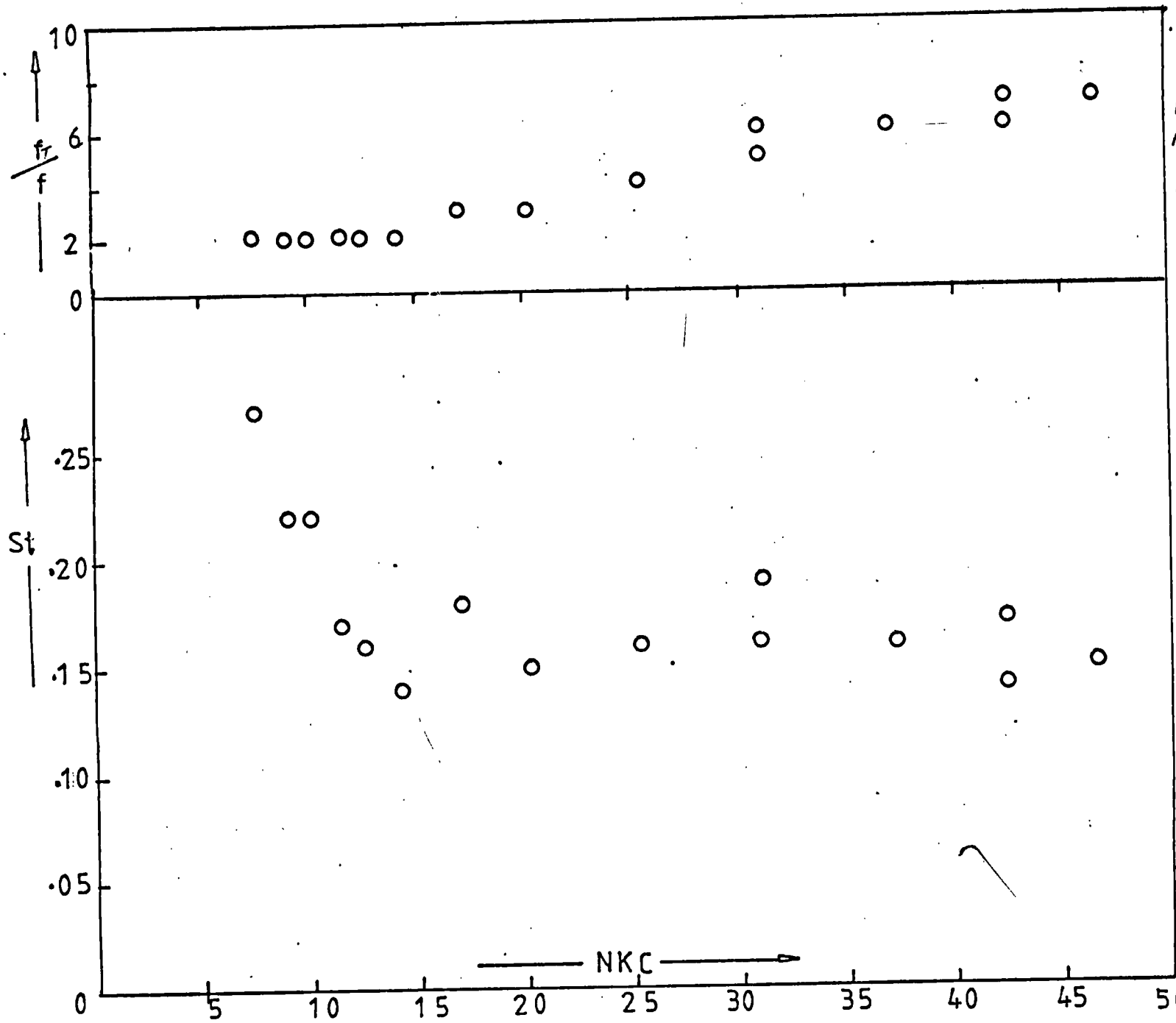

VARIATION OF FREQUENCY OF TRANSVERSE FORCE WITH NKC

RESULTS ON THE CIRCULAR CYLINDER (β=451)

VARIATION OF STROUHAL NO. WITH NKC

FIG : 4.76

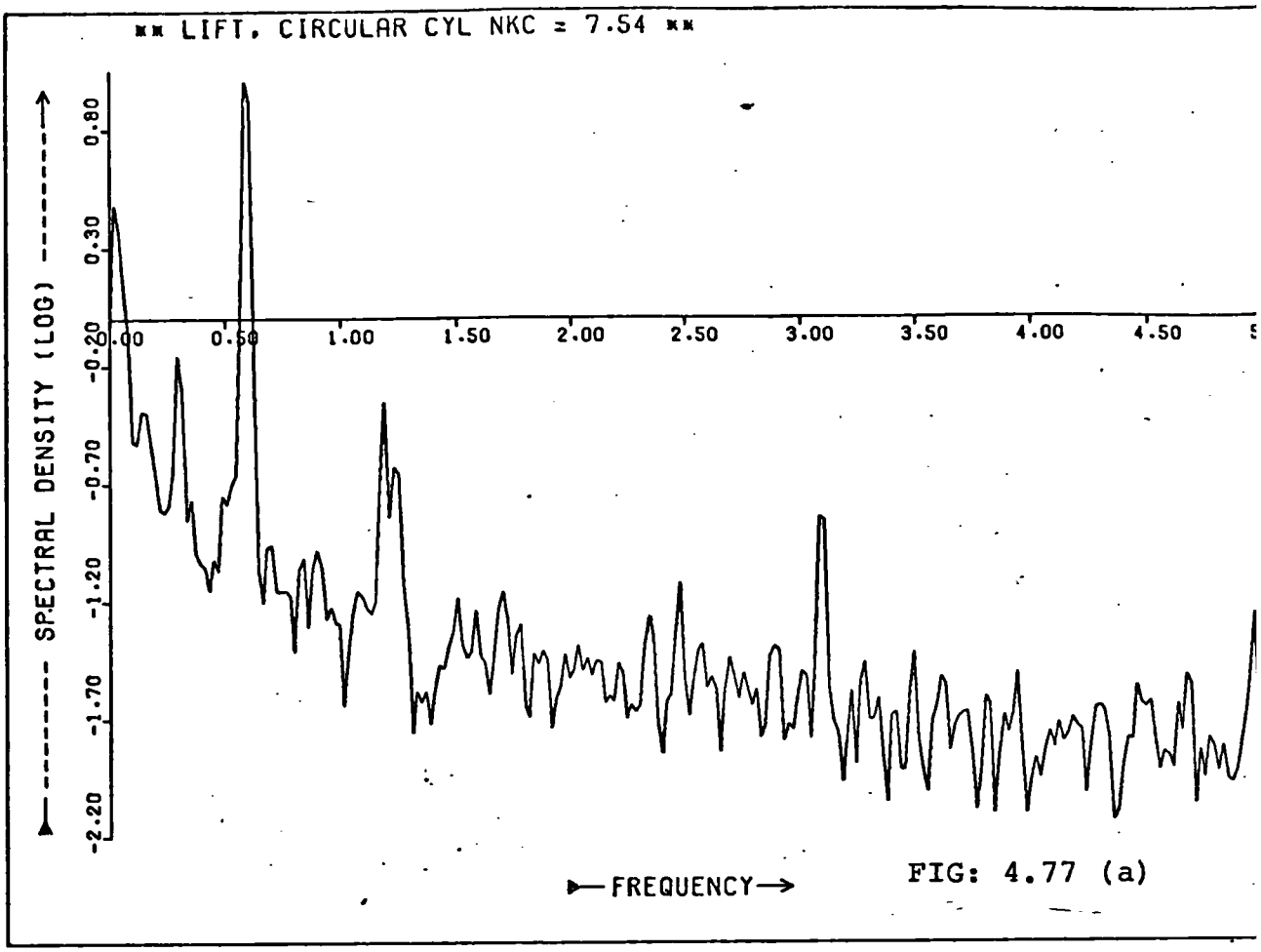

FIG: 4.77 (a)

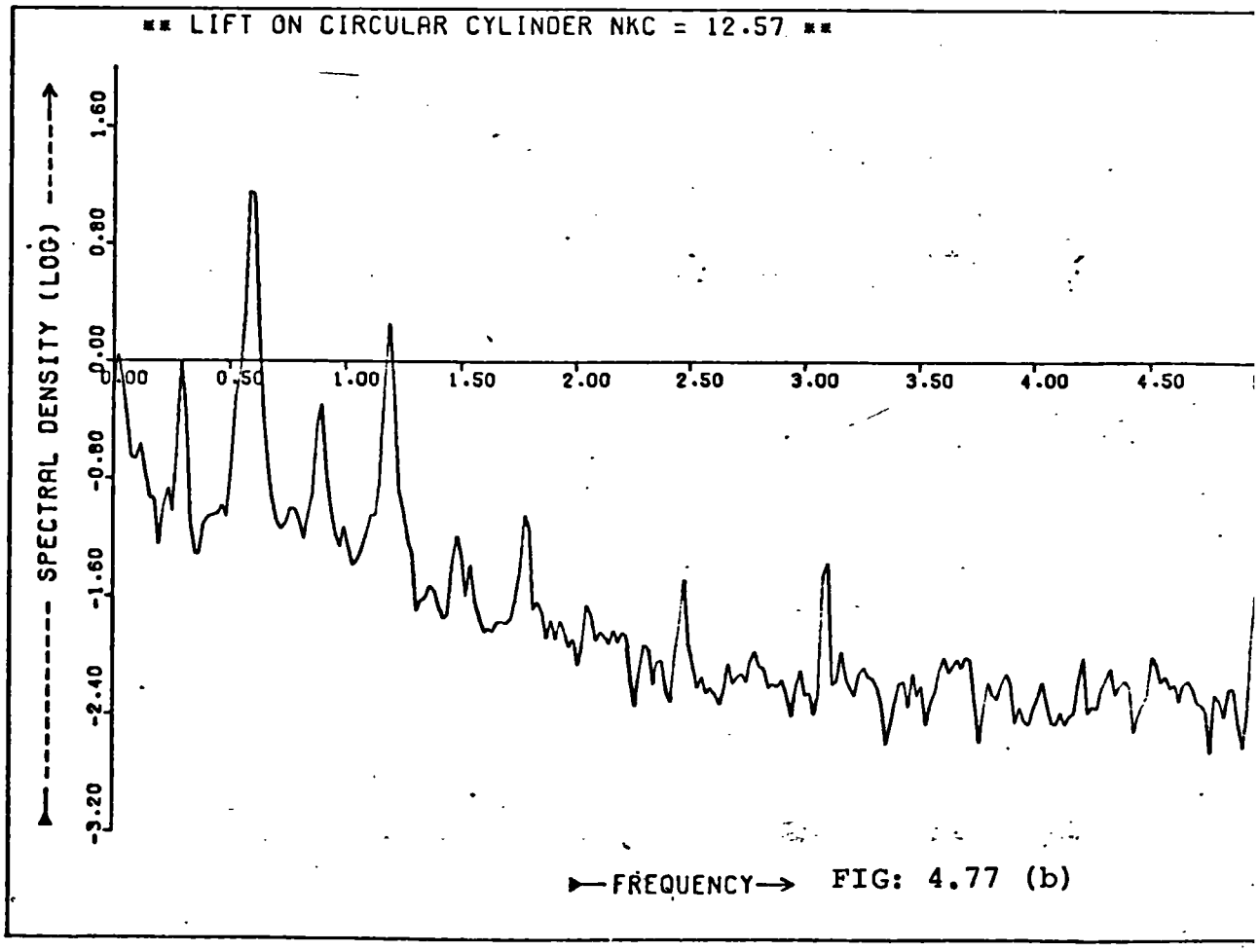

FIG: 4.77 (b)

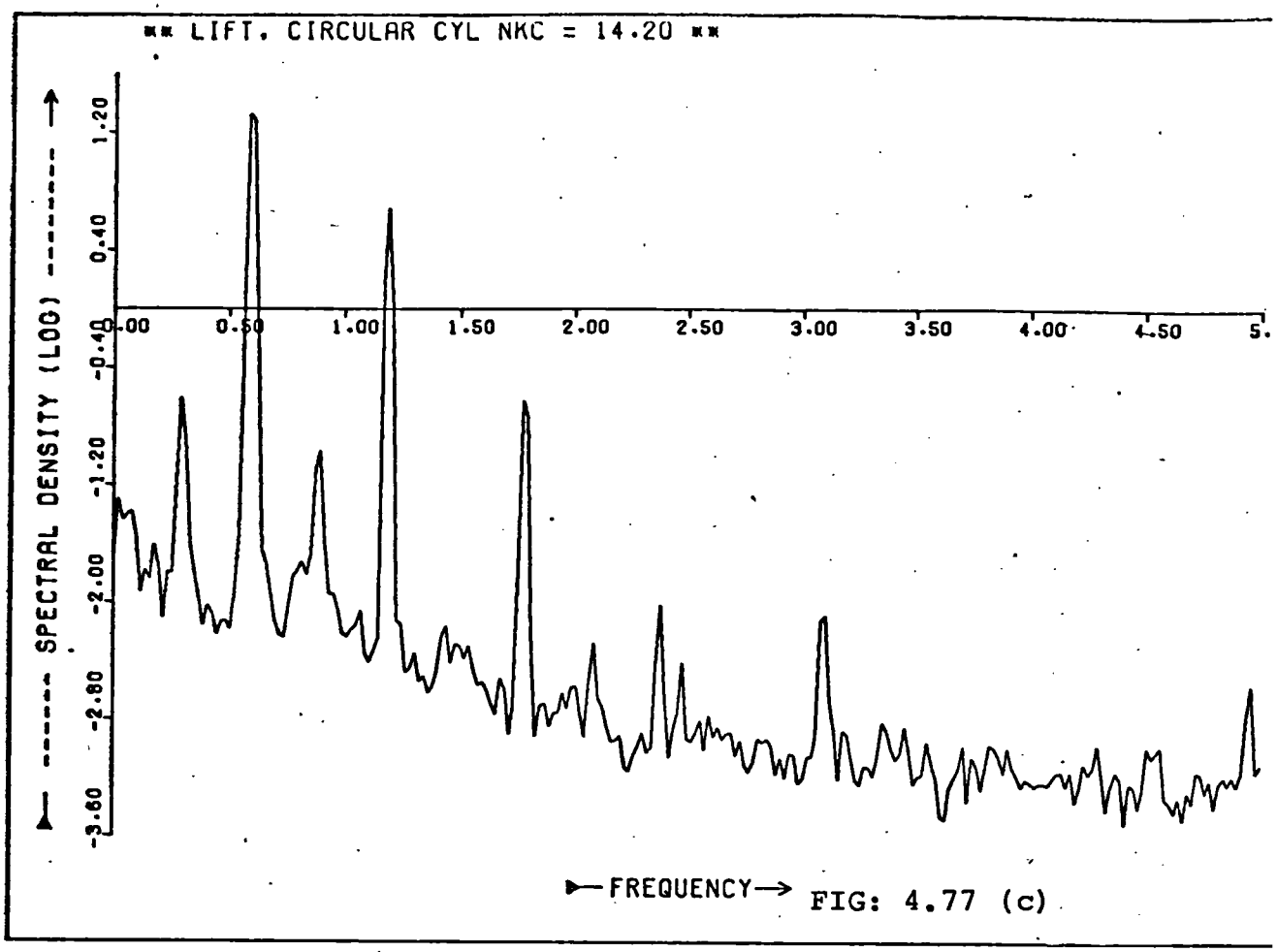

FIG: 4.77 (c)

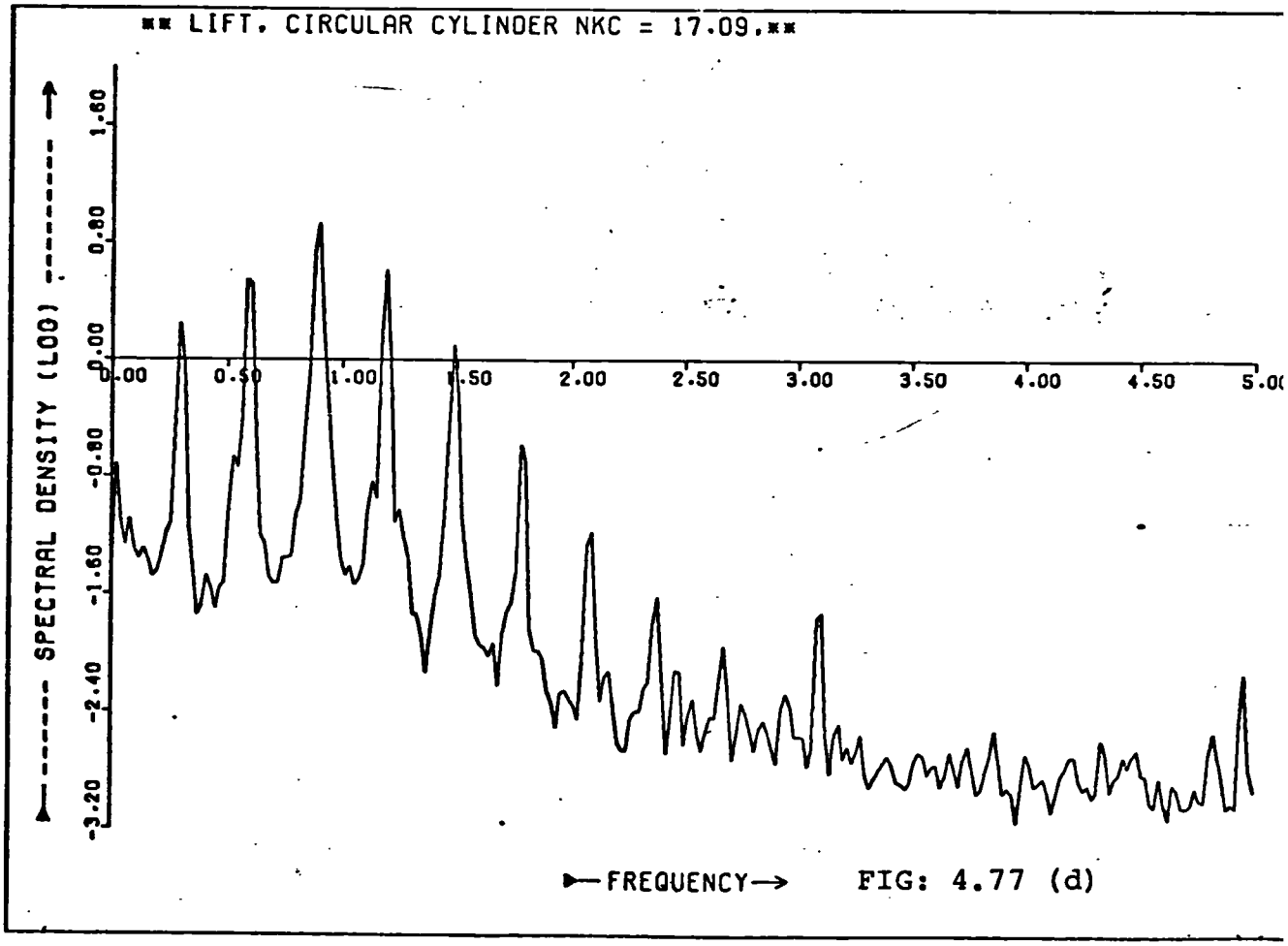

FIG: 4.77 (d)

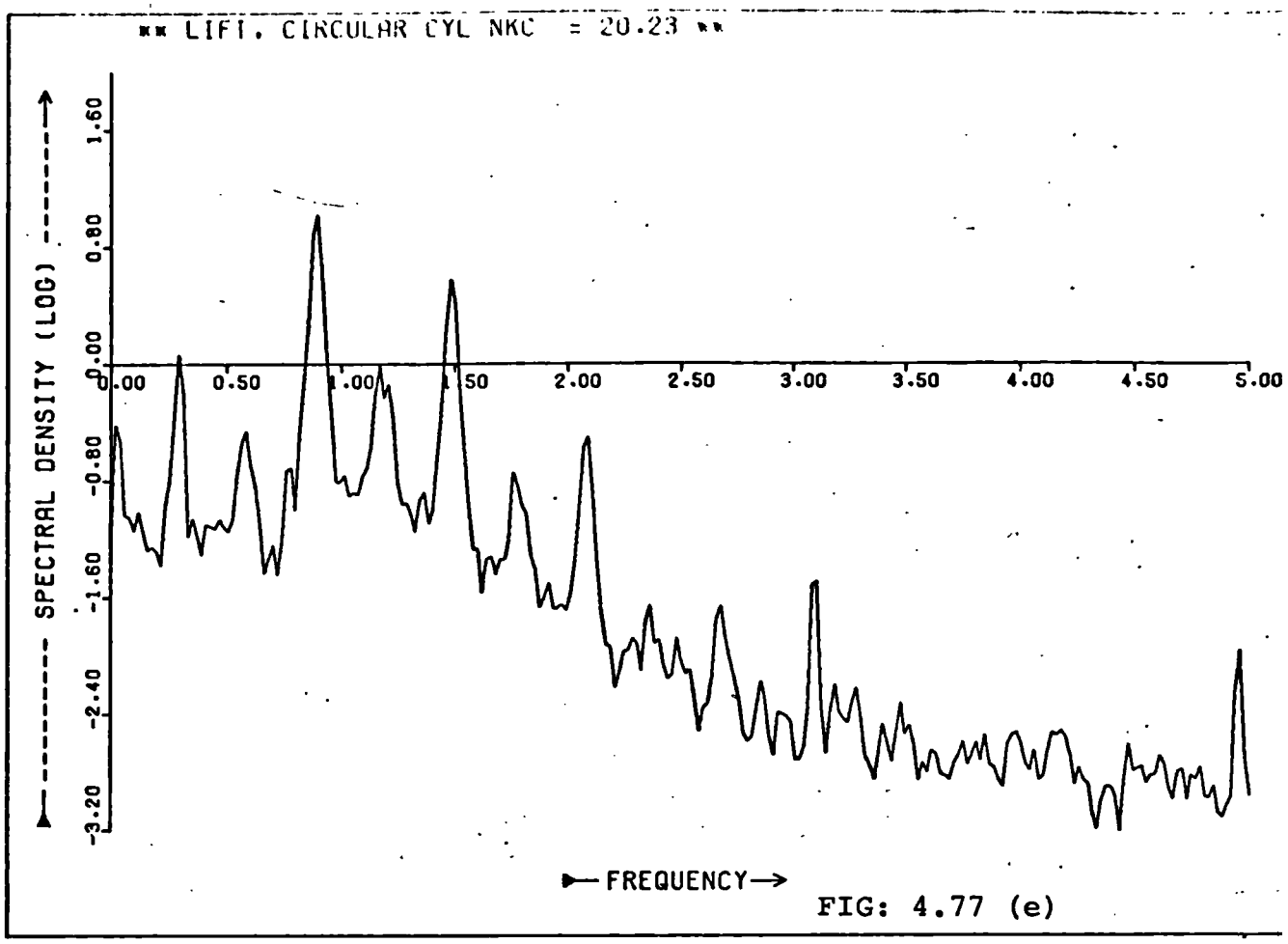

FIG: 4.77 (e)

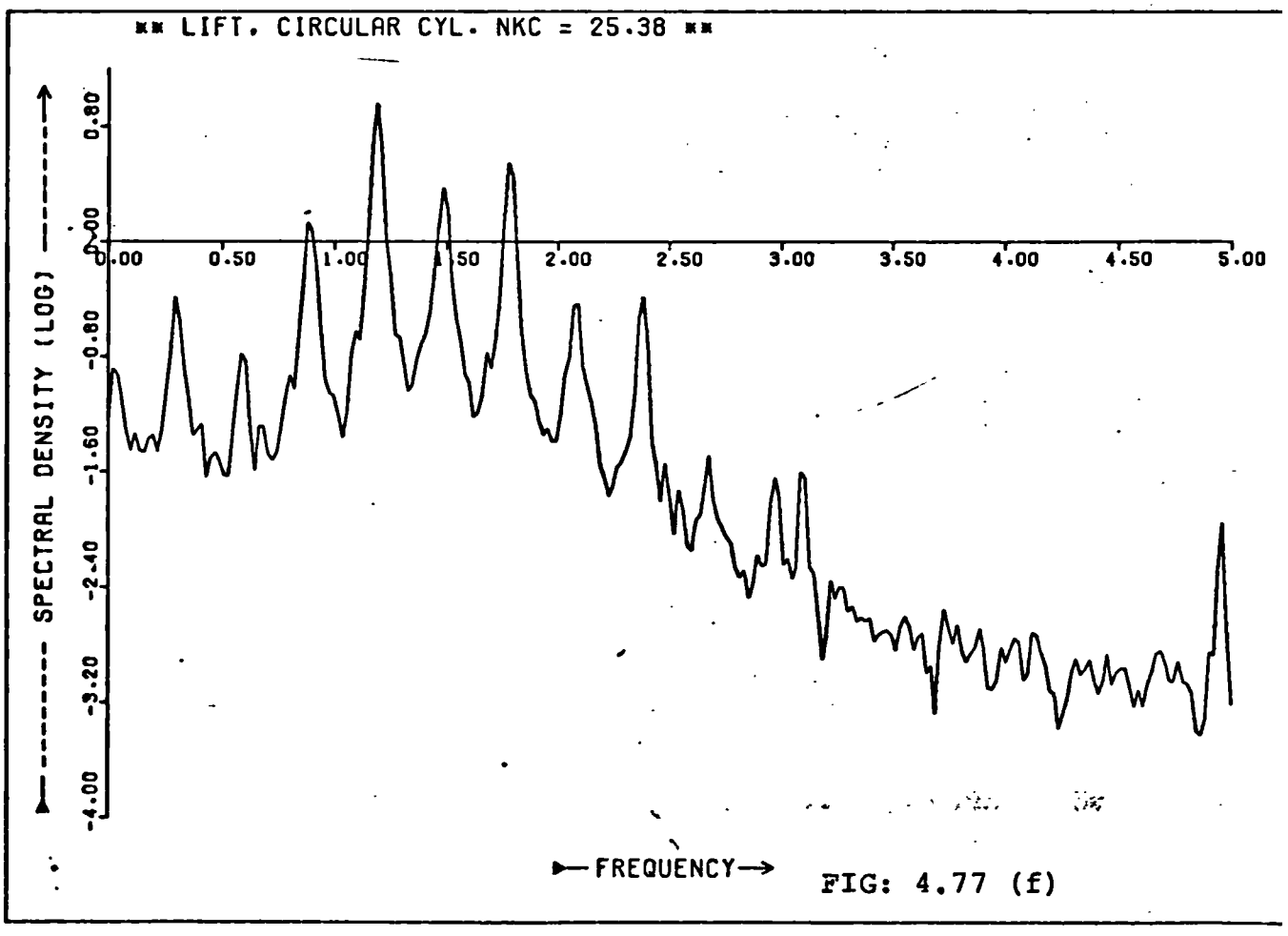

FIG: 4.77 (f)

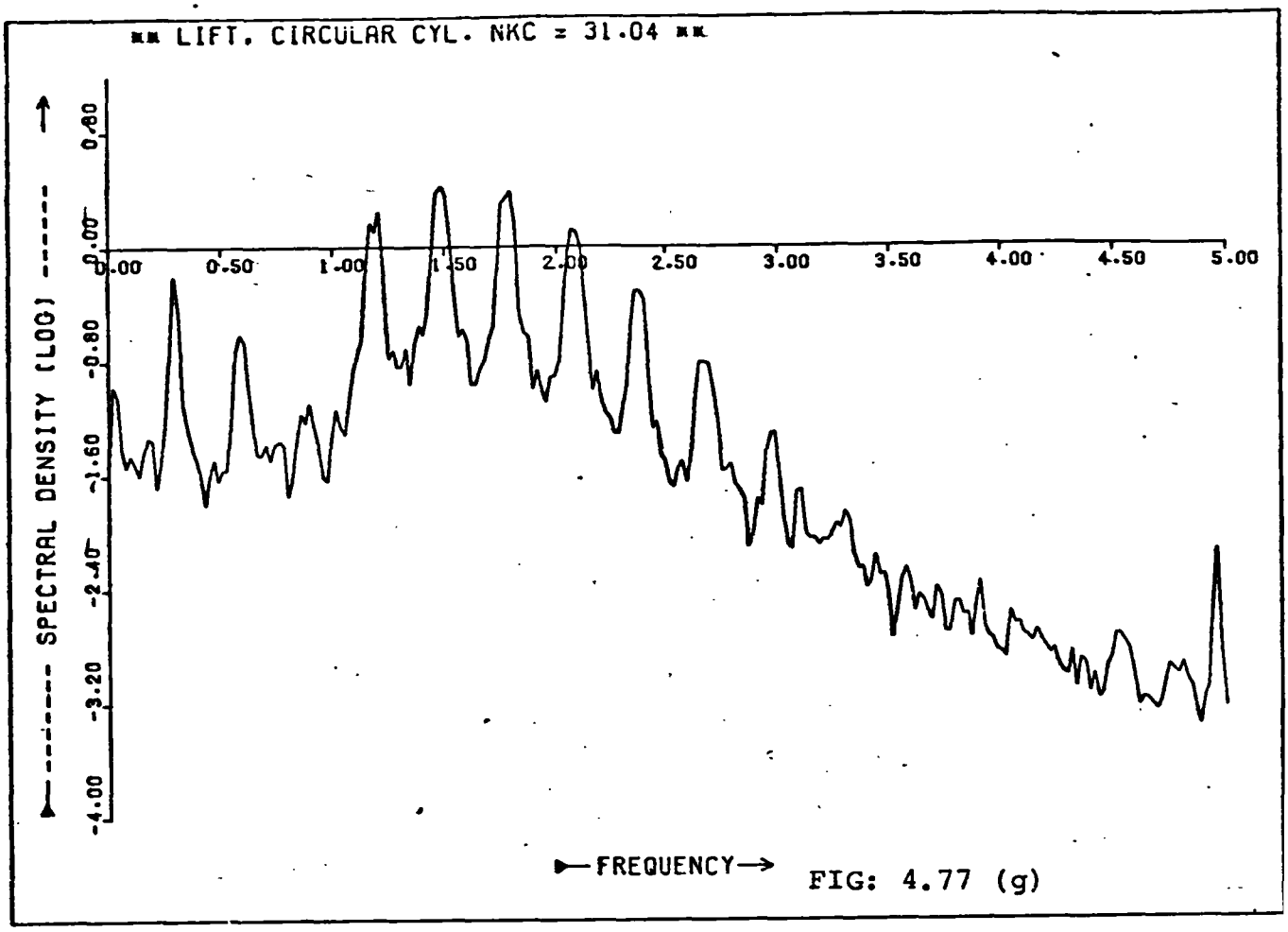

FIG: 4.77 (g)

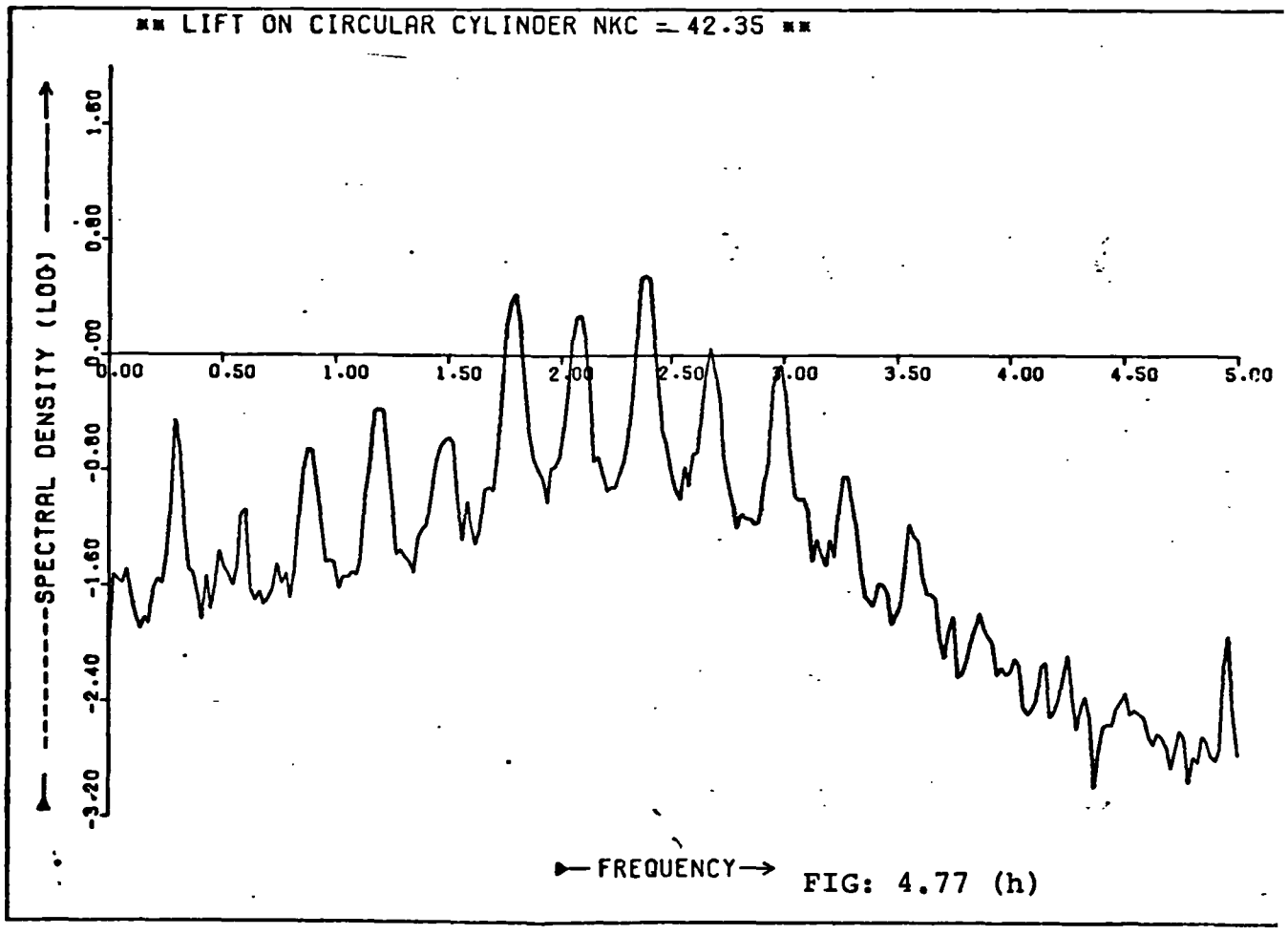

FIG: 4.77 (h)

FIG: 4.78

VARIATION OF LIFT ON DIAMOND SECTION

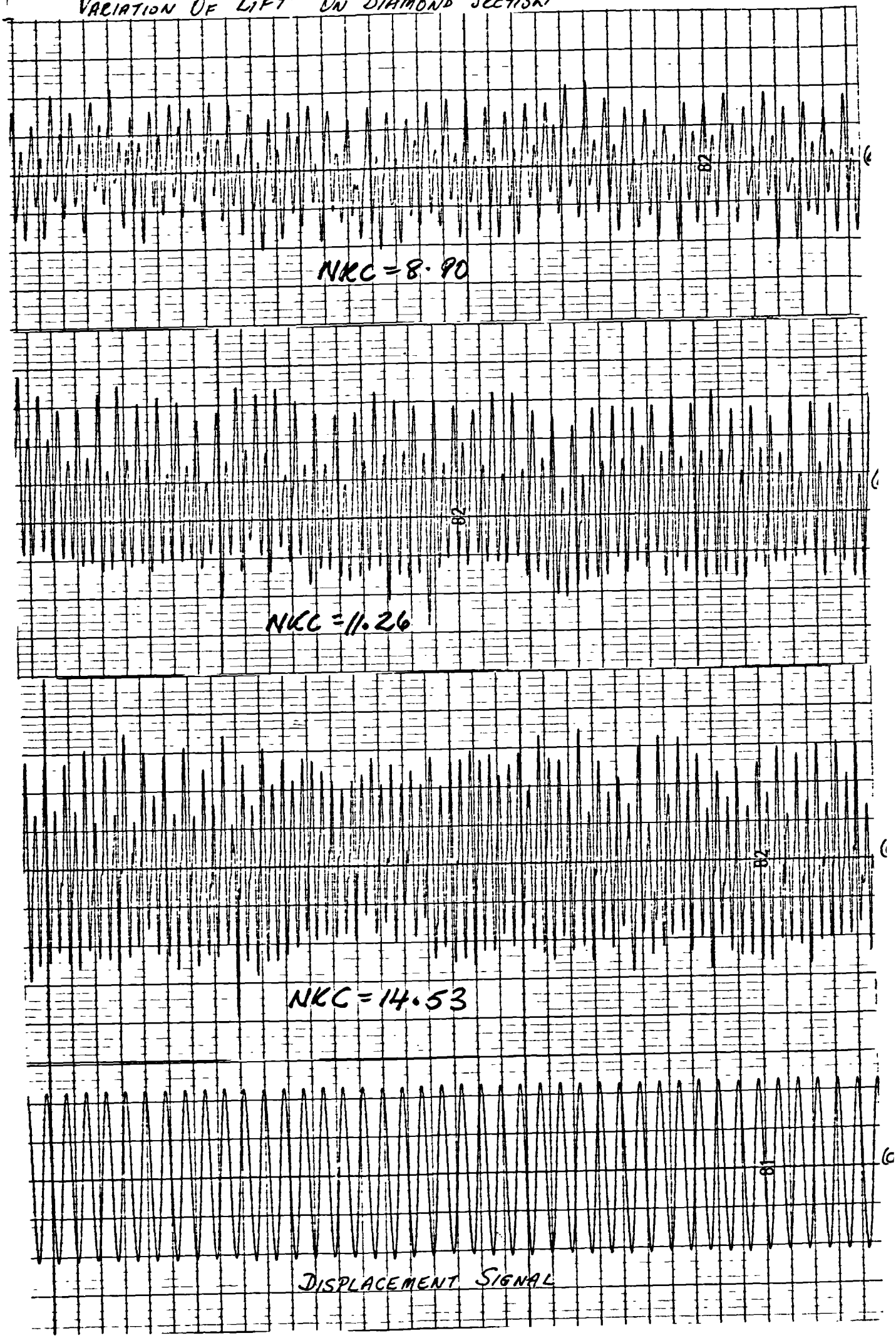

FIG: 4.78 (e) – 4.78 (h)

VARIATION OF LIFT ON DIAMOND SECTION

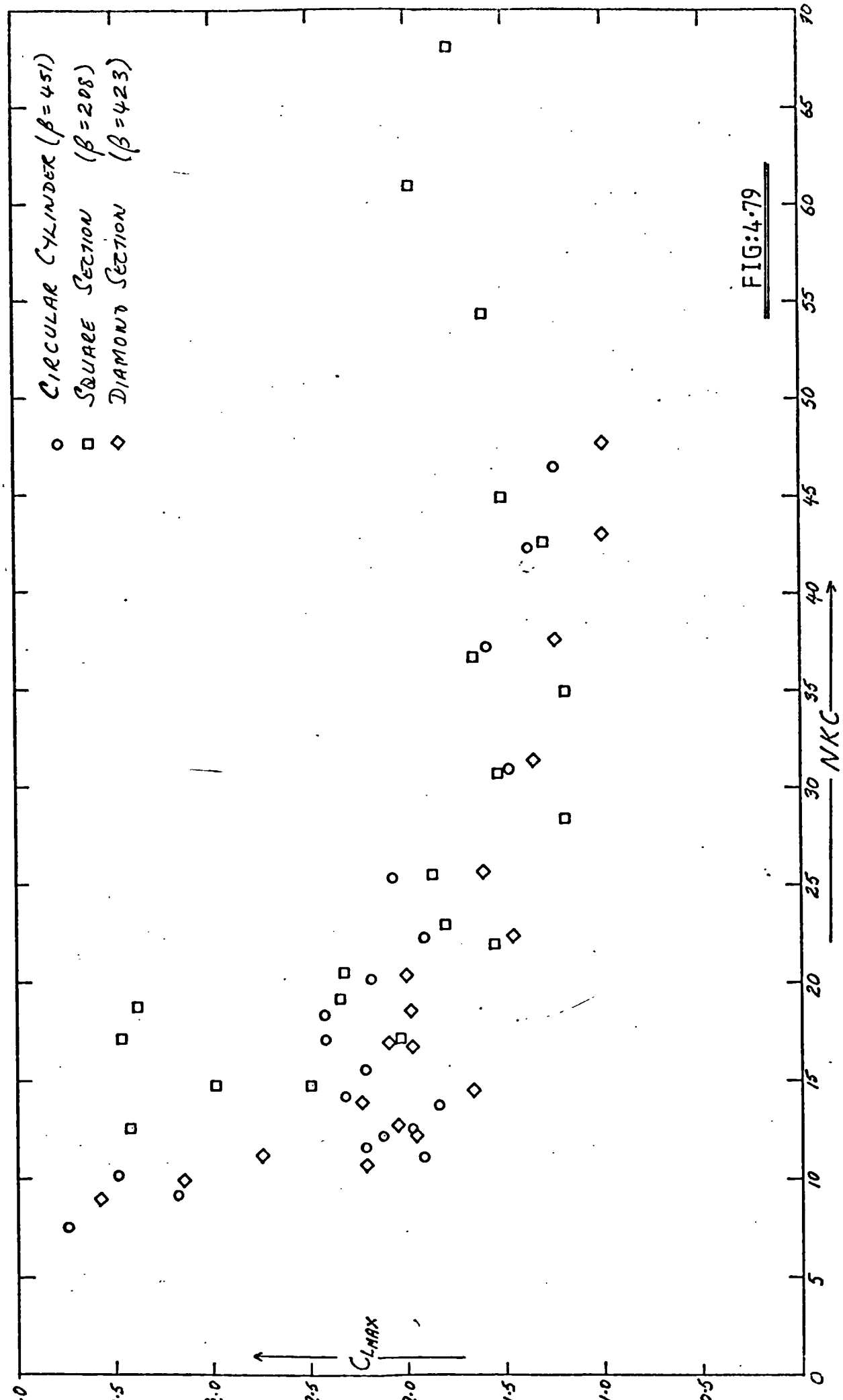
CIRCULAR CYLINDER (β=451)
SQUARE SECTION (β=208)
DIAMOND SECTION (β=423)
C_{LMAX}
NKC
4.0
3.5
3.0
2.5
2.0
1.5
1.0
0.5
0
5
10
15
20
25
30
35
40
45
50
55
60
65
70

FIG:4.79

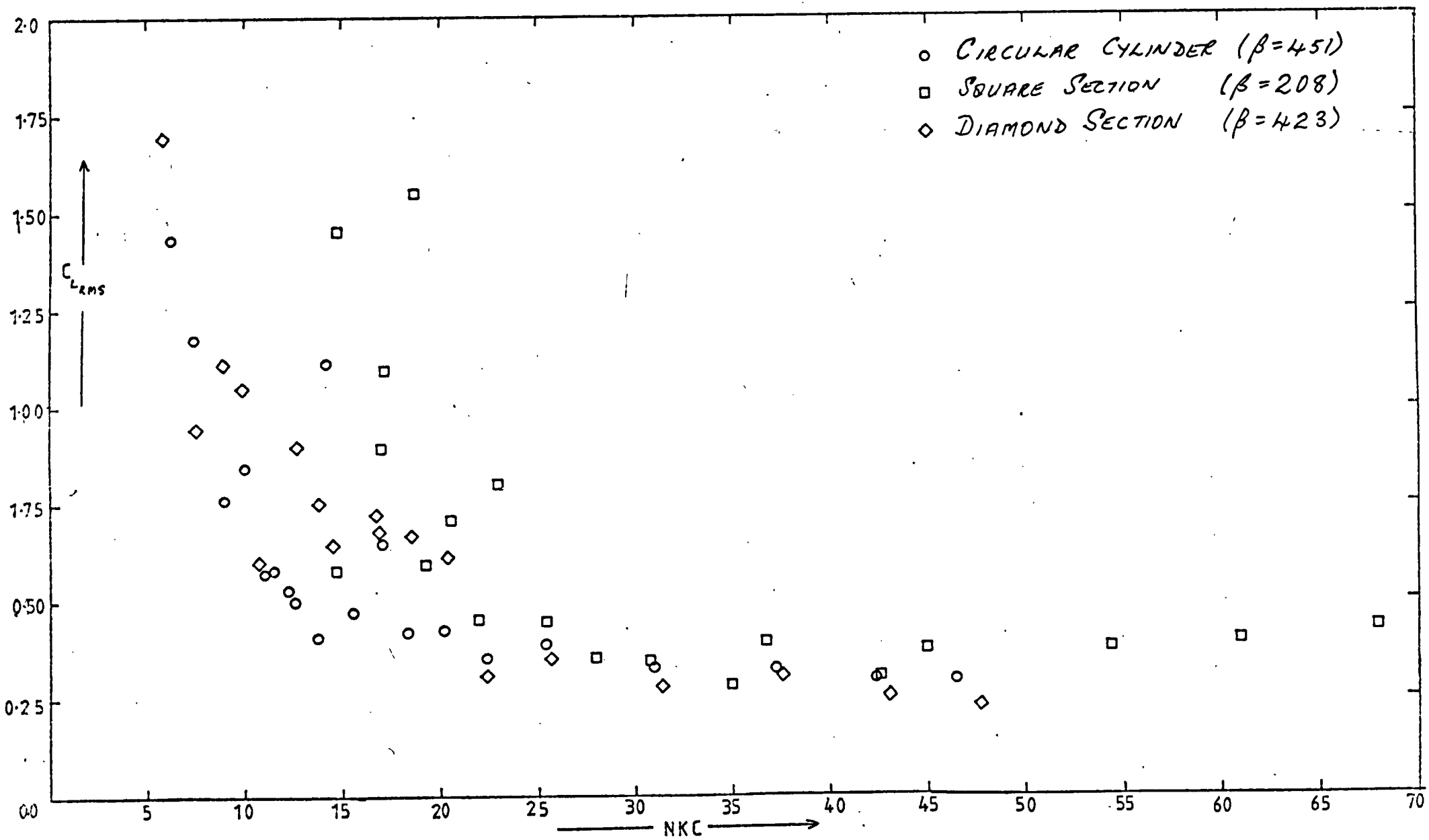
CIRCULAR CYLINDER (β=451)
SQUARE SECTION (β=208)
DIAMOND SECTION (β=423)
$C_{L_{RMS}}$
2·0
1·75
1·50
1·25
1·00
0·75
0·50
0·25
0·0
5
10
15
20
25
30
35
40
45
50
55
60
65
70
NKC

FIG : 4·80

VARIATION OF LIFT ON DIAMOND SECTION DURING A CYCLE.

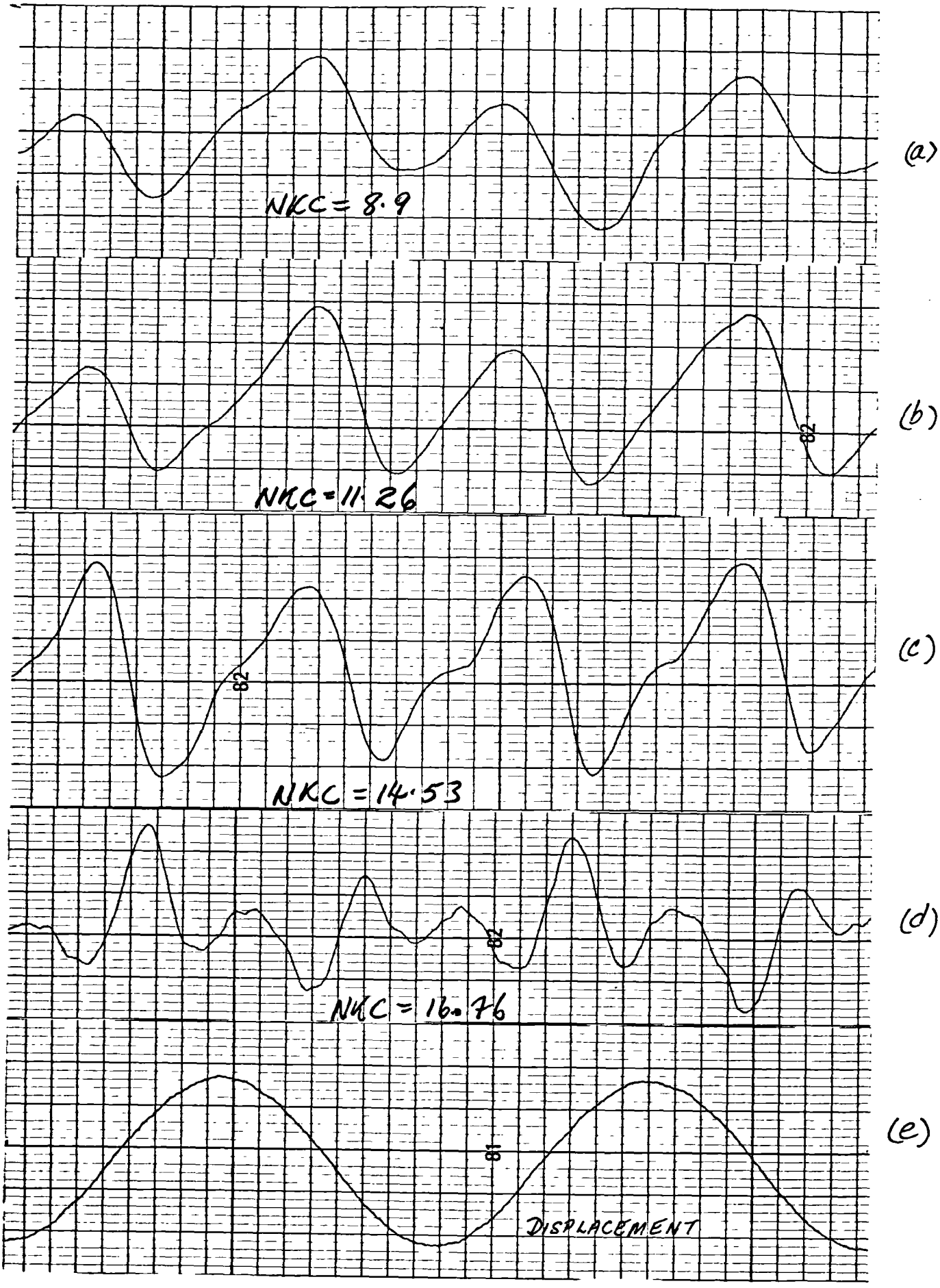

FIG: 4.81
VARIATION OF LIFT ON DIAMOND SECTION DURING A CYCLE

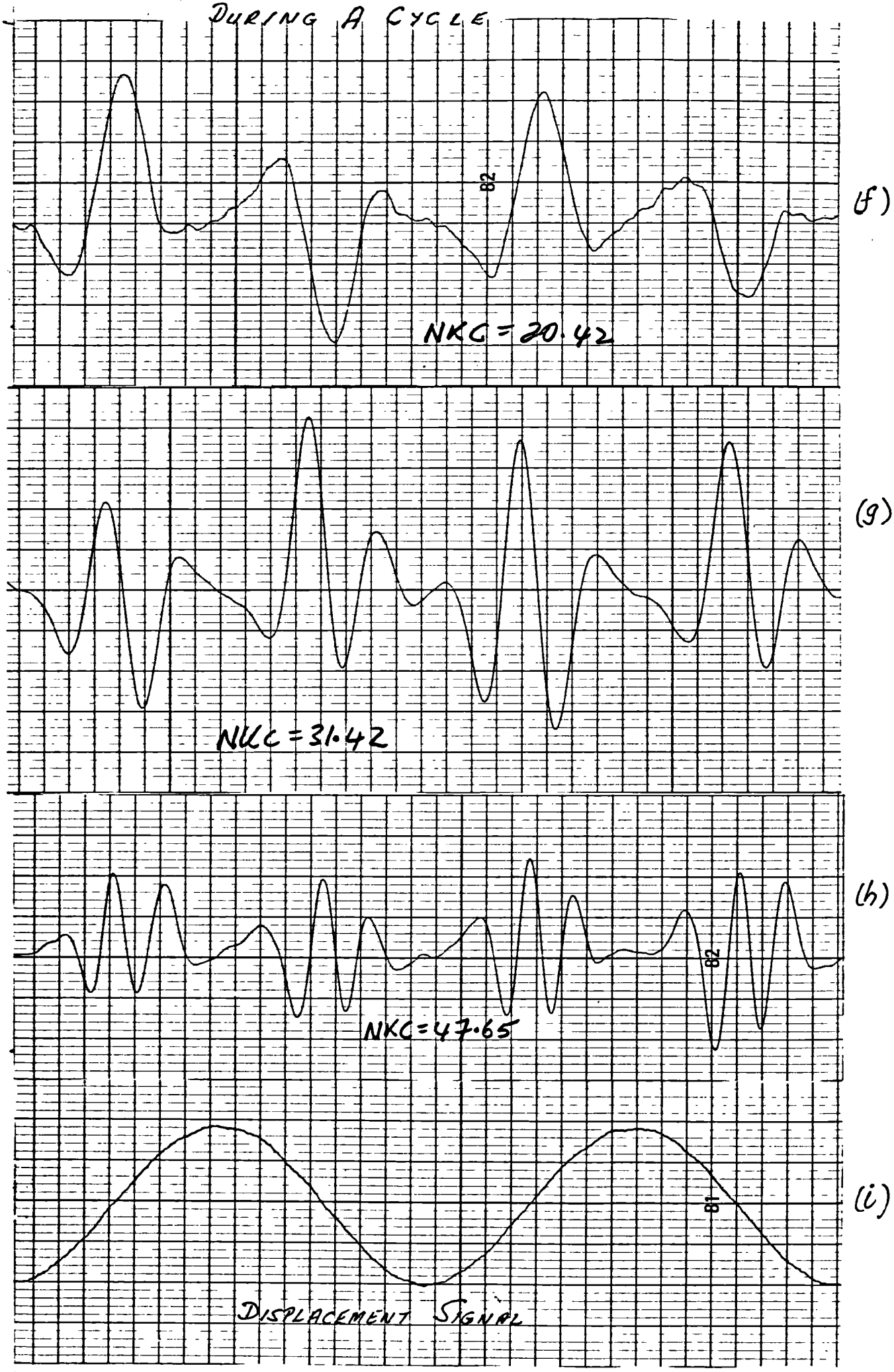

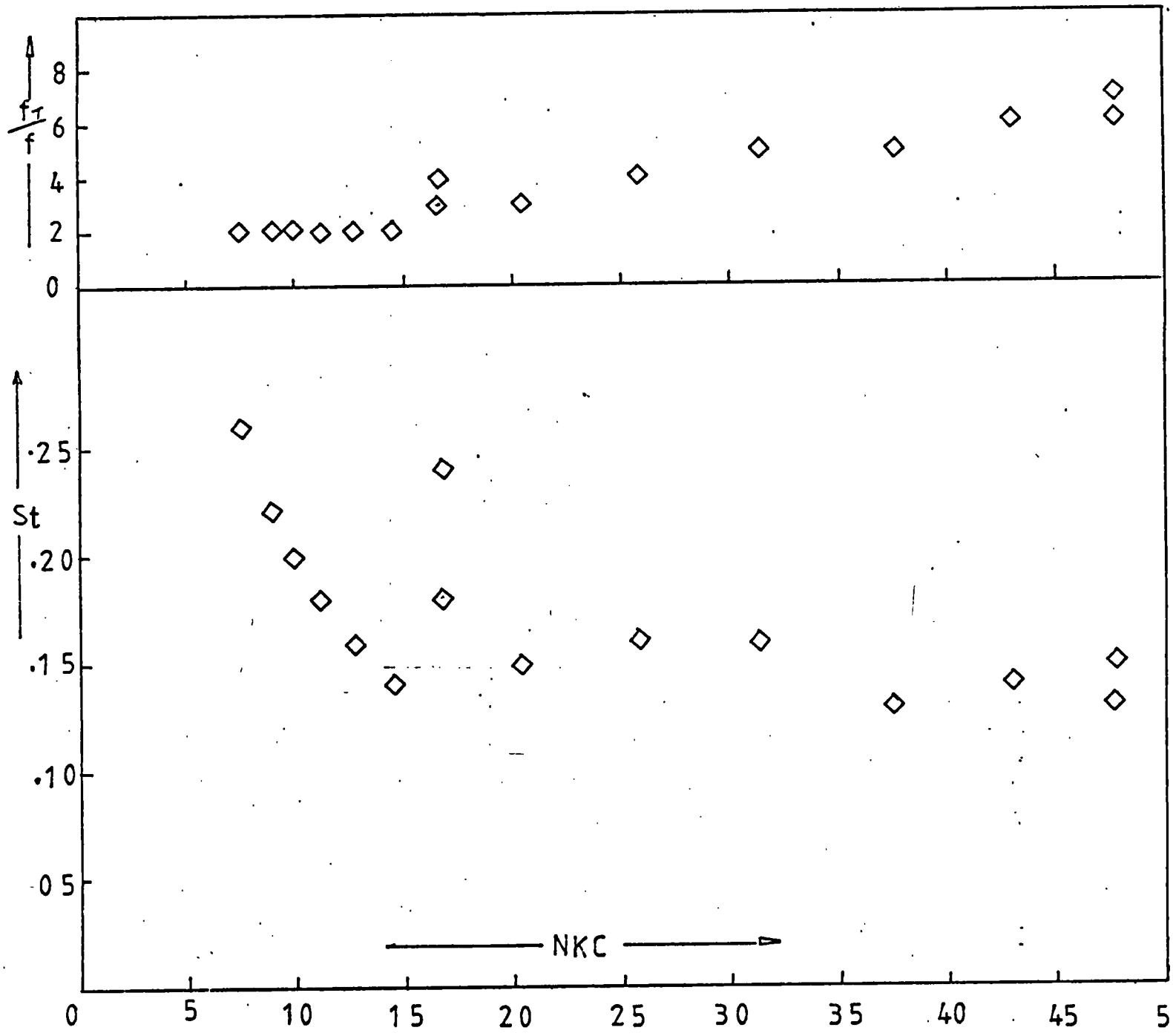

VARIATION OF FREQUENCY OF TRANSVERSE FORCE WITH NKC

RESULTS FOR DIAMOND SECTION ($\beta = 423$)

VARIATION OF STROUHAL NO. WITH NKC

FIG : 4·82

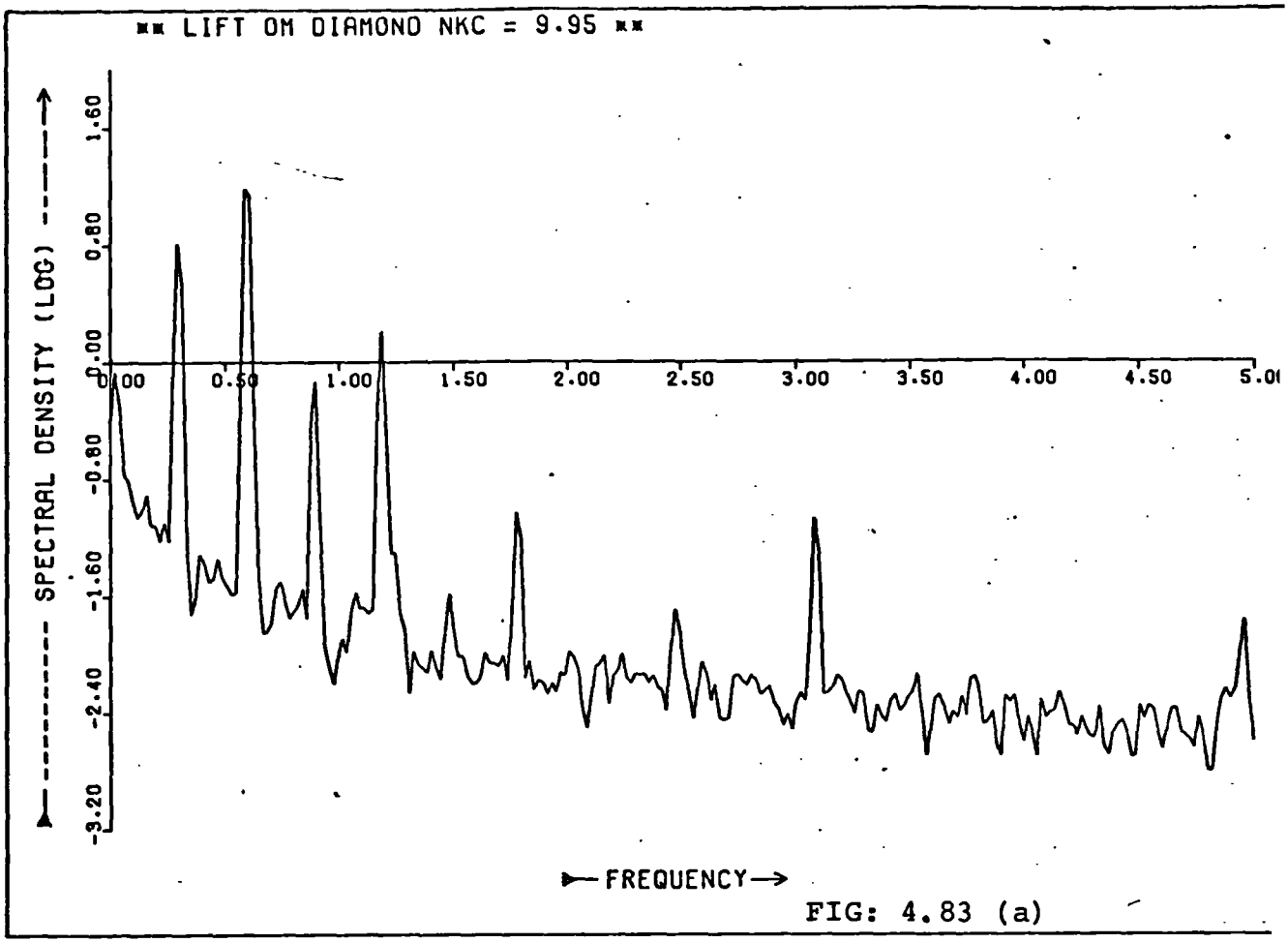

FIG: 4.83 (a)

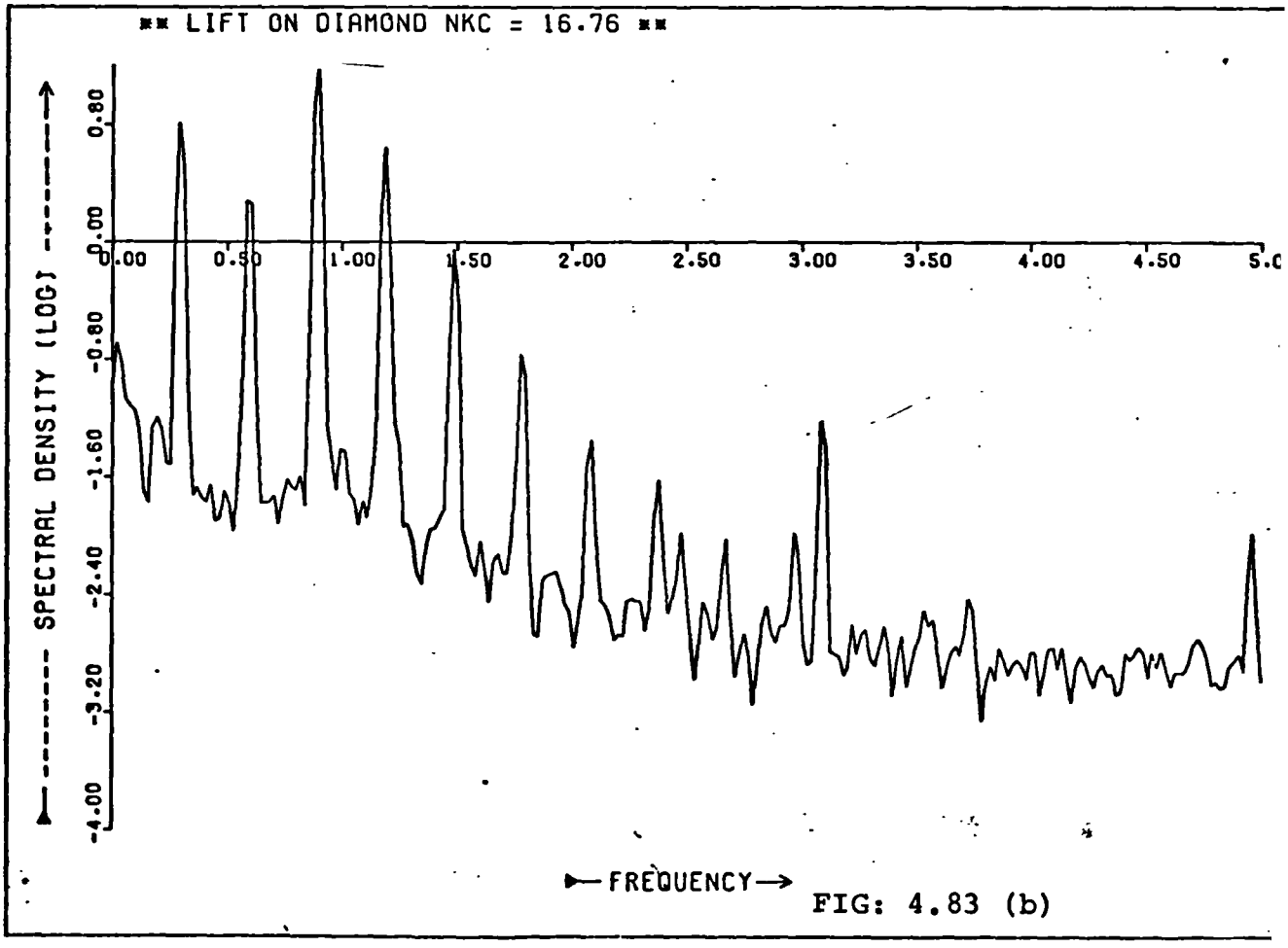

FIG: 4.83 (b)

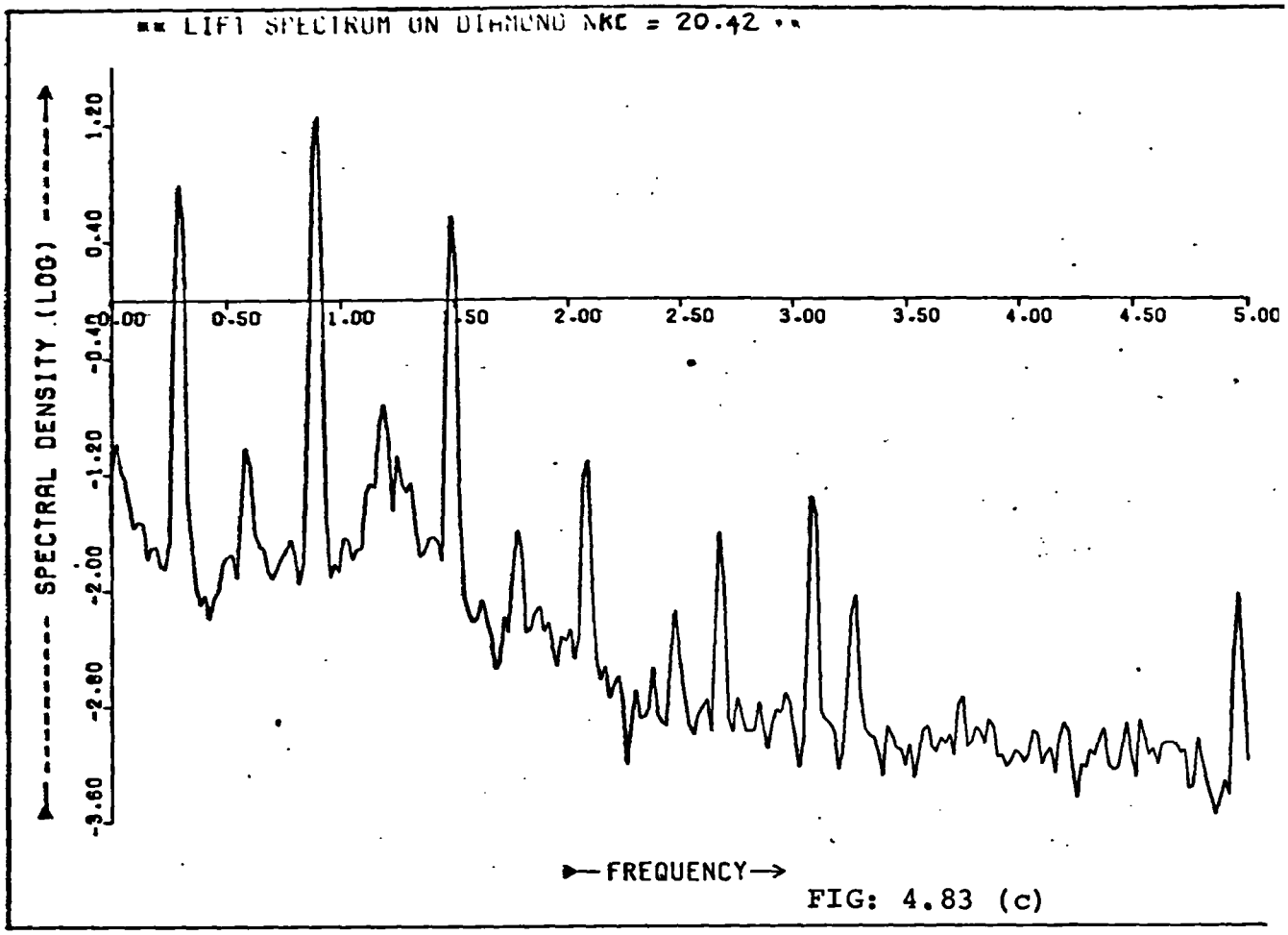

FIG: 4.83 (c)

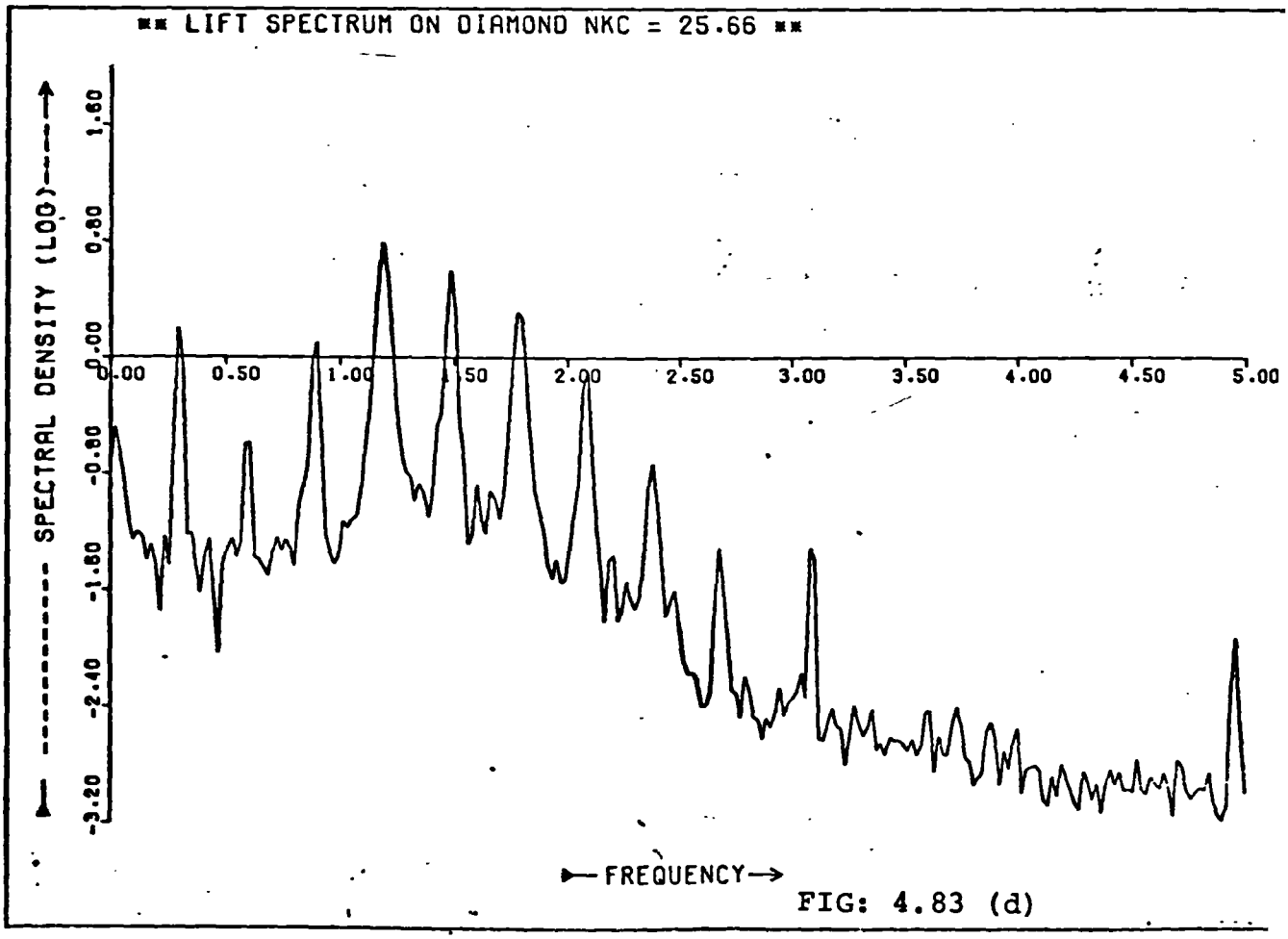

FIG: 4.83 (d)

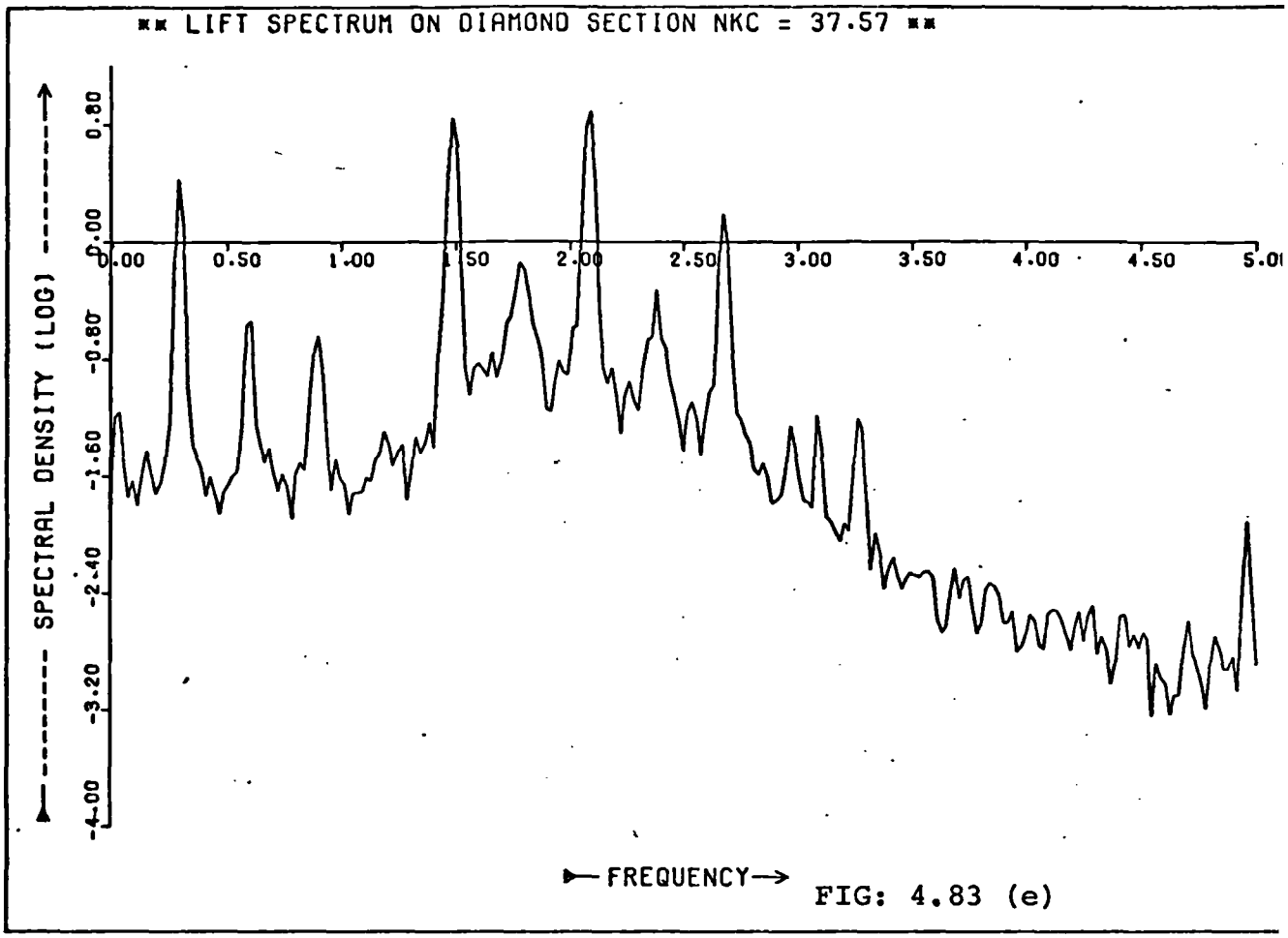

FIG: 4.83 (e)

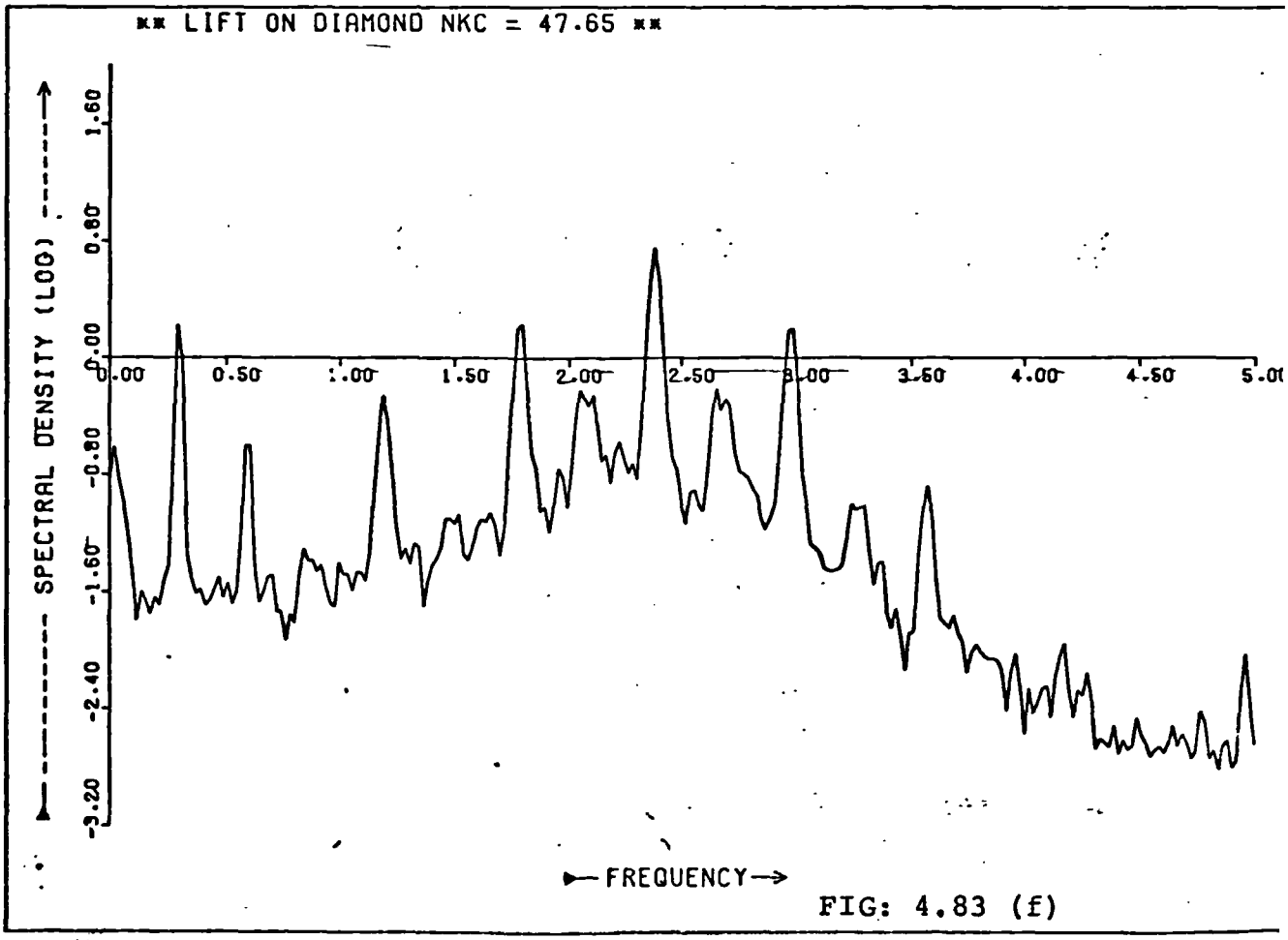

FIG: 4.83 (f)

FIG:4.84

VARIATION OF LIFT ON THE SQUARE SECTION

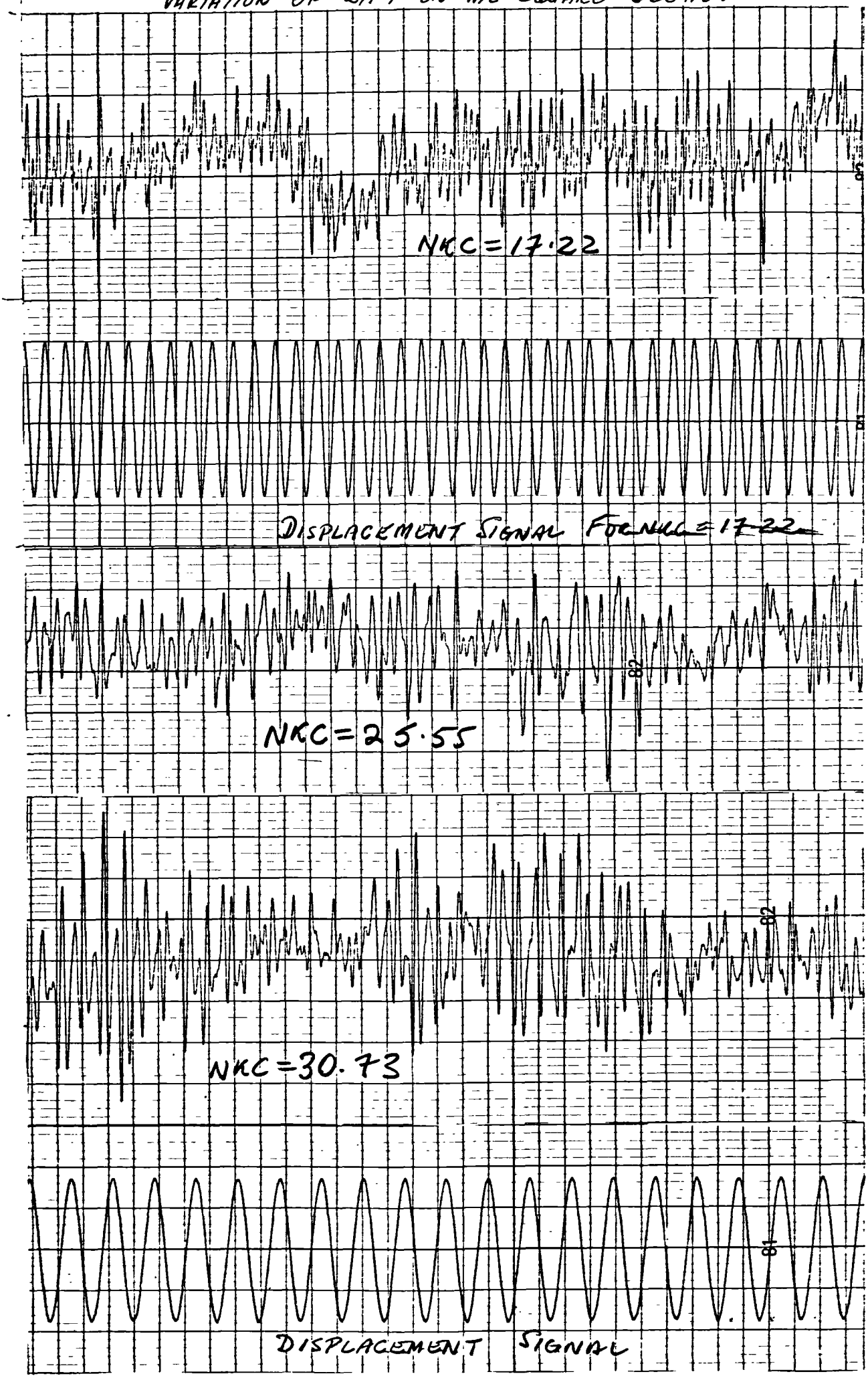

FIG: 4·84

VARIATION OF LIFT ON THE SQUARE SECTION

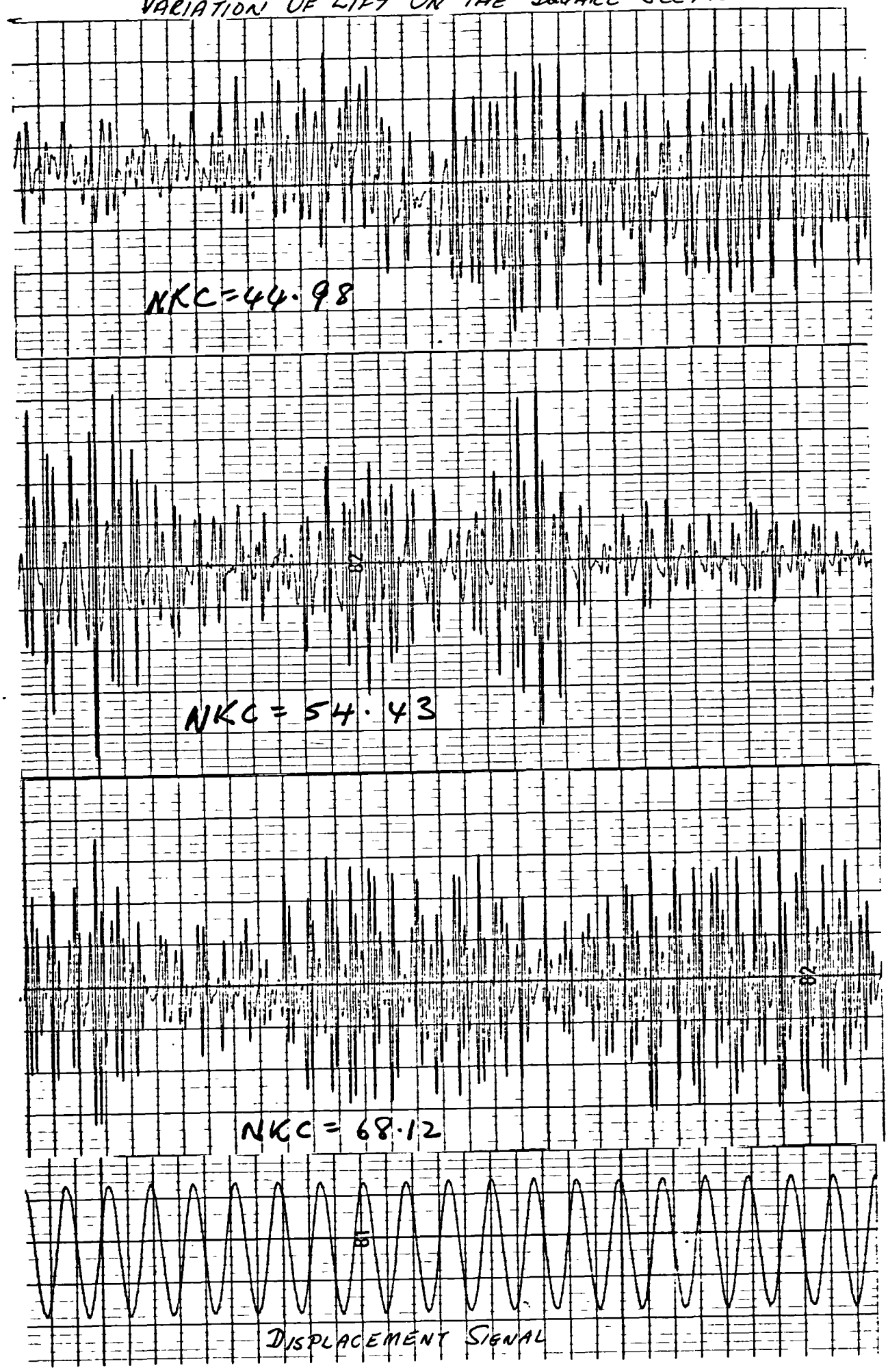

FIG: 4·85

VARIATION OF LIFT ON SQUARE SECTION DUEING A CYCLE.

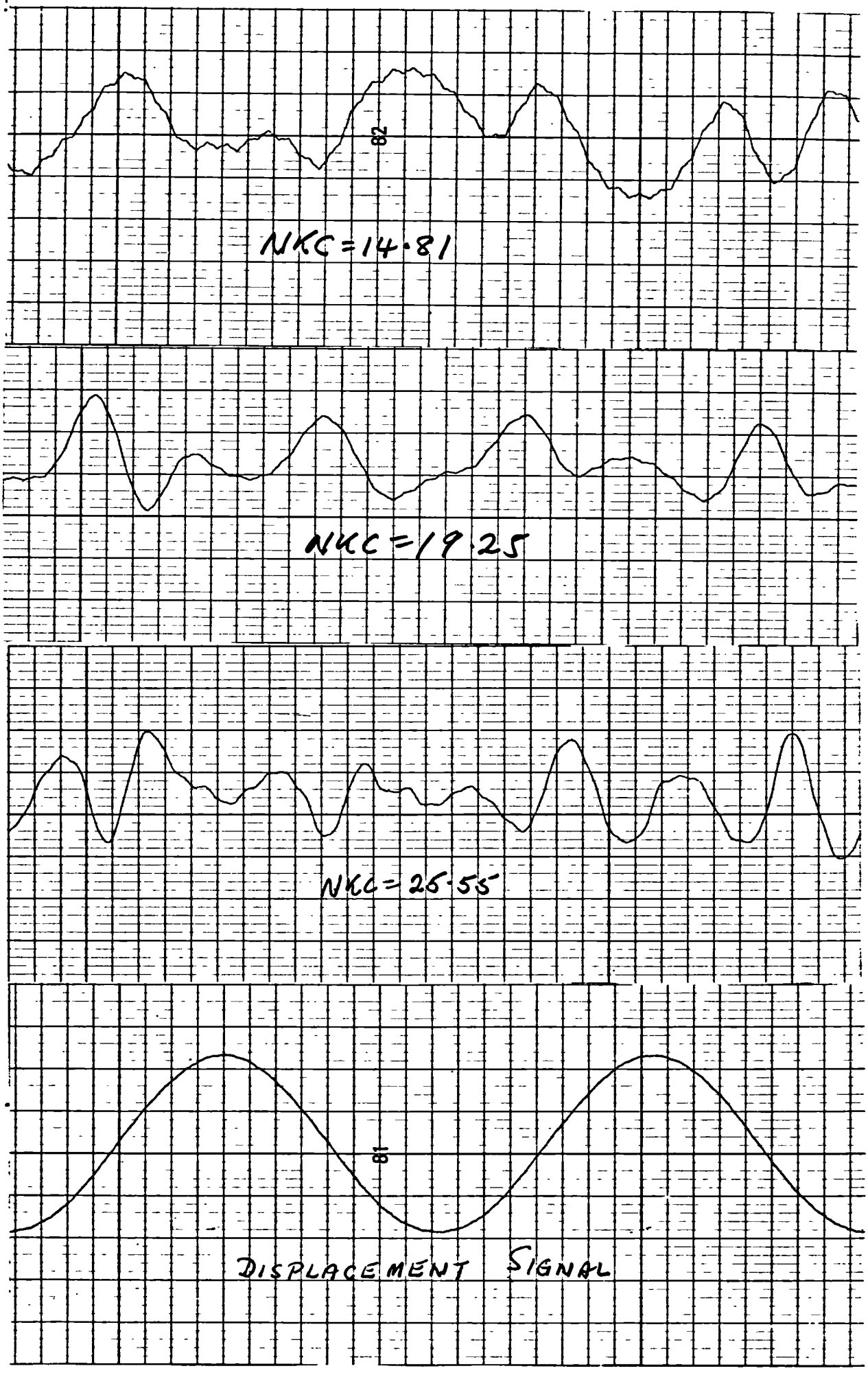

FIG. 4.83

VARIATION OF LIFT ON SQUARE SECTION DUCING A CYCLE

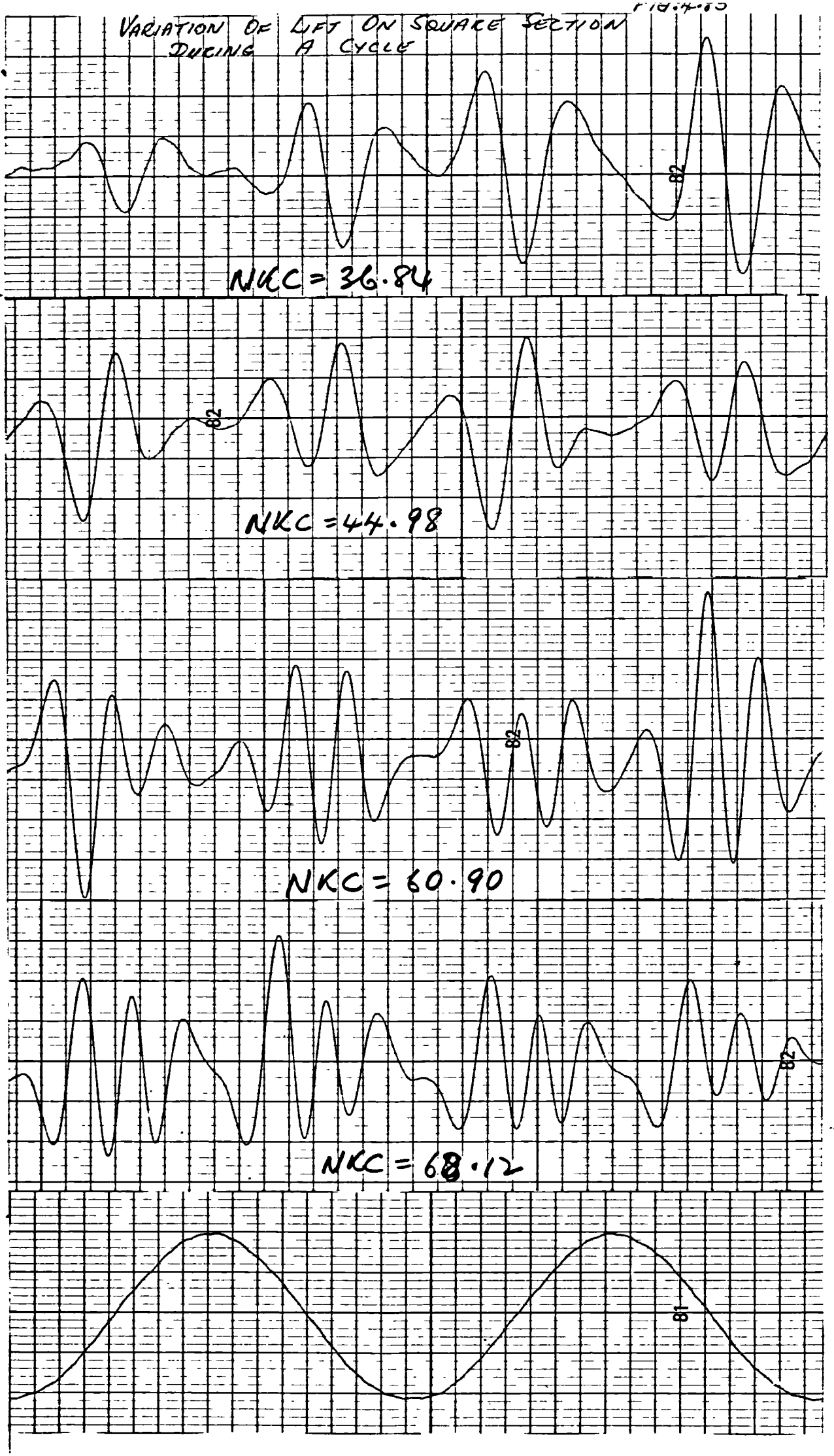

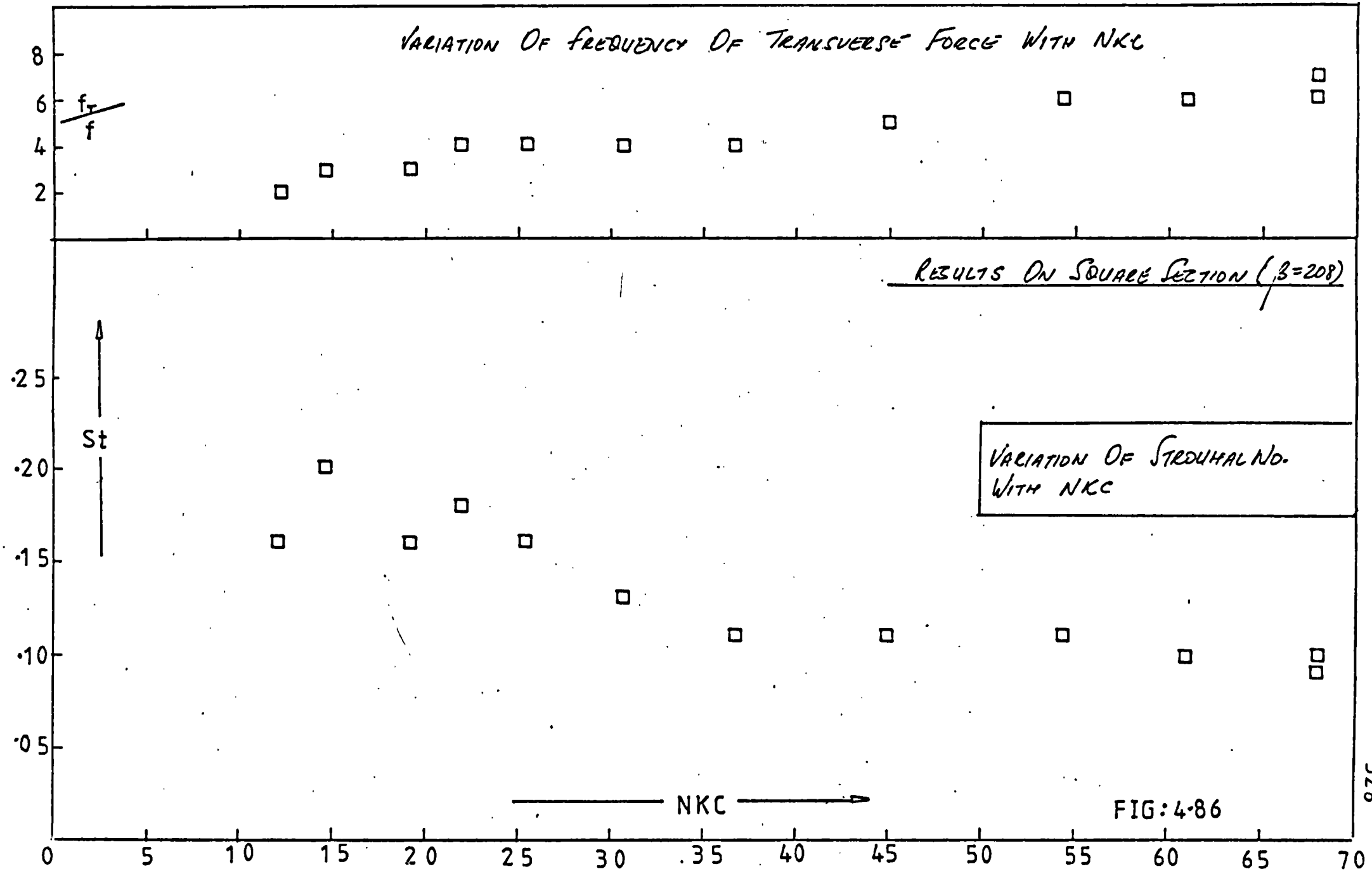
VARIATION OF FREQUENCY OF TRANSVERSE FORCE WITH NKC
$\frac{f_T}{f}$
8
6
4
2
RESULTS ON SQUARE SECTION (β=208)
St
·25
·20
·15
·10
·05
VARIATION OF STROUHAL NO. WITH NKC
NKC
0
5
10
15
20
25
30
35
40
45
50
55
60
65
70

FIG: 4·86

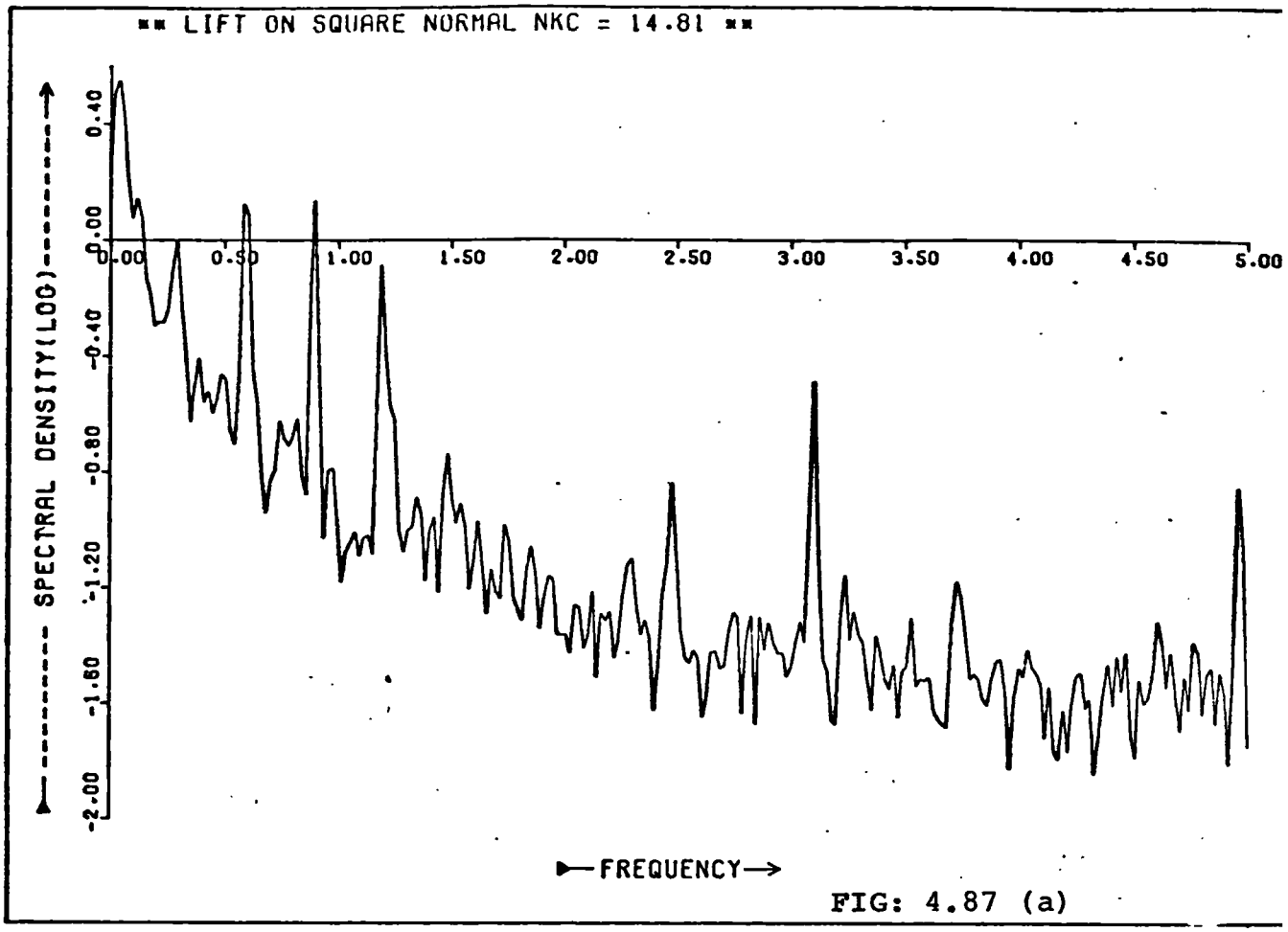

FIG: 4.87 (a)

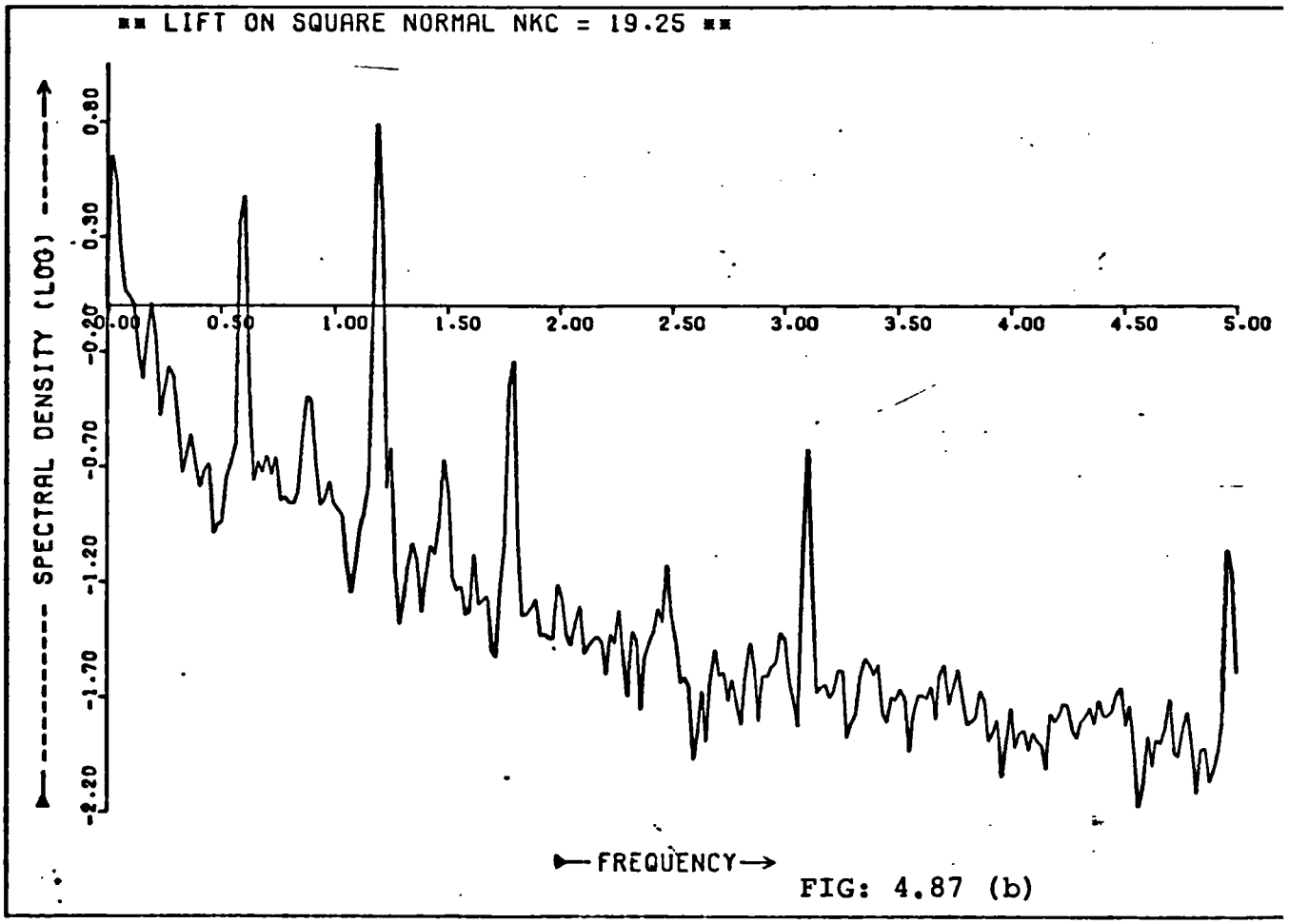

FIG: 4.87 (b)

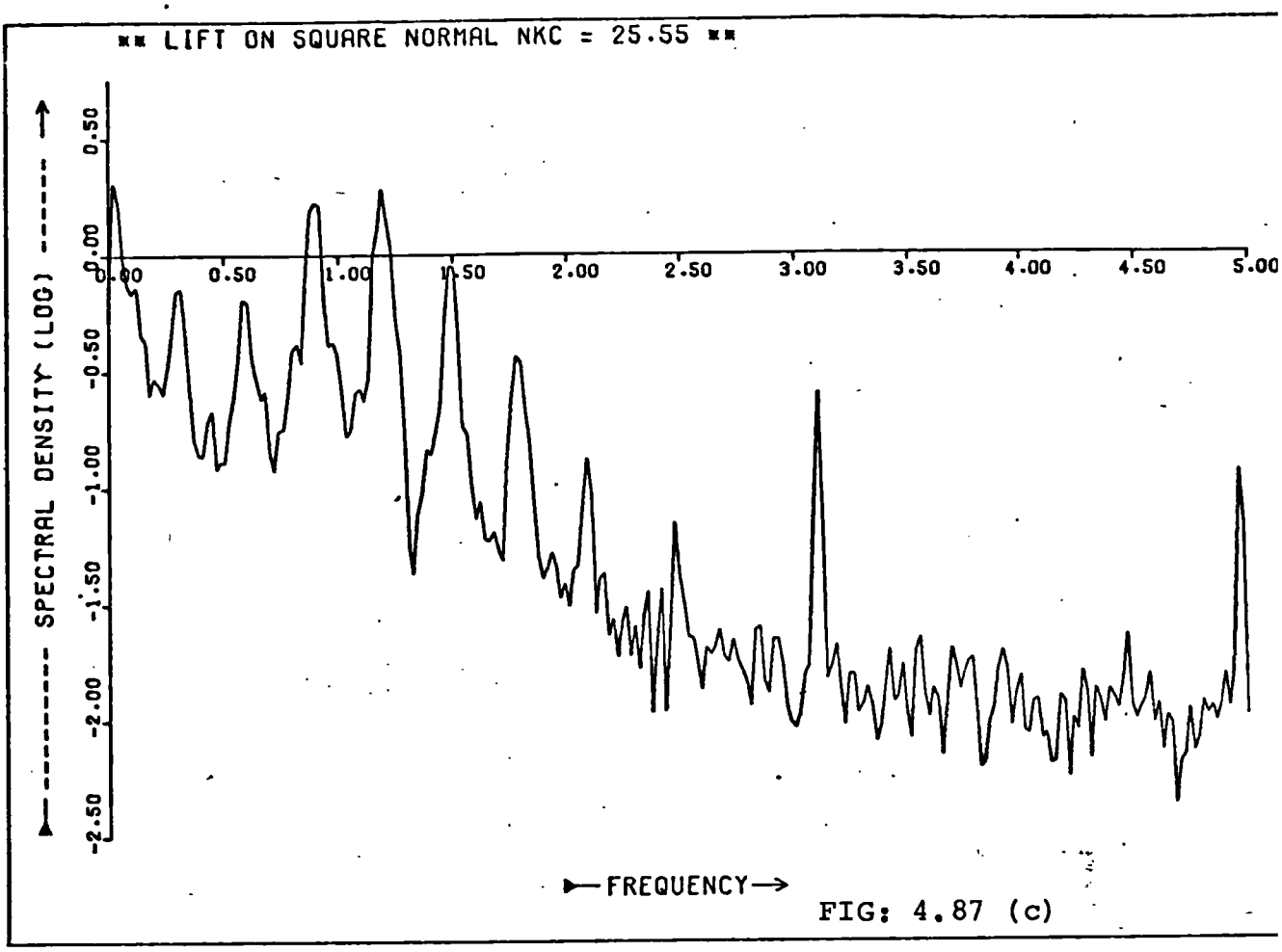

FIG: 4.87 (c)

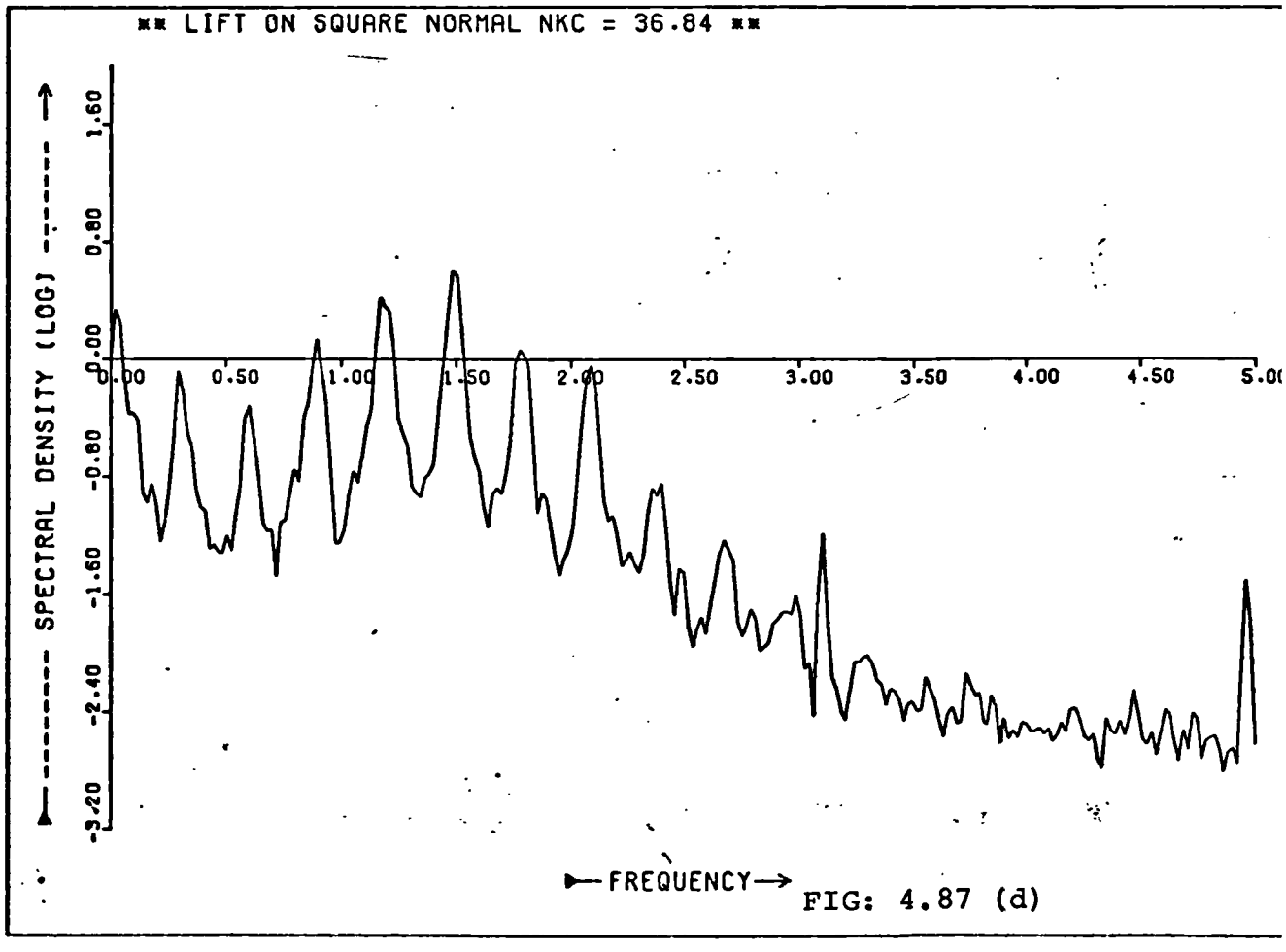

FIG: 4.87 (d)

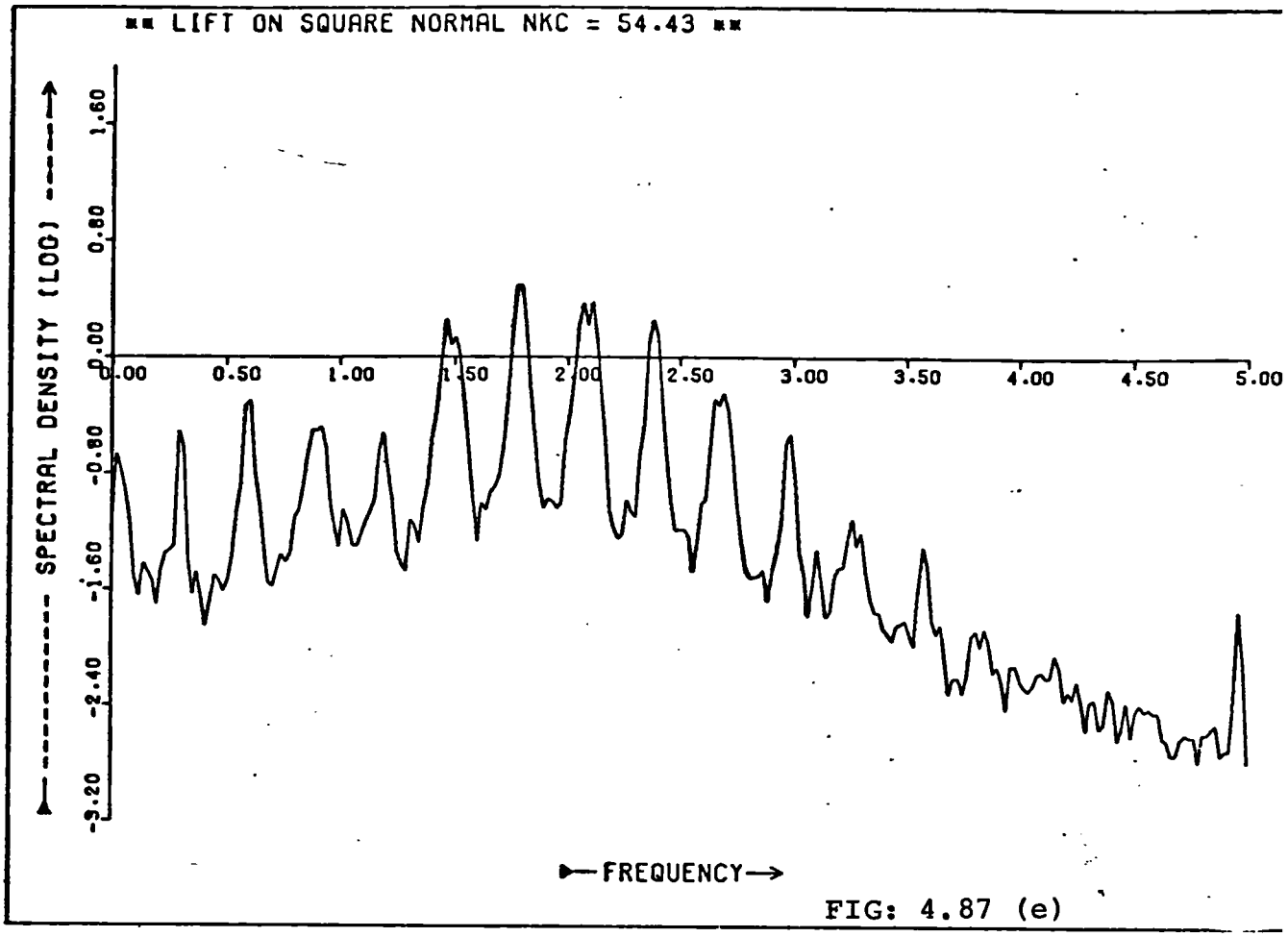

FIG: 4.87 (e)

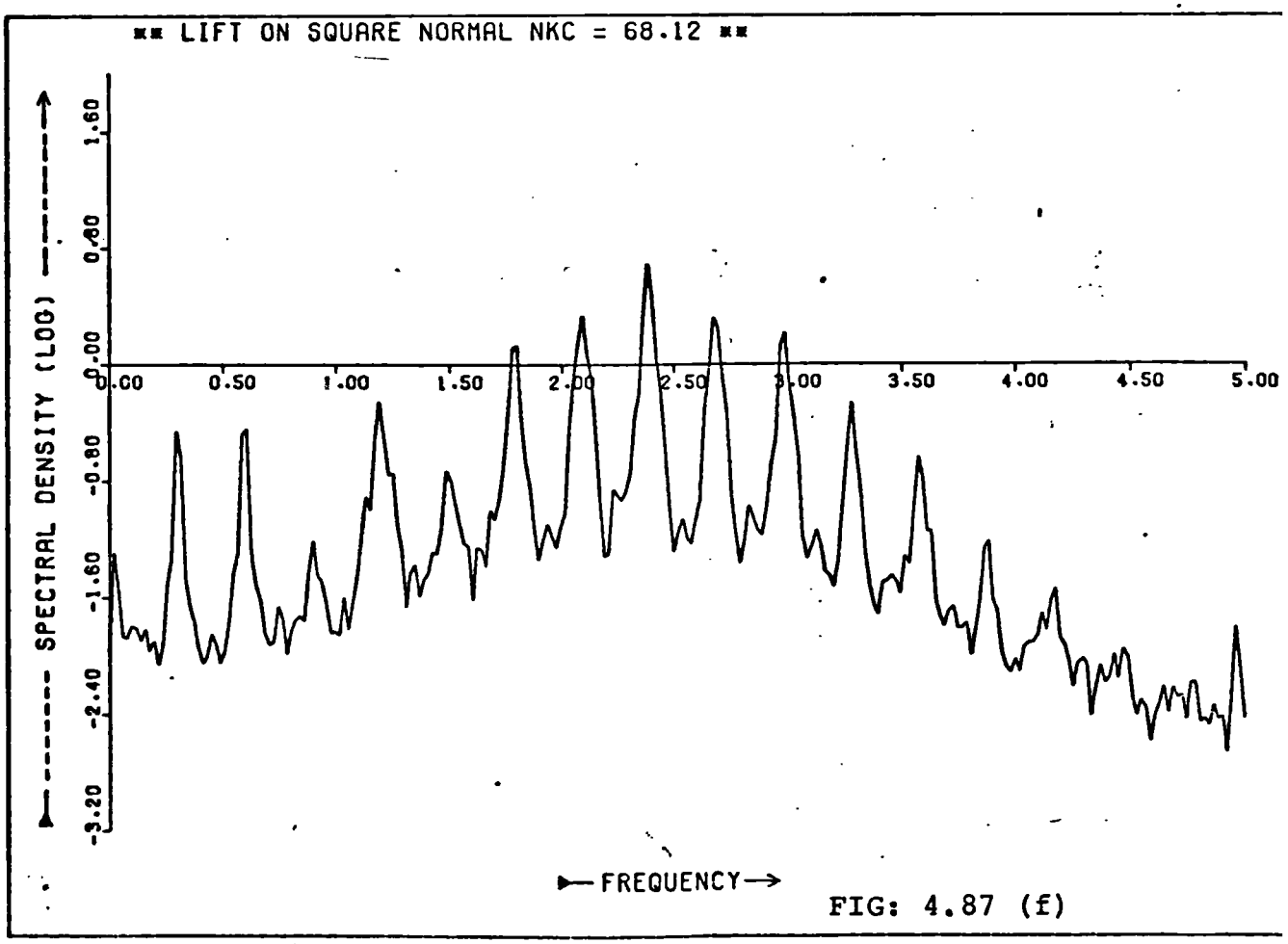

FIG: 4.87 (f)

NOTATION USED DURING FLOW VISUALISATION

① FLOW DEFINED BY : $U = -U_m \cos\theta$, WHERE $\theta = 2\pi t/T$ AND T = PERIOD OF OSCILLATIONS.

② FLOW FROM LEFT TO RIGHT DEFINED AS POSITIVE.

③ CLOCKWISE CIRCULATION (Q) DEFINED AS POSITIVE, AND GIVEN THE SYMBOL 'O'.

④ ANTI-CLOCKWISE CIRCULATION, (G) DEFINED AS NEGATIVE AND GIVEN THE SYMBOL '□'.

⑤ APPROXIMATELY 43 FRAMES OF MOTION PICTURE REPRESENTS A CYCLE. THEREFORE THE NUMBERS BELOW AND IN FIGURES 5.4, 5.8, AND 5.11 REPRESENT THE FRAME NUMBER. FRAME ①, DENOTES APPROXIMATELY THE START OF A CYCLE, WITH THE VELOCITY FROM RIGHT TO LEFT AND MAXIMUM.

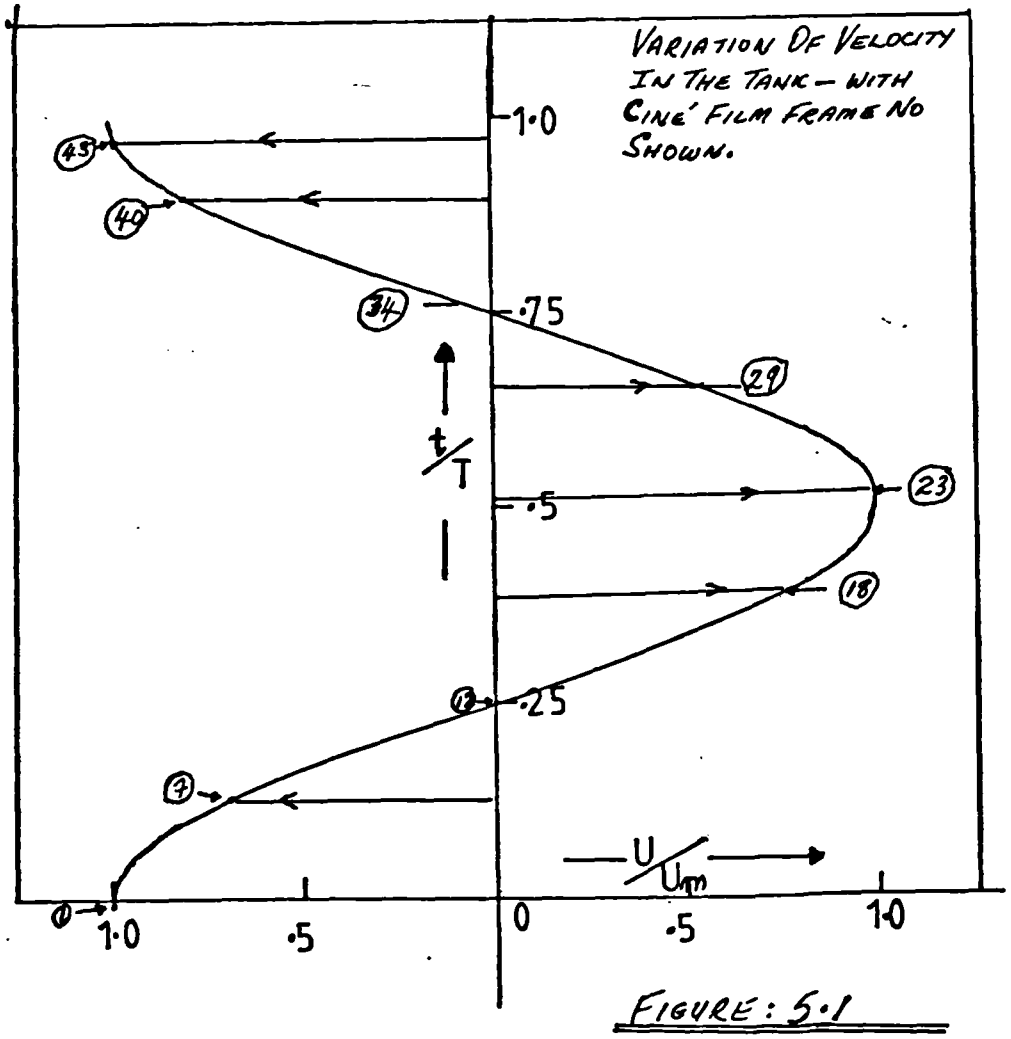

FIGURE: 5·1

SYMMETRIC PAIR : NKC < 4

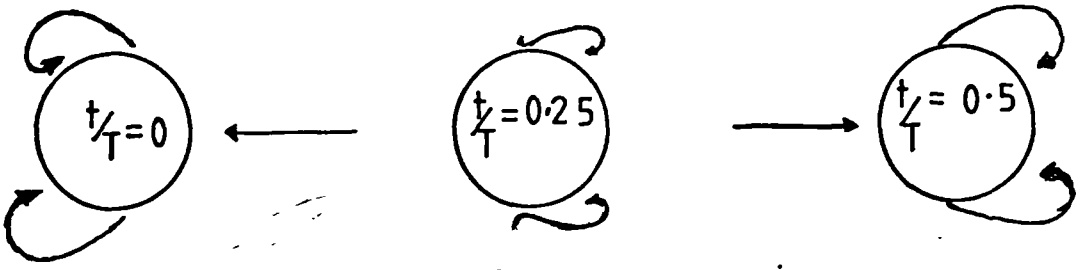

FIG : 5·2(a)

ASYMMETRIC REGION : 8 > NKC > 4

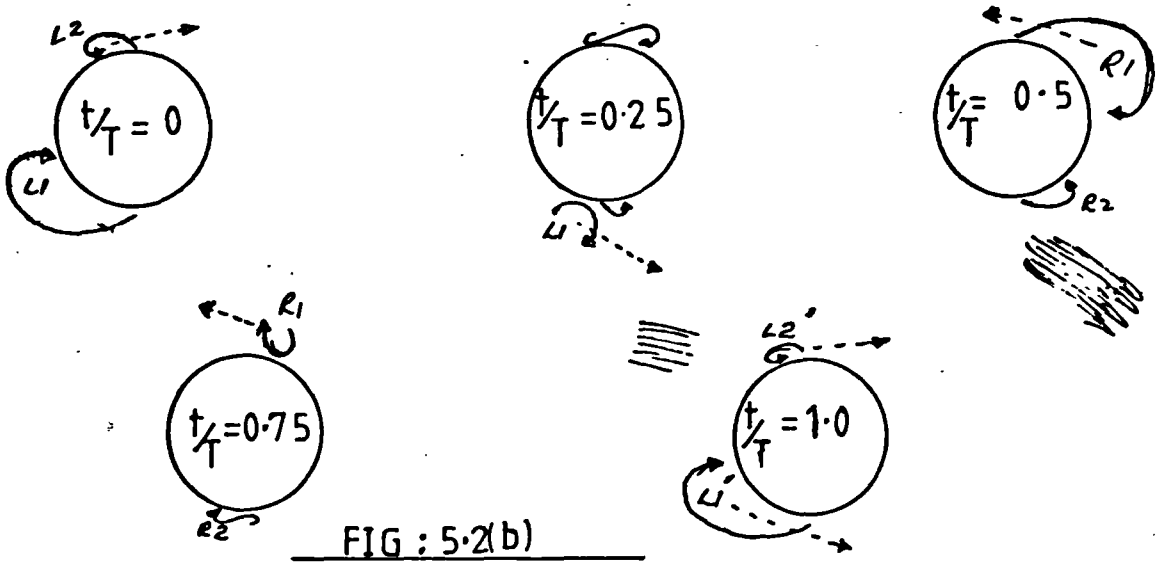

FIG : 5·2(b)

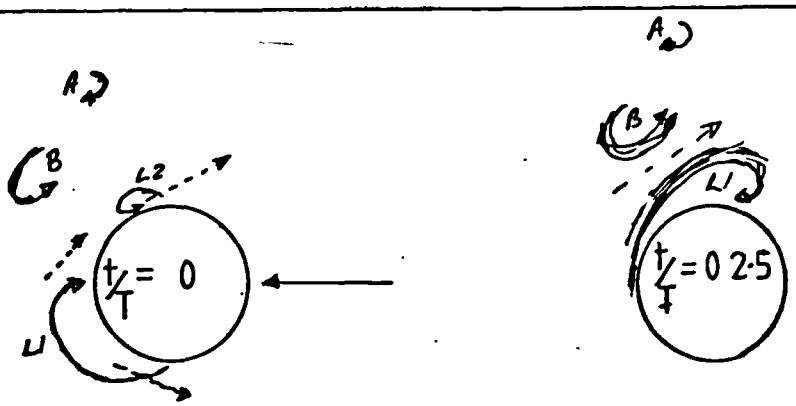

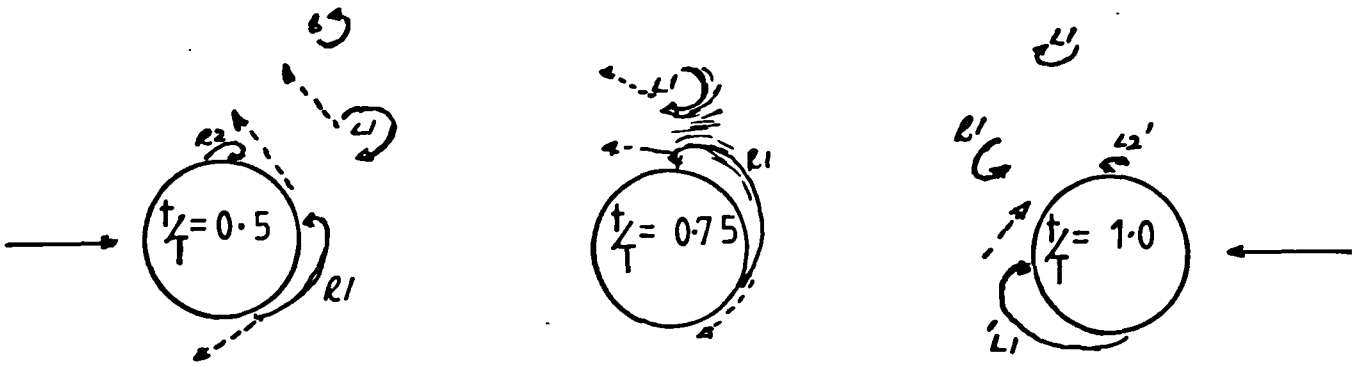

SIDEWAYS VORTEX STREET : 15 > NKC > 8

FIG : 5·2(c)

CYCLIC REGION : 25 > NKC > 15

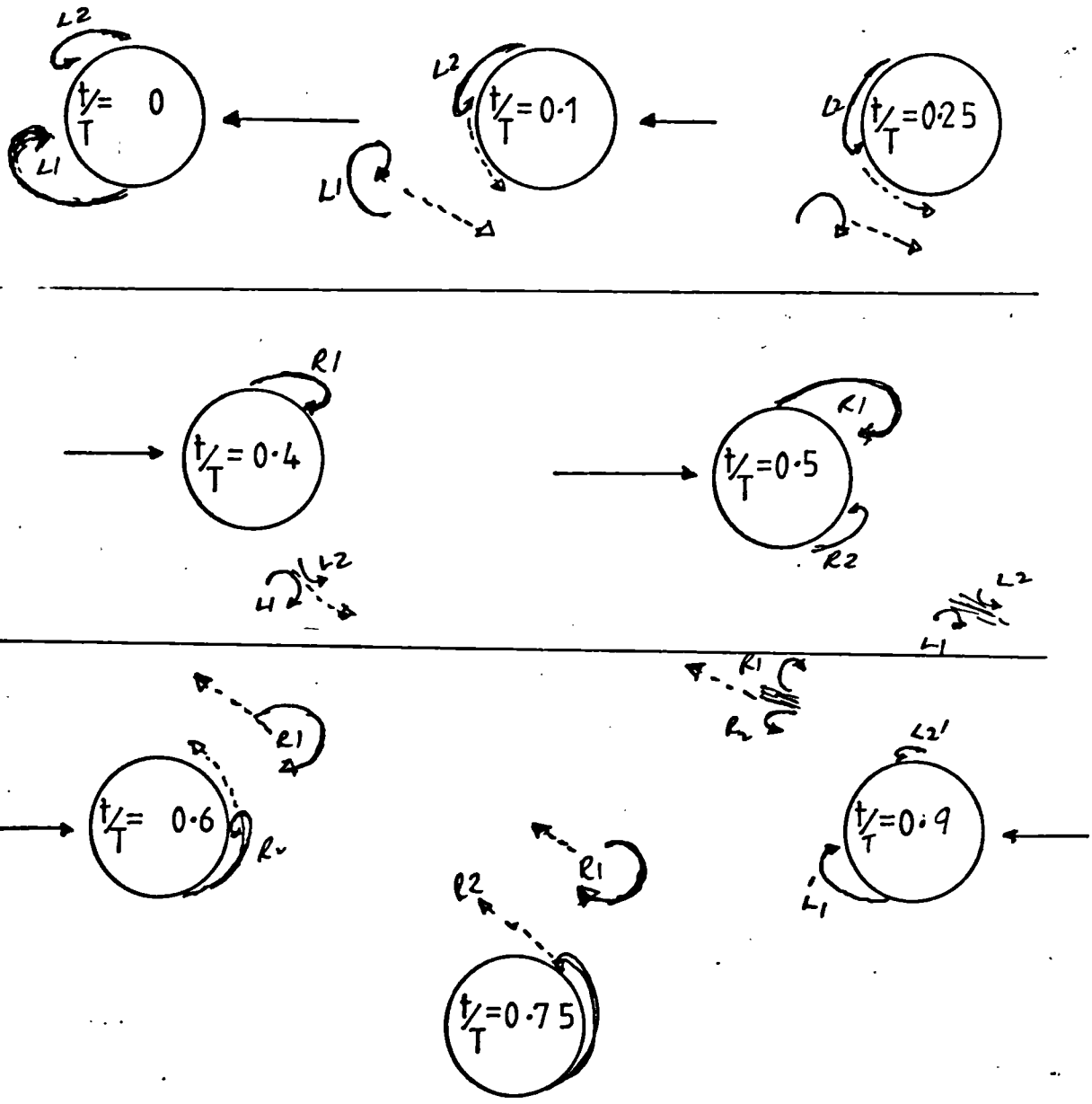

FIG : 5·2(d)

CIRCULAR CYLINDER $\beta = 451$

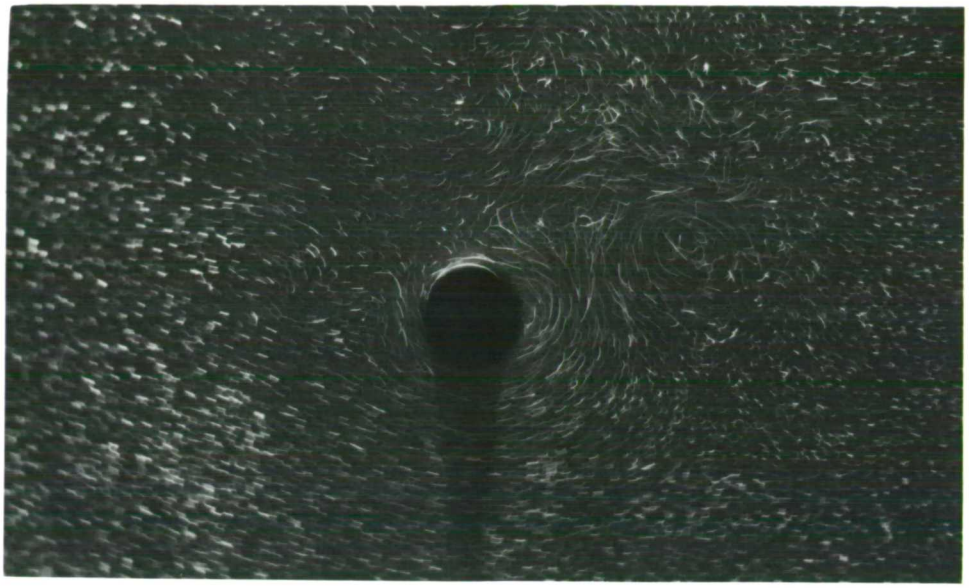

Sideways
Vortex Street
NKC = 11·0
$t/T \approx 0{\cdot}7$

FIG : 5·3(a)

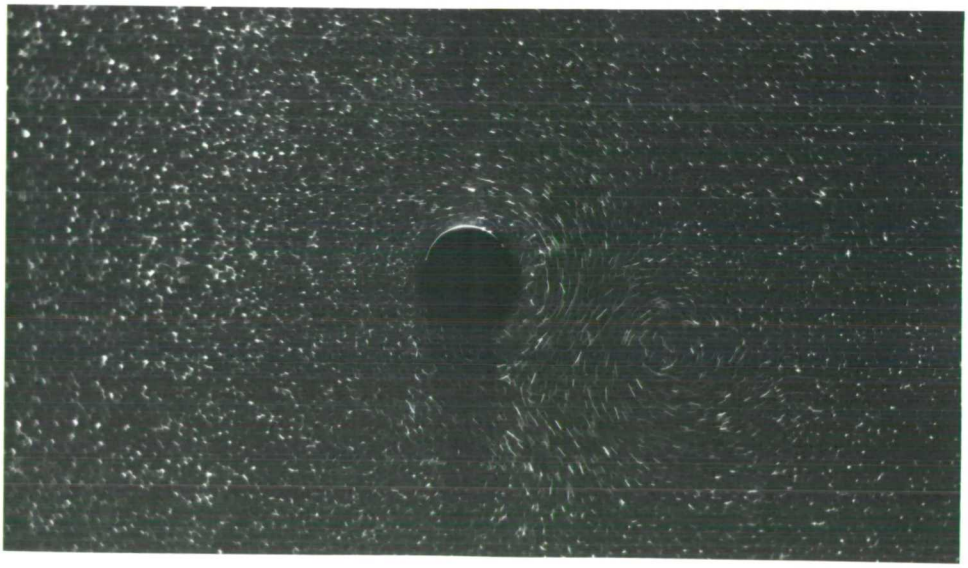

Cyclic Region
NKC = 17·02
$t/T \approx 0\ 75$

FIG : 5·3(b)

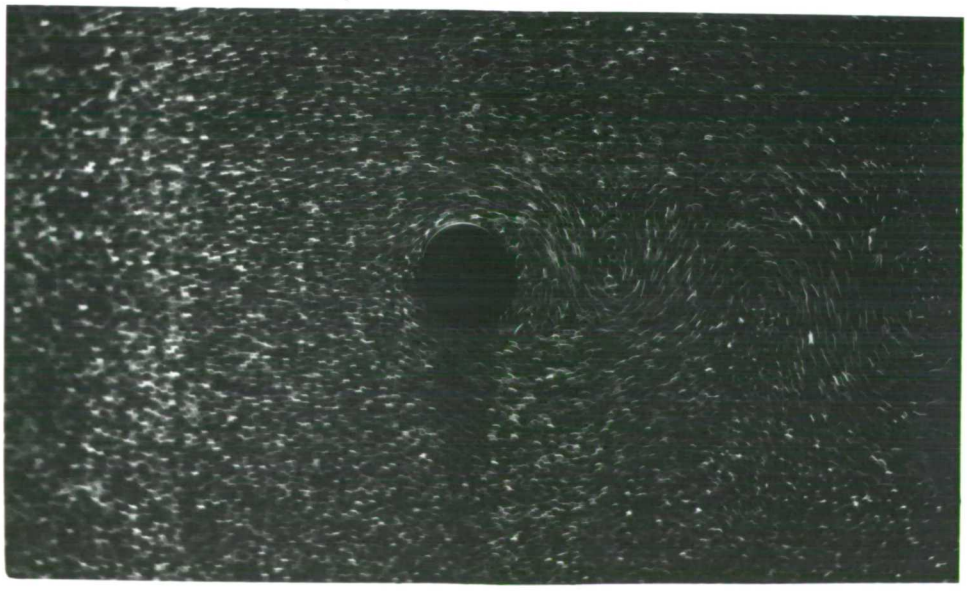

Pseudo Karman
Vortex Street
NKC = 52·9
$t/T \approx 0 \cdot 7$

FIG : 5·3 (c)

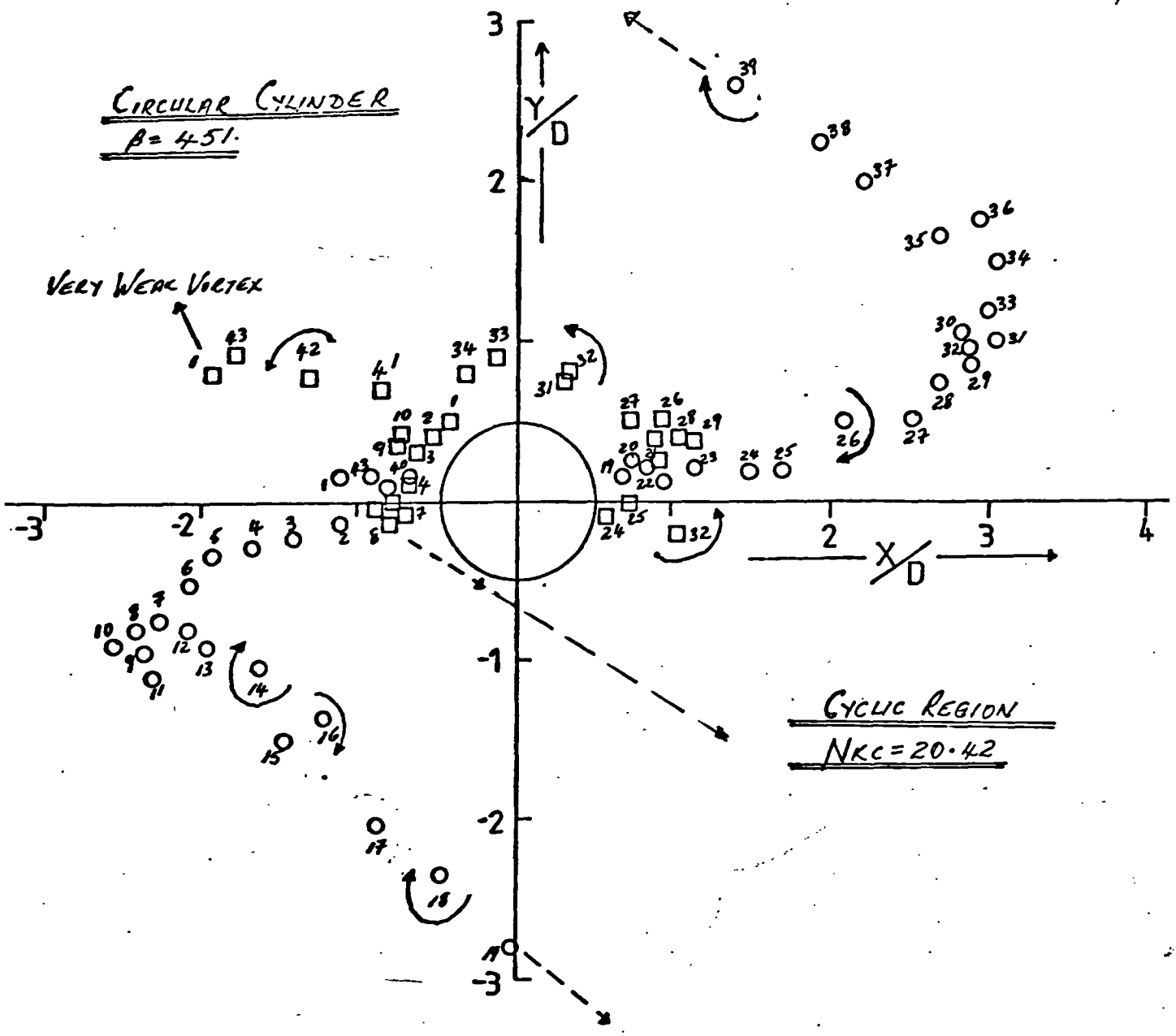

VORTEX POSITIONS DURING A CYCLE

See Fig: 5.1 For Notation

FIGURE: 5.4

FLOW PATTERN AROUND THE FLAT PLATES

NKC < 3 : SYMMETRIC PAIR

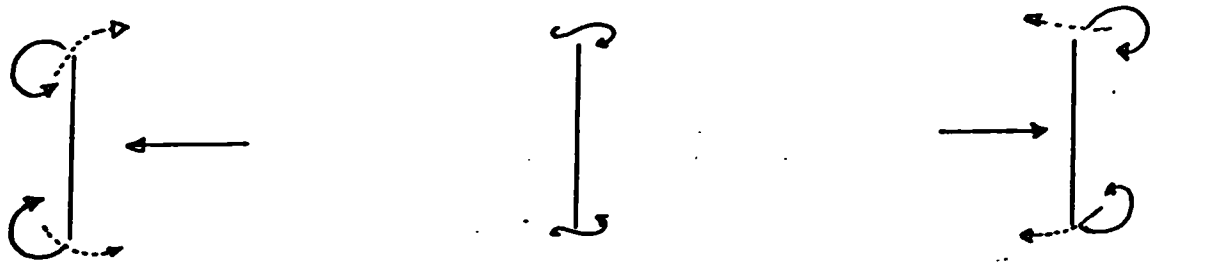

FIGURE : 5.5 (a)

---

7 < NKC < 4 : ASYMMETRIC REGION

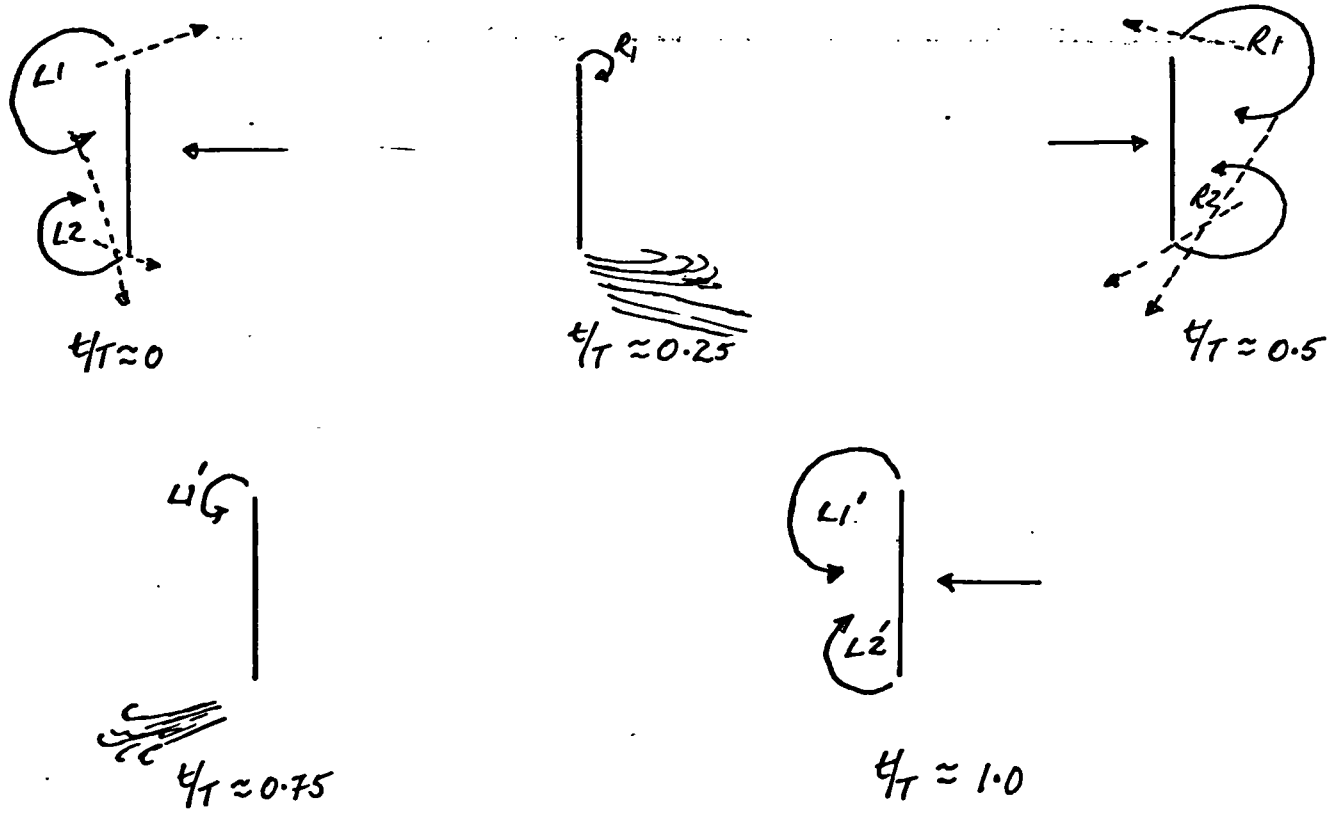

FIGURE : 5.5 (b)

25 > NKC > 7 : Cyclic Region

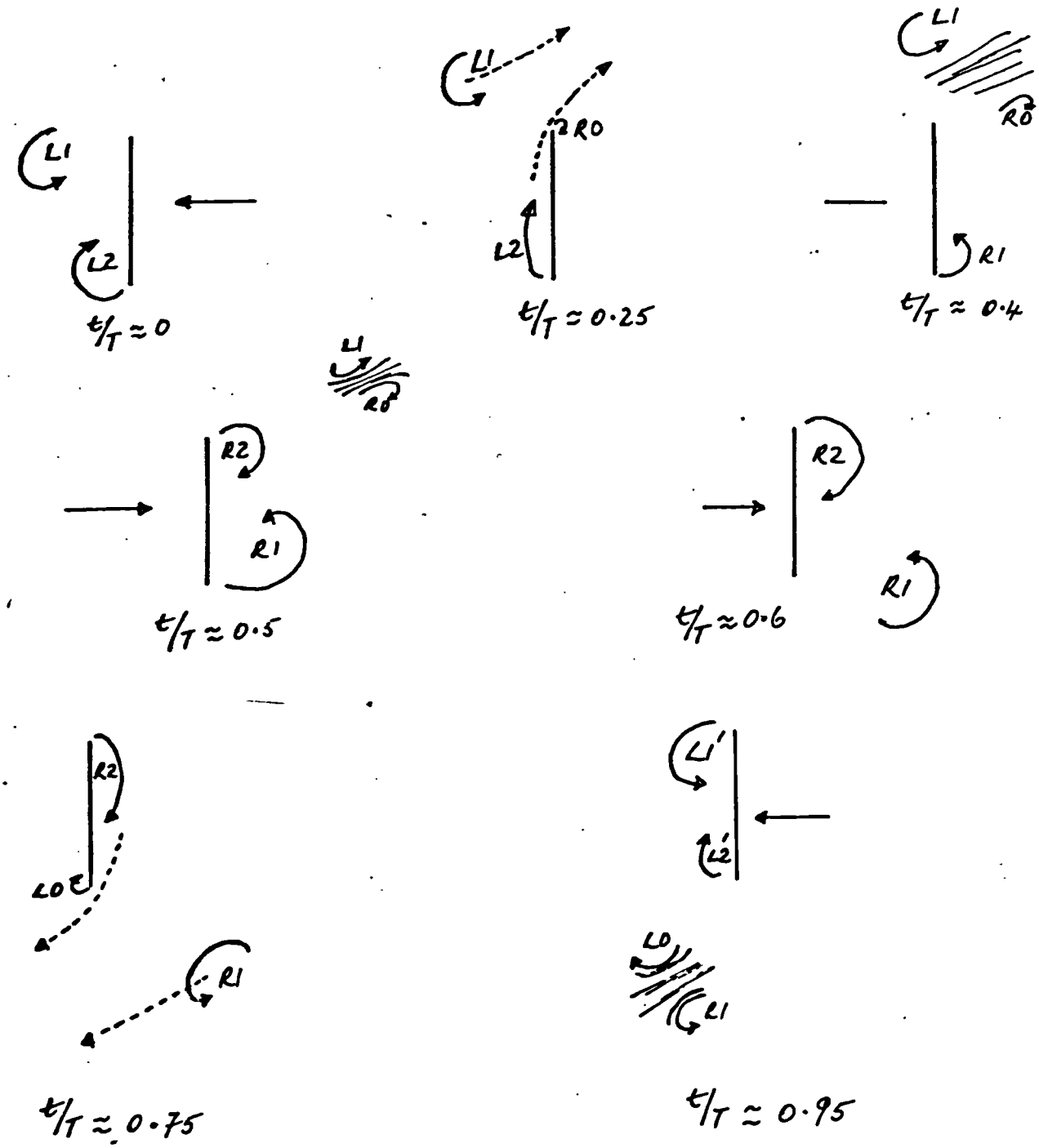

Figure : 5.5 (c)

FLAT PLATE : $\beta = 1685 \cdot 8$: CYCLIC REGION

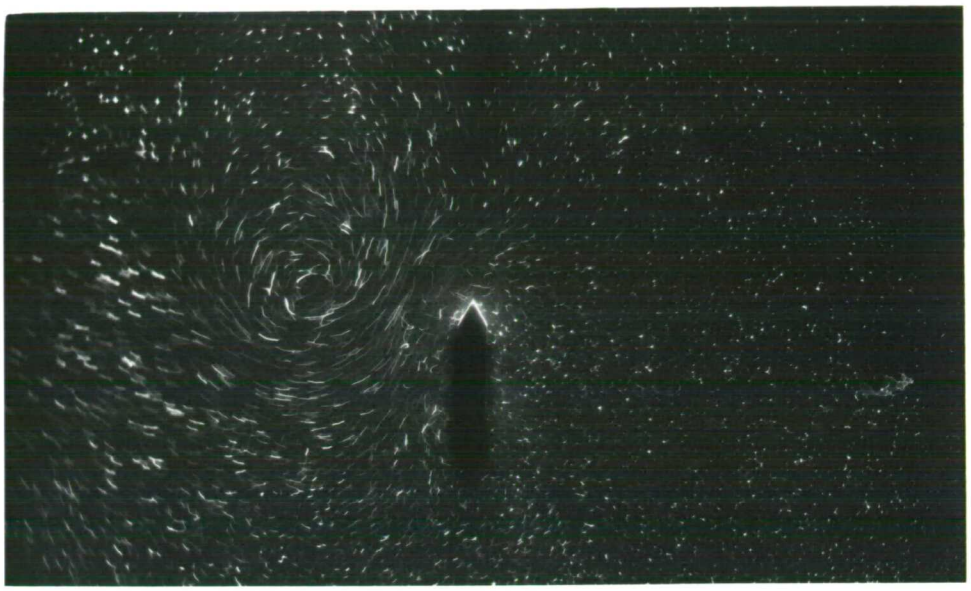

$t/T \approx 0 \cdot 25$

FIG : 5·6(a)

$t/T \approx 0 \cdot 48$

FIG : 5·6(b)

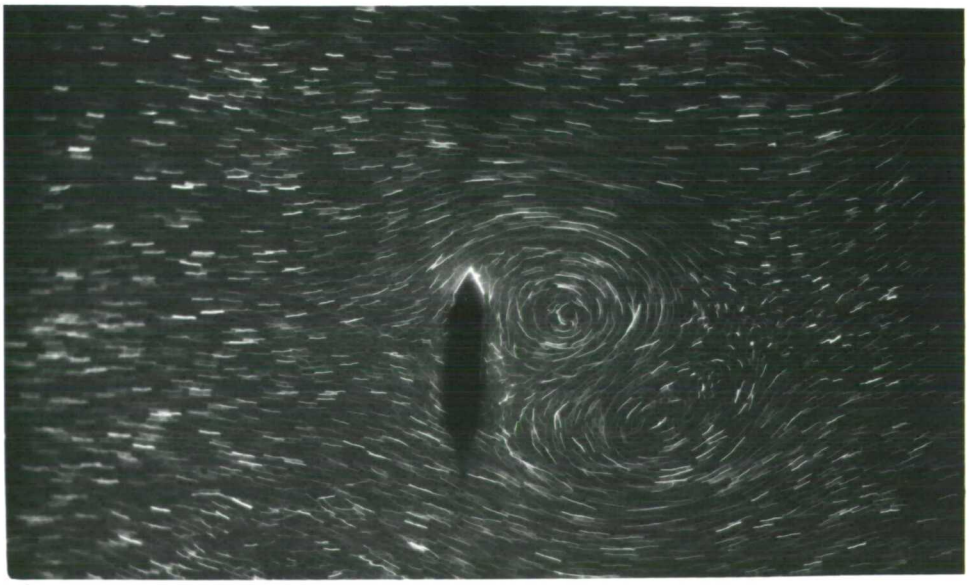

$t/T \approx 0 \cdot 55$

FIG : 5·6(c)

Rotation Clockwise :

NKC = 14·8

FLAT PLATE : β =1685·8 : CYCLIC REGION

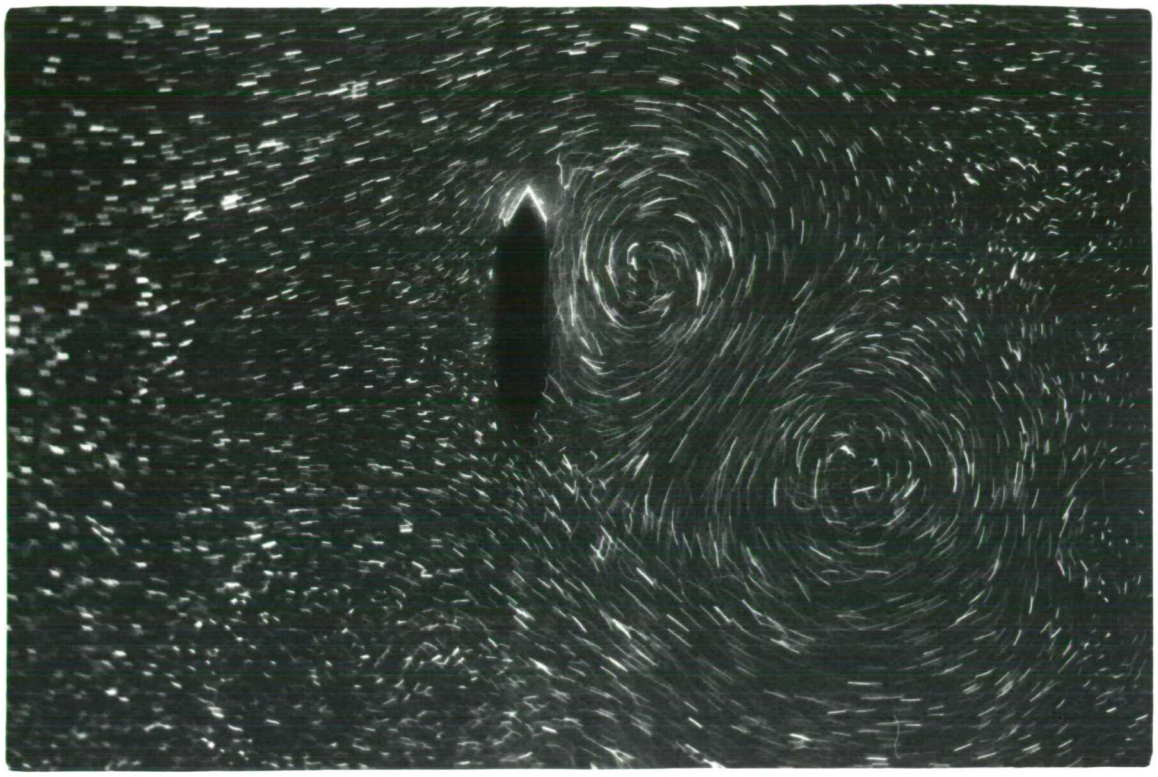

$t/T \approx 0 \cdot 65$ FIG : 5·6(d)

Rotation Clockwise : NKC = 14·8

$t/T \approx 0 \cdot 73$ FIG : 5·6(e)

FLAT PLATE : $\beta = 1685 \cdot 8$: CYCLIC REGION

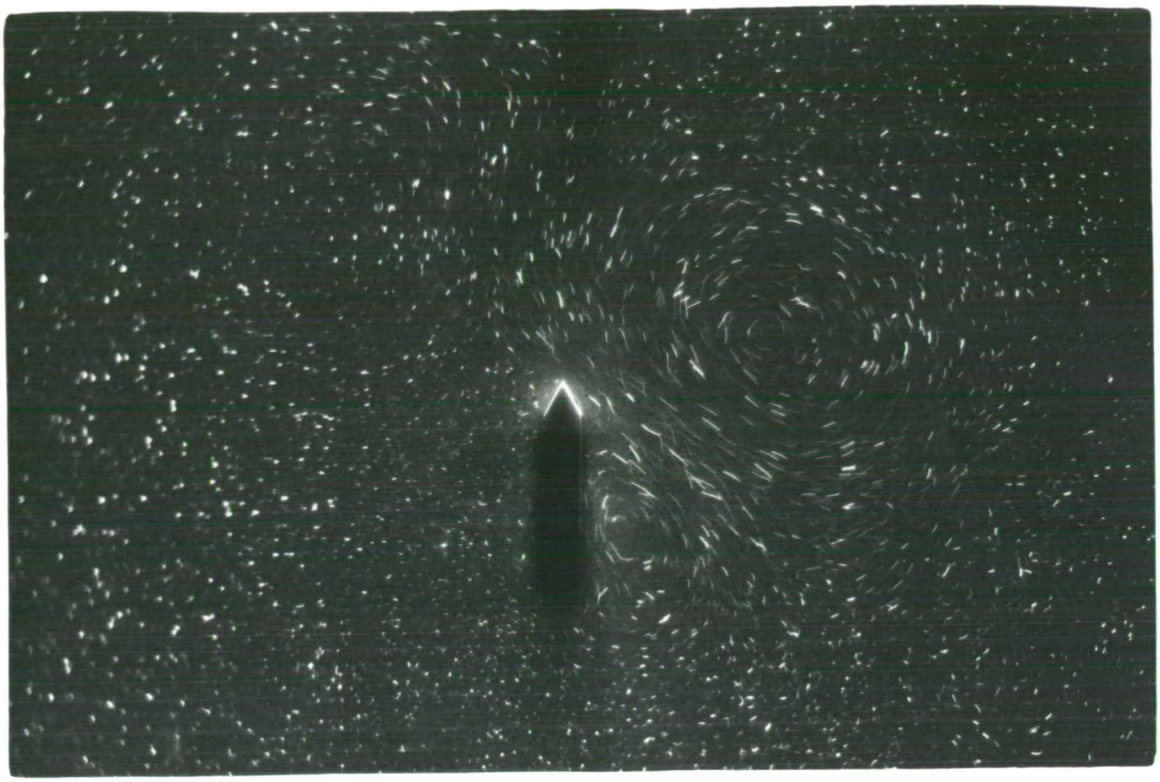

$t/T \approx 0 \cdot 75$ FIG : 5·7 (a)

Rotation Anti - Clockwise : NKC = 8·0

$t/T \approx 0 \cdot 85$ FIG : 5·7(b)

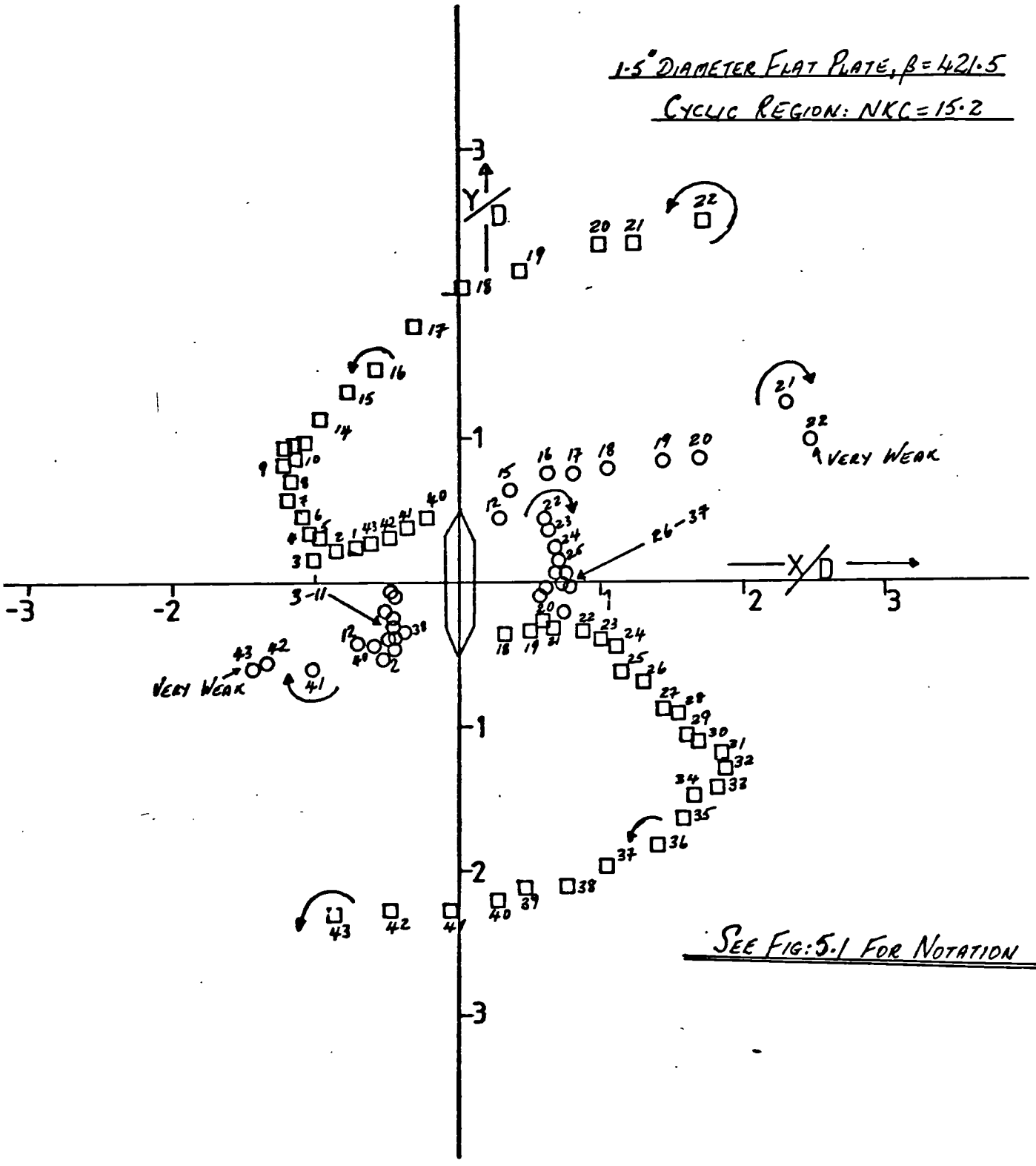

VORTEX POSITIONS DURING A CYCLE

FIGURE: 5.8a

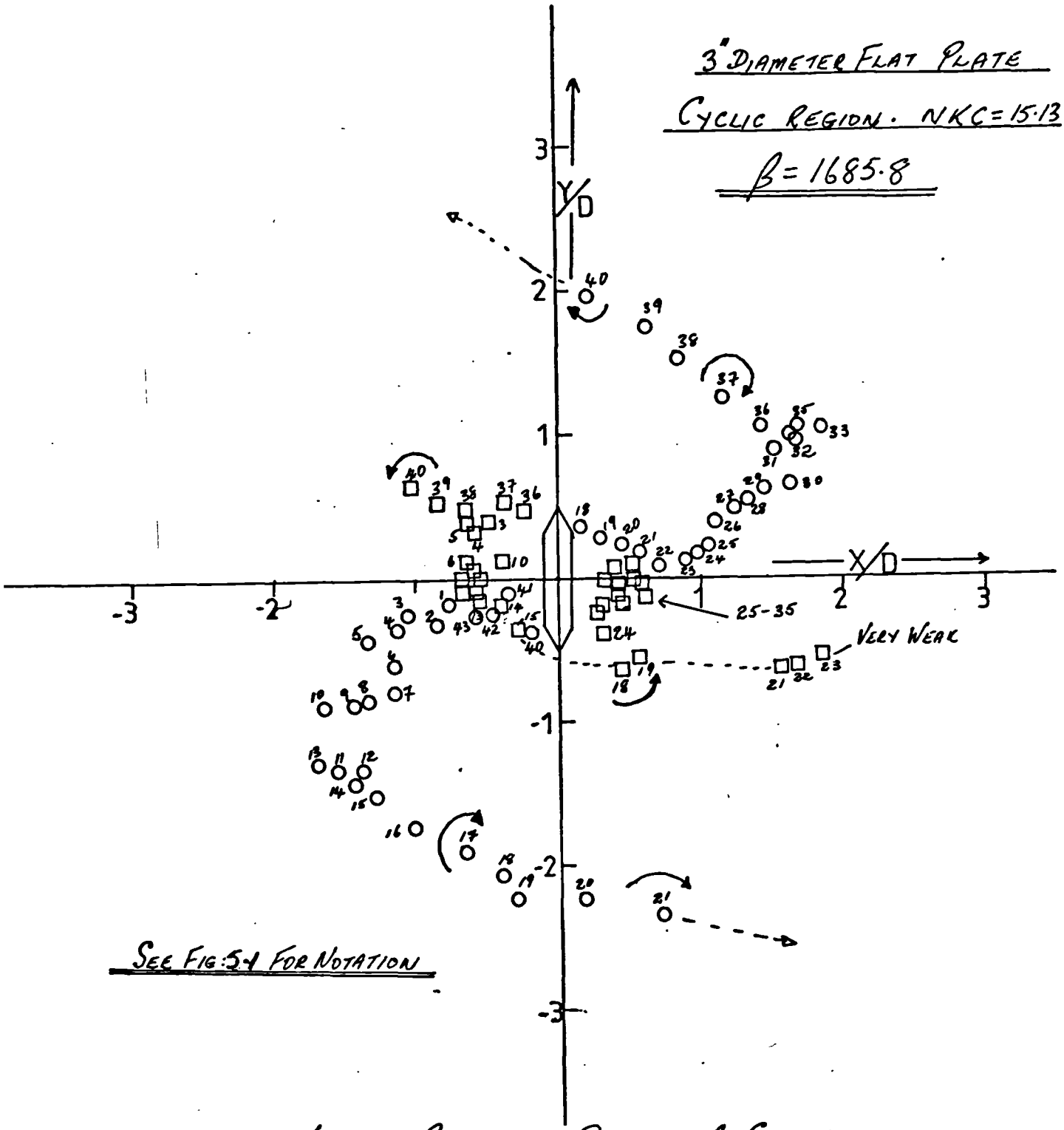

VORTEX POSITIONS DURING A CYCLE

FIGURE: 5-8b

NKC < 4 : SYMMETRIC REGION

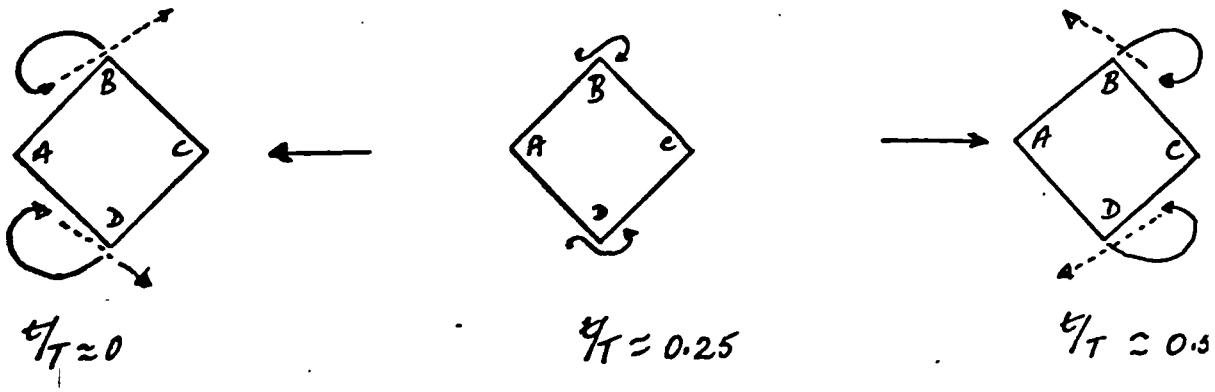

FIG : 5·9(a)

87 > NKC > 4 : ASYMMETRIC REGION

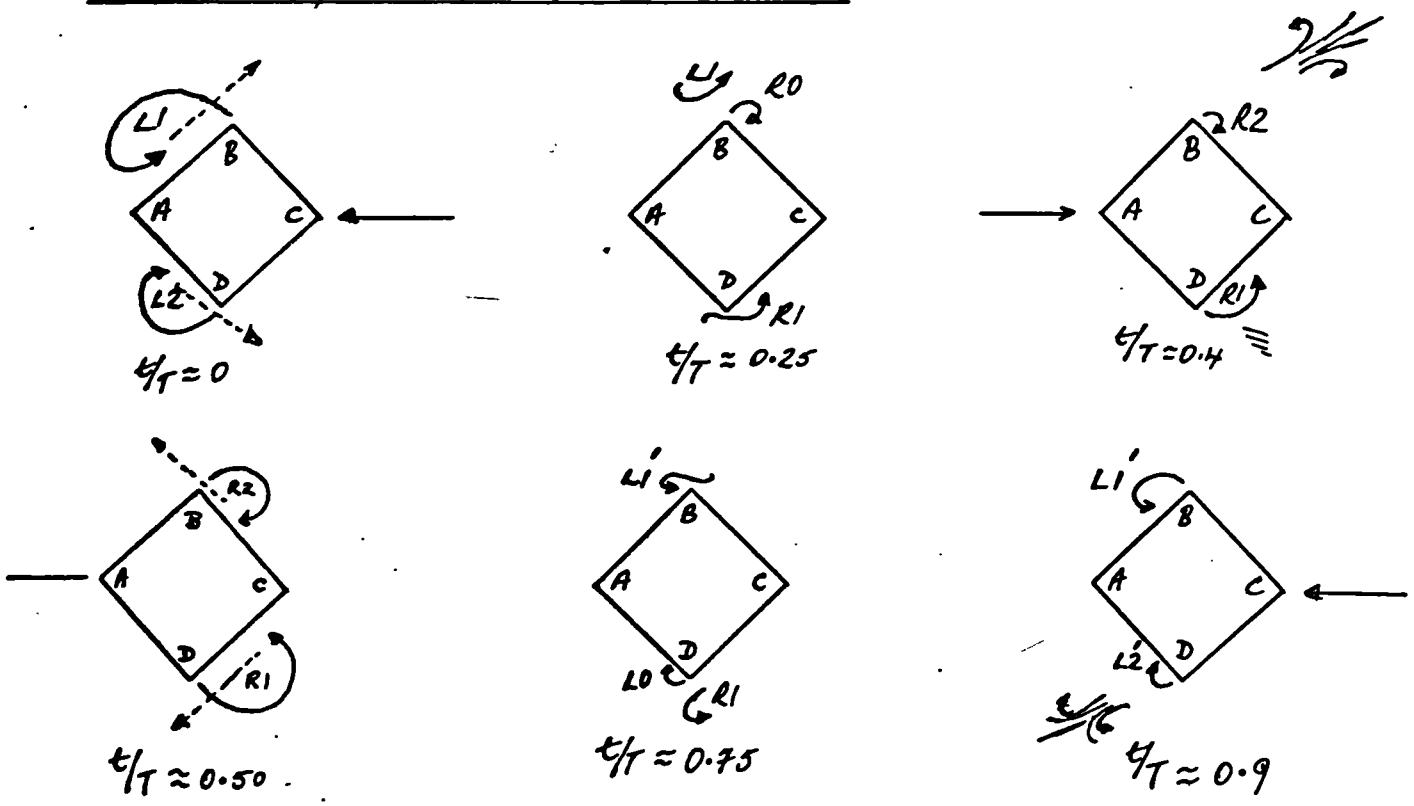

FIG : 5·9(b)

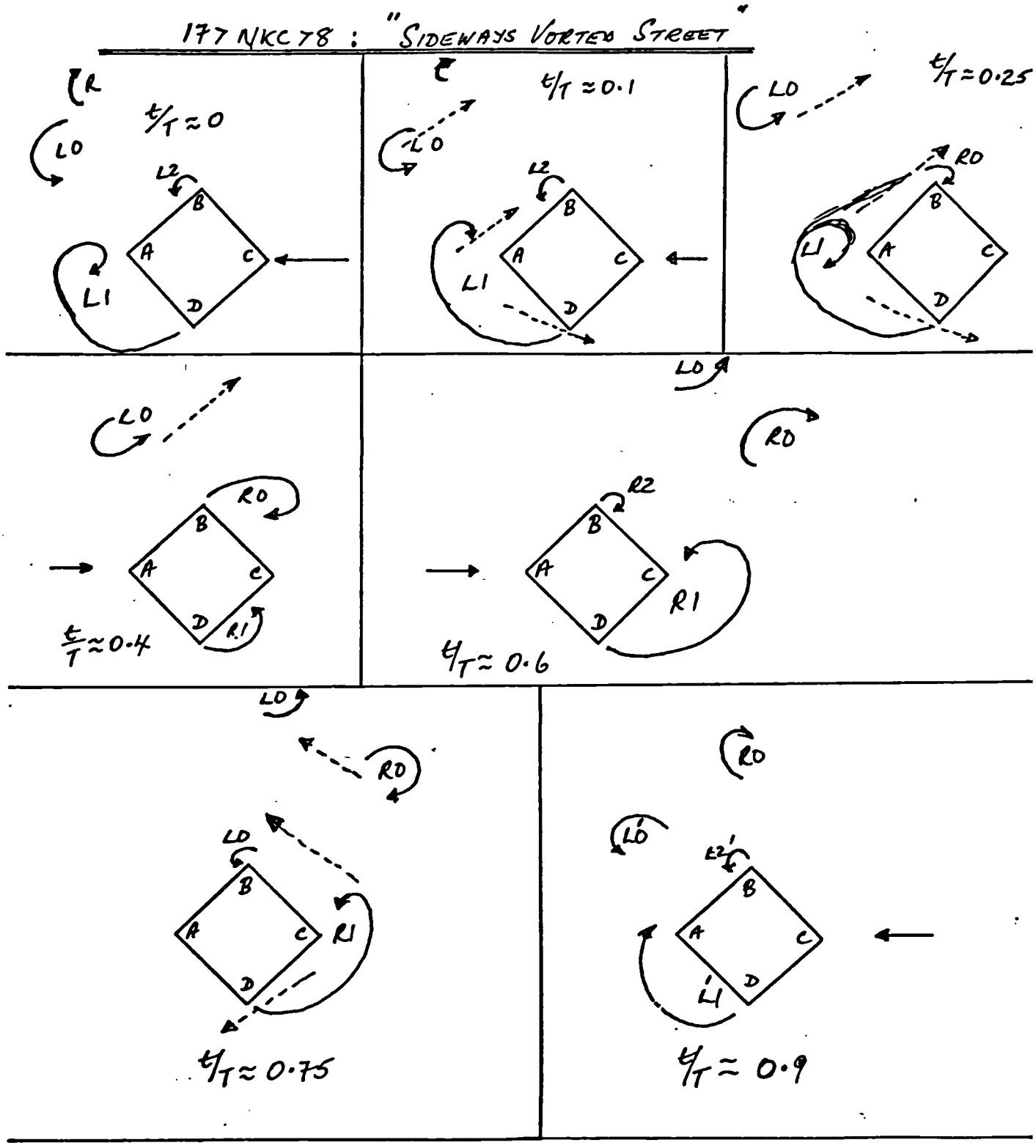
177 NKC 78 : "SIDEWAYS VORTEX STREET"
t/T ≈ 0
t/T ≈ 0.1
t/T = 0.25
t/T ≈ 0.4
t/T ≈ 0.6
t/T ≈ 0.75
t/T ≈ 0.9
A
B
C
D

FIG : 5.9(c)

25 > NKC > 17 : Cyclic Region

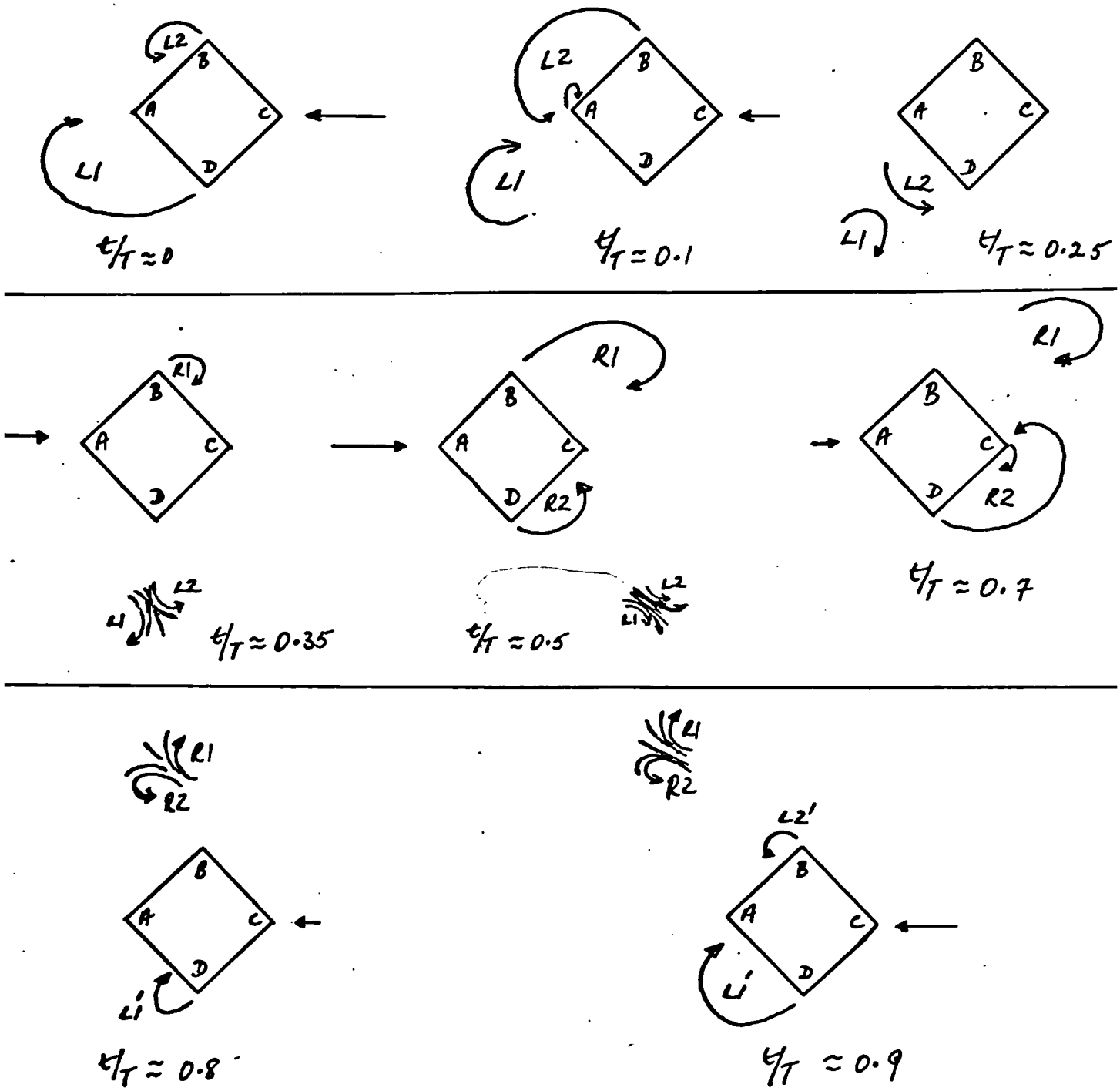

FIG : 5·9(d)

DIAMOND SECTION $\beta = 422 \cdot 7$

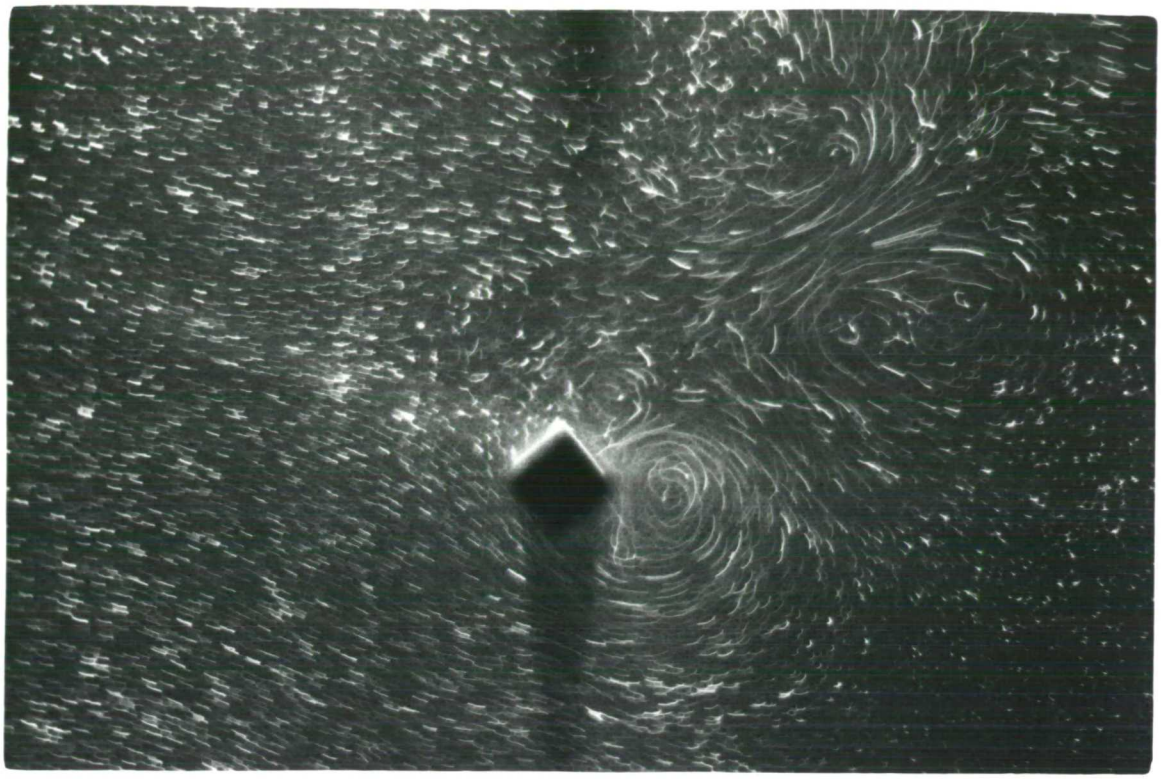

FIG: 5·10(a). Sideways Vortex Street. NKC = 13·61: $t/T \approx 0 \cdot 68$

FIG: 5·10(b) Pseudo Karman Vortex Street

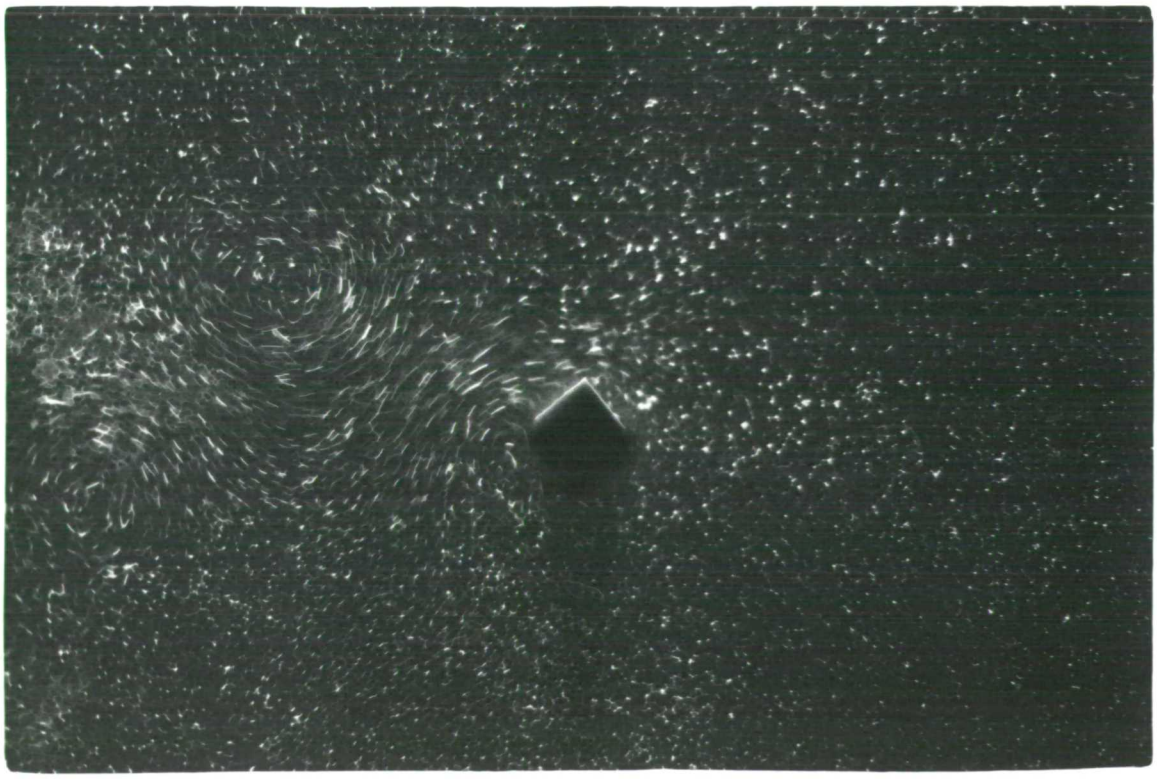

NKC = 52·1 $t/T \approx 0 \cdot 25$

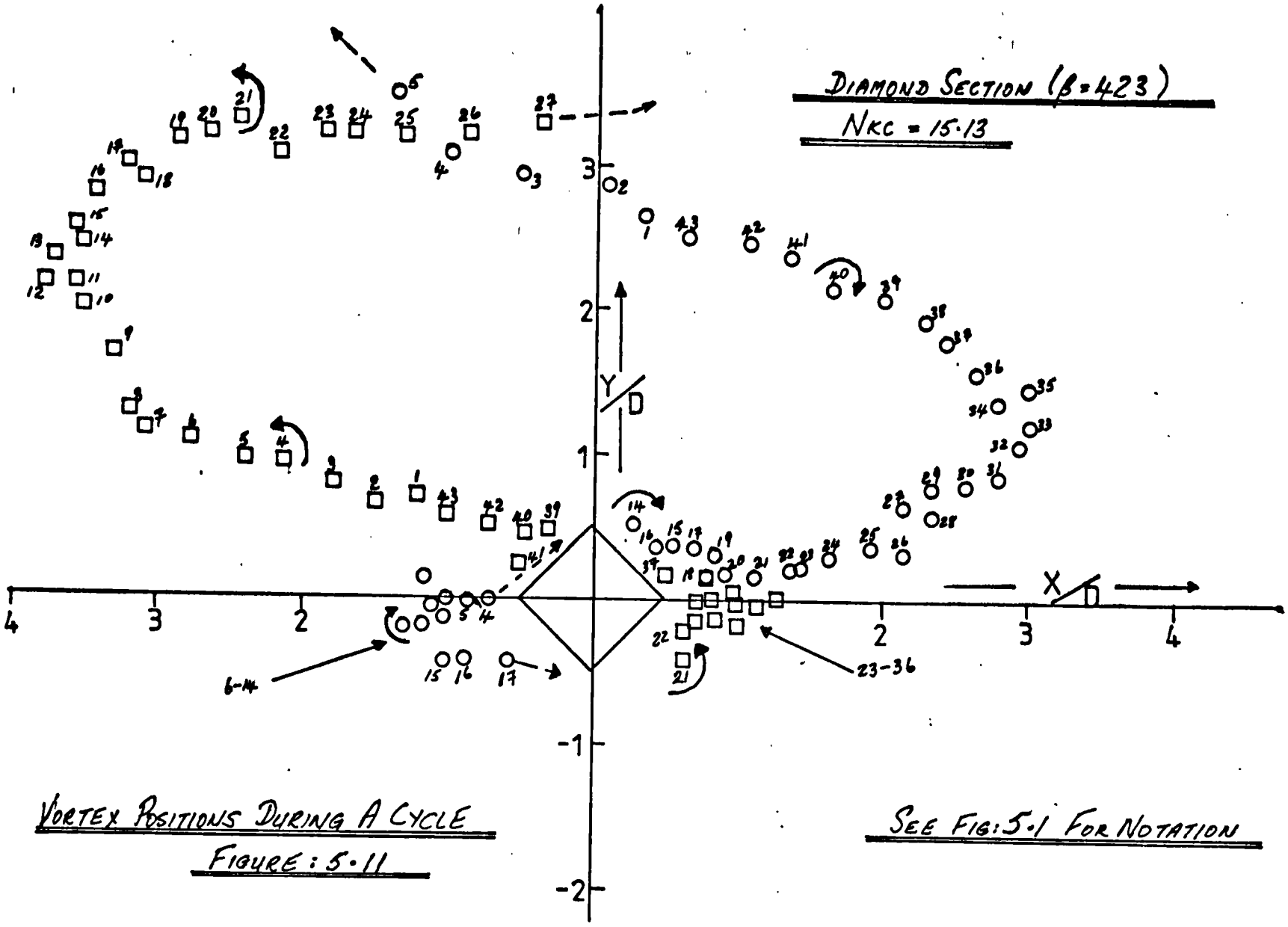

VORTEX POSITIONS DURING A CYCLE

FIGURE : 5·11

NKC < 5 : SYMMETRIC REGION

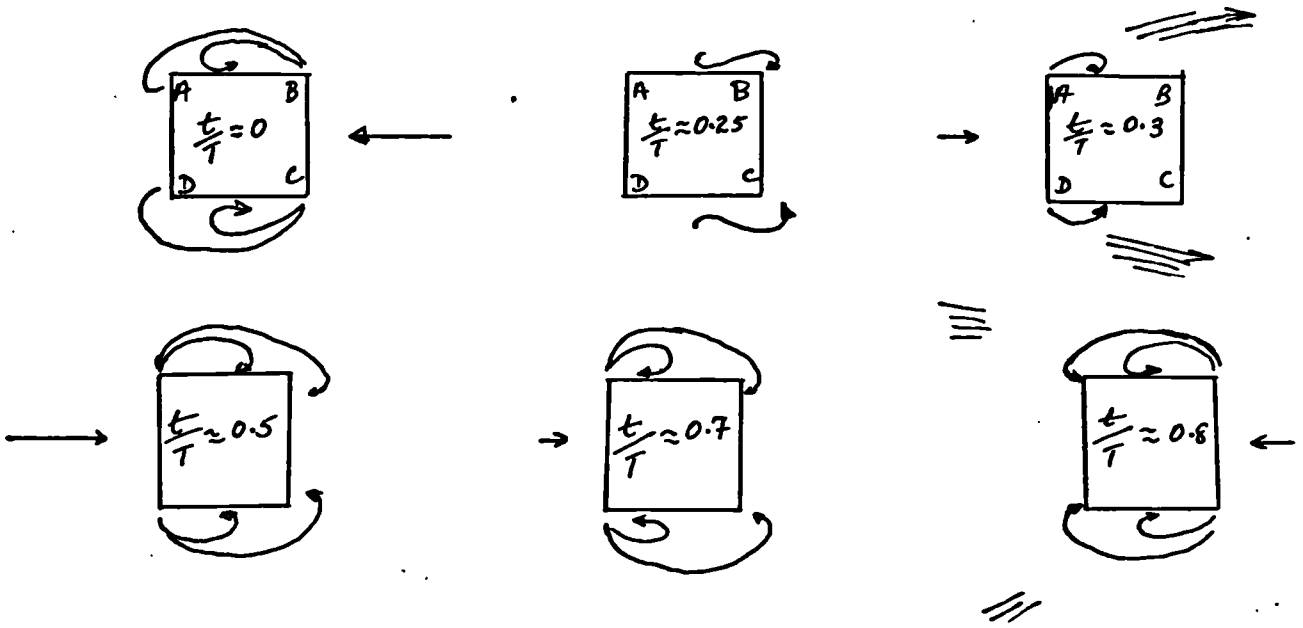

FIG : 5·12(a)

ASYMMETRIC REGION I : 12 > NKC > 5

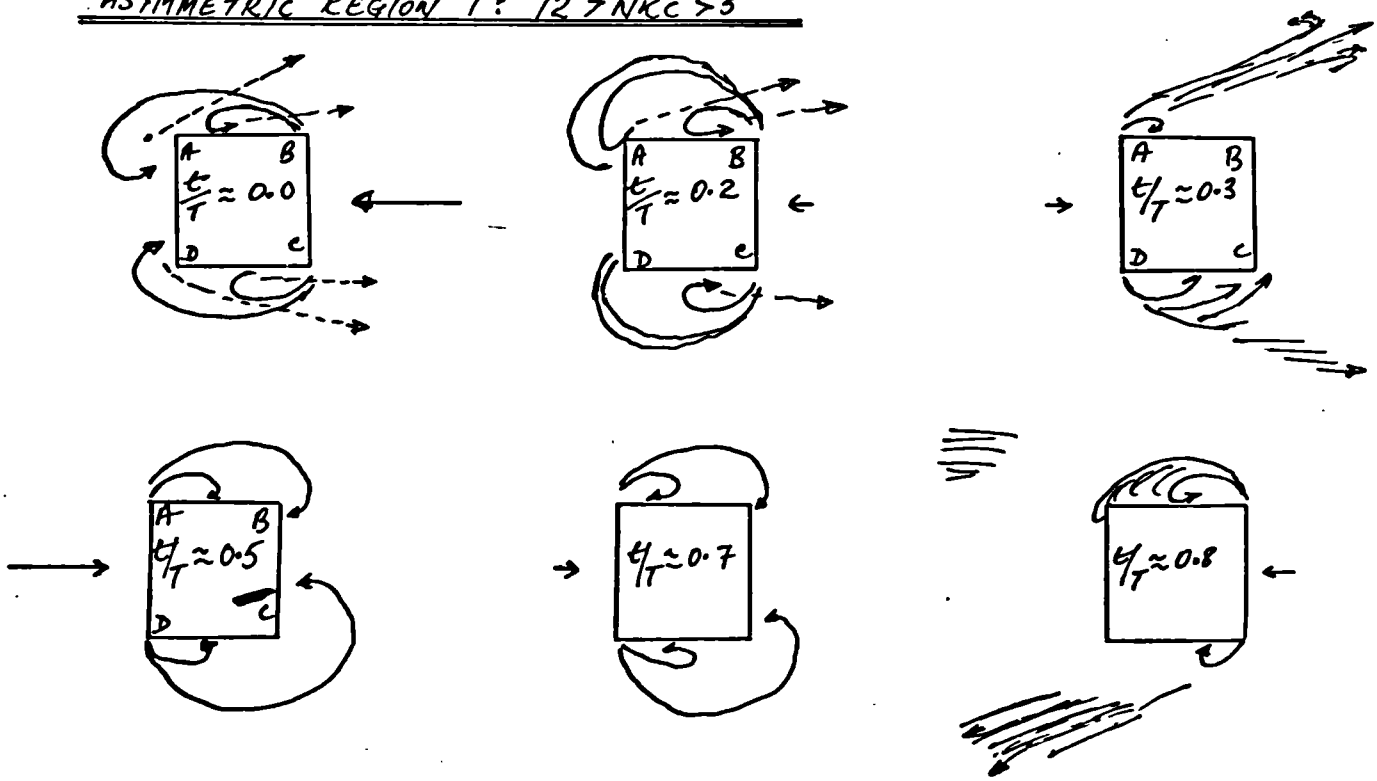

FIG : 5·12(b)

ASYMMETRIC REGION: 2 : 17 > NKC > 12

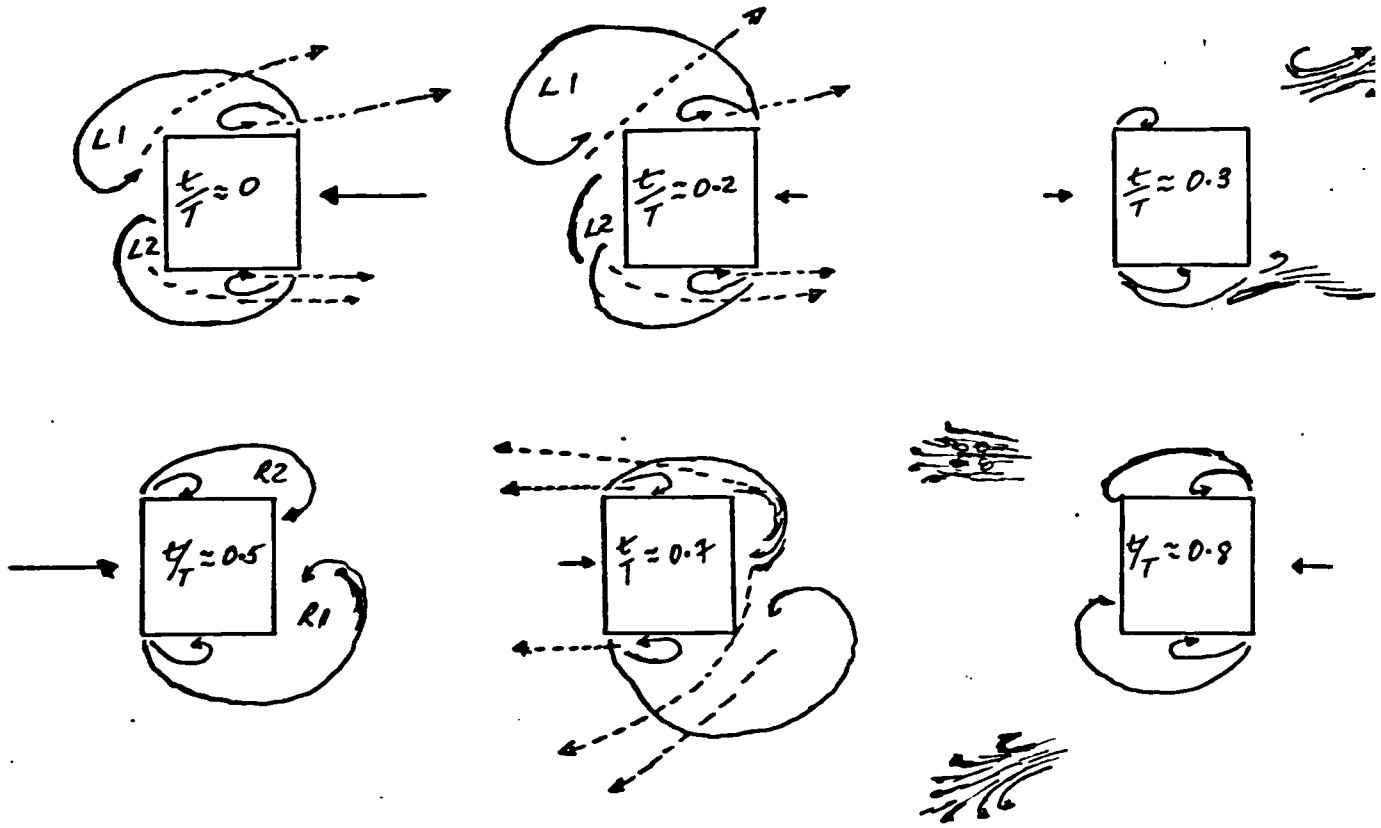

FIG : 5·12(c)

ASYMMETRIC REGION : 3 — 25 > NKC > 17

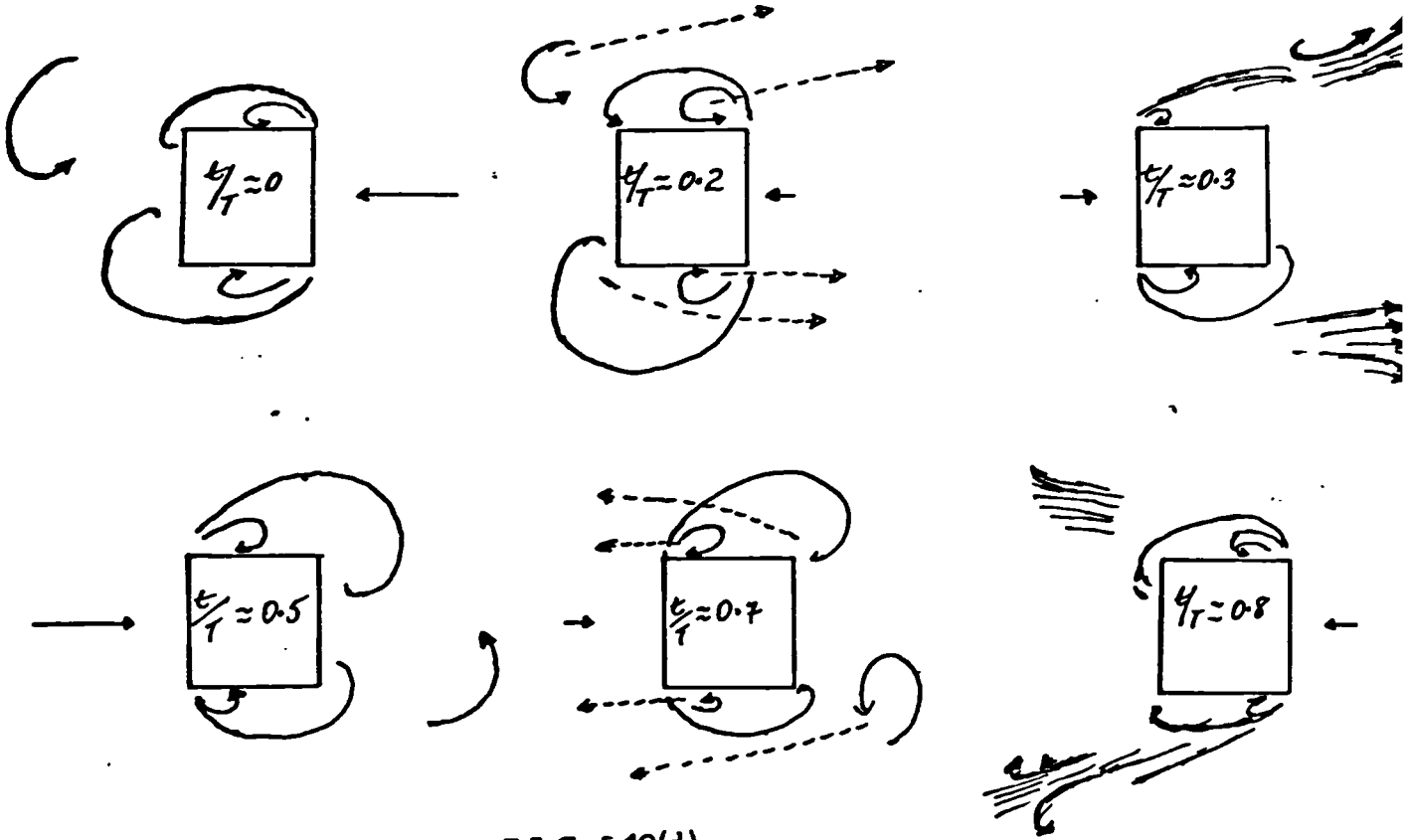

FIG : 5·12(d)

SQUARE SECTION β = 208

FIG : 5·13(a) $t/T \approx 0{\cdot}15$

NKC = 60·72 : Pseudo Karman Vortex Street

FIG : 5·13(b) $t/T \approx 0{\cdot}30$

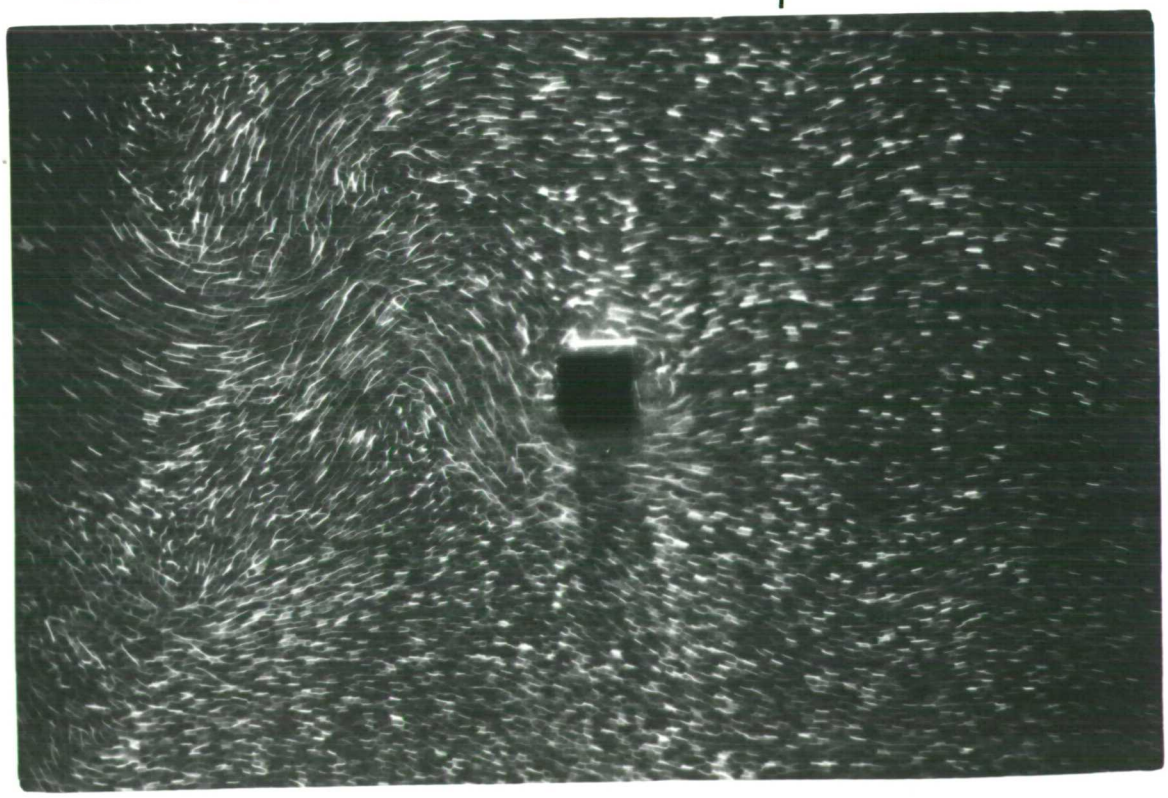

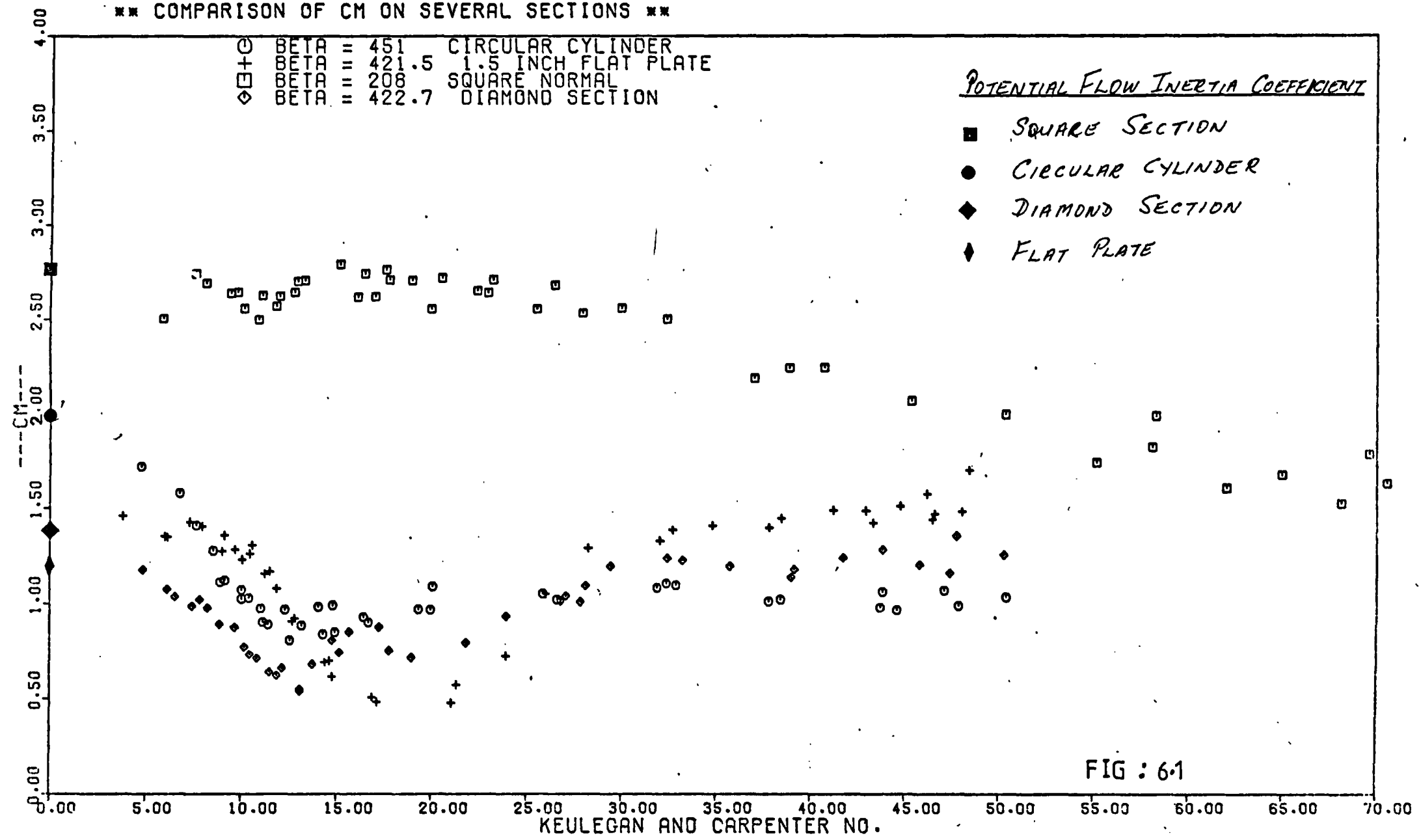
** COMPARISON OF CM ON SEVERAL SECTIONS **
BETA = 451 CIRCULAR CYLINDER
BETA = 421.5 1.5 INCH FLAT PLATE
BETA = 208 SQUARE NORMAL
BETA = 422.7 DIAMOND SECTION
POTENTIAL FLOW INERTIA COEFFICIENT
SQUARE SECTION
CIRCULAR CYLINDER
DIAMOND SECTION
FLAT PLATE
---CM---
0.00
0.50
1.00
1.50
2.00
2.50
3.00
3.50
4.00
0.00
5.00
10.00
15.00
20.00
25.00
30.00
35.00
40.00
45.00
50.00
55.00
60.00
65.00
70.00
KEULEGAN AND CARPENTER NO.

FIG : 6.1

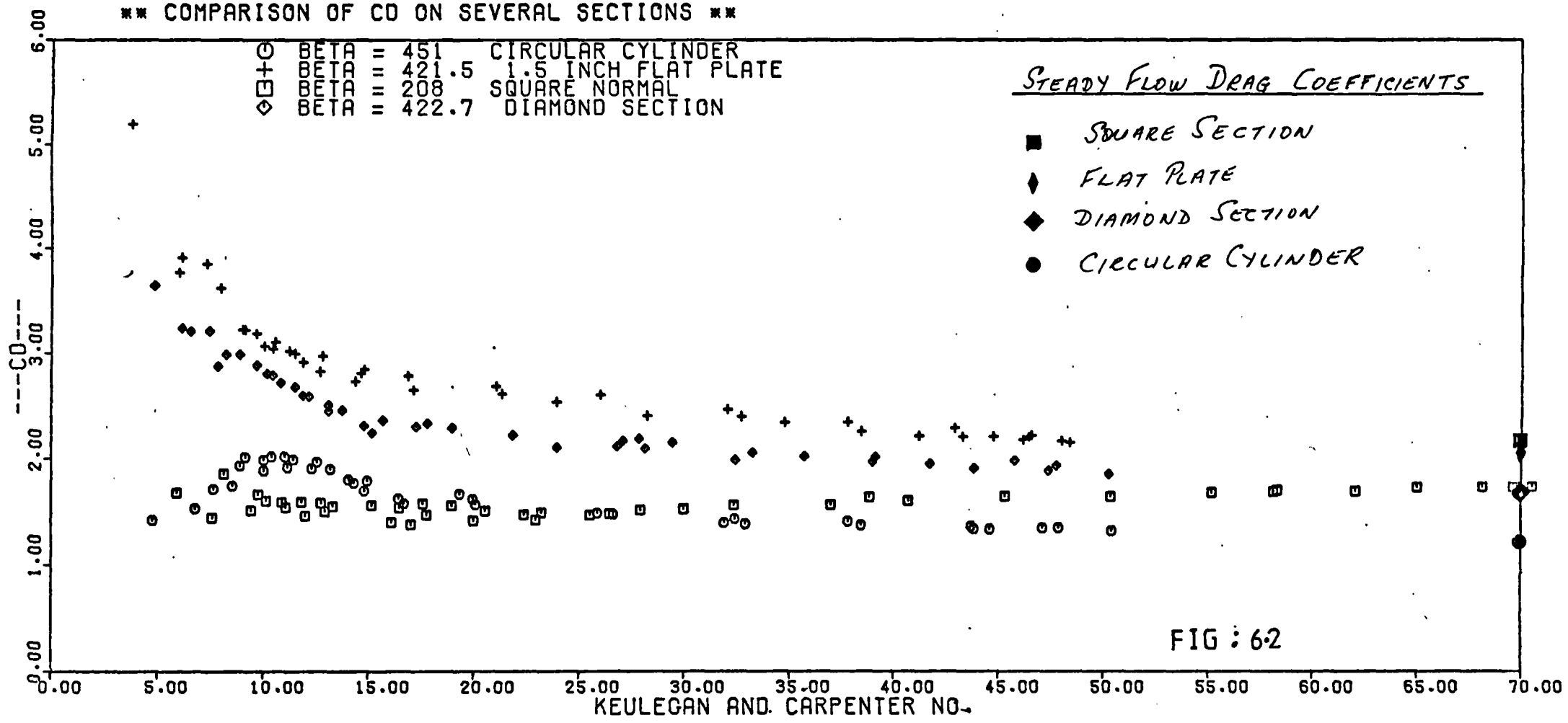
** COMPARISON OF CD ON SEVERAL SECTIONS **
BETA = 451 CIRCULAR CYLINDER
BETA = 421.5 1.5 INCH FLAT PLATE
BETA = 208 SQUARE NORMAL
BETA = 422.7 DIAMOND SECTION
STEADY FLOW DRAG COEFFICIENTS
SQUARE SECTION
FLAT PLATE
DIAMOND SECTION
CIRCULAR CYLINDER
---CD---
0.00
1.00
2.00
3.00
4.00
5.00
6.00
0.00
5.00
10.00
15.00
20.00
25.00
30.00
35.00
40.00
45.00
50.00
55.00
60.00
65.00
70.00
KEULEGAN AND CARPENTER NO.

FIG : 6·2

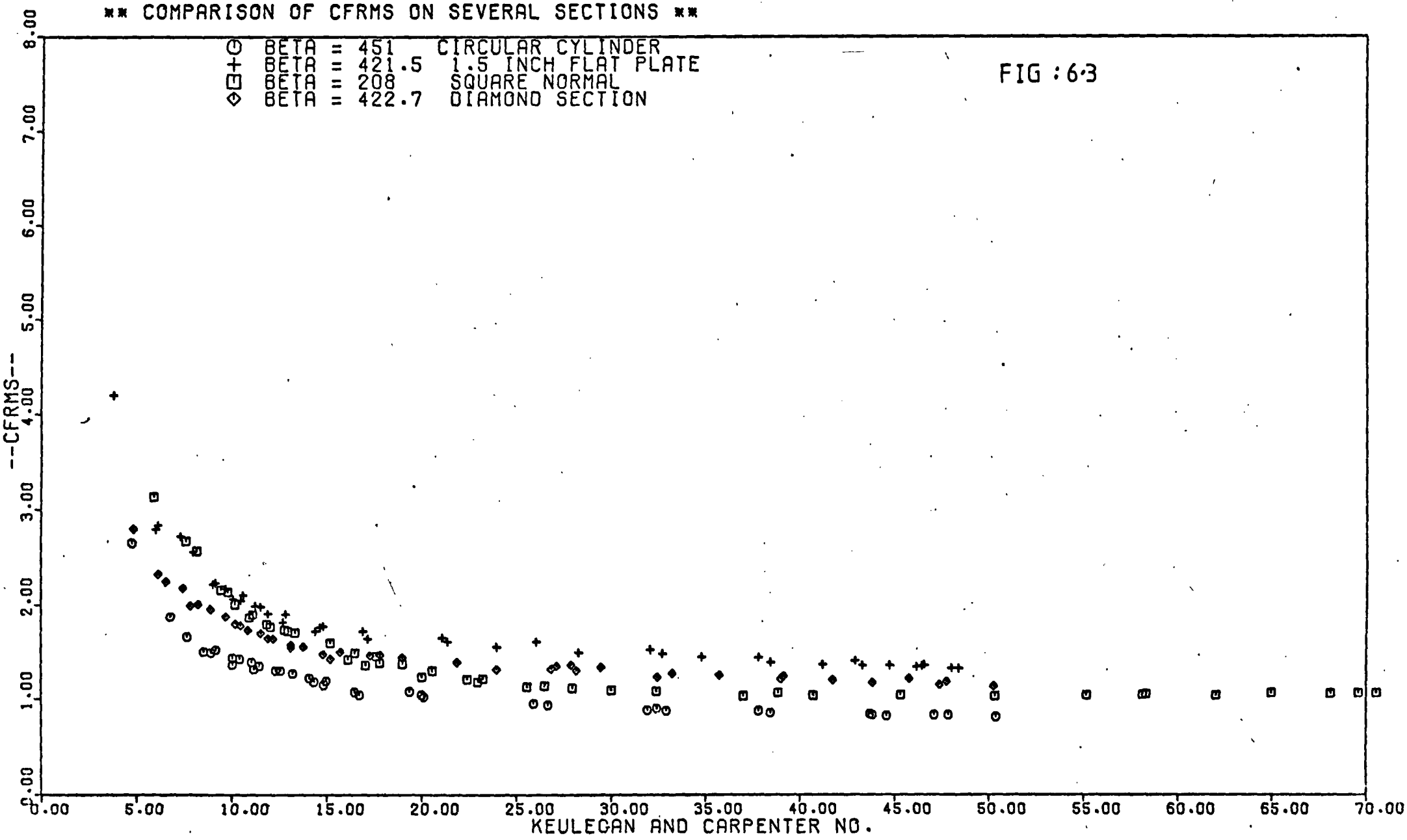
** COMPARISON OF CFRMS ON SEVERAL SECTIONS **
BETA = 451 CIRCULAR CYLINDER
BETA = 421.5 1.5 INCH FLAT PLATE
BETA = 208 SQUARE NORMAL
BETA = 422.7 DIAMOND SECTION
FIG : 6·3
--CFRMS--
0.00
1.00
2.00
3.00
4.00
5.00
6.00
7.00
8.00
0.00
5.00
10.00
15.00
20.00
25.00
30.00
35.00
40.00
45.00
50.00
55.00
60.00
65.00
70.00
KEULEGAN AND CARPENTER NO.

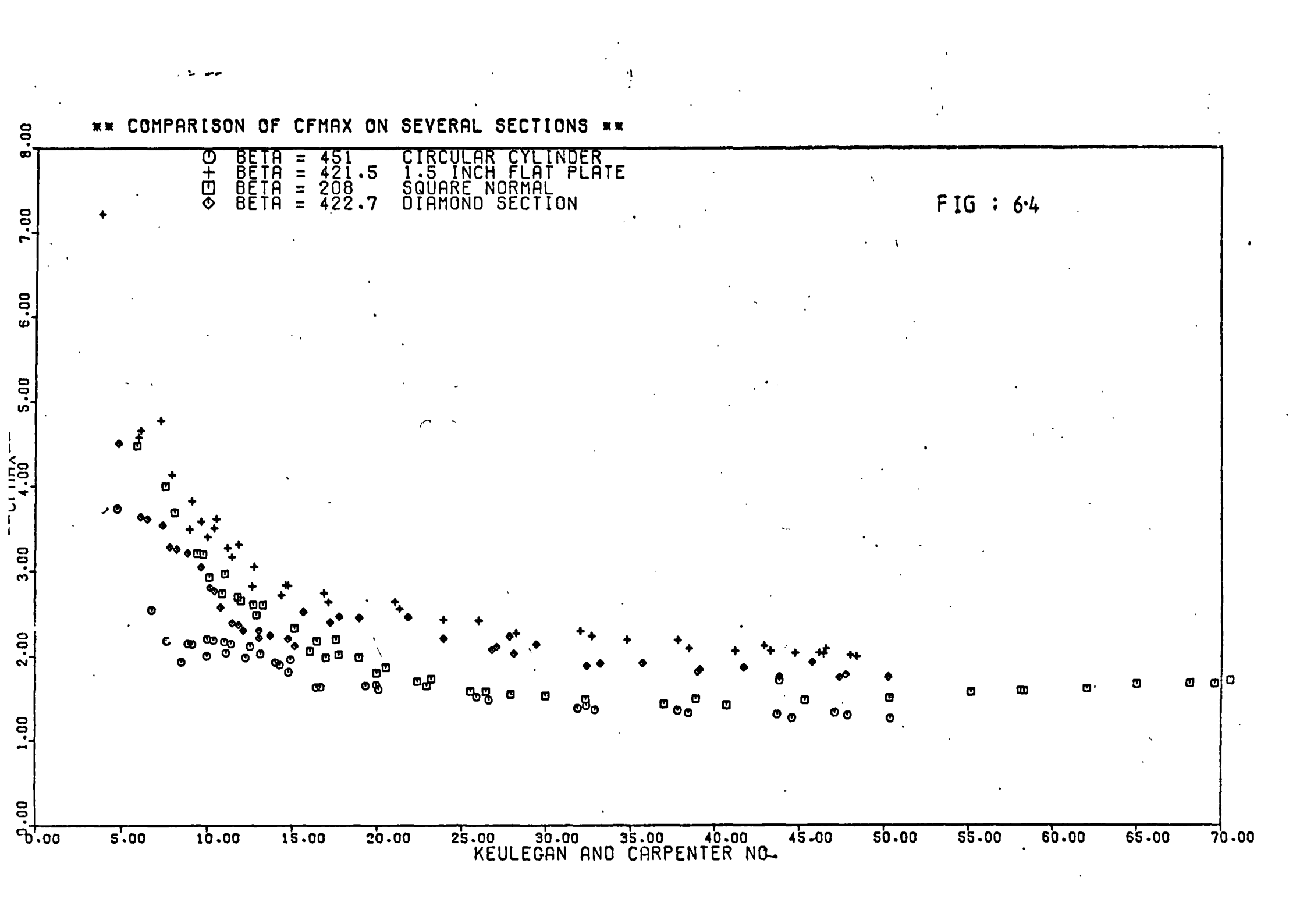
** COMPARISON OF CFMAX ON SEVERAL SECTIONS **
BETA = 451 CIRCULAR CYLINDER
BETA = 421.5 1.5 INCH FLAT PLATE
BETA = 208 SQUARE NORMAL
BETA = 422.7 DIAMOND SECTION
FIG : 6·4
CFMAX
0.00
1.00
2.00
3.00
4.00
5.00
6.00
7.00
8.00
0.00
5.00
10.00
15.00
20.00
25.00
30.00
35.00
40.00
45.00
50.00
55.00
60.00
65.00
70.00
KEULEGAN AND CARPENTER NO.

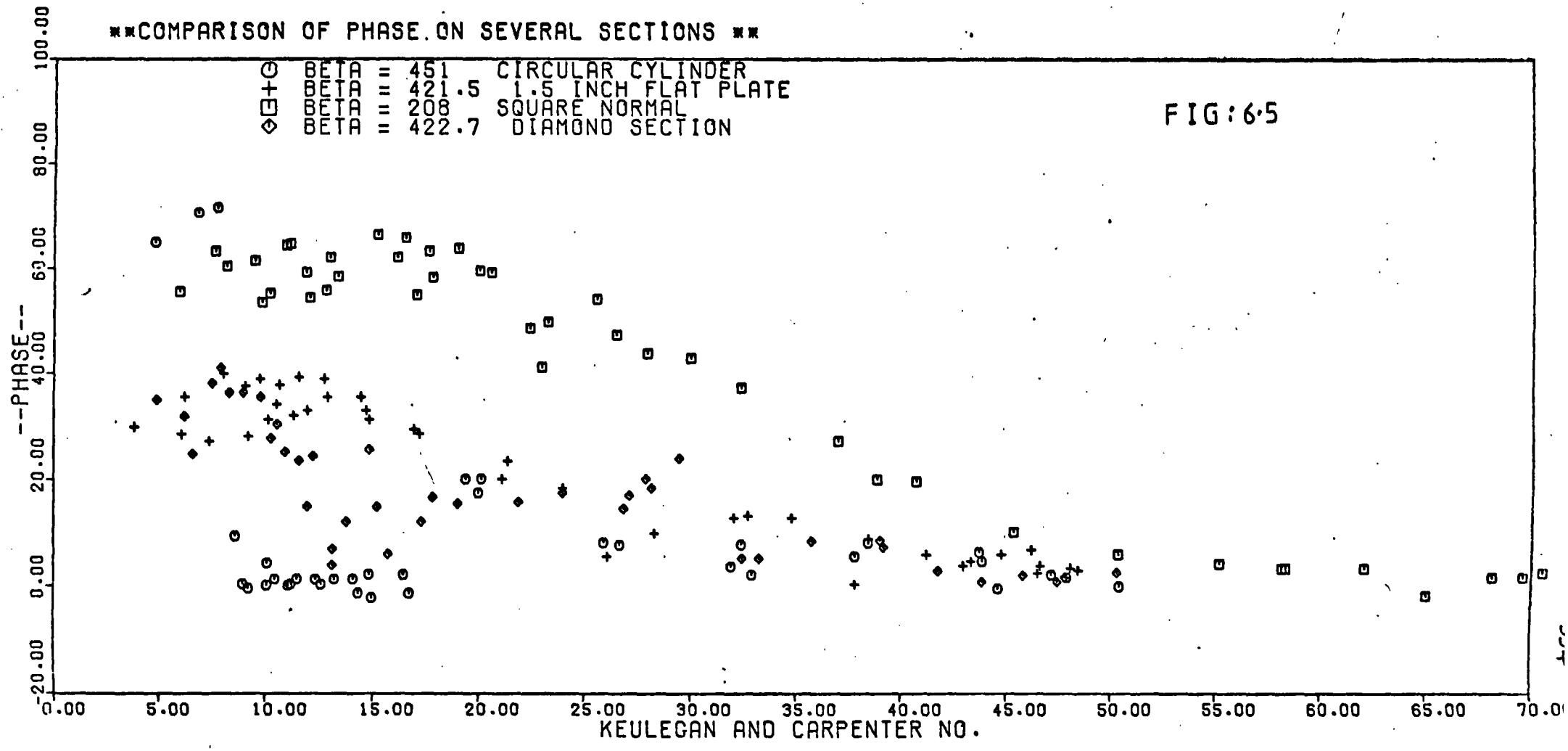
**COMPARISON OF PHASE ON SEVERAL SECTIONS **
BETA = 451 CIRCULAR CYLINDER
BETA = 421.5 1.5 INCH FLAT PLATE
BETA = 208 SQUARE NORMAL
BETA = 422.7 DIAMOND SECTION
FIG:6·5
--PHASE--
100.00
80.00
60.00
40.00
20.00
0.00
-20.00
0.00
5.00
10.00
15.00
20.00
25.00
30.00
35.00
40.00
45.00
50.00
55.00
60.00
65.00
70.00
KEULEGAN AND CARPENTER NO.

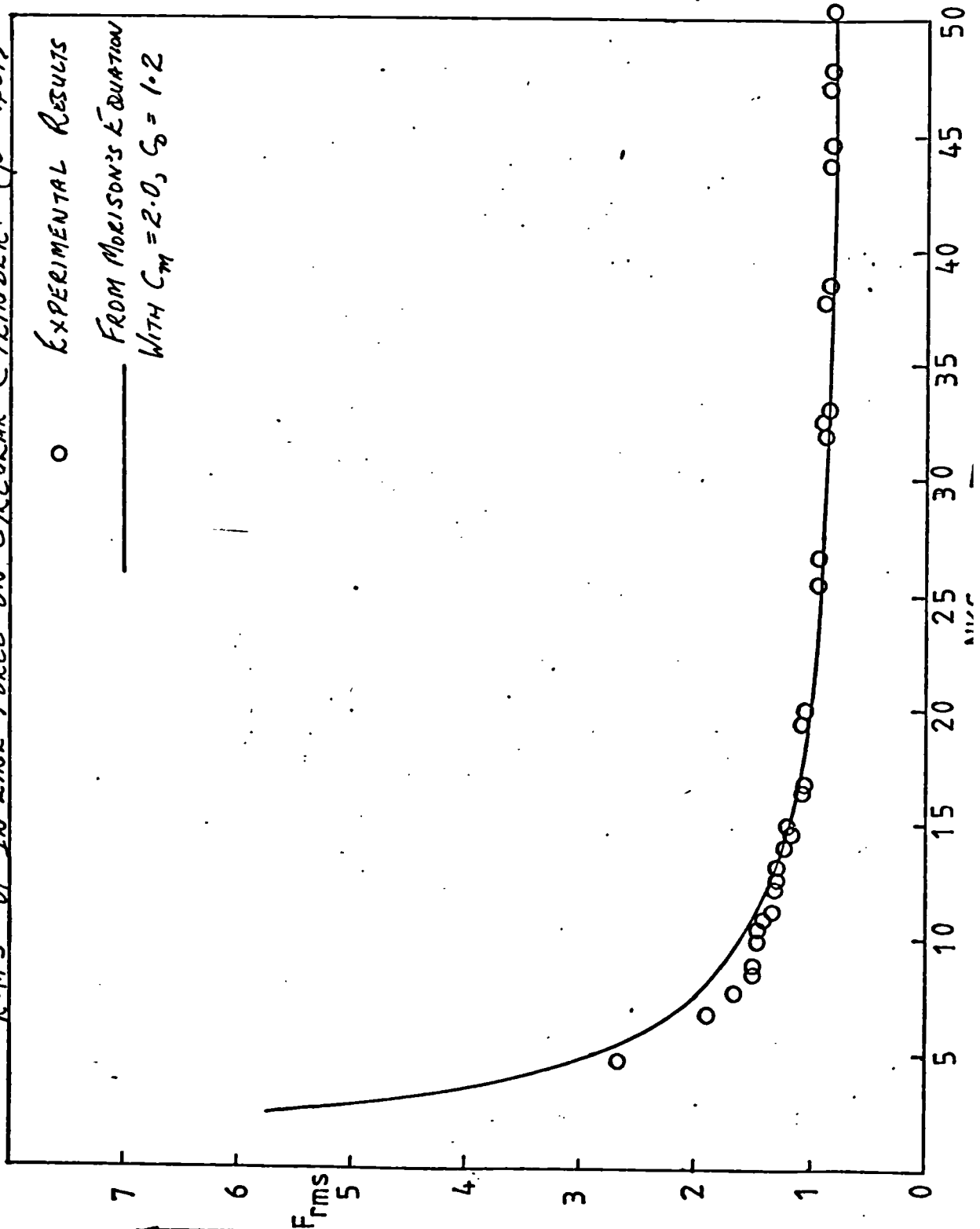
R.M.S OF IN LINE FORCE ON CIRCULAR CYLINDER (β = 451)
O EXPERIMENTAL RESULTS
FROM MORISON'S EQUATION WITH C_M = 2·0, C_D = 1·2
$C_{F_{rms}}$
0
1
2
3
4
5
6
7
5
10
15
20
25
30
35
40
45
50

FIG : 66

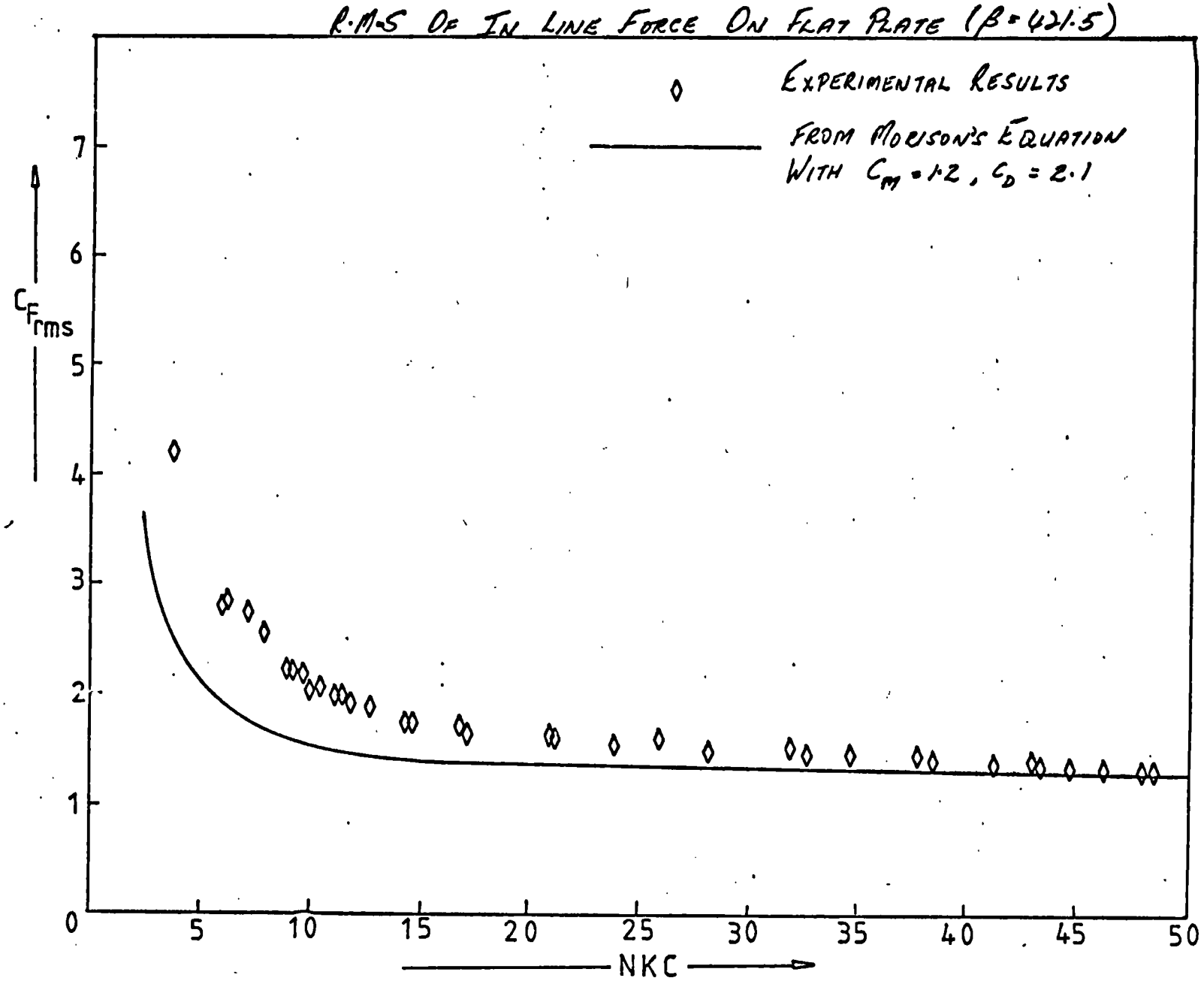
R·M·S OF IN LINE FORCE ON FLAT PLATE (β = 421·5)
EXPERIMENTAL RESULTS
FROM MORISON'S EQUATION
WITH $C_M = 1.2$, $C_D = 2.1$
$C_{F_{rms}}$
0
1
2
3
4
5
6
7
5
10
15
20
25
30
35
40
45
50
NKC

FIG: 6·7

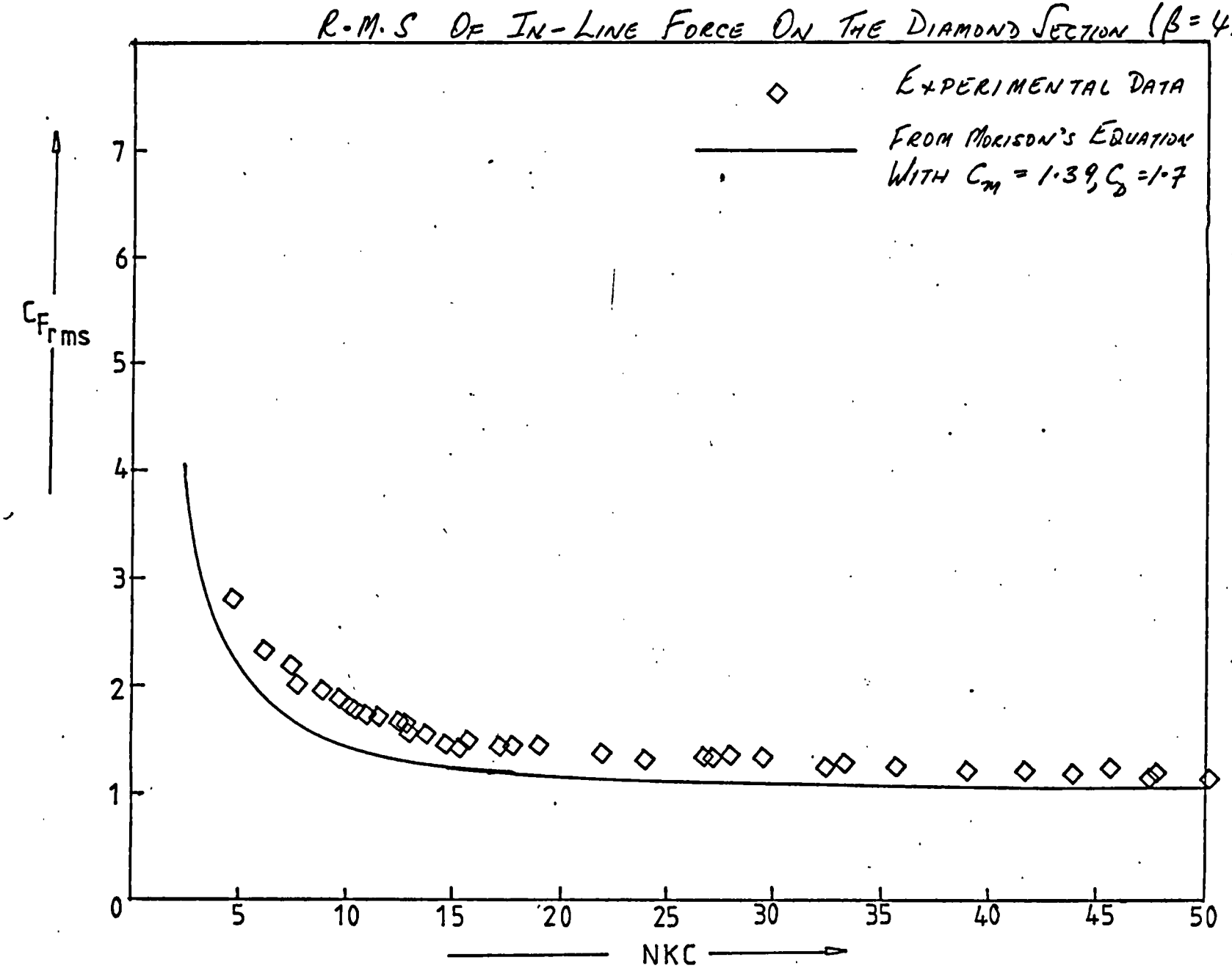
R.M.S OF IN-LINE FORCE ON THE DIAMOND SECTION (β = 422.7)
EXPERIMENTAL DATA
FROM MORISON'S EQUATION WITH $C_M = 1.39, C_D = 1.7$
$C_{F_{rms}}$
0
1
2
3
4
5
6
7
5
10
15
20
25
30
35
40
45
50
NKC

FIG : 6·8

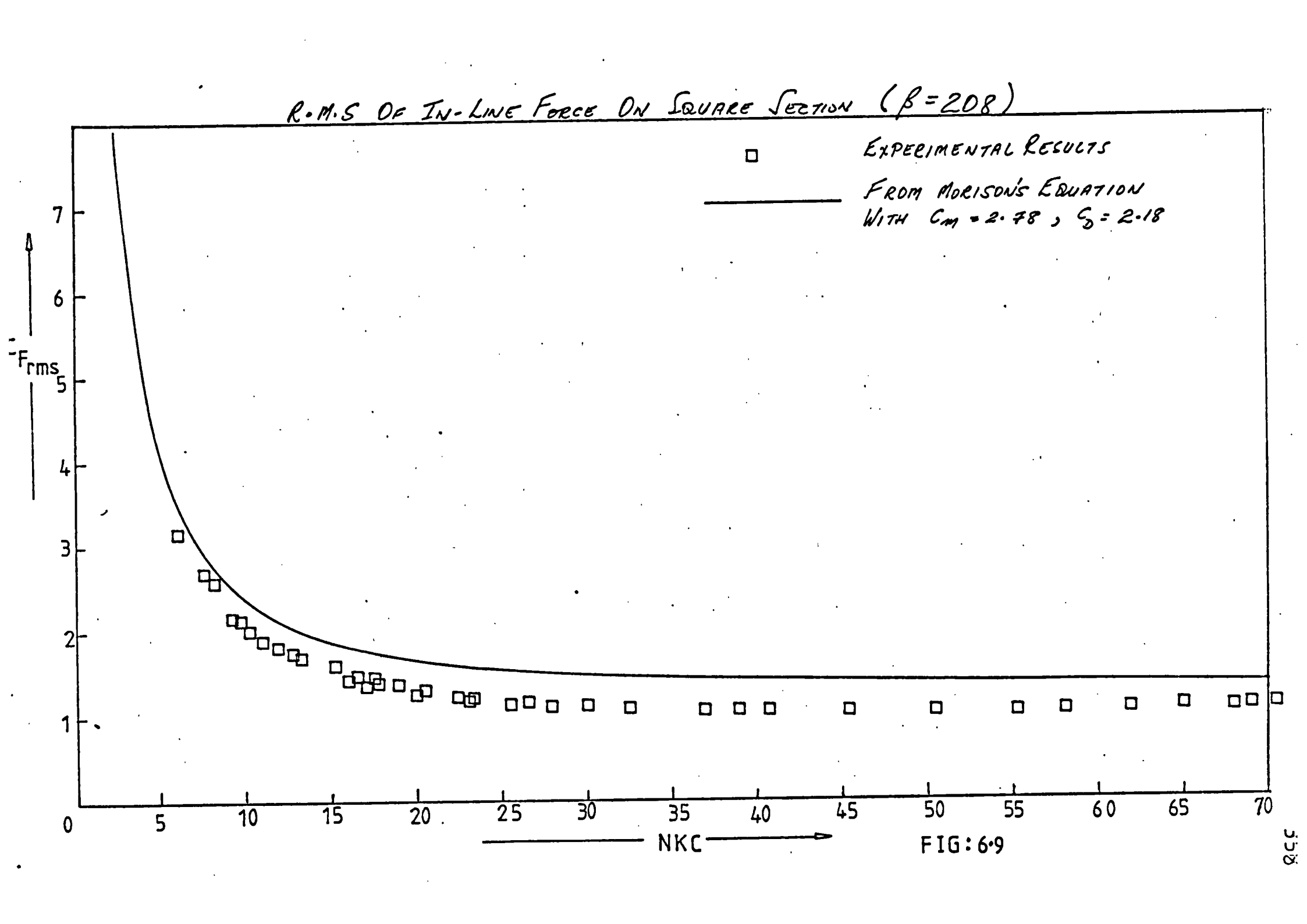
R.M.S OF IN-LINE FORCE ON SQUARE SECTION (β=208)
EXPERIMENTAL RESULTS
FROM MORISON'S EQUATION
WITH $C_M = 2.78$, $C_D = 2.18$
F_{rms}
0
1
2
3
4
5
6
7
5
10
15
20
25
30
35
40
45
50
55
60
65
70
NKC

FIG: 6·9